

Comprehensive Treatise of Electrochemistry

*Volume 6
Electrodics: Transport*

Edited by

Ernest Yeager

*Case Western Reserve University
Cleveland, Ohio*

J. O'M. Bockris

*Texas A&M University
College Station, Texas*

Brian E. Conway

*University of Ottawa
Ottawa, Ontario, Canada*

S. Sarangapani

*Union Carbide Corporation
Parma, Ohio*

 Springer

Comprehensive Treatise of Electrochemistry

*Volume 6
Electrodics: Transport*

COMPREHENSIVE TREATISE OF ELECTROCHEMISTRY

- Volume 1 **THE DOUBLE LAYER**
Edited by J. O'M. Bockris, Brian E. Conway, and Ernest Yeager
- Volume 2 **ELECTROCHEMICAL PROCESSING**
Edited by J. O'M. Bockris, Brian E. Conway, Ernest Yeager, and
Ralph E. White
- Volume 3 **ELECTROCHEMICAL ENERGY CONVERSION AND STORAGE**
Edited by J. O'M. Bockris, Brian E. Conway, Ernest Yeager, and
Ralph E. White
- Volume 4 **ELECTROCHEMICAL MATERIALS SCIENCE**
Edited by J. O'M. Bockris, Brian E. Conway, Ernest Yeager, and
Ralph E. White
- Volume 5 **THERMODYNAMIC AND TRANSPORT PROPERTIES OF
AQUEOUS AND MOLTEN ELECTROLYTES**
Edited by Brian E. Conway, J. O'M. Bockris, and Ernest Yeager
- Volume 6 **ELECTRODICS: TRANSPORT**
Edited by Ernest Yeager, J. O'M. Bockris, Brian E. Conway,
and S. Sarangapani
- Volume 7 **KINETICS AND MECHANISMS OF ELECTRODE PROCESSES**
Edited by Brian E. Conway, J. O'M. Bockris, Ernest Yeager,
S. U. M. Khan, and Ralph E. White

Comprehensive Treatise of Electrochemistry

Volume 6

Electrodics: Transport

Edited by

Ernest Yeager

*Case Western Reserve University
Cleveland, Ohio*

J. O'M. Bockris

*Texas A&M University
College Station, Texas*

Brian E. Conway

*University of Ottawa
Ottawa, Ontario, Canada*

S. Sarangapani

*Union Carbide Corporation
Parma, Ohio*

SPRINGER SCIENCE+BUSINESS MEDIA, LLC

Library of Congress Cataloging in Publication Data

Main entry under title:

Electrodics, transport.

(Comprehensive treatise of electrochemistry; v. 6)

Includes bibliographical references and index.

1. Electrodes. 2. Transport theory. I. Yeager, Ernest B., 1924-

QD552.C64 vol. 6 [DQ571]

541.37s

82-13144

ISBN 978-1-4615-6692-2

ISBN 978-1-4615-6690-8 (eBook)

DOI 10.1007/978-1-4615-6690-8

© 1983 Springer Science+Business Media New York

Originally published by Plenum Press, New York in 1983

Softcover reprint of the hardcover 1st edition 1983

All rights reserved

No part of this book may be reproduced, stored in a retrieval system, or transmitted in any form or by any means, electronic, mechanical, photocopying, microfilming, recording, or otherwise, without written permission from the Publisher

This volume is dedicated in memory of

PROFESSOR NORBERT IBL

of the Eidgenössische Technische Hochschule Zürich. Professor Ibl was the author of three chapters in this volume of the Treatise and offered much counsel to the editors in the organization of this volume. Professor Ibl was a pioneer in the development of electrochemical engineering and contributed much to this field through the training of many students as well as his original research in this area.

The Editors

Contributors

- A. J. Arvia**, Instituto de Investigaciones Físicoquímicas, Teóricas y Aplicadas (INIFTA), Sucursal 4, Casilla de Correo 16, 1900 La Plata, Argentina
- Yu. G. Chirkov**, Institute of Electrochemistry, Academy of Sciences of the USSR, Moscow
- Yu. A. Chizmadzhev**, Institute of Electrochemistry, Academy of Sciences of the USSR, Moscow
- O. Dossenbach**, Laboratory of Industrial and Engineering Chemistry, Swiss Federal Institute of Technology, Universitätstrasse 6, 8092 Zurich, Switzerland
- F. Goodridge**, Department of Chemical Engineering, Merz Court, Claremont Road, University of Newcastle upon Tyne, Newcastle upon Tyne NE1 7RU, England
- N. Ibl**, Laboratory of Industrial and Engineering Chemistry, Swiss Federal Institute of Technology, Universitätstrasse 6, 8092 Zurich, Switzerland, deceased
- S. L. Marchiano**, Instituto de Investigaciones Físicoquímicas, Teóricas y Aplicadas (INIFTA), Sucursal 4, Casilla de Correo 16, 1900 La Plata, Argentina
- H. Vogt**, Fachbereich Verfahrenstechnik der Technischen Fachhochschule Berlin, D-1000 Berlin 65
- A. R. Wright**, Department of Chemical Engineering, Merz Court, Claremont Road, University of Newcastle upon Tyne, Newcastle upon Tyne NE1 7RU, England

Preface to Comprehensive Treatise of Electrochemistry

Electrochemistry is one of the oldest defined areas in physical science, and there was a time, less than 50 years ago, when one saw "Institute of Electrochemistry and Physical Chemistry" in the chemistry buildings of European universities. But after early brilliant developments in electrode processes at the beginning of the twentieth century and in solution chemistry during the 1930s, electrochemistry fell into a period of decline which lasted for several decades. Electrochemical systems were too complex for the theoretical concepts of the quantum theory. They were too little understood at a phenomenological level to allow the ubiquity in application in so many fields to be comprehended.

However, a new growth began faintly in the late 1940s, and clearly in the 1950s. This growth was exemplified by the formation in 1949 of what is now called The International Society for Electrochemistry. The usefulness of electrochemistry as a basis for understanding conservation was the focal point in the founding of this Society. Another very important event was the choice by NASA in 1958 of fuel cells to provide the auxiliary power for space vehicles.

With the new era of diminishing usefulness of the fossil fuels upon us, the role of electrochemical technology is widened (energy storage, conversion, enhanced attention to conservation, direct use of electricity from nuclear-solar plants, finding materials which interface well with hydrogen). This strong new interest is not only in the technological applications of electrochemistry. Quantum chemists have taken an interest in redox processes. Organic chemists are interested in situations where the energy of electrons is as easily controlled as it is at electrodes. Some biological processes are now seen in electrodic terms, with electron transfer to and from materials which would earlier have been considered to be insulators.

It is now time for a comprehensive treatise to look at the whole field of electrochemistry.

The present treatise was conceived in 1974, and the earliest invitations to authors for contributions were made in 1975. The completion of the early volumes has been delayed by various factors.

There has been no attempt to make each article emphasize the most recent situation at the expense of an overall statement of the modern view. This treatise is not a collection of articles from *Recent Advances in Electrochemistry* or *Modern Aspects of Electrochemistry*. It is an attempt at making a mature statement about the present position in the vast area of what is best looked at as a new interdisciplinary field.

Texas A & M University
University of Ottawa
Case Western Reserve University
Texas A & M University

John O'M. Bockris
Brian E. Conway
Ernest B. Yeager
Ralph E. White

Preface to Volume 6

The past three decades have seen the rapid evolution of the transport aspects of electrochemical engineering into a formal part of electrochemistry as well as chemical engineering. With minor exceptions, however, this subject has not been systematically covered in any treatise or recent electrochemical text. The editors believe that the treatment in this volume will serve the function.

Chapter 1 presents a formal general framework for the overall principles of mass and charge in electrochemical systems. Chapters 2, 3, and 4 are concerned with more specific aspects of mass and charge transfer at electrodes, while Chapters 5, 6, and 7 are directed to the special topics of porous electrodes, flow-through electrodes, fluidized bed electrodes, and gas evolution in electrode systems.

The nomenclature and symbols in this volume conform with the recommendations of the IUPAC in the Manual of Symbols and Terminology for Physicochemical Quantities and Units, 1979 edition, published by Pergamon Press Ltd., Oxford, England, as prepared by the IUPAC Commission I-1. In a few instances there may be deviations from the symbols used in other volumes of the Treatise because of the overlapping use of symbols in different disciplines. A list of generally used symbols is given in the beginning of this volume. For chapters in which deviations have occurred or further symbols been introduced, an auxiliary notation list is also included with the chapter.

The editors owe special thanks to Professor N. Ibl, of Eidgenossische Technische Hochschule Zurich for his major contributions in both helping with the organizational aspects of this volume as well as contributing several chapters. All of the chapters in this volume have also been reviewed by external reviewers to whom the editors express their appreciation. Finally, the editors acknowledge the help of James O'Connor of Kennametal, Inc.

(Latrobe, Pennsylvania) in the preparation of the subject and author indices for this volume.

Case Western Reserve University
Texas A & M University
University of Ottawa
Union Carbide Corporation

Ernest B. Yeager
John O'M. Bockris
Brian E. Conway
S. Sarangapani

Contents

1. Fundamentals of Transport Phenomena in Electrolytic Systems

N. Ibl

1. Introduction	1
2. Fundamental Equations of Mass Transport: General Form	4
2.1. Flux and Velocity of a Species	4
2.2. Driving Forces	4
2.3. Relationship Between Fluxes and Driving Forces	5
2.4. Systems of Reference	7
2.5. Friction Coefficients	9
2.6. Conservation Equations	10
2.7. Recapitulation of Basic Equations and Comparison with Number of Variables	13
2.8. Scope of Applications of Generalized Equations	15
3. Fundamental Equations of Mass Transport: Approximation of Ideal and Dilute Solutions	16
3.1. Dilute Solutions	16
3.2. Ideal Dilute Solution	17
4. Charge Transport	18
4.1. Electric Current in Solution	18
4.2. Electrode Current	20
4.3. Local and Average Electrode Current Density	22
4.4. Current Efficiency	22
4.5. Electric Mobility; Conductivity	23
4.6. Transport Number	25
4.7. Transport of Charges through the Diffusion Layer	27
5. Elimination of Electric Potential from the Basic Equations	31
5.1. Ideal Dilute Solution	31
5.2. Nonideal, Concentrated Solutions of a Single Electrolyte	33
5.3. Remarks about the Diffusion Coefficients	35
5.4. Interfacial Flux Densities; Interfacial Velocities	37

6. Topics Related to the Electroneutrality Condition	39
6.1. Validity of the Electroneutrality Condition and Application of Poisson's Law	39
6.2. Concept of Interfacial Quantities	41
6.3. Overlap of the Diffusion Layer and the Double Layer	42
7. Some General Concepts Related to Mass and Charge Transport	43
7.1. Diffusion Potential	43
7.2. Concentration Overpotential	44
7.3. Mass Transport Control	47
8. Determination of Quantities of Practical Interest: Theoretical and Semi- empirical Methods	50
8.1. Quantities of Practical Interest	50
8.2. Outline of Theoretical Method	51
8.3. Semiempirical Procedures	54
9. Simplified Approach to Mass Transport in Electrolytic Systems	54
9.1. Approximation of the Ideal Dilute Solution and the Problem of the Diffusion Coefficient	54
9.2. Problem of the Species	56
10. Historical Note	58
11. Scope of Volume 6	61
<i>References</i>	62

2. Diffusion in the Absence of Convection: Steady State and Nonsteady State

S. L. Marchiano and A. J. Arvia

1. Transport Phenomena in Electrochemical Systems	65
2. Migration Flux	68
3. Diffusional Flux	68
4. Convective Flux	72
5. General Expression of the Mass Transfer Equation	72
5.1. Limiting Cases of Equation (27)	73
5.2. Migration Contribution	74
6. Pure Diffusion and the Mathematical Solution of the Diffusion Equation	75
7. Stationary State	77
7.1. Infinite-Plane Interface	78
7.2. Spherical Shell	80
7.3. Cylindrical Interface	81
8. Resolution of the Fick Equation: The Nonstationary State	82
8.1. Boundary Conditions for the Nonstationary Solutions under a Potent- tial Step Perturbation	82
8.2. Nonstationary Concentration Distribution Equation: Ideal Semi- infinite Plane Diffusion	84
8.3. Spherical Diffusion	90
8.4. Expanding Sphere Electrode	92
8.5. Cylindrical Diffusion	100

9. Solution of the Diffusion Equation under a Constant Flux: Galvanostatic Conditions	103
9.1. Reversible Electrochemical Reaction	105
9.2. Irreversible Electrochemical Process	106
9.3. Consecutive Diffusion-Controlled Electrochemical Reactions	107
9.4. Instantaneous Current Pulse	113
10. Diffusion Equation with Time-Dependent Boundary Conditions	114
10.1. Linear Potential/Time Perturbation	115
10.2. Mathematical Procedures	116
10.3. Solution by the Laplace Transform Method	116
10.4. Reversible Reaction	118
10.5. Irreversible and Quasireversible Electrochemical Reactions	121
11. Time-Dependent Boundary Conditions: Sinusoidal Perturbations	125
11.1. Potential Sinusoidal Perturbation	126
11.2. Sinusoidal Current Perturbation	128
<i>References</i>	129

3. Convective Mass Transport

N. Ibl and O. Dossenbach

1. Introduction	133
1.1. Convective Mass Transport: Qualitative Considerations	137
1.2. Nernst Model for the Diffusion Layer	139
1.3. Mass Transfer Coefficient	140
1.4. Application Example for the Nernst Model	140
1.5. Current-Voltage Curve: Limiting Current	141
1.6. Historical Note	142
2. Theoretical Approach Based on Fundamental Equations	143
2.1. Basic Equations	143
2.2. Prandtl Boundary-Layer Simplifications	146
2.3. Mass Transfer to a Plate in Laminar Flow	147
3. Dimensional Analysis	155
3.1. Principle	155
3.2. Dimensionless Groups	156
3.3. π -Theorem	157
3.4. Application Examples	158
3.5. Concluding Remarks	160
4. Analogy between Mass, Heat, and Momentum Transport	161
4.1. General Aspects	161
4.2. Application Example for a Theoretical Approach	164
4.3. Remarks on the Boundary Layers for Mass, Heat, and Momentum Transport	167
4.4. Advantage of Using Dimensionless Groups in Analogy Considerations	168
4.5. Considerations on Analogy with Momentum Transport	170
5. Mass Transport in Turbulent Flow	172
5.1. Fluctuating and Time-Averaged Quantities	172

5.2. Mass Transport Correlations	176
5.3. General Remarks	180
6. Influence of Migration on Limiting Currents	182
6.1. Introduction	182
6.2. Theoretical Approach	184
6.3. Approximate Method	190
7. Selected Systems of Interest to the Electrochemist	192
7.1. Introduction	192
7.2. Industrial Processes	192
7.3. Natural Convection	192
7.4. Channel Flow	200
8. Mass Transport Coupled with Chemical Reactions	205
9. Examples of Practical Calculations	208
9.1. Introduction	208
9.2. Copper Deposition in a Channel Cell	210
9.3. Copper Deposition Under Natural Convection Conditions	214
9.4. Concluding Remarks	216
10. Evaluation of Interfacial Concentrations	218
11. Applications of Convective Mass Transport Theory	220
11.1. Generalities	220
11.2. Electrochemical Systems as Models for Transport Measurements	220
11.3. Limitation of Reaction Rate by Mass Transport: Optimization	223
11.4. Scaling-Up Effects	230
<i>References</i>	234

4. Current Distribution

N. Ibl

1. Introduction: Practical Importance of Current and Potential Distribution	239
2. Experimental Methods	241
3. Main Types of Current and Potential Distributions	242
4. Outline of Theory of Primary and Secondary Distribution	243
5. Primary Distribution	245
5.1. Boundary Conditions	245
5.2. Kasper Method	246
5.3. Further Examples of Primary Distribution: Analytical Solutions for Plane Parallel and Disk Electrodes	247
5.4. Numerical Integration of the Laplace Equation	251
5.5. Some General Aspects of Primary Distribution	254
6. Secondary Distribution	255
6.1. Qualitative Considerations	255
6.2. Semiquantitative Concepts and Tests Used in Electroplating	258
6.3. Quantitative Treatment	260
7. Distribution with Finite Electrode Conductivity, Three-Dimensional Elec- trodes	277
7.1. Current Distribution	277
7.2. Variation of Potential	287

8. Tertiary Distribution	289
8.1. General Remarks	289
8.2. Distribution Over a Microprofile—Microscopic Throwing Power	290
8.3. Distribution Over a Macroprofile—Macroscopic Throwing Power	291
8.4. Case of Three-Dimensional Electrodes	296
8.5. Particular Case of Limiting Current—Mass Transport Control	299
9. Influence of a Few Other Kinds of Overpotentials	303
10. Current Distribution for the Case of Simultaneous Electrode Reactions	304
11. Historical Note	308
<i>References</i>	310

5. Porous Electrodes

Yu. A. Chizmadzhev and Yu. G. Chirkov

1. Introduction	317
1.1. Porous Electrode	318
1.2. Types of Porous Electrodes	320
2. Porous Media	321
2.1. Properties of Porous Media	321
2.2. Experimental Methods for Determining Characteristics of Porous Media	325
3. Capillary Equilibrium	330
3.1. Branching Processes	333
3.2. Lattice Models	335
3.3. Experimental Facts	342
4. Transport Processes	345
4.1. Convective Diffusion	345
4.2. Diffusion in Gases	353
4.3. Effective Electrical Conductivity	357
5. Electrochemical Activity of Electrodes	362
5.1. Two-Phase Electrodes	362
5.2. Three-Phase Hydrophilic Electrodes	368
5.3. Hydrophobic Electrodes	378
6. Conclusion	384
<i>References</i>	385

6. Porous Flow-Through and Fluidized-Bed Electrodes

F. Goodridge and A. R. Wright

1. Introduction	393
1.1. Aims and Treatment of the Chapter	393
1.2. General Considerations	394
2. Hydrodynamic and Mass Transfer Aspects of Three-Dimensional Electrodes	398
2.1. Hydrodynamic Aspects	398
2.2. Mass Transfer Aspects	404

3. Monopolar Three-Dimensional Electrodes	407
3.1. Mathematical Models	407
3.2. Industrial Aspects	425
4. Bipolar Three-Dimensional Electrodes	429
4.1. Mathematical Models	430
4.2. Experimental Aspects	436
4.3. Industrial Aspects	438
<i>References</i>	440

7. Gas-Evolving Electrodes

Helmut Vogt

1. Characterization of Gas-Evolving Electrodes	445
2. Regimes in Gas Evolution	446
3. Analogy with Boiling	447
4. Nucleate Gas Evolution	447
4.1. Nucleation	447
4.2. Bubble Growth	449
4.3. Bubble Departure	453
5. Mass Transfer	455
5.1. Empirical Correlations	456
5.2. Theoretical Approaches	456
5.3. Mass Transfer with Superposition of Liquid Bulk Flow	464
6. Heat Transfer	465
7. Film Gas Evolution	466
8. Bubble-Filled Electrolytes	471
8.1. Effective Conductivity	471
8.2. Rising Velocity of Gas Bubbles	473
8.3. Current Distribution and Ohmic Resistance	476
8.4. Influence of Temperature and Pressure	480
8.5. Electrode Geometry and Flow Conditions	481
<i>References</i>	483
 <i>Annotated Author Index</i>	 491
<i>Subject Index</i>	493

Notation

<i>a</i>	thermal diffusivity ($\text{m}^2 \text{s}^{-1}$)	<i>j</i> ₀	exchange current density (A m^{-2})
<i>a</i>	activity (mol kg^{-1})	<i>j</i> _x	local current density (A m^{-2})
<i>b</i>	electrode breadth (m)	<i>j</i> _{lim}	average limiting-current density (A m^{-2})
<i>c</i> _B	concentration of substance B (mol m^{-3})	<i>j</i> _∞	current density at infinite distance from edge of electrode (A m^{-2})
<i>c</i> '	wave velocity (m s^{-1})	<i>j</i> *	transfer current in three-dimensional electrode
cn	coordination number	<i>k</i>	thermal conductivity ($\text{kg m s}^{-2} \text{K}^{-1}$); rate constant (cm s^{-1})
<i>c</i> _p	specific heat ($\text{J kg}^{-1} \text{K}^{-1}$)	<i>k</i> _d	mass transfer coefficient (m s^{-1})
<i>d</i>	bubble departure diameter (m); specific gravity (dimensionless)	<i>l</i>	electrode length or height (m); characteristic length
<i>d</i> _h	hydraulic diameter (m)	<i>m</i>	mass; number of a layer of sites; number of components
<i>e</i>	charge of an electron (A s)	<i>n</i>	charge number of the cell reaction (dimensionless, positive); number of independent species (dimensionless); cell number
<i>f</i>	dimensionless velocity profile at plate electrode; roughness factor		
<i>g</i>	gravitational constant (9.81 m s^{-2}); porosity		
<i>h</i>	heat transfer coefficient ($\text{W m}^{-2} \text{K}^{-1}$); distance between electrodes (m)		
<i>j</i>	current density in solution (A m^{-2})		
<i>j</i>	average current density flowing through electrode (A m^{-2})		

n'	total number of species	y	direction perpendicular to electrode
p	pressure (Pa)		
q	heat flux density (W m^{-2}); volume flow rate ($\text{cm}^3 \text{s}^{-1}$)	y^* z	dimensionless distance direction parallel to electrode and perpendicular to flow
r_0	disk radius (m)		
r	radius (m); radial distance on disk electrode (m); pore radius; grain radius; ratio of supporting electrolyte concentration to total concentration (normalities)	z_a z_B z_C	number of active nucleation sites charge number of an ion B (dimensionless, positive for cations, negative for anions); number of adhering bubbles
s	electrode spacing (m); cross-sectional area of a pore (m^2); number of supercritical pores	A C	number of bubbles formed by coalescence area (m^2) dimensionless concentration
t	time (s); transport number (dimensionless)	C_d \mathcal{D}	double-layer capacitance diffusion coefficient based on thermodynamic driving force ($\text{m}^2 \text{s}^{-1}$)
t_B	residence time (s)		
t_W	waiting time (s)		
T	temperature (K)		
u^*	mechanical mobility ($\text{mol m s}^{-1} \text{N}^{-1}$)	D^*	effective diffusion coefficient of nonideal concentrated solution based on concentration gradient ($\text{m}^2 \text{s}^{-1}$)
u	electric mobility ($\text{m}^2 \text{s}^{-1} \text{V}^{-1}$)		
v	velocity (m s^{-1}); potential sweep rate (V s^{-1}); molecular volume	\bar{D}	integral (average) diffusion coefficient based on concentration gradients ($\text{m}^2 \text{s}^{-1}$)
$v_{B,r}^*$	rate of production of species B by homogeneous reaction r ($\text{mol m}^{-3} \text{s}^{-1}$)	D	diffusion coefficient of ideal dilute solution ($\text{m}^2 \text{s}^{-1}$)
w	width of the electrode (m)	E	strength of the electric field (V m^{-1})
x	direction parallel to electrode and to flow; number of moles of a species per mole of solution.	E E_0 F	electrode potential relative to solution (V) standard potential (V) Faraday constant ($96,500 \text{ A s mol}^{-1}$);

	adhesion force (kg m s^{-2})	R, R^*	ideal gas constant ($\text{J mol}^{-1} \text{K}^{-1}$)
$\Delta\tilde{G}$	driving force (affinity) (J mol^{-1})	R	number of homogeneous reactions; polarization resistance ($\Omega \text{ m}^2$)
H	Henry's law constant ($\text{kg m}^{-1} \text{s}^{-2}$)	R_a, R'_a	activation resistance ($\Omega \text{ m}^2$)
I	current (A)	R_B	departure bubble radius (m)
J	total current density in three-dimensional electrode (A m^{-2})	R_e	electrolyte resistance ($\Omega \text{ m}^2$)
K	permeability ($\text{cm}^3 \text{S}^{-1}$)	S_0	specific inner surface (m^{-1})
K_{ij}	interaction coefficient between species i and j ($\text{J m}^{-5} \text{s}$)	T	temperature (K)
L	characteristic length, electrode length (m); hydrodynamic and mass transfer entrance lengths (m); phenomenological coefficient ($\text{mol}^2 \text{J}^{-1} \text{m}^{-1} \text{s}^{-1}$); length of diffusion path (m)	V	volume (m^3)
L_h, L_M	hydrodynamic and mass transfer entrance lengths (m)	\dot{V}_G	gas volume flow rate ($\text{m}^3 \text{s}^{-1}$)
M	molar mass (kg mol^{-1})	Z	drag coefficient (dimensionless)
N	flux density ($\text{mol m}^{-2} \text{s}^{-1}$)	Z_f	faradaic impedance (Ω)
N	mass flux density ($\text{mol m}^{-2} \text{s}^{-1}$)	α	transfer coefficient; j/j_{lim} ; densification coefficient ($\text{m}^3 \text{mol}^{-1}$)
$N_{B,e}, \bar{N}_{B,e}$	local and average interfacial flux density of species B (perpendicular to interface) ($\text{mol m}^{-2} \text{s}^{-1}$)	β	constant in Tafel equation (V)
$\bar{N}_{B,\text{lim}}$	limiting average interfacial flux density of species B excluding migration ($\text{mol m}^{-2} \text{s}^{-1}$)	β'	thermal expansion coefficient
P	pressure ($\text{kg m}^{-1} \text{s}^{-2}$)	γ	dimensionless parameter; interfacial tension (N m^{-1}); activity coefficient, molality basis
		$\delta, \delta_T, \delta_V$	diffusion, thermal and hydrodynamic boundary layer thickness (m)
		$\varepsilon, \varepsilon_M$	turbulent transport coefficients ($\text{m}^2 \text{s}^{-1}$)
		ε	relative dielectric constant
		ε_0	permittivity of vacuum ($\text{A s V}^{-1} \text{m}^{-1}$)
		ν	contact angle

η	overpotential (V); similarity variable; rotational elliptic coordinate	ξ	rate of homogeneous reaction (mol s^{-1})
θ	current efficiency (dimensionless); fractional surface coverage (dimensionless)	ρ^*	space charge (A s m^{-3})
κ	specific conductivity ($\Omega^{-1} \text{m}^{-1}$)	ρ	density (kg m^{-3})
κ^*	effective specific conductivity ($\Omega^{-1} \text{m}^{-1}$)	τ	shear stress, momentum flux density (N m^{-2}); wave period; transition time
λ	wavelength (m); mean free path (m)	ϕ	electrical potential (V)
λ_B	ionic conductivity of species B ($\text{ohm}^{-1} \text{m}^2 \text{mol}^{-1}$)	ϕ_m	electric potential of metallic phase (V)
μ	dynamic viscosity ($\text{kg m}^{-1} \text{s}^{-1}$); chemical potential (J mol^{-1})	ϕ_l	electric potential of solution (V)
$\tilde{\mu}$	electrochemical potential (J mol^{-1})	$\Delta\phi$	potential difference across the interface (V)
ν	kinematic viscosity ($\text{m}^2 \text{s}^{-1}$)	χ	constant in Tafel equation (V); volume fraction (dimensionless)
ν	$\nu_+ + \nu_-$ (dimensionless)	ω	mass fraction (dimensionless); frequency of the ac signal (HZ)
ν_+, ν_-	number of moles of cations and anions, respectively, generated in the dissociation of one mole of neutral electrolyte (dimensionless)	ζ	friction factor
ν_i	stoichiometric coefficients of electrode reaction or of homogeneous reaction in solution (positive for products, negative for reactants (dimensionless)	Dimensionless Groups	
ξ	rotational elliptic coordinate; normalized concentration	f	friction factor; $f = 2\tau/\rho v_0^2$
		Sh	Sherwood number; $\text{Sh} = N_{B,e}x/D_B(c_{B,e} - c_{B,0})$
		$\overline{\text{Sh}}$	Sherwood number (average); $\overline{N}_{B,e}l/D_B(c_{B,e} - c_{B,0})$
		Nu	Nusselt number; $\text{Nu} = q_e l / a p c_p (T_0 - T_e)$
		Sc	Schmidt number; $\text{Sc} = \nu / D_B$
		Re	Reynolds number; $\text{Re} = vl/\nu$
		Re_x	vx/ν , Reynolds number (local)

Gr	Grashof number; $Gr = g(\rho_0 - \rho_e)L^3/\rho_0\nu^2$
j_D	Chilton–Colburn factor for mass transfer $j_D = Sh/Re Sc^{1/3}$
j_H	Chilton–Colburn factor for heat transfer $j_H = Nu/Re Pr^{1/3}$
Kn	Knudsen number λ/l
Pr	Prandtl number; $Pr = \nu/a$
Lf	Le Goff number; $Lf = 2j_D/f = 2j_H/f$
Wa	Wagner number
Wa'	Wagner number with two conductivities

Subscripts

A, B	species A, B (A = solvent)
b	mass average
e	electrode–solution interface
i	i th species
j	j th species
k	k th electrode reaction
k	reaction k
lim	limiting
m	migration
m	molar average
n	direction perpendicular to electrode
o	bulk solution
r	reaction r
r	r th homogeneous chemical reaction in solution

s	neutral electrolyte (e.g., $CuSO_4$)
t, T	total
$+, -$	cations and anions, respectively

Superscripts

	In general, denotes frame of reference:
A	velocity of solvent as reference
b	mass average (barycentric) velocity v_b as reference
m	molar average velocity v_m as reference
o	velocity v_o as reference

Vector Notation

∇	nabla operator
∇c	gradient of concentration (components: $\partial c/\partial x, \partial c/\partial y, \partial c/\partial z$)
$\nabla \cdot \mathbf{N}$	divergence of flux density = $\partial N_x/\partial x + \partial N_y/\partial y + \partial N_z/\partial z$
$\nabla^2 c$	divergence of the gradient of concentration = $\partial^2 c/\partial x^2 + \partial^2 c/\partial y^2 + \partial^2 c/\partial z^2$

Vectors are in bold type.

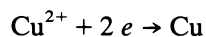
1

Fundamentals of Transport Phenomena in Electrolytic Systems

N. IBL

1. Introduction

In any electrolysis the species consumed (or generated) at the electrode must be transported toward it (or carried away). Let us consider as an example the electrodeposition of copper from a CuSO_4 solution. The copper ions migrate toward the cathode under the influence of the electric field. However, the sulfate ions migrate also (in the opposite direction) and carry part of the current. Meanwhile, at the cathode–solution interface, in the absence of secondary reactions, the whole of the electric current going through the electrode is due to the discharge of the copper ions:



Thus, there is a deficit in the transport balance. From, say, 10 Cu atoms deposited only 4 are transported by electric migration toward the cathode because the transport number of Cu^{2+} in the solution considered is about 0.4. The remaining 6 must reach the cathode by another transport mechanism, namely *diffusion*. This is a molecular mode of transport which tends to equalize

concentrations and which is set up only if concentration differences exist. Therefore, a depleted layer of Cu^{2+} ions must build up near the cathode. It is called the *diffusion layer*. The above result may be generalized: In the vicinity of an electrode through which an electric current flows, there is a diffusion layer in which the concentration of the solution is different from its value in the bulk. It is smaller or larger depending upon whether the species considered is consumed or generated at the electrode.

After the electrolysis current is switched on, the diffusion layer is set up and extends progressively toward the interior of the solution; i.e., its thickness grows with time. If there is convection (i.e., if there is a hydrodynamic flow), the stirring equalizes the concentrations at some distance from the electrode and the diffusion layer stops growing when it reaches the stirred region. A steady state is then established in which the concentration curve (Figure 1) and the thickness of the diffusion layer remain constant (independent of time). This thickness depends on the hydrodynamic conditions.

In general, ionic mass transport takes place by *diffusion, migration, and convection*. Diffusion is effective in the immediate vicinity of the electrode where there is no convection because of the friction forces at the interface. At increasing distance from the electrode, mass transport by convection becomes more and more important compared to diffusion. Beyond the diffusion layer, there are no concentration gradients and therefore no transport by diffusion. Finally, mass transport by electric migration takes place, in principle, both inside and outside of the diffusion layer.

Let us now consider again our example of copper deposition and let us increase, under otherwise identical conditions, the current density by increasing the voltage applied to the electrolysis cell. The rate of removal of the metal from the solution becomes larger, but the fraction of the current carried by the Cu^{2+} ions due to the electric field remains constant; i.e., the contribution of the migration to the transport does not change. Therefore, in the vicinity

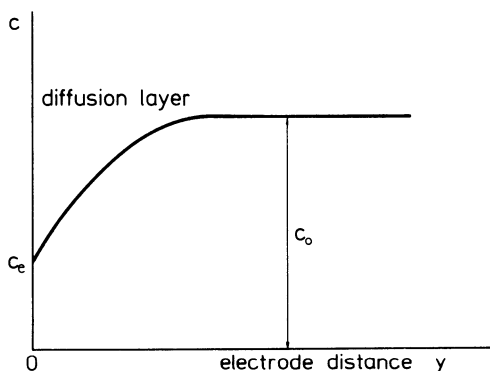


Figure 1. Concentration field near the cathode in the deposition of Cu from a CuSO_4 solution.

of the electrode the diffusion must be accelerated, and the result is that the concentration difference between the bulk and the interface must become larger; i.e., the concentration c_e at the interface of the cathode drops. Upon further increase of the current density, c_e finally becomes zero and the current which is then flowing is the *limiting current* of copper deposition. Any further increase in the applied voltage can lead to a current increase through a new reaction only—i.e., in the present case hydrogen evolution. The limiting current corresponds to the maximum rate at which an electrode reaction can be carried out under given hydrodynamic conditions.

At the limiting current the rate of the electrode reaction no longer depends on the kinetic parameter of that reaction (charge-transfer coefficient, exchange-current density). It is controlled by the mass transport. The transport phenomena thus play an important role in electrochemical kinetics. On the other hand, the limiting current is usually proportional to the bulk concentration of the species reacting at the interface, and its measurement can thus be used for the determination of this concentration. A number of analytical applications of electrochemistry are based on this fact. Let us further mention that in industrial electrolysis the limiting current determines the maximum utilization of the electrolytic cells and thus the minimum investment cost. These three aspects illustrate the role of the transport phenomena in the fields of electrochemical kinetics, electroanalytical chemistry, and electrochemical engineering. Their generally great importance in electrochemistry will become more apparent later in the respective chapters.

In the above introduction we have emphasized the link between mass transport and electrolysis (taken in the conventional sense). However, electrolytic mass transport also plays an essential role in the theory of subjects where such a link is unimportant or nonexistent (semiconductors, transport through membranes and ion exchangers, bioelectrochemistry).

In this volume, mass transport in electrolytic systems is reviewed. The subject is divided into a number of chapters corresponding to various subfields. However, there are some general concepts and basic equations common to these subfields and they constitute the stepping stone for the treatment given in Chapters 2 to 7. These common fundamentals will be presented in the following sections. We will start by writing the general equations and then show the validity conditions of the relationships more commonly used in practice. We will restrict ourselves to volume mass transport; surface diffusion will not be considered. Attention will be focused on fluid electrolytic systems and our concrete examples will refer to such systems, but, in principle, the equations presented are valid also for solid ionic conductors and semiconductors. In particular, Section 2 is fundamental for transport through membranes and ion exchangers. However, Section 2 may be skipped by readers who are interested only in an approximate treatment as commonly used in the case of aqueous electrolytic solutions.

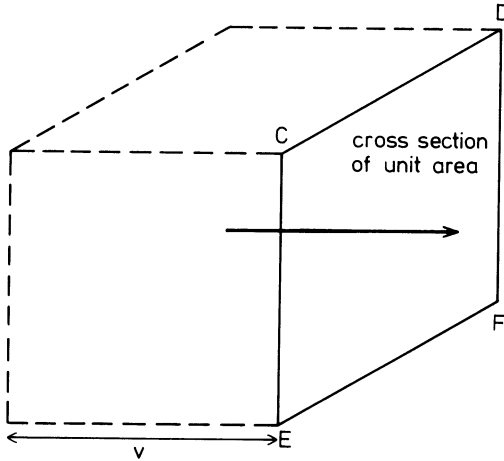


Figure 2. Derivation of relationship between flux density and velocity.

2. Fundamental Equations of Mass Transport : General Form

2.1. Flux and Velocity of a Species

We consider a multicomponent phase with species A, B, C, The flux density, or simply flux, \mathbf{N}_B of species B (at a given point of the fluid) is a vector that indicates the direction in which B moves, and its intensity is equal to the number of moles of species B which pass per unit time through a surface of unit area perpendicular to \mathbf{N}_B . The number of moles which pass per unit time through any infinitesimal surface of area $d\mathbf{A}$ is given by the scalar product of \mathbf{N}_B and of the vector $d\mathbf{A}$ representing the surface.

\mathbf{v}_B , the velocity of species B (m s^{-1}) is an average, macroscopic velocity, to be distinguished from the velocity of the individual molecules. \mathbf{v}_B is related in a simple manner to the flux density. Let us consider the surface CDEF of unit area perpendicular to \mathbf{v} (Figure 2). An amount of substance B found within the distance v crosses the surface per unit time. This amount is given by the concentration times the velocity. We thus have

$$\mathbf{N}_B = c_B \mathbf{v}_B \quad (1)$$

In general, \mathbf{N}_B is a function of location (x, y, z) and time.

2.2. Driving Forces

The species in an electrolytic solution move under the influence of the driving forces acting upon them. At constant temperature and pressure these

forces are the *gradients*[†] of the electrochemical potentials $\nabla\tilde{\mu}_i$. Indeed, the electrochemical potential

$$\tilde{\mu}_i = \mu_i + z_i F \phi \quad (2)$$

has the dimension of energy per mole, whereas the energy is a force times a length. Therefore, $\nabla\tilde{\mu}_i$ has the dimension of a force per mole. The situation is analogous to the one encountered in an electrical system, where the electric potential ϕ is an energy per unit charge and the field $\nabla\phi$ is the electric force per unit charge. $\nabla\tilde{\mu}_i$ is a generalized force in the sense of irreversible thermodynamics.⁽³⁻⁵⁾ We may note that it includes the electric force acting on an ionic species. This is readily seen by deriving Eq. (2) with respect to location (x, y, z) :

$$\nabla\tilde{\mu}_i = \nabla\mu_i + z_i F \nabla\phi \quad (2')$$

where z_i is the elemental charge of species i , F is the Faraday constant, and $z_i F$ is the electric charge carried by a mole of i . $z_i F \nabla\phi$ is then the electric force acting on 1 mole of i .

2.3. Relationship Between Fluxes and Driving Forces

The flux of a species B depends on the $\nabla\tilde{\mu}_i$ of any species i present in the solution. According to irreversible thermodynamics, not too far away from equilibrium there is a linear relationship between the fluxes and the driving forces.⁽³⁻⁵⁾ For a system at constant temperature and pressure we can write

$$\mathbf{N}_B^0 = \mathbf{N}_B - c_B \mathbf{v}_0 = - \sum_{i \neq A} L_{Bi}^0 \nabla\tilde{\mu}_i \quad \text{with } i = B, C, \dots \quad (3)$$

where the superscript 0 denotes the reference system (see below). The proportionality factors L_{Bi}^0 are called *phenomenological coefficients*. They are independent of the driving forces but functions of the composition of the phase, the temperature, and the pressure.

Let us note that the numerical values of the velocities \mathbf{v} depend on the frame of reference. From Eq. (1) it follows that the values of the fluxes, and therefore also those of the phenomenological coefficients, depend on the frame of reference. In Eq. (3) \mathbf{N}_B^0 represents a flux density relative to a frame of reference which moves at velocity \mathbf{v}_0 whereas \mathbf{N}_B is a flux density taken with respect to a fixed frame. More precisely, \mathbf{N}_B^0 and \mathbf{N}_B are relative to two frames of reference, the velocity of which differs by \mathbf{v}_0 . The most commonly used systems of reference are discussed in Section 2.4.

Note that the $\nabla\tilde{\mu}_i$ of Eq. (3) are not independent. They are linked through the Gibbs–Duhem equation which expresses the fact that the chemical and the electrochemical potentials are homogeneous functions of degree

[†] The reader not familiar with vector notation is referred to the Appendix in Newman's book⁽¹⁾ and to treatises on mathematics.⁽²⁾ (See also the Notation list.)

zero in the mole numbers n_i :

$$\sum_i n_i d\tilde{\mu}_i = 0 \quad \text{at constant } T \text{ and } P \quad (4)$$

The $\tilde{\mu}_i$ are functions of state and the difference $d\tilde{\mu}_i$ in the $\tilde{\mu}_i$ values between two points of the fluid at distance $d\mathbf{r}$ is

$$d\tilde{\mu}_i = \nabla \tilde{\mu}_i \cdot d\mathbf{r}$$

and we have

$$\sum \mu_i d\mu_i = \sum_i n_i \cdot \nabla \tilde{\mu}_i d\mathbf{r} = d\mathbf{r} \cdot \sum_i n_i \nabla \tilde{\mu}_i = 0$$

or

$$\sum_i n_i \nabla \tilde{\mu}_i = 0$$

One can thus eliminate one driving force from Eq. (3). In Eq. (3) we have produced unambiguous values of the phenomenological coefficients by omitting $\nabla \tilde{\mu}_A$ from the set of driving forces. This requires

$$L_{Bi}^0 = 0 \quad \text{for } i = A$$

i.e., $i = A$ is omitted from the sum in Eq. (3). $\nabla \tilde{\mu}_B$ is the *force conjugate* with the flux of B, \mathbf{N}_B^0 . The conjugate forces and fluxes determine the rate of local entropy production \dot{s} :

$$\sum_i \mathbf{N}_i^0 \cdot \nabla \mu_i = T\dot{s} \quad (5)$$

\dot{s} is the local rate of increase of the entropy density due to irreversible processes inside the volume element considered. If the composition of the volume element is independent of time (steady-state mass transport), the production of entropy corresponds to an increase in temperature of the volume, provided there is no exchange of heat with the environment of the volume.

In Eq. (3) L_{BB}^0 ($i = B$) is the coefficient conjugated with species B. The L_{Bi}^0 ($i \neq B$) are *coupling coefficients*. They express the influence of the driving forces other than that of the conjugated one. According to *Onsager's reciprocal law*, the matrix of the coupling coefficients is symmetric: $L_{Bi}^0 = L_{iB}^0$. Note, however, that there are many ways of defining the fluxes and driving forces. Onsager's law is valid only for adequately chosen systems. In particular, all fluxes and driving forces must be independent.

Generalized forces other than those considered in Eq. (3) can influence the flux of species B. In writing this equation we have assumed constant temperature T and pressure P [which is implied in writing the Gibbs–Duhem equation in the form (4)]. Therefore the $\nabla \tilde{\mu}_i$ appearing in our equations apply to constant T and P and represent in fact a $(\nabla \tilde{\mu}_i)_{T,P}$. The influence of pressure can be taken into account by writing $(\nabla \tilde{\mu}_i)_T$ instead of $(\nabla \tilde{\mu}_i)_{T,P}$ and remembering that $(d\mu_i)_T = (d\mu_i)_{T,P} + v_i dP$, where v_i is the partial molar volume of species

i. Thus in a system with a pressure gradient we have a driving force $v_i \nabla P$ in addition to $(\nabla \tilde{\mu}_i)_{T,P}$ and a corresponding additional term in Eq. (3). This may play a role in the transport of electrolytes through membranes as encountered in the desalination of water by hyperfiltration (reverse osmosis). However, usually one can neglect the influence of ∇P on the fluxes present in electrolytic systems. Likewise, a temperature gradient causes an additional driving force, which is to be taken into account by an additional term in Eq. (3).

In the following, we will not consider the influence of ∇T or ∇P on electrolytic mass transport and we will always write $\nabla \tilde{\mu}_i$ instead of $(\nabla \tilde{\mu}_i)_{T,P}$ for the sake of simplicity. Furthermore, we will disregard the effects of external forces such as gravity or centrifugal forces (or consider them as virtually compensated by ∇P). Even in electrolytic systems, however, it may be necessary to take the influence of such forces, as well as that of ∇P , into account when applying the equation expressing the conservation of momentum (see Section 2.6). Of course, another external force which is particularly important in electrolytic systems is that exerted by the electric field $\nabla \phi$ on charged species. However, this is included in $\nabla \tilde{\mu}_i$ for the reasons already mentioned.

2.4. Systems of Reference

As mentioned in Section 2.3, the numerical values of the phenomenological coefficients depend on the frame of reference, with the various conventions that are in use. One possibility is to select the velocity of one of the species as reference, say that of species A. Then $\mathbf{v} = \mathbf{v}_A$ and Eq. (3) takes the form

$$\mathbf{N}_B^{\wedge} = \mathbf{N}_B - c_B \mathbf{v}_A = - \sum_{i \neq A} L_{Bi}^{\wedge} \nabla \tilde{\mu}_i \quad \text{with } i = B, C, \dots \quad (3')$$

where L_{BA}^{\wedge} is zero because of the Gibbs–Duhem equation (see Section 2.3). With this velocity of reference the flux of species A, $\mathbf{N}_A^{\wedge} = \mathbf{N}_A - c_A \mathbf{v}_A$ is zero by definition, and all the corresponding phenomenological coefficients are also zero:

$$L_{Ai}^{\wedge} = 0$$

Another possibility is to use an average velocity as velocity of reference.^(1,6) The most commonly used ones are the *mass average* (or *barycentric*)† velocity \mathbf{v}_b (which is the velocity at which the center of gravity moves):

$$\mathbf{v}_b = \rho^{-1} \sum_i c_i M_i \mathbf{v}_i \quad i = A, B, C, \dots \quad (6)$$

† The usage in transport nomenclature is at present not uniform. Alternate names will be given and semantic remarks made occasionally as we proceed in the development of our subject. A more complete survey of the terminology of electrolytic mass transport is to be found in a review paper by Roy.⁽⁶⁾ The definitions and the nomenclature proposed by the International Union of Pure and Applied Chemistry is given in Reference 19.

and the *molar average* velocity \mathbf{v}_m

$$\mathbf{v}_m = c_T^{-1} \sum_i c_i \mathbf{v}_i = c_T^{-1} \sum_i \mathbf{N}_i \quad i = A, B, C, \dots \quad (7)$$

with

$$c_T = \sum_i c_i$$

where M_i is the molar mass, c_T the total concentration (mol m^{-3}), and ρ the average density (kg m^{-3}).

For instance, the flux of species B referred to the molar average velocity is

$$\mathbf{N}_B^m = \mathbf{N}_B - c_B \mathbf{v}_m \quad (8a)$$

or

$$\mathbf{N}_B = c_B \mathbf{v}_m + \mathbf{N}_B^m = c_B \mathbf{v}_m - \sum_{i \neq A} L_{Bi}^m \nabla \tilde{\mu}_i \quad i = B, C \quad (8b)$$

The fluxes referred to the barycentric velocity are best expressed as fluxes of mass (e.g., the mass flux of B being obtained by simply multiplying the molar flux by the molar mass). Mass fluxes are more convenient than molar ones when used in conjunction with relationships such as Eq. (15). The numerical values of the coefficients L_{Bi} are different in the two cases because they are expressed in the units $\text{mol}^2 (\text{J ms})^{-1}$ and $\text{kg}^2 (\text{J ms})^{-1}$. The similarities and differences between the mass and the molar systems are discussed in more detail by Roy.⁽⁶⁾ Note that because of Eqs. (8a) and (7) we have

$$\sum_i \mathbf{N}_i^m = 0 \quad (9)$$

The sum of all fluxes *referred to the average velocity* is zero. This can be interpreted as follows. In Eq. (8b) the term $c_B \mathbf{v}_m$ represents a flux connected with the *bulk movement of the fluid* (convective flux) whereas $\mathbf{N}_B^m = -\sum_i L_{Bi}^m \nabla \tilde{\mu}_i$ is a flux *relative* to the average velocity and is due to the $\nabla \tilde{\mu}_i$, i.e., to forces internal to the system. In summation, the effects of these forces cancel. This does not mean, however, that the average velocity (e.g., taken relative to the container of the fluid) is zero. The value of this velocity is determined by the fact that it must fulfill the condition of conservation of momentum (see Section 2.6).

Because of Eq. (9), one can express one of the fluxes, for instance, that of A, in terms of the other fluxes. If we consider n species there are only $n - 1$ independent equations such as (8b). Further, we may apply the Gibbs–Duhem equation and eliminate one of the $\nabla \tilde{\mu}_i$, for instance, $\nabla \tilde{\mu}_A$, as was done in Eq. (3). This requires $L_{Bi}^m = 0$ for $i = A$; i.e., $i = A$ is omitted in the sum of Eq. (8b). Equation (8b) thus generates $(n - 1)^2$ phenomenological coefficients such as L_{Bi}^m . The number of independent coefficients is further restricted by Onsager's reciprocal law (see Section 2.5).

Note that in the case when the flux is referred to the velocity of a species, there are likewise $n - 1$ independent equations such as (3)[†] because this equation need not be written for the species taken as the reference. Let us consider a simple example—a binary mixture of water (A) and sucrose (B). If the water is taken as reference we have

$$L_{AA}^A = L_{AB}^A = L_{BA}^A = 0$$

and the Eq. (3') reduces to

$$\mathbf{N}_B^A = -L_{BB}^A \nabla \tilde{\mu}_B \quad (3'')$$

In this case there is only one independent driving force and one independent phenomenological coefficient.

2.5. Friction Coefficients

An alternative way of presenting the mass transport phenomena is to consider the *friction* between two species, B and A, which is due to the molecular motion of these two species. The driving force given by the gradient $\nabla \tilde{\mu}_B$ of the electrochemical potential of B must overcome the friction forces between B and all the other species in the solution. Per unit volume this driving force is $c_B \nabla \tilde{\mu}_B$. On the other hand, the friction forces are proportional to the velocity differences $\mathbf{v}_i - \mathbf{v}_B$. Thus we have

$$\begin{aligned} c_B \nabla \tilde{\mu}_B &= \sum_{i \neq B} K_{Bi} (\mathbf{v}_i - \mathbf{v}_B) \\ &= RT \sum_{i \neq B} c_B c_i (c_T \mathcal{D}_{Bi})^{-1} (\mathbf{v}_i - \mathbf{v}_B) \end{aligned} \quad (10a)$$

K_{Bi} is the coefficient of friction between species B and i . Equation (10a) further introduces the interaction diffusion coefficients \mathcal{D}_{Bi} (between B and i), which are more commonly used than the friction coefficients.

Because of Newton's principle of action and reaction we have

$$\mathcal{D}_{Bi} = \mathcal{D}_{iB} \quad \text{and} \quad K_{Bi} = K_{iB} \quad (10b)$$

From Eq. (10b) and noting[‡] that $\mathcal{D}_{BB} = 0$, it is seen that for a system with n species the number of independent coefficients defined by the above equations is $\frac{1}{2}n(n - 1)$.

As mentioned earlier, we may note that the Gibbs–Duhem equation similarly restricts the number of independent transport coefficients defined

[†] The coupling in Eq. (3) arising in the case of chemical reactions between the species will be briefly considered in Section 9.2.

[‡] In addition, one has the Gibbs–Duhem equation but this is not an independent condition because it is automatically fulfilled through Eq. (10b) as can be readily seen by making the sum of Eq. (10a) for all species, which yields $\sum_i c_i \nabla \tilde{\mu}_i = 0$. It follows from this, however, that there are not n but only $n - 1$ independent equations in the form of (10a).

by Eq. (3) (Section 2.3). It can be readily shown that the number of these coefficients is again $\frac{1}{2}n(n-1)$. In fact, Eqs. (3) and (10a) are alternative, equivalent forms of the fundamental relationships between fluxes and driving forces. The coefficients \mathcal{D}_{Bi} and L_{Bi} of the two sets of equations are linked by simple correlations.^(1,11) Equation (10a) has the advantage of being more illustrative because it shows the equality between the driving force and the friction resistance. On the other hand, Eq. (3) is much more convenient to use in the derivation of the relationships expressing the conservation of mass, which will be discussed in the next section.

2.6. Conservation Equations

The equations of Sections 2.3 and 2.5 are usually not sufficient to calculate the quantities of practical interest for given experimental conditions. One has to consider, in addition, one or more of the equations expressing the conservation of mass, momentum, and energy.

Let us first deal with the basic equation derived from the principle of *conservation of mass*. We make a mass balance of species B for an infinitesimal volume ($dx dy dz$) (Figure 3). The change of the amount of substance of species B contained in the volume with time t , is given by the difference between the fluxes of B entering and leaving the volume (see caption of Figure 3) and by the amount of B generated or consumed in the volume. We have

$$\frac{dc_B}{dt} = -\nabla \cdot \mathbf{N}_B^0 + \sum_r v_{B,r}^* \quad (11a)$$

$v_{B,r}^*$ is the number of moles of species B produced (or consumed) per unit time and per unit volume through the homogeneous reaction r taking place in the solution. The summation extends over all reactions in which B participates,† and dc_B/dt is the change of concentration of species B with time at the point of the solution considered. This point moves with the velocity of the reference frame, \mathbf{v}_0 ; i.e., it is the overall time change in concentration seen by an “observer” moving at velocity \mathbf{v}_0 . Let us also calculate the change in concentration $\partial c_B/\partial t$ at a fixed point (e.g., fixed with respect to the container of an electrolytic solution). If \mathbf{v}_0 is taken relative to the container we can write

$$\mathbf{N}_B^0 = \mathbf{N}_B - c_B \mathbf{v}_0 \quad (3)$$

† In irreversible thermodynamics the generation (or consumption) of a species by a homogeneous reaction is regarded as a flux, the driving force being the affinity ΔG of the reaction. This force has been omitted in writing Eq. (3) although homogeneous chemical reactions often occur as part of the overall electrochemical processes. The reason is that \mathbf{N}_B is a vector whereas the flux corresponding to a chemical reaction is a scalar (at least in an isotropic medium). According to the Curie theorem there can be no coupling between quantities represented by vectors and scalars. Homogeneous reactions therefore appear only as source terms in the relationships expressing the conservation of mass.

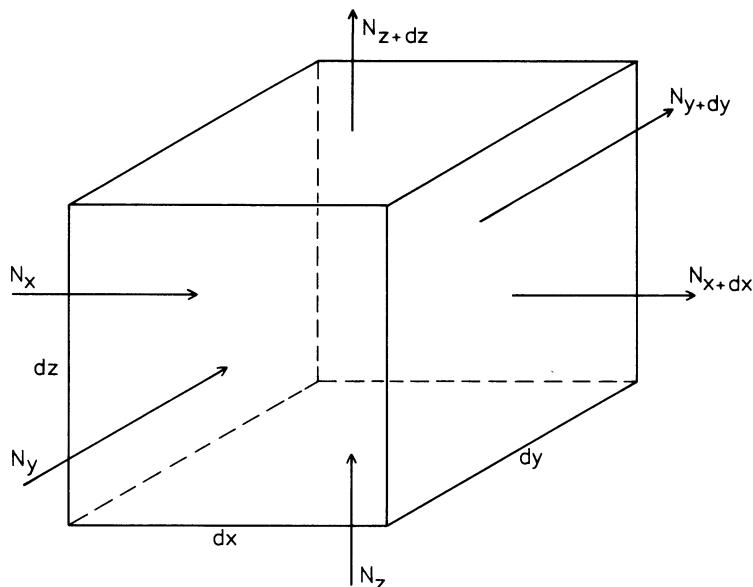


Figure 3. Volume element for derivation of conservation equation. The concentration change due to the difference between the amount of species B entering and leaving the volume element is

$$\begin{aligned} \frac{\partial c_B}{\partial t} &= \frac{1}{dx dy dz} [(N_{x+dx} - N_x) dy dz + (N_{y+dy} - N_y) dx dz \\ &\quad + (N_{z+dz} - N_z) dx dy] \\ &= -\frac{1}{dx dy dz} \left(\frac{\partial N_x}{\partial x} dx dy dz + \frac{\partial N_y}{\partial y} dy dx dz + \frac{\partial N_z}{\partial z} dz dx dy \right) = -\nabla \cdot \mathbf{N}_B \end{aligned}$$

and

$$\nabla \cdot \mathbf{N}_B^0 = \nabla \cdot \mathbf{N}_B - \nabla \cdot c_B \mathbf{v}_0$$

so that

$$\frac{\partial c_B}{\partial t} = \frac{dc_B}{dt} + \nabla \cdot c_B \mathbf{v}_0 = -\nabla \cdot \mathbf{N}_B + \sum_r v_{Br}^* \quad (11b)$$

$\partial c_B / \partial t$ is the change in concentration with time seen by an observer looking through a window into the container. Comparison of (11b) and (11a) shows that the change of the reference frame involves an additional term $\nabla \cdot c_B \mathbf{v}_0$. This represents the change in concentration with time seen by an observer moving at the velocity \mathbf{v}_0 , because the *observer is moving*.

When Eq. (11a) is used in conjunction with Eq. (15), it is of advantage to refer the fluxes to the barycentric velocity \mathbf{v}_b and to use the mass system of units instead of the molar one. ($^* \mathbf{N}_B$ is the flux density of B in $\text{kg m}^{-2} \text{s}^{-1}$,

ρ_B the mass concentration of B in kg m^{-3} , $v_{B,r}^*$ the amount of B produced in $\text{kg m}^{-3} \text{ s}^{-1}$.) Equation (11a) then takes the form

$$\frac{d\rho_B}{dt} = -\nabla \cdot \mathbf{N}_B^b + \sum_r v_{B,r}^* \quad (11c)$$

In addition, for ionic species one has the electroneutrality condition

$$\sum_i z_i c_i = 0 \quad (12)$$

where z_i is the ionic charge (positive for cations, negative for anions).

In principle, it is the integration of Eq. (11a), with the appropriate boundary conditions, which yields the quantities of practical interest (see Section 2.8). However, the fluxes of the species are expressed relative to a reference velocity, which, for the purpose of the present discussion, is conveniently taken as the mass average velocity defined in Section 2.4. This velocity must be known in order to perform mass transfer calculations. In many systems, the velocity distribution is determined by momentum considerations. Therefore, in addition to Eq. (11a) one must take into account the mechanics of the fluid. They are governed by two basic relationships: the equations of continuity and of Navier–Stokes.

An overall mass balance for an infinitesimal volume yields

$$\frac{\partial \rho}{\partial t} = -\nabla \cdot (\rho \mathbf{v}_b) \quad (13)$$

where ρ is the average density of the fluid. In Eqs. (13) and (15) $\partial \rho / \partial t$ and $\partial(\rho \mathbf{v}_b) / \partial t$ refer to a fixed point if \mathbf{v}_b is the velocity referred to a coordinate system linked with a container at rest. In electrolytic systems the fluid, to a good approximation, can usually be considered as incompressible; i.e., the density is independent of location and time. Equation (13) thus reduces to

$$\nabla \cdot \mathbf{v}_b = 0 \quad (14)$$

This is the *continuity equation* of hydrodynamics.

The Navier–Stokes equation is a consequence of Newton's law, expressed as the principle of *conservation of momentum*. We again take the balance for an infinitesimal volume, $dx dy dz$. The change with time of the amount of momentum contained in the volume $[\partial(\rho \mathbf{v}_b) / \partial t]$ is given by the difference between the momentum fluxes entering and leaving the volume and by the external forces acting on the volume [which correspond to the source term $\sum_r v_{B,r}^*$ in Eq. (11a)]. For a *Newtonian incompressible fluid*[†] with a dynamic viscosity μ we have

$$\frac{\partial(\rho \mathbf{v}_b)}{\partial t} = -\mathbf{v}_b \cdot \nabla(\rho \mathbf{v}_b) + \mu \nabla^2 \mathbf{v}_b - \nabla p + \rho \mathbf{g} \quad (15a)$$

[†] A Newtonian fluid is one in which the viscosity is independent of the shear stress.⁽⁸⁾

∇p is the gradient of the hydrostatic pressure and $\rho \mathbf{g}$ the force of gravity per unit volume. $\mu \nabla^2 \mathbf{v}_b$ is the shear stress acting on the faces of the infinitesimal volume. The shear stress can also be regarded as the divergence of the flux of momentum entering and leaving the volume. This aspect, which points out the analogy between mass and momentum transport, will be worked out more fully in Chapter 3. For a more detailed discussion of the Navier–Stokes equation the reader is referred to the literature.^{(1,8–10)†}

In some circumstances heat transport has to be considered in addition to mass and momentum transport. A conservation equation analogous to Eq. (11a) holds for heat transport. More attention will be given to this mode of transport in Chapter 7 and Chapter 3 (Section 3.4), mainly from the viewpoint of the analogy with mass transport. However, heat transport in electrolytic systems will not be treated any further in this volume.

2.7. Recapitulation of Basic Equations and Comparison with Number of Variables

It is of interest at this stage to recapitulate the general basic relationships presented in the preceding sections and to compare their number to that of the unknowns in the usual electrolytic mass transport problems. As we have seen in Section 2.4, in the case of n species there are $n - 1$ independent equations for the fluxes [Eq. (3)]. If homogeneous reactions between the species take place, n is the number of “independent” species which, in a solution at equilibrium, is equal to $n' - R$ (where n' is the total number of species and R the number of chemical equilibria in which they are involved). We will return to this question in Section 9.2.

The number of independent coefficients L_{Bi} or \mathcal{D}_{Bi} is restricted by the Gibbs–Duhem equation and by Onsager’s reciprocal law and is equal to $\frac{1}{2}n(n - 1)$ (Section 2.5).

The driving forces in Eq. (3) can be written [see Eq. (2)]

$$\nabla \tilde{\mu}_i = \nabla \mu_i + z_i F \nabla \phi = RT \nabla \ln a_i + z_i F \nabla \phi \quad (15b)$$

The independent equations (3) include as variables $n - 1$ flux densities \mathbf{N} , $n - 1$ activities a_i of the species, the potential ϕ , and the reference velocity \mathbf{v}_0 , which we will take as the mass average velocity $\mathbf{v}_0 = \mathbf{v}_b$ in what follows. Thus, there are $2n$ variables which are usually unknown. Indeed, they are local values at a given instant (i.e., dependent on x, y, z, t) and are determined only in a general way by the external conditions imposed on the system. They represent fields which, in a general approach, have to be calculated by

† Applying the principle of conservation of momentum to the average velocity and coupling the resulting equation with the relationships expressing the conservation of mass is the classical procedure. An alternate approach involving equations expressing the conservation of momentum for the *individual species* has been discussed in the literature in recent years. It is reviewed in the book by Slattery.⁽⁷⁾

integrating differential equations with appropriate boundary conditions. The latter will be discussed in Section 8.2. For the moment, let us ascertain whether we have enough equations to solve the problem. In addition to the $n - 1$ equations for the fluxes we need $n + 1$ further relationships. One is provided by the electroneutrality condition[†] (12) which is usually exploited to eliminate the electric potential (see Sections 5.1 and 5.2). Furthermore, the relationship expressing the conservation of momentum, Eq. (15a), offers itself for the calculation of the mass average velocity \mathbf{v}_b (velocity of the center of gravity). Finally, we have the conservation of mass equations [(11a) Section 2.6] which can be written for each species. We need $n - 1$ such equations and this number is certainly available since there are $n - 1$ independent flux densities in these equations.

However, the situation is simple only if no homogeneous chemical reactions take place within the diffusion field, since then all $v_{B,r}^*$ in Eq. (11a) are nil. For each species taking part in a homogeneous reaction additional variables $v_{B,r}^*$ are introduced in Eq. (11a). Let us examine how to deal with these additional unknowns, remembering that in the case of R homogeneous reactions the total number of species is $n' = n + R$. The source terms $v_{B,r}^*$ in Eq. (11a) are linked by the stoichiometry of the reactions involved. For each reaction r we can write, for a species B taking part in that reaction,

$$v_{B,r}^* = \nu_{B,r} \dot{\xi}_r V^{-1} \quad (15c)$$

where $\nu_{B,r}$ is the stoichiometric number of species B in reaction r , V the volume, and $\dot{\xi}_r$ the rate of reaction r . We have thus reduced the source terms $v_{B,r}^*$ to R variables $\dot{\xi}_r$. Furthermore, we can apply the conservation of mass principle to each reaction r :

$$\sum_i \nu_{B,r} M_B \dot{\xi}_r V^{-1} = 0 \quad (15d)$$

where the summation extends over all species engaged in reaction r and the M_B terms are the molar masses. There are R equations for (15d).

Now, before proceeding further, we have to distinguish two cases: (a) the phase is at equilibrium with respect to homogeneous reactions (i.e., these reactions are very fast compared to the rate of mass transport so that they are virtually at equilibrium); (b) the phase is not at equilibrium, i.e., some or all of the homogeneous reactions are irreversible.

In case (a) we have R equilibrium equations ($\Delta G = 0$), in addition to the R equations for (15d). Therefore, we can both eliminate the R unknowns $\dot{\xi}_r$ and reduce the number of equations for (11a) by R . We have thus eliminated all the source terms in Eq. (11a) and we still have $n - 1 = n' - R - 1$ independent equations for (11a).

[†] In the rare case where the electroneutrality of the solution is not a sufficient approximation, Poisson's equation (71) has to be used instead. The validity of the electroneutrality condition is discussed in Section 6.1.

In case (b), when none of the reactions is at equilibrium, we are missing the R equilibrium conditions. We must replace them by R kinetic laws which allow us to express the R reaction rates $\dot{\xi}_r$ in terms of the activities of the species. If these laws are available we can eliminate all the $\dot{\xi}_r$ and use the R equations for (15d) to reduce the number of equations for (11a) by R . Again, we still have $n - 1$ independent equations for (11a).

Therefore, independently of whether homogeneous reactions between the species are present or not, we have $n - 1$ equations for (11a), $n - 1$ equations for (3), the electroneutrality condition (12), and the equation expressing the conservation of momentum (15a). This is enough to determine the $2n$ unknowns of the game. We may conclude that the fundamental equations presented in the previous sections are sufficient, in principle, to solve the problem of electrolytic mass transport. We do not need the equation expressing the conservation of energy, provided the system is at constant temperature. If temperature gradients are present an additional equation is necessary, which is provided by the conservation of energy principle.

2.8. Scope of Applications of Generalized Equations

The general form of the fundamental equations presented in the preceding sections is very complicated and difficult to apply. In practice, more or less drastic simplifications of various kinds are made. The most commonly used approximation is that of the ideal and dilute solution, which will be discussed in more detail in the next section. In particular, the coupling terms in Eq. (3) are usually neglected in electrolytic mass transport. However, there are important cases where such simplifications are too far from reality.

This often applies, for instance, to fused salts⁽³²⁾ where the mole fraction of the component in which one is interested may not be sufficiently small compared to 1. An extreme situation is that of the melt of a single salt such as fused NaCl. As an example we will briefly discuss in Section 4.6 the consequence of this peculiar state of affairs for a specific transport quantity—the transport number.

Another category of systems where dilute solution theory often can not be applied are membranes. An example is the transport of water and of NaCl through the membranes used in hyperfiltration for the desalination of water. In this case the coupling coefficients L_{Bi} ($i \neq B$) and the corresponding coupling fluxes cannot be ignored. A review of this problem has been given by Bennion and Rhee.⁽¹¹⁾ Another example where the coupling coefficients may be of importance are the membranes encountered in bioelectrochemistry and, more generally, in biology. It can be that the species flows in the direction opposite to that of the conjugated force; i.e., that, B flows contrary to the gradient of $\tilde{\mu}_B$ (active transport).^(24,26) This is due to a special coupling mechanism involving a reaction with a carrier which transports the species across the membrane.

3. Fundamental Equations of Mass Transport : Approximation of Ideal and Dilute Solutions

3.1. Dilute Solutions

If a species B (and all other species except the solvent) are present at low concentration in a solvent A the friction between B and all other species, except the solvent, can be ignored. Therefore, in Eq. (10a) all K_{Bi} ($i \neq A$) and all \mathcal{D}_{Bi} ($i \neq A$) are negligible. This equation thus reduces to

$$c_B \nabla \tilde{\mu}_B = RTc_Bc_A(c_T\mathcal{D}_{BA})^{-1}(\mathbf{v}_A - \mathbf{v}_B)$$

or

$$\mathbf{N}_B^A = \mathbf{N}_B - c_B\mathbf{v}_A = c_B(\mathbf{v}_B - \mathbf{v}_A) = -(RTc_A)^{-1}c_T\mathcal{D}_{BC}c_B \nabla \tilde{\mu}_B \quad (16a)$$

Equation (16a) can also be obtained from Eq. (3') (Section 2.4) taking into account that in a dilute solution the coupling coefficients L_{Bi} ($i \neq B$) are negligible and that[†] \mathcal{D}_B is given by

$$\mathcal{D}_{BA}^A = \mathcal{D}_B = L_{BB}^A RTc_A(c_Bc_T)^{-1} \quad (16b)$$

The use of \mathcal{D} instead of L in Eq. (16a) has the advantage that the first of these two coefficients is much less concentration dependent than the second one.

In electrolytic systems, the flux density is usually separated into a chemical and an electric term by taking into account Eq. (2), which relates the electrochemical to the chemical and to the electric potential. If we also remember that μ can be expressed in terms of activities a ($\nabla\mu_B = RT \nabla \ln a_B$), Eq. (16a) takes the form

$$\mathbf{N}_B^A = \mathbf{N}_B - c_B\mathbf{v}_A = -c_Tc_Bc_A^{-1}\mathcal{D}_B \nabla \ln a_B - z_B F(RT)^{-1}c_Tc_B\mathcal{D}_{BC}^{-1} \nabla \phi \quad (17a)$$

where $\nabla\phi$ is the gradient of the electric potential, i.e., the electric field. The first term on the right-hand side is a *diffusion flux*.[‡] It is the movement of species B, relative to the solvent, due to the action of the gradient of the *chemical potential*. The second term is a *migration flux*, due to the action of the gradient of the *electric potential*.

In the case of ionic species a complication arises because the individual ionic activities are not known. The result is that the electric potential is *not* unambiguously given and a convention has to be used. In his book, which presents an excellent review on transport phenomena in electrolytic systems

[†] \mathcal{D}_B is the interaction diffusion coefficient between B and the solvent A. According to Eq. (10a) it should be written as $\mathcal{D}_{B,A}^A$. However, since there are no other interactions to be considered than that with the solvent, the second subscript A may be dropped without ambiguity for the sake of simplicity. We also drop the superscript A because in dilute solutions the solvent is usually taken as the reference for the definition of the diffusion coefficients.

[‡] In some books this term is called *chemical diffusion* and the migration term *electric diffusion*.

Newman⁽¹⁾ has shown that an expedient solution is to arbitrarily refer the potential to one of the ionic species in the solution.

If the solution is very dilute, $c_T \cong c_A$ and \mathbf{v}_A coincides with the average velocities defined in Section 2.4. The velocity of the solvent can thus be regarded as the velocity of the medium as a whole. We denote it by \mathbf{v} and take it relative to a frame of reference that is fixed with respect to the container of the solution.

$$\mathbf{N}_B^A = -c_B \mathcal{D}_B \nabla \ln a_B - F(RT)^{-1} z_B c_B \mathcal{D}_B \nabla \phi \quad (17b)$$

and

$$\mathbf{N}_B = -c_B \mathcal{D}_B \nabla \ln a_B - F(RT)^{-1} z_B c_B \mathcal{D}_B \nabla \phi + c_B \mathbf{v} \quad (18)$$

In these equations \mathbf{N}_B^A is the flux density referred to the fluid and \mathbf{N}_B that referred to a frame of reference fixed with respect to the container. The term $c_B \mathbf{v}$, usually referred to as a *convective flux density*, is often introduced through the argument that the dissolved species is dragged along by the hydrodynamic stream of the system. In reality, it comes from the definition of the diffusion coefficients (which are commonly referred to the solvent in the case of dilute solutions) as well as from the fact that the fluxes are usually referred to a fixed frame. It is this change in the considered frame of reference which introduces the term $c_B \mathbf{v}$.

Note that for a very dilute solution ($c_T \cong c_A$) the relationship between \mathcal{D}_B and L_B [Eq. (16a)] simplifies to

$$D_B = L_B RT / c_B \quad (16c)$$

3.2. Ideal Dilute Solution

If the solution is ideal in addition to being dilute, the activities can be replaced by the concentrations and $\nabla \ln a_B$ can be written $c_B^{-1} \nabla c_B$. Equation (18) thus takes the form

$$\mathbf{N}_B = -D_B \nabla c_B - F(RT)^{-1} z_B c_B D_B \nabla \phi + c_B \mathbf{v} \quad (19)$$

where D_B is the diffusion coefficient of species B in the ideal dilute solution of species B in solvent A.

For the x component (in a rectangular coordinate system) we have

$$(\mathbf{N}_B)_x = -D_B \frac{\partial c_B}{\partial x} - z_B F(RT)^{-1} c_B D_B \frac{\partial \phi}{\partial x} + c_B v_x \quad (20)$$

The first, second, and third terms on the right-hand side of Eqs. (19) and (20) represent, respectively, the fluxes by diffusion, by migration, and by convection. Furthermore, in the case of an ideal dilute solution, the conservation equation (11b) (also called the equation of change) can be combined with Eq. (19). We also take into account that in electrolytic systems the fluid is

usually incompressible and that Eq. (14) therefore applies; from this it follows that

$$\nabla \cdot (c_B \mathbf{v}) = c_B \nabla \cdot \mathbf{v} + \mathbf{v} \cdot \nabla c_B = \mathbf{v} \cdot \nabla c_B$$

Equation (11b) can therefore be written in the form

$$\frac{\partial c_B}{\partial t} = D_B \nabla^2 c_B + F(RT)^{-1} z_B D_B \nabla \cdot (c_B \nabla \phi) \mathbf{v} \cdot \nabla c_B + \sum_r v_{Br}^* \quad (21)$$

In Eq. (21) $\partial c_B / \partial t$ denotes the change in concentration at a point fixed with respect to the container, if \mathbf{v} is the velocity with respect to the container. Equations (19) and (21) are the most important fundamental equations for mass transport in electrolytic systems.

4. Charge Transport

4.1. Electric Current in Solution

In the preceding sections we have been dealing with the transport of mass. Of even greater direct interest to the electrochemist is the electric current, i.e., the transport of charges. In fact, the flux of an ionic species B represents at the same time a flux of charges. The current flowing through the solution is linked by simple relationships of proportionality with the fluxes of the ionic species in the mixture. If the fluxes are expressed in moles, the proportionality factor is the charge of a mole, $z_B F$. From Eq. (3) we obtain

$$\mathbf{j}_B^0 = z_B F \mathbf{N}_B^0 = \mathbf{j}_B - z_B F c_B \mathbf{v}_0 \quad (22)$$

\mathbf{j}_B^0 is the partial current density associated with species B. It is a vector that indicates the direction in which the charges transported by the species B flow and that gives the number of these charges going through a plane oriented perpendicular to the vector, divided by time and area.

In general, the current density of a species depends on the reference frame, which is indicated by a superscript (see Section 2.4): \mathbf{j}_B^0 is the current density of B referred to the frame of velocity \mathbf{v}_0 and \mathbf{j}_B is the current density referred to another frame, the velocity of which differs from the first one by \mathbf{v}_0 . For example, the second one may be a frame fixed with respect to the recipient and the first one may be the solvent of velocity \mathbf{v}_A relative to the recipient.

The total current density at a point in the solution is the sum of the current densities of all the species at that point:

$$\mathbf{j} = \sum_i \mathbf{j}_i^0 = \sum_i \mathbf{j}_i - F \mathbf{v}_0 \sum_i z_i c_i = \sum_i \mathbf{j}_i \quad (23)$$

\mathbf{j} is a function of location and time.

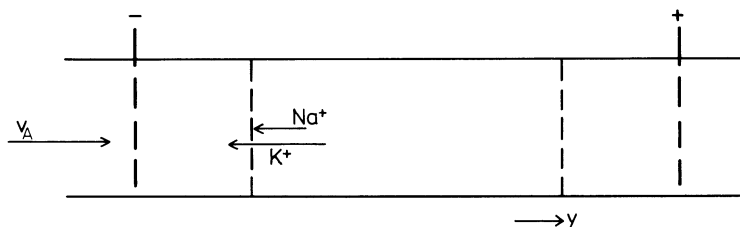


Figure 4. Illustration of role of reference frame on the separation of ionic species by counter current ionophoresis.

In contrast to the \mathbf{j}_i , the total current density is *independent of the reference velocity selected* [because of the electroneutrality condition $\sum_i z_i c_i = 0$, the term $Fv_0 \sum_i z_i c_i$ in Eq. (23) is nil]. Let us clarify the physical meaning of this somewhat puzzling theoretical conclusion by a concrete example. We consider countercurrent ionophoresis, a method in which ionic species are separated by applying an electric field.^(54,55) The principle is shown in Figure 4, where the system is a dilute solution of NaCl and KCl. There are no concentration gradients but there is a uniform hydrodynamic flow of velocity v_A in the y direction relative to the cell walls. The solution flows from the cathode toward the anode, thus counteracting the migration of the cations. We now consider two systems of reference: (a) the flowing solution (reference velocity v_A) and (b) the cell (reference velocity $v = 0$).

In case (a) we have for the Na^+ ions ($z = 1$)

$$N_{\text{Na}^+}^{\wedge} = N_{\text{Na}^+} - c_{\text{Na}^+} v_A = -F(RT)^{-1} c_{\text{Na}^+} D_{\text{Na}^+} \frac{\partial \phi}{\partial y} \quad (24)$$

$$\begin{aligned} j_{\text{Na}^+}^{\wedge} &= F N_{\text{Na}^+}^{\wedge} - F c_{\text{Na}^+} v_A = j_{\text{Na}^+} - F c_{\text{Na}^+} v_A \\ &= -F^2 (RT)^{-1} c_{\text{Na}^+} D_{\text{Na}^+} \frac{\partial \phi}{\partial y} \end{aligned} \quad (25)$$

In the absence of a concentration gradient the electric field determines the flux density of Na^+ relative to the moving solution. The partial current density of Na^+ , $j_{\text{Na}^+}^{\wedge}$, represents the number of charges transported by the ions of Na^+ and crossing a plane perpendicular to y , moving at the velocity of the solution v_A (divided by time and area).

In case (b) the frame of reference is stationary (the velocity of the cell walls having been taken as equal to zero). Therefore,

$$j_{\text{Na}^+}^{\text{s}} = j_{\text{Na}^+} = j_{\text{Na}^+}^{\wedge} + F c_{\text{Na}^+} v_A \quad (26)$$

$j_{\text{Na}^+}^{\text{s}}$ represents the number of charges transported by the Na^+ ions and crossing a stationary plane perpendicular to y (divided by time and area). It differs from the number of charges crossing the moving plane in case (a) by the amount $F c_{\text{Na}^+} v_A$.

However, the total current density ($j = j_{\text{Na}^+} + j_{\text{K}^+} + j_{\text{Cl}^-}$) is the same for the two frames of reference; i.e. the *total* number of charges crossing the stationary plane is the *same* as for the plane moving at the velocity of the solution. The reason is that the difference in the cationic currents for the two frames of reference is compensated by the difference in the anionic current.

Thus the total current density does not depend on the value of the flow velocity of the solution. The ionic current density $j_{\text{Na}^+}^{\text{A}}$ is also independent of v_{A} but *not* $j_{\text{Na}^+}^{\text{s}}$. For a certain value of v_{A} , $j_{\text{Na}^+}^{\text{s}}$ is zero. Under these conditions the Na^+ ions cannot leave the cathode compartment, in contrast to K^+ ions, and a separation of the two cationic species results. The method is quite sensitive and has been even used for the separation of isotopes. The value of v_{A} at which $j_{\text{Na}^+}^{\text{s}}$ is zero depends on the electric field $\partial\phi/\partial y$ but not on c_{Na^+} as can be seen by comparing Eqs. (25) and (26).

4.2. Electrode Current

One of the most commonly measured quantities in electrochemistry is the electric current flowing from the electrode to the external circuit. The total electrode current I is given by the number of electric charges crossing the electrode–solution interface divided by time. We have

$$I = \int_A dI \quad (27)$$

where dI is an elementary current flowing through an elementary area dA of the electrode–solution interface. The integration extends over the whole electrode surface A . The electrode current density at a given point of the interface is

$$j = dI/dA \quad (28)$$

Both the total electrode current and the electrode current density are scalar quantities, in contrast to the current flowing within the solution. They are linked by the relationship

$$j = (\mathbf{j}_e)_y \quad (29)$$

where $(\mathbf{j}_e)_y$ is the component perpendicular to the interface of the total current density in the solution immediately adjacent to the interface, which is denoted by the subscript e .

The electrode current density can also be expressed in terms of the flux density of any one of the species taking part in the electrode reaction. We can write this in a general way as



where the ν_i are the stoichiometric coefficients (positive for products, negative for reactants), and n is the charge number of the electrode reaction which is taken as a positive number.⁽¹²⁾ If there is only one electrochemical reaction

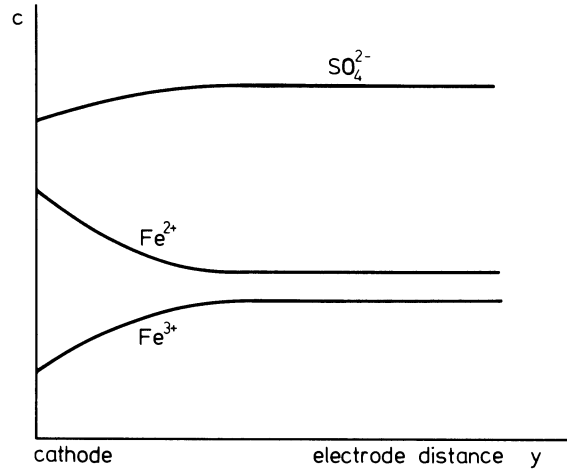


Figure 5. Concentration profiles in the reduction of Fe^{3+} ions from a solution of $\text{Fe}_2(\text{SO}_4)_3 + \text{FeSO}_4$.

taking place at the interface we have

$$j = n\nu_{\text{B}}^{-1}F(\mathbf{N}_{\text{B}})_{y,e} \quad (31)$$

where $(\mathbf{N}_{\text{B}})_{y,e}$ is the component normal to the interface of the interfacial flux density of species B.†

According to the recommendations of the International Union of Pure and Applied Chemistry (IUPAC),⁽¹²⁾ an anodic current is positive, a cathodic current negative. With the convention that the normal distance vector points into the electrolytic solution, the electrode reaction must then be written in such a way that the ratio n/ν_{B} is positive if species B is consumed in a cathodic reaction or produced in an anodic reaction. Otherwise, the reaction has to be written so that n/ν_{B} is negative.

Let us illustrate the important equation (31) by an example. We consider the reduction of Fe^{3+} ions at a Pt electrode in a sulfate solution



We have

$$n = 1; \quad \nu_{\text{Fe}^{3+}} = +1; \quad \nu_{\text{Fe}^{2+}} = -1; \quad \nu_{\text{SO}_4^{2-}} = 0$$

If the reaction runs from right to left, i.e., if the electrode acts as cathode, Eq. (31) yields

$$j/F = (\mathbf{N}_{\text{Fe}^{3+}})_{y,e} = -(\mathbf{N}_{\text{Fe}^{2+}})_{y,e} \quad (33a)$$

$$(\mathbf{N}_{\text{SO}_4^{2-}})_{y,e} = (Fn)^{-1}\nu_{\text{SO}_4^{2-}}j = 0 \quad (33b)$$

The interfacial flux densities of the Fe^{3+} and of the Fe^{2+} ions must be equal and of opposite sign. The concentration profiles in the solution close to the electrode are shown schematically in Figure 5 and will be discussed in Section 4.7.

† See Section 6.2 for a more precise discussion of the concept of interfacial flux density and concentration.

4.3. Local and Average Electrode Current Density

Equation (31) applies to a given spot of the electrode surface. Depending on the circumstances, the electrode current density may, or may not, vary along the electrode surface. In the first case, we have to distinguish between the local value and the average current density, which is equal to I/A . The area A used in the calculation of the average value from the measured total electrode current needs to be specified—geometric projected area (without taking into account roughness) or more or less true area (taking into account roughness by means of an adequate factor).

The current distribution over the electrode is closely linked with the distribution of the current density and of the potential within the solution. It will be treated more thoroughly in Chapter 4.

4.4. Current Efficiency

In Section 4.2 we have assumed that a single reaction takes place at the electrode. In practice, especially in technical applications, there are often several simultaneous electrode reactions. We can then assign to each reaction k a partial current density j_k . It is given by the stoichiometry of that reaction and by the amount of substance generated or consumed per unit time by this reaction. For a species B which takes part in only one of the simultaneous reactions, the interfacial flux density of B can be linked with the partial current density of the corresponding reaction by Eq. (31).

The total current is the sum of the partial currents: $j = \sum_m j_k$. The instantaneous current efficiency for reaction k , θ_k , is then defined as

$$\theta_k = j_k / \sum_m j_k \quad (34a)$$

The overall or average current efficiency for a reaction k over a given electrolysis period is the ratio of the number of coulombs required for reaction k , Q_k , to the total coulombs passed

$$\theta_k = Q_k / \sum_m Q_k \quad (34b)$$

Since anodic currents are positive and cathodic currents negative, the current efficiency may be larger than 1 if cathodic and anodic reactions take place simultaneously. A particular case is that of corrosion where no current flows through the external circuit. The cathodic and anodic currents then exactly compensate each other. The electrochemical aspects of corrosion are treated in Volume 4.

In industrial applications an important quantity is the material yield of a species B. It is the amount of substance of B produced, divided by the quantity of charges that has flowed through the electrodes. For reaction k it

is given by $\theta_k \nu_{B,k} / n_k F$ (provided there is no chemical reaction that is consecutive to the electrode reaction and that consumes or produces species B).

Note that the distribution of the partial current densities over the electrode surface may be different from that of the total current density.

4.5. Electric Mobility; Conductivity

Let us now return to the electric current within the solution and write Eq. (22) in a more specific form. We consider the case where there are *no gradients of the chemical potential* in the solution. From Eqs. (2), (3), and (22) we obtain

$$\mathbf{j}_B^0 = -z_B F^2 \nabla \phi \sum_{i \neq A} z_i L_{Bi}^0 \quad (35)$$

\mathbf{j}_B^0 is the current density of species B due to migration under the influence of an electric field, relative to the reference velocity \mathbf{v}_0 . Traditionally, it is customary in electrochemistry to link the migration current to the electric field through the electric mobility u_B^0 , defined as the velocity of an ionic species when the electric field $\nabla \phi$ is equal to unity.

We have

$$\mathbf{v}_B - \mathbf{v}_0 = -u_B^0 \nabla \phi \quad \text{and} \quad \mathbf{j}_B^0 = z_B F c_B (\mathbf{v}_B - \mathbf{v}_0) \quad (36)$$

Comparison of Eq. (35) with (36) yields†

$$u_B^0 = F (c_B)^{-1} \sum_{i \neq A} z_i L_{Bi}^0 \quad (37)$$

In the general case of Section 2 the mobility depends on the phenomenological coefficients of all species. Because of relationship (16b) between L_{Bi} and \mathcal{D}_{Bi} , Eq. (37) could also be expressed in terms of the interaction diffusion coefficients. Furthermore, it is seen that the value of the *mobility depends on the reference velocity*. This remark is of importance for the definition of the mobility in molten salts (see also Section 4.6).

In the case of an ideal dilute solution, the mobility depends only on the interaction coefficient between the species B considered and the solution. In principle, it still depends on the reference velocity. However, in the case of ideal dilute solutions this is usually taken to be the velocity of the solvent and the superscript 0 can be dropped without ambiguity. Thus, we can write Eq. (37) as

$$u_B = z_B F (c_B)^{-1} L_B = z_B F D_B / RT \quad (38)$$

where we have taken into account Eq. (16c). Note that because of our

† Species A is omitted from the summation for a number of equations in Sections 4.5 and 4.6 because of the Gibbs–Duhem equation which allows the elimination of one of the fluxes (see Section 2.3).

convention for the sign of z the mobility as defined above has a positive sign for cations and a negative sign for anions. Again for the case of an ideal dilute solution the relationship giving the current density of species B [Eq. (37)] reduces to

$$\mathbf{j}_B^0 = -z_B^2 F^2 L_B^0 \nabla \phi = -z_B^2 F^2 (RT)^{-1} c_B \nabla \phi \quad (39)$$

Let us now consider the total current density \mathbf{j} . From Eqs. (2), (3), (19), (22), and (23) we obtain a relationship that expresses \mathbf{j} in terms of the electric field $\nabla \phi$ and of the chemical potentials or concentration gradients. If we put

$$\kappa = F^2 \sum_i \sum_{j \neq A} z_i z_j L_{ij}^0 \quad (40)$$

we can write

$$\mathbf{j} = \sum \mathbf{j}_i^0 = -F \sum_i \sum_{j \neq A} z_i L_{ij}^0 \nabla \mu_j - \kappa \nabla \phi \quad (41a)$$

or for an ideal dilute solution

$$\mathbf{j} = -F \sum_i z_i D_i \nabla c_i - \kappa \nabla \phi \quad (41b)$$

In the absence of concentration gradients this reduces to

$$\mathbf{j} = -\kappa \nabla \phi = -F^2 \nabla \phi \sum_i \sum_{j \neq A} z_i z_j L_{ij}^0 \quad (41c)$$

The proportionality factor κ which relates the current to $\nabla \phi$ is usually called the conductivity. Equation (40) shows that it is linked in a simple manner to the transport properties of the solution. We may note that, in contrast to the mobility, the conductivity does *not* depend on the choice of the reference frame.

In the case of an ideal dilute solution, Eq. (40) reduces to

$$\begin{aligned} \kappa &= F^2 \sum_i z_i^2 L_i = F^2 (RT)^{-1} \sum_i z_i^2 c_i D_i \\ &= F \sum_i z_i c_i u_i \end{aligned} \quad (40')$$

This equation expresses the conductivity in terms of the three coefficients most commonly used to describe ionic transport properties in electrolytic systems (i.e., u , L , D).

We may note a fourth equivalent transport quantity often employed in electrochemistry—the ionic conductivity λ

$$\lambda_B = z_B F u_B \quad (42)$$

Finally, a fifth quantity encountered in papers on mass transport is the *mechanical mobility* u_B^* : It is the velocity taken by the ionic species when the force acting on 1 mole is equal to 1 (in contrast to the electric mobility which

is the velocity for a unit field). The following equation can easily be derived from this definition:

$$u_B^* = u_B(z_B F)^{-1} \quad (43)$$

In fact, all of the five above-mentioned quantities (u , L , D , λ , u^*) represent one and the same transport property of the ionic species. In the case of an ideal dilute solution they are linked together by simple relationships:

$$D_B = u_B RT(z_B F)^{-1} = \lambda_B RT(z_B F)^{-2} = u_B^* RT = RTc_B^{-1} L_B \quad (44)$$

4.6. Transport Number

In the absence of concentration gradients, the vectors of the current densities of all species have the same direction as the electric field. We can then define a scalar quantity, the transport (or transference) number[†] of species B, as the ratio of the current transported by that species and the total current:

$$t_B^0 = \frac{j_B^0}{j} = z_B \sum_{i \neq A} z_i L_{Bi}^0 / \sum_i \sum_{j \neq A} z_i z_j L_{ij}^0 \quad (45)$$

The value of the transport number depends on the reference velocity: t_B^0 is the transport number relative to velocity v_0 .

In solid ionic conductors it is convenient to take the fixed ions of the lattice as the reference frame. In a fused salt AB, such as NaCl, we may take either the cation A or the anion B as reference. In the first case, the transport number of A is zero and that of B is one; in the second case, the transport number of A is one and that of B is zero. Similarly, in the first case the mobility of A is zero; in the second case the mobility of B is zero. In both cases the mobility of the counter ions is equal to κ/zFc . [It may be easily shown that Eq. (40b) holds even though the system is not ideal.] It has been shown by Sinistri⁽¹³⁾ that the choice of reference systems other than the above-mentioned ones also leads to trivial values of t and u in the case of a single salt melt.

With melts having three ionic species (such as NaCl, KCl) the choice of any one of them is *a priori* equally convenient.

[†] Both terms—*transport* and *transference* number—are encountered in the literature. IUPAC recommends the name transport number. A similar situation prevails more generally with respect to the terms *mass transport* and *mass transfer*. They are often used indifferently in the literature. From the viewpoint of economy of language it would be preferable to exploit the availability of two expressions to distinguish between different processes. It has been suggested⁽¹⁹⁾ that the term mass transport be used when one is dealing with phenomena taking place within the solution, including the diffusion layer whereas mass transfer would be used more specifically to designate the phenomena taking place at the interface proper, which in most cases involved an exchange of mass between the adjacent phases.

In the case of ideal dilute solutions it is customary to take the velocity of the solvent as reference and the superscript and second subscripts can be dropped without ambiguity, as pointed out earlier. Equation (45) reduces to

$$t_B = z_B^2 L_B / \sum_i z_i^2 L_i = z_B c_B u_B / \sum_i z_i c_i u_i \quad (46)$$

This is the classical equation for the transport number. The number referred to the solvent or to another species is often called Hittorf's transport number (see Section 10), whereas those referred to an average velocity and to the container are sometimes called true (or absolute) and external transport number, respectively.

Note that according to Eq. (46) t_B is a positive number between 0 and 1. This is due to the fact that in the absence of concentration gradients \mathbf{j}_B^0 and \mathbf{j} [see Eq. (45)] have the same direction, and in the approximation of the ideal dilute solution they also have the same sign so that $0 < \mathbf{j}_B^0 / \mathbf{j} < 1$.

Even in the approximation of an ideal dilute solution a complication sometimes arises because of the problem of the species (see Section 9.2). The definition given by Eq. (45) or (46) involves no difficulty if one is dealing with a species that has a uniform charge number and the concentration of which can be determined analytically. However, this is not always the case. Let us consider a system of complex and simple ions linked through equilibria which establish themselves very fast (as in the case of Cd in a iodide solution containing Cd^{2+} , CdI_3^- , I^- , etc.). In this example it is possible to determine analytically only the overall concentration of either cadmium or iodine, which we call a constituent C of the solution:

$$c_{\text{Cd}} = c_{\text{Cd}^{2+}} + c_{\text{CdI}_3^-} + \cdots \quad \text{or} \quad c_{\text{I}} = c_{\text{I}^-} + 3c_{\text{CdI}_3^-} + \cdots$$

(More generally $c_C = \sum \nu_i c_i$, where ν_i is the number of moles of the considered constituent contained in 1 mole of i .) It is convenient to regard the ensemble of all particles of a constituent C (in our example Cd or I) as a single species (see Section 9.2) and to define a transport number t_C of the constituent. In a Hittorf-type experiment (see Volume 5, Chapter 3) one can indeed measure the total flux density N_C of C. (In our example, $N_C = N_{\text{Cd}} = N_{\text{Cd}^{2+}} + N_{\text{CdI}_3^-} + \cdots$ or $N_C = N_{\text{I}} = N_{\text{I}^-} + 3N_{\text{CdI}_3^-} + \cdots$; more generally $N_C = \sum_i \nu_i N_i$.) However, in applying the definition of the transport number given by Eq. (45) ($t_C = \mathbf{j}_C^0 / \mathbf{j}$, with $\mathbf{j}_C^0 = z_C F N_C$), one faces the problem of the value to be assigned to the charge number z_C because some of the particles of the constituent are part of a complex ion having a charge number different from that of the uncomplexed constituent. By definition, one multiplies each N_i with $z_C \nu_i F$, taking for z_C the charge number of the uncomplexed constituent (in our example $z_C = +2$ or $z_C = -1$), independently of whether it is present in the uncomplexed or complex state. In our example, $\mathbf{j}_{\text{Cd}}^0 = 2F(N_{\text{Cd}^{2+}} + N_{\text{CdI}_3^-} + \cdots)$ and $\mathbf{j}_{\text{I}}^0 = -F(N_{\text{I}^-} + 3N_{\text{CdI}_3^-} + \cdots)$. Since the N_i may have different signs (as is the case in our example for $N_{\text{Cd}^{2+}}$ and $N_{\text{CdI}_3^-}$), the result of the above definition

is that j_C^0 and j do not necessarily have the same sign (in contrast to the usual case, where z_B is equal to the charge number of the migrating ion considered). It can then be easily shown that if one applies the above definition to all constituents of the mixture (say Cd^{2+} and I^-) the sum $\sum t_C$ for all constituents is still equal to 1, but the transport numbers themselves can be negative or larger than 1 [whereas for a simple ion according to Eq. (46) t_B is necessarily a positive number between 0 and 1]. We shall refrain from a further discussion of this problem and refer the reader to the literature.⁽⁵³⁾ The transport numbers are also discussed more fully in Volume 5, Chapter 3. Furthermore, we will return more generally to the problem of the species in Section 9.2.

4.7. Transport of Charges through the Diffusion Layer

The transport number describes the fraction of the current transported by a species in the absence of a concentration gradient. We now consider the case where such a gradient is present; i.e., we deal with the transport of charges through the diffusion layer. A quantitative understanding of the peculiar situation that may be encountered there is important for many applications of electrochemistry.

For the sake of simplicity we restrict ourselves to ideal dilute solutions. The cell has plane parallel electrodes and the current flows from the anode to the cathode, perpendicularly to the electrodes. First we consider the same example as in Section 1 (deposition of Cu from a CuSO_4 solution, without concomitant hydrogen evolution) (Figure 1). In the interior of the solution, outside of the diffusion layer, the fraction of the electric current associated with the Cu^{2+} ions is given by their transport number.

In contrast to a metallic conductor, in an electrolytic solution the current divides itself among the carriers present (in our example between the Cu^{2+} and the SO_4^{2-} ions). However, in the solution in the immediate vicinity of the interface, the *whole* current is carried by the Cu^{2+} ions, because this is the only species which reacts at the electrode. This is possible because in the diffusion layer mass transport by diffusion occurs in addition to transport by migration and acts in the same direction. Part of the current is due to diffusion and part to ionic migration, but it is carried by a single species. Across the diffusion layer, we have a continuous transition from a conductor with several carriers of electricity to one of the first kind in which there is only one carrier of electricity. Furthermore, when one approaches the electrode, the mass transport by convection decays because of the friction at the wall and is progressively replaced by diffusion. This affects the Cu^{2+} and SO_4^{2-} ions in the same way: Because of the electroneutrality of convective mass transport (see Section 4.1) the latter does not modify the distribution of the current between the cations and anions.

Let us now examine more closely the situation with respect to the anions. They do not react at the electrode whose surface is "adiabatic" with respect

to the SO_4^{2-} ions (i.e., the mass associated with them does not cross the interface). The flux density of SO_4^{2-} at the interface must therefore be zero. This comes about because the electric force and the “diffusion” force now act in opposite directions. At the interface the first two terms on the right-hand side of Eq. (20) cancel and \mathbf{v} is zero, so that $\mathbf{N}_{\text{SO}_4^{2-}} = 0$. Therefore, at the interface, the SO_4^{2-} ions do not contribute to the transport of the current.

An extreme case is that shown in Figure 6. The CuSO_4 solution is electrolyzed with two copper electrodes. Copper is deposited on one side and dissolved at the other. The whole solution is at rest with respect to the electrodes and a steady state is established. Then, in Eq. (55) to be derived later (see Section 5), $\partial c_B / \partial t = 0$, $v_{Br}^* = 0$, and $v = 0$; ∇c reduces to $\partial^2 c / \partial y^2$ (linear diffusion) and the integration is very simple, yielding a straight line for the concentration profile over the whole interelectrode distance. This demonstrates that once the steady state has established itself, the cathodic and anodic diffusion layers have merged. In this case, throughout the whole solution the charges are transported from the anode to the cathode solely by the Cu^{2+} ions: *Only the cations move*; the anions are standing still everywhere, as if they were fixed ions of the lattice in the ionic conduction through solids.

Let us note that the concentrations of the Cu^{2+} and of the SO_4^{2-} ions must be equal in any point of the solution because of the electroneutrality condition. We have thus drawn only one line for the concentration profile.

A more complicated situation arises if two cationic species are present in the solution, as is the case in the cathodic reduction of Fe^{3+} ions to Fe^{2+} ions in a sulfate solution, which was considered in Section 4.2 [Eq. (32)]. The Fe^{3+} ions are consumed, while the Fe^{2+} ions are generated at the interface. Therefore the diffusion layer is depleted with respect to Fe^{3+} and enriched with respect to Fe^{2+} . We now have three different concentration profiles (Figure 5), one of which is not independent of the other two because of the electroneutrality condition.

We consider first the flux densities through a plane in the solution located in the immediate vicinity of the cathode. Within a plane there can be no

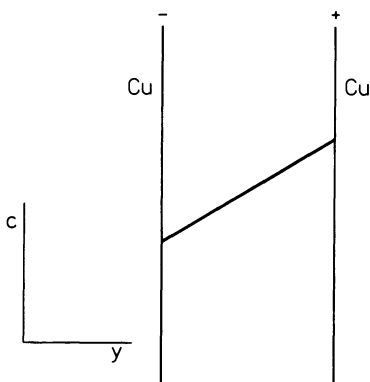


Figure 6. Concentration profile in the steady-state electrolysis of a CuSO_4 solution with Cu electrodes without convection.

accumulation of matter. Therefore, the interfacial flux densities of Fe^{3+} and Fe^{2+} must be equal and of opposite sign [Eq. (33a)]. This does not mean, however, that the concentration gradients are equal. Indeed, examination of Eq. (20) (with $v = 0$ at the interface) shows that the concentration gradients are different for a given N if the diffusion coefficients are different. However, the difference between the D values for Fe^{3+} and Fe^{2+} is such that the effect is a secondary one. But there is another effect which is much more important in the present example. The electric field drags both Fe^{2+} and Fe^{3+} ions toward the cathode. However, in the first case this helps to supply Fe^{3+} ions to the electrode, whereas in the second case it hinders the transport of Fe^{2+} ions away from the cathode.† The absolute value of the concentration gradient of Fe^{2+} must therefore be larger‡ than for Fe^{3+} if the fluxes of the two species are to be equal (and if $D_{\text{Fe}^{2+}} \cong D_{\text{Fe}^{3+}}$). As in our first example the interfacial electric current in the solution is carried by the cations only (to the exclusion of the anions) but it is associated with *both* cationic species. It is equal to the difference between the currents associated with the fluxes of the Fe^{3+} and Fe^{2+} ions, which are in opposite directions. This difference is equal to the current flowing through the electrode.

As a third example we will discuss the case of a concentrated supporting excess electrolyte which is of considerable practical importance. Let us consider again, as in our first example, the deposition of copper from a CuSO_4 solution without concomitant hydrogen evolution. However, the solution now contains Na_2SO_4 , the concentration of which is very much larger than that of CuSO_4 . The Na^+ ions are not discharged at the cathode. For this reason one sometimes encounters the term *indifferent electrolyte* (in German, *Leitelektrolyt*) instead of supporting electrolyte. Figure 7 shows schematically the concentration profiles. We have

$$j = j_{\text{Cu}^{2+}} + j_{\text{Na}^+} + j_{\text{SO}_4^{2-}} \tag{47}$$

Outside of the diffusion layer because of $c_{\text{Cu}^{2+}} \ll c_{\text{SO}_4^{2-}}, c_{\text{Na}^+}$, and the fact that the mobilities and diffusion coefficients of the three ionic species are similar,§ it follows from Eqs. (45) and (46) that

$$j_{\text{Cu}^{2+}} = jt_{\text{Cu}^{2+}} \cong 0 \quad j_{\text{Cu}^{2+}} \ll j \tag{48}$$

† A similar situation is encountered in the cathodic reduction of an anionic metallic complex such as $\text{Ag}(\text{CN})_2^-$. At first sight it may seem surprising that it is possible to deposit the metal from such a solution because the metal migrates away from the cathode under the influence of the electric field. In reality, a concentration gradient is set up which overcomes the influence of migration.

‡ At the interface $v = 0$ because of the friction at the electrode. For equal N the concentration gradients therefore depend (in addition to the small influence of the diffusion coefficients) on the ratio of the concentrations, $c_{\text{Fe}^{3+}}/c_{\text{Fe}^{2+}}$. But in any case the electric migration tends to make the concentration profile of Fe^{2+} steeper than that for Fe^{3+} .

§ The diffusion coefficients of most ionic species in aqueous solutions are of the same order of magnitude.

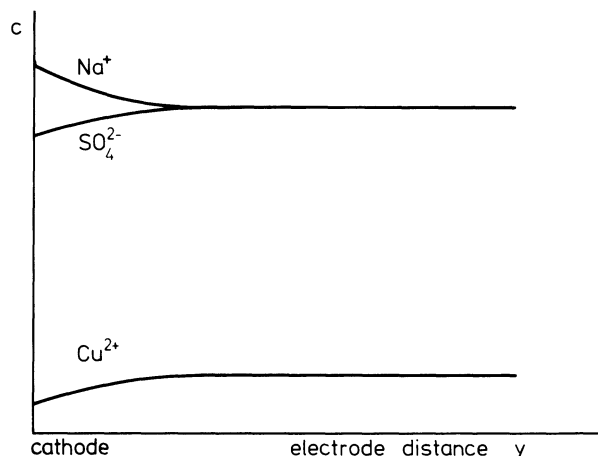


Figure 7. Concentration profile in the reduction of Cu^{2+} from a solution with excess of indifferent electrolyte (Na_2SO_4 ; concentration of Na_2SO_4 not drawn to scale).

The current is virtually carried entirely by the Na^+ and SO_4^{2-} ions. In the diffusion layer, the concentration gradients are such that they counteract the electric migration of the SO_4^{2-} and Na^+ ions, and j_{Na^+} and $j_{\text{SO}_4^{2-}}$ progressively decay when one approaches the interface where $j_{\text{Na}^+} = j_{\text{SO}_4^{2-}} = 0$. At the same time the current carried by the Cu^{2+} ions increases progressively because of the diffusion, and finally it is equal to the whole current at the interface, as in the first example of this section.

However, now the current of the Cu^{2+} ions due to migration is negligible. This can be shown as follows. The second term on the right-hand side of Eq. (20) is approximately of the same magnitude in the diffusion layer and in the bulk (or smaller). This is due to the fact that the concentration of Cu^{2+} is smaller in the diffusion layer and the electric field $d\phi/dy$ is about the same due to the high conductivity of the solution and to the small *relative* changes in the concentrations of Na^+ and SO_4^{2-} (see also Section 6.1). Therefore, the current of Cu^{2+} due to migration is about the same in the diffusion layer as in the bulk (or smaller). According to Eq. (48) the migration current of Cu^{2+} in the bulk is much smaller than the whole current which remains the same throughout the diffusion layer. Therefore, at the interface, the contribution of the migration to the total current is negligible: The latter is a pure diffusion current of the Cu^{2+} ions. This is an important conclusion. Systems with excess indifferent electrolyte are commonly used in electroanalytical chemistry, especially in polarography, and in many studies of electrode kinetics.

To conclude this section let us note that arguments similar to those developed above can be used to discuss the transport of charges in solid ionic conductors and in semiconductors (among others, to discuss the situation in

the diffusion layer near the interface between a *pn* semiconductor). In the latter case the electrons of the conduction band play the role of the anions, the positive holes the role of the cations.

5. Elimination of Electric Potential from the Basic Equations

5.1. Ideal Dilute Solution

Let us now return to the fundamental mass transport equations. In Section 3.2 we have presented a simplified version by restricting ourselves to ideal dilute solutions. A further simplification of these equations is achieved if we consider two extreme cases: (a) that of an excess of indifferent electrolyte and (b) that of the solution of a single binary electrolyte (such as a CuSO_4 solution without other salts present).

In case (a) the second term on the right-hand side of Eq. (19) is negligible for the species present in minor concentration (see end of Section 4.7). The conservation equation (21) thus takes the form

$$\frac{\partial c_B}{\partial t} = D_B \nabla^2 c_B - \mathbf{v} \cdot \nabla c_B - \sum_r v_{Br}^* \quad (49)$$

In case (b) one can eliminate the potential from the fundamental equations with the help of the electroneutrality condition, $\sum_i z_i c_i = 0$. Denoting with subscripts + and - the cation and anion, respectively, Eqs. (23), (22), and (19) [see also Eq. (4)] yield for a binary electrolyte (where $z_+ F c_+ = -z_- F c_-$)

$$\mathbf{j}_+ = z_+ F D_+ \nabla c_+ - F^2 (RT)^{-1} z_+^2 D_+ c_+ \nabla \phi + z_+ F c_+ \mathbf{v} \quad (50)$$

$$\begin{aligned} \mathbf{j} &= \mathbf{j}_+ + \mathbf{j}_- = -z_+ F D_+ \nabla c_+ - z_- F D_- \nabla c_- \\ &\quad - F^2 (RT)^{-1} (z_+^2 D_+ c_+ + z_-^2 D_- c_-) \nabla \phi + F \mathbf{v} (z_+ c_+ + z_- c_-) \\ &= -z_+ F (D_+ - D_-) \nabla c_+ - \kappa \nabla \phi \end{aligned} \quad (51)$$

where κ is the conductivity or

$$\nabla \phi = -j/\kappa - z_+ F (D_+ - D_-) \kappa^{-1} \nabla c_+ \quad (52)$$

Introducing this value of $\nabla \phi$ into Eq. (50) and remembering the electroneutrality condition as well as the definition of the transport number [Eq. (46)] we get

$$\mathbf{j}_+ = z_+ F D_+ \nabla c_+ + j t_+ + z_+ F \mathbf{v} c_+ = z_+ F N_+ \quad (53)$$

where

$$D = \frac{(z_+ - z_-) D_+ D_-}{z_+ D_+ - z_- D_-} \quad (54)$$

is the diffusion coefficient of the neutral electrolyte.

In the case of a single binary electrolyte, the migration term can be simply expressed in terms of the transport number even in the presence of a concentration gradient. It remains constant across the diffusion layer even if the electric field $\nabla\phi$ strongly varies. This is not the case for an excess of indifferent electrolyte, but it may be so for a single binary electrolyte, especially at or near the limiting current (see Section 1).

We now consider the conservation equation. We make a mass balance for the cations or anions (see Figure 3) ∇j is zero because of the conservation of charges (there is no time change of a space charge). Taking into account that the concentration c of the neutral electrolyte is simply proportional to the ionic concentration c_+ and c_- , we obtain (for an incompressible fluid)[†]

$$\frac{\partial c}{\partial t} = D \nabla^2 c - \mathbf{v} \cdot \nabla c + \sum_r v_r^* \quad (55)$$

The equations for an excess of indifferent electrolyte [Eq. (49)] and for a single electrolyte [Eq. (55)] differ only in the diffusion coefficients which appear in these relationships. In the first case it is the diffusion coefficient of the ionic species. In the second case it is the diffusion coefficient of the neutral electrolyte (e.g., of CuSO_4). This is a kind of average between the individual diffusion coefficients of the two ionic species, taking into account the fact that the concentration gradients of the two species are not independent because of the electroneutrality condition (for $z_+ = -z_-$ they must be equal). A remarkable feature of Eqs. (49) and (55) is that the term with the electric field which is characteristic of electrolytic mass transport does not appear in them. This not only constitutes a decisive simplification of the fundamental differential equations of mass transport in electrolysis, but it also means that *the conservation equation [Eq. (49) or (55)] is now the same as for nonelectrolytic systems*. This result is of great practical consequence. One can directly *transpose* to electrolytic systems the numerous solutions of the conservation equation which have been obtained in physical chemistry at large or in connection with chemical engineering. One can also make use of the analogy with heat and momentum transport. This analogy will be discussed in more detail in Chapter 3.

Equations (49) and (55) are the forms of the conservation equation which have been by far most commonly used in electrolytic mass transport problems. It must be recalled, however, that they are strictly valid only in the limiting cases of a single binary electrolyte solution on the one hand, and of a minor species in a solution with excess indifferent electrolyte on the other hand. In practice, they are often used as a first approximation in the intermediate cases where the concentration of the ionic species considered is of the same order

[†] For a 1-1 electrolyte $c = c_+ = c_-$. For a 2-1 electrolyte, such as CuCl_2 , $c = c_+ = c_-/2$. In Eq. (55) v_r^* is the number of moles of neutral electrolyte produced or consumed per unit time and per unit volume by reaction r .

of magnitude as that of other species present in the solution. The tricky problem of the integration of the more complete Eq. (21) (which includes the term with the electric potential) has been treated only recently for a few cases mainly by Newman. An example of this much more sophisticated calculation will be discussed in Chapter 3.

5.2. Nonideal, Concentrated Solutions of a Single Electrolyte

The discussion in the preceding section was restricted to ideal dilute solutions. However, in the last decade the theory of mass transport in electrolysis with concentrated solutions has made considerable progress, thanks mainly to the work of Newman, Tobias, Bennion,^(1,30) and others.^(33,34) We shall deal with the solution of a single electrolyte which is amenable to a relatively simple treatment. As in the case of the ideal solution, one can eliminate the potential by means of the electroneutrality condition [Eq. (12)]. From Eqs. (3'), (10), (22), and (23) and remembering the relationship between μ and the activity a (see Section 3.1) one obtains, upon some rearrangement,⁽¹⁾

$$\begin{aligned} \mathbf{j}_+ = z_+ F \mathbf{N}_+ = -z_+ F \nu_+ \mathcal{D} c_T (f_{+-} c_A)^{-1} \nabla c f_{+-} + \mathbf{j} t_+^A \\ + z_+ F \nu_+ c \mathbf{v}_A \end{aligned} \quad (56)$$

with a similar equation for the anion.

In this equation c_A and \mathbf{v}_A are the concentration and velocity of the solvent, respectively; c_T is the total concentration and c the concentration of the neutral electrolyte, which is linked with c_+ and c_- by $c = c_+/\nu_+ = c_-/\nu_-$ (i.e., ν_+ and ν_- are the number of cations and anions formed when 1 molecule of neutral electrolyte dissociates). f_{+-} is the mean molar activity coefficient and $c f_{+-}$ thus represents the activity of the neutral electrolyte.

\mathcal{D} is the diffusion coefficient of the neutral electrolyte,

$$\mathcal{D} = \frac{\mathcal{D}_{A^+} \mathcal{D}_{A^-} (z_+ - z_-)}{z_+ \mathcal{D}_{A^+} - z_- \mathcal{D}_{A^-}} \quad (57)$$

It is defined in a way quite similar to that for the diffusion coefficient of the neutral electrolyte in an ideal dilute solution [Eq. (54)]. It represents a kind of average between the individual ionic diffusion coefficients \mathcal{D}_{A^+} and \mathcal{D}_{A^-} (which are the interaction diffusion coefficients between the solvent A and the cations and anions, respectively).[†] t_+^A is the transport number (referred to the solvent). According to Eqs. (45) and (16b) applied to the solution of a single electrolyte, t_+^A is given by

$$t_+^A = \frac{z_+ \mathcal{D}_{A^+}}{z_+ \mathcal{D}_{A^+} - z_- \mathcal{D}_{A^-}} \quad (58)$$

[†] In addition, we have an interaction diffusion coefficient \mathcal{D}_{+-} between cations and anions but this does not enter into Eq. (57) (see Section 5.3).

In contrast to the case of the ideal dilute solution, t_+^{\wedge} is not necessarily constant across the diffusion layer. Therefore, it does not drop out when the conservation equation is derived from Eq. (56).

$$\begin{aligned} \frac{\partial c}{\partial t} = & \nabla \cdot \mathcal{D}_{cT}(f_{+-}c_A)^{-1} \nabla c f_{+-} - \nabla \cdot c \mathbf{v}_A \\ & - \mathbf{j} \cdot \nabla t_+^{\wedge} (z_+ F \nu_+)^{-1} + v_r^* \end{aligned} \quad (59)$$

Equations (59) and (56) are the analogs of Eqs. (53) and (55), which are valid for an ideal dilute solution only. They are somewhat more complicated[†] than the latter ones but the main result is preserved. Namely, the electric potential no longer appears in the equations so they can be written in terms of the concentration of the neutral electrolyte, and the tricky problem of the individual ionic activities (see Section 3.1) is avoided. The main difference compared to ideal dilute solutions is that diffusion coefficients based on thermodynamic driving forces enter into Eqs. (56)–(59).

An alternative possibility is to use, even in the case of concentrated solutions, an effective diffusion coefficient D^* based on concentration gradients. It is the quantity most directly accessible to experiment. In the classical methods (involving porous cups or optical systems), the diffusion coefficient is measured in the interior of a solution that is at rest with respect to the container; i.e., the whole volume of the solution is fixed and the mass average velocity, taken with respect to the container, is zero. This suggests that D^* be defined by the relationship

$$\mathbf{N}_s = -D^* \nabla c \quad (60)$$

where c is the concentration of the neutral electrolyte and \mathbf{N}_s its flux density. D^* is linked with \mathcal{D} by the relationship^(1,30)

$$D^* = \mathcal{D}_{cTc}^{-1} \left(1 + \frac{d \ln \gamma_{+-}}{d \ln m} \right) \quad (61)$$

where γ_{+-} is the mean activity coefficient on the molal scale and m is the molality (moles of electrolyte per kg of solvent). The gradient of the chemical potential of the neutral electrolyte $\nabla \mu$ can be expressed as⁽¹⁾

$$\mathcal{D}_{cTc}(\nu RTc_A)^{-1} \nabla \mu = D^* \left(1 - \frac{d \ln c_A}{d \ln c} \right) \nabla c \quad (62)$$

where $\nu = \nu_+ + \nu_-$.

[†] The complication does not only come from the term $(z_+ F \nu_+)^{-1} \mathbf{j} \cdot \nabla t_+^{\wedge}$ (which is not zero in the case of a concentrated solution). In addition, one has to write $\nabla \cdot c \mathbf{v}_A (= \mathbf{v} \cdot \nabla c + c \nabla \cdot \mathbf{v}_A)$ instead of $\mathbf{v}_A \cdot \nabla c$ because in a concentrated solution $\nabla \cdot \mathbf{v}_A$ is not necessarily zero even for an incompressible fluid. In contrast to this, $\nabla \cdot \mathbf{v}_b$ is zero even in a concentrated solution (Section 2.6) and thus need not be considered in Eq. (60).

We now express the flux in terms of D^* and of the mass fraction of the salt, $\omega_s = (\rho_+ + \rho_-)/\rho$, as the driving force. We further use the mass average velocity as reference. We thus obtain an equation that is expedient for the use in conjunction with the conservation of momentum equation [Eq. (15a)] in an *ab ovo* calculation of the quantities of practical interest (see Section 8.2). One can write for the cations

$$\mathbf{N}_+ = -\nu_+ \rho D M^{-1} \nabla \omega_e + \frac{\mathbf{j} t_+^b}{z_+ F} + c_+ \mathbf{v}_b \quad (63)$$

where t_+^b is the transport number referred to the mass average velocity and M the molar mass of the neutral electrolyte. A similar relationship holds for the anion.

The above equations pave the way for a quantitative treatment of mass transport in concentrated single electrolyte solutions, which are unfortunately the ones most commonly encountered in practice, especially in industrial systems. With modern computers it is possible to perform a complete calculation starting from the basic equations, at least for relatively simple hydrodynamic conditions, in spite of the great complication of the variation of D^* across the diffusion layer, i.e., over the integration path. An example of such a computation is to be found in a paper by Newman and Hsueh.⁽³¹⁾ However, by and large, very few calculations of this kind have been done so far.

5.3. Remarks about the Diffusion Coefficients

In the case of a solution with a single electrolyte, there are three species: the cations, the anions, and the solvent. According to Section 2.5 the number of independent diffusion coefficients is thus $\frac{1}{2}n(n-1) = 3$. We have two diffusion coefficients, \mathcal{D}_{A^+} and \mathcal{D}_{A^-} , which describe the interaction between the solvent and the cations and anions, respectively. The third coefficient, \mathcal{D}_{+-} , is characteristic for the interaction between cations and anions. It is interesting to note that \mathcal{D}_{+-} does not appear in the equations for the transport number [Eq. (58)] nor in that for the diffusion coefficient of the neutral electrolyte [Eq. (57)]. These two transport properties depend only on the friction between the solvent and the ions. However, \mathcal{D}_{+-} influences the conductivity κ of the solution, as can be readily seen from Eqs. (40) and (16b) applied to a single electrolyte solution.

In the case of a concentrated electrolyte \mathcal{D} , t_+ (or t_-), and κ represent three different transport properties, which are accessible to experimental determination. From the measured values of \mathcal{D} , t_+ , and κ one can calculate \mathcal{D}_{A^+} , \mathcal{D}_{A^-} , and \mathcal{D}_{+-} by means of Eqs. (57), (58), and (40). Experimental results are available for a number of systems over a wide range of concentration, for instance, for aqueous KCl between 10^{-4} and about 5 moles/liter.⁽¹⁾ In this range \mathcal{D}_{A^+} and \mathcal{D}_{A^-} are both about $2 \times 10^{-5} \text{ cm}^2 \text{ s}^{-1}$ and vary little

with concentration, whereas \mathcal{D}_{+-} strongly increases from 1.5×10^{-8} to $5 \times 10^{-6} \text{ cm}^2 \text{ s}^{-1}$ and thus becomes of the same order of magnitude as \mathcal{D}_{A^+} or \mathcal{D}_{A^-} in concentrated solutions.

In addition to the diffusion coefficients \mathcal{D} based on thermodynamic driving forces we have used in the preceding section a kind of effective diffusion coefficient D^* based on concentration gradients [Eq. (60)] and which is formally analogous to the diffusion coefficient D for dilute solutions, but should not be confused with the latter. The differences in properties should be noted. \mathcal{D} , \mathcal{D}_{A^+} , \mathcal{D}_{A^-} , and \mathcal{D}_{+-} are *functions of state* and depend on concentrations, temperature, and (in principle) pressure, but are independent of concentration gradients. The D_s are also functions of state but are *independent* of concentration. However, as can be easily seen from Eq. (61), D^* is not a function of state and depends on *both* concentrations and concentration gradients, as well as on temperature. This complicates the integration of differential equations based on D^* , such as Eq. (60).

It is useful at this stage to recapitulate quite generally the various diffusion coefficients and transport coefficients which we have encountered so far. They are summarized in Table 1. Additional variants can be generated by changing the reference velocity. Table 1 also includes the integral diffusion coefficient which we will discuss later in Section 9.1. Further diffusion and transport coefficients have been defined in the literature. In all, there is a bewildering

Table 1
Transport Coefficients

L_{Bi}^0	Phenomenological coefficients, based on thermodynamic driving force, referred to velocity $v_0(\text{J}^{-1} \text{ mol}^2 \text{ m}^{-1} \text{ s}^{-1})$, [Eq. (3)]
K_{Bi}	Friction coefficient between species B and i (kg s m^{-2}), [Eq. (10)]
\mathcal{D}_{Bi}^0	Interaction diffusion coefficient between species B and i , based on thermodynamic driving force, referred to velocity $v_0(\text{m}^2 \text{ s}^{-1})$ [Eq. (10)]
\mathcal{D}_B	Diffusion coefficient of species B in dilute solution, based on thermodynamic driving force, referred to solvent ($\text{m}^2 \text{ s}^{-1}$) [Eq. (16)]
D^*	Effective diffusion coefficient of nonideal concentrated solution based on concentration gradient ($\text{m}^2 \text{ s}^{-1}$) [Eq. (61)]
\bar{D}	Integral (average) diffusion coefficient, based on concentration gradients ($\text{m}^2 \text{ s}^{-1}$) (Section 9.1)
D_B	Diffusion coefficient of species B in ideal dilute solution, based on concentration gradients, referred to solvent ($\text{m}^2 \text{ s}^{-1}$) [Eq. (19)]
D	$D_+D_-(z_+ - z_-)/(z_+D_+ - z_-D_-)$ diffusion coefficient of neutral electrolyte, based on concentration gradient, referred to solvent ($\text{m}^2 \text{ s}^{-1}$) [Eq. (54)]
μ_B	Electric mobility of species B, based on electric driving force, usually referred to velocity of solvent ($\text{m}^2 \text{ s}^{-1} \text{ V}^{-1}$) [Eq. (37)]
μ_B^*	Mechanical mobility of species B, based on mechanical, driving force, usually referred to velocity of solvent ($\text{kg}^{-1} \text{ s mol}$) [Eq. (43)]
λ_B	Ionic conductivity of species B, usually referred to velocity of solvent ($\text{ohm}^{-1} \text{ m}^2 \text{ mol}^{-1}$) [Eq. (42)]

number of them. They are all essentially equivalent but, depending on the circumstances, one or the other may be more convenient to use. It is important to remember that their numerical values are usually different. When making numerical calculations with the help of coefficients found in the literature one should take care to ascertain which *kind* of coefficient has been tabulated.

5.4. Interfacial Flux Densities; Interfacial Velocities

As we have seen in Section 4.2 the interfacial flux densities are linked in a simple manner with the electrode current density, which is, beside the potential, the most commonly measured quantity in electrochemistry. In the case of an ideal dilute solution one obtains from Eq. (31) combined with Eq. (19) or (53)

$$j = -n\nu_B^{-1} D_B F \left(\frac{dc_B}{dy} \right)_e \quad (64)$$

$$j = -(1 - t_B)^{-1} z_B F D \left(\frac{dc_B}{dy} \right)_e \quad (65)$$

where $(dc_B/dy)_e$ is the interfacial concentration gradient of B perpendicular to the interface.

The first relationship pertains to a minor reacting species B in an excess of supporting electrolyte. The second equation applies to a solution with a binary electrolyte.† Here, D denotes the diffusion coefficient of the neutral electrolyte and B denotes the cation or the anion, depending upon whether the first or the second one is the species which reacts at the electrode.

The transport number t_B is necessarily smaller than 1 and the factor $(1 - t_B)^{-1}$ in Eq. (65) is thus larger than 1. Therefore, under otherwise identical conditions, the current is larger than in the presence of a supporting electrolyte. The reason is that in the case of a binary electrolyte, electric migration contributes to the transport of the reacting ionic species toward (or away from) the electrode.‡

In Eqs. (64) and (65) no convection term appears. Indeed, in a dilute solution the average velocities are virtually equal to the velocity of the solvent

† In deriving Eq. (65) it has been taken into account that in the case of a binary single electrolyte, only electrode reactions such as $\text{Cu} \rightarrow \text{Cu}^{2+} + 2e$ or $2\text{Cl}^- \rightarrow \text{Cl}_2 + 2e$ are possible. [Redox reactions such as $\text{Fe}^{3+} + e \rightarrow \text{Fe}^{2+}$ or the reduction of a complex ion such as $\text{Cu}(\text{CN})_4^{2-}$ are excluded, because a *third* ionic species would be generated at the electrode and the diffusion layer would no longer consist of a binary single electrolyte.] Under these conditions $n\nu_B^{-1}$ is equal to z_B and the relationship for the electrode current is simplified accordingly.

‡ Note that the reverse is also possible: In the cathodic reduction of $\text{Cu}(\text{CN})_4^{2-}$, for example, the migration slows down the transport of the reacting species toward the cathode and thus decreases the current. However, we have excluded this case in deriving Eq. (65) because then a third ionic species would be generated at the cathode (CN^-) (see preceding footnote).

\mathbf{v}_A (Section 3.1), and the latter is zero at the interface because of the friction forces (see Chapter 3) and because no solvent flows through the interface.

In contrast to this, in the case of a concentrated solution, a nonnegligible convection term may exist even at the interface. In the case of a binary electrolyte solution, we now have to apply Eq. (63) where \mathbf{v}_b is given by

$$\mathbf{v}_b = \rho^{-1}(\rho_+\mathbf{v}_+ + \rho_-\mathbf{v}_- + \rho_A\mathbf{v}_A) \quad (66)$$

Let us consider for the sake of concreteness a cathodic metal deposition. At the cathode solution, interface $\rho_A\mathbf{v}_A$ and $\rho_-\mathbf{v}_-$ in Eq. (66) is zero but the mass flux density of the cations, $\rho_+\mathbf{v}_+$, is not since the mass associated with the cations crosses the interface. Equation (66) reduces to

$$v_b = \frac{\rho_+v_+}{\rho} = \omega_+v_+ \quad (67)$$

In a concentrated solution the mass fraction of the cations is not negligibly small; i.e., we may have to take into account that $\dagger v_b^*$ is not zero at the interface. This means that the mass flux of the reacting species itself (which crosses the interface) constitutes a nonnegligible convective term, which modifies the value of N at the interface and therefore increases the current flowing through the interface.

From Eqs. (63) and (67) it follows upon rearrangement that (remembering that $N_+ = c_+v_+ = M_+\rho_+v_+$)

$$N_+ = (1 - \omega_+)^{-1}(-\nu_+\rho DM^{-1} \nabla \mu_s + jt_+/z_+F) \quad (68)$$

or if we take into account that $jt_+/z_+F = N_+$

$$N_+ = -(1 - \omega_+ - t_+^b)^{-1}\nu_+\rho DM^{-1} \nabla \mu_s \quad (69)$$

From Eq. (68) it is seen that the interfacial velocity increases the interfacial flux density of the reacting cations (and thus their limiting current density) by the factor $(1 - \omega_+)^{-1}$. For a 1 M CuSO_4 solution ω_+ is 0.05 and N_+ is increased by about 6%. The above effect may be of importance especially in the electrolysis of fused salts, in particular, for the case of single salt melts such as NaCl.

In addition to the above effect, the interfacial velocity also affects the boundary condition to be applied in the integration of the equation expressing the conservation of momentum [Eq. (15a)] (see Section 8.2). The complications caused by the interfacial velocity have been treated by Acrivos⁽³⁵⁾ (see also Reference 31).

\dagger In Eq. (67) the velocity has not been taken as a vector because at the interface only the velocity component perpendicular to the interface is of importance.

6. Topics Related to the Electroneutrality Condition

6.1. Validity of the Electroneutrality Condition and Application of Poisson's Law

In the preceding sections we have repeatedly made use of the electroneutrality equation (12). It is about time to digress on the validity conditions of this relationship. The departure from electroneutrality corresponds to the space charge ρ^* (amount of free, or excess, charges divided by volume):

$$F \sum_i z_i c_i = \rho^* \quad (70)$$

On the other hand, the space charge is related to the electric potential by Poisson's law:

$$\nabla^2 \phi = \rho^* / \epsilon \epsilon_0 \quad (71)$$

ϵ is the dielectric constant of the medium relative to vacuum and is a dimensionless number. If SI units are used, the value of the permittivity for a vacuum, ϵ_0 , is $8.86 \times 10^{-12} \text{ A s V}^{-1} \text{ m}^{-1}$. If one uses the electrostatic system of units, $\epsilon \epsilon_0$ has to be replaced by $(4\pi)^{-1}$.

From Eq. (71) it is seen that the electroneutrality equation is strictly valid only if there is no gradient of the electric field $\nabla \phi$. Let us examine how far this is indeed the case. The principle of conservation of electric charges and Eq. (41b) yield for an ideal dilute solution

$$\frac{\partial \rho^*}{\partial t} = -\nabla \cdot \mathbf{j} = F \nabla \cdot \sum_i z_i D_i \nabla c_i + \kappa \nabla^2 \phi + \nabla \phi \cdot \nabla \kappa \quad (72)$$

If there is no capacitive current (i.e., no charging of the liquid volume element considered and therefore no change of ρ^* with time), we can write

$$\nabla^2 \phi = -\kappa^{-1} \nabla \kappa \cdot \nabla \phi - \kappa^{-1} F \nabla \cdot \sum_i z_i D_i \nabla c_i \quad (73a)$$

or

$$\nabla^2 \phi = -\kappa^{-1} \nabla \kappa \cdot \nabla \phi \quad (73b)$$

in the absence of concentration gradients.

If the concentrations and thus κ are constant, it follows from Eq. (73a) that $\nabla^2 \phi$ and therefore, because of Eq. (71), also ρ^* are zero: In the absence of concentration gradients the electroneutrality condition is strictly fulfilled.

If concentration gradients are present, we have to consider the term $F \nabla \cdot \sum_i z_i D_i \nabla c_i$. It is zero if the diffusion coefficients of all species are equal and if we accept at least as a first approximation, the principle of electroneutrality. For the sake of simplicity let us first restrict ourselves to that case. Equation (73b) then remains valid even if concentration gradients are present. However, across the diffusion layer there is a change of concentrations and

thus of κ ; therefore $\nabla^2\phi$ is not zero. In the presence of concentration gradients there is a space charge. We will now evaluate the magnitude of this effect. It is particularly small in the case of an excess of indifferent electrolyte (such as the example of a $\text{CuSO}_4 + \text{Na}_2\text{SO}_4$ solution considered toward the end of Section 4.7). Indeed, under these conditions the relative change of the overall concentration across the diffusion layer is small (Figure 7), and the same is true of the relative change in conductivity. Therefore, according to Eq. (73b) $\nabla^2\phi$ is small.† The fact that the field strength is nearly constant across the diffusion layer has been utilized already in our discussion of the influence of an indifferent electrolyte on the charge transport in Section 4.7. The constancy of the field strength is also important in connection with the measurement of electrode potentials (see Section 7.2).

On the other hand, in the case of a solution of a single binary electrolyte (such as CuSO_4 without additions), the relative concentration change, and therefore the relative change of κ across the diffusion layer, may be quite large, particularly at or near a cathodic limiting current. These are the cases where the values of $\nabla^2\phi$ are expected to be largest.

We have developed our argument for the case of equal diffusion coefficients. However, even if this is not true the main conclusion that we have reached so far remains essentially correct: The variation of the electric field across the diffusion layer and the departure from electroneutrality strongly decreases if an excess of indifferent electrolyte is added to a single salt solution. Indeed, the diffusion coefficients of most ionic species in aqueous solutions do not differ very much (except for H^+ and OH^- ions), and the additional term $F\nabla \cdot \sum_i z_i D_i \nabla c_i$ [which appears in Eq. (73a) when the D_i are not equal] is usually relatively small.

Let us now evaluate numerically the departure from electroneutrality in an unfavorable case—that of a single binary electrolyte. For the sake of simplicity, we consider the example of Figure 6 with a 1:1 electrolyte (such as AgNO_3) and assume ideal dilute solution behavior. For convection-free, steady-state linear mass transport, without homogeneous reaction in the solution ($\partial c/\partial t = \mathbf{v} \cdot \sum_r v_r^* = 0$), Eq. (55) reduces to

$$\frac{d^2c}{dy^2} = 0 \quad (74)$$

Integration between the limits

$$c = c_e \quad \text{at } y = 0, \quad c = c_{\text{av}} \quad \text{at } y = L/2$$

where L is the distance between the electrodes, yields

$$c = c_e + \frac{(c_{\text{av}} - c_e)y}{L/2} \quad (75)$$

† One may argue that the value of $\nabla^2\phi$ also depends on $\nabla\phi$. However, if we add a supporting electrolyte to, say, a CuSO_4 solution, $\nabla\phi$ is decreased for a given current, so that the conclusion given in the main text remains valid.

On the other hand, the potential can be calculated by applying Eq. (19) to the anions, for which $j_- = 0$:

$$Fc \frac{d\phi}{dy} = RT \frac{dc}{dy} \quad (76)$$

Integration shows that ϕ is proportional to $\ln c$. Whereas the concentration profile is linear, the potential is *not* a linear function of y .

The steepness of the concentration and potential profile depends on the magnitude of the electrolysis current j . We will express our results in terms of the fraction α of the limiting current j_{lim} flowing through the cell. Since for $j = j_{\text{lim}}$ $c_e = 0$, it follows from Eq. (65)† that

$$\frac{c_{\text{av}} - c_e}{c_{\text{av}}} = \frac{j}{j_{\text{lim}}} = \alpha \quad (77)$$

Combining Eqs. (75), (76), (77), (70), and (71) we obtain, upon differentiation,

$$\frac{d^2\phi}{dy^2} = -\frac{4RT\alpha^2}{F[L(1-\alpha) + 2\alpha y]^2} = \frac{\rho^*}{\epsilon\epsilon_0} = (\epsilon\epsilon_0)^{-1}F \sum_i z_i c_i \quad (78)$$

This equation gives the departure from electroneutrality as a function of α and y . At 25°C and for an aqueous solution ϵ is 78.3 and RT/F is equal to 0.0257 V. For $L = 0.1$ mm and (a) $\alpha = 0.05$, $y = 0.05$ mm, (b) $\alpha = 0.99$, $y = 0$, we obtain for $d^2\phi/dy^2$ 2.57 and 1.0×10^7 V cm⁻², respectively. There is thus quite a strong gradient of the electric field $d\phi/dy$. Nevertheless, because of the very large value of the Faraday constant, the departure from the electroneutrality condition is quite small. According to Eq. (78), for the above examples, the difference between the amount of cations and anions is 1.85×10^{-13} and 7.2×10^{-7} eq/liter. This is negligible compared to the concentrations commonly encountered in electrolysis. We may thus conclude that in most cases one can safely use the electroneutrality condition in electrolytic mass transport problems. Exceptions are systems with very thin diffusion layers or solutions of a very dilute binary electrolyte (see Section 6.3).

Let us note that in contrast to the diffusion layer the electroneutrality condition does not hold in the electric double layer. The distinction between double layer and diffusion layer will be discussed in Sections 6.2 and 6.3.

6.2. Concept of Interfacial Quantities

In electrolytic mass transport one often refers to interfacial values (i.e., at the interface of the electrode and solution)—interfacial concentration or interfacial flux density. They play a role in the concentration overpotential

† In Eqs. (74)–(77) c represents the concentration of the neutral 1–1 electrolyte ($c = c_+ = c_-$).

This assumes that the electroneutrality condition is valid at least as a first approximation. This assumption is also implied in the use of Eq. (73a). The continuation of our argument will show *a posteriori* that this premise is indeed fulfilled.

(see Section 7.2) and appear as boundary conditions (see Section 8) in the integration of the differential equations of mass transport, with the qualification "at $y = 0$ " (when the origin of the coordinate axis is on the interface). What exactly is meant by that? Obviously, one wants to designate by $y = 0$ a point of the solution as close to the interface as possible. However, one also usually wishes to apply the electroneutrality equation. Therefore, $y = 0$ means more precisely a point near the interface, just outside of the electric double layer, at a distance l such that the electroneutrality condition is fulfilled. In moderately concentrated aqueous solutions, the double layer thickness is of the order of nanometers, whereas the thickness of the diffusion layer ranges from 1 to 1000 μm . Therefore, in the mathematical treatment of mass transport the above-mentioned distance l is negligible compared to the length of the diffusion path over which the integration of the differential equations is performed.

Therefore, in general, the distinction between double layer and diffusion layer is no problem. However, under some circumstances the overlap of the two layers has to be considered.

6.3. Overlap of the Diffusion Layer and the Double Layer

The thickness of the electric double layer increases with decreasing ionic concentration in the solution (see Chapter 3 of Vol. 1). On the other hand, the departure from electroneutrality, which is given by $(\sum_i z_i c_i)/(\sum_j z_j c_j)$ also increases with decreasing ionic concentration for a given $d^2\phi/dy^2$. The problem of the overlap of the diffusion layer and the double layer is therefore most likely to come up in the case of very dilute systems, when the bulk ionic concentration is very small, or at or near the electrode, at current densities close to the limiting value where the interfacial concentration of the reacting species is low.

Indeed, Eq. (78) shows that $d^2\phi/dy^2$ and therefore $\sum_i z_i c_i$ increases (a) with decreasing y (i.e., close to a cathode), (b) when the thickness of the diffusion layer L decreases, (c) when α increases, i.e., when one approaches the limiting current (where for $y \rightarrow 0$ the value of $d^2\phi/dy^2$ tends toward infinity), and (d) when ε is smaller (as it may be the case in nonaqueous solvents). For the purpose of illustration let us consider the following numerical example: $L = 1 \mu\text{m}$ (which is the thickness of the diffusion layer that may be attained in a strongly agitated aqueous solution), $y = 0.1 \mu\text{m}$ (which corresponds to an electrode distance equal to 1/10 the thickness of the diffusion layer), and $\alpha = 0.95$. According to Eq. (78) $\sum_i z_i c_i$ is then 1.1×10^{-5} eq/liter. With a bulk concentration of 10^{-4} eq/liter, c at $y = L/10$ is 1.5×10^{-5} eq/liter. $\sum_i z_i c_i$ and c are now of the same order. This result applies to a solution of binary electrolyte. In the case of excess indifferent electrolyte (as commonly used in electroanalysis), the above effect does not occur (or to a small extent only), even if the reacting species is present in small concentration.

Nevertheless we may conclude that under exceptional circumstances the distinction between diffusion layer and double layer becomes hazy and the departure from electroneutrality then has to be considered in mass transport calculations. The problem of the structure of the outer parts of the double layer in such cases has been treated by Newman.^(17,18)

7. Some General Concepts Related to Mass and Charge Transport

7.1. Diffusion Potential

Diffusion layers in electrolytes can also occur elsewhere than near an electrode. This is the case when two different solutions are brought into contact, for example, a KCl and NaCl solution or two solutions of NaCl of different concentrations. The NaCl diffuses into the less-concentrated solution. An electric field can be set up in such a diffusion layer even if no net electric current is flowing through the solution. This is readily seen by writing the equation for the total current [Eq. (41a)] for $j = 0$.

$$\nabla\phi = -\frac{1}{\kappa} \left(F \sum_i D_i z_i \nabla c_i \right) \quad (79)$$

The field $\nabla\phi$ is zero only when all diffusion coefficients are equal. The integral of $\nabla\phi$ over the diffusion layer is called the diffusion (or junction) potential.

Its occurrence can be qualitatively explained as follows. In the above example of two NaCl solutions of different concentrations the Na^+ ions have a higher mobility than the Cl^- ions. Under the influence of the same driving concentration difference they tend to diffuse faster and to overpass the Cl^- ions. This results in a separation of charges and thus an electric field is set up. This field slows down the faster species and accelerates the slower one, so that both species diffuse at the same rate. The diffusion process is electroneutral since no net current is flowing through the system.

An argument similar to that developed in Section 6.1 shows that, although the diffusion potential can be regarded as being due to the formation of a space charge, the departure from electroneutrality is negligible: The sum $\sum_i z_i c_i$ is virtually zero, as compared to the concentrations of the species.

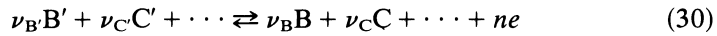
The magnitude of the diffusion potential is relatively small in most cases. Nevertheless, it plays an important role in potentiometry (pH determinations, etc.) and more generally in emf measurements.

It is seen from Eq. (79) that, in general, $\nabla\phi$ decreases if the conductivity becomes larger. Let us consider a 0.01 *M* NaCl solution which diffuses into a 0.0001 *M* solution of the same salt, and let us add to the first solution a large amount of KCl so that it has a concentration of KCl of 1 mole/liter. The mobilities of K^+ and Cl^- are about the same. Therefore, the strong

concentration gradient of K^+ and Cl^- ions which is set up hardly increases the term $\sum_i D_i z_i \nabla c_i$ (because $D_{K^+} \nabla c_{K^+} \cong D_{Cl^-} \nabla c_{Cl^-}$). The numerator in Eq. (79) remains essentially the same but the total concentration and therefore the conductivity κ strongly increases, resulting in a large decrease of the diffusion potential. Addition of a supporting electrolyte with equal cationic and anionic mobilities is a popular and practical way of minimizing the diffusion potential.

7.2. Concentration Overpotential

Let us now return to the situation where a diffusion layer develops near an electrode. As a consequence of the difference between the interfacial and bulk concentrations, the equilibrium potential of an electrode under current flow (E_j) is not the same as for zero current (E_0). This shift in potential is given by Nernst's law [Eq. (83), Section 8.2]. For a generalized electrode reaction of the form



we have

$$E_j - E_0 = \frac{RT}{nF} \ln \left[\frac{\prod (a_i^{\nu_i})_e}{\prod (a_i^{\nu_i})_0} \right] \quad (80)$$

In the simple example of copper deposition from an ideal dilute $CuSO_4$ solution, this relationship reduces to

$$E_j - E_0 = \frac{RT}{nF} \ln \frac{(c_{Cu^{2+}})_e}{(c_{Cu^{2+}})_0} \quad (81)$$

The subscript e denotes the interfacial value under current flow, and 0 the values of the concentrations or activities before the current is switched on. In many instances the initial concentrations c_0 are those that prevail later in the bulk solution.

$E_j - E_0$ is a contribution to the total overpotential, due to the difference between the concentrations at the interface and those in the bulk solution. In turn, this concentration difference is caused by the slowness of the mass transport and by the resulting buildup of a diffusion layer. Another effect linked with the mass transport is the potential difference that develops over the diffusion layer due to the differences in the diffusion coefficients of the species involved (diffusion potential) (see Section 7.1). If (as is usually the case) the electrode potential under current flow is measured with respect to a reference electrode located outside the diffusion layer, then the potential difference linked with the diffusion potential is included in the measurement.

Thus it appears adequate to lump this effect together with the shift in equilibrium potential $E_j - E_0$ given by Eq. (80) and to call the sum of the two *concentration overpotential*.[†]

IUPAC recommends the following definition of the concentration overpotential⁽¹⁹⁾: "The concentration overpotential of an electrode reaction at current density j is basically the difference in electrode potentials across the diffusion layer. More precisely, it is the potential of a reference electrode (of the same electrode reaction as the working electrode) with the concentrations which establish themselves at the interface at current density j , relative to the potential of a similar reference electrode with the concentrations of the bulk solution. From such a measured potential difference, with current flowing, one needs to subtract the ohmic potential drop prevailing between two electrodes." This definition corresponds to that given in the preceding paragraph. However, it is an operational definition which, in general, is to be preferred to a theoretical one. But in the present case it is difficult to live up to it experimentally. In practice, one may proceed as follows: One calculates the concentration overpotential as the open circuit potential of a concentration cell where the electrodes are both equilibrated with respect to the given electrode reaction. One compartment of the concentration cell has the bulk solution concentrations and the other compartment has the concentrations that would have been established at the interface of the working electrode and that can be deduced from mass transport theory. The junction assumed in the calculation should approximate the concentration profiles existing in the diffusion layer under current flow.

The above procedure yields the concentration overpotential as defined by IUPAC. In principle, it is also possible to determine it by a direct experiment, by measuring under current flow the potential difference between the working electrode and a reference electrode located outside the diffusion layer. However, concentration overpotential should be the only one present; i.e., all other types of overpotential, in particular activation overpotential should be negligible. In practice, this condition is seldom fulfilled to a good approximation. In addition, in a concrete situation one does not know whether or not it is fulfilled. Furthermore, if the measurement is made under current flow, it contains an ohmic potential drop which, according to the IUPAC definition, should not be included in the concentration overpotential.

The separation of the ohmic drop is a tricky problem. One problem is that the ohmic potential drop is ill-defined. If the working electrode is connected to the reference electrode through a Luggin capillary, the ohmic drop included in the measurement depends on the location of the tip of the

[†] In the literature there is no agreement on the definition of the concentration overpotential. In most textbooks,⁽²⁰⁻²³⁾ it is regarded as being the value of $E_j - E_0$ given by Eq. (80); in Newman's book⁽¹⁾ the diffusion potential is included.

capillary. If it is situated outside the diffusion layer, the measurement includes some of the ohmic drop in the bulk solution. If, in contrast to this, the capillary is located very close to the electrode there is a shielding effect and a modification of the local electrode potential near the tip of the capillary (see Chapter 4 on current and potential distribution) so that a value different from the average one is measured.

Let us mention two possibilities to correct for the ohmic drop:

- (a) One measures the electrode potential for various electrode–capillary tip distances and extrapolates to zero distance. We will return to this at the end of Section 7.2.
- (b) One interrupts the current and measures immediately after cutoff. The ohmic potential drop is thus eliminated. However, the activation overpotential does not drop instantaneously to zero. Another effect is the relaxation of the interfacial concentrations during the off-time. The method works only if a compromise between these two effects can be found.

The ohmic drop over the diffusion layer can be regarded as the potential drop that would prevail in the diffusion layer (for the same current) if all diffusion coefficients were equal. In fact, this part of the overall potential difference across the diffusion layer is very difficult to distinguish from the contribution due to an inequality of the diffusion coefficients. In practice, however, there is often no need for this distinction.

In kinetic studies especially, one is interested mainly in separating from the total overpotential the contributions that are not related to the reactions taking place at the electrode–solution interface. This includes both the concentration overpotential and the ohmic drop. Thus it is sufficient to determine the overall potential difference across the diffusion layer (including the ohmic drop and the diffusion potential) and the value of $E_j - E_0$ as given by Eq. (80), the interfacial concentrations being obtained from mass transport theory. In this connection an interesting conclusion may be drawn from the basic equations developed in this chapter. It is of advantage to add an excess of supporting electrolyte because then the potential drop across the diffusion layer decreases substantially and the field becomes more uniform (see Section 6.1). Under these conditions it becomes easier to determine this potential drop by varying the distance of the tip of the capillary and extrapolating to zero distance, if, as is often the case, the overpotential is measured by connecting the working electrode with the reference electrode by means of a Luggin capillary. The experimental methods for its measurement are treated in more detail in Chapters 1 and 2, Volume 6, and will not be discussed here.

Let us conclude this section with a semantic remark. Instead of concentration overpotential the expressions *transport overpotential* or *diffusion overpotential* are often found in the literature. According to the IUPAC nomenclature recommendations,⁽¹⁹⁾ these terms should not be used indifferently. The name transport overpotential should be restricted to cases where no

homogeneous reaction takes place in the diffusion layer. If, in addition, the magnitude of the interfacial concentrations is not influenced by any migration terms, the concentration overpotential may (but need not) be called diffusion overpotential.

7.3. Mass Transport Control

The concept of mass transport control plays an important role in electrochemical kinetics and electroanalysis. It is used to indicate that the rate-controlling step of an electrochemical process is the mass transport to or from the interface and not a reaction taking place at the interface or in the volume of the solution. One often reads the statement that there is mass transport control if the transport is slow compared to the rate of a consecutive electrode reaction. In reality, such a statement is ambiguous, if not misleading. Indeed, the number of moles of a species reacting at the electrode per unit time must be necessarily equal to the number of moles transported to (or from) the electrode per unit time, because in the interfacial plane[†] at $y = 0$ (as defined in Section 6.2) there can be no accumulation of substance (even under *unsteady*-state conditions): The electrode current (or the amount of substance consumed or produced in the charge-transfer reaction) is necessarily linked with the interfacial flux densities by the simple relationships given in Section 4.2.

A more precise characterization is as follows. The term *transport control* refers to conditions where, in a controlled-potential experiment, the current, and in a controlled-current experiment the electrode potential, are solely determined by the rate of mass transfer to (or away from) the electrode. For instance, the current measured in a controlled potential experiment is then called a transport-controlled current. Under conditions of transport control there is no influence of the kinetics of a reaction taking place at the electrode or in the volume of the solution. Except at the limiting current, this implies that the electrode reaction and homogeneous reactions, if present, are virtually at equilibrium (in spite of the current flow). This means that the reaction rate allowed by the slow mass transport is so small that the equilibrium of the chemical or electrochemical reactions is not disturbed.

An important consequence is that, in a transport-controlled experiment, below the limiting current the electrode potential can be calculated from the Nernst equation. However, although the electrode reaction is virtually at equilibrium its rate is not zero; but the reaction proceeds reversibly. This

[†] This interfacial plane is to be distinguished from the interface proper, which includes the electrode surface and the double layer in which there can be, under unsteady-state conditions, an accumulation of matter with time, due to adsorption. However, in calculations dealing with the mass transport in the volume of the solution, the interfacial plane to be considered is the boundary of the region to which the continuum equations and the electroneutrality condition can be applied.

should not be misunderstood as the whole process being reversible. This is not the case. But the irreversibility does not lie at the electrode; it is within the diffusion layer.

An interesting aspect is the connection of the concept of the mass transport control with the driving force of the process.⁽²⁵⁾ In the case of a chemical reaction, the driving force (or affinity) is given by $\sum \nu_i \mu_i$ and the equilibrium condition is $\sum \nu_i \mu_i = 0$. In the case of an electrochemical reaction, the μ_i terms are replaced by the electrochemical potentials $\tilde{\mu}_i$, which are linked with the chemical potential μ and the electric potential ϕ through Eq. (2'). For a reaction such as Eq. (30), the driving force is†

$$\Delta \tilde{G} = \sum \nu_i \tilde{\mu}_i = (\sum \nu_i \tilde{\mu}_i)_{\text{react}} + (\sum \nu_i \mu_i)_{\text{prod}} \quad (82)$$

At equilibrium $\Delta \tilde{G} = 0$, from which one can easily derive the Nernst equation, (83), if one remembers Eq. (2'), the relationship between μ and the activity ($\mu = \mu_0 + RT \ln a$), and the fact that $\sum z_i \nu_i = n$. If the electrochemical reaction is to run, $\Delta \tilde{G}$ must be negative; i.e., $(\sum_i |\nu_i| \mu_i)_{\text{react}} > (\sum_i |\nu_i| \mu_i)_{\text{prod}}$. This situation is shown schematically in Figure 8. The overall electrochemical reaction can be split into two parts: (i) the electrode reaction proper (involving the charge exchange at the interface) and (ii) the mass transport through the diffusion layer.

Correspondingly, we can split up the overall driving force:

$$\Delta \tilde{G} = \Delta \tilde{G}_1 + \Delta \tilde{G}_2$$

$\Delta \tilde{G}_1$ represents the driving force for the electrode reaction proper and $\Delta \tilde{G}_2$ that for the mass transport across the diffusion layer. If the electrode reaction is reversible, the "force" $\Delta \tilde{G}_1$ needed to drive it is negligible and we have $\Delta \tilde{G} \cong \Delta \tilde{G}_2$. Therefore, when the process is mass transport controlled, virtually the whole driving force is used to overcome the resistance due to the slowness of the mass transport and which lies in the diffusion layer (Figure 8a). Conversely, if the electrode reaction is strongly irreversible, we have the reverse situation: The major part of the total $\Delta \tilde{G}$ lies at the interface to overcome the resistance due to the slowness of the electrode reaction (Figure 8b). The situation is analogous to that of two electric resistors of very different resistances in series. The same electric current flows through both but there is a very small potential drop over the resistor with the small resistance and a very large potential drop over the resistor with the large resistance. The latter corresponds in the chemical or electrochemical analogy to the rate-determining step.

Let us return to the important exception of the limiting current which is reached in a certain potential range in a controlled-potential experiment (see Section 1). As already mentioned, in that case there is always mass transport

† Note that according to our sign convention the stoichiometric coefficients ν_i are positive for products and negative for reactants so that in Eq. (82) $(\sum \nu_i \tilde{\mu}_i)_{\text{react}}$ is negative. Note also that the μ of the metal electrons is to be included in the summation.

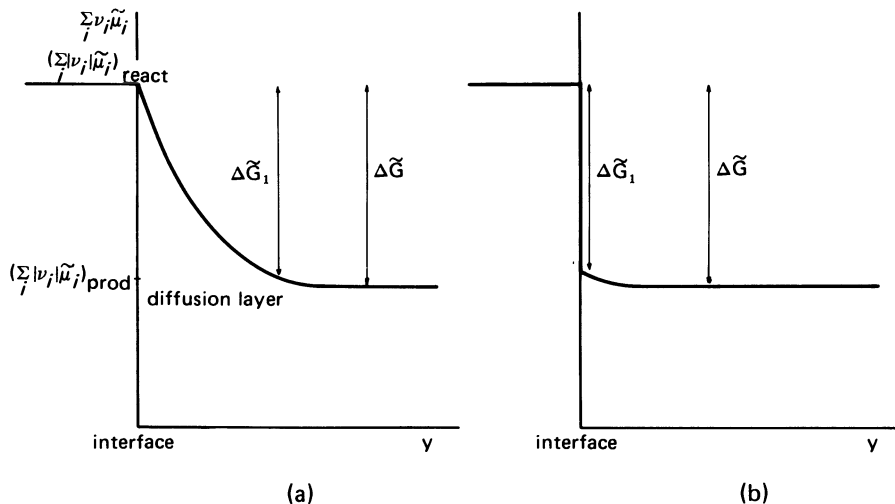


Figure 8. Distribution of total driving force ΔG between reaction at interface and transport process below limiting current: (a) transport control (reversible electrode reaction); (b) irreversible electrode reaction (kinetic control).

control of the current, even if the electrode reaction is *not* at equilibrium. Indeed, at the limiting current one is in a potential range where the interfacial concentration of the reacting species is zero[†] independent of the degree of irreversibility of the electrode reaction and of the applied electrode potential (within a certain range). Therefore, the concentration difference between bulk solution and interface, which determines the driving force for the diffusion toward the electrode, is also independent of those quantities. The rate of mass transport thus depends solely on the transport properties of the system (diffusion coefficients, hydrodynamic conditions). As we have seen at the beginning of this section, the rate of mass transport necessarily corresponds to the electrode current (and to the rate of the charge-transfer reaction at the electrode). Therefore, the limiting current is governed solely by the mass transport and is independent of the irreversibility of the electrode reaction or of the potential (within a certain range).

In contrast to the above situation, below the limiting current in a controlled-potential experiment, under conditions of transport control, the current not only depends on the transport properties but also on the value of the applied potential. Indeed, the latter determines through the Nernst

[†] Let us note that the interfacial concentration is not necessarily zero at the limiting current. It depends on the definition. If one considers as limiting current that which flows when a plateau on the steady-state current voltage curve is reached it may happen that this does not correspond to zero interfacial concentration. In this volume we will restrict the term limiting current to the cases where the interfacial concentration is zero.

equation the interfacial concentration and thus the driving force for the mass transport. The rate of mass transport, and thus also the current, are finally governed by *both* the transport properties and the applied potential. The situation is similar to that which one has in nonelectrolytic mass transport control, such as in the dissolution of NaCl in water. Under conditions of transport control, the equilibrium at the surface of the dissolving crystals is established; i.e., the solution is saturated at the interface crystal–solution. This determines the interfacial concentration and thus the driving force for the mass transport. The dissolution rate depends both on the equilibrium constant (which in our example is the solubility) and on the transport properties. The peculiarity of electrochemistry resides in the fact that the equilibrium can be easily modified by varying the applied potential and that one can reach a range in which the equilibrium concentration is negligible compared to the bulk value (limiting current), so that the driving force for the mass transport no longer depends on the actual equilibrium value.

Let us again conclude this section with a semantic remark. If, under conditions of transport control, the migration term in Eq. (19) is negligible, the term transport control may (but need not) be replaced by diffusion control.⁽¹⁹⁾ The expression diffusion control (diffusion current, etc.) is often used in polarography and related methods. Finally, the term mixed control is used instead of transport control if the measured quantity is determined *both* by the mass transport *and* by the kinetics of a reaction.

8. Determination of Quantities of Practical Interest: Theoretical and Semiempirical Methods

8.1. Quantities of Practical Interest

In electrochemical experiments one usually controls either (a) the *electrode current* or (b) the *potential* (of an electrode or of a cell). The controlled quantity may be constant or any function of time. One wishes then to calculate in case (a) the *potential* for a given current, and in case (b) the *current* for a given potential.

In principle, this calculation always involves mass transport considerations. However, their role may be negligible in the case of a strongly irreversible electrode reaction, when the concentrations in the diffusion layer differ little from those in the bulk. Conversely, when the heterogeneous and homogeneous reactions involved are at equilibrium, the quantities of practical interest can be calculated from the laws of mass transport alone, without kinetic considerations. The same is true of the limiting current, irrespective of whether the electrode reaction is reversible or not. These are the cases of transport control discussed in Section 7.3.

8.2. Outline of Theoretical Method

A complete *ab ovo* calculation has to start from the conservation equation, either in its general form (11a) or in a simplified version such as Eq. (21), (49), or (55). In order to avoid a complicated discussion that may obscure the main issues, we will assume that the differential equations (49) or (55) (ideal dilute solutions, excess of supporting electrolyte, or solution with a binary electrolyte) can be applied.

Their integration requires a specification of the boundary conditions (which play the same role as the integration constants in simpler differential equations). One of these conditions usually describes the situation in the bulk of the solution and indicates that the concentrations at a large distance from the electrode are known and constant (see Figure 1).[†] The boundary conditions that pertain to the situation at the electrode–solution interface depend upon whether the current or the potential of the electrode is controlled.

In case (a), controlled current, one can make a statement regarding the *concentration gradients at the interface*. Indeed, when there is only one electrode reaction,[‡] the electrode current density is linked with the interfacial fluxes of the species taking part in that reaction by Eq. (31). We have already derived earlier (Section 5.4) the equations

$$j = n\nu_B^{-1}FD_B\left(\frac{dc_B}{dy}\right)_e \quad (64)$$

for an excess of supporting electrolyte and

$$j(1 - t_B) = -z_BFD\left(\frac{dc_B}{dy}\right)_e \quad (65)$$

for a solution with a binary electrolyte.

In these equations, $(dc_B/dy)_e$ is the interfacial concentration gradient of a species taking part in the electrode reaction. Thus, we have a boundary condition expressed in terms of interfacial concentration gradients, which are determined by the current applied to the electrode.§ However, it must be

[†] It may be noted that, in some instances, there is no bulk electrolyte (with zero concentration gradients) in the above sense, because the region to which Eq. (49) or (55) is to be applied is not restricted to a simple diffusion layer of the kind shown in Figure 1. This is the case for the mass transport situation illustrated by Figure 6, or for the diffusion in the voids of a porous electrode. The boundary of the region to which Eq. (49) or (55) is to be applied then has to be shifted further away from the considered electrode, and the corresponding boundary conditions modified accordingly.

[‡] In the case of several simultaneous electrode reactions, the current efficiency must be known and the j terms appearing in Eq. (31) are then the current densities corresponding to the individual electrode reactions.

§ When the solution is concentrated (instead of dilute as assumed here) and the interfacial flux densities are high, the interfacial velocities discussed in Section 5.4 may play a role, and Eq. (66) or (61) may have to be used instead of (65).

noted that the current density appearing in Eqs. (64) and (65) is, in principle, a *local value* whereas the controlled quantity is the *overall* electrode current. One often avoids this difficulty by assuming a uniform current distribution over the interface. It must be emphasized that the accuracy of this approximation depends on the geometry of the system, the steepness of the current voltage curve, and the conductivity of the solution; i.e., on the factors that govern the current and potential distribution in the solution (see Chapter 4). A more precise statement regarding the boundary condition at the interface requires a knowledge of this distribution, and therefore implies the solution of the problem, which is complicated because it has to be achieved by some iterative procedure.

In case (b), controlled potential, one can make a statement regarding the *interfacial concentrations*. For a reversible electrode reaction they are given by the Nernst equation:

$$E = E_0 + \frac{RT}{nF} \ln [\prod (c_i^{\nu_i})_e] \quad (83)$$

which has been written here in a general way, corresponding to reaction (30).

In a simple case such as the deposition of copper from a CuSO_4 solution, the potential unambiguously determines the interfacial concentration of the reacting species, and one may formulate the boundary condition at the interface by stating that the concentration has a known value given by the electrode potential through Eq. (83). However, for a redox reaction such as $\text{Fe}^{2+} \rightarrow \text{Fe}^{3+} + e$, or for a metal deposition with amalgam formation, the potential determines through the Nernst equation only the ratio (or the product) of the interfacial concentrations. One then needs to write down an additional condition, which is given by the fact that the interfacial flux of *any* species involved in the electrode reaction is linked with the electrode current by means of Eq. (31). For example, for the reduction of Fe^{3+} to Fe^{2+} ions in an excess supporting electrolyte, remembering Eqs. (33a) and (80), we can write the boundary condition at the interface as follows

$$\begin{aligned} (c_{\text{Fe}^{3+}}/c_{\text{Fe}^{2+}})_e &= e^{(E-E_0)F/RT} \quad (E - E_0 \text{ given}) \\ (N_{\text{Fe}^{3+}})_e &= -(N_{\text{Fe}^{2+}})_e \end{aligned} \quad (84)$$

or

$$D_{\text{Fe}^{3+}} \left(\frac{dc_{\text{Fe}^{3+}}}{dy} \right)_e = -D_{\text{Fe}^{2+}} \left(\frac{dc_{\text{Fe}^{2+}}}{dy} \right)_e \quad (85)$$

Note that the same complication as for the case of controlled current arises here because of the problem of nonuniform distribution. The potential is controlled by means of the Luggin capillary only for a spot of the working electrode, and the potential jump across the electric double layer may vary

along the interface, depending on the factors governing the potential and current distribution (see Chapter 4). Again, this difficulty is overcome by assuming that $E - E_0$, and thus the concentrations, are constant along the interface. Depending upon the circumstances, however, this approximation may be a poor one and it is important to check whether the assumption made is acceptable or not.

Let us restrict ourselves to the case of a single electrode reaction and to a situation that can be approximated by a uniform current or potential distribution. It can then be easily seen that there is an important difference between the case of controlled current and that of controlled potential. In the first case the electrode current determines in a simple manner the interfacial concentration gradients independently of whether the electrode reaction is reversible or not. In a controlled-potential experiment, however, one can deduce the boundary condition from Eq. (83) in a simple way *only* if the electrode reaction is *virtually at equilibrium*. If this is not the case, one has to combine Eq. (83) with a relationship describing the electrode kinetics, and the formulation of the boundary condition becomes more complicated. An important exception is the case where the whole electrode works under limiting-current conditions. The boundary condition is then simply that the interfacial concentration of the consumed species is zero (or more precisely negligible as compared to the bulk concentration) everywhere along the interface and no complication arises from the fact that the electrode reaction may be irreversible.

Once the boundary conditions have been decided, one can proceed with the integration of Eq. (49) or (55). In a system with convection ($\mathbf{v} \neq 0$), the calculation requires knowledge of the velocity field, $\mathbf{v} = f(x, y, z, t)$. In an *ab ovo* computation it is obtained by integrating the Navier–Stokes equation (15). For a dilute solution with forced convection this can be done independently of the mass transport problem. In natural convection, due to the concentration differences present in the solution, the integration of the Navier–Stokes equation is coupled with that of Eq. (49) or (55). Such a coupling may also have to be considered in the case of concentrated solutions and high flux densities of the species reacting at the electrode. Indeed, with a dilute solution one has the boundary condition that the average flow velocity \mathbf{v}_b (taken relative to the electrode) is zero at the electrode–solution interface because of the friction forces (see Chapter 3). However, for a concentrated solution, \mathbf{v}_b at the interface may have a significant component perpendicular to the interface due to the flux of the reacting species (see Section 5.4). The integration of the Navier–Stokes equation is then linked with that of the mass conservation equation.

The integration of Eq. (49) or (55) finally yields the concentration field, $c = f(x, y, z, t)$. In some cases it might be desirable to calculate the concentration field for the various species present, but often it suffices to do so only for one of the reacting species.

The concentration field may be of interest by itself, but usually one is interested in the practically important quantities mentioned in Section 8.1. Once the concentration field is known, it is easy to calculate from it, for a controlled-potential experiment, the interfacial concentration gradient and thus the current, and for a controlled-current experiment, the interfacial concentrations. Knowledge of the latter is important for the evaluation of the concentration overpotential. In the case of a single reversible electrode reaction this determines the electrode potential. Otherwise, kinetic parameters have to be considered in addition.

In the case of a boundary condition of zero interfacial concentration, the concentration field can be used to calculate the interfacial concentration gradient and thus the limiting current. This is the most common application of mass transport theory.

In Chapters 2 and 3, examples will be given of a complete calculation of the quantities of practical interest through the integration of the fundamental differential equations (which is usually carried out by some approximate method). A review of the general methods employed has been given by Newman.⁽²⁷⁾

8.3. Semiempirical Procedures

In many cases (especially in the presence of a hydrodynamic flow under turbulent conditions), the integration of the fundamental differential equations is much too complicated and one has to resort to experiment. The most common technique is the determination of the limiting current by recording the current–voltage curve. In general, the limiting current density is a function of concentration, of the diffusion coefficient, and, in a system with convective mass transport, of the variables that govern the hydrodynamic flow. The determination of the complete relationship between the limiting current and all variables involved is very time consuming. The experimental investigation and the presentation of the results can be simplified by using dimensional analysis. It is useful for the extrapolation of the measurements to a broader range and to establish generalized correlations. Since this method is mainly of importance in convective mass transport, it will be outlined in Chapter 3.

9. Simplified Approach to Mass Transport in Electrolytic Systems

9.1. Approximation of the Ideal Dilute Solution and the Problem of the Diffusion Coefficient

The calculation of the numerical value of the quantities of practical interest mentioned in the preceding section requires knowledge of the diffusion

coefficient. In the case of an ideal dilute solution, it is independent of concentration. This applies to the individual ionic diffusion coefficient as well as to the diffusion coefficient of an electrolyte (see Section 5.1, cases a and b). Both can be calculated [through Eqs. (44) and (54)] from the conductivities, for which many good values are available. A satisfactory agreement is often observed in the case of species of low concentrations in an excess of indifferent electrolyte, as encountered in polarography and related methods.⁽⁴⁰⁾ In general, the systems encountered in practice can very seldom be regarded as ideal dilute with a clean conscience. Considerable progress has been achieved in recent years in dealing with the problem of nonideal solutions (see Sections 3.1 and 5.2) and numerical applications are increasing in number, but they are still very scarce. In present practice, one usually accepts (more or less tacitly) the myth of the ideal dilute solution, because it is so difficult to do better. In reality this is not as bad as it may seem at first sight. First, the departures from ideality are often moderate in the most common electrolytic systems. Second, the use of the equations for ideal dilute solutions has the advantage of avoiding the difficulty of the single-ion activities and the resulting problem of the definition of the electric potential mentioned in Section 3.1. They show clearly the major effects whereas the relationships involving the thermodynamic driving forces and the coupling terms (see Sections 2, 3.1, and 5.2) often tend to obscure the main issues. Third, the accuracy can be substantially improved by using adequate diffusion coefficients.

The actual values of the quantities of practical interest can differ from those calculated from relationships similar to Eqs. (49) and (55) for several possible reasons. Reasons such as the contribution of migration different from that implied in these equations; a nonnegligible interfacial velocity (Sections 5.2 and 5.4); and variation of transport properties over the diffusion path due to the dependence on concentration. However, it has been shown that one can express as a correction factor to the mass transport rate the influence of nonzero interfacial velocity and migration in the diffusion layer in the cases intermediate between a great excess of indifferent electrolyte and a binary electrolyte.^(22,31,35,39) This factor is the same for channel, or pipe flow and rotating disk, when the Schmidt number $\mu/\rho D$ (see Chapter 3) tends to infinity. This is usually the case for aqueous solutions. Similarly, for such systems a single effective diffusion coefficient should apply to mass transfer at the limiting rate for high Schmidt numbers, even though the physical properties vary with composition in the diffusion layer.^(1,57)

In view of this state of affairs Newman⁽¹⁾ has suggested that a fair approximation can be achieved in computations based on Eq. (49) or (55) (or equivalent relationships) by using effective (or integral) diffusion coefficients calculated from measured limiting currents by means of relationships derived from precisely these equations. These measurements should have been made with concentrations and hydrodynamic systems as close as possible to those at hand. For example, diffusion coefficients determined with

the rotating disk electrode are appropriate in calculations concerning pipe or channel flows. In polarography and related techniques, one may use diffusion coefficients measured by the Cottrell method involving electrolysis with unsteady-state mass transport in a stagnant solution contained in a capillary (see Chapter 2, Sections 8a and 8b). However, diffusion coefficients obtained by the porous cup method or by optical techniques are much less suited because the mass transport situation is rather different from that prevailing in electrolytic systems. Such data should be used only if more appropriate ones are not available.

The diffusion coefficients obtained with the porous cup or optical method can be differential or integral values, depending upon whether the concentration difference over the diffusion path is small or large compared to the concentration level.† In the first case, the most valid approximation is to use data applying to an *average* concentration of the diffusion layer (i.e., to a value corresponding to the mean of the concentration at both ends of the diffusion layer).

Many measurements of diffusion coefficients and transport numbers have been made over the years. Nevertheless, the desired values are often lacking or difficult to find. Useful sources of information are References 36–38. However, no comprehensive, critical compilation of transport data for electrolytes is available. It would be beneficial if such work were done and the results stored in a modern data bank to make them readily accessible.

9.2. Problem of the Species

Many multicomponent solutions include a number of species that are not independent of each other. Let us consider as an example cadmium deposition from an aqueous cadmium iodide solution with some free iodine. We may consider the following species: Cd^{2+} , CdI^+ , CdI_2 , CdI_3^- , CdI_4^{2-} , I_2 , I_3^- , H_2O . Reactions of the following kind occur between them:



At equilibrium, the concentrations are linked by the corresponding relationships expressing the law of mass action, and the chemical potentials fulfill the condition $\Delta G = 0$. This means that in a system with n' species only the concentrations of n species must be given in order to completely define the composition, $n' - n$ being equal to the number R of independent equations (86) which can be written. The figure n corresponds to the number of independent components in the classical phase rule. In our case it determines in part the number of independent equations (3) or (19) which can be written since the concentrations of R species can be expressed in terms of concentrations of other species. Furthermore, one of the equations drops out because

the fluxes are referred to a reference velocity (see Section 2.4): For a phase at equilibrium the number of independent Equations (3) or (19) is therefore $n - R - 1$. The number of independent equations expressing the conservation of mass [Eq. (49) or (21)] is likewise restricted by the above considerations (see Section 2.7).

What is the consequence of this state of affairs from the viewpoint of practical calculations? We first consider the case of a phase at equilibrium [i.e., the rates of the reactions described by equations such as (86) are very fast and the equilibrium is virtually undisturbed].

(a) One possibility is to write the Eq. (49) for all species considered, reducing the number of these equations by means of the restricting conditions indicated above (see also Section 2.7). Often one is interested only in some of the species—usually those that react at the electrode. The concentration profiles of the other species need to be considered only inasmuch as they influence the former ones. In the example mentioned at the beginning of this section (cadmium deposition from a iodide bath), one has to write Eq. (49) at least for all species containing Cd, but the problem can be simplified by using the law of mass action to eliminate a number of concentrations. Nevertheless, the procedure is extremely tedious and requires a detailed knowledge of the equilibrium constants and of the individual diffusion coefficients involved. These data are frequently not available. Often one does not even know which species are present. Are the hydrated ions to be considered as a species distinct from the naked ions? Should one distinguish between ions of different degrees of hydration? In fact, it is to a large extent *arbitrary* which assemblages of particles are regarded as a separate entity. In a sense, a species is whatever we define it to be. In reality, it matters little what one does, provided the diffusion coefficients of the species envisaged are about the same. Fortunately, the diffusion coefficients in aqueous solutions (which are the most commonly encountered ones in electrochemistry) are, in general, of the same order of magnitude and are often not very different. This suggests the following procedure.

(b) Instead of making efforts to consider all species separately, one lumps together a number of species of interest. For instance, in the aforementioned example of cadmium deposition, one is interested in the transport of the cadmium toward the cathode. All species containing Cd are lumped together and this ensemble is considered as a single component. Equations such as (49) are then written in terms of this single component, the concentration being taken as the total number of moles of cadmium per unit volume. Obviously the diffusion coefficient to be used now has the character of an effective or integral value. It is a kind of average between the individual diffusion coefficients. Furthermore, it depends on the relative amounts of the individual species present, which may vary across the diffusion layer because the equilibria in this layer can be more or less shifted due to the generation

or consumption of certain species at the electrode. The error involved in practical computations based on this approach will be smaller the less different the individual diffusion coefficients are and the less the chemical equilibria in the diffusion layer are shifted compared to the bulk solution. Furthermore, the best approximation will be achieved if one uses diffusion coefficients determined as indicated in Section 9.1, i.e., measured for bulk concentration and hydrodynamic conditions as close as possible to those at hand.

In the previous discussion it was assumed that the diffusion layer is at equilibrium with respect to homogeneous chemical reactions. When this is not the case, the situation is a very different one. Equation (49) (or similar relationships written for the various species involved) is now no longer linked through the law of mass action. The source term $v_{Br}^* = \nu_{Br} V^{-1} \xi$ in these equations [see also Eq. (15b)] is no longer determined by the equilibrium constant; ξ must be expressed by a kinetic law. Under these conditions the approach suggested under (b) above is inadequate in problems where one needs to know the concentration distribution of a species involved in an irreversible homogeneous reaction.

Let us consider an electrolysis in which a reaction of the type $C \rightarrow A + B$ takes place in the diffusion layer and only B reacts at the electrode in the range of applied potentials. A well-defined limiting current plateau may be observed in the current-voltage curve, even though the overall process is not (or at least not purely) transport controlled. A well-known system of this sort is aqueous formaldehyde, which is present predominantly as hydrate (methylene glycol), but only the free aldehyde is readily reducible cathodically. Let us assume that we want to calculate the limiting current in channel flow at a specified hydrodynamic velocity and we envisage doing this by applying the mass transport correlations valid for this type of flow (see Chapter 3, Sections 7.4 and 9.2). The result may be quite wrong, even if one uses an effective diffusion coefficient measured for similar bulk concentrations and hydrodynamic conditions, for example, with a rotating disk. The reason is that if the reaction $C \rightarrow A + B$ is irreversible, the limiting current depends in general on the kinetics of that reaction. In a theoretical treatment starting from the fundamental equations, one has to write the conservation equation separately for that species, and introduce a value of v_{Br}^* given by the kinetics of the reaction. Examples of systems of this sort will be discussed at various places throughout this volume (see, for instance, Section 8, Chapter 3).

10. Historical Note

Before we conclude this chapter, let us digress for a glimpse at the early history of electrolytic mass transport and diffusion. The basic relationships for diffusion (i.e., the flux equation and the conservation equation) are often referred to as Fick's first and second law. Indeed, the simplest version of these

laws,

$$N_B = -D \frac{dc_B}{dx}$$

$$\frac{dc_B}{dt} = D_B \frac{d^2c_B}{dx^2}$$

was formulated by him in 1855.⁽⁴¹⁾ In his youth Fick was fascinated by mathematics but later studied medicine under the influence of an elder brother. In 1852 he followed his former teacher, Carl Ludwig, to Switzerland where Ludwig had just been appointed professor of anatomy at the University of Zurich.⁽²⁹⁾ Three years later, at the age of 26, Fick published his well-known paper. In fact, his main contribution was to point out clearly the analogy of the diffusion law with Ohm's law for the conduction of electricity and with Fourier's law for heat conduction, which had already been known for 30 years.⁽⁴²⁾ The proportionality between flux and concentration gradient itself had been already understood earlier by Graham, who wrote in 1850⁽⁴³⁾: "the quantities diffused appear to be closely in proportion . . . to the quantity of salt in the solution." An even earlier precursor of Fick was Berthollet⁽⁴⁴⁾ who, in 1803, described the phenomena of diffusion and recognized the analogy with the propagation of heat, which he states as being proportional to the temperature difference. He thus anticipated both Fick's and Fourier's law.†

At about the same time as Fick was dealing with the diffusion of uncharged species, Hittorf studied intensively the migration of ions and developed his classical method for the determination of transport numbers.⁽¹⁴⁾ His merit was to show that by measuring the concentration changes taking place in the cathodic and anodic compartments one could draw conclusions regarding the ratios of the migration rates of the cations and anions. Hittorf's main papers⁽¹⁴⁾ appeared in the years 1853–1859. However, his ideas were to remain almost unnoticed for quite a while to come. According to Ostwald⁽⁴⁵⁾ they were ignored on purpose, because the scientific establishment of the time was jealous of the success of a very young unknown man in solving a problem where his elder colleagues had failed. However, Hittorf's theory received a striking confirmation when, about 20 years later, Kohlrausch developed accurate techniques for the measurement of the conductivity of electrolytic solutions and established the principle of the independent migration of ionic species.

Transport equations showing *both* the diffusion and the migration term appear in two remarkable papers by Nernst⁽¹⁶⁾ and Planck,⁽¹⁵⁾ published in 1888 and 1890, respectively. Nernst discussed the diffusion of the cations and anions of an electrolyte, showing that in the absence of an electric current, due to the electric forces, both these ions must move at one and the same

† According to Berthollet, Newton already regarded it as probable that the quantity of heat given up by a body to its surroundings is proportional to their temperature difference.

rate, intermediate between those corresponding to the mobilities of the two ionic species. He derived the equation connecting the diffusion coefficient D of an electrolyte [Eq. (54)] with the transport coefficients of the cation and anion. He showed that all the experimental values of D available to him were in very good agreement with those calculated from the ionic mobilities deduced somewhat earlier by Kohlrausch from conductivity measurements. He rightly regarded this as a further decisive confirmation of the views put forward by the German school of electrochemists in the second half of the century. The driving force for diffusion was called osmotic pressure rather than chemical potential, but the essential features of the mechanism of electrolytic mass transport were obviously well known around 1890. It is interesting that the mechanism of the passage of current through an electrolytic solution was correctly understood at a time when the ideas about the phenomena involved in the electric conductivity of metals were still quite hazy.⁽¹⁵⁾

Apart from the convective and source terms (which were not considered), the basic equations for electrolytic mass transport in dilute solutions [i.e., the flux equation (19) and conservation equation (21)] were presented by Planck in 1890 much in the same way as we do it today. He also examined the validity of the electroneutrality condition and showed quantitatively, by applying Poisson's law, that under usual circumstances the space charge due to $\nabla^2\phi$ is completely negligible compared to the total ionic charge. That is, the assumption of electroneutrality is a very good approximation. Furthermore, Planck clearly recognized the important fact that, for a binary electrolyte (in contrast to a multicomponent system), diffusion proceeds in the same way, independent of whether an electric current flows through the solution or not [which follows from the absence of the potential in Eq. (55)].

Soon after followed the first integrations of the differential mass transport equations with the purpose of calculating the electrode current or the concentration overpotential. In 1897, Salomon⁽⁴⁶⁾ calculated the transport-controlled current for steady-state convection-free electrolysis with a supporting electrolyte. A decade later, Eucken⁽⁴⁷⁾ treated the same problem for the case of a binary electrolyte and included the influence of the electric potential in his derivation. He showed theoretically that under these conditions, because of the contribution of migration, the limiting current of cation discharge is larger than in the presence of supporting electrolyte. The basic concept of the limiting current and that of the equivalent diffusion layer in a stirred bath had been introduced somewhat earlier by Brunner⁽⁴⁸⁾ and Nernst.⁽⁴⁹⁾ In 1903 Cottrell computed from the fundamental equations the limiting current for convection-free unsteady-state conditions,⁽⁵⁰⁾ and in 1901 Sand⁽⁵¹⁾ calculated, for a constant applied current, the change in interfacial concentration with time, and the time interval necessary for its decrease to zero. In 1910 Rosebrugh and Miller, in a comprehensive paper,⁽⁵²⁾ generalized Sand's results. They included in their consideration the case where the spreading of the diffusion layer toward the interior of the bath is prevented by convection,

as well as a variety of cases where the applied current is a periodic function of time. The major basic concepts, and the main lines of approach to problems of electrolytic mass transport, were therefore already well developed at the dawn of this century. However, the treatments presented until 1910 did not include any quantitative consideration based on hydrodynamic theory (which will be discussed in Chapter 3). This came very much later.

11. Scope of Volume 6

In this chapter we have developed the fundamental equations of electrolytic mass transport, starting from their general form (Sections 2.3 and 2.6), and showing later how they simplify for a moderately dilute solution (Section 3.1), for an ideal and dilute solution (Section 3.2), and for a single electrolyte or an excess of supporting electrolyte (Section 5). Equations (19) and (21) of Section 3.2, as well as Eqs. (53) and (55) [or (49)] of Section 5.1 (or some simplified version of them) are the relationships most commonly used in the literature, explicitly or implicitly. The first two [(19) and (21)] include three transport terms corresponding to diffusion, migration, and convection. The integration of Eq. (21) (which yields the quantities of practical interest as discussed in Section 8) depends on whether or not all three terms are taken into account.

In Chapter 2 the case of transport *without* convection will be treated; i.e., the terms $c\mathbf{v}$ and $\mathbf{v} \cdot \nabla c$ can be neglected in Eqs. (19) and (21), respectively. This type of problem is particularly important in electroanalysis and in the study of electrode kinetics.

Chapter 3 deals with *convective mass transport*; i.e., the terms $c\mathbf{v}$ and $\mathbf{v} \cdot \nabla c$ have to be taken into account. This is the case most commonly encountered in industrial electrolysis. However, it also has important applications in electroanalysis and in the study of electrode kinetics.

In both Chapters 2 and 3 the migration term with the electric potential, $zFD(RT)^{-1}c \nabla\phi$ and $zFD(RT)^{-1}\nabla \cdot c \nabla\phi$ will be usually ignored; i.e., the basic equations will be Eqs. (55) and (49), which correspond to the limiting cases of a single binary electrolyte and of an excess supporting electrolyte, respectively. The intermediate solutions, where the term with ϕ cannot be eliminated, will be briefly discussed in Section 6 of Chapter 3.

On the other hand, an opposite extreme case is that in which the concentration gradients *are negligible* and the migration term with $\nabla\phi$ is decisive. This is the approach used in the classical theory of current distribution which will be presented in Chapter 4.

Finally, Chapters 5, 6, and 7 deal with three particular systems that are most relevant for industrial electrochemistry: porous electrodes, three dimensional electrodes, and gas evolving cells.

References

1. J. Newman, *Electrochemical Systems*, Prentice-Hall, Englewood Cliffs, New Jersey (1973).
2. H. Margenau and G. M. Murphy, *The Mathematics of Physics and Chemistry*, Van Nostrand, New York (1964).
3. P. Haase, *Thermodynamik der Irreversiblen Prozesse*, Steinkopff, Darmstadt (1963). English translation: *Thermodynamics of Irreversible Processes*, Addison-Wesley, Boston (1969).
4. P. Chartier, M. Gross, and K. S. Spiegler, *Applications de la thermodynamique du non-équilibre*, Hermann, Paris (1975).
5. I. Prigogine, *Introduction to Thermodynamics of Irreversible Processes*, C. Thomas, Springfield, IL (1955).
6. A. S. Roy, *Adv. Heat Trans.* **12**, 195 (1976).
7. J. C. Slattery, *Momentum, Energy and Mass Transfer in Continua*, McGraw-Hill, New York (1972).
8. R. B. Byrd, W. E. Stewart, and E. N. Lightfoot, *Transport Phenomena*, Wiley, New York (1960).
9. V. G. Levich, *Physicochemical Hydrodynamics*, Prentice-Hall, Englewood Cliffs, New Jersey (1962).
10. H. Schlichting, *Boundary Layer Theory*, McGraw-Hill, New York (1968).
11. D. N. Bennion and B. W. Rhee, *I. & EC Fundamentals* **8**, 36 (1969).
12. IUPAC Manual of Symbols and Terminology for Physicochemical Quantities and Units: Appendix III, Electrochemical Nomenclature (R. Parsons), *Pure Appl. Chem.* **37**, 501 (1974).
13. C. Sinistri, *J. Phys. Chem.* **66**, 1600 (1962).
14. W. Hittorf, *Pogg. Ann. Phys.* **89**, 177 (1853); **98**, 1 (1856); **103**, 1 (1858); **106**, 337, 513 (1859).
15. M. Planck, *Wied. Ann.* **39**, 161 (1890).
16. W. Nernst, *Z. Phys. Chem.* **2**, 613 (1888).
17. J. Newman, *Trans. Faraday Soc.* **61**, 2229 (1965).
18. W. H. Smyrl and J. Newman, *Trans. Faraday Soc.* **63**, 207 (1967).
19. N. Ibl, IUPAC-Provisional Document No. 59 (July 1977), *Transport Phenomena in Electrolytic Systems*.
20. G. Milazzo, *Electrochimie*, Dunod, Paris (1969).
21. J. O'M. Bockris and A. K. N. Reddy, *Modern Electrochemistry*, Plenum, New York (1970).
22. J. Newman, *Indus. Eng. Chem. Fund.* **5**, 525 (1966).
23. G. Kortüm, *Lehrbuch der Electrochemie*, Verlag Chemie, Weinheim (1957).
24. K. J. Vetter, *Electrochemical Kinetics*, Academic, New York (1967).
25. N. Ibl, *Chimia* **23**, 245 (1969).
26. A. Katchelsky, *Biophysics and Other Topics*, p. 337 ff, Academic, New York (1976).
27. J. Newman, In: *Electroanalytical Chemistry, A Series of Advances*, A. J. Bard, Ed., Vol. 6, p. 187, Marcel Dekker, New York (1973).
28. R. Paterson, In: *Membranes and Ion Transport*, Vol. 1, p. 141 ff, E. E. Bitton, Ed., Wiley-Interscience, New York (1970).
29. E. L. Cussler, *Multicomponent Diffusion*, Elsevier, New York (1976).
30. J. Newman, D. Bennion, and C. W. Tobias, *Ber. Bunsenges. Phys. Chem.* **69**, 608 (1965); **70**, 493 (1966).
31. J. Newman and L. Hsueh, *Electrochimica Acta* **12**, 417 (1967).
32. J. Richter, *Ber. Bunsenges.* **78**, 973 (1974).
33. D. G. Miller, *J. Phys. Chem.* **70**, 2639 (1966).
34. R. Haase and J. Richter, *Z. Naturforsch. A* **22**, 1761 (1967).
35. A. Acrivos, *J. Fluid Mech.* **12**, 337 (1962).
36. Landolt-Börnstein, *Zahlenwerte und Funktionen aus Physik, Chemie* 6th ed., Vol. 2, Part 7, Springer, Berlin (1960).

37. R. A. Robinson and R. H. Stookes, *Electrolytic Solutions*, Butterworth, London (1965).
38. T. W. Chapman and J. Newman, Lawrence Radiation Laboratory, University of California, Berkeley (May 1968) (UCRL-17767) (see also UCRL-17768) (Nov. 1968).
39. J. Newman, *Int. J. Heat Mass Trans.* **10**, 938 (1967).
40. J. Heyrovsky and J. Kuta, *Principles of Polarography*, Academic Press, New York (1965).
41. A. E. Fick, *Pogg. Ann.* **94**, 59 (1855).
42. J. B. J. Fourier, *Theorie Analytique de la Chaleur*, Paris (1822).
43. T. Graham, *Philos. Trans. R. Soc. Lond.* **140**, 1 (1850).
44. C. L. Berthollet, *Essai de Statique Chimique*, Part I, Chap. IV of Sec. V, in particular pp. 410, 412, 414, 418, 181, Paris (1803).
45. W. Ostwald, *Vorträge über die Geschichte der Elektrochemie, Leitlinien der Chemie*, p. 181, Akademische Verlagsgesellschaft, Leipzig (1906).
46. E. Salomon, *Z. Phys. Chem.* **24**, 55 (1897).
47. A. Eucken, *Z. Phys. Chem.* **59**, 72 (1907).
48. E. Brunner, *Z. Phys. Chem.* **56**, 321 (1906).
49. W. Nernst, *Z. Phys. Chem.* **47**, 52 (1904).
50. F. C. Cottrell, *Z. Phys. Chem. (Leipzig)* **42**, 358 (1903).
51. H. J. S. Sand, *Philos. Mag.* **1**, 45 (1901).
52. T. R. Rosebrugh and W. L. Miller, *J. Phys. Chem.* **14**, 816 (1910).
53. M. Spiro, In: *Physical Methods of Chemistry*, Vol. 1, Part IIA, Chapter IV (p. 205), A. Weissberger and B. W. Rossiter, Eds., Wiley, New York (1971).
54. W. Preetz, In: *Fortschritte der chemischen Forschung*, Vol. 11, p. 411 ff, Springer, Berlin (1968–69).
55. W. Preetz, *Talanta* **13**, 1649 (1966).
56. E. Spenke, *Elektronische Halbleiter*, 2. Aufl., Springer, Berlin (1965).
57. A. Acrivos, *Phys. Fluids* **3**, 657 (1960).

2

Diffusion in the Absence of Convection : Steady State and Nonsteady State

SUSANA L. MARCHIANO and ALEJANDRO J. ARVIA

1. Transport Phenomena in Electrochemical Systems

Electrochemical processes occurring at the electrode–electrolyte interface involve either a solid–solid, liquid–liquid, solid–liquid, or gas–liquid–solid interfaces. The rate at which reactants arrive at the reaction surface plays an important role in the kinetics of heterogeneous reactions, including electrochemical reactions. Therefore, transport phenomena (migration, diffusion, and convection) are quite relevant in most cases as they contribute to the kinetics of the overall processes occurring at each electrode of any electrochemical cell. Transport phenomena become important in different fields of applied electrochemistry, such as electrochemical cell design, current distribution, and optimization problems, but they are also of fundamental importance for the methodological approach of electrochemical kinetics when the understanding of the electrochemical reactions at the molecular mechanistic level is attempted.^(1–3)

SUSANA L. MARCHIANO and ALEJANDRO J. ARVIA • Instituto de Investigaciones Físicoquímicas, Teóricas y Aplicadas (INIFTA), Sucursal 4, Casilla de Correo 16, 1900 La Plata, Argentina.

From a detailed knowledge of the transport processes it is possible to obtain the concentration profile at any instant of any of the species participating in the overall reaction. This certainly includes the instantaneous interfacial concentration value of the reacting species.

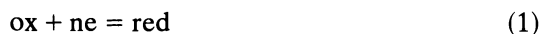
The concentration of the reacting species at the electrode surface is determined either by the flux (current density) or the potential across the interface, or both, depending on the working conditions of the experiments. These electrical parameters in the case of the stationary state adjust themselves to particular sets of values which are bound to well-defined time-independent concentration distributions.⁽⁴⁾ On the other hand, the relaxation techniques, which are particularly useful in electrochemical kinetics, may be employed either under potential-, current-, or charge-controlled conditions.

The perturbation variable, in the case of current or the potential, may correspond either to a constant value such as in the case of a constant current step or a constant potential step function, or to a time-dependent function. In the first case, for some kinetic studies the value of the relaxation variable can usually be extrapolated to $t = 0$, where the surface concentration of the reacting species corresponds to that of the bulk of the solution. The perturbation variable can also be programmed according to various time-dependent functions, such as a linear potential sweep, a single potential pulse, and so forth.^(1,5)

When any of the electrochemical variables, namely, either the current (flux) or the potential, are time-dependent, the concentration profile is also time-dependent, and its own relaxation is determined either by the rate of the proper electrochemical reaction, by the rate of mass transport, or both simultaneously. The phenomenological relationships thus derived are particularly important in obtaining reliable kinetic parameters, such as the exchange current density (j_0), the transfer coefficient (α), the reaction orders, and others, which serve as the basis for a mechanistic interpretation of a particular electrochemical reaction.

The present chapter is exclusively focused on diffusion as far as it is related to the electrochemical processes. Transport processes such as migration and convection, as well as convective diffusion, are dealt with in another chapter of the present volume.

In what follows the diffusion processes occurring at the reaction interface are analyzed, in most cases, on the basis of the simple electrochemical reaction



where ox and red are, respectively, the oxidized and reduced states of the soluble species participating in the electron-transfer step and the electrolyte solution is assumed to behave as an incompressible fluid.^(4,6,7) The rate equation of reaction (1) in terms of current density (j) is⁽²⁾

$$-j = nF[k_{\text{red}}^{\circ}c_{\text{ox},e} \exp(-\alpha_c FE/RT) - k_{\text{ox}}^{\circ}c_{\text{red},e} \exp(\alpha_a FE/RT)] \quad (2)$$

where k_{red}° and k_{ox}° are the rate constants for reaction (1) in both directions

when $E = 0$, $c_{\text{ox},e}$ and $c_{\text{red},e}$ are the surface concentrations of ox and red, respectively; α_c and α_a are the apparent cathodic and anodic transfer coefficients, respectively, and E is the potential applied to the interface measured against the reversible hydrogen electrode. The surface concentrations, although not usually known, can be either calculated or, in some particular cases, determined by optical techniques.^(8,9) The concentration to be used in kinetic relationships such as Eq. (2) is different from the bulk concentration because the latter still in the region where the mass transport, is usually not the same as the interfacial concentration. Thus, one has to distinguish, in principle, between the surface concentration and the interfacial driving force for diffusion was called osmotic pressure rather than chemical potential, but the essential features of the mechanism of electrolytic mass transport were obviously well known around 1890. It is interesting that the of the electrical double layer; i.e., still in the region where the electroneutrality condition is virtually fulfilled and the mass transport equations can be applied in the usual form. The surface and interfacial concentration can be the same but they may be different if complications, such as specific adsorption, occur.⁽¹⁰⁻¹³⁾

In the absence of specific adsorption, the concentration of reactants and products at the surface is determined exclusively by the relative rates of the forward and backward steps of reaction (1)—the transport rate of ox from the solution side toward the electrode surface and the transport rate of red in the reverse direction. When the resistance associated with the rate of consumption of ox (or production of red) is sufficiently larger than the resistance related to the transport of ox (or red), the concentration of both species at the surface will be practically equal to their respective bulk concentrations at any instant from the initiation of the reaction. The reverse situation implies that concentration gradients of ox and red start to build up from $t = 0$ at the reaction interface. The intermediate situation is the one most usually found in electrochemistry. Therefore, the general scheme of reaction can be put forward as follows:

$$\begin{aligned} (\text{ox})_{\text{solution}} &= (\text{ox})_{\text{electrode}} \\ (\text{ox})_{\text{electrode}} + ne &= (\text{red})_{\text{electrode}} \\ (\text{red})_{\text{electrode}} &= (\text{red})_{\text{solution}} \end{aligned} \quad (3)$$

The total flux (N_T), defined as the number of moles of a particular species which passes across a unit arbitrary area (interface) per unit of time, can be expressed as the sum of three independent contributions due to migration (N_m), diffusion (N_d) and convection (N_c):⁽⁴⁾

$$N_T = N_m + N_d + N_c \quad (4)$$

Depending on the operation conditions, namely, the presence or absence of a supporting electrolyte, the stirring of the system, the applied potential, the

time scale of the perturbing and relaxation variables, etc., the contribution of each term in Eq. (4) may be considerably different.

2. Migration Flux

The migration flux involves the transport of charged species through one of the phases under the influence of the electrical field. The resultant z -charged ion movement occurs in a direction parallel to the electric field at a rate (N_m) that depends both on E , the strength of the field, and on u_B , the ion mobility of the species B^(4,14,15):

$$N_{B,m} = z_B u_B E c_{B,0} \quad (5)$$

The ion mobility is related to its diffusion coefficient (D_B) through the Einstein–Stokes relationship^(16,17):

$$u_B = D_B F / RT \quad (6)$$

where F is the Faraday constant, R the universal gas constant, and T the absolute temperature. Therefore, $N_{B,m}$ is given by

$$N_{B,m} = z_B D_B F E c_{B,0} / RT \quad (7)$$

and in terms of the electrical potential:

$$N_{B,m} = -(z_B F / RT) D_B c_{B,0} \nabla \phi \quad (8)$$

where ϕ is the inner electric potential.

3. Diffusional Flux

The diffusional flux can be qualitatively defined as the transport of one species within a phase from one region of high concentration to another region of lower concentration. The transport process continues by the random walk of the corresponding species until a homogeneous concentration is attained.

The diffusional transport of the species B perpendicular through a reference plane of an isotropic substance is proportional to its concentration gradient.^(7,18,19)

$$N_{B,d} = -D_B \frac{\partial c_B}{\partial x} \quad (9)$$

where the negative sign indicates a diffusion toward the reference surface. Equation (9) is Fick's first law for unidirectional diffusion within an isotropic medium. It can be generalized to a three-dimensional diffusional flux and written in vectorial notation as follows:

$$N_{B,d} = -D_B \nabla c_B \quad (10)$$

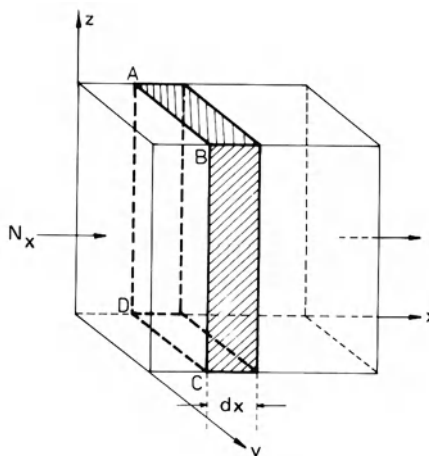


Figure 1. Scheme for the unidirectional flux balance.

The form of the operator ∇ depends on the choice of a suitable coordinate system for each particular case. Equation (10) is, however, strictly valid in a few particular instances related to time-independent diffusional transport.

Most of the diffusional processes of electrochemical interest generally involve time-dependent concentration characteristics. In order to deduce the concentration/time relationship, let us consider a unit volume element ($dx dy dz$) whose axes are parallel to the Cartesian axes (Figure 1). The sides of the parallelepiped normally placed with respect to the x axes are of unit area and they are separated by the distance dx . The diffusing flux which enters the plane ABCD is N_x and that which leaves the volume element through the opposite face is $N_x + (\partial N_x / \partial x) dx$. The amount of species accumulated within the volume element due to the x -directional flux is

$$-\frac{\partial N_x}{\partial x} dx = N_x - \left(N_x + \frac{\partial N_x}{\partial x} dx \right) \quad (11)$$

Taking into account that the accumulation of diffusing species in the reference volume can be expressed in terms of the rate change of the concentration, one obtains

$$\frac{\partial c_B}{\partial t} dx = -\frac{\partial(N_d)x}{\partial x} dx \quad (12)$$

Equation (12) is obviously valid for the other two directions. Therefore, after considering Eq. (9), the overall rate process is given in Cartesian coordinates by

$$\frac{\partial c_B}{\partial t} = \frac{\partial}{\partial x} \left(D_B \frac{\partial c_B}{\partial x} \right) + \frac{\partial}{\partial y} \left(D_B \frac{\partial c_B}{\partial y} \right) + \frac{\partial}{\partial z} \left(D_B \frac{\partial c_B}{\partial z} \right) \quad (13)$$

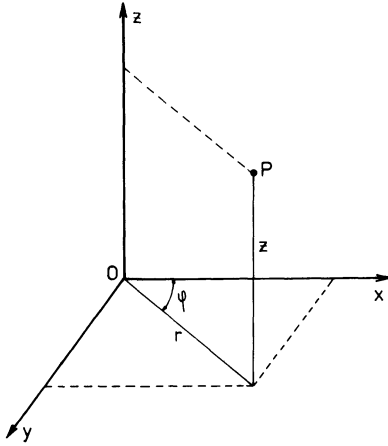


Figure 2. Cylindrical coordinate system.

Equation (13) can be expressed in vectorial notation as follows:

$$\frac{\partial c_B}{\partial t} = \text{div} (D_B \text{grad } c_B) \quad (14)$$

Equation (14) is Fick's second diffusion law and, as it is presented, is independent of the chosen system of coordinates. The coordinates, however, must be chosen according to the symmetry characteristics of the system. Thus, for a cylindrical coordinate system (r, ψ, z) (Figure 2), Eq. (14) becomes

$$\frac{\partial c_B}{\partial t} = \frac{1}{r} \left[\frac{\partial}{\partial r} \left(D_B r \frac{\partial c_B}{\partial r} \right) + \frac{\partial}{\partial \psi} \left(\frac{D_B}{r} \frac{\partial c_B}{\partial \psi} \right) + \frac{\partial}{\partial z} \left(D_B r \frac{\partial c_B}{\partial z} \right) \right] \quad (15)$$

Equation (15) is obtained from Eq. (13) with the following set of transform equations:

$$\begin{aligned} x &= r \cos \psi \\ y &= r \sin \psi \\ z &= z \end{aligned} \quad (16)$$

Analogously, for a spherical symmetry (Figure 3), Eq. (13) can be written as follows:

$$\frac{\partial c_B}{\partial t} = \frac{1}{r^2} \left[\frac{\partial}{\partial r} \left(D_B r^2 \frac{\partial c_B}{\partial r} \right) + \frac{1}{\sin \theta} \frac{\partial}{\partial \theta} \left(D_B \sin \theta \frac{\partial c_B}{\partial \theta} \right) + \frac{1}{\sin^2 \theta} \frac{\partial}{\partial \psi} \left(D_B \frac{\partial c_B}{\partial \psi} \right) \right] \quad (17)$$

after taking into account the corresponding transform equations:

$$\begin{aligned} x &= r \sin \theta \cos \psi \\ y &= r \sin \theta \sin \psi \\ z &= r \cos \theta \end{aligned} \quad (18)$$

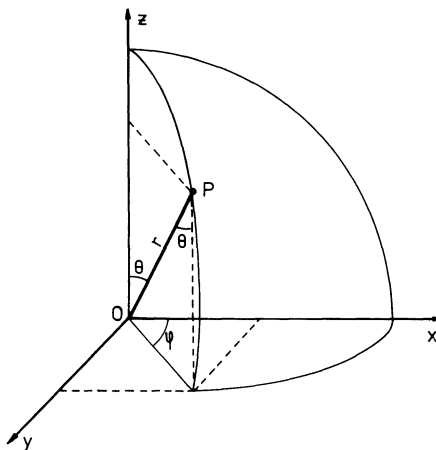


Figure 3. Spherical coordinate system.

Equations (13), (15), and (17) are particular forms of the continuity equation which applies to many other phenomena.^(7,18,19)

According to the thermodynamics of irreversible processes, the unidirectional diffusional flux for a real solution without the influence of external forces is given by the expression^(12,16,17)

$$\mathbf{N}_{B,d} = -L_B c_B \frac{d}{dx} (RT \ln \gamma_B c_B) = -L_B RT \frac{dc_B}{dx} \left(1 + \frac{c_B}{\gamma_B} \frac{d\gamma_B}{dc_B} \right) \quad (19)$$

where L_B is a phenomenological coefficient. For a real solution, the diffusion coefficient of the species B is given by

$$D_B = -L_B RT \left(1 + \frac{d \ln \gamma_B}{d \ln c_B} \right) \quad (20)$$

Equation (20) yields the diffusion coefficient as a function of the concentration of the diffusing species. Nevertheless, in solutions of high ionic strength involving, for example, a supporting electrolyte, for the minor components $(\partial \ln \gamma_B / \partial \ln c_B) \approx 0$. Accordingly, as a limiting case for the ideal solution

$$D_B = -L_B RT \quad (21)$$

Therefore, the diffusional flux equation written

$$\frac{\partial c_B}{\partial t} = D_B \nabla^2 c_B \quad (22)$$

implies a concentration-independent diffusion coefficient. This approximation is usually satisfied by electrochemical systems, although it is objectionable from a rigorous standpoint in dealing with real systems.

4. Convective Flux

The convective flux of the species B ($\mathbf{N}_{B,c}$) is produced by macroscopic streams of fluid which carry species B toward the transfer plane.^(4,7,18,19) The convective flux is given by the expression

$$\mathbf{N}_c = \mathbf{v}c_B \quad (23)$$

where \mathbf{v} means the fluid velocity. The expression of \mathbf{v} depends on the type of forces which cause the fluid displacement and the explicit dependences of each of its components along a particular coordinate as a function of time. Local density in a gravitational field due to concentration and thermal gradients in a homogeneous phase, and external forces, such as mechanical or magnetic forces,^(20,21) contribute to the convective flux. The instantaneous space distribution of the velocity components along each coordinate are obtained by solving the Navier–Stokes equation for each symmetry.^(6,22)

5. General Expression of the Mass Transfer Equation

The sum of the three fluxes just defined independently, corresponding to migration, diffusion, and convection, furnishes according to expression (4) the total flux for the species B:

$$\mathbf{N}_T = -z_B u_B F c_B \nabla \phi - D_B \nabla c_B + \mathbf{v}c_B \quad (24)$$

Equation (24) is the general expression for the transport of matter.

On applying Eq. (24) to electrochemical processes it is convenient to deal with the fluxes in terms of current density (j), i.e., electrical current per unit electrode surface area:

$$j = -nF|\mathbf{N}_T| \quad (25)$$

Equations (24) and (25) can be extended to an electrochemical system of multiple diffusing particles by admitting that there are no mutual interactions of the various moving species.^(3,23)

Taking into account Eqs. (7), (22), and (23) for the flux of species B, the rate of change of its concentration in the elementary unit volume is

$$\frac{\partial c_B}{\partial t} = D_B \nabla^2 c_B - \mathbf{v} \cdot \nabla c_B + \frac{z_B D_B F}{RT} \nabla \cdot (\nabla \phi c_B) \quad (26)$$

This equation is valid only for an incompressible fluid and a concentration- and distance-independent diffusion coefficient.

Equation (26) becomes even more general when it includes the possibility that within the elementary reference volume there is either a source or a sink of the species B due to an homogeneous chemical reaction. If $\pm R_B$ is the rate

of such a process, where the + sign stands for the source and the - sign for the sink, Eq. (26) results in

$$\frac{\partial c_B}{\partial t} = D_B \nabla^2 c_B - \mathbf{v} \cdot \nabla c_B + \frac{z_B D_B F}{RT} \nabla \cdot (\nabla \phi c_B) \pm R_B \quad (27)$$

Equation (27) is the general expression for the material balance of species B. This second-order partial differential equation with variable coefficients can be analytically solved only in a few cases of a simple geometry if some reasonable assumptions are made to make the mathematical problem easier to handle. Certainly Eq. (27) is valid for each moving species present in the electrochemical system.^(3,4)

5.1. Limiting Cases of Equation (27)

From the material balance equation (27) in the absence of a homogeneous chemical reaction ($\pm R_B = 0$), simple expressions are derived. The migration flux term can be disregarded in two particular cases—(i) when the electrochemical system contains a supporting electrolyte at a suitable concentration and (ii) for a binary electrolyte.^(3,4) In the former case, the migration contribution of the reacting species B is negligibly small compared to that of the supporting electrolyte. For the binary electrolyte (case ii) the migration term is dropped out through the mathematical operational procedure, but its physical contribution is automatically included by defining an effective diffusion coefficient that takes into account the migration effect.

Case (i): The migration contribution of species B to the mass transport process is minimized when other ionic species at concentrations very much larger than that of the species B are present in the electrolyte solution. The supporting electrolyte increases the electrical conductivity of the solution, taking on itself almost all of the migration current. Ideally, it must be electrochemically inactive in the range of potentials where the species B of interest reacts. Under these circumstances, the mass transport of species B occurs as if it were a neutral particle. Then, under stationary conditions ($\delta c_B / \delta t = 0$) from Eq. (27) becomes⁽⁴⁾

$$\mathbf{v} \cdot \nabla c_B = D_B \nabla^2 c_B \quad (28)$$

Equation (28) is the convective-diffusion differential equation, which yields the concentration distribution and is better fulfilled the larger the ratio between the supporting electrolyte concentration and the concentration of species B. Thus, when the latter ratio is 10^3 , $\mathbf{N}_m = 10^{-3} \mathbf{N}_T$. The incidence of the migration contribution to the mass transport has been evaluated in detail in the literature.^(3,4,23)

Case (ii): Let us consider a binary electrolyte solution, c_+ and c_- being the concentration of each component.⁽⁴⁾ The electroneutrality condition is

$$z_+ c_+ + z_- c_- = 0 \quad (29)$$

so that a reduced concentration, c , can be defined:

$$c = -\frac{c_+}{z_-} = \frac{c_-}{z_+} \quad (30)$$

The material balance equation (26) applied to each species, in terms of c , results in

$$\frac{\partial c}{\partial t} + \mathbf{v} \cdot \nabla c = D_+ \nabla^2 c - \frac{z_+ D_+ F}{RT} c \nabla \cdot \nabla \phi \quad (31)$$

and

$$\frac{\partial c}{\partial t} + \mathbf{v} \cdot \nabla c = D_- \nabla^2 c + \frac{z_- D_- F}{RT} c \nabla \cdot \nabla \phi \quad (32)$$

By subtracting Eq. (31) from Eq. (32) and after replacing the latter into Eq. (26), one obtains

$$\frac{\partial c}{\partial t} = D \nabla^2 c + \mathbf{v} \cdot \nabla c \quad (33)$$

where D , the effective diffusion coefficient, is

$$D = \frac{D_+ D_- (z_+ - z_-)}{z_+ D_+ - z_- D_-} \quad (34)$$

The migration term is formally absent in Eq. (33). Notwithstanding, expression (34) considers the influence of both the counterion and the charge of species (+) and (-).

5.2. Migration Contribution

Under certain circumstances, the total flux (current flowing through the cell) can be associated with a concentration gradient of the reacting species approaching zero ($\nabla c_B \rightarrow 0$), and, therefore, the diffusional contribution, compared to that corresponding to an interfacial concentration of the reacting species equal to zero, can be negligible. Then, the diffusional contribution does not play a significant role in the total current in the cell. The entire solution may be characterized by the conductivity of the solution, and, therefore, the current distribution can be determined just by solving a purely electrical problem,^(3,4) through either Laplace or Poisson equations. See Chapter 4 in this volume.

On the other hand, if the current in the cell is comparable to the diffusional limiting current, the contribution of the distribution of the reactant concentration becomes increasingly more important than the chemical and electrical contributions in the overall rate of the electrochemical process. Then, the current distribution is determined by resolution of the mass transport differential equations.

When the concentration of the supporting electrolyte is low compared to that of the reacting species, the presence of an electric field in the diffusion layer can produce either an increase or a decrease in the flux toward the surface due to the contribution of migration. Under these circumstances, within the diffusion layer, migration and diffusion contribute to the mass transport process.^(3,4)

The problem of diffusion plus nonnegligible migration in the absence of convection is particularly relevant for a solid electrolyte. See Chapter 9 in Volume 3.

6. Pure Diffusion and the Mathematical Solution of the Diffusion Equation

When, besides migration, the contribution of convection is also cancelled in Eqs. (24) and (26), diffusion remains as the only driving force for the transport phenomena. Under these conditions, Eqs. (24) and (26) yield Fick's first and second law, respectively.

The fluid movement due to any kind of forced convection in unstirred solutions is eliminated by means of a vibration-free experimental device as the forced convective flux is cancelled when $v = 0$. Nevertheless, natural convection produced by density gradients in a gravitational field also contributes to bulk transport of the electrolyte. However, its influence can be practically cancelled by a number of different procedures such as electrolyte jellying and electrolyte stratification, employing a small-area indicating electrode, or by perturbing the system during a relatively short time.^(1,4) Under these circumstances either no density gradients can be established or the system is unable to produce a massive displacement of the electrolyte during the short perturbation periods.

Another interesting situation is the diffusion which occurs where a concentration gradient of the reacting species exists on the surface.⁽²⁾ This diffusional process, which corresponds to surface diffusion, is important in electrocrystallization. In dealing with a solid electrolyte, convection effects being absent, diffusion and migration are the only terms left in Eqs. (24) and (27).⁽¹⁹⁾

The general mathematical solution of the diffusion equations for any set of boundary conditions is relatively easier when the diffusion coefficient is taken as a constant. These solutions have one or two standard forms. Thus, for short times, solutions of either the error-function-type or integrals related to it are found, while for long times solutions given in terms of trigonometric series are satisfactorily convergent. For cylindrical-shaped surfaces, these series transform into Bessel equations.^(18,19,24)

To solve the Fick equations, the usual mathematical procedures are employed. They are expressed in terms of a coordinate system which, while

suiting the geometry of the system, yield the simplest expression whose solution can be straightforwardly interpreted. Therefore, Eqs. (13), (15), and (17) are those to be solved for the cases of the planar, spherical, and cylindrical geometries, respectively. In other special cases a more adequate system of coordinates must be chosen. Thus, for particular problems the partial differential equation takes the form of a simple unidirectional diffusion equation.

The initial and boundary conditions depend upon the operational form of the system. The most frequently encountered problems of diffusion in electrochemistry involve instantaneous sources, continuous sources, or extended initial distributions.⁽¹⁹⁾ The three types of problems just referred to can be achieved in electrochemical systems either through current, charge, or potential control.⁽¹⁾

Let us first consider a plane electrode of infinite dimensions located at $x = 0$, where the diffusion process takes place in one direction on both plane surfaces (infinite linear diffusion). At $t = 0$ a constant potential E is applied at which the electrochemical reaction (1) proceeds at an infinite rate, so that a concentration profile of both ox and red species are instantaneously established on both sides of the plane. At the potential E , the interfacial concentration ratio of ox and red, at $x = 0$, is therefore constant.

Then, the ox species diffuses from $x \rightarrow \infty$ to $x = 0$ and from $x \rightarrow -\infty$ to $x = 0$ or vice versa, depending on the direction of the reaction. The diffusion of red occurs in the reverse direction. Under these circumstances, the boundary conditions are expressed by the concentration of the ox species at two positions, namely, at a value of $x > 0$ and at a value of $x < 0$, respectively, and by the equality of fluxes for ox and red at $x = 0$ on both plane surfaces ($N_{\text{ox}} = -N_{\text{red}}$). When the diffusion takes place only toward positive x values, it corresponds to semi-infinite linear diffusion.

Situations such as those of infinite linear diffusion or semi-infinite linear diffusion can be induced by a punctual source, like the perturbation of the electrochemical interface with an ideal instantaneous pulse current function or by means of a continuous constant flux source located at the interface ($x = 0$). This latter situation is practically approached when the electrochemical interface is perturbed with a step current function (galvanostatic method). Then, the initial condition depends on each particular case, but the boundary condition which expresses the continuous flux is

$$D_B \left(\frac{\partial c_B}{\partial x} \right)_{x=0} = \text{const} \quad (35)$$

Sometimes the mathematical solution of the diffusion equation implies time-dependent boundary conditions. This case is encountered, in general, in the electrochemical methods with dynamic electrical variables (e.g., square-wave polarography and linear potential sweeps technique) and in the perturba-

tion of the electrochemical interface with sinusoidal functions as in the case of the faradaic impedance method.^(11,25,26)

When the Fick law is applied to an electrochemical system under a potential-controlled perturbation, the degree of irreversibility of the reaction is explicitly given as a boundary condition in contrast with the current-controlled perturbation conditions. Thus, when the electrode reaction behaves reversibly ($j_0 \geq 10^{-3} \text{ A cm}^{-2}$), the interfacial concentration ratio of the reacting species is determined by the applied potential. The resulting interfacial concentration ratio applied-potential relationship is a boundary condition of the problem. On the other hand, under either intermediate kinetic conditions ($10^{-3} \geq j_0 \geq 10^{-7} \text{ A cm}^{-2}$), or in the case of an irreversible reaction ($j_0 \leq 10^{-7} \text{ A cm}^{-2}$) the interfacial concentration is determined by the rate of the electrochemical reaction.

In the following section the mathematical solutions of Fick's equation for different geometries under a stationary state is considered first. Then the problem under a nonstationary state is considered.

7. Stationary State

A system that has reached a stationary state for diffusion involves time-independent local concentration values. This condition is expressed by

$$\frac{\partial c_B}{\partial t} = 0 \quad (36)$$

The stationary state under pure diffusion is only an approximation. At the initiation of diffusion, large variations of either the flux toward the interface or the local concentration are produced. On the other hand, at long times, either the increase or the depletion of concentration of the reacting species at the interface causes density gradients in the gravitational field, which generate the bulk fluid motions of natural convection. Under these circumstances, the stationary state is achieved by a complex transport mechanism (convective diffusion) rather than by diffusion alone.

However, sometimes in electrochemical kinetics the analysis of the system concerns a quasistationary condition. Then, it is convenient to solve the diffusion equation as if one were dealing with a stationary state. These solutions are of special interest in regard to diffusion through membranes as well as to hydrogen diffusion in metals. Therefore, the diffusion equation reduces to

$$D_B \nabla^2 c_B = 0 \quad (37)$$

which is applied independently to each component of the system. The following deals with the classical solutions of Eq. (37) for those well-defined, simple-geometry interfaces often encountered in experimental electrochemistry.

7.1. Infinite-Plane Interface

Let us consider an infinite-plane interface where diffusion of the reacting species takes place along the x axis (Figure 4). Then, Eq. (22) applied to the unidirectional diffusion with condition (36) becomes

$$\frac{d^2 c_B}{dx^2} = 0 \quad (38)$$

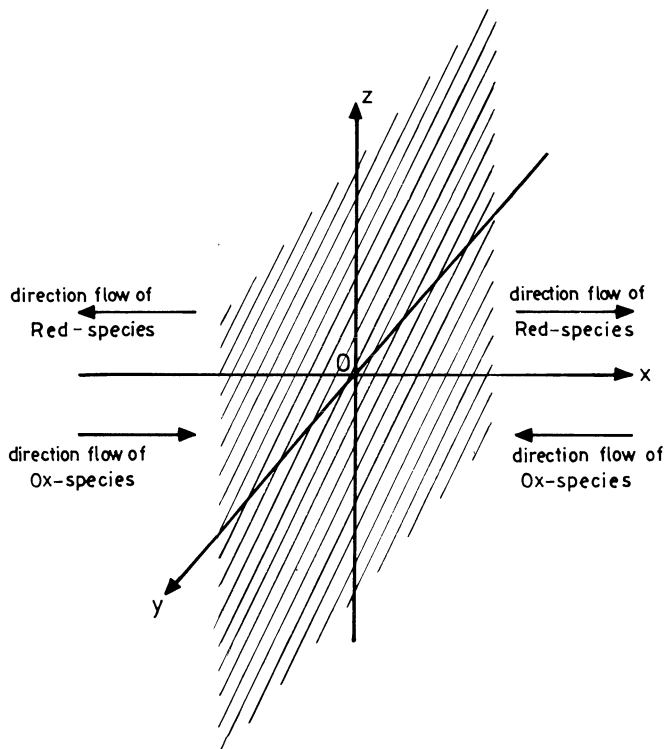
By solving Eq. (38),

$$\frac{dc_B}{dx} = K_0 \quad (39)$$

and

$$c_B = K_0 + K_1 x \quad (40)$$

where K_0 and K_1 are integration constants. Accordingly, the concentration profile is represented by a straight line, since the concentration gradient is a constant. The constants K_0 and K_1 depend upon the boundary conditions.



Equations (39) and (40) are especially interesting for diffusion through membranes. For a membrane whose thickness is l (Figure 5) the boundary conditions must be given for both faces of the membrane, namely, at $x = 0$ and at $x = l$, where $c_{B,0}$ and $c_{B,l}$ are, respectively, the concentrations of the species B at each plane. Then the concentration distribution results:

$$\frac{c_{B,0} - c_B}{c_{B,0} - c_{B,l}} = \frac{x}{l} \tag{41}$$

and the current density associated with ion B, referred to one face of the membrane, is

$$j_B = -n_B F D_B \left(\frac{\partial c_B}{\partial x} \right)_{x=0} = -n_B F D_B \left(\frac{c_{B,0} - c_{B,l}}{l} \right) \tag{42}$$

According to Eq. (42), l is the diffusion layer thickness in the membrane, which is equal to the membrane thickness.

The plane-interface diffusion equation can be applied to real systems as long as the diffusion distance is much larger than the microscopic unevenness of the plane. Furthermore, it can be extended to other different geometries provided the radius of curvature of the surface is very much larger than the diffusion distance.

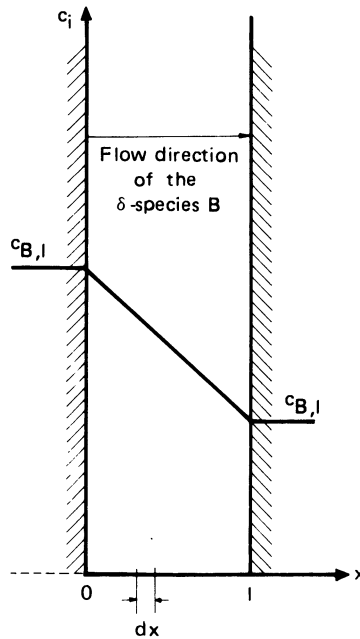


Figure 5. Steady-state unidirectional flow between two infinite-plane plates at a distance l .

7.2. Spherical Shell

To solve the problem of radial diffusion through a spherical shell (Figure 6), Eq. (17) is reduced on the assumption of a constant diffusion coefficient and stationary-state conditions to

$$\frac{d}{dr}\left(r^2 \frac{dc_B}{dr}\right) = 0 \quad (43)$$

its solution being

$$c_B = A + \frac{B}{r} \quad (44)$$

where the integration constants A and B come out from the corresponding boundary conditions. The r coordinate is bound to the condition $r_b \geq r \geq r_a$, r_a and r_b being the radii of the spheres which determine the spherical shell. $c_{B,a}$ and $c_{B,b}$ are the concentrations of the reacting species at r_a and r_b , respectively. Hence the concentration distribution within the shell is

$$c_B = \frac{r_a c_{B,a}(r_b - r) + r_b c_{B,b}(r - r_a)}{r(r_b - r_a)} \quad (45)$$

The total current (I) which flows through the outer sphere is

$$I = -n_B F 4\pi D_B \frac{r_a r_b}{r_b - r_a} (c_{B,b} - c_{B,a}) \quad (46)$$

and the charge is given by the product $I\tau$, where τ is the duration of the perturbation. Equation (46) gives the total current through the outer sphere.

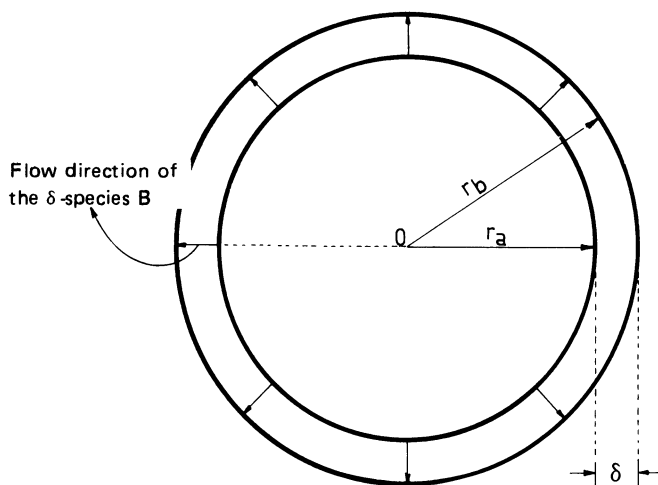


Figure 6. Radial flow in a spherical shell.

7.3. Cylindrical Interface

Let us consider a radial diffusion through a cylindrical shell of thickness $\delta = r_b - r_a$ (Figure 7), where r_b and r_a are now the radii of the outer and inner concentric cylinders, respectively. The diffusion equation in cylindrical coordinates for a stationary flux is

$$\frac{\partial}{\partial r} \left(D_B r \frac{dc_B}{dr} \right) = 0 \tag{47}$$

which is immediately solved on the assumption of a concentration- and distance-independent diffusion coefficient to give

$$c_B = A + B \ln r \tag{48}$$

When $r = r_a$, $c_b = c_{B,a}$ and $r = r_b$, $c_b = c_{B,b}$, the concentration distribution is

$$c_B = \frac{c_{B,a} \ln (r_b/r) + c_{B,b} \ln (r/r_a)}{\ln (r_b/r_a)} \tag{49}$$

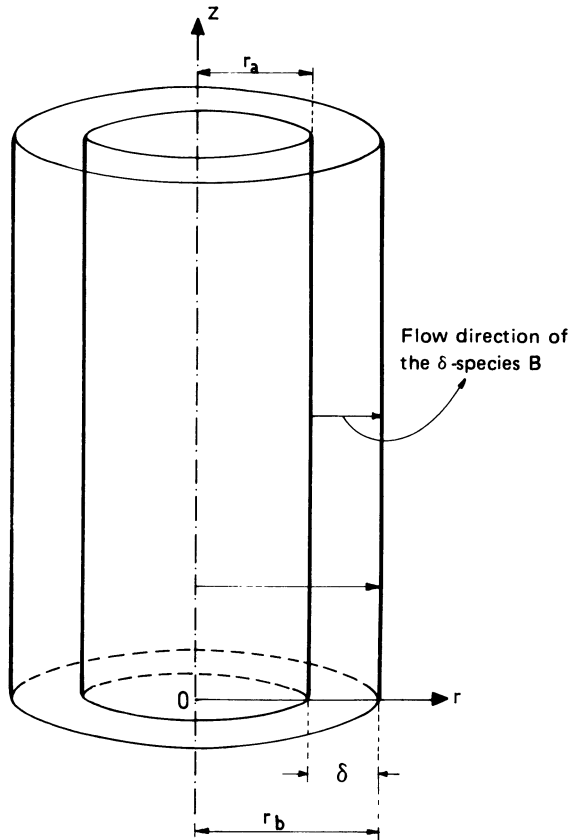


Figure 7. Radial flow in a cylindrical shell.

Analogously, the current per unit length of cylinder is

$$j = - \frac{n_{\text{B}} F 2 \pi D_{\text{B}} (c_{\text{B},b} - c_{\text{B},a})}{\ln (r_b / r_a)} \quad (50)$$

and the charge flowing during the time τ , per unit length, is equal to the product $j\tau$. In the cases of the cylindrical or spherical shells, δ represents the true diffusional layer thickness. When $\delta \ll r_a$, both Eqs. (45) and (49) involve as a limiting case that of the semi-infinite plane.

8. Resolution of the Fick Equation : The Nonstationary State

In dealing with the kinetics of processes occurring at the electrochemical interface, it is quite important to establish its response under different perturbations of the electrical variables. One variable is under control while the other relaxes. Usually the relaxation variable is followed during the period of perturbation, as is the case for the linear potential sweep methods, but it might be also interesting to follow the variation of the relaxation variable for a longer period than that of the perturbation function. The latter case is encountered, for example, when either a potential pulse or a current pulse is used.

During all these processes diffusion plays an important role, and, therefore, resolution of the Fick equation under a nonstationary state is quite relevant, particularly in the field of electrochemical kinetics. Moreover, to a great extent the type of solutions obtained furnish the quantitative basis for a large number of electrochemical methods.

8.1. Boundary Conditions for the Nonstationary Solutions under Potential Step Perturbation

The boundary conditions for the solution of the Fick equation depend on the perturbation program as well as the kinetic characteristics of the reaction. Let us consider that reaction (1) occurs at an interface that is perturbed at $t = 0$ with a potential step of magnitude E . Reaction (1) can be considered either as a completely reversible or irreversible electrochemical reaction.

8.1.1. Reversible Electrochemical Reaction

Let us consider reaction (1) as a reversible process. Initially ($t = 0$), the concentration of ox is constant and equal to the bulk concentration, while that of red may be either constant or equal to zero. Thus, the initial condition

is either, at $t = 0$, $0 \leq n \leq \infty$:

$$c_{\text{ox}} = c_{\text{ox},0} \quad , \quad c_{\text{red}} = 0 \quad (51a)$$

or

$$c_{\text{ox}} = c_{\text{ox},0} \quad , \quad c_{\text{red}} = c_{\text{red},0} \quad (51b)$$

where n defines the coordinate perpendicular to the electrode plane. $n = x$ in Cartesian coordinates and $n = r - r_0$ in either spherical or cylindrical coordinates, r_0 being the corresponding surface radius.

The boundary conditions refer to the concentration of each reacting species at the interface ($n = 0$) which depend upon the electrode potential. The latter, as it is measured, corresponds to the overall potential drop at the interface measured against a reference electrode.

In general, when the electrode potential is negative with respect to the equilibrium potential (cathodic reaction), the concentration of the ox species decreases at the reaction interface, while that of the red species increases—both attaining a constant value. Moreover, when the potential is sufficiently negative, a null concentration of the ox species may be reached at $n = 0$. Then

$$t > 0, E \rightarrow -\infty, n = 0: \quad c_{\text{ox}} = c_{\text{ox},e} = 0 \quad (52)$$

For a reversible reaction this condition is approached with a relatively small potential shift from the equilibrium value. In the bulk of the solution, the boundary conditions depend on the initial composition of the solution and are given by, at $t > 0$, $n \rightarrow \infty$,

$$c_{\text{ox}} = c_{\text{ox},0}, \quad c_{\text{red}} = 0 \quad (53a)$$

or

$$c_{\text{ox}} = c_{\text{ox},0}, \quad c_{\text{red}} = c_{\text{red},0} \quad (53b)$$

When the potential shift from the equilibrium value is relatively small so that the surface concentration of the reacting species remains finite, the application of Fick's equation to both the ox and red species requires two initial [Eq. (51)] and four boundary conditions. Now the $c_{\text{ox}}/c_{\text{red}}$ ratio at $n = 0$ is determined by the Nernst equation:

$$\frac{c_{\text{ox},e}}{c_{\text{red},e}} = \theta = \frac{\gamma_{\text{red}}}{\gamma_{\text{ox}}} \exp \left[\frac{nF}{RT} (E - E_0) \right] \quad (54)$$

where the γ_{red} and γ_{ox} are the activity coefficients and E_0 is the standard potential for the couple. Another boundary condition is related to the equality of ox and red fluxes at the electrode plane. Therefore,

$$D_{\text{ox}} \left(\frac{\partial c_{\text{ox}}}{\partial n} \right)_{n=0} + D_{\text{red}} \left(\frac{\partial c_{\text{red}}}{\partial n} \right)_{n=0} = 0 \quad (55)$$

and the boundary conditions at $n \rightarrow \infty$ are given by (53). A third possibility corresponds to the formation of a solid metallic product on the electrode surface.⁽¹⁾ As a first approximation, the solution of the equation is then obtained for the case of a totally covered surface, so that the activity of the solid is unity.

8.1.2. Irreversible Electrochemical Reaction

The first attempts to solve this problem yielding only approximate solutions were based upon the Nernst diffusion layer concept.⁽²⁷⁻³⁰⁾ Later, more rigorous mathematical procedures were introduced for the semi-infinite plane diffusion⁽³¹⁻³⁸⁾ as well as for diffusion toward the sphere surface.^(32,39,40) In either case first-order charge-transfer reactions shall be considered.

When the electrochemical reaction (1) is highly irreversible, the initial and boundary conditions corresponding to $n \rightarrow \infty$ are the same as described for the reversible case [Eqs. (51) and (53)] but those related to the electrode surface ($n = 0$) are different. The concentration of the reacting species at the interface is determined through the rate equation of reaction (1). For a simple first-order process occurring in both directions, the reaction rate is given by Eq. (2). Therefore, taking into account the material balance at $n = 0$, the following boundary condition results:

$$D_{\text{ox}} \left(\frac{\partial c_{\text{ox}}}{\partial n} \right)_{n=0} = k_{\text{R}} c_{\text{ox},e} - k_0 c_{\text{red},e} \quad (56)$$

where the k_{R} and k_0 terms are the formal potential-dependent rate constants for the forward and backward reactions. The second boundary condition at $n = 0$ is certainly the same as for the reversible case, namely, Eq. (55).

8.2. Nonstationary Concentration Distribution Equation: Ideal Semi-infinite Plane Diffusion

Solution of Fick's equation for semi-infinite linear diffusion toward a plane is important because it can be reasonably extended to a number of electrodes of different geometries commonly used in experimental measurements. Furthermore, this model proves useful in tackling the mathematics of diffusion problems involving relatively more complex electrochemical reactions. The complexity may arise either because of the type of electrical perturbation or of the characteristics of the electrode process.

8.2.1. Reversible Electrochemical Reaction

Let us consider the simple electrochemical reaction (1) taking place on an ideal semi-infinite plane electrode (Figure 8), the reactant diffusing perpendicularly toward this plane (unidirectional diffusion). Let us assume that the magnitude of the perturbing potential is large enough to produce the electrochemical reaction in one direction only and to make the interfacial con-

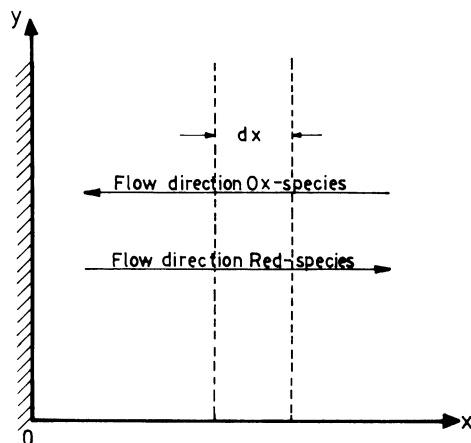


Figure 8. Diffusion toward an ideal semi-infinite plane plate electrode—semi-infinite diffusion.

centration of the reacting species virtually zero. In this case only the diffusion equation involving the ox species (for the cathodic reaction) should be considered. Then the mathematical solution of the differential equation requires just one initial and two boundary conditions. The initial and boundary conditions are already established by Eqs. (51)–(53) and the diffusion equation, for a constant diffusion coefficient, is

$$\frac{\partial c_{\text{ox}}}{\partial t} = D_{\text{ox}} \frac{\partial^2 c_{\text{ox}}}{\partial x^2} \quad (57)$$

Different mathematical procedures can be followed to solve Eq. (57) with the previously mentioned boundary conditions. One of them considers that the solution of the differential equation is the superposition of the solutions of an infinite number of linear (punctual) sources. Another method, widely used in electrochemistry involves the application of a Laplace transform.

The concentration distribution of the ox species at any instant, which comes out from Eq. (57), is

$$c_{\text{ox}} = c_{\text{ox},0} \text{erfc}[x/2(D_{\text{ox}}t)^{1/2}] \quad (58)$$

Equation (58) is represented in Figure 9 for different values of t . For $t \rightarrow 0$ the largest concentration change of the reacting species is located within a short distance adjacent to the reaction plane. As t increases, the concentration gradient decreases due to the larger distance at which the bulk concentration of the reacting species is reached. As t approaches infinity, the bulk concentration is only reached at $x = \infty$.

Once the concentration distribution equation is known, the flux of ox toward the electrode surface is obtained from the equation

$$\frac{\partial c_{\text{ox}}}{\partial x} = \frac{2}{\pi^{1/2}} \exp - \left(\frac{x}{2(D_{\text{ox}}t)^{1/2}} \right)^2 \frac{c_{\text{ox},0}}{2(D_{\text{ox}}t)^{1/2}} \quad (59)$$

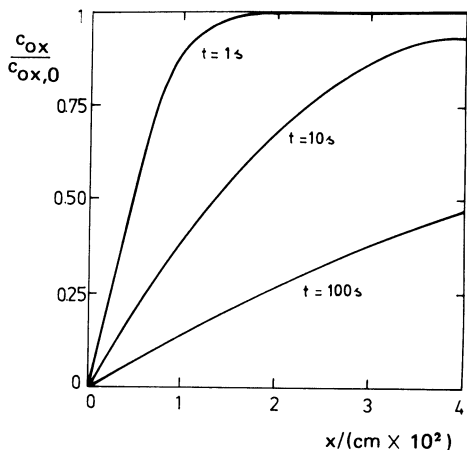


Figure 9. Plot of Eq. (58) for various times of electrolysis. $D_{\text{ox}} = 10^{-5} \text{ cm}^2 \text{ s}^{-1}$

Consequently, the flux of the reactant at the plane interface ($x = 0$) in terms of the limiting current density, j_{lim} , is

$$j_{\text{lim}} = -nFD_{\text{ox}} \left(\frac{dc_{\text{ox}}}{dx} \right)_{x=0} = -nF \frac{c_{\text{ox},0} D_{\text{ox}}^{1/2}}{(\pi t)^{1/2}} \quad (60)$$

Hence, under a constant potential, the semi-infinite diffusion of any species which reacts very fast at the electrode according to reaction (1) provokes an instantaneous current jump that steadily decreases as t increases, approaching a $j_{\text{lim}} = 0$ value when $t \rightarrow \infty$. Moreover, the product $j_{\text{lim}} t^{1/2}$ is a constant at any time and is linearly related to the concentration of the reacting species. Equation (60), although involving the determination of an instantaneous current, permits the practical evaluation of either $c_{\text{ox},0}$ or D_{ox} .

The verification of the theory requires an experimental device actually fitting semi-infinite diffusion conditions. The interference of free convection can be eliminated if the electrochemical process produces the stratification of the electrolyte. On this basis quite reliable results have been reported for the $[\text{Fe}(\text{CN})_6]^{4-}/[\text{Fe}(\text{CN})_6]^{3-}$ redox system⁽⁴¹⁾ and for the electrodeposition of silver, both on platinum electrodes.⁽⁴²⁾ At equimolar concentration, the cathodic reaction occurring in the former system $[\text{Fe}(\text{CN})_6]^{3-} + e = [\text{Fe}(\text{CN})_6]^{4-}$ has been studied with the working electrode facing upward, in contrast with the reverse reaction where, for the same concentration, the density of $\text{K}_4\text{Fe}(\text{CN})_6$ is somewhat larger than that of $\text{K}_3\text{Fe}(\text{CN})_6$.

The solution of Eq. (58) carried out with the same initial and boundary conditions as Eqs. (51) and (53)–(55) gives the following concentration distribution equations for the ox and the red species, both soluble and initially present in solution:

$$c_{\text{ox}} = c_{\text{ox},0} \frac{\xi\theta + \text{erf}(x/D_{\text{ox}}^{1/2} t^{1/2})}{1 + \xi\theta} \quad (61)$$

$$c_{\text{red}} = c_{\text{ox},0} \frac{\xi \operatorname{erfc}(x/D_{\text{red}}^{1/2}t^{1/2})}{1 + \xi\theta} \tag{62}$$

where $\xi = (D_{\text{ox}}/D_{\text{red}})^{1/2}$. The concentration ratio, $c_{\text{ox},0}/c_{\text{red},0} = \theta$, at the surface depends on the applied potential. Equation (58) is included in Eq. (61) since for $E = -\infty$, $\theta = 0$. At $x = 0$, from Eqs. (61) and (62) one gets

$$c_{\text{ox},e} = c_{\text{ox},0} \frac{\xi\theta}{1 + \xi\theta} \tag{63}$$

$$c_{\text{red},e} = c_{\text{ox},0} \frac{\xi}{1 + \xi\theta} \tag{64}$$

According to these equations, when $E = E_0$, if the $\gamma_{\text{ox}}/\gamma_{\text{red}}$ ratio is unity, then $c_{\text{ox},e} = c_{\text{red},e}$ at $x = 0$ [Eq. (54)]. The concentration profiles as given by Eqs. (61) and (62) are depicted in Figure 10. The reactant concentration has a minimum value at $x = 0$ and approaches asymptotically the bulk concentration as x increases. The reverse occurs with the concentration of the reaction product. The distance at which the limiting concentration values are attained depends quite markedly on the time elapsed and to a minor extent on the value of θ . The current density expression for this case is

$$j = -nFD_{\text{ox}}^{1/2} c_{\text{ox},0} \frac{1}{\pi^{1/2} t^{1/2} (1 + \xi\theta)} \tag{65}$$

Therefore, the current density given by Eq. (65) for the same value of $c_{\text{ox},0}$ is lower than that given by Eq. (60), which is valid when $c_{\text{ox},e} = 0$. From both

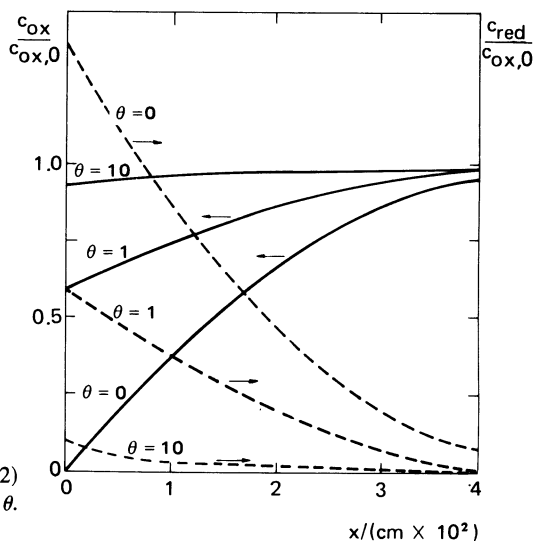


Figure 10. Plot of Eqs. (61) and (62) at $t = 10$ s, for various values of θ . $D_{\text{ox}} = 2 \times 10^{-5} \text{ cm}^2 \text{ s}^{-1} = 2 D_{\text{red}}$.

expressions (65) and (60) one obtains

$$j = \frac{j_{\text{lim}}}{1 + \xi\theta} \quad (66)$$

Equation (66) contains the current–potential relationship of the reversible electrochemical process represented by Eq. (1). Then,

$$E = E_0 - \frac{RT}{nF} \ln \frac{\gamma_{\text{red}} \left(\frac{D_{\text{ox}}}{D_{\text{red}}} \right)^{1/2}}{\gamma_{\text{ox}}} + \frac{RT}{nF} \ln \frac{j_{\text{lim}} - j}{j} \quad (67)$$

Obviously, to test Eq. (67) the currents must be read at the same intervals of time counted from the application of the potential step. When $j = \frac{1}{2}j_{\text{lim}}$, $E = E_{1/2}$:

$$E_{1/2} = E_0 - \frac{RT}{nF} \ln \frac{\gamma_{\text{red}} \left(\frac{D_{\text{ox}}}{D_{\text{red}}} \right)^{1/2}}{\gamma_{\text{ox}}} \quad (68)$$

$E_{1/2}$ represents the half-wave potential—a magnitude, which for the reversible electrochemical reaction, is independent of the time at which the current is read and characteristic of the electrochemical system. Thus,

$$E = E_{1/2} + \frac{RT}{nF} \ln \frac{j_{\text{lim}} - j}{j} \quad (69)$$

The expression of $E_{1/2}$ is different when the process becomes more complex than that represented by reaction (1). This is the case, for example, when either hydrogen-ion discharge participates in the ox to red electrochemical process or for the electroreduction of a complex ion in the presence of a large excess of a complex substance with the formation of an amalgam.⁽¹⁾ In any case, Eq. (69) is still valid independently of the operational conditions.

8.2.2. Irreversible Electrochemical Reactions

Let us consider now reaction (1) as an irreversible electrochemical reaction,⁽⁴³⁾ namely, the resistance to the diffusion rate of the reacting species is of the same order of magnitude as that of the proper electrochemical process. Under these circumstances Eq. (57) is solved taking into account the initial and boundary conditions given by Eqs. (51), (53), (55), and (56). The mathematical solution yields the equation for the current density related to the reduction of ox^(1,5):

$$j = J_k \exp(\lambda^2 t) \operatorname{erfc}(\lambda t^{1/2}) \quad (70)$$

where

$$J_k = -nF[k_{\text{red}}^{\circ} c_{\text{ox},0} \exp(-\alpha_c FE/RT) - k_{\text{ox}}^{\circ} c_{\text{red},0} \exp(\alpha_a FE/RT)] \quad (71)$$

and

$$\lambda = \frac{k_{\text{red}}^{\circ}}{D_{\text{ox}}^{1/2}} \exp\left(\frac{-\alpha_c FE}{RT}\right) + \frac{k_{\text{ox}}^{\circ}}{D_{\text{red}}^{1/2}} \exp\left(\frac{\alpha_a FE}{RT}\right) \quad (72)$$

where k_{red}° and k_{ox}° are the standard-state rate constants. It is convenient to write both equations in terms of j_0 , the standard exchange current density, and the overpotential, η , which is defined as $\eta = E - E_0'$, where E is the irreversible electrochemical potential and E_0' the reversible standard value.

$$J_k = -j_0[\exp(-\alpha_c F\eta/RT) - \exp(\alpha_a F\eta/RT)] \quad (73)$$

and

$$\lambda = \frac{j_0}{nF} \left[\frac{\exp(-\alpha_c F\eta/RT)}{c_{\text{ox},0} D_{\text{ox}}^{1/2}} + \frac{\exp(\alpha_a F\eta/RT)}{c_{\text{red},0} D_{\text{red}}^{1/2}} \right] \quad (74)$$

Equation (70), which appears to be rather complex, implies different limiting cases which are convenient to deal with independently. Thus, by expanding the $\exp(\lambda^2 t) \operatorname{erfc}(\lambda t^{1/2})$ terms:

$$\begin{aligned} & \exp(\lambda^2 t) \operatorname{erfc}(\lambda t^{1/2}) \\ &= \frac{1}{\pi^{1/2} \lambda t^{1/2}} \left[1 - \frac{1}{2\lambda^2 t} + \frac{1 \times 3}{(2\lambda^2 t)^2} - \frac{1 \times 3 \times 5}{(2\lambda^2 t)^3} + \dots \right] \end{aligned} \quad (75)$$

When $\lambda t^{1/2} > 5$, Eq. (70) yields

$$j = \frac{J_k}{\pi^{1/2} \lambda t^{1/2}} \quad (76)$$

Equation (76), when $c_{\text{red},0} = 0$, gives

$$(j)_{\lambda t^{1/2} > 5} = -\frac{nFc_{\text{ox},0}^{1/2} D_{\text{red}}^{1/2} D_{\text{ox}}^{1/2}}{\pi^{1/2} t^{1/2}} \frac{1}{D_{\text{red}}^{1/2} + (k_{\text{ox}}^{\circ}/k_{\text{red}}^{\circ}) D_{\text{ox}}^{1/2} \exp(FE/RT)} \quad (77)$$

Another situation emerges when the second term on the right-hand side of Eqs. (73) and (74) is negligible as compared to the first one. Then, one obtains

$$j = -nFc_{\text{ox}} k_{\text{red}}^{\circ} \exp\left(-\frac{\alpha_c FE}{RT}\right) \exp\left(\frac{k_{\text{red}}^2 t}{D_{\text{ox}}}\right) \operatorname{erfc}\left(\frac{k_{\text{red}} t^{1/2}}{D_{\text{ox}}^{1/2}}\right) \quad (78)$$

Equation (78) is applicable when red is a metal. Both Eqs. (76) and (78), at high negative potentials, approach the linear j vs. $t^{-1/2}$ plot predicted for a simple reversible process.

When $\lambda t^{1/2} < 1$, Eq. (70) reduces to

$$j = J_k \left(1 - \frac{2\lambda t^{1/2}}{\pi^{1/2}} \right) \quad (79)$$

This equation still contains the contribution of the reverse reaction. The extrapolated value of j at $t = 0$ depends on E and allows the calculation of j_0 (or k_0) if the value of α_c is independently determined. When $\lambda t^{1/2} \ll 1$ (the electrochemical reaction is very slow), one obtains

$$j = J_k \quad (80)$$

the transient is represented by a step function. The equations for the variation of current under a potentiostatic step perturbation function for more complex mechanisms of reaction are given in the literature⁽⁵⁾ and discussed in greater detail in other chapters of this book.

The differential diffusion equations for higher-order irreversible processes permit only an exact numerical solution. The analytical solutions are approximate.⁽⁴⁴⁻⁴⁷⁾ After comparing the exact numerical solution and the approximate analytical one it is concluded that the coincidence range depends on the pseudo-order of the reaction with respect to the reactant, on the initial concentration, and on the overpotential, but it is independent of the exchange current density and of the transfer coefficient. The lower the pseudo-order, the smaller the coincidence range. The higher the concentration, the larger the time range where the approximate equation is valid. Finally, the discrepancy increases as the overpotential increases.

8.3. Spherical Diffusion

Let us consider the unidirectional radial diffusion of the reacting species through a spherical shell of radius r_0 so that the concentration changes may be produced either for $r < r_0$ or for $r > r_0$ (Figure 11). In electrochemistry, the solution of the diffusion equation for the second condition is the most important one. The diffusion equation in spherical coordinates [Eq. (17)] can be solved for the simple reaction (1), taking into account the initial and boundary conditions already set up [Eqs. (51)–(53)]. Now $n = r - r_0$, where r_0 stands for the radius of the spherical interface. The concentration distribution equation is^(24,48-50)

$$c_{\text{ox}} = c_{\text{ox},0} - (c_{\text{ox},0} - c_{\text{ox},e}) \frac{r_0}{r} + (c_{\text{ox},0} - c_{\text{ox},e}) \frac{r_0}{r} \frac{2}{\sqrt{\pi}} \int_0^\lambda \exp(-y^2) dy \quad (81)$$

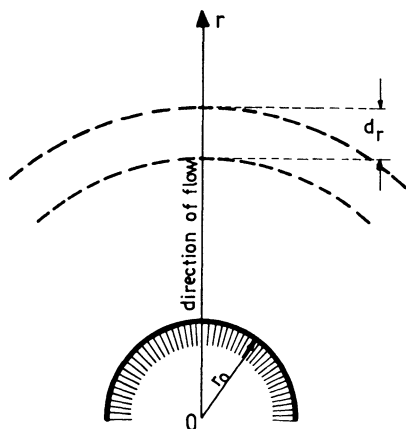


Figure 11. Radial flow toward the surface of the sphere.

since $(2/\sqrt{\pi}) \int_0^\lambda e^{-y^2} dy = \text{erf}(\lambda)$ and $1 - \text{erf}(\lambda) = \text{erfc}(\lambda)$ where $\lambda = [(r - r_0)/2](D_{\text{ox}}t)^{1/2}$. When $c_{\text{ox},e} = 0$,

$$c_{\text{ox}} = c_{\text{ox},0} \left(1 - \frac{r_0}{r} \right) + c_{\text{ox},0} \frac{r_0}{r} \frac{2}{\sqrt{\pi}} \int_0^\lambda \exp(-y^2) dy \quad (82)$$

The latter equation can be expressed in a simpler form as

$$c_{\text{ox}} = c_{\text{ox},0} \left\{ 1 - \frac{r_0}{r} \text{erfc} \left[\frac{r - r_0}{2(D_{\text{ox}}t)^{1/2}} \right] \right\} \quad (83)$$

The development of the concentration profiles according to Eq. (83) is seen in Figure 12. From Eq. (83) the time-independent term in the concentration distribution equation is therefore

$$(c_{\text{ox}})_{t \rightarrow \infty} = c_{\text{ox},0} \left(1 - \frac{r_0}{r} \right) \quad (84)$$

By deriving Eq. (83) at $r = r_0$, the current density related to the flux of the ox species is obtained:

$$-j = nFD_{\text{ox}}^{1/2} c_{\text{ox},0} \frac{1}{\pi^{1/2} t^{1/2}} + nFD_{\text{ox}} c_{\text{ox},0} \frac{1}{r_0} \quad (85)$$

According to Eq. (85), the spherical diffusion implies a stationary current at $t \rightarrow \infty$. The time-independent current density is given by

$$(j)_{t \rightarrow \infty} = -nFD_{\text{ox}} c_{\text{ox},0} \frac{1}{r_0} \quad (86)$$

This relationship holds when $r_0 \ll (\pi t)^{1/2}$. Otherwise, when $r_0 \gg (\pi t)^{1/2}$ the spherical diffusion approaches the condition of the semi-infinite linear diffusion to the plane [Eq. (60)].

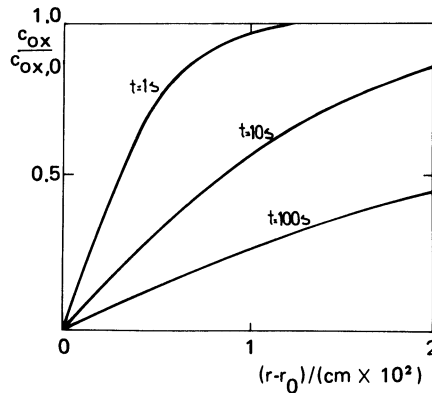


Figure 12. Plot of Eq. (83) for various times of electrolysis. $r_0 = 0.1 \text{ cm}$ and $D_{\text{ox}} = 10^{-5} \text{ cm}^2 \text{ s}^{-1}$.

The experimental test of Eq. (85) always yields currents larger than those predicted.⁽⁵¹⁾ Equation (85) has been applied to both the dropping mercury electrode and the hanging mercury electrode in the absence of kinetic effects.^(43,52-56) However, it fails either at $t \rightarrow 0$ or $t \rightarrow \infty$ because of the convective effects. In the former case, the potential applied to the electrode changes the surface tension of the liquid metal and produces a convective flow within the bulk of the metal. In the latter case, the influence of convection arises from the density gradients originated in the electrolyte side of the interface. At short times there is also a relatively large contribution of the double-layer charging effect. The use of microelectrodes to surmount in part the interference of convection requires, however, experiments made in a relatively short time.^(57,58)

8.4. Expanding Sphere Electrode

8.4.1. The Ilkovic Equation

The first quantitative treatment of diffusion toward an expanding sphere, which is exemplified by the dropping mercury electrode (dme),⁽⁵⁹⁻⁶¹⁾ was presented by Ilkovic.^(62,63) The problem was solved on the assumption that the dme behaves as a plane electrode with an area equal to that of the surface of the drop. The effect of the expansion of the mercury drop producing the compression of the diffusion layer was taken into account by introducing a correction factor equal to $(7/3)^{1/2}$. The maximum diffusion current flowing through the dme depends linearly on the concentration of the reacting species and on the hydrostatic pressure of the mercury column.

A rather more rigorous model for the dme (Figure 5)^(60,64,65) consists of a sphere of radius r_1 which is immersed in a solution volume, V , comprised between the radii r_0 and r_1 . However, in this case the diffusion equation must be corrected by considering a convective term that results from the advance of the spherical surface toward the solution as the sphere expands. There is then a lateral tangential movement of the fluid, and, because of the continuity equation $\nabla \cdot \mathbf{v} = 0$, there must be a flow of liquid and therefore a flux of matter relative to the interface. This additional flux increases the current to a value higher than it would have been without taking into consideration the above effect. Nevertheless, since the diffusion occurs radially and the sphere also expands into the solution, the diffusion layer thickness is always much smaller than r_0 . Hence, the differential equation for unidirectional planar diffusion can be extended to the present system. Thus, the corrected diffusion equation for the ox species becomes^(50,60)

$$\frac{\partial c_{\text{ox}}}{\partial t} = D_{\text{ox}} \frac{\partial^2 c_{\text{ox}}}{\partial x^2} - \mathbf{v} \cdot \frac{\partial c_{\text{ox}}}{\partial x} \quad (87)$$

where $x = r - r_0$. To evaluate \mathbf{v} , the fluid velocity (rate of change of the radial

coordinate), the time dependence of the spherical surface must be considered. However, as the surface increases, due to the expansion sphere, the diffusion layer thickness must decrease to keep the volume V constant. Consequently, at the same reference time, the current density obtained on an expanding sphere electrode is larger than that of the corresponding static sphere. The volume of solution in the spherical shell $r - r_0$ is

$$V = \frac{4}{3}\pi[(r_0 + x)^3 - r_0^3] \quad (88)$$

After expanding the binomial and neglecting the higher-order terms in x , for $x \ll r_0$, Eq. (88) becomes

$$V = 4\pi r_0^2 x = Ax \quad (89)$$

where the area A is a function of time. Then

$$\frac{dV}{dt} = A \frac{dx}{dt} + x \frac{dA}{dt} = 0 \quad (90)$$

and

$$|v| = \frac{dx}{dt} = -\frac{x}{A} \frac{dA}{dt} \quad (91)$$

Furthermore, A can be expressed in terms of m , the mercury flow, as follows:

$$V_d = \frac{4}{3}\pi r_0^3 = \frac{mt}{\rho} \quad (92)$$

where V_d is the volume of the mercury drop and ρ the mercury density. Equation (92) yields the radius of the mercury drop as a function of time in terms of known magnitudes. Then, the expression for A in terms of r_0 is

$$A = 4\pi r_0^2 = 4\pi \left(\frac{3}{4\pi}\right)^{2/3} \left(\frac{1}{\rho}\right)^{2/3} (mt)^{2/3} \quad (93)$$

For the dme, $\rho = 13.56 \text{ g cm}^{-3}$ at 25°C ; therefore,

$$A = 0.85(mt)^{2/3} \quad (94)$$

and

$$\frac{dA}{dt} = \frac{2}{3}(0.85)(mt)^{2/3} t^{-1} \quad (95)$$

By replacing the expressions for A and dA/dt into Eq. (91) one obtains

$$|v| = \frac{dx}{dt} = -\frac{2}{3} \frac{x}{t} \quad (96)$$

Therefore, the diffusion differential equation (87) becomes

$$\frac{\partial c_{\text{ox}}}{\partial t} = D_{\text{ox}} \frac{\partial^2 c_{\text{ox}}}{\partial x^2} + \frac{2x}{3t} \frac{\partial c_{\text{ox}}}{\partial x} \quad (97)$$

On the assumption that the surface concentration is constant at $t = 0$, $(I)_b$, the instantaneous current, is

$$(I)_t = \frac{-nFAD_{\text{ox}}^{1/2}(c_{\text{ox},0} - c_{\text{ox},e})}{(3/7)^{1/2}(\pi t)^{1/2}} \quad (98)$$

Taking into account the expression (94) for A :

$$(I)_t = -0.732 nF(c_{\text{ox},0} - c_{\text{ox},e})D_{\text{ox}}^{1/2}m^{2/3}t^{1/6} \quad (99)$$

where $(I)_t$ is in amperes, F in coulomb/mole, A in cm^2 , D in $\text{cm}^2 \text{s}^{-1}$, m in g s^{-1} , c_{ox} in mole cm^{-3} , and t in seconds. When $c_{\text{ox},e} = 0$, $(I)_t = (I_{\text{lim}})_b$, Eq. (99) gives the limiting current at the dme:

$$(I_{\text{lim}})_t = -0.732 nFc_{\text{ox},0}D_{\text{ox}}^{1/2}m^{2/3}t^{1/6} \quad (100)$$

This equation, in contrast to the case of the plane, exhibits a parabolic current-time relationship.^(50,60,62,63) The mean current, (\bar{I}) , at the dme is immediately obtained by averaging Eq. (100) between $t = 0$ and $t = \tau$, where τ is the lifetime of the mercury drop:

$$(\bar{I}) = \frac{1}{\tau} \int_0^\tau (I)_t dt = -0.627 nF(c_{\text{ox},0} - c_{\text{ox},e})D_{\text{ox}}^{1/2}m^{2/3}\tau^{1/6} \quad (101)$$

Therefore, the following ratio results:

$$(\bar{I}) = \frac{6}{7}(I)_\tau \quad (102)$$

A similar relationship is obtained for (\bar{I}_{lim}) , the average limiting current:

$$(\bar{I}_{\text{lim}}) = 0.627 nFc_{\text{ox},0}D_{\text{ox}}^{1/2}m^{2/3}\tau^{1/6} \quad (103)$$

The fair validity of these equations and the reproducibility of the dme are the basis for their use in electrochemical kinetics, particularly in polarography.

The Ilkovic equation involves the following constant⁽⁶⁰⁾:

$$\mathcal{I} = \frac{(K_{\text{II}})}{c_{\text{ox},0}m^{2/3}t^{1/6}} = -0.627 nFD_{\text{ox}}^{1/2} \quad (104)$$

The value of the constant can be obtained either from (\bar{I}_{lim}) and t or from D_{ox} . The values resulting from these calculations show a discrepancy of about $\pm 5\%$ which is attributed to the mathematical simplifications of the models for the expanding sphere, on one side, and to the more involved situation encountered at the dme. For example, the curvature of the drop which was neglected in Eq. (87) may have an appreciable influence.⁽⁶¹⁾

The sphericity correction was introduced in the following way.⁽⁶⁰⁾ To Eq. (100), which determines the current density after correction for the advance of the drop surface resembling the semi-infinite plane model, the stationary term of the flux equation corresponding to the radial diffusion to the sphere was added. For the latter r_0 was taken from Eq. (93). Finally, the average current density equation, after integrating between 0 and τ results⁽⁶⁵⁾:

$$(\bar{I}_{\text{lim}})_{\text{corr}} = -0.627 nF c_{\text{ox},0} D_{\text{ox}}^{1/2} m^{2/3} \tau^{1/6} \left(1 + \frac{AD_{\text{ox}}^{1/2} \tau^{1/6}}{m^{1/3}} \right) \quad (105)$$

A further advance toward a rigorous solution of the radial diffusion equation applied to the expanding sphere is obtained after including in the differential equation the expansion term, namely,^(66,67)

$$\frac{\partial c_{\text{ox}}}{\partial t} = D_{\text{ox}} \left[\frac{\partial^2 c_{\text{ox}}}{\partial r^2} + \frac{2}{r} \frac{\partial c_{\text{ox}}}{\partial r} \right] - v_r \frac{\partial c_{\text{ox}}}{\partial r} \quad (106)$$

The first and the second terms on the right-hand side of Eq. (106) refer to the diffusion to a static sphere, while the third term corresponds to the convective contribution of the expanding sphere. If the radius increases according to

$$r^3 = a^3 t + \text{const} \quad (107)$$

then

$$v_r = \frac{a^2}{3r^2} \quad (108)$$

where

$$a = \left(\frac{3}{4\pi} \frac{m}{\rho} \right)^{1/3} \quad (109)$$

Therefore the following initial and boundary conditions are considered:

$$t = 0, r \geq 0: \quad c_{\text{ox}} = c_{\text{ox},0} \quad (110)$$

and

$$t > 0, r \rightarrow \infty: \quad c_{\text{ox}} = c_{\text{ox},0} \quad (111)$$

The concentration of the ox species on the electrode surface is constant, and the radial coordinate of the surface is time dependent. Therefore,

$$t > 0, r = at^{1/3}: \quad c_{\text{ox}} = c_{\text{ox},e} \quad (112)$$

Introducing Eq. (108) into Eq. (106), the expression for the instantaneous current after Koutecky⁽⁶⁶⁾ is

$$(I)_t = 0.732 nF (c_{\text{ox},0} - c_{\text{ox},e}) D_{\text{ox}}^{1/2} m^{2/3} t^{1/6} \times \left[1 + 3.4 \frac{D_{\text{ox}}^{1/2} t^{1/6}}{m^{1/3}} + 1.5 \left(\frac{D_{\text{ox}}^{1/2} t^{1/6}}{m^{1/3}} \right)^2 \right] \quad (113)$$

and for the average current

$$(\bar{I}) = -0.627 nF(c_{\text{ox},0} - c_{\text{ox},e})D_{\text{ox}}^{1/2} m^{2/3} \tau^{1/6} \times \left[1 + 3.4 \frac{D_{\text{ox}}^{1/2} \tau^{1/6}}{m^{1/3}} + 1.5 \left(\frac{D_{\text{ox}}^{1/2} \tau^{1/6}}{m^{1/3}} \right)^2 \right] \quad (114)$$

Another mathematical solution of the diffusion equation for the expanding sphere has been proposed by Levich.⁽⁴⁾ The corresponding average current at the dme then results:

$$(\bar{I}) = (\bar{I})_{\text{Ilkovic}} \left(1 + 3.39 \frac{D_{\text{ox}}^{1/2} \tau^{1/6}}{m^{1/3}} \right) \quad (115)$$

8.4.2. Irreversible Reactions and Spherical Diffusion

The problem of reaction (1), involving a system that initially contains the soluble species ox and red as an irreversible process occurring on an expanding sphere electrode, was solved in terms of the semi-infinite linear diffusion equation for a plane plus a convective term, as already done in the case of the reversible process.^(68,69) The curvature effect can only be ignored when the measurements imply short time intervals and the faradaic current is large. Accordingly, the differential equations for each reacting species are given in terms of Eq. (87) applied to each reacting species. The initial conditions for both ox and red are the same as already given (51). The boundary conditions at the bulk of the solution are expressed by Eq. (53) and those corresponding to the interface are given by Eqs. (55) and (56). Equation (56) represents the irreversibility of the electrode reaction. The solution given by Koutecky^(68,70,71) is

$$I_{\text{ir}} = I_{\text{rev}} F(\chi) \quad (116)$$

where I_{ir} is the current obtained for the irreversible process and I_{rev} refers to the current which would be measured if the process behaves reversibly. $F(\chi)$ is a tabulated function, the variable χ being,⁽⁶⁰⁾

$$\chi = \left(\frac{12}{7} \right)^{1/2} \left[\frac{k_{\text{red}}}{(D_{\text{ox}})^{1/2}} + \frac{k_{\text{ox}}}{(D_{\text{red}})^{1/2}} \right] t^{1/2} \quad (117)$$

The approximate expression for the average (mean) current is

$$\bar{I}_{\text{ir}} = \bar{I}_{\text{rev}} \frac{0.886 [k_{\text{red}}/(D_{\text{ox}})^{1/2} + k_{\text{ox}}/(D_{\text{red}})^{1/2}] \tau^{1/2}}{1 + 0.886 [k_{\text{red}}/(D_{\text{ox}})^{1/2} + k_{\text{ox}}/(D_{\text{red}})^{1/2}] \tau^{1/2}} \quad (118)$$

For a hanging drop electrode the convective term of Eq. (87) is dropped out although the influence of the curvature of the drop must be considered.⁽⁷²⁾

The shielding effect due to the capillary tip and the influence of natural convection are also neglected.⁽⁷²⁾ Then, the corresponding differential

equations are

$$\frac{\partial c_{\text{ox}}}{\partial t} = D_{\text{ox}} \left(\frac{\partial^2 c_{\text{ox}}}{\partial r^2} + \frac{2}{r} \frac{\partial c_{\text{ox}}}{\partial r} \right) \quad (119)$$

$$\frac{\partial c_{\text{red}}}{\partial t} = D_{\text{red}} \left(\frac{\partial^2 c_{\text{red}}}{\partial r^2} + \frac{2}{r} \frac{\partial c_{\text{red}}}{\partial r} \right) \quad (120)$$

The initial and boundary conditions already considered for the expanding sphere are also valid in the present case [Eqs. (51), (53), (55), and (56)]. The solution in terms of j , derived from the Laplace transform on assuming that $D_{\text{ox}} = D_{\text{red}} = D$, is

$$\begin{aligned} j = & -\frac{nF(k_{\text{red}}c_{\text{ox},0} - k_{\text{ox}}c_{\text{red},0})}{1 + (r_0/D)(k_{\text{red}} + k_{\text{ox}})} \left\{ 1 + \frac{r_0(k_{\text{red}} + k_{\text{ox}})}{D} \right. \\ & \times \exp \left[\left(\frac{1}{r_0} + \frac{k_{\text{red}} + k_{\text{ox}}}{D} \right)^2 Dt \right] \\ & \left. \times \operatorname{erfc} \left[\left(\frac{1}{r_0} + \frac{k_{\text{red}} + k_{\text{ox}}}{D} \right) (Dt)^{1/2} \right] \right\} \end{aligned} \quad (121)$$

Equation (121) approaches that of the plane electrode under semi-infinite linear diffusion when either $r_0 \rightarrow \infty$ or $t \rightarrow 0$.

The analysis of Eq. (121) in terms of a simple totally irreversible electrochemical reaction is made as usual, by neglecting the term of the rate equation belonging to the reverse process. After introducing the following dimensionless parameters

$$\lambda = \frac{k_{\text{red}}r_0}{D_{\text{ox}}} \quad (122)$$

and

$$T = \frac{Dt}{r_0^2} \quad (123)$$

Eq. (121) becomes

$$\frac{-jr_0}{nFDc_{\text{ox},0}} = \frac{1 + \lambda \exp[(\lambda + 1)^2 T] \operatorname{erfc}[(\lambda + 1)T^{1/2}]}{1 + 1/\lambda} \quad (124)$$

When $T = 0$ ($t = 0$), Eq. (124) reduces to Eq. (70). Moreover, after a McLaurin series expansion of the term $\exp(x^2) \operatorname{erfc}(x)$, the resulting current is proportional to $T^{1/2}$ at short times. Thus, a plot of the data in this way would facilitate the extrapolation of the current at $t = 0$.⁽⁷²⁾

The validity of these equations has been tested with the electrochemical reduction of the iodate ion in aqueous solution at pH 7.2 on the hanging drop mercury electrode.⁽⁷²⁾

More general equations are derived when the diffusion coefficients of each species are used. Then, the concentration distribution equations are⁽⁷³⁾

$$\begin{aligned}
 c_{\text{ox}} &= c_{\text{ox},0} - \frac{A}{k^{1/2}(\xi - \mu)} \left\{ \frac{(D_{\text{red}})^{1/2}}{r_0} \left(\frac{1}{\mu} - \frac{1}{\xi} \right) \right. \\
 &+ \left[1 - \frac{(D_{\text{red}})^{1/2}}{r_0 \mu} \right] \exp(\mu^2 t) \operatorname{erfc}(\mu t^{1/2}) \\
 &\left. - \left[1 - \frac{(D_{\text{red}})^{1/2}}{r_0 \xi} \right] \exp(\xi^2 t) \operatorname{erfc}(\xi t^{1/2}) \right\} \quad (125)
 \end{aligned}$$

and

$$\begin{aligned}
 c_{\text{red}} &= c_{\text{red},0} + \frac{A}{(\xi - \mu)} \left[\frac{(D_{\text{ox}})^{1/2}}{r_0} \left(\frac{1}{\mu} - \frac{1}{\xi} \right) \right. \\
 &+ \left(1 - \frac{(D_{\text{ox}})^{1/2}}{r_0 \mu} \right) \exp(\mu^2 t) \operatorname{erfc}(\mu t^{1/2}) \\
 &\left. - \left[1 - \frac{(D_{\text{ox}})^{1/2}}{r_0 \xi} \right] \exp(\xi^2 t) \operatorname{erfc}(\xi t^{1/2}) \right] \quad (126)
 \end{aligned}$$

where

$$A = \frac{j_0 \exp(-\alpha_c F \eta / RT)}{n F D_{\text{ox}}^{1/2}} - \frac{j_0 \exp(\alpha_a F \eta / RT) K^{1/2}}{n F D_{\text{red}}^{1/2}} \quad (127)$$

and $K = D_{\text{ox}}/D_{\text{red}}$. Correspondingly, the current density is given by

$$\begin{aligned}
 \frac{j}{j_{t=0}} &= \frac{1}{1 + r_0 \lambda_r + r_0 \lambda_0} + \frac{1}{\xi - \mu} \left\{ \frac{[(D_{\text{red}})^{1/2} - r_0 \xi][(D_{\text{ox}})^{1/2} - r_0 \xi]}{r_0^2 \xi} \right. \\
 &\times \exp(\xi^2 t) \operatorname{erfc}(\xi t^{1/2}) - \frac{(D_{\text{red}} - r_0 \mu)[(D_{\text{ox}})^{1/2} - r_0 \mu]}{r_0^2 \mu} \\
 &\left. \times \exp(\mu^2 t) \operatorname{erfc}(\mu t^{1/2}) \right\} \quad (128)
 \end{aligned}$$

where

$$\begin{aligned}
 \mu &= \frac{1}{2} \left(\lambda + \frac{(D_{\text{ox}})^{1/2} + (D_{\text{red}})^{1/2}}{r_0} + \left\{ \lambda^2 + \frac{[(D_{\text{ox}})^{1/2} - (D_{\text{red}})^{1/2}]^2}{r_0^2} \right. \right. \\
 &\left. \left. - \frac{2[\lambda_R (D_{\text{red}})^{1/2} - \lambda_0 (D_{\text{ox}})^{1/2}][(D_{\text{red}})^{1/2} - (D_{\text{ox}})^{1/2}]}{r_0} \right\}^{1/2} \right) \quad (129)
 \end{aligned}$$

$$\lambda = \lambda_0 (D_{\text{ox}})^{1/2} + \lambda_R (D_{\text{red}})^{1/2} \quad (130)$$

$$\lambda_0 = \frac{j_0 \exp(-\alpha_c F \eta / RT)}{n F D_{\text{ox}} c_{\text{ox},0}} \quad (131)$$

$$\lambda_R = \frac{j_0 \exp(\alpha_a F \eta / RT)}{n F D_{\text{red}} c_{\text{red},0}} \quad (132)$$

$$\xi = \frac{1}{2} \left(\lambda + \frac{(D_{\text{ox}})^{1/2} + (D_{\text{red}})^{1/2}}{r_0} - \left\{ \lambda^2 + \frac{[(D_{\text{ox}})^{1/2} - (D_{\text{red}})^{1/2}]^2}{r_0^2} - \frac{2}{r_0} [\lambda_R (D_{\text{red}})^{1/2} - \lambda_0 (D_{\text{ox}})^{1/2}] [(D_{\text{red}})^{1/2} - (D_{\text{ox}})^{1/2}] \right\}^{1/2} \right) \quad (133)$$

$$j_{t=0} = j_0 \left[\exp\left(\frac{-\alpha_c F \eta}{RT}\right) - \exp\left(\frac{\alpha_a F \eta}{RT}\right) \right] = -n F (\lambda_0 D_{\text{ox}} c_{\text{ox},0} - \lambda_R D_{\text{red}} c_{\text{red},0}) \quad (134)$$

The short-time solution is obtained by use of the approximation $\exp(x^2) \operatorname{erfc}(x) \approx 1 - (2/\pi^{1/2})x + x^2$, which is valid for small values of x . Then

$$j = j_{t=0} \left[1 - \frac{2\lambda t^{1/2}}{\pi^{1/2}} + \left(1 + \frac{\lambda_R D_{\text{red}} + \lambda_0 D_{\text{ox}}}{r_0 \lambda^2} \right) \lambda^2 t \right] \quad (135)$$

The long-time solution comes out after making use of the approximation $\exp(x^2) \operatorname{erfc}(x) = \pi^{-1/2} x^{-1}$, which is valid for large values of x . The result is

$$j = \frac{j_{t=0}}{1 + r_0 \lambda_R + r_0 \lambda_0} \left\{ 1 + \frac{r_0^2 [\lambda_R / (D_{\text{red}})^{1/2} + \lambda_0 / (D_{\text{ox}})^{1/2}]}{1 + r_0 \lambda_R + r_0 \lambda_0} \frac{1}{(\pi t)^{1/2}} \right\} \quad (136)$$

Then, according to this equation, the current depends linearly on $t^{-1/2}$:

$$j = j_{t \rightarrow \infty} + \sigma t^{-1/2} \quad (137)$$

which yields $j_{t \rightarrow \infty}$, the extrapolated current at $t \rightarrow \infty$:

$$(j)_{t \rightarrow \infty} = \frac{(j)_{t=0}}{1 + r_0 \lambda_R + r_0 \lambda_0} \quad (138)$$

The slope σ corresponds to

$$\sigma = \frac{r_0^2 [\lambda_R / (D_{\text{red}})^{1/2} + \lambda_0 / (D_{\text{ox}})^{1/2}]}{\pi^{1/2} (1 + r_0 \lambda_R + r_0 \lambda_0)^2} (j)_{t=0} \quad (139)$$

Under these circumstances, a constant current implies a mass-transfer-controlled electrochemical process and no kinetic parameter of the proper electrochemical reaction can be derived. Nevertheless, if the electrode surface area is small, the reaction behaves as a charge-transfer-controlled process at any time.

A general treatment of voltammetry at an expanding spherical electrode in accord with any power law was given by Oldham^(40,74,75) which yields an equation of very wide generality. The solution of the latter gives the equations already established for both the stationary electrode and dme.

8.5. Cylindrical Diffusion

Cylindrical electrodes are seldom employed in electrochemistry, except when either wires or small rods are used as working electrodes. Nevertheless, the solution of the pertaining diffusion problem is interesting in order to evaluate the geometry influence in the rate of diffusion-controlled processes.

8.5.1. Reversible Reaction

Let us consider reaction (1) under reversible conditions occurring at the electrochemically active surface of a cylinder which extends to infinity parallel to the cylinder axis. The diffusion of the reacting species occurs radially so that the diffusion equation becomes

$$\frac{\partial c_{\text{ox}}}{\partial t} = D_{\text{ox}} \left(\frac{\partial^2 c_{\text{ox}}}{\partial r^2} + \frac{1}{r} \frac{\partial c_{\text{ox}}}{\partial r} \right) \quad (140)$$

The initial and boundary conditions are given by the expressions (51), (52), and (53) where $n = r - r_0$. After the usual procedures, the concentration distribution equation results^(24,76):

$$c_{\text{ox}} = -\frac{2}{\pi} c_{\text{ox},0} \int_0^\infty \exp(-D_{\text{ox}} u^2 t) \times \frac{J_0(u, r) Y_0(u, r_0) - Y_0(u, r) J_0(u, r_0)}{J_0^2(u, r_0) - Y_0^2(u, r_0)} \frac{du}{u} \quad (141)$$

where u is an auxiliary variable and $J_0(u, r)$ and $Y_0(u, r)$ are, respectively, zero-order Bessel functions of the first and second class. The integrals were evaluated by Jaeger and Clarke.⁽⁷⁷⁾ The limiting current density is obtained from (141) in the usual way:

$$j_{\text{lim}} = -\frac{4nFD_{\text{ox}}c_{\text{ox},0}}{\pi^2 r_0} \int_0^\infty \frac{\exp(-D_{\text{ox}} u^2 t)}{J_0^2(u, r_0) + Y_0^2(u, r_0)} \frac{du}{u} \quad (142)$$

From Eq. (142) two limiting cases arise, namely, for $t \rightarrow 0$,

$$j = -nFD_{\text{ox}}c_{\text{ox},0} \frac{1}{r_0} \left(\frac{1}{\pi^{1/2} \phi^{1/2}} + \frac{1}{2} - \frac{1}{4} \left(\frac{\phi}{\pi} \right)^{1/2} + \frac{1}{8} \phi - \dots \right) \quad (143)$$

and for $t \rightarrow \infty$,

$$j = -nFD_{\text{ox}}c_{\text{ox},0} \frac{2}{r_0} \left\{ \frac{1}{\ln(4\phi) - 2\gamma} - \frac{1}{[\ln(4\phi) - 2\gamma]^2} + \dots \right\} \quad (144)$$

where $\phi = D_{\text{ox}}t/r^2$ and γ is the Euler-Mascheroni constant, equal to 0.5772.

From Eqs. (143) and (144) one concludes that for $t \rightarrow 0$ the linear diffusional equation for the plane is approached, while for $t \rightarrow \infty$, the limiting current density is given by

$$j_{\text{lim}} = -nFD_{\text{ox}}c_{\text{ox},0} \frac{2}{r_0} \left[\frac{1}{\ln(4D_{\text{ox}}t/r_0^2)} \right] \quad (145)$$

Equation (145) shows that the current density approaches zero very slowly because of the logarithmic function. By using a platinum-wire electrode sealed to the end of a glass tube, a virtually constant current after a sufficiently long time was observed.⁽⁴¹⁾ Notwithstanding, the possible contribution of a convective effect in the measurements is far from being discarded.⁽⁴²⁾

8.5.2. Irreversible Reactions and Diffusion Toward a Cylinder

The diffusional problem related to reaction (1) as an irreversible electrochemical reaction occurring at a cylindrical surface electrode, although involving a simple first-order irreversible reaction, admits no exact analytical solution.⁽⁷³⁾ The differential equation (140) was solved by Johnson and Barnartt^(51,73) for both species ox and red with the boundary conditions (51), (53), and (55). The other boundary conditions for $t > 0$ and $r = r_0$ are related to the reaction rate through the current density in the form

$$t > 0, r = r_0: \quad j = nFD_{\text{red}} \frac{\partial c_{\text{red}}}{\partial r} = -nFD_{\text{ox}} \frac{\partial c_{\text{ox}}}{\partial r} \quad (146)$$

Then the system of equations can be solved, in principle, by the Laplace transform, but the analytical reverse transform to obtain c_{red} and c_{ox} is difficult. The inverse transform can be obtained for particular cases only, yielding an exact solution. On the other hand, approximate analytical solutions are derived for times much shorter than the smallest of r_0^2/D_{ox} , r_0^2/D_{red} , $r_0/\lambda(D_{\text{red}})^{1/2}$, and $r_0/\lambda(D_{\text{ox}})^{1/2}$, where λ is given by Eq. (72).

The equation for the transformed current density $\bar{j}(s)$, is

$$\begin{aligned} \bar{j}(s) = j_{t=0} / \sqrt{s} & \left[\sqrt{s} + \frac{\lambda_0(D_{\text{ox}})^{1/2} K_0((s/D_{\text{ox}})^{1/2} r_0)}{K_1((s/D_{\text{ox}})^{1/2} r_0)} \right. \\ & \left. + \frac{\lambda_R(D_{\text{red}})^{1/2} K_0(s/D_{\text{red}})^{1/2} r_0}{K_1((s/D_{\text{red}})^{1/2} r_0)} \right] \end{aligned} \quad (147)$$

where $K_0(x)$ is the modified Bessel function of the second kind of order zero, and $K_1(x)$ is the modified Bessel function of the second kind of order 1. Equation (147) can be inverse transformed in the following limiting cases. For $t \rightarrow 0$ ($s \rightarrow \infty$), it becomes

$$\bar{j}(s) \rightarrow \frac{j_{t=0}}{s + \lambda(s)^{1/2} - (\lambda_0 D_{\text{ox}} + \lambda_R D_{\text{red}})/2r_0} \quad (148)$$

which can be analytically inverted to yield

$$\begin{aligned} \frac{j(t)}{j_{t=0}} = \frac{1 + \delta}{2\delta} \exp \left[\left(\frac{1 + \delta}{2} \right)^2 \lambda^2 t \right] \operatorname{erfc} \left[\left(\frac{1 + \delta}{2} \right) \lambda t^{1/2} \right] \\ - \frac{1 - \delta}{2\delta} \exp \left[\left(\frac{1 - \delta}{2} \right)^2 \lambda^2 t \right] \operatorname{erfc} \left[\left(\frac{1 - \delta}{2} \right) \lambda t^{1/2} \right] \end{aligned} \quad (149)$$

where

$$\delta = \left[\frac{1 + 2(\lambda_R D_{\text{red}} + \lambda_0 D_{\text{ox}})}{r_0 \lambda^2} \right]^{1/2} \quad (150)$$

After a series expansion of $\exp(x^2) \operatorname{erfc}(x)$, for $x \ll 1$, one obtains

$$\frac{j(t)}{j_{t=0}} \approx 1 - \frac{2}{\sqrt{\pi}} \lambda \sqrt{t} + \left(1 + \frac{\lambda_R D_{\text{red}} + \lambda_0 D_{\text{ox}}}{2r_0 \lambda^2} \right) \lambda^2 t \quad (151)$$

Similarly, the concentrations of the ox and red species at the surface, for $t \rightarrow 0$, are, respectively,

$$c_{\text{ox},e} \approx c_{\text{ox},0} - \frac{j_{t=0}}{F(D_{\text{ox}})^{1/2}} \left\{ \frac{2t^{1/2}}{\sqrt{\pi}} - \left[1 + \frac{(D_{\text{ox}})^{1/2}}{2r_0 \lambda} \right] \lambda t \right\} \quad (152)$$

and

$$c_{\text{red},e} \approx c_{\text{red},0} + \frac{j_{t=0}}{F(D_{\text{red}})^{1/2}} \left\{ \frac{2t^{1/2}}{\pi^{1/2}} - \left[1 + \frac{(D_{\text{red}})^{1/2}}{2r_0 \lambda} \right] \lambda t \right\} \quad (153)$$

Comparative plots of these equations are given in Figure 13 for the plane, spherical, and cylindrical electrodes. This comparison is made taking into account the numerical solutions of the transformed equations when $a = (D^{1/2})/\lambda$ and $D_{\text{red}} = D_{\text{ox}} = D$, according to the Papoulis method.⁽⁷⁸⁾ Then, one observes a coincidence of the three functions when $\lambda t^{1/2} \rightarrow 0$. In contrast, when $\lambda t^{1/2} \rightarrow \infty$, their differences are such that the values of $j_{t \rightarrow \infty}$ for the plane are larger than those derived for the sphere, under comparable conditions.

A generalized rigorous numerical procedure and approximate methods for the solution of the boundary-value problems concerning diffusion toward

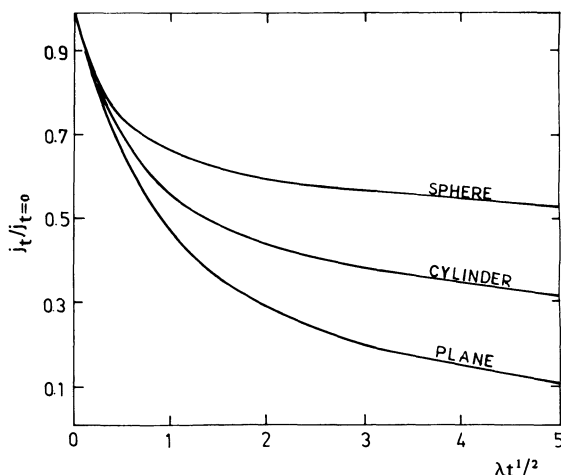


Figure 13. Constant potential current–time relationships for spherical, cylindrical, and plane electrodes. [From Reference 73].

planar, spherical, and dme at constant potential are given by Guidelli.^(79,80) Comparison between the rigorous and approximate solutions reveals a satisfactory degree of accuracy attainable by the approximate methods based on the direct substitution of suitable power series of time into the boundary conditions defining the diffusional problem.

9. Solution of the Diffusion Equation under a Constant Flux: Galvanostatic Conditions

Constant-current techniques are widely used in electrochemical kinetics and also in electroanalysis. Their applications are based upon the mathematical solution of Fick's equation under constant flux. These solutions were reported a long time ago.⁽⁸¹⁻⁸⁴⁾

An electrochemical reaction under a constant flux implies that the reactant is consumed at a constant rate, and consequently a concentration profile of that species is established in a direction perpendicular to the electrode surface. The concentration distribution is independent of the type of reaction taking place, be it a reversible or an irreversible process. The equations to be solved are the same as Eqs. (13), (15), and (17), according to the electrode geometry.

Let us consider reaction (1) with only the ox species initially present in a still solution yielding the soluble red species—the reaction occurring at an infinite plane electrode. This model can be easily extended to other electrode shapes if the electrolysis lasts for a short time, such that the thickness of the diffusion layer remains much smaller than the curvature radius of either a spherical or cylindrical electrode surface. The boundary condition at $x \rightarrow \infty$ remains the same as given for a potential step perturbation [Eq. (53)]. At $x = 0$ one of the boundary conditions is given by Eq. (55) and the remaining one is

$$\left(\frac{\partial c_{\text{ox}}}{\partial x}\right)_{x=0} = \lambda = \frac{-j}{nFD_{\text{ox}}} \quad (154)$$

The concentration distribution equation of the reactant was obtained by Weber,⁽⁸⁴⁾ Sand,⁽⁸³⁾ and Rosebrugh and Miller⁽⁸²⁾ and for both the reactant and product by Karaoglanoff.⁽⁸¹⁾ By solving the diffusion equation (58) with the initial and boundary conditions (51), (53), (55), and (154), the concentration of the ox species is

$$c_{\text{ox}} = c_{\text{ox},0} - \frac{s}{\pi^{1/2}(D_{\text{ox}})^{1/2}} \int_0^t \exp\left(-\frac{x^2}{4D_{\text{ox}}t}\right) \frac{dt}{t} \quad (155)$$

where s , the constant flux toward the electrode surface, is

$$s = -\frac{j}{nF} = \lambda D_{\text{ox}} \quad (156)$$

The migration contribution can be neglected in solutions containing a relatively large concentration of the supporting electrolyte. After solving the integral of Eq. (155), the following concentration distribution equations are obtained for the reactant and product, respectively:

$$c_{\text{ox}} = c_{\text{ox},0} - \frac{2\lambda(D_{\text{ox}})^{1/2}t^{1/2}}{\pi^{1/2}} \exp\left(-\frac{x^2}{4D_{\text{ox}}t}\right) + \lambda x \operatorname{erfc}\left(\frac{x}{2(D_{\text{ox}})^{1/2}t^{1/2}}\right) \quad (157)$$

and

$$c_{\text{red}} = \frac{2\lambda D_{\text{ox}}t^{1/2}}{\pi^{1/2}(D_{\text{red}})^{1/2}} \exp\left(-\frac{x^2}{4D_{\text{red}}t}\right) - \frac{\lambda x D_{\text{ox}}}{D_{\text{red}}} \operatorname{erfc}\left(\frac{x}{2(D_{\text{red}})^{1/2}t^{1/2}}\right) \quad (158)$$

When the product of the reaction is initially present, its initial concentration enters the corresponding distribution equation. If the initial concentration is denoted by $c_{\text{red},0}$, Eq. (158) becomes

$$c_{\text{red}} = c_{\text{red},0} + \frac{2\lambda D_{\text{ox}}t^{1/2}}{\pi^{1/2}(D_{\text{red}})^{1/2}} \exp\left(-\frac{x^2}{4D_{\text{red}}t}\right) - \lambda x \frac{D_{\text{ox}}}{D_{\text{red}}} \operatorname{erfc}\left(\frac{x}{2(D_{\text{red}})^{1/2}t^{1/2}}\right) \quad (159)$$

As the process occurs at a constant rate ($j = \text{const}$), the change in concentration also takes place at a constant rate ($\partial c_{\text{ox}}/\partial t = \text{const}$) at $x = 0$. At a fixed time, the concentration of the ox species approaches $c_{\text{ox},0}$ when x increases. The value of x required for $c_{\text{ox}} = c_{\text{ox},0}$ increases as the electrochemical process advances.

At the electrode surface the reactant concentration is given by

$$c_{\text{ox},e} = c_{\text{ox},0} - \frac{2\lambda(D_{\text{ox}})^{1/2}t^{1/2}}{\pi^{1/2}} \quad (160)$$

and it becomes nil when $t = \tau$; namely,

$$c_{\text{ox},0} = \frac{2\lambda(D_{\text{ox}})^{1/2}\tau^{1/2}}{\pi^{1/2}} \quad (161)$$

where τ is defined as the transition time.⁽⁸⁵⁾

On the other hand, the concentration of products depends upon the diffusion coefficients of both species but it is independent of the reactant concentration. Thus, from Eq. (158), at $x = 0$,

$$c_{\text{red},e} = \frac{2\lambda D_{\text{ox}}t^{1/2}}{\pi^{1/2}(D_{\text{red}})^{1/2}} \quad (162)$$

After introducing Eq. (154) into Eq. (161), the Sand expression is obtained:

$$\frac{-j\tau^{1/2}}{c_{\text{ox},0}} = \frac{\pi^{1/2}nF(D_{\text{ox}})^{1/2}}{2} \quad (163)$$

The $j\tau^{1/2}/c_{\text{ox},0}$ ratio is a constant which depends only on the electrochemical

system. For a simple reaction, this constant is independent of the degree of reversibility and the total concentration of the reacting species. In contrast, for complex electrochemical reactions the $j\tau^{1/2}$ term depends on the bulk concentration of the reacting species.

9.1. Reversible Electrochemical Reaction

When reaction (1) proceeds as a reversible electrochemical reaction, the concentrations of ox and red at the electrode surface are related to the potential according to the Nernst equation:

$$E = E_0 + \frac{RT}{nF} \ln \frac{\gamma_{\text{ox}} c_{\text{ox},e}}{\gamma_{\text{red}} c_{\text{red},e}} \quad (164)$$

The potential–time relationship resulting for a current step function is immediately obtained by replacing the concentrations for ox and red at $x = 0$ in Eq. (164) by those given in Eqs. (160) and (162). Thus, one obtains

$$E = E_0 + \frac{RT}{nF} \ln \left(\frac{\gamma_{\text{ox}}}{\gamma_{\text{red}}} \right) \left(\frac{D_{\text{red}}}{D_{\text{ox}}} \right)^{1/2} + \frac{RT}{nF} \ln \frac{[c_{\text{ox},0} + 2jt^{1/2}/\pi^{1/2}F(D_{\text{ox}})^{1/2}]}{[-2jt^{1/2}/\pi^{1/2}F(D_{\text{ox}})^{1/2}]} \quad (165)$$

In this equation the sum of the first two terms on the right-hand side corresponds to the half-wave potential of the electrochemical reaction as usually defined in polarography.^(1,61) Equation (165) can be more simply expressed as follows after considering Eqs. (154) and (161):

$$E = E_{1/2} + \frac{RT}{nF} \ln \frac{\tau^{1/2} - t^{1/2}}{t^{1/2}} \quad (166)$$

Thus, when $t = \tau$, the potential should become infinite unless another electrochemical reaction is involved at a potential larger than that related to reaction (1). According to this expression, the half-wave potential is determined in the potential–time profile at $t = \tau/4$.^(1,86,87)

Although the mathematics of the diffusional process under a constant flux was known since the beginning of this century, the experimental test of equations such as (163) and (166) was achieved with some success as recently as the 1950 decade. All previous attempts had failed due to improper experimental designs which involved other contributions such as migration and free convection.^(88,89) The validity of Sand's equation has been claimed for times as large as 290 s.⁽⁹⁰⁾ On the other hand, when the transition times are very short, the correction for the double-layer charging becomes increasingly important.

The potential–time relationship is slightly different than that given by Eq. (166) when both the ox and the red species are initially present in the

solution. Then,

$$E = E_{1/2} + \frac{RT}{nF} \ln \left[\frac{\tau^{1/2} - t^{1/2}}{(c_{\text{red},0}/c_{\text{ox},0})\tau^{1/2} + t^{1/2}} \right] \quad (167)$$

On the other hand, it is interesting to note that the abrupt change of the potential–time profile when the red species is initially absent is not observed when the red species is initially present. When the red species is insoluble, the potential–time profile is then given by the following equation:

$$E = E_0 + \frac{RT}{nF} \ln \left[\frac{-2j}{nF(D_{\text{ox}})^{1/2} \pi^{1/2}} \right] + \frac{RT}{nF} \ln (\tau^{1/2} - t^{1/2}) \quad (168)$$

9.2. Irreversible Electrochemical Process

Let us assume that reaction (1) represents an irreversible electrochemical process.⁽⁹¹⁾ The corresponding rate equation can be now conveniently expressed as

$$j = -nF(k_{\text{red}}c_{\text{ox},e} - k_{\text{ox}}c_{\text{red},e}) \quad (169)$$

where the rate constants k_{red} and k_{ox} are potential dependent according to

$$k_{\text{red}} = k_{\text{red}}^{\circ} \exp \left(-\frac{\alpha_c FE}{RT} \right) \quad (170)$$

and

$$k_{\text{ox}} = k_{\text{ox}}^{\circ} \exp \left(\frac{\alpha_a FE}{RT} \right) \quad (171)$$

The concentrations of the ox and red species at $x = 0$ can be obtained from Eqs. (160) and (162). Substitution of these expressions into Eq. (169) results in the potential–time relationship as a function of current density:

$$\begin{aligned} \frac{-j}{nF} = & k_{\text{red}}^{\circ} \left[c_{\text{ox},0} + \frac{2jt^{1/2}}{\pi^{1/2} nF(D_{\text{ox}})^{1/2}} \right] \exp \left(-\frac{\alpha_c FE}{RT} \right) \\ & + k_{\text{ox}}^{\circ} \left[\frac{2jt^{1/2}}{\pi^{1/2} nF(D_{\text{red}})^{1/2}} \right] \exp \left(\frac{\alpha_a FE}{RT} \right) \end{aligned} \quad (172)$$

Different limiting situations are derived from Eq. (172), depending on the degree of reversibility of the test reaction. Thus, when the potential is relatively far from its equilibrium value, one of the terms on the right-hand side of Eq. (172) may be eliminated. Let us consider a sufficiently high cathodic potential, so that the following equation is valid:

$$-\frac{j}{nF} = k_{\text{red}}^{\circ} \left[c_{\text{ox},0} + \frac{2jt^{1/2}}{\pi^{1/2} nF(D_{\text{ox}})^{1/2}} \right] \exp \left(-\frac{\alpha_c FE}{RT} \right) \quad (173)$$

then, from Eq. (173) at $j = \text{const}$, the following expression is obtained:

$$E = \frac{-RT}{\alpha_c F} \ln \left(\frac{F c_{\text{ox},e} k_{\text{red}}^{\circ}}{-j} \right) + \frac{RT}{\alpha_c F} \ln \left[1 - \left(1 - \frac{t}{\tau} \right)^{1/2} \right] \quad (174)$$

In this case, the potential-time relationship explicitly depends on the kinetic parameters of the electrochemical reaction. At $t = 0$, Eq. (174) is

$$E_{t=0} = \frac{-RT}{\alpha_c F} \ln \left(\frac{F k_{\text{red}} c_{\text{ox},0}}{-j} \right) \quad (175)$$

Hence, the initial potential depends on the magnitude of the current step and on the concentration of the reacting species. According to Eq. (175), a plot of $E_{t=0}/\log(Fk_{\text{red}}c_{\text{ox},0}/j)$, obtained at different concentrations of the reactant, yields α_c the transfer coefficient assisting the cathodic reaction.

9.3. Consecutive Diffusion-Controlled Electrochemical Reactions

It is interesting to establish the concentration distribution near the electrochemical interface of the different species related to a set of consecutive reactions occurring under a constant current. For a diffusion-controlled process, the concentration profile of the reactant pertaining to the first process remains unaltered as the following stages occur, but the concentration distribution of the species involved in a given stage is sensitive to the preceding ones. There are many cases that can be considered as consecutive electrochemical reactions, but only the following four are referred to here; namely, (i) the initial reaction followed by the reoxidation of the reaction product (by reversing the current step function); (ii) a consecutive reaction involving two different substances; (iii) the step-by-step electroreduction of a single species; and (iv) consecutive reactions involving an arbitrary number of reacting species.

For consecutive reactions, the concentrations of species entering into the first reaction appear in the boundary conditions of the following step and so forth. Then, a different solution of the diffusional problem is obtained, depending on the type of process considered.

9.3.1. Electrochemical Reoxidation of the Reaction Product

Let us consider that the ox species is electrochemically reduced to the red species at a constant current. When $t = \tau$, at $x = 0$, $c_{\text{ox},e} = 0$. Now if at the instant τ_1 the current is reversed, the electrochemical reoxidation of red occurs.⁽⁸⁶⁾ The concentration of the latter at $x = 0$ is given by Eq. (158) after making $t = \tau_1$. The time τ_1 is taken now as the starting point for time-counting, so that

$$t' = t - \tau_1 \quad (176)$$

Then, as the reacting species is now red, one of the boundary conditions at

$x = 0$ is given by Eq. (55) and the remaining one becomes

$$\left(\frac{\partial c_{\text{red}}}{\partial x}\right)_{x=0} = \frac{j'}{nFD_{\text{red}}} = \lambda' \quad (177)$$

where j' represents the reversal current step. The initial condition comes from Eq. (158) when $t' = 0$ (or $t = \tau_1$):

$$\begin{aligned} (c_{\text{red}})_{t'=0} = & -\frac{2j(D_{\text{red}})^{1/2}\tau_1^{1/2}}{n\pi^{1/2}F} \exp\left(-\frac{x^2}{4D_{\text{red}}\tau_1}\right) \\ & + \frac{jx}{nFD_{\text{red}}} \operatorname{erfc}\left[\frac{x}{2(D_{\text{red}})^{1/2}\tau_1^{1/2}}\right] \end{aligned} \quad (178)$$

The boundary conditions at $x \rightarrow \infty$ are the same corresponding to the electroreduction of the ox species [Eq. (53)]. The diffusion equation with the new initial and boundary conditions is solved by using the Fourier cosine transform. Accordingly, the concentration distribution equation is given by the following relationship:

$$\begin{aligned} c_{\text{red}} = & \frac{-2j}{nFD_{\text{red}}}\left[\frac{D_{\text{red}}(\tau_1 + t')}{\pi}\right]^{1/2} \exp\left[-\frac{x^2}{4D_{\text{red}}(\tau_1 + t')}\right] + \frac{jx}{nFD_{\text{red}}} \\ & \times \operatorname{erfc}\left\{\frac{x}{2[D_{\text{red}}(\tau_1 + t')]^{1/2}}\right\} + 2\left(\frac{j-j'}{nFD_{\text{red}}}\right)\left(\frac{D_{\text{red}}t'}{\pi}\right)^{1/2} \\ & \times \exp\left(-\frac{x^2}{4D_{\text{red}}t'}\right) - \left(\frac{j'-j}{nFD_{\text{red}}}\right)x \operatorname{erfc}\left[\frac{x}{2(D_{\text{red}}t')^{1/2}}\right] \end{aligned} \quad (179)$$

According to this equation a plot of c_{red} vs. x , at a constant t exhibits a maximum at $x \neq 0$, since red species diffuses out to the bulk of the solution. When $t' = \tau_2$, the concentration of red becomes zero at $x = 0$, for a preset value of j' . From Eq. (179), when $c_{\text{red}} = 0$ one obtains under the present conditions the transition time:

$$\tau_2 = \frac{(j/nFD_{\text{red}})^2\tau_1}{[(j' - j)/nFD_{\text{red}}]^2 - (j/nFD_{\text{red}})^2} \quad (180)$$

By choosing $j' = -j$, one obtains $\tau_2 = \tau_1/3$. On the other hand, substitution of Eq. (179) and an equivalent equation for $(c_{\text{ox},e})_{t=t'}$ into Eq. (164) yields, after rearranging the terms, the corresponding potential-time relationship:

$$E = E_0 + \frac{RT}{nF} \ln \frac{c_{\text{ox},0} + \frac{2j}{nFD_{\text{ox}}}\left[\frac{D_{\text{ox}}(\tau_1 + t')}{\pi}\right]^{1/2} - \frac{4j}{nFD_{\text{ox}}}\left(\frac{D_{\text{ox}}t'}{\pi}\right)^{1/2}}{\frac{-2j'}{nFD_{\text{red}}}\left[\frac{D_{\text{red}}(\tau_1 + t')}{\pi}\right]^{1/2} + \frac{4j}{nFD_{\text{red}}}\left(\frac{D_{\text{red}}t'}{\pi}\right)^{1/2}} \quad (181)$$

Equation (181) can be simplified as follows if $c_{\text{ox},0}$ is given in terms of τ_1 [Eq. (163)]:

$$E = E_{1/2} + \frac{RT}{nF} \ln \frac{\tau_1^{1/2} - [(\tau_1 + t')^{1/2} - 2(t')^{1/2}]}{(\tau_1 + t')^{1/2} - 2(t')^{1/2}} \quad (182)$$

9.3.2. Consecutive Reactions Involving Different Substances

Let us consider an electrochemical system (86) containing initially just two soluble species ox_1 and ox_2 which are electroreduced to red_1 and red_2 , respectively, at potentials quite apart from each other, according to the following simple reactions:



The products are also soluble.

The concentration distributions of the ox_1 and the red_1 species are given by the same expressions already given for the simple reaction [Eqs. (157) and (158)], since the occurrence of the second process has no influence on the former one. In contrast, the second process is affected by the first process; when the potential of the second process is attained the concentration of the ox_1 species becomes zero at $x = 0$, but the diffusion of ox toward the electrode surface continues. Therefore, the sum of the partial currents of reactions (183) and (184) corresponds to the total applied current (j_1) and this determines the initial and boundary conditions $x = 0$.

In this case, a new time scale referred to τ_1 is introduced. Then, the initial conditions are

$$t' = 0, 0 \leq x \leq \infty: \quad c_{\text{ox}_2} = c_{\text{ox}_2,0} \quad (185)$$

$$c_{\text{ox}_1} = c_{\text{ox}_1,0} + \frac{2j\tau_1^{1/2}}{n_1 F (D_{\text{ox}_1})^{1/2}} \exp\left(-\frac{x^2}{4D_{\text{ox}_1}\tau_1}\right) - \frac{jx}{n_1 F D_{\text{ox}_1}} \operatorname{erfc}\left[\frac{x}{2(D_{\text{ox}_1}\tau_1)^{1/2}}\right] \quad (186)$$

and the boundary conditions at $x = 0$ are

$$t' > 0, x = 0: \quad c_{\text{ox}_1} = c_{\text{ox}_1,e} = 0 \quad (187)$$

and

$$n_1 D_{\text{ox}_1} \left(\frac{\partial c_{\text{ox}_1}}{\partial x}\right)_{x=0} + n_2 D_{\text{ox}_2} \left(\frac{\partial c_{\text{ox}_2}}{\partial x}\right)_{x=0} = \frac{-j}{(n_1 + n_2)F} \quad (188)$$

together with

$$x \rightarrow \infty: \quad c_{\text{ox}_1} = c_{\text{ox}_1,0} \quad \text{and} \quad c_{\text{ox}_2} = c_{\text{ox}_2,0} \quad (189)$$

The first term of the left-hand side of Eq. (188) is derived by solving the diffusion equation for conditions $c_{\text{ox}_1, e} = 0$ when $t \geq \tau_1$.

The second term of Eq. (188) is obtained by applying either the Laplace transform or the Fourier transform method:

$$\left(\frac{\partial c_{\text{ox}_2}}{\partial x}\right)_{x=0}^{\wedge} = \frac{-j}{n_2 F D_{\text{ox}_2}} \left(\frac{1}{2} - \frac{1}{\pi} \arcsin \frac{\tau_1 - t'}{\tau_1 + t'}\right) \quad (190)$$

This equation is now replaced into the boundary-layer equation (188). After introducing the function $h(x, t')$, defined as

$$h(x, t') = c_{\text{ox}_2, 0} - c_{\text{ox}_2} \quad (191)$$

into Fick's equation, the latter can be solved by using the Laplace transform, after applying the convolution theorem. The following equation results for $x = 0$:

$$c_{\text{ox}_2, e} = c_{\text{ox}_2, 0} + \frac{2j}{\pi^{1/2} n_2 F (D_{\text{ox}_2})^{1/2}} [(\tau_1 + t')^{1/2} - \tau_1^{1/2}] \quad (192)$$

$c_{\text{ox}_2} = 0$ when $t' = \tau_2$. That is,

$$\tau_2 = \left(\frac{\pi^{1/2} n_2 F (D_{\text{ox}_2})^{1/2} c_{\text{ox}_2, 0}^{\circ}}{2j}\right)^2 - 2 \left(\frac{\pi^{1/2} n_2 F (D_{\text{ox}_2})^{1/2} c_{\text{ox}_2, 0}^{\circ}}{2j}\right) \tau_1^{1/2} \quad (193)$$

The transition time of the second process depends on the concentration of the ox_2 species and on the transition time of the former stage. As an example, when $n_1 = n_2$, $c_{\text{ox}_1, 0} = c_{\text{ox}_2, 0}$ and $D_{\text{ox}_1} = D_{\text{ox}_2}$, one obtains $\tau_2 = 3\tau_1$. For this case, the following relationship is obeyed:

$$-j[(\tau_1 + \tau_2)^{1/2} - \tau_1^{1/2}] = \text{const} \quad (194)$$

Besides, $(\tau_1 + \tau_2)^{1/2} - \tau_1^{1/2}$ is proportional to the concentration of the ox_2 species.

9.3.3. Step-by-Step Electroreduction of a Single Species

Now let us consider the following sequence of electrochemical reactions⁽⁸⁶⁾:



As considered in the previous cases, the potential-time relationship for the former step is that established by Eq. (167). When the potential of the second stage is sufficiently different than that of the first stage, the first transition time is definitely reached before the initiation of the second stage. On reaching the potential of the second stage, the direct electroreduction of ox_1 to red_2 becomes feasible, involving the transfer of $(n_1 + n_2)$ charges per mole of the ox_1 species. This reaction occurs simultaneously with the second reaction if

the reactant red_1 is available. The applied current step involves, therefore, two contributions and can be expressed as follows:

$$-j_{t>\tau_1} = (n_1 + n_2)FD_{\text{ox}} \left(\frac{\partial c_{\text{ox}_1}}{\partial x} \right)_{x=0} + n_2 FD_{\text{red}_1} \left(\frac{\partial c_{\text{red}_1}}{\partial x} \right)_{x=0} \quad (197)$$

where the time t' has been defined previously. Following a procedure similar to that described in case (ii), one of the boundary conditions becomes

$$\left(\frac{\partial c_{\text{red}_1}}{\partial x} \right)_{x=0} = \frac{-j}{n_1 FD_{\text{red}_1}} + \frac{(n_1 + n_2)j}{n_1 n_2 FD_{\text{red}_1}} \left(\frac{1}{2} + \frac{1}{\pi} \arcsin \frac{\tau_1 - t'}{\tau_1 + t'} \right) \quad (198)$$

c_{red_1} is evaluated as in the earlier cases by using the Laplace transform. Then, the concentration of the red_1 species at $x = 0$ is

$$c_{\text{red}_1,e} = \frac{-2j}{\pi^{1/2} n_2 F (D_{\text{red}_1})^{1/2}} \left[\frac{n_1 + n_2}{n_1} \tau_1^{1/2} - (\tau_1 + t')^{1/2} \right] \quad (199)$$

From this equation, when $c_{\text{red}_1,e} = 0$, the following relationship for the transition time results:

$$\tau_2 = \tau_1 \left[2 \left(\frac{n_2}{n_1} \right) + \left(\frac{n_2}{n_1} \right)^2 \right] \quad (200)$$

To obtain the concentration of red_2 at $x = 0$, the following boundary condition is required:

$$D_{\text{ox}_1} \left(\frac{\partial c_{\text{ox}_1}}{\partial x} \right)_{x=0, t>\tau_1} + D_{\text{red}_1} \left(\frac{\partial c_{\text{red}_1}}{\partial x} \right)_{x=0, t>\tau_1} + D_{\text{red}_2} \left(\frac{\partial c_{\text{red}_2}}{\partial x} \right)_{x=0, t>\tau_1} = 0 \quad (201)$$

together with the initial condition $(c_{\text{red}_2})_{t=t'} = 0$. Thus, the following equation results:

$$(c_{\text{red}_2,e})_{t'>0} = \frac{-2j}{\pi^{1/2} n_2 F (D_{\text{red}_2})^{1/2}} [(\tau_1 + t')^{1/2} - \tau_1^{1/2}] \quad (202)$$

and the corresponding potential-time equation is

$$E = (E_{1/2})_{\text{red}_1/\text{red}_2} + \frac{RT}{n_2 F} \ln \frac{(\tau_1 + \tau_2)^{1/2} - (\tau_1 + t')^{1/2}}{(\tau_1 + t')^{1/2} - \tau_1^{1/2}} \quad (203)$$

$(E_{1/2})_{\text{red}_1/\text{red}_2}$ is defined in the same way as $E_{1/2}$ for the simple reaction. The time at which $E = (E_{1/2})_{\text{red}_1/\text{red}_2}$ is obtained by making the argument of the logarithm of Eq. (203) unity. After rearrangement and simple transformations,

$$(t')_{E_{1/2}} = \frac{\tau_2}{4} + \frac{1}{2} \frac{n_2}{n_1} \tau_1 \quad (204)$$

Then when $n_1 = n_2$, $\tau_2 = 3\tau_1$ and $E_{1/2}$ is observed at $t' = 5\tau_2/12$. Therefore, this time is 5/4th of the transition time found for the reduction of a single species according to reaction (1).

9.3.4. Reaction Involving an Arbitrary Number of Reacting Species

When the system contains a large number of reacting species,⁽⁸⁸⁾ each one participating in a single diffusion-controlled reversible electrochemical process at a definite potential, the following initial and boundary conditions are required to solve the diffusion problem under a constant flux:

$$t = 0, 0 \leq x \leq \infty: \quad c_{\text{ox}_i} = c_{\text{ox}_i,0}, \quad c_{\text{red}_i} = c_{\text{red}_i,0} \quad (205)$$

$$t > 0, x = 0: \quad j = -\sum_i n_i F D_{\text{ox}_i} \left(\frac{\partial c_{\text{ox}_i}}{\partial x} \right)_{x=0} \quad (206)$$

$$D_{\text{ox}} \left(\frac{\partial c_{\text{ox}}}{\partial x} \right)_{x=0} + D_{\text{red}} \left(\frac{\partial c_{\text{red}}}{\partial x} \right)_{x=0} = 0$$

$$t > 0, x \rightarrow \infty: \quad c_{\text{ox}_i} = c_{\text{ox}_i,0}, \quad c_{\text{red}_i} = c_{\text{red}_i,0} \quad (207)$$

The expressions for the concentration of the different species at $x = 0$ are obtained after solving the mathematical problem by applying the Laplace transform. Thus, one obtains

$$c_{\text{ox}_i,e} = c_{\text{ox}_i,0} + \frac{\gamma_{\text{red}_i} K_i c_{\text{red}_i,0} - \gamma_{\text{ox}_i} c_{\text{ox}_i,0}}{\gamma_{\text{ox}_i} + \gamma_{\text{red}_i} K_i (D_{\text{ox}_i}/D_{\text{red}_i})^{1/2}} \quad (208)$$

$$c_{\text{red}_i,e} = c_{\text{red}_i,0} - \left(\frac{D_{\text{ox}_i}}{D_{\text{red}_i}} \right)^{1/2} \frac{\gamma_{\text{red}_i} K_i c_{\text{red}_i,0} - \gamma_{\text{ox}_i} c_{\text{ox}_i,0}}{\gamma_{\text{ox}_i} + \gamma_{\text{red}_i} K_i (D_{\text{ox}_i}/D_{\text{red}_i})^{1/2}} \quad (209)$$

where

$$K_i = \left(\frac{\gamma_{\text{ox}_i}}{\gamma_{\text{red}_i}} \right) \left(\frac{D_{\text{red}_i}}{D_{\text{ox}_i}} \right)^{1/2} \exp \left[\frac{n_i F}{RT} (E - E_{1/2,i}) \right] \quad (210)$$

and

$$E_{1/2,i} = E_{0,i} + \frac{RT}{n_i F} \ln \left(\frac{\gamma_{\text{ox}_i}}{\gamma_{\text{red}_i}} \right) \left(\frac{D_{\text{red}_i}}{D_{\text{ox}_i}} \right)^{1/2} \quad (211)$$

The general equation for potential-time curves in the case of an arbitrary number of reducible (or oxidizable) substances is

$$\frac{2jt^{1/2}}{\pi^{1/2}} = -\sum_{i=1}^p \frac{n_i F (D_{\text{ox}_i})^{1/2} c_{\text{ox}_i,0}}{2} \left[1 + \tanh \left(-\frac{n_i F (E - E_{1/2,i})}{2RT} \right) \right] \quad (212)$$

The right-hand side of Eq. (212) is proportional to the mean current observed for the stepwise composite polarographic waves with the same system. From the relationships of the polarographic reversible reduction of each species one obtains

$$I_i = \frac{I_{\text{lim},i}}{2} \left[1 + \tanh \left(-\frac{n_i F (E - E_{1/2,i})}{2RT} \right) \right] \quad (213)$$

and

$$I_{\text{lim},i} = (P)n_i(D_{\text{ox}})^{1/2}c_{\text{ox},i,0} \quad (214)$$

where P , the polarographic constant, is given by $0.607m^{2/3}t^{1/6}$. Equation (212) can be written in the form

$$t^{1/2} = \sum_{i=1}^n \frac{\pi^{1/2}I_i}{2Pj} \quad (215)$$

The p th system participates in the electrode reaction after the $(p-1)$ th reducible species is depleted at the electrode surface. Then, from (215) we get the result

$$T_p^{1/2} = \frac{\pi^{1/2}}{2Pj} (I_{\text{lim},1} + I_{\text{lim},2} + \cdots + I_{\text{lim},p}) \quad (216)$$

with

$$T_p = \sum_{i=1}^p \tau_i \quad (217)$$

where τ_i is the transition time for the i th system. From Eq. (216) one obtains

$$T_p^{1/2} - T_{p-1}^{1/2} = - \frac{\pi^{1/2}n_p F (D_{\text{ox},p})^{1/2} c_{\text{ox},p,0}}{2j} \quad (218)$$

which is the general formula for the particular case of two substances already seen. The potential-time relationship for the p th system comes from Eqs. (215) and (218):

$$E = E_{1/2,p} + \frac{RT}{nF} \ln \frac{T_p^{1/2} - t^{1/2}}{t^{1/2} - T_{p-1}^{1/2}} \quad (219)$$

The polarographic half-wave potential is observed at time t_p :

$$t_p = \left(\frac{T_p^{1/2} + T_{p-1}^{1/2}}{2} \right)^2 \quad (220)$$

The foregoing equations are useful in developing a graphical procedure for the analysis of potential-time curves.⁽⁸⁸⁾

The different equations derived in this section are employed in the chronopotentiometric techniques, a review related to them having been recently published.⁽⁹²⁾

9.4. Instantaneous Current Pulse

Another important diffusion problem is that resulting from the perturbation of the electrochemical interface with a current pulse of infinitely small length. When reaction (1) is a reversible electrochemical process, this type of

perturbation program generates an excess of product and a deficit of reactant at the electrode plane with respect to their corresponding bulk concentrations. Therefore, diffusion processes set in, lasting in until the concentration gradients disappear. Let us consider for simplicity only the case of a semi-infinite plane electrochemical surface. It is obvious that the mathematical solution of the diffusion equation is closely bound to that resulting from the previously obtained current step perturbation, since the time derivative of a step function is an instantaneous pulse. Then, at $t = 0$, the constant flux of each species switched on, is related to j_{pulse} , the corresponding instantaneous pulse flux,

$$j_{\text{pulse}} = \frac{K dj_{\text{step}}}{dt} \quad (221)$$

where K denotes the relationship between the characteristics of the perturbation function corresponding to the pulse and the step. This equation is immediately solved through the Laplace transform. For the simple example of a metal that dissolves anodically by the current pulse (instantaneous plane source of metal ions),⁽¹²⁾ the space-time concentration distribution becomes

$$c_{\text{Me}^{z+}} = c_{\text{Me}^{z+},0} + \frac{s}{(\pi D_{\text{Me}^{z+}})^{1/2}} \exp\left(-\frac{x^2}{4D_{\text{Me}^{z+}}t}\right) \quad (222)$$

where $c_{\text{Me}^{z+}}$ and $D_{\text{Me}^{z+}}$, the concentration and diffusion coefficient, respectively, refer to Me^{z+} , the metal-ion species generated by the current pulse.

Equation (222), when $c_{\text{Me}^{z+},0} = 0$ at $t = 0$, results in

$$c_{\text{Me}^{z+}} = \frac{s}{(\pi D_{\text{Me}^{z+}})^{1/2}} \exp\left(-\frac{x^2}{4D_{\text{Me}^{z+}}t}\right) \quad (223)$$

where s , the Laplace transform of the pulse flux, is the flux under a constant current step. In the present case, it corresponds to the total concentration of diffusing ions produced on the $x = 0$ plane at $t = 0$. Then Eq. (223) in terms of N , the number of ions, is

$$N = \frac{N_{\text{total}}}{(\pi D_{\text{Me}^{z+}})^{1/2}} \exp\left(\frac{-x^2}{4D_{\text{Me}^{z+}}t}\right) \quad (224)$$

At any given time a semi-bell-shaped distribution curve is found. The height of the curve at $x = 0$ decreases as t increases, while simultaneously the spread of ions along the distance x increases.

10. Diffusion Equation with Time-Dependent Boundary Conditions

The electrochemical interface can be perturbed with different potential-time functions. For each particular function there is a definite current-time

response of the system which depends to a large extent on the kinetics of the electrode reaction. There are different potential–time programs that are convenient for electrochemical kinetic studies, particularly, the linear potential–time, the triangular potential–time, and the sinusoidal potential–time perturbation functions. These functions can be applied either as a single potential sweep or as repetitive potential sweeps. The single potential sweep implies that after each perturbation, the system is allowed to recover its initial conditions before applying another perturbation. On the other hand, for pure diffusion the repetitive potential sweeps produce after a few cycles a quasi-stationary average concentration of the reacting species at the interface which differs from the initial one. The difference of concentration depends naturally on the perturbation conditions. The experimental techniques related to repetitive perturbations are the repetitive triangular potential sweep voltammetry and polarography, oscillographic polarography, differential pulse polarography, and faradaic impedance methods.

When the perturbation program at the interface is more complex, and when influences such as the double-layer capacity and ohmic drop contributions are considered, the corresponding differential equations are either nonlinear or they involve variable coefficients. Under these circumstances the mathematical solution is only achieved through the application of approximate methods.

The following paragraphs refer to different types of time-dependent perturbations on the assumption that the electric double-layer and ohmic drop contributions are absent.

10.1. Linear Potential/Time Perturbation

The theory of both single linear-potential sweep and triangular-potential sweep perturbations applied to electrochemical reactions involving diffusion were first developed for the dme on the assumption that its smooth surface could be considered in terms of the semi-infinite unidirectional plane interface model.^(94–98) The analysis was also extended to repetitive triangular-potential sweeps.⁽⁹⁹⁾ The pertaining equations were extended to solid electrodes of different geometries.^(40,100)

The linear-potential sweep starts at a potential where there is no faradaic current through the electrode–solution interface. The changing potential reaches the region where, as the electrochemical reaction occurs, the current increases. Simultaneously, as long as the reaction proceeds and the latter involves a diffusion contribution, the concentration of the reacting species at the electrode decreases. Therefore, there are two antagonistic effects on the current due to the increasing potential and the decreasing concentration of the reacting species at the electrode plane, since the rate of arrival of the latter from the bulk becomes insufficient to balance its consumption by the electrode process. Then the consumption rate of the reacting species prevails, the faradaic current decreasing as the potential increases. The current–time

response, therefore, is relatively complex and it exhibits a net current peak at a definite potential.

For a simple reversible process, such as that expressed by reaction (1), the current decreases after the maximum and reaches a stationary limiting value. The potential at which the limiting current is attained increases as the rate of the potential sweep increases. Let us compare this behavior with that of the potential-step perturbation previously discussed.

Under a potential-step perturbation within the lapse where the system is practically convection-free, the surface concentration adjusts to a constant value, which corresponds to the applied potential, but the diffusion layer thickness increases (relaxation of the diffusion layer). Conversely, during the potential sweep both the surface concentration and the diffusion-layer thickness change. The former decreases according to a defined concentration-time profile, while the latter increases.⁽⁶⁰⁾

10.2. Mathematical Procedures

The mathematical solution of the differential equations pertaining to diffusion with the time-dependent boundary conditions are mainly obtained by using three methods; namely, (i) the application of the Laplace transform; (ii) the numerical solutions obtained through the finite-difference method; and (iii) the conversion of the boundary-value problem into an integral equation.⁽⁹⁶⁾

The first procedure is applicable to reversible and catalytic reactions⁽¹⁰¹⁻¹⁰⁴⁾ rendering for these reactions definite integrals that can only be numerically solved. The second method yields only numerical values that are tabulated for different reaction mechanisms and kinetic conditions.^(92,97,105,106) The third method is the most general one. The integral equations can be solved either by series^(13,43,100,104,107) or numerically.^(33,95,99,108-110) In all these methods the application of numerical solutions is required at least in the final step.

Let us consider again the simple redox electrochemical reaction (1) involving two soluble species. The unidirectional differential diffusion equations for the ox and the red species are given through Eq. (57) applied to each species. The corresponding initial condition is the same as that given in expression (51), and the boundary conditions in the bulk of the solution at $t \geq 0$ correspond to those given by Eq. (53). At $x = 0$, one boundary condition is related to the balance of fluxes [Eq. (55)].

10.3. Solution by the Laplace Transform Method

By applying the Laplace transform to the set of Fick's differential equations [Eq. (57)], corresponding to each reacting species, and taking into account the boundary conditions just mentioned, the following equations are

obtained:

$$\text{At } x = 0, \quad s(\bar{c}_{\text{ox}} - c_{\text{ox},0}) = D_{\text{ox}} \left(\frac{\partial^2 \bar{c}_{\text{ox}}}{\partial x^2} \right) \quad (225a)$$

$$s(\bar{c}_{\text{red}} - c_{\text{red},0}) = D_{\text{red}} \left(\frac{\partial^2 \bar{c}_{\text{red}}}{\partial x^2} \right) \quad (225b)$$

$$D_{\text{ox}} \frac{\partial \bar{c}_{\text{ox}}}{\partial x} - D_{\text{red}} \frac{\partial \bar{c}_{\text{red}}}{\partial x} = \rho(s) \quad (226)$$

And at $x \rightarrow \infty$,

$$\bar{c}_{\text{ox}} = c_{\text{ox},0} \quad (227)$$

$$\bar{c}_{\text{red}} = c_{\text{red},0}$$

where

$$\rho(s) = \mathcal{L}[I(t)/nFA]$$

$$\bar{c}_{\text{ox}} = \mathcal{L}c_{\text{ox}} \quad (228)$$

$$\bar{c}_{\text{red}} = \mathcal{L}c_{\text{red}}$$

and A is the electrode area.

By solving the set of transformed equations one obtains

$$\bar{c}_{\text{ox}} = c_{\text{ox},0} - \frac{1}{(D_{\text{ox}})^{1/2}} \frac{\bar{\rho}(s)}{s^{1/2}} \exp \left[-s^{1/2} \left(\frac{x^2}{D_{\text{ox}}} \right)^{1/2} \right] \quad (229)$$

and

$$\bar{c}_{\text{red}} = c_{\text{red},0} + \frac{1}{(D_{\text{red}})^{1/2}} \frac{\bar{\rho}(s)}{s^{1/2}} \exp \left[-s^{1/2} \left(\frac{x^2}{D_{\text{red}}} \right)^{1/2} \right] \quad (230)$$

The surface concentrations of the different species are given by the following transform equations:

$$(\bar{c}_{\text{ox}})_{x=0} = c_{\text{ox},0} - \frac{1}{(D_{\text{ox}})^{1/2}} \frac{\bar{\rho}(s)}{s^{1/2}} \quad (231)$$

and

$$(\bar{c}_{\text{red}})_{x=0} = c_{\text{red},0} + \frac{1}{(D_{\text{red}})^{1/2}} \frac{\bar{\rho}(s)}{s^{1/2}} \quad (232)$$

the inverse transform is obtained by applying the convolution theorem:

$$c_{\text{ox},e} = c_{\text{ox},0} - \frac{1}{\pi^{1/2} (D_{\text{ox}})^{1/2}} \int_0^t \frac{\phi(\tau)}{(t-\tau)^{1/2}} d\tau \quad (233)$$

and

$$c_{\text{red},e} = c_{\text{red},0} + \frac{1}{\pi^{1/2} (D_{\text{red}})^{1/2}} \int_0^t \frac{\phi(\tau)}{(t-\tau)^{1/2}} d\tau \quad (234)$$

where

$$\phi(t) = -D_{\text{ox}} \left(\frac{\partial c_{\text{ox}}}{\partial x} \right)_{x=0} = D_{\text{red}} \left(\frac{\partial c_{\text{red}}}{\partial x} \right)_{x=0} = \frac{I(t)}{nFA} \quad (235)$$

The concentration distribution equations (231) and (232) just derived are independent of the rate of the electrochemical reaction since only the boundary conditions (53) and (55) were considered.

10.4. Reversible Reaction

For the case of reaction (1) behaving as a reversible process, the secondary boundary condition at $x = 0$ results from the Nernst equation which relates c_{ox} and c_{red} at equilibrium [Eq. (54)]. The mathematical development is similar to that already indicated for the potentiostatic step, but instead of having a constant potential equation, it implies now a time-dependent potential. For a linear potential sweep the potential–time program is given by

$$E = E_i - vt \quad (236)$$

E_i being the initial potential at which no current flows and v the rate of the potential sweep. Certainly, the initial potential satisfies the equilibrium equations,

$$E_i = E_0 + \frac{RT}{nF} \ln \frac{\gamma_{\text{ox}} c_{\text{ox},e}}{\gamma_{\text{red}} c_{\text{red},e}} \quad (237)$$

For a symmetric triangular potential perturbation, the potential–time perturbation function is

$$E = E_i - 2v\lambda + vt \quad (238)$$

which is valid for $t > \lambda$, where $\lambda = t/2$ corresponds to the time of initiation of the reverse potential sweep.

According to Eq. (236) and (237) or (238), the boundary condition (54) is then

$$\frac{c_{\text{ox},e}}{c_{\text{red},e}} = \theta S_\lambda(t) \quad (239)$$

where

$$\theta = \exp \left[\frac{nF(E_i - E^0)}{RT} \right] \quad (240)$$

and

$$t \leq \lambda, \quad S_\lambda(t) = \exp(-at) \quad (241)$$

$$t > \lambda, \quad S_\lambda(t) = \exp(at - 2a\lambda) \quad (242)$$

with

$$a = \frac{nFv}{RT} \quad (243)$$

The unknown time-dependent function involved in the concentration distribution equations (233) and (234) can now be solved. By means of the boundary condition already seen, the concentration term is eliminated from Eqs. (233) and (234). The expression for $S_\lambda(t)$ is taken either for the potential changing in the negative reaction ($\lambda \leq t$) or vice versa ($\lambda \geq t$) [Eqs. (241) or (242)]. When $c_{\text{red},0} = 0$, the following equation is obtained:

$$\int_0^t \frac{\phi(\tau)}{(t-\tau)^{1/2}} d\tau = \frac{c_{\text{ox},0} \pi^{1/2} (D_{\text{ox}})^{1/2}}{1 + \gamma \theta S_\lambda(t)} \quad (244)$$

where $\gamma = (D_{\text{ox}}/D_{\text{red}})^{1/2}$.

By a proper change of variables, Eq. (244) can be written in a dimensionless form. Thus, if

$$\begin{aligned} \tau &= \frac{z}{a} \\ \phi(t) &= g(at) \end{aligned} \quad (245)$$

and

$$g(at) = c_{\text{ox},0} (\pi D_{\text{ox}} a)^{1/2} \chi(at) \quad (246)$$

Then, the dimensionless form of Eq. (244) is

$$\int_0^{at} \frac{\chi(z)}{(at-z)^{1/2}} dz = \frac{1}{1 + \gamma \theta S_{a\lambda}(at)} \quad (247)$$

Equation (247) is an Abel integral equation, a particular case of the Volterra integral equation. This type of equation can be solved either analytically or by power series, or by numerical methods. For the latter, the dimensionless form is the most suitable one. From Eqs. (235), (245), and (244), the following equation for the current is derived:

$$I = -nFAc_{\text{ox},0} (\pi D_{\text{ox}} a)^{1/2} \chi(at) \quad (248)$$

The $\chi(at)$ function is obtained either analytically or by power series, or numerically.

10.4.1. Analytical Solution for $\chi(at)$

Solution of the Abel integral equation (96) yields

$$\chi(at) = \frac{L(0)}{\pi(at)^{1/2}} + \frac{1}{\pi} \int_0^{at} \frac{1}{(at-z)^{1/2}} \left[\frac{dL(at)}{d(at)} \right]_{at=z} dz \quad (249)$$

where $L(at)$ represents the right-hand side of Eq. (247) for $at = 0$. Substitution of the definition of $S_\lambda(at)$ gives

$$\chi(at) = \frac{1}{\pi(at)^{1/2}(1 + \gamma \theta)} + \frac{1}{4\pi} \int_0^{at} \frac{dz}{(at-z)^{1/2} \cosh^2 [\ln(\gamma \theta - z)/2]} \quad (250)$$

But the integral equation involved in the right-hand side of Eq. (250) must be numerically solved, and to eliminate the singular point at $at = z$ either a change of variables⁽⁸¹⁾ or an integration by parts is done.⁽¹⁰³⁾

When the electrochemical problem involves a reversible reaction yielding an insoluble product,⁽⁸⁶⁾ only the differential equation (57) for the reactant concentration is required. The same extends obviously to the initial and boundary conditions. Now, there is only one condition at $x = 0$, which is determined by the Nernst equation:

$$c_{\text{ox},e} = \exp \left[\frac{nF(E_i - E_0)}{RT} \right] \exp \left(-\frac{nFvt}{RT} \right) = \theta \exp(-at) \quad (251)$$

By using the Laplace transform the following equation is derived:

$$j = \frac{-2}{\sqrt{\pi}} \frac{(nF)^{3/2}}{(RT)^{1/2}} c_{\text{ox},0} (D_{\text{ox}})^{1/2} v^{1/2} \phi \left[\left(\frac{nFvt}{RT} \right)^{1/2} \right] \quad (252)$$

where $\phi(\chi) = \exp(-\chi^2) \int_0^\alpha \exp(z^2) dz$. Its values are tabulated.⁽¹¹¹⁾ The maximum value of $\phi(\alpha)$ is proportional to the current peak height (j_{peak}) which is given by

$$j_{\text{peak}} = - (nF)^{3/2} \left(\frac{vD_{\text{ox}}}{RT} \right)^{1/2} c_{\text{ox},0} [\phi(\chi)]_{\text{max}} \quad (253)$$

Different values of $\phi(\chi)_{\text{max}}$ are reported, depending on the mathematical method employed. Thus, the values are 0.4463⁽⁹⁶⁾ and 0.5410.⁽¹⁰⁹⁾ According to Berzins and Delahay in the equation for j_{peak} , at 25°C,⁽¹⁰¹⁾

$$J_{\text{peak}} = -367n^{3/2} c_{\text{ox},0} (D_{\text{ox}})^{1/2} v^{1/2} \quad (254)$$

where j_{peak} is in A cm^{-2} , $c_{\text{ox},0}$ in mole/liter, D_{ox} in $\text{cm}^2 \text{s}^{-1}$, and v in V s^{-1} .

10.4.2. Numerical Solution of $\chi(at)$

The numerical solution of Eq. (247) is achieved by dividing the integration range into N equally spaced subintervals ($z = \delta\nu$) from $t = 0$ to $at = M$. The order number of the subintervals, n , is $n = at/\delta$ where $\delta = M/N$. Then, Eq. (247) becomes

$$\delta^{1/2} \int_0^n \frac{\chi(\delta\nu)}{(n-\nu)^{1/2}} d\nu = \frac{1}{1 + \gamma\theta S_\delta(\delta n)} \quad (255)$$

After an integration by parts, the singular point of Eq. (255) at $n = \nu$ is obtained:

$$\int_0^n \frac{\chi(\delta\nu) d\nu}{(n-\nu)^{1/2}} = 2 \left\{ \chi(0)n^{1/2} + \int_0^n (n-\nu)^{1/2} d[\chi(\delta\nu)] \right\} \quad (256)$$

By replacing the integral on the right-hand side of Eq. (256) by its sum and after eliminating the values corresponding to $i = 0$ and $i = n$, one derives

$$2\delta^{1/2} \left\{ \chi(1)n^{1/2} + \sum_{i=1}^{n-1} (n-1)^{1/2} [\chi(i+1) - \chi(i)] \right\} = \frac{1}{1 + \gamma\theta S_{\delta\lambda}(\delta n)} \quad (257)$$

This relationship defines N algebraic equations in $\chi(n)$. When $\delta_n \leq \delta_\lambda$, $S_{\delta\lambda}/\delta n$ becomes equal to $\exp(-\delta n)$, while for $\delta_n > \delta_\lambda$ the function becomes equal to $\exp(\delta_n - 2\delta\lambda)$. This calculation procedure yields the function $\chi(at)$ both for a single linear-potential sweep and for the repetitive sweeps. The numerical solutions of the equation are tabulated in terms of $(E - E_{1/2})n_i$ and $\pi^{1/2}\chi(at)$.⁽⁹⁶⁾

10.4.3. Series Solution of $\chi(at)$

Either the faradaic current or $\chi(at)$, the current determining function, is given in terms of a series that converges very rapidly for large potential excursions.⁽¹³⁾ One proposed series is

$$\chi(at) = \frac{1}{\sqrt{\pi}} \sum_{i=1}^{\infty} (-1)^{i+1} \sqrt{i} \exp \left[-\frac{inF(E - E_{1/2})}{RT} \right] \quad (258)$$

which for $nFat/RT \geq 5$ can be written

$$\chi(at) = x - \sqrt{2} x^2 + \sqrt{3} x^3 - \sqrt{4} x^4 + \dots \quad (259)$$

where

$$x = \exp \left[\frac{nF(E - E_{1/2})}{RT} \right] \quad (260)$$

10.5. Irreversible and Quasirreversible Electrochemical Reactions

When reaction (1) is irreversible, the boundary condition at $x = 0$ and $t > 0$ is that indicated by Eq. (56) together with E given either by Eq. (236) or (238). For sufficiently large cathodic potentials ($E \rightarrow -\infty$), the term of the rate equation corresponding to the reverse reaction can be neglected so that the boundary condition (56) is simplified:

$$f(t) = D_{\text{ox}} \left(\frac{\partial c_{\text{ox}}}{\partial x} \right)_{x=0} = k_{\text{red}}^{\circ} c_{\text{ox},e} \exp \left(-\frac{\alpha_c FE}{RT} \right) \quad (261)$$

Under a linear-potential sweep it is convenient to refer the rate constant to the initial potential [Eq. (236)]:

$$k_i = k_{\text{red}}^{\circ} \exp \left(-\frac{\alpha_c FE_i}{RT} \right) \quad (262)$$

Then, Eq. (261) becomes

$$f(t) = k_i c_{\text{ox},e} \exp(bt) \quad (263)$$

where $b = (\alpha_c F/RT)v$. The concentration distribution equation derived from Eq. (247) is obtained by applying Duhamel's method^(24,108)

$$c_{\text{ox}} = c_{\text{ox},0} - \frac{1}{(\pi D_{\text{ox}})^{1/2}} \int_0^t f(t-\tau) \exp\left(-\frac{x^2}{4D_{\text{ox}}\tau}\right) \frac{d\tau}{\tau^{1/2}} \quad (264)$$

where τ is an auxiliary time value. From Eq. (263), the concentration distribution equation can be transformed into an integral equation. Thus, for

$$\exp(u) = \frac{(\pi b D_{\text{ox}})^{1/2}}{k_i} \quad (265)$$

and $a = b(t-\tau)$, one obtains

$$1 - \int_0^{bt} \frac{\chi(z) dz}{(bt-z)^{1/2}} = \exp(u-bt)\chi(bt) \quad (266)$$

After fixing certain values of u and different values of bt , values of the function $\chi(bt)$ are obtained after a series expansion.^(96,108) From the following relationships,

$$bt = \frac{\alpha_c F(E_i - E)}{RT} \quad (267)$$

and

$$j = -nFc_{\text{ox},0}(\pi D_{\text{ox}}b)^{1/2}\chi(bt) \quad (268)$$

the current density-potential curves of the irreversible process are traced.

After replacing b from Eq. (267) and $\chi(bt)$ for $\chi(bt)_{\text{max}}$ the peak current results:

$$I_{\text{peak}} = -\text{const} \times \pi^{1/2} nF \left(\frac{\alpha_c F}{RT}\right)^{1/2} A(D_{\text{ox}})^{1/2} c_{\text{ox},0} v^{1/2} \quad (269)$$

where the $(\pi^{1/2} \times \text{const})$ factor depends on the number of terms used in the series expansion. The following values for the constant have been reported: 0.4998,⁽¹⁰⁸⁾ 0.4958,⁽⁹⁸⁾ and 0.496.⁽¹⁰⁹⁾

Matsuda and Ayabe⁽¹⁰⁹⁾ derived the expression of $\chi(bt)$ taking into account the boundary condition (56). After replacing in Eq. (56) the concentrations at $x=0$ according to expressions (229) and (230) and dividing both members by the following relationship,

$$\frac{k_{\text{red}}^{\circ}}{(D_{\text{ox}})^{1/2}} \exp\left(-\frac{\alpha_c FE}{RT}\right) - \frac{k_{\text{ox}}^{\circ}}{(D_{\text{red}})^{1/2}} \exp\left(\frac{\alpha_a FE}{RT}\right) \quad (270)$$

the Volterra integral is obtained:

$$\frac{1}{\left(\frac{k_{\text{red}}\gamma_{\text{ox}}}{D_{\text{ox}}}\right)^{\alpha_a} \left(\frac{k_{\text{ox}}\gamma_{\text{red}}}{D_{\text{red}}}\right)^{\alpha_c}} \frac{\phi(t)}{\exp\left[-\frac{\alpha_c F(E - E_{1/2})}{RT}\right] + \exp\left[\frac{\alpha_a F(E - E_{1/2})}{RT}\right]}$$

$$= \frac{(D_{\text{ox}})^{1/2} c_{\text{ox},0} - (D_{\text{red}})^{1/2} c_{\text{red},0} \exp\left[\frac{nF(E - E_{1/2})}{RT}\right]}{1 + \exp\left[\frac{nF(E - E_{1/2})}{RT}\right]}$$

$$- \frac{1}{\pi^{1/2}} \int_0^t \frac{\phi(s)}{\sqrt{t-s}} ds \quad (271)$$

Equation (271) is simplified after introducing the new variables:

$$\xi = -\frac{nF(E - E_{1/2})}{RT} = \frac{nFvt}{RT} - a \quad (272)$$

$$\zeta = -\frac{nF(E(s) - E_{1/2})}{RT} = \frac{nFvs}{RT} - a \quad (273)$$

where

$$a = \frac{nF(E_0 - E_{1/2})}{RT} = \ln \frac{c_{\text{ox},0} \left(\frac{D_{\text{ox}}}{D_{\text{red}}}\right)^{1/2}}{c_{\text{red},0}} \quad (274)$$

and

$$\psi(\xi) = \frac{\phi(\xi)}{(D_{\text{ox}})^{1/2} c_{\text{ox},0} (nFv/RT)} \quad (275)$$

Thus, the following integral equation results:

$$\frac{1}{\Lambda \exp(\alpha\xi) + \exp[-(1-\alpha)\xi]} = \frac{1 - \exp[-(\xi + a)]}{1 + \exp(-\xi)} - \frac{1}{\pi^{1/2}} \int_{-a}^{\xi} \frac{\psi(\zeta)}{(\xi - \zeta)^{1/2}} d\zeta \quad (276)$$

with

$$\Lambda = \frac{[k_{\text{red}}\gamma_{\text{ox}}/(D_{\text{ox}})^{1/2}]^{\alpha_a} [k_{\text{ox}}\gamma_{\text{red}}/(D_{\text{red}})^{1/2}]^{\alpha_c}}{nFv/RT} \quad (277)$$

The behavior of the function depends upon the values of Λ , α_a , α_c , and a , but when $E_0 - E_{1/2} > 300/n$ mV, $\psi(\xi)$ becomes independent of a . Under this condition, regarding the values of Λ , α_a , and α_c , three different cases are distinguished.

When $\Lambda > 15$, the following integral-differential equation results:

$$\psi(\xi) = \frac{1 + \exp(-a)}{4\pi^{1/2}} \int_{-a}^{\xi} \frac{1}{\cosh^2(\eta/2)} \frac{d\eta}{(\xi - \eta)^{1/2}} - \frac{1}{\Lambda\pi^{1/2}} \int_{-a}^{\xi} \frac{d}{d\eta} \left[\frac{\psi(\eta)}{\exp(\alpha_c\eta) + \exp(-\alpha_a\eta)} \right] \frac{d\eta}{(\xi - \eta)^{1/2}} \quad (278)$$

which can be solved as a power series in Λ .

$$\psi(\xi) = 1 - \exp(-a) \left[f_0(\xi) + \sum_{l=1}^{\infty} (-1)^l f_l(\xi) \right] \quad (279)$$

An approximate numerical calculation yields $f_1(\xi)/f_0(\xi) \approx 0.4$ for $l > 1$. Therefore, for $\Lambda \approx 15$, the Λ -containing terms in Eq. (278) can be eliminated within a 1–2% error⁽¹⁰⁹⁾ and then the integral equation is

$$\psi_{\text{rev}}(\xi) = \frac{1 + \exp(-a)}{4\pi^{1/2}} \int_0^{\xi} \frac{1}{\cosh^2(\eta/2)} \frac{d\eta}{(\xi - \eta)^{1/2}} \quad (280)$$

In terms of the new variables, Eq. (280) becomes

$$\psi_{\text{rev}}(\xi) = \frac{1 + \exp(-a)}{2\pi^{1/2}} \int_0^{\sqrt{\xi+a}} \frac{d\eta}{\cosh^2[(\xi - \eta^2)/2]} \quad (281)$$

These equations correspond to the limiting case of a reversible process, since they involve no parameters related to the kinetics of the proper electron-transfer reaction. Equation (281) is transformed into a sum after applying the Euler–McLaurin method. When the initial potential is far from $E_{1/2}$, that is, $a > 12$, $\psi_{\text{rev}}(\xi)$ becomes independent of a . Then the equation to be numerically solved is

$$\psi_{\text{rev}}(\xi) = \frac{h}{2\pi^{1/2}} \left(\frac{1}{2} \frac{1}{\cosh^2(\xi/2)} + \sum_{l=1}^{\infty} \frac{1}{\cosh^2\{[\xi - (lh)^2]/2\}} \right) \quad (282)$$

and for $h = 0.1$, the resulting $\psi_{\text{rev}}(\xi)_{\text{max}}$ is 0.447, a value close to that reported by Matsuda and Ayabe.⁽¹⁰⁹⁾ Hence, at 25°C, the equation for j_{peak} results in

$$j_{\text{peak}} = -269n^{2/3}c_{\text{ox},0}D_{\text{ox}}^{1/2}v^{1/2} \quad (283)$$

When $\Lambda < 10^{-2(1+\alpha_c)}$, the reaction behaves as an irreversible process, and the current density equation is

$$j = -nFc_{\text{ox},0}D_{\text{ox}}^{1/2} \left(\frac{\alpha_c Fv}{RT} \right)^{1/2} \psi_{\text{ir}} \left\{ - \left[\frac{\alpha_c F(E - E_{1/2})}{RT} \right] + \ln \Lambda^* \right\} \quad (284)$$

where $\Lambda^* = \Lambda/\alpha_c^{1/2}$ and $\psi_{\text{ir}}(\chi)$ changes accordingly with the argument. The current peak value, related to $\psi_{\text{ir}}(\chi)_{\text{max}}$ is

$$j_{\text{peak}} = -0.496nFc_{\text{ox},0}(D_{\text{ox}})^{1/2} \left(\frac{\alpha_c Fv}{RT} \right)^{1/2} \quad (285)$$

Values of Λ are between the two limiting cases just referred to, $15 \geq \Lambda \geq 10^{-2(1+\alpha_c)}$, correspond to quasireversible processes.⁽¹⁰⁹⁾

Diffusional problems under a linear-potential sweep have also been solved for more complex electrochemical processes on a spherical surface,⁽¹⁰⁶⁾ on an expanding sphere,⁽⁹⁹⁾ and on a cylindrical surface.⁽⁹²⁾ Their solutions are mostly based on the application of the mathematical solutions given in the present chapter as well as on the application of computational procedures beyond the scope of the present text.^(112,113)

11. Time-Dependent Boundary Conditions: Sinusoidal Perturbations

The electrochemical interface can be perturbed with a sinusoidal current or with a sinusoidal potential. This signal can also be superimposed on a dc level or modulated on a linear time-dependent base function, as in the case of the potential in alternating current (ac) polarography.^(26,114,115)

The theory of perturbing the interface with a sinusoidal potential was developed by Breyer, Gutmann, and Bauer.^(114,116) In this case, when the perturbing potential covers a small amplitude, the current induced at the interface consists of the algebraic sum of two components—one alternating component (ac) and one direct current (dc) component. When an ac flux is controlling the interface behavior, such as in ac chronopotentiometry,^(60,117) the net flux through the interface is the sum of an ac and a dc component, but in this case a large ac potential component contributes in the region of the transition time together with the dc component.⁽¹¹⁸⁾ The mathematical resolution of both problems to obtain the integral equation for the surface concentration of the reacting species follows the same pattern.

Let us again consider reaction (1) involving both ox and red as soluble species on a plane electrode. The corresponding diffusional equations are bound to the initial and boundary conditions given by Eqs. (51) and (53), respectively. The boundary conditions at $x = 0$ change accordingly, the perturbed variable being either the potential or the current. In any case, the integral surface concentration distribution equations for both the ox and the red species are obtained after the Laplace transform. They are given by, respectively,⁽²⁶⁾

$$c_{\text{ox},e} = c_{\text{ox},0} + \int_0^t \frac{I(t-u) du}{nFA(\pi D_{\text{ox}}u)^{1/2}} \quad (286)$$

$$c_{\text{red},e} = c_{\text{red},0} - \int_0^t \frac{I(t-u) du}{nFA(\pi D_{\text{red}}u)^{1/2}} \quad (287)$$

The perturbed function is usually imposed on a dc component, therefore, the concentration of any species will primarily change according to the dc component but will fluctuate in phase with the applied ac signal.

11.1. Potential Sinusoidal Perturbation

Modern ac polarography^(38,97) consists of the modulation of a dc linear-potential sweep with different perturbations, namely, triangular, square, or sinusoidal potential waves.^(38,64,97,105,114,116,119-124) An exact solution of this problem has been obtained for reaction (1) under reversible conditions with a sinusoidal controlled perturbation.⁽⁹⁹⁾

$$E(t) = E_{dc} - \Delta E \sin \omega t \quad (288)$$

ΔE is the amplitude of the perturbation and ω its frequency. For simplicity, let us assume that the reduced form is initially absent from the solution ($c_{red,0} = 0$). The boundary conditions at $x = 0$ and $t > 0$ are

$$-D_{ox} \left(\frac{\partial c_{ox}}{\partial x} \right)_{x=0} = D_{red} \left(\frac{\partial c_{red}}{\partial x} \right)_{x=0} = \frac{I(t)}{nFA} \quad (289)$$

and

$$c_{ox,e} = c_{red,e} \left(\frac{\gamma_{ox}}{\gamma_{red}} \right) \left(\frac{D_{red}}{D_{ox}} \right)^{1/2} \exp \left[\frac{nF(E - E_{1/2})}{RT} \right] \quad (290)$$

The latter expression implies a Nernstein response of reaction (1). After replacing in Eq. (290) the concentration as given in expression (286) and (287), the following integral equation results⁽²⁶⁾

$$\begin{aligned} & \exp \left[-\frac{nF(E - E_{1/2})}{RT} \right] \left[1 + \int \frac{I}{nFAc_{ox,0}(D_{ox})^{1/2}} \frac{t-u}{(\pi u)^{1/2}} du \right] \\ & = - \int \frac{I}{nFAc_{ox,0}(D_{ox})^{1/2}} \frac{t-u}{(\pi u)^{1/2}} du \end{aligned} \quad (291)$$

By introducing expression (288) into the exponential of Eq. (291), one obtains

$$\exp \left[-\frac{nF(E - E_{1/2})}{RT} \right] = \exp \left[-\frac{nF(E_{dc} - E_{1/2})}{RT} \right] \exp \left(\frac{nF\Delta E}{RT} \right) \sin \omega t \quad (292)$$

The first exponential on the right-hand side contains a time-independent exponent which involves the dc potential component. In contrast, the second one is time dependent and can be conveniently expressed as a series expression:

$$\exp \left(\frac{nF\Delta E}{RT} \sin \omega t \right) = \sum_{p=0}^{\infty} \left(\frac{nF\Delta E}{RT} \right)^p \left(\frac{\sin \omega t}{p!} \right)^p \quad (293)$$

$$\psi(t) = \sum_{p=0}^{\infty} \psi_p(t) \left(\frac{nF\Delta E}{RT} \right)^p \quad (294)$$

$$p = 0, 1, 2, 3, \dots \quad (295)$$

where

$$\psi(t) = \frac{-I}{nFAc_{ox,0}(D_{ox})^{1/2}} \quad (296)$$

After substituting Eqs. (293) and (294) in Eq. (291) and equating coefficients of equal power of ψ_p , the system of integral equations is obtained:

$$\begin{aligned} \frac{\exp(-J)(\sin \omega t)^p}{p!} - \sum_{r=0}^p (-J) \frac{(\sin \omega t)^r}{r!} \int_0^t \psi_{p-r} \frac{t-u}{(\pi u)^{1/2}} du \\ = \int_0^t \frac{\psi_p(t-u)}{(\pi u)^{1/2}} du \end{aligned} \quad (297)$$

and

$$J = \frac{nF}{RT}(E_{dc} - E_{1/2}) \quad (298)$$

p represents the various faradaic components ($k = 0$ for dc, $k = 1$ for the fundamental harmonic ac, etc.) according to

$$P = 2q + k \quad (q = 0, 1, 2, 3, \dots) \quad (299)$$

When $P = 0$ ($k = 0$), the dc component results:

$$\int_0^t \psi_0 \frac{(t-u)}{(\pi u)^{1/2}} du = \frac{1}{1 + \exp(J)} \quad (300)$$

By solving the problem through the Laplace transform one obtains

$$j_{dc} = \frac{-nFc_{ox,0}D_{ox}^{1/2}}{[1 + \exp(J)](\pi t)^{1/2}} \quad (301)$$

which corresponds to the current response for reaction (1) on a plane electrode under a potentiostatic step function.

For $p = 1$, at small amplitude perturbations, the equation for the fundamental harmonics is

$$I(\omega t) = -\frac{n^2F^2Ac_{ox,0}(\omega D_{ox})^{1/2}\Delta E \sin(\omega t + \pi/4)}{4RT \cosh^2(J/2)} \quad (302)$$

Small-amplitude ac signal perturbations are usually employed in ac polarography and in faradaic impedance techniques, where equations such as (302) are generally applied. This equation corresponds to a faradaic impedance z_t , given by^(25,26)

$$Z_t = \frac{4RT \cosh^2(J/2)}{n^2F^2Ac_{ox,0}(\omega D_{ox})^{1/2}} \quad (303)$$

which is equivalent to a series RC circuit with

$$R_t = \frac{1}{\omega C_f} = \frac{4RT \cosh^2(J/2)}{n^2 F^2 A c_{\text{ox},0} (\omega D_{\text{ox}})^{1/2}} \quad (304)$$

Mathematical solutions also exist for ac perturbations involving relatively large amplitudes⁽⁹⁹⁾ and larger values of p , either for the dc component ($p = 2, 4, 6, \dots$) or for the ac fundamental harmonics ($p = 3, 5, 7, \dots$).

11.2. Sinusoidal Current Perturbation

The mathematical description of this problem for a simple reversible process occurring at a plane electrode is given for the conditions of chronopotentiometry with a superimposed alternating current of constant amplitude.⁽¹²⁵⁾ In this case, the flux of the ox species is the sum of the dc and ac components. Thus at $x = 0$,

$$-D_{\text{ox}} \left(\frac{\partial c_{\text{ox}}}{\partial x} \right)_{x=0} = \frac{I_{\text{dc}} + \Delta I \sin \omega t}{nFA} = \frac{I}{nF} \quad (305)$$

where ΔI is the amplitude and ω is the frequency of the ac signal. The initial and the other boundary conditions are given by Eqs. (51) and (53). By solving the diffusion equation for linear diffusion with those conditions, the concentration of the ox species at $x = 0$ is given by

$$c_{\text{ox},e} = c_{\text{ox},0} + \frac{1}{nFA(D_{\text{ox}})^{1/2}} \left[\frac{2I_{\text{dc}}t^{1/2}}{\pi^{1/2}} + \frac{\Delta I}{\omega^{1/2}} \sin \left(\omega t - \frac{\pi}{4} \right) \right] \quad (306)$$

$$c_{\text{red},e} = \frac{-1}{nFA(D_{\text{red}})^{1/2}} \left[\frac{2I_{\text{dc}}t^{1/2}}{\pi^{1/2}} + \frac{\Delta I}{\omega^{1/2}} \sin \left(\omega t - \frac{\pi}{4} \right) \right] \quad (307)$$

For the reversible reaction, the potential is the sum of a slowly varying component which changes, as in the case of conventional chronopotentiometry,⁽¹⁾ plus an ac component which has the same frequency as the current. Then

$$E_{\text{ac}} = E_{\text{dc}} + \frac{RT}{nF} \ln \left\{ \frac{1 - [k \sin(\omega t - \pi/4)]/(\tau^{1/2} - t^{1/2})}{1 + [k \sin(\omega t - \pi/4)]/t^{1/2}} \right\} \quad (308)$$

$$k = \frac{\pi^{1/2} \Delta I}{2I_{\text{dc}} \omega^{1/2}} \quad (309)$$

and

$$E_{\text{dc}} = E_{1/2} + \frac{RT}{nF} \ln \left(\frac{\tau^{1/2} - t^{1/2}}{t^{1/2}} \right) \quad (310)$$

The term $I_{\text{dc}} \tau^{1/2}$ is also given by expression (163). The second term on the right-hand side of Eq. (309) represents the ac potential contribution which,

when the argument is small, allows the series expansion of the log term, yielding

$$E_{ac} = -\frac{RT}{nF} \frac{\tau^{1/2}}{t^{1/2}(\tau^{1/2} - t^{1/2})} \frac{\pi^{1/2} \Delta I}{2I_{dc} \omega^{1/2}} \sin\left(\omega t - \frac{\pi}{4}\right) \quad (311)$$

which is -45° out of phase with respect to the current. The transition time can be detected more easily from the variations of the ac potential than from conventional potential-time curves.^(125,126)

The theory of sinusoidal perturbations, either potential-controlled or current-controlled, has been extended to quasireversible first-order reactions, irreversible reactions, and more complex electrochemical processes.^(25,26,93,127)

Their analysis, however, is beyond the scope of the present chapter.

Auxiliary Notation

E_0	standard electrode potential
E'_0	reversible electrode potential
$E_{1/2}$	half-wave potential
k°	standard rate constant
k	potential-dependent rate constant
m	rate of flow mercury
V_d	volume of mercury drop
γ	Euler-Macheroni constant
λ	time at which scan is reversed

References

1. P. Delahay, *New Instrumental Methods in Electrochemistry*, Interscience, New York (1962).
2. K. J. Vetter, *Electrochemical Kinetics*, Academic Press, New York (1967).
3. J. S. Newman, *Electrochemical Systems*, Prentice-Hall, Englewood Cliffs, NJ (1973).
4. V. G. Levich, *Physicochemical Hydrodynamics*, Prentice-Hall, Englewood Cliffs, NJ (1962).
5. H. R. Thirsk and J. A. Harrison, *A Guide to the Study of Electrode Kinetics*, Academic Press, London (1972).
6. H. Schlichting, *Boundary Layer Theory*, McGraw-Hill, New York (1955).
7. R. B. Bird, W. E. Stewart, and E. N. Lightfoot, *Transport Phenomena*, Wiley, New York (1960).
8. T. Kuwana and N. Winograd, In: *Electroanalytical Chemistry*, A. J. Bard, Ed., Vol. 7, p. 1, Dekker, New York (1974).
9. N. Winograd and T. Kuwana, *J. Electroanal. Chem.* **23**, 333 (1969).
10. B. E. Conway, *Theory and Principle of Electrode Processes*, Ronald Press, New York (1965).
11. P. Delahay, *Double Layer and Electrode Kinetics*, Interscience, New York (1965).
12. J. O'M. Bockris and A. K. N. Reddy, *Modern Electrochemistry*, vols. I and II, Plenum Press, New York (1970).
13. W. H. Reinmuth, *Anal. Chem.* **34**, 1446 (1962).
14. H. S. Harned and B. B. Owen, *The Physical Chemistry of Electrolytic Solutions*, Reinhold, New York (1957).

15. R. A. Robinson and R. H. Stokes, *Electrolyte Solutions*, Butterworth, London (1970).
16. S. R. de Groot, *Thermodynamics of Irreversible Processes*, North Holland, Amsterdam (1951).
17. I. Prigogine, *Introduction to Thermodynamics of Irreversible Processes*, Interscience, New York (1967).
18. J. Crank, *The Mathematics of Diffusion*, Clarendon Press, Oxford (1964).
19. W. Jost, *Diffusion*, Academic Press, New York (1960).
20. T. Z. Fahiday, *Chem. Eng. J.* **7**, 21 (1974).
21. J. A. Shercliff, *A Textbook of Magnetohydrodynamics*, Pergamon Press, London (1965).
22. N. Curle, *The Laminar Boundary Layer Equations*, Clarendon Press, Oxford (1962).
23. J. Newman, In: *Electroanalytical Chemistry*, A. J. Bard, Ed., Vol. 6, p. 187, Dekker, New York (1973).
24. H. S. Carslaw and J. C. Jaeger, *Conduction of Heat in Solids*, Oxford University Press, Oxford (1947).
25. M. Sluyters-Rehbach and J. H. Sluyters, In: *Electroanalytical Chemistry*, A. J. Bard, Ed., Vol. 4, p. 1, Dekker, New York (1970).
26. D. E. Smith, In: *Electroanalytical Chemistry*, A. J. Bard, Ed., Vol. 1, p. 1, Dekker, New York (1966).
27. H. Eyring, L. Marker, and T. C. Kwoh, *J. Phys. Chem.* **53**, 187 (1949).
28. N. Tanaka and R. Tamamushi, *Bull. Chem. Soc. Jap.* **22**, 187 (1949).
29. N. Tanaka and R. Tamamushi, *Bull. Chem. Soc. Jap.* **22**, 1227 (1949).
30. N. Tanaka and R. Tamamushi, *Bull. Chem. Soc. Jap.* **23**, 110 (1950).
31. P. Delahay, *J. Am. Chem. Soc.* **73**, 4994 (1951).
32. P. Delahay and J. E. Strassner, *J. Am. Chem. Soc.* **73**, 5219 (1951).
33. P. Delahay, *J. Am. Chem. Soc.* **75**, 1430 (1953).
34. M. G. Evans and N. S. Hush, *J. Chem. Phys.* **49**, C159 (1952).
35. T. Kambara and I. Tachi, *Bull. Chem. Soc. Jap.* **25**, 135 (1952).
36. M. Smutek, *Chem. Listy* **45**, 241 (1951).
37. M. Smutek, *Coll. Czech. Chem. Commun.* **18**, 771 (1953).
38. M. Smutek, *Coll. Czech. Chem. Commun.* **20**, 247 (1955).
39. H. Matsuda and Y. Ayabe, *Bull. Chem. Soc. Jap.* **28**, 422 (1955).
40. K. B. Oldham, *Anal. Chem.* **41**, 936 (1969).
41. H. A. Laitinen and I. M. Kolthoff, *J. Phys. Chem.* **45**, 1061 (1941).
42. D. Lydersen, *Acta Chim. Scand.* **3**, 259 (1949).
43. H. Gerischer and W. Vielstich, *Z. Phys. Chem. NF* **3**, 16 (1955).
44. S. Barnartt, *J. Phys. Chem.* **70**, 412 (1966).
45. R. Parsons, *Trans. Faraday Soc.* **47**, 1332 (1951).
46. S. Barnartt, *Electrochim. Acta* **11**, 1531 (1966).
47. S. Barnartt and C. A. Johnson, *Trans. Faraday Soc.* **63**, 431 (1967).
48. E. L. Lederer, *Kolloid. Z.* **44**, 128 (1928).
49. E. L. Lederer, *Kolloid. Z.* **46**, 169 (1928).
50. D. MacGillivray and E. K. Rideal, *Rec. Trav. Chim.* **56**, 1013 (1937).
51. C. A. Johnson and S. Barnartt, *J. Phys. Chem.* **73**, 3374 (1969).
52. H. Gerischer and K. Stanbach, *Z. Phys. Chem. NF* **6**, 118 (1956).
53. H. A. Laitinen and I. M. Kolthoff, *J. Am. Chem. Soc.* **61**, 3344 (1939).
54. I. Shain and K. J. Martin, *J. Phys. Chem.* **65**, 254 (1961).
55. E. M. Skobets and N. S. Kavetskii, *Zh. Fiz. Khim.* **24**, 1486 (1950).
56. W. Vielstich and H. Gerischer, *Z. Phys. Chem. NF* **4**, 10 (1955).
57. T. Berzins and P. Delahay, *J. Am. Chem. Soc.* **77**, 6448 (1955).
58. H. Gerischer, *Z. Phys. Chem.* **202**, 302 (1953).
59. J. Heyrovsky and D. Ilkovic, *Coll. Czech. Chem. Commun.* **7**, 198 (1935).
60. J. Heyrovsky and J. Kuta, *Principles of Polarography*, Academic Press, New York (1966).

61. I. M. Kolthoff and J. J. Lingane, *Polarography*, Interscience, New York (1952).
62. D. Ilkovic, *Coll. Czech. Chem. Commun.* **6**, 498 (1934).
63. D. Ilkovic, *J. Chim. Phys.* **35**, 129 (1938).
64. J. Heyrovsky and R. Kalvoda, *Oszillographische Polarographie mit Wechselstrom*, Akademie Verlag, Berlin (1960).
65. J. J. Lingane and B. A. Loveridge, *J. Am. Chem. Soc.* **72**, 438 (1950).
66. J. Koutecky, *Czech. J. Phys.* **2**, 50 (1953).
67. H. Matsuda, *Bull. Chem. Soc. Jap.* **26**, 342 (1953).
68. J. Koutecky, *Chem. Listy* **47**, 323 (1953).
69. N. Mejman, *Zh. Fiz. Khim.* **22**, 1454 (1948).
70. J. Koutecky, *Coll. Czech. Chem. Commun.* **20**, 980 (1955).
71. J. Weber and J. Koutecky, *Chem. Listy*, **49**, 562 (1955).
72. I. Shain, K. J. Martin, and J. W. Ross, *J. Phys. Chem.* **65**, 259 (1961).
73. C. A. Johnson and S. Barnartt, *J. Phys. Chem.* **71**, 1637 (1967).
74. K. B. Oldham, *Anal. Chem.* **41**, 1904 (1969).
75. K. B. Oldham and J. Spanier, *J. Electroanal. Chem.* **26**, 331 (1970).
76. A. Ruis, S. Polo, and J. Llopis, *Anal. Fis. Quím.* **45**, 1029 (1949).
77. J. C. Jaeger and M. Clarke, *Proc. R. Soc. Edinburgh A* **61**, 229 (1942).
78. A. Papoulis, *Q. Appl. Math.* **14**, 405 (1957).
79. R. Guidelli, *J. Electroanal. Chem.* **33**, 291 (1971).
80. R. Guidelli, *J. Electroanal. Chem.* **33**, 303 (1971).
81. Z. Karaoglanoff, *Z. Elektrochem.* **12**, 5 (1906).
82. T. R. Rosebrugh and W. L. Miller, *J. Phys. Chem.* **14**, 816 (1910).
83. H. J. S. Sand, *Philos. Mag.* **1**, 45 (1901).
84. H. F. Weber, *Wied. Ann.* **7**, 536 (1879).
85. J. A. V. Butler and G. Armstrong, *Proc. R. Soc. Lond. A* **139**, 406 (1933).
86. T. Berzins and P. Delahay, *J. Am. Chem. Soc.* **75**, 4205 (1953).
87. P. Delahay and C. C. Mattax, *J. Am. Chem. Soc.* **76**, 874 (1954).
88. T. Kambara and I. Tachi, *J. Phys. Chem.* **61**, 1405 (1957).
89. R. C. Turner and C. A. Winkler, *J. Electrochem. Soc.* **99**, 78 (1952).
90. T. Rabockai, *Anal. Lett.* **9**, 341 (1976).
91. P. Delahay and T. Berzins, *J. Am. Chem. Soc.* **75**, 2486 (1953).
92. M. M. Nicholson, *J. Am. Chem. Soc.* **76**, 2539 (1954).
93. R. K. Jain, H. C. Gaur, and B. J. Welch, *J. Electroanal. Chem.* **79**, 211 (1977).
94. Y. P. Gokhshtein, *Dokl. Akad. Nauk SSSR* **126**, 598 (1959).
95. A. Y. Gokhshtein and Y. P. Gokhshtein, *Dokl. Akad. Nauk SSSR* **131**, 601 (1960).
96. R. S. Nicholson and I. Shain, *Anal. Chem.* **36**, 706 (1964).
97. J. E. B. Randles, *Trans. Faraday Soc.* **44**, 327 (1948).
98. A. Sevick, *Coll. Czech. Chem. Commun.* **13**, 349 (1948).
99. H. Matsuda, *Z. Elektrochem.* **61**, 489 (1957).
100. W. H. Reinmuth, *Anal. Chem.* **33**, 185 (1961).
101. T. Berzins and P. Delahay, *J. Am. Chem. Soc.* **75**, 555 (1953).
102. J. Koutecky, *Coll. Czech. Chem. Commun.* **21**, 433 (1956).
103. W. H. Reinmuth, *J. Am. Chem. Soc.* **79**, 6358 (1957).
104. J. Weber, *Coll. Czech. Chem. Commun.* **24**, 1770 (1959).
105. R. P. De Mars and I. Shain, *J. Am. Chem. Soc.* **81**, 2654 (1959).
106. R. P. Frankenthal and I. Shain, *J. Am. Chem. Soc.* **78**, 2969 (1956).
107. W. H. Reinmuth, *Anal. Chem.* **34**, 1453 (1962).
108. P. Delahay, *J. Am. Chem. Soc.* **75**, 1190 (1953).
109. H. Matsuda and Y. Ayabe, *Z. Elektrochem.* **59**, 494 (1955).
110. J. M. Saveant and E. Vianello, In: *Advances in Polarography*, J. S. Longmuir, Ed., Vol. 1, p. 367, Pergamon Press, New York (1960).

111. W. L. Miller and A. R. Gordon, *J. Phys. Chem.* **35**, 2785 (1931).
112. W. Felberg, In: *Electroanalytical Chemistry*, A. J. Bard, Ed., Vol. 3, p. 200, Dekker, New York (1969).
113. J. A. Mattson, H. B. Mark, and H. C. MacDonald, *Electrochemistry, Calculations, Simulation and Instrumentation*, Dekker, New York (1972).
114. B. Breyer and H. H. Bauer, *Alternating Current Polarography and Tensammetry*, Interscience, New York (1963).
115. T. Kambara, *Leybold Polarography. Ber.* **2**, 41 (1957).
116. B. Breyer, F. Gutmann, and H. H. Bauer, *Ost. Chem. Z.* **57**, 67 (1956).
117. J. Heyrovsky, *Chem. Listy* **35**, 155 (1941).
118. J. Heyrovsky, *Discuss. Faraday Soc.* **1**, 212 (1947).
119. J. E. B. Randles, *Discuss. Faraday Soc.* **1**, 47 (1947).
120. D. C. Grahame, *J. Am. Chem. Soc.* **63**, 1207 (1941).
121. B. Ershler, *Discuss. Faraday Soc.* **1**, 269 (1947).
122. H. Matsuda, *Z. Elektrochem.* **60**, 617 (1956).
123. K. Micka, *Z. Phys. Chem.* **206**, 345 (1957).
124. J. Heyrovsky and S. Forejt, *Oscillographica Polarographie*, SNTC, Prague (1953).
125. Y. Takemori, T. Kambara, M. Senda, and I. Tachi, *J. Phys. Chem.* **61**, 968 (1957).
126. M. Fournier, *C. R. Acad. Sci. (Paris)* **232**, 1673 (1951).
127. N. P. Bansal and J. A. Plambeck, *J. Electroanal. Chem.* **78**, 205 (1977).

3

Convective Mass Transport

N. IBL and O. DOSENBACH

1. Introduction

1.1. Convective Mass Transport: Qualitative Considerations

This chapter deals with convective mass transport, i.e., a hydrodynamic flow in the electrolyte system. Let us start by a few qualitative remarks. As an example, we consider the electrolysis of a solution of $\text{CuSO}_4 + \text{H}_2\text{SO}_4$ in a cell with two plane, parallel, copper electrodes. The solution streams parallel to the electrode in laminar flow. Copper is deposited at the cathode. The concentration of H_2SO_4 is much larger than that of CuSO_4 so that migration of the Cu^{2+} ions is negligible. Near each of the electrodes a diffusion layer builds up in which the concentration of the Cu^{2+} is different from its value in the bulk (Section 1, Chapter 1). Similarly, a hydrodynamic boundary layer is established in which the flow velocity is different from its value in the bulk solution. The reason is that, due to the viscous forces, there can be no slip of the liquid at a wall; i.e., the flow velocity at a stationary interface electrode solution is zero. Figure 1 is a schematic of the velocity and concentration profiles near the cathode.

The slowing down of the liquid due to the friction forces at the electrode becomes more and more effective downstream: Near the leading edge ($x = 0$) only the layers immediately adjacent to the wall are retarded in their movement by the action of the wall. However, further downstream these layers of

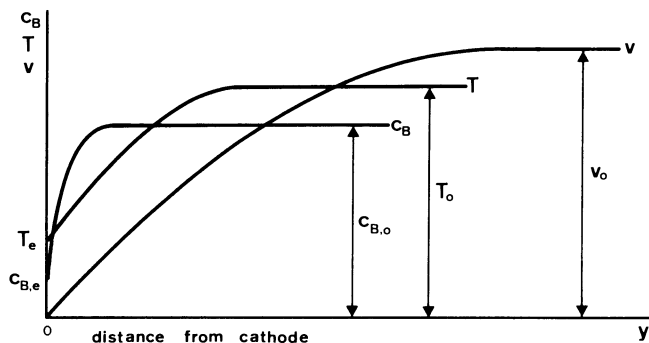


Figure 1. Concentration, temperature, and velocity profiles near a cathode.

low velocity slow down in turn, through the viscous forces, layers of liquid located further away from the electrode. Therefore, at increasing distance x from the leading edge, the zone with decreased velocity extends more and more into the interior of the solution. The thickness δ_v of the hydrodynamic boundary layer thus becomes larger at increasing x (Figure 2).

The liquid flowing into the diffusion layer carries Cu^{2+} ions of the bulk concentration $c_{B,0}$: A flux of electroactive species equal to $c_{B,0}v_0$ (where v_0 is the flow velocity parallel to the electrode) thus enters the diffusion layer.[†] This convective flux accelerates the mass transport toward the cathode (as compared to the case of a quiescent liquid, where the transport proceeds by diffusion and migration only). The supply of cations by convection compensates for the cations discharged at the cathode. This establishes a steady state which in our example is reached after a time of the order of 10–60 s. Figure 3 shows a mass balance over the whole diffusion layer for steady-state conditions.[‡] In this stationary state the concentration profile is independent of time. This is in contrast to the situation without convection where the

[†] In the above argument and in the mass balance of Figure 3 we have considered, for the sake of simplicity, conditions (excess of indifferent electrolyte, see Section 5, Chapter 1) in which the migration is negligible. If this is not so (e.g., in the case of a solution of CuSO_4 only) a flux due to migration enters into the diffusion layer through the plane AB . However, this flux is smaller than the amount of Cu^{2+} ions discharged per unit time at the cathode and there is a deficit in the mass balance of the diffusion layer. In the steady state this deficit is compensated by the balance of the convective fluxes entering and leaving the control volume $ABCD$. The argument becomes somewhat more complicated but remains essentially the same as that developed on pp. 134 and 135–136 for the case of a negligible migration flux.

[‡] Note that although the flow is on the whole parallel to the electrode there is a velocity component v_y near the electrode in the y direction perpendicular to the electrode. This effect is due to the slowing down of the liquid downstream and can be easily deduced from a mass balance for the liquid. Thus, there is a flux of the electroactive species leaving the diffusion layer both in the x and y directions. It is the difference between these fluxes and the flux entering the diffusion layer in the x direction at the leading edge which is available to compensate the above mentioned deficit in the mass balance.

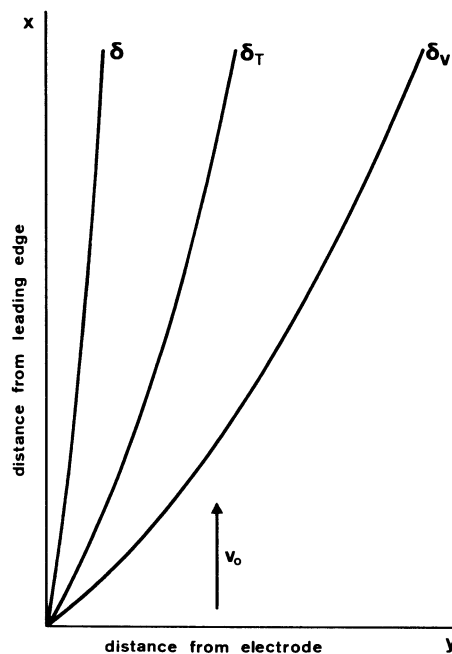


Figure 2. Influence of location on boundary-layer thickness in laminar flow along an electrode. δ , δ_T , and δ_v are the thicknesses of the diffusion, thermal and hydrodynamic boundary layers, respectively.

diffusion layer keeps on growing because the cations removed from the layer at the cathode cannot be compensated from outside of the diffusion layer, so that the overall amount of Cu^{2+} ions present in the diffusion layer must continuously decrease with time; i.e., the thickness of the diffusion layer increases (see Section 1, Chapter 1).

The steady state in convective transport is the situation most commonly encountered in industrial electrolytic systems. The thickness of the diffusion layer in the steady state depends on the kind and velocity of the hydrodynamic flow: The more effective the stirring, the thinner the diffusion layer and the faster the transport toward the cathode. A consequence is that in the example of Figures 1 and 2, the diffusion layer becomes thicker downstream due to the aforementioned slowing down of the convective stream with increasing distance from the leading edge. The thicknesses of the diffusion layer δ and the hydrodynamic boundary layer δ_v both increase downstream (Figure 2). We will discuss more quantitatively later how the two layers are related (Section 4.5). For the moment, let us point out that the variation of the thickness of the diffusion layer along the electrode is another characteristic feature of convective mass transport, in contrast to convection-free electrolysis. In the latter case, with the cell geometry of Figure 1, the diffusion layer would be uniform (except for small edge effects at both ends). In convective mass transport there are also systems in which the thickness of the diffusion layer is constant over the electrode, but, in general, the hydrodynamic flow may cause a nonuniformity of the diffusion layer and thus a variation of the

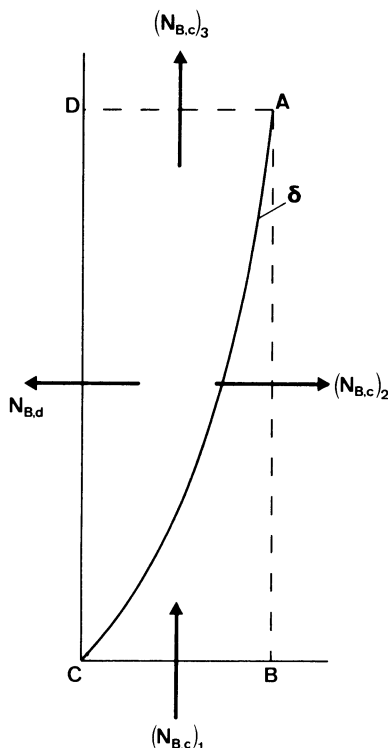


Figure 3. Mass balance for boundary layer (steady-state). $ABCD$, control volume; $N_{B,d}$, diffusion flux out of control volume; $N_{B,c}$, convective fluxes in and out (concentration times flow velocity). (For a definition of these fluxes, see Chapter 1, Sections 2.1, 3.1, and 3.2.) In the steady state, $N_{B,d} + (N_{B,c})_1 = (N_{B,c})_2 + (N_{B,c})_3$.

rate of mass transport or of interfacial concentrations over the electrode surface.

Before we turn toward the quantitative treatment of the problem, let us make a few more qualitative remarks about the mechanism of convective mass transport. In Figure 3 we have made a mass balance for the whole diffusion layer. We will get further insight by considering a volume element $dx dy dz$ within the diffusion layer (Figure 4). The velocity v_x decreases downstream and so does the flux density $v_x c_B$: The amount of electroactive species entering the volume from below is larger than that leaving at the upper end.† The difference between the two is available for diffusion toward the cathode: It serves to increase the diffusion flux toward the cathode over the distance dy . The increase in diffusion flux when one approaches the cathode can also be seen from Figure 1. The concentration gradient increases

† In reality, the situation is more complicated because there is also a fluid flow v_y away from the cathode (see second footnote on p. 134) and this flow carries species B. Part of the decrease of the convective flux of B in the x direction serves to increase the convective flux of B in the y direction over the distance dy . But this does not change the conclusion of the argument developed in the main text. Quantitatively, the mass balance for the infinitesimal volume $dx dy dz$ is described by the differential equation (2.6) (see Section 2.1) (see also Figure 3, Chapter 1).

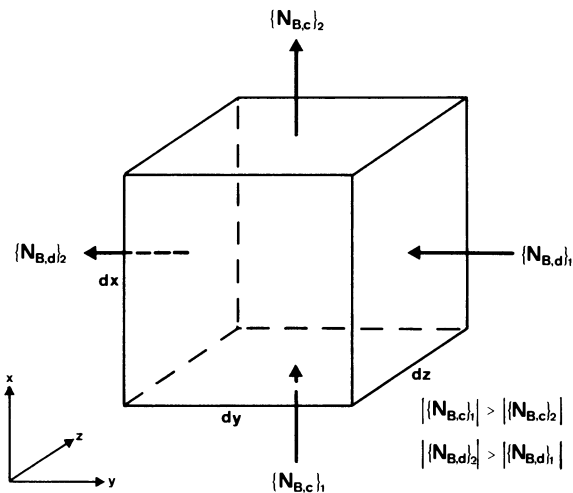


Figure 4. Volume element in diffusion layer for qualitative discussion [see also Section 2.1 and Eq. (1)].

toward the cathode and so does the diffusion flux which is proportional to the concentration gradient according to Fick's first law. In each volume element, in the steady state, the increase in the diffusion flux over the distance dy is compensated by the decrease of the convective flux over the distance dx . Within the diffusion layer the convective flux in the x direction is progressively converted (at least partly) to a diffusion flux in the y direction. In the outer parts of the diffusion layer, the concentration gradient and the diffusion flux are very small and mass transport by convection is predominant. On the other hand, very close to the electrode the flow velocity tends to zero (Figure 1) and transport by convection is negligible. In this region the diffusion flux can no longer increase with decreasing y : The concentration profile is a straight line which is the situation characteristic of steady-state convection-free diffusion.

This state of affairs suggests a simplified view of the diffusion layer which dates back to the dawn of this century and which was first expressed by Brunner⁽¹⁾ and Nernst.⁽²⁾

1.2. Nernst Model for the Diffusion Layer

The linear part of the concentration profile is extended until the concentration in the bulk solution is reached. The diffusion layer is thus approximated by the broken line shown in Figure 5. In physical chemistry, this model is called the Nernst diffusion layer; in chemical engineering, the equivalent or effective diffusion layer. The leading idea is that the solution can be roughly divided into two parts: a thin layer near the electrode with no convection on the one hand, and the bulk solution where the stirring ensures perfect mixing—

i.e., uniform concentration, on the other hand. Thus it is assumed that the transition from transport by convection to that by diffusion occurs abruptly at point *C*. In reality, as we have seen, this transition is progressive and the true concentration profile is not a straight line. Nevertheless, the model of an adhering unmoved layer has proved quite useful and been popular during many years in physical chemistry and electrochemistry. One advantage is that it allows the assignment, in a simple and unambiguous manner, of a thickness δ to the diffusion layer, as shown on Figure 5. In contrast to this, in the case of the true profile (continuous line in Figure 5) the thickness of the diffusion layer is undefined because the concentration tends asymptotically to the bulk value $c_{B,0}$. One has thus to recourse to some arbitrary definition anyhow, such as that the thickness of the diffusion layer is the distance from the electrode at which $(c_B - c_{B,e})/(c_{B,0} - c_{B,e}) = 0.99$. Such an arbitrary definition is no more expedient than that given by the Nernst model. However, it should be recognized that the Nernst diffusion layer has a fictitious character. Nevertheless, the thickness of this layer is, in general, related to and representative of any "true" diffusion layer thickness which we may define.

An effective hydrodynamic boundary layer of thickness δ_v can be defined in a way quite similar to that for the diffusion layer. It is represented by the linear velocity profile (broken line) of Figure 5.

The Nernst model further gives simple expressions for the interfacial flux density $N_{B,e}$. For an electroactive species B present in small concentration (excess of indifferent electrolyte) one obtains (see also Section 5.4, Chapter 1)

$$N_{B,e} = -D_B \left(\frac{dc_B}{dy} \right)_e = -D_B \frac{c_{B,0} - c_{B,e}}{\delta} \quad (1)$$

where D_B is the diffusion coefficient of the species reacting at the electrode.

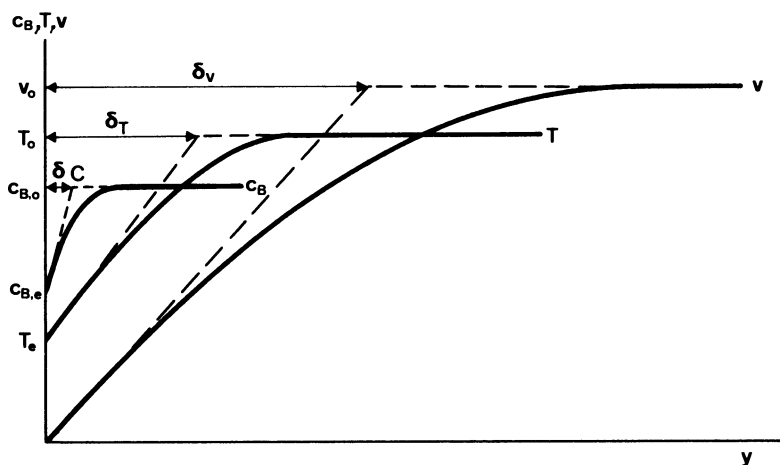


Figure 5. Nernst approximation: ---, linear approximation of the profiles; —, true profiles.

The current density, for the deposition of a metal, is

$$j = -z_B F D_B \frac{c_{B,0} - c_{B,e}}{\delta} \quad (2)$$

where z_B is the charge number of the metallic ions. In the case of the solution of a single electrolyte we have (see Section 5.4, Chapter 1)

$$N_{B,e} = -(1 - t_B)^{-1} D (c_{B,0} - c_{B,e}) / \delta \quad (3)$$

and

$$j = -(1 - t_B)^{-1} z_B F D (c_{B,0} - c_{B,e}) / \delta \quad (4)$$

where t_B is the transport number of the metallic cations.

Equations (1), (2), (3), and (4) are similar to Ohm's law for the conduction of electricity: The interfacial flux density is proportional to $c_{B,0} - c_{B,e}$ which can be regarded as the driving force for the mass transport of the metallic cations to the cathode. It is inversely proportional to the thickness of the diffusion layer which can be regarded as a resistance to the mass transport: The longer the diffusion path the smaller the mass transport rate. By and large, the equivalent thickness δ of the diffusion layer, just as the true thickness, is smaller the more effective the convection is.

It should be noted at this point that the proportionality between $N_{B,e}$ and $c_{B,0} - c_{B,e}$ suggested by the Nernst model applies only if δ is independent of $c_{B,0} - c_{B,e}$. The model by itself does not allow us to decide whether or not this is true. It turns out, however, that this is generally the case, both for convective and convection-free mass transport. A variety of electroanalytical methods (polarography and related techniques) are based upon this fact. However, there are exceptions, such as the case of natural convection, which will be discussed in Section 7.

1.3. Mass Transfer Coefficient

In chemical engineering the proportionality between $N_{B,e}$ and $c_{B,0} - c_{B,e}$ is often expressed in another manner; namely, by means of the mass transfer coefficient k_d

$$N_{B,e} = -k_d (c_{B,0} - c_{B,e}) \quad (5)$$

Comparison of Eqs. (1) and (5) shows that

$$k_d = D_B / \delta \quad (6a)$$

Equation (1) and (5) both show the proportionality between $N_{B,e}$ and $c_{B,0} - c_{B,e}$. However, in the first case it is expressed in terms of a "resistance" δ and in the second case in terms of a "conductivity" k_d . The two representations are equivalent. In this context the thickness of the Nernst fictitious layer can be regarded as being only another way of expressing the mass transfer

coefficient. However, it is more illustrative than the latter and this has probably contributed to its widespread use in electrochemistry so far.

Note that Eqs. (5) and (6a) apply to a case where there is no migration (excess of supporting electrolyte). In the case of a binary electrolyte, the contribution of migration has to be taken into account. From Eq. (3) it follows that

$$N_{B,e} = -D(c_{B,0} - c_{B,e})/\delta + N_{B,e}t_B \quad (6b)$$

The second term on the right-hand side can be regarded as a migration term and the first term as a transport term excluding migration. Since the mass transfer coefficient is usually employed in conjunction with nonelectrolytic systems, we equate the first term $D(c_{B,0} - c_{B,e})/\delta$ to $k_d(c_{B,0} - c_{B,e})$:

$$N_{B,e} = -k_d(c_{B,0} - c_{B,e}) + N_{B,e}t_B \quad (6c)$$

or

$$N_{B,e} = -(1 - t_B)^{-1}k_d(c_{B,0} - c_{B,e}) \quad (6d)$$

In the case of a binary electrolyte the proportionality factor between the total flux density and the concentration differences is not k_d but $(1 - t_B)^{-1}k_d$.

1.4. Application Example for the Nernst Model

The proportionality between $N_{B,e}$ and $c_{B,0} - c_{B,e}$ can be used to derive a relationship describing the current dependence of the concentration overpotential, for example, in the deposition of a metal from a solution containing in addition to the metallic cation B of charge z_B an excess of indifferent electrolyte. We consider the steady state in a convective mass transport system such as that considered in Section 1.1 (see also Figure 5). The equivalent diffusion layer thickness δ is independent of $c_{B,0} - c_{B,e}$. Therefore, if one increases the current density j applied to the electrode, $c_{B,0} - c_{B,e}$ must increase according to Eq. (2). The interfacial concentration $c_{B,e}$ thus decreases at increasing current density and drops to zero at the limiting current density j_{lim} . The latter is thus given by

$$j_{\text{lim}} = -z_B F D_B c_{B,0} / \delta \quad (7)$$

On the other hand, below the limiting current one may apply Eq. (2). Now the concentration overpotential η_c is given by†

$$\eta_c = \frac{RT}{z_B F} \ln \frac{c_{B,e}}{c_{B,0}} = \frac{RT}{z_B F} \ln \left(1 - \frac{c_{B,0} - c_{B,e}}{c_{B,0}} \right) \quad (8)$$

† As was pointed out in Section 7.2, Chapter 1, one may wish to include in the concentration overpotential the potential drop across the diffusion layer due to the different mobilities of the diffusing species. However, in the case of an excess of supporting electrolyte, the latter effect is small and Eq. (8) can be used as an approximation for the concentration overpotential, independent of how one wishes to define it.

The bulk concentration $c_{B,0}$ can be eliminated by expressing it through the limiting current with the help of Eq. (7). Combination of Eqs. (2), (7) and (8) yields

$$\eta_c = \frac{RT}{z_B F} \ln \left(1 - \frac{j}{j_{\text{lim}}} \right) \quad (9)$$

This equation gives the relationship between η_c and the current density j . At the limiting current η_c becomes infinite.

This example shows that the Nernst model results in conclusions of practical interest. Its chief weakness is that it is not able to provide any information about the actual value of δ or about its dependence on the hydrodynamic regime or on the flow velocity. This can only be obtained experimentally or by applying the modern theory of hydrodynamics to the problem of convective mass transport.

1.5. Current–Voltage Curve : Limiting Current

In Figure 6 the current density as given by Eq. (9) is plotted schematically as a function of η_c (solid line). It represents the current–voltage curve for steady-state conditions in a stirred electrolyte, in the case where there is only concentration overpotential due to the slowness of the mass transport. When j approaches j_{lim} , $\ln(1 - j/j_{\text{lim}})$ tends toward $\ln 0$ and η_c increases very fast. One observes on the current–voltage curve a horizontal segment (plateau) that corresponds to the limiting current (see also Section 1, Chapter 1). Except in the case of natural convection (see Section 7.3) the height of the plateau is usually proportional to the bulk concentration $c_{B,0}$ of the species consumed at the electrode (in the example of Section 1.4 to the concentration of metallic ions). One can thus deduce the concentration from an experimental determination of the current–voltage curve. This method is used in electroanalysis.

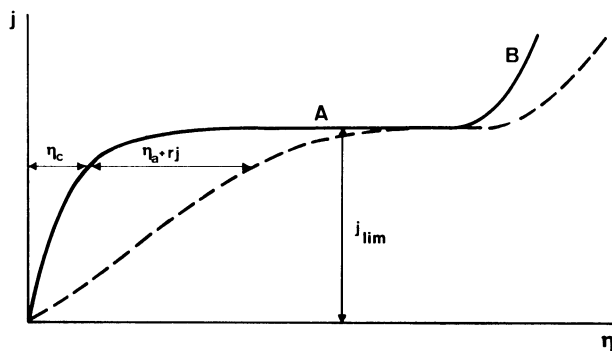


Figure 6. Current–voltage curve: —, for a concentration overpotential only; ---, with activation overpotential and ohmic drop in addition.

The length of plateau A is limited by the occurrence of an additional reaction. In the example of Section 1.4 the first reaction is the deposition of metal, for example, copper. Once the potential is sufficiently negative, there is, in addition, hydrogen evolution and the total current increases over the value of j_{lim} (which corresponds to the maximum rate of mass transport of Cu^{2+} toward the cathode at $c_{\text{Cu}^{2+},e} = 0$ (part B of the curve). In order to observe a well-defined limiting-current plateau, the reversible potentials of the two possible reactions should not be too close. Otherwise, the plateau is too short and eventually disappears.

Another reason for a smearing of the curve is the occurrence of overpotentials other than concentration overpotential (e.g. activation overpotential η_a due to the slowness of the charge exchange reaction at the interface). This overpotential adds itself to η_c and one obtains the broken line of Figure 6. Furthermore, even if a Luggin capillary with reference electrode is used for the measurement of the electrode potential (see Chapter 2, Volume x), there is an ohmic drop in the solution close to the working electrode, which is included in the potential measurement. This causes a further shift of the measured current–voltage curve to the right. Such effects decrease the accuracy of the determination of the limiting current and often smear out the curve to such an extent that virtually no measurable plateau is obtained even if the reversible potentials of the competing reactions are quite different. In electroanalysis, one minimizes these effects by using solutions that are dilute with respect to the species reacting at the electrode and concentrated with respect to indifferent (nonreacting) species. This strongly decreases both components of the ohmic drop rj —the resistance r through the high concentration of indifferent electrolyte, the current density j through the small concentration of the reacting species. Furthermore, in electroanalysis, mercury electrodes are often used because in this case η_a for most reactions (but not for hydrogen evolution) is much smaller than at solid electrodes.

In order to obtain accurately measurable limiting currents, the hydrodynamic conditions must be well defined. A popular arrangement is the rotating disk electrode (see Section 11).

1.6. Historical Note

The application of hydrodynamic theory to electrochemical systems started only after World War II. It has been fostered by the early and detailed work of Levich.^(3,4) Further pioneer papers are those by Wagner⁽⁵⁾ who calculated in 1949 the limiting current for vertical electrodes under the condition of natural convection, by Wilke, Eisenberg and Tobias⁽⁶⁾ who determined experimentally in 1954 the influence of the relevant hydrodynamic parameters on the limiting current in natural convection and at rotating cylinders. In 1947 Agar⁽⁷⁾ and in 1955 Ibl⁽⁸⁾ applied dimensional analysis to electrochemical systems. Ibl, Barrada, and Trümpler⁽⁹⁾ in 1954 measured

interferometrically the thickness of the diffusion layer in electrolysis with natural convection and showed it to be in good agreement with theory. In 1954 Vielstich⁽¹⁰⁾ discussed the relationship between the diffusion layer and the hydrodynamic boundary layer. Later, the Berkeley School (Tobias, Newman, and others) contributed decisively to the further development of the application of hydrodynamic theory to electrochemical systems. Many other authors published in the field in the last 20 years. At least part of this work will be quoted in the following sections as well as in Chapters 5 and 6.

The theoretical approach to convective mass transport in electrolytic systems will be sketched in the next sections.

2. Theoretical Approach Based on Fundamental Equations

2.1. Basic Equations

In this section, as well as in all other sections of this Chapter, we will restrict ourselves to the case of an ideal dilute solution and consider a situation where the electric potential can be eliminated from the basic equations. As has been pointed out in Section 5.1 of Chapter 1, this simplification is strictly valid in the two limiting cases of (a) a single (binary) electrolyte solution and (b) an electroactive species present in small concentration compared to the overall concentration (excess of indifferent electrolyte).

The fundamental equations for the flux density under these conditions have been established in Sections 3.2 and 5.1 of Chapter 1 [see, in particular, Eq. (53)]:

$$\mathbf{N}_B = -D_B \nabla c_B + c_B \mathbf{v} \quad (\text{case b}) \quad (10)$$

$$\mathbf{N}_+ = -D \nabla c_+ + \mathbf{v} c_+ + \frac{\mathbf{j}_+}{z_+ F} \quad (\text{case a}) \quad (11)$$

where D_B and D are the diffusion coefficients of the minority species and of the neutral electrolyte [Eq. (54)], respectively. The subscript + refers to the cations. A relationship similar to (11) holds for the anions. The first terms on the right-hand side of Eq. (10) and (11) correspond to mass transport by diffusion; the second terms correspond to mass transport by convection, and the third term in Eq. (11) to mass transport by electric migration.

The equation expressing the conservation of mass in an incompressible liquid can be written [Eqs. (49) and (55) of Section 5.1, Chapter 1]

$$\frac{\partial c}{\partial t} = D \nabla^2 c - \mathbf{v} \cdot \nabla c + \sum_r v_r^* \quad (\text{case a}) \quad (12)$$

$$\frac{\partial c_B}{\partial t} = D_B \nabla^2 c_B - \mathbf{v} \cdot \nabla c_B + \sum_r v_{B,r}^* \quad (\text{case b}) \quad (13)$$

c_B and c are the concentrations of the minority species and of the neutral electrolyte, respectively. $\partial c/\partial t$ is the change of concentration with time at a given point of the solution. On the right-hand side, the first term is the change in the diffusion flux density over a volume element around the point considered (Figure 4); the second term is the change in convective flux density and $\sum_r v_B^*$ is a source term, taking into account the generation or consumption of the species considered by a chemical reaction taking place in the diffusion layer.

Note that Eqs. (12) and (13) are formally identical. In the following we will retain only Eq. (13) (excess of indifferent electrolyte), it being understood that the equation can be used also for a single electrolyte (with a somewhat different meaning of the diffusion coefficient). In the following sections we will consider cases where the steady state is established and there are no chemical reactions taking place in the diffusion layer. Equation (13) thus reduces to

$$D_B \nabla^2 c_B = \mathbf{v} \cdot \nabla c_B \quad (14)$$

or, written in Cartesian coordinates

$$D_B \left(\frac{\partial^2 c_B}{\partial x^2} + \frac{\partial^2 c_B}{\partial y^2} + \frac{\partial^2 c_B}{\partial z^2} \right) = v_x \frac{\partial c_B}{\partial x} + v_y \frac{\partial c_B}{\partial y} + v_z \frac{\partial c_B}{\partial z} \quad (15)$$

It is seen that in the steady state, in the absence of a chemical reaction, the change in the diffusion flux [left-hand side Eq. (15)] is compensated by the change in the convective flux (right-hand side). This effect has been discussed in a more illustrative manner in Section 1.1.

In order to obtain the quantities of practical interest (i.e., the limiting current or the current density at a given value of the concentration overpotential, the interfacial concentration, and the concentration overpotential at a given current density), Eq. (14) must be integrated with the appropriate boundary conditions (see Section 8, Chapter 1). This requires knowledge of the velocity field [$\mathbf{v} = f(x, y, z)$]. In a complete *ab ovo* calculation, this field can be obtained by integrating the continuity equations and Navier–Stokes equations which have been presented in Section 2.6 of Chapter 1 for an incompressible Newtonian liquid [Eqs. (14) and (15a)]. For a dilute solution, we can equate the mass average velocity \mathbf{v}_b to the velocity of the solvent and thus write Eq. (14) and (15a) of Chapter 1 in the form

$$\nabla \cdot \mathbf{v} = \frac{\partial v_x}{\partial x} + \frac{\partial v_y}{\partial y} + \frac{\partial v_z}{\partial z} = 0 \quad (\text{continuity equation}) \quad (16)$$

$$\frac{\partial(\rho \mathbf{v})}{\partial t} = -\mathbf{v} \cdot \nabla(\rho \mathbf{v}) + \nu \nabla^2(\rho \mathbf{v}) - \nabla p + \rho \mathbf{g} \quad (\text{Navier–Stokes equation}) \quad (17)$$

where ρ is the density of the liquid and ν the kinematic viscosity ($\text{m}^2 \text{s}^{-1}$), ∇p is the gradient of the hydrostatic pressure, and $\rho \mathbf{g}$ the force of gravity per unit volume. $\partial(\rho \mathbf{v})/\partial t = \rho \partial \mathbf{v}/\partial t$ represents the change of flow velocity with time at a given point of the solution.

Equation (17) follows from Newton's law of motion, expressed as the principle of conservation of momentum. The latter is a vector and Eq. (17) involves the gradient of this vector. Thus, the equation has a tensorial character. However, we can reduce it to a vectorial form similar to that of the equation of conservation of matter [Eq. (14)] by writing Eq. (17) in terms of the components v_x , v_y , v_z of the velocity vector.

$$\begin{aligned} \frac{\partial(\rho v_x)}{\partial t} = \nu \left[\frac{\partial^2(\rho v_x)}{\partial x^2} + \frac{\partial^2(\rho v_x)}{\partial y^2} + \frac{\partial^2(\rho v_x)}{\partial z^2} \right] \\ - v_x \frac{\partial(\rho v_x)}{\partial x} - v_y \frac{\partial(\rho v_x)}{\partial y} - v_z \frac{\partial(\rho v_x)}{\partial z} - \frac{dp_x}{dx} + \rho g_x \end{aligned} \quad (17a)$$

$$\begin{aligned} \frac{\partial(\rho v_y)}{\partial t} = \nu \left[\frac{\partial^2(\rho v_y)}{\partial x^2} + \frac{\partial^2(\rho v_y)}{\partial y^2} + \frac{\partial^2(\rho v_y)}{\partial z^2} \right] \\ - v_x \frac{\partial(\rho v_y)}{\partial x} - v_y \frac{\partial(\rho v_y)}{\partial y} - v_z \frac{\partial(\rho v_y)}{\partial z} - \frac{dp_y}{dy} + \rho g_y \end{aligned} \quad (17b)$$

$$\begin{aligned} \frac{\partial(\rho v_z)}{\partial t} = \nu \left[\frac{\partial^2(\rho v_z)}{\partial x^2} + \frac{\partial^2(\rho v_z)}{\partial y^2} + \frac{\partial^2(\rho v_z)}{\partial z^2} \right] \\ - v_x \frac{\partial(\rho v_z)}{\partial x} - v_y \frac{\partial(\rho v_z)}{\partial y} - v_z \frac{\partial(\rho v_z)}{\partial z} - \frac{dp_z}{dz} + \rho g_z \end{aligned} \quad (17c)$$

In Eqs. (17a)–(17c) the Navier–Stokes relationship has been written in such a way that the analogy with the equation for the conservation of mass [Eq. (13)] is particularly striking. We will return to this interesting and important aspect in Section 4. We will also discuss in that connection the physical meaning of the various terms of Eqs. (17a)–(17c).

In many cases the terms ∇p and $\rho \mathbf{g}$ approximately cancel (as in hydrostatics). We will further restrict ourselves to steady-state conditions where the velocity field is independent of time, i.e., $\partial(\rho \mathbf{v})/\partial t = 0$. Equations (17a) and (17b) thus reduce to

$$\nu \left[\frac{\partial^2(\rho v_x)}{\partial x^2} + \frac{\partial^2(\rho v_x)}{\partial y^2} + \frac{\partial^2(\rho v_x)}{\partial z^2} \right] = v_x \frac{\partial(\rho v_x)}{\partial x} + v_y \frac{\partial(\rho v_x)}{\partial y} + v_z \frac{\partial(\rho v_x)}{\partial z} \quad (18a)$$

$$\nu \left[\frac{\partial^2(\rho v_y)}{\partial x^2} + \frac{\partial^2(\rho v_y)}{\partial y^2} + \frac{\partial^2(\rho v_y)}{\partial z^2} \right] = v_x \frac{\partial(\rho v_y)}{\partial x} + v_y \frac{\partial(\rho v_y)}{\partial y} + v_z \frac{\partial(\rho v_y)}{\partial z} \quad (18b)$$

with a similar equation for the z component of \mathbf{v} .

The velocity field is obtained by integrating Eqs. (17) or (18) with the appropriate boundary conditions (usually $\mathbf{v} = 0$ at the electrode surface). The values of v so obtained are introduced into Eqs. (12) and (13) or (15) and the latter are then integrated. In spite of the simplified situation considered in Eqs. (15) and (18) (steady state, absence of chemical reaction, elimination

of the electric field), the integration of these differential equations is, because of their nonlinear character, a formidable affair, even in the era of the computer. Additional simplifications are usually made.

2.2. Prandtl Boundary-Layer Simplifications

Decisive progress in the integration of the Navier–Stokes equation was made around 1904 when Prandtl introduced the boundary-layer simplifications which are today named after him. The leading idea is as follows. The thickness of the diffusion layer and of the hydrodynamic boundary layer is very small compared to the dimensions of the interface; i.e., in the example of Figure 2 δ and δ_v are small compared to the width and length of the electrode. Therefore, the average concentration gradient $\partial c_B/\partial y$ in the direction perpendicular to the electrode is very much larger than those in the directions parallel to the electrode, $\partial c_B/\partial x$ and $\partial c_B/\partial z$. We can thus also write $\partial^2 c_B/\partial y^2 \gg \partial^2 c_B/\partial x^2$ and $\partial^2 c_B/\partial y^2 \gg \partial^2 c_B/\partial z^2$, so that the terms $\partial^2 c_B/\partial x^2$ and $\partial^2 c_B/\partial z^2$ in Eq. (15) can be neglected. The same argument shows that $\partial^2(\rho v_x)/\partial x^2$, $\partial^2(\rho v_x)/\partial z^2$, $\partial^2(\rho v_y)/\partial x^2$, and $\partial^2(\rho v_y)/\partial z^2$ can be dropped in the Navier–Stokes equation [Eq. (17a), (17b), (18a), and (18b)]. Furthermore, some of the terms involving the first derivatives of the concentration and of the velocity with respect to distance can be neglected.

The validity of the boundary-layer simplifications can be verified *a posteriori* by assuming them as a first approximation and by checking that the solution obtained yields very thin diffusion and hydrodynamic boundary layers.

In the next section we will apply the boundary-layer simplifications to the quantitative treatment of mass transfer to a plane electrode in laminar flow. Further simplifications arise here, because c_B and \mathbf{v} are virtually constant in the z direction perpendicular to the flow and parallel to the electrode. Equation (15) thus reduces to

$$D_B \frac{\partial^2 c_B}{\partial y^2} = v_x \frac{\partial c_B}{\partial x} + v_y \frac{\partial c_B}{\partial y} \quad (19)$$

For a constant fluid density the momentum equation pertaining to this flow system, Eq. (18a), reduces to

$$\nu \frac{\partial^2 v_x}{\partial y^2} = v_x \frac{\partial v_x}{\partial x} + v_y \frac{\partial v_x}{\partial y} \quad (20)$$

Before we proceed with the quantitative treatment of our example, let us point out that the theoretical approach outlined above is based on differential equations from which the electric potential has been eliminated (see Section 5, Chapter 1). *The peculiarity of the electrochemical systems is thus lacking in these equations.* The only aspect specific to electrochemistry arises in the connection of the interfacial flux density with the electrode

current, which has been discussed in Section 4.2 of Chapter 1 and which will be recalled occasionally in the next sections. It is thus possible to readily transpose to electrochemistry the numerous empirical or theoretical mass transport correlations that have been established in physical chemistry or chemical engineering at large. In principle, it would suffice to refer to the pertinent textbooks⁽¹¹⁻¹⁶⁾ and be content here to deal with a few specific aspects, such as the connection between the interfacial concentration gradient and electrode current or the experimental methodology for the electrochemical determination of mass transport coefficients. Nevertheless, we will discuss in the following section the theory of some hydrodynamic systems of particular interest to electrochemists. It should be understood that, for many flow systems not mentioned here, the nonelectrolytic correlations can be applied. Finally, we will devote some attention in Section 6 to the theoretically very complicated case intermediate between the solution of a single electrolyte and an excess of indifferent electrolyte, where the electric potential cannot be eliminated from the basic equations and which thus has specifically electrochemical features.

2.3. Mass Transfer to a Plate in Laminar Flow

We consider a plane electrode along which an electrolyte flows in parallel flow. From the leading edge ($x = 0$) a diffusion layer and a hydrodynamic boundary layer develop (Figure 2). The mass transport to the electrode is calculated by integrating the mass conservation equation by the method outlined in Section 8.2 of Chapter 1. We assume the situation to be such that the requirements for the validity of Eq. (19) enumerated in Sections 2.1 and 2.2 (boundary-layer simplifications, ideal dilute solution, steady state, excess of supporting electrolyte, etc.) are fulfilled with a sufficient approximation. Equation (19) is thus our starting differential equation. The boundary conditions for its integration depend on the experimental situation. We consider the case of an electrolysis with a prescribed, constant interfacial concentration of the species B consumed (or generated) at the electrode.† Outside of the diffusion layer there is a uniform concentration, $c_{B,0}$. The boundary conditions are

$$x = 0: \quad c_B = c_{B,0} \quad (21a)$$

$$y \rightarrow \infty: \quad c_B = c_{B,0} \quad (21b)$$

$$y = 0: \quad c_B = c_{B,e} \quad (21c)$$

The profiles of the velocity components v_x and v_y in the neighborhood of the

† This case is realized at the limiting current or, more generally, in a potentiostatic experiment (i.e., at a constant electrode potential, independent of x) in the absence of any overpotentials other than concentration overpotential. For a more detailed discussion of the boundary conditions the reader is referred to Section 8.1 of Chapter 1.

electrode are obtained from the integration of the Navier–Stokes equation (20) together with the continuity equation:

$$\frac{\partial v_x}{\partial x} + \frac{\partial v_y}{\partial y} = 0 \quad (22)$$

We consider the case where the hydrodynamic boundary layer is thin compared to the distance between the electrodes. That is, there is a region outside the boundary layer where the flow velocity v_0 is uniform. We further note that the flow velocity is zero at a stationary solid interface because of the friction forces (see beginning of Section 1.1). Therefore the boundary conditions for the integration of Eqs. (20) and (22) are

$$x = 0: \quad v_x = v_0 \quad (23a)$$

$$y = \infty: \quad v_x = v_0 \quad (23b)$$

$$y = 0: \quad v_x = 0 \quad (23c)$$

The main difficulty in the integration of a set of equations such as (19), (20), and (22) is their partial differential character involving two spatial coordinates, x and y . However, it is often possible to reduce such partial differential equations to ordinary ones by introducing a dimensionless group, also called *similarity variable*. It combines the effect of the two independent variables x and y , thus reducing the number of variables of the problem (see also Section 3). With an appropriate choice, the dependent variables (v_x , v_y , c_B) may become functions of the above similarity variable only.†

The starting point is the generally accepted fact that in such boundary layers the velocity and also the concentration profiles at various points along the plate are similar. Therefore, the velocity and concentration at any point along the plate should be a unique function of a normalized wall distance $\eta = y/\delta$. In order to determine how the boundary-layer thickness δ depends on the relevant parameters, we make an order-of-magnitude analysis of the momentum equation (20). If we linearize $v_y = f(y)$ the derivative $\partial v_y/\partial y$ is equal to $v_{y=\delta}/\delta$, and this is the order of magnitude of $\partial v_y/\partial y$. Similarly, $\partial v_x/\partial x$ is of the order of $(v_0 - v_x)/x \approx v_0/x$ (v_x is small as compared to v_0 over most of the boundary layer). We may thus write Eq. (22) in the approximate form:

$$\frac{v_0}{x} + \frac{v_y}{\delta} \approx 0 \quad (24)$$

from which we obtain

$$v_{y=\delta} \approx \frac{v_0 \delta}{x} \quad (25)$$

v_y is also of this order of magnitude.

† The reader interested in a detailed treatment of the flat-plate problem is referred to Schlichting's book.⁽²¹⁾ An approximate solution of the mass transport problem for the flat plate using the von Karman–Pohlhausen integral method has been given by Wranglen.⁽¹⁷⁾

Finally, using these orders of magnitude, the analysis of the momentum equation yields

$$v_0 \frac{v_0}{x} + \frac{v_0 \delta}{x} \frac{v_0}{\delta} \approx \nu \frac{v_0}{\delta^2}$$

or

$$\delta \sim \left(\frac{\nu x}{v_0} \right)^{1/2} \tag{26}$$

With this expression our similarity variable becomes

$$\eta = y(v_0/\nu x)^{1/2} \tag{27}$$

We now introduce it into the mass transfer boundary-layer equation (19) in order to reduce it to an ordinary differential equation. We further define a dimensionless concentration

$$C_B = \frac{c_B - c_{B,e}}{c_{B,0} - c_{B,e}} \tag{28}$$

Finally we profit from the fact that the solution of the flow problem of the flat plate is known. We can express the velocity components v_x and v_y in terms of a function f of the similarity variable η :

$$v_x = v_0 f \tag{29}$$

$$v_y = \frac{1}{2} v_0 \left(\frac{v_0}{\nu x} \right)^{-1/2} x^{-1} \left(\eta f - \int_0^\eta f d\eta \right) \tag{30}$$

where Eqs. (29) and (30) satisfy the continuity equation.

With the definition of the similarity variable η [Eq. (27)], the derivatives of the concentration in Eq. (19) become

$$\frac{\partial c_B}{\partial x} = -\frac{1}{2} x^{-1} (c_{B,0} - c_{B,e}) C'_B \tag{31a}$$

$$\frac{\partial c_B}{\partial y} = \left(\frac{v_0}{\nu x} \right)^{1/2} (c_{B,0} - c_{B,e}) C'_B \tag{31b}$$

$$\frac{\partial c_B}{\partial y^2} = v_0 \nu^{-1} x^{-1} (c_{B,0} - c_{B,e}) C''_B \tag{31c}$$

where the primes denote differentiation with respect to η . With Eqs. (28)–(31c) inserted into (19) the mass transport boundary-layer equation becomes

$$C''_B - \frac{1}{2} Sc C'_B \int_0^\eta f d\eta = 0 \tag{32}$$

where $Sc = \nu/D_B$ is the dimensionless Schmidt number. With the boundary conditions

$$C_B = 0, \quad \text{at } \eta = 0 \quad (33a)$$

$$C_B = 1, \quad \text{at } \eta \rightarrow \infty \quad (33b)$$

the complete solution of Eq. (32) is

$$C_B = \frac{\int_0^\eta \exp\left[-\frac{Sc}{2} \int_0^\eta \left(\int_0^\eta f d\eta\right) d\eta\right] d\eta}{\int_0^\infty \exp\left[-\frac{Sc}{2} \int_0^\eta \left(\int_0^\eta f d\eta\right) d\eta\right] d\eta} \quad (34)$$

As already mentioned earlier the hydrodynamic problem of the plate has been solved and the generalized velocity profile $f(\eta)$ is available in the form of tables.^(18,19) This allows Eq. (34) to be integrated numerically. Figure 7 shows the concentration profiles obtained by Eckert and Drewitz⁽²⁰⁾ in dimensionless form for different values of the Schmidt number.

As one can see in Figure 7 the diffusion layer becomes thinner with increasing Schmidt numbers. This is not only the case for the flow along a plate but is true for other geometries as well. We will discuss this in more detail in Section 4. For the moment, let us note that at high Sc values (as

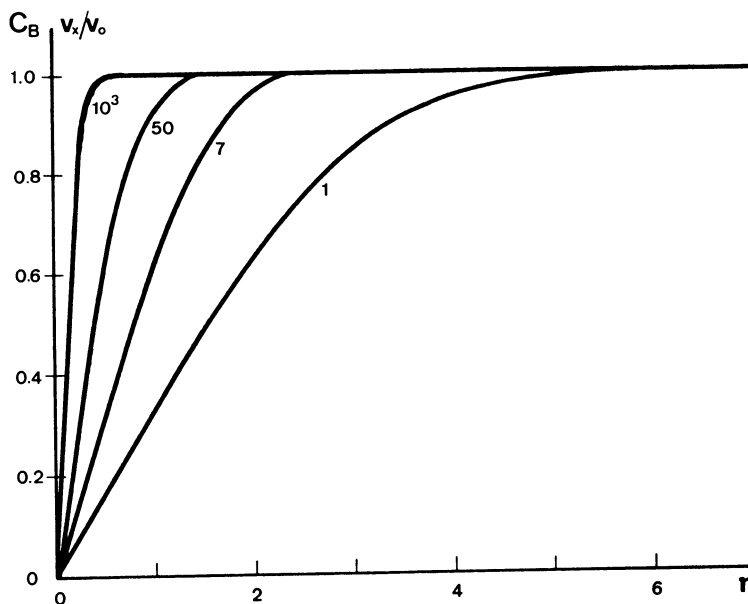


Figure 7. Dimensionless concentration profiles at the plate electrode. Parameter is the Schmidt number. The curve for $Sc = 1$ also represents the velocity profile.

they prevail in aqueous solutions) the thickness of the diffusion layer is much smaller than that of the hydrodynamic boundary layer. The diffusion layer lies entirely within a practically linear part of the velocity profile, and therefore the latter can in our calculation be approximated by the first term of its Taylor expansion in the dimensionless distance η :

$$f(\eta) \approx \left[\frac{\partial f(\eta)}{\partial \eta} \right]_{\eta=0} \times \eta \quad (35)$$

The value of the slope of the velocity profile at the origin is $0.332^{(21)}$

$$f(\eta) \approx 0.332\eta \quad (36)$$

With this approximation the concentration profile (34) becomes

$$C_B = \frac{\int_0^\eta \exp(-2.77 \times 10^{-2} Sc \eta^3) d\eta}{\int_0^\infty \exp(-2.77 \times 10^{-2} Sc \eta^3) d\eta} \quad (37)$$

The integral in the denominator can be expressed in terms of a gamma function if we make the following substitution:

$$t = 2.77 \times 10^{-2} Sc \eta^3 \quad (38)$$

Then

$$\int_0^\infty \exp(-2.77 \times 10^{-2} Sc \eta^3) d\eta = (2.77 \times 10^{-2} Sc)^{-1/3} \frac{1}{3} \int_0^\infty t^{-2/3} \exp(-t) dt \quad (39)$$

With

$$\frac{1}{3} \int_0^\infty t^{-2/3} \exp(-t) dt = \frac{1}{3} \Gamma\left(\frac{1}{3}\right) = \Gamma\left(\frac{4}{3}\right) = 0.893 \quad (40)$$

Eq. (37) becomes

$$C_B = 0.339 Sc^{1/3} \int_0^\eta \exp(-2.77 \times 10^{-2} Sc \eta^3) d\eta \quad (41)$$

Frequent use of this kind of approximation is made in the calculation of concentration profiles in laminar convective diffusion systems. It can be applied if the diffusion layer is thin compared to the hydrodynamic boundary layer, which is the case at high Schmidt numbers. The possibility of replacing the generally complicated velocity profiles by a simple function (in many cases a straight line) allows us to simplify the convection terms in the conservation equation and to make its integration considerably easier.

Let us now evaluate the interfacial flux density $N_{B,e}$ of the species B which is the quantity of practical interest in our problem, since it is related directly to the electrolysis current density. We can disregard convection because at a solid electrode surface the interfacial flow velocity is zero, and

therefore the contribution of convection to mass transport vanishes. The diffusion flux is [Eq. (1)]

$$N_{B,e} = N_{\text{diff}} = -D_B \left(\frac{\partial c_B}{\partial y} \right)_e \quad (1)$$

or in terms of our dimensionless variables C_B and η [Eqs. (27), (28), and (31b)],

$$N_{B,e} = -D_B \frac{\partial \eta}{\partial y} (c_{B,0} - c_{B,e})(C'_B)_e \quad (42)$$

The dimensionless concentration gradient at the surface is obtained by differentiating Eq. (34):

$$(C'_B)_e = \frac{\left\{ \exp \left[-\frac{\text{Sc}}{2} \int \left(\int_0^\eta f d\eta \right) d\eta \right] \right\}_e}{\int_0^\infty \exp \left[-\frac{\text{Sc}}{2} \int \left(\int_0^\eta f d\eta \right) d\eta \right] d\eta} \quad (43)$$

The gradient depends on the Schmidt number in a complicated way. However, we can again simplify the problem by means of the high-Schmidt-number approximation. We replace Eq. (34) by (41):

$$(C'_B)_e = 0.339 \text{Sc}^{1/3} [\exp(-2.77 \times 10^{-2} \text{Sc} \eta^3)]_e \quad (44)$$

For the interface, $\eta = 0$ and the term in parentheses is 1. We get

$$(C'_B)_e = 0.339 \text{Sc}^{1/3} \quad (45)$$

Introducing (45) into (42),

$$N_{B,e} = -0.339 D_B \text{Sc}^{1/3} (c_{B,0} - c_{B,e}) \frac{\partial \eta}{\partial y} \quad (46)$$

and finally, taking into account the definition of η [Eq. (27)] and of the Schmidt number, $\text{Sc} = \nu/D_B$, we get

$$N_{B,e} = -0.339 (c_{B,0} - c_{B,e}) D_B^{2/3} \nu^{-1/6} v_0^{1/2} x^{-1/2} \quad (47)$$

Equation (47) gives the mass flux density toward the electrode. $N_{B,e}$ is a local value; it decreases downstream with the square root of the distance from the leading edge. This behavior is, of course, linked with the fact that, due to friction, convection becomes more and more ineffective downstream—a fact we have already discussed qualitatively in Section 1.1. The result of our calculation is also in accordance with the Nernst model (see Section 1) in that the mass transfer rate is proportional to the concentration difference between the bulk and the interface. We can therefore calculate the thickness of the Nernst diffusion layer δ and the mass transfer coefficient k_d from (47), (1), and (5):

$$\delta = 2.95 (D_B/\nu)^{1/3} (\nu x/v_0)^{1/2}; \quad k_d = 0.339 D_B (\nu/D_B)^{1/3} (v_0/\nu x)^{1/2} \quad (48a)$$

Corresponding to the decrease of the flux density the thickness of the diffusion layer increases downstream.

As pointed out previously, these results are valid for higher Schmidt numbers. At lower values of Sc the dependence of $N_{B,e}$, δ , and k_d on Sc is more complicated. However, the influence of Sc is not very large. For instance, at $Sc \approx 1$ a good approximation for δ and k_d is⁽²¹⁾

$$\delta = 3.01(D_B/\nu)^{1/3}(\nu x/v_0)^{1/2}; \quad k_d = 0.332D_B(\nu/D_B)^{1/3}(v_0/\nu x)^{1/2} \quad (48b)$$

Let us finally calculate the average flux density $\bar{N}_{B,e}$ over a plate of length l :

$$\bar{N}_{B,e} = l^{-1} \int_0^l N_{B,e} dx \quad (49)$$

With the expression for the local flux density (47),

$$\bar{N}_{B,e} = -0.678(c_{B,0} - c_{B,e})D_B^{2/3}\nu^{-1/6}v_0^{1/2}l^{-1/2} \quad (50)$$

We have assumed at the beginning that species B are consumed in an electrochemical reaction at the interface. The treatment of the problem so far has had no particular electrochemical features due to the assumption of an excess of indifferent electrolyte. We can now use the *nonelectrolytic* solution of the mass transport equation to calculate the average electric current density at an electrode with a constant interfacial concentration:

$$\bar{j} = z_B F \bar{N}_{B,e} \quad (51)$$

Introducing (50) into this equation,

$$\bar{j} = -0.678z_B F(c_{B,0} - c_{B,e})D_B^{2/3}\nu^{-1/6}v_0^{1/2}l^{-1/2} \quad (52)$$

(We can of course obtain the local current density j exactly the same way by multiplying $N_{B,e}$ by $z_B F$).

The total current I at an electrode of length l and width b is given by

$$I = \bar{j}lb \quad (53)$$

$$I = -0.678z_B F(c_{B,0} - c_{B,e})D_B^{2/3}\nu^{-1/6}v_0^{1/2}bl^{1/2} \quad (54)$$

Note that Eqs. (52) and (54) apply only to the case of the discharge of cations of charge z_B at the cathode from a solution with an excess of supporting electrolyte (see Sections 1.2 and 5.4, Chapter 1). For more complicated electrode reactions (including redox processes) one has to use instead of Eqs. (51) and (1) the more general equations (64) and (31) of Chapter 1. For a metal deposition from a binary electrolyte, Eq. (52) becomes [because of Eq. (65) of Chapter 1]

$$\bar{j} = -0.678(1 - t_B)^{-1}z_B F(c_{B,0} - c_{B,e})D^{2/3}\nu^{-1/6}v_0^{1/2}l^{-1/2} \quad (52')$$

where D is the diffusion coefficient of the neutral electrolyte.

Let us complete this section by a brief outline of the solution of the flat-plate problem for the case of a uniform electrode current density. In Section 8 of Chapter 1 the possibility of realizing such a condition was discussed. Usually it corresponds to a constant-current experiment well below the limiting current. In this case, the interfacial concentration is the quantity of practical interest since it allows us to calculate the electrode potential. The situation regarding the hydrodynamics and mass transport mechanisms in the boundary layer is exactly the same as in the example treated above. Therefore we have to solve the same set of differential equations [(19), (21), (22)]. The only difference concerns the boundary condition (21c): Instead of a constant interfacial concentration of B we now have a constant interfacial concentration gradient which is given by the imposed current density. Thus, the new boundary condition is

$$\frac{dc_B}{dy} = -j(z_B F D_B)^{-1} \quad \text{at } y = 0 \quad (55)$$

For the solution of this problem we define the dimensionless concentration as

$$C_B = \frac{c_B}{c_{B,0}} \quad (56)$$

With this definition, the dimensionless differential equation and the boundary condition describing the situation far from the electrode have the same form as in the previous treatment [Eqs. (32) and (33b)]. The dimensionless form of boundary condition (55) is

$$C'_B = -j(z_B F D_B c_{B,0})^{-1} (v_0/\nu x)^{-1/2} \quad \text{at } \eta = 0 \quad (55')$$

With the linear approximation for the dimensionless velocity profile (35) (high Schmidt number), the integration of Eq. (32) with boundary conditions (33b) and (55') yields the following concentration profile:

$$C_B = 1 + j(z_B F D_B c_{B,0})^{-1} \left(\frac{v_0}{\nu x}\right)^{-1/2} \int_{\eta}^{\infty} \exp(-2.77 \times 10^{-2} \text{Sc } \eta^3) d\eta \quad (57)$$

The integral can be split into two parts, one of which can be expressed in terms of a gamma function [see Eqs. (38)–(40)]. Equation (57) then takes the form

$$C_B = 1 + j(z_B F D_B c_{B,0})^{-1} \left(\frac{v_0}{\nu x}\right)^{-1/2} \times \left[2.951 \text{Sc}^{-1/3} - \int_0^{\eta} \exp(-2.77 \times 10^{-2} \text{Sc } \eta^3) d\eta \right] \quad (58)$$

Since we wish to calculate the interfacial concentration of B we have to evaluate the integral in (58) for $\eta = 0$. Replacing the integrand by its Taylor

expansion about the origin yields

$$\int_0^{\eta} \exp(-2.77 \times 10^{-2} \text{Sc} \eta^3) d\eta = \eta \quad (59)$$

Inserting (59) into (58), setting $\eta = 0$, and remembering the definitions of C_B and Sc , we finally obtain for the interfacial concentration of c_B :

$$c_{B,e} = c_{B,0} + 2.95j(z_B F)^{-1} D_B^{-2/3} \nu^{1/6} v_0^{-1/2} x^{1/2} \quad (60)$$

Equation (60) describes the *variation of the interfacial concentration of species B with the relevant parameters for a given electrode current density*. In particular, it shows that this concentration varies along the electrode. For example, for a cathodic reaction the current density has a negative sign (Section 5, Chapter 1) and $c_{B,e}$ can be shown to decrease downstream. This result corresponds to the decrease in current density along the plate in the constant-potential experiment [Eq. (47)]. In the latter case (constant-potential) the increasing depletion of the diffusion layer results in a decrease of the interfacial flux density, whereas in the former case (constant-current) a decrease of the interfacial concentration is needed in order that the driving concentration gradient at the interface can be maintained constant.

3. Dimensional Analysis

3.1. Principle

When the hydrodynamic conditions are complex, a complete calculation starting from the basic equations is too cumbersome or not possible even in the computer era. This applies, in particular, to the turbulent-flow regime (see Section 5). Experimental or semiempirical correlations then have to be used. A great help in establishing them is provided by dimensional analysis.⁽²²⁻²⁸⁾ The leading idea is as follows. Any equation that describes properly a physical phenomenon must be so constructed that calculations made with it are independent of the size of the fundamental units which have been arbitrarily introduced by man to measure mass, length, and time. The equation must remain valid independently of whether we have expressed the length in millimeters or kilometers, the time in seconds or centuries. Consequently, the terms of a physically significant relationship must be homogeneous with respect to the fundamental units. In contrast to the derived units (such as velocity), the fundamental units are those that cannot be reduced to other units and are defined by comparison with a standard. In mechanical or mass transport problems the fundamental units are those of mass (or amount of substance), length, and time.

Let us consider as a simple example the period T of a swinging pendulum. We may expect that the period depends on its length l (m), mass m (kg), and

acceleration of gravity g (m s^{-2}):

$$T = f(m, l, g) \quad (61)$$

There is only one way of writing this equation if it is to be homogeneous; namely,

$$T = K(l/g)^{1/2} \quad (62)$$

It can be easily seen that the mass does not enter into the equation at all; otherwise the period of the pendulum would depend upon whether we express the mass in g or kg. The value of the numerical constant K remains unknown. But, in principle, it can be determined by a single experiment whereas the experimenter who would have approached our problem without the above argument would have had to carry out an incomparably larger number of measurements to obtain Eq. (62). Of course, in the present example it would have been easy to derive expression (62) from the basic equations of mechanics.

The principle which allows us to make a far-reaching statement regarding the relationship in which we are interested will remain valid for any complicated differential equation that we may be unable to integrate. Of course, in order to apply dimensional analysis one must first know the variables in play. However, we hardly ever approach our problem without some prior knowledge. Consciously or unconsciously, we make use of a lot of experience, both ours and that of the generations before us. In mass, heat, and momentum transport the fundamental differential equations, describing the phenomena involved, are well established and the relevant variables are thus determined. Indeed, the applications of dimensional analysis are particularly popular in these fields.

3.2. Dimensionless Groups

Let us now assume in a general way that we know the variables a_2, a_3, \dots, a_j on which a quantity a_1 depends, and let us write the relationship connecting them in the implicit form:

$$f(a_1, a_2, \dots, a_j) = 0 \quad (63)$$

It is shown in dimensional analysis that if this equation is independent of the size of the fundamental units, it must be possible to write it in terms of new dimensionless variables A_1, A_2, \dots, A_i

$$F(A_1, A_2, \dots, A_i) = 0 \quad (64)$$

where

$$A_i = a_1^{m_{i1}} a_2^{m_{i2}} \dots a_j^{m_{ij}} \quad (65)$$

The new variables A_i are obtained by multiplying the original variables a_j

Table 1
Dimensional Matrix for Mass Transport to a Plate in Laminar Flow

	M (α)	L (β)	T (γ)
$\bar{N}_{B,e}$	1	-2	-1
$c_{B,0} - c_{B,e}$	1	-3	0
l	0	1	0
v_0	0	1	-1
D_B	0	2	-1
ν	0	2	-1

with each other and raising them to some power (which may be positive, negative, or zero).

The only condition is that the group thus formed is independent of the size of the fundamental units, i.e., is a pure number. If we write the dimensional formula of a_i in the classical way (assuming that the fundamental units are those of mass M, length L, and time T),[†]

$$a_i = M^{\alpha_i} L^{\beta_i} T^{\gamma_i} \tag{66}$$

The condition that A_i is dimensionless requires

$$\sum_j m_{ij} \alpha_j = 0; \quad \sum_j m_{ij} \beta_j = 0; \quad \sum_j m_{ij} \gamma_j = 0 \tag{67}$$

The $\alpha_j, \beta_j, \gamma_j$ of all “dimensional” quantities a_j can be written in the form of a matrix called a dimensional matrix (Table 1).

3.3. π Theorem

An essential question is: How many dimensionless groups A_i have to be introduced instead of the original variables in order to describe the problem entirely? According to the π theorem the necessary number r of dimensionless variables is equal to the number n of the original variables a_j minus the rank p of the dimensional matrix: $r = n - p$. In the majority of cases, the rank of the dimensional matrix is equal to the number of fundamental units, which is three in mass transport problems—i.e., $r = n - 3$.

Note that the π theorem determines only the number of dimensionless groups. In eqs. (67) the $\alpha_j, \beta_j,$ and γ_j are known but not the m_i . For each dimensionless group A_i to be introduced, the number of unknown exponents is equal to n and is usually larger than the number of Eqs. (67) which is equal

[†] The exponents α, β, γ indicate how a derived quantity changes when the size of the fundamental units is changed. For example, for the density $[\rho] = [ML^{-3}]$ the unit of ρ becomes 10 times larger if the unit of the mass is increased by a factor of 10; but it becomes 1000 times smaller if the unit of length is made 10 times larger.

to the number of fundamental units. Therefore, one or more exponents m_i are to be set arbitrarily. The result is that the dimensionless groups for a given problem can be usually selected in a great variety of ways. Their choice is governed by considerations of convenience. For example, it is expedient to have dimensionless groups with m_i values as small as possible. Let us now illustrate the application of dimensional analysis by two examples from the field of mass transport. We will consider mass transport excluding migration in the remaining part of this section; $N_{B,e}$ denotes an interfacial flux density in which migration takes no part.

3.4. Application Examples

Case a: We consider the case of electrolysis with linear diffusion (without convection and migration) to a plane electrode (See section 8, Chapter 2). If the concentration difference $c_{B,0} - c_{B,e}$ between bulk and interface is fixed (controlled-potential experiment), we ask for the variation of the interfacial flux density $N_{B,e}$ with time t . If $N_{B,e}$ is fixed (controlled-current experiment), we ask for the variation of $c_{B,0} - c_{B,e}$ with time. Let us assume that the edge effects are negligible and the diffusion layer can extend indefinitely into the interior of the solution (no influence of a counterwall). Thus, there is no characteristic length involved. Since we ask for the flux density at a certain spot (located at the interface), $N_{B,e}$ is not a function of any length. The same is true of $c_{B,0} - c_{B,e}$. We further know the fundamental differential equation of the problem

$$\frac{\partial c_B}{\partial t} = D_B \frac{\partial^2 c_B}{\partial y^2} \quad (68)$$

which involves the diffusion coefficient D_B . We may thus conclude that there are four relevant variables: $N_{B,e}$ [$\text{ML}^{-2}\text{T}^{-1}$], $c_{B,0} - c_{B,e}$ [ML^{-3}], t [T], and D_B [L^2T^{-1}]. According to the π theorem we need $4 - 3$, i.e., only one dimensionless group A to describe the problem:

$$A = N_{B,e}^{m_1} (c_{B,0} - c_{B,e})^{m_2} t^{m_3} D_B^{m_4} = K = \text{const} \quad (69)$$

Since we have only three equations (67) and four exponents m_i one of them must be set arbitrarily. For the sake of simplicity we write $m_1 = 1$. We thus have

$$1 + m_2 = -2 - 3m_2 + 2m_4 = -1 + m_3 - m_4 = 0 \quad (70)$$

$$A = N_{B,e} (c_{B,0} - c_{B,e})^{-1} t^{1/2} D_B^{-1/2} = K \quad (71)$$

If we remember that $N_{B,e}$ is proportional to the electrolysis current density, it is seen that Eq. (71) is identical with Cottrell's relationship (controlled-potential) and Sand's equation (controlled-current) [Eqs. (60) and (163) of Chapter 2]. Dimensional analysis thus enables us to derive in a very simple way these two important relationships, except for the numerical value of K . This could, in principle, be determined by a single experiment. Or it can be

obtained through the much more difficult integration of Eq. (68). It turns out that K is $\pi^{-1/2}$ in the first case, and $\frac{1}{2}\pi^{-1/2}$ in the second case.

Case b: Our second example is the flat electrode in parallel flow considered in Section 2.3. We are interested in the average interfacial flux density, $\bar{N}_{B,e}$, which establishes itself at a given value of the concentration difference $c_{B,0} - c_{B,e}$ between bulk and interface. $\bar{N}_{B,e}$ is not a function of the coordinates x, y, z and thus we need not take these variables into account. The problem may still depend on certain characteristic lengths, which in our case could be the distance from the counterelectrode and the width and length of the working electrode. If the counterelectrode is sufficiently far away, its distance does not play any role and the electrode width can also be left out for reasons of symmetry provided that the width is sufficiently large. We thus retain only the length l of the working electrode in the direction of the flow.† Inspection of the differential equations for mass and momentum transport [Eqs. (19) and (20)] indicates that as further variables we have the given $c_{B,0} - c_{B,e}$ and the given flow velocity v_0 , the diffusion coefficient D_B and the kinematic viscosity ν . We thus have six variables, the dimensions of which are shown in the dimensional matrix of Table 1. According to the π theorem, we need $6 - 3$, i.e., 3 dimensionless groups of the form

$$A_i = \bar{N}_{B,e}^{m_{i1}} (c_{B,0} - c_{B,e})^{m_{i2}} l^{m_{i3}} v_0^{m_{i4}} D_B^{m_{i5}} \nu^{m_{i6}} \quad (72)$$

We have only three Eqs. (67) to determine the six exponents m_i involved in each of the three A_i ; i.e., we have to set arbitrarily the values of three exponents for each A_i . We select three variables as the main ones and arrange the dimensionless groups in such a way that each of them contains only one of the main variables and this with the power 1. We choose as main variables $\bar{N}_{B,e}$, v_0 , and ν . We thus set

$$m_{11} = 1, \quad m_{14} = m_{16} = 0 \quad (\text{for } A_1)$$

$$m_{21} = m_{26} = 0, \quad m_{24} = 1 \quad (\text{for } A_2);$$

$$m_{31} = m_{34} = 0, \quad m_{36} = 1 \quad (\text{for } A_3)$$

Applying Eqs. (67) we now obtain

$$A_1 = \bar{N}_{B,e} l / D_B (c_{B,e} - c_{B,0}) = \bar{\text{Sh}} \quad (\text{Sherwood number}^\ddagger) \quad (73)$$

$$A_2 = v_0 l / \nu = \text{Re} \quad (\text{Reynolds number}) \quad (74)$$

$$A_3 = \nu / D_B = \text{Sc} \quad (\text{Schmidt number}) \quad (75)$$

† The dependence of $\bar{N}_{B,e}$ on l is also suggested by the general experience of convective mass transport (change of thickness of the hydrodynamic boundary layer along the surface; see Section 1). If one is uncertain about whether a variable is relevant or not, it is safer to include it and to accept the risk that one has unnecessarily increased the number of dimensionless groups by one.

‡ In particular, in the older literature $\bar{\text{Sh}}$ is often called the Nusselt number for mass transport^(8,29,30) and denoted by Nu^* . Note further that in Eq. (73) $\bar{N}_{B,e}$ is the interfacial flux density excluding migration.

The Sherwood number can be regarded as a normalized (or “adimensionalized”) flux density or mass transfer rate, the Reynolds number as a normalized (or “adimensionalized”) flow velocity. The meaning of the Schmidt number will be discussed in Section 4.3.

Instead of the relationship connecting the six original variables

$$f(\bar{N}_{B,e}, (c_{B,0} - c_{B,e}), v_0, l, \nu, D_B) = 0 \quad (76)$$

one can now write

$$F(\bar{Sh}, Re, Sc) = 0 \quad (77)$$

The function $F()$ is not known better than $f()$, but it involves only three variables instead of six. In the case of laminar flow along a plate, the functions $f()$ and $F()$ can be obtained by integrating the fundamental equations. Rewriting Eq. (50) in terms of \bar{Sh} , Re , and Sc we have

$$\bar{Sh} = 0.678 Re^{1/2} Sc^{1/3} \quad (78a)$$

However, in turbulent flow the basic equations are not amenable to an analytical solution and the relationship connecting the variables has to be determined experimentally (see Section 5). Equation (77) is then very much superior to Eq. (76).

Note that we could have described our problem by many sets of three dimensionless groups other than \bar{Sh} , Re , and Sc . But the latter three are those most commonly used in convective mass transport. Other frequently employed dimensionless groups will be mentioned later in the corresponding sections throughout this volume.

In the above example it may happen that another characteristic length, for example, the interelectrode distance l' , plays a role. Re and Sh can then be formed with l or l' . In order to describe the problem entirely we have to introduce an additional dimensionless group such as l'/l .

We may note that Eq. (78a) yields an average value of the Sherwood number. We can also define a local value

$$Sh = N_{B,e}x/D_B(c_{B,e} - c_{B,0}) \quad (78b)$$

which is then given, for $Sc \approx 1$, by

$$Sh = 0.332 Re_x^{1/2} Sc^{1/3} \quad (78c)$$

where Re_x is the local Reynolds number formed with the distance from the leading edge x .

3.5. Concluding Remarks

By and large, it can be said that dimensional analysis provides, on a broad basis, a powerful approach to physical problems. Its general applicability is both its strength and weakness. Dimensional analysis can be used in any

problem, provided the relevant variables and their dimensions are known. However, it yields only a partial solution. The functional relationship between the variables remains basically unknown. Yet the use of dimensionless groups has decisive advantages that we will briefly review.

(i) The diminution of the number of variables facilitates drastically the experimental determination of the desired relationship. This advantage is the more impressive the smaller the number of dimensionless groups to be introduced.

(ii) The smaller number of variables allows a much simpler graphical representation of the experimental data. Dimensional analysis puts order into our measurements. Without this structuring principle Reynolds would never have been able to achieve a neat correlation of his results.

(iii) The dimensionless groups are very useful in modelling. Consider for instance in our example of the flow along a plate, a model and a scaled-up version with different values l_1 and l_2 of the characteristic length but with flow velocities so adjusted that $v_2/v_1 = l_1/l_2$. The Reynolds numbers are then the same in both cases. At constant Sc , the Sherwood numbers are also the same. It is thus possible to predict the behavior of the scaled-up version from that of the model without having to determine the whole correlation between Sh , Re , and Sc . The two systems are then said to be similar. The method of modelling is widely used in certain branches of engineering. Its theory and, more generally, the introduction of dimensionless groups are often derived from the principle of similitude rather than from that of dimensional analysis. In reality, the two methods are only different aspects of one and the same basic idea and are essentially equivalent. In the derivation of Section 2.3 we have made use of the method of similitude.

(iv) The dimensionless groups are most convenient when one wishes to make use of the analogy between mass, heat, and momentum transport which will be discussed in the next section.

A more detailed treatment of the method of dimensional analysis is to be found in a number of monographs and textbooks.⁽²²⁻²⁸⁾ An early discussion of the application of the method to electrochemistry has been made by Agar⁽⁷⁾ and Ibl.^(8,29) More recently, it was used in connection with the optimization of electrochemical systems.⁽³¹⁾

4. Analogy between Mass, Heat, and Momentum Transport

4.1. General Aspects

The equation for the mass flux density N_B in an ideal dilute solution has been recalled in Section 2.1. A relationship quite similar to Eq. (10) holds for the *heat flux density* \mathbf{q} (which is defined quite similarly to N_B as the vector that indicates the direction in which the heat flows and the amount of heat

flowing, divided by time and area):

$$\mathbf{q} = -a \nabla(\rho c_p T) + \mathbf{v}(\rho c_p T) \quad (79)$$

The product of fluid density ρ (kg m^{-3}), specific heat c_p ($\text{J kg}^{-1} \text{K}^{-1}$), and temperature T , i.e., $\rho c_p T$, represents the amount of energy per unit volume and can be regarded as the *concentration of energy*, analogous to c_B (which is the concentration of species B). The first term on the right-hand side of Eq. (79) is the heat flux by conduction, analogous to the diffusion flux. It is proportional to the gradient of the “concentration” of energy, the proportionality factor being a which is the thermal diffusivity. The second term on the right-hand side represents the heat transport by convection, analogous to the term $c_B \mathbf{v}$ of Eq. (10).

In the case of momentum transport, the analogy is complicated by the fact that the momentum $m\mathbf{v}$ is a vector, in contrast to the amount of heat or of matter. To work out the analogy we have to consider the components of momentum along the three spatial coordinate axes (mv_x, mv_y, mv_z), which are scalar quantities. In a way this corresponds to a situation that we would have in the case of mass transport, three different species (where, however, these concentrations may be independent, whereas v_x, v_y , and v_z are related through the continuity equation (16)). The *momentum flux density* ($\text{kg m}^{-1} \text{s}^{-2}$) is defined similarly to \mathbf{N}_B : $\boldsymbol{\tau}_x$ is a vector that indicates the direction in which the x component of momentum flows at a given point of the fluid and that gives the amount of momentum flowing, divided by time and area (similar definitions holding for $\boldsymbol{\tau}_y$ and $\boldsymbol{\tau}_z$). Physically, $\boldsymbol{\tau}_x$ has the following meaning. We consider for a given point a surface element represented by the vector† $d\mathbf{A}$. The scalar product $\boldsymbol{\tau}_x \cdot d\mathbf{A}$ for that point gives the x component of the friction force acting on that surface element. Similarly, $\boldsymbol{\tau}_y \cdot d\mathbf{A}$ and $\boldsymbol{\tau}_z \cdot d\mathbf{A}$ give the y and z components of that force. The *momentum flux density* $(\boldsymbol{\tau}_x)_e$ at the electrode solution interface corresponds to the x component of the *shear stress* acting on the electrode.

The relationships for $\boldsymbol{\tau}_x, \boldsymbol{\tau}_y$, and $\boldsymbol{\tau}_z$ are analogous to those for \mathbf{q} and \mathbf{N}_B . For example, for $\boldsymbol{\tau}_x$ we have

$$\boldsymbol{\tau}_x = -\nu \nabla(\rho v_x) + (\rho v_x)\mathbf{v} \quad (80)$$

ρv_x (amount of momentum per unit volume) can be regarded as the *concentration of the x component of momentum*. The first term on the right-hand side is the momentum flux due to the viscous drag (friction) and is analogous to diffusion. It is proportional to the gradient of the “concentration” of momentum, the proportionality factor being the kinematic viscosity ν . The second term on the right-hand side represents momentum transport by convection and is analogous to the term $c_B \mathbf{v}$ of Eq. (10).

† The vector $d\mathbf{A}$ is perpendicular to the surface element and its intensity is equal to the area of the element.

The second terms on the right-hand side of Eqs. (10), (79), and (80) represent *macroscopic* transport processes, in which the transported quantity is dragged along by the hydrodynamic flow. In contrast to this, the first terms correspond to *molecular* transport processes: diffusion, heat conduction, or momentum transport by viscous drag. They are *equalizing* processes (*Ausgleichsvorgänge*), due to molecular motion. Because of this random movement the particles are exchanged between the various parts of the fluid. The exchanged particles carry with them their properties: amount of energy (which is related to temperature), momentum (which is related to flow velocity), and chemical potential (which is related to molar concentration). These properties are thus also exchanged between adjacent parts of the fluid and the result is a tendency to render uniform, over the whole fluid, the distribution of these properties; i.e., to render uniform the molar concentration, the temperature, and the flow velocity. The macroscopically observable equalizing processes through which this is achieved are the aforementioned phenomena of diffusion, heat conduction, and viscous drag. The corresponding kinetic parameters are D_B , a , and ν ; their meaning will be discussed further toward the end of this section. Note that all of them have the same dimension L^2T^{-1} . This underlines again the analogy of mass, heat, and momentum transport.

A further cornerstone of the analogy structure is provided by the *conservation law* which holds for each of the three transport phenomena considered. Application of the conservation principle (see Section 2.6, Chapter 1) to an infinitesimal volume element yields, in the case of mass transport, Eq. (13) and, in the case of momentum transport, Eq. (17a) (which is the Navier–Stokes equation written for the x component of momentum). In the case of heat, an energy balance for an infinitesimal volume element yields (for an incompressible fluid) the similar equation

$$\frac{\partial(\rho c_p T)}{\partial t} = a \nabla^2(\rho c_p T) - \mathbf{v} \cdot \nabla(\rho c_p T) + \Phi \quad (81)$$

The left-hand sides of Eqs. (13), (81), and (17a) represent, for a given point of the fluid, the change with time of the concentration of a species, of energy, or of momentum, respectively. The first and the second terms on the right-hand sides of these equations correspond to the molecular and convective transport modes, respectively. The third term on the right-hand sides represent a source or a sink. In the case of Eq. (13) (mass transport) it corresponds to the generation taking place in the volume element considered. In Eq. (81) the dissipation term Φ represents the amount of heat generated or consumed (divided by time and volume), due for example, to a chemical reaction or to the ohmic effect of the passage of an electric current through the fluid. Finally, in Eq. (17a) the source term is the x component of the resultant external forces acting, per unit volume, on the fluid at the point considered. In the most usual case where the external forces reduce to the hydrostatic pressure

and the gravity force, the source term is given by $-dp_x/dx + \rho g_x$, as indicated in Eq. (17a). Similarly, the corresponding term in Eq. (17b) represents the y component of the external forces. The meaning of the source term in the Navier–Stokes equation can be derived from Newton’s law of motion applied to a volume element and expressed in terms of the forces being equal to change of momentum with time.

It should be pointed out at this stage that the perfect symmetry between the basic equations for mass transport and those for the other transport phenomena applies only to ideal dilute solutions. The situation is much more complicated if one has to consider the conjugate mass fluxes discussed in Section 2 of Chapter 1 or the interfacial velocities mentioned in Section 5.4 of Chapter 1. However, in electrolytic transport one uses in most cases the simpler equations (12) and (13) (or their further simplified versions). Furthermore, one usually assumes D_B and ν to be constant within the boundary layer. Under these circumstances not only the basic differential equations are formally the same for mass, heat, and momentum transport, but also the solution of these equations is the same in the three cases, provided that one considers corresponding conditions, in particular, equivalent boundary conditions. This is of great practical importance because it allows us in many cases to predict convective mass transport in electrolysis from calculations or measurements of heat and momentum transport (i.e., from heat exchange rates and shearing stresses) or vice versa.

Let us first demonstrate the benefit of the analogy argument in an example of a theoretical treatment.

4.2. Application Example for a Theoretical Approach

Let us consider as a concrete example mass transport to a plate in longitudinal laminar flow. The basic differential equations for mass transport have been integrated in Section 2.3. For a constant interfacial concentration, steady-state conditions, and $Sc \approx 1$, one obtains the following relationship for the local mass transfer coefficient k_d and the equivalent thickness of the diffusion layer at distance x from the leading edge [Eq. (48b)]:

$$k_d = 0.332D_B(\nu/D_B)^{1/3}(v_0/\nu x)^{1/2}; \quad \delta = 3.01(D_B/\nu)^{1/3}(\nu x/v_0)^{1/2} \quad (82)$$

Let us now consider the heat exchange at a plate in laminar flow under the same hydrodynamic and geometric conditions as those assumed in Section 2.3. To further preserve the symmetry of the two problems, we will regard the generation or consumption of heat within the system as negligible [i.e., $\Phi = 0$ in (81)] just as we assumed there is no chemical reaction in the solution in deriving Eq. (82) [i.e., $v_B^* = 0$ in Eq. (12) and (13)]. The fundamental differential equation for heat transport [Eq. (81)] is formally identical with that for mass transport [Eqs. (12) and (13)], with $\rho c_p T$ replacing c_B and a

replacing D_B . To the mass transfer at the interface (i.e., the amount of matter removed from or supplied to the liquid phase) corresponds the heat exchanged between the plate and the fluid. The first is given by the interfacial mass flux density $N_{B,e}$, the second one by the interfacial heat flux density, q_e ($\text{J m}^{-2} \text{s}^{-1}$). Dividing through by the difference between the temperature T_0 in the bulk of the fluid and that at the interface T_e we obtain the heat transfer coefficient:

$$h = q_e / (T_0 - T_e) \quad (83a)$$

which is similar to the mass transfer coefficient k_d . Near the interface a temperature boundary layer develops with a temperature profile similar to the concentration profile in the diffusion layer (Figures 1 and 2). Let the temperature in the bulk of the fluid (T_0) and that at the plate (T_e) be maintained at a given constant value. This corresponds to the boundary condition $c_B = c_{B,0}$ for $y = \infty$ and $c_B = c_{B,e}$ for $y = 0$ in the mass transport problem of Section 2.3. If the bulk of the fluid and the plate are maintained at given constant temperatures ($T = T_0$ for $y = \infty$, $T = T_e$ for $y = 0$), the boundary conditions correspond to those considered at the beginning of Section 2.3. Therefore, not only the fundamental equations (79), (81), (10), and (13) but also the boundary conditions are formally the same. The integration of Eq. (81) (with the Prandtl boundary-layer simplifications; see Section 2.2) yields the same result as that given by Eq. (82):

$$h = 0.332a(\nu/a)^{1/3}(v_0/\nu x)^{1/2}; \quad \delta_T = 3.01(a/\nu)^{1/3}(\nu x/v_0)^{1/2} \quad (84)$$

h plays the same role in heat transfer as k_d in mass transfer.

Strictly speaking the quantity corresponding to k_d is not h but rather k_c which is defined as the ratio of q_e to the driving *heat concentration* difference between bulk and interface $\rho c_p(T_0 - T_e)$

$$k_c = q_e / \rho c_p(T_0 - T_e) = h / \rho c_p \quad (83b)$$

k_c and k_d have the same dimension, namely, that of a velocity, m s^{-1} . However, traditionally in the heat transfer literature, h is more commonly used than k_c but, in principle, they are equivalent.

We have chosen the equation analogous to Eq. (82) [(48b)] which is valid for $\text{Sc} \approx 1$ because the dimensionless group Pr which corresponds to the Schmidt number Sc in heat transfer ($\text{Pr} = \nu/a$, see later) is of the order of 1 rather than 1000.

δ_T is the thickness of the equivalent temperature boundary layer, approximated by a straight line for the temperature profile, analogous to that of the Nernst diffusion layer (Figure 5).

Obviously, we can turn the problem around: If we find in the literature the solution of the heat transport equation (81) yielding Eqs. (84) we can deduce from this, without any further calculations, that Eqs. (82) hold for mass transport with corresponding boundary conditions. This is of great practical importance because (especially in the past) more correlations have

been established (theoretically or experimentally) for heat than for mass transfer. An excellent review of heat conduction in a great variety of situations has been given by Carslaw and Jaeger⁽³²⁾, while a comprehensive compilation of correlations for convective heat transfer are to be found in the books by McAdams⁽³³⁾ and others.⁽³⁴⁻³⁶⁾

Finally let us discuss, from the viewpoint of analogy, the momentum transport at a plate under the hydrodynamic conditions considered in Section 2.3. The laminar flow along the x axis, parallel to the plate, exerts on the plate a viscous drag, or friction force in the x direction (also called shear stress). The force per unit electrode area, τ_x , is equal to the amount of momentum (along the x axis) transferred from the fluid to the wall, per unit electrode area and per unit time. It corresponds to the amount of mass, or of heat, transferred at the interface in the case of mass or heat transport, respectively. It is equal to the interfacial flux density of the x component of momentum (mv_x): $\tau_x = J_x$. Note that we are dealing with the component of momentum along the axis parallel to the electrode (i.e., the latter is pushed in the direction parallel to itself), but the flux of momentum goes in the y direction, perpendicular to the plate, just as in the case for the fluxes of mass and heat, $N_{B,e}$ and q_e . The driving force for $N_{B,e}$ is the molar concentration difference $c_{B,0} - c_{B,e}$ over the diffusion layer, and, similarly, the driving force for the flux of momentum is the difference in the momentum concentrations ρv over the hydrodynamic boundary layer, which develops near the plate, with a velocity profile similar to the concentration profile (Figures 1 and 2). However, whereas $c_{B,e}$ can have any value, the interfacial flow velocity at a stationary wall must be zero because of the friction forces (see Section 1.1), and the driving momentum concentration difference reduces to ρv_0 , where v_0 is the velocity outside the boundary layer. Therefore, in order to obtain a quantity corresponding to k_d , we do not divide the flux density by a concentration difference $c_{B,0} - c_{B,e}$, but simply by the momentum concentration in the bulk ρv_0 , yielding $\tau_x/\rho v_0$. It is the quantity corresponding to k_d and k_c and has the same dimension as the latter, namely, that of a velocity, m s^{-1} .

It is calculated by integrating Eq. (17a) in which the source term, $-dp_x/dx - \rho g_x$, is dropped because we consider a case with no external forces. Equation (17a) is then formally the same as Eq. (13) for $\sum_r v_{Br}^* = 0$ (with ρv_x instead of c_B and v instead of D_B). With the boundary-layer simplifications, Eqs. (17a) and (13) reduce for steady-state conditions to Eqs. (20) and (19), respectively—the similitude of which has already been noted in Section 2.3. The boundary conditions given by Eqs. (23a)–(23c) are also formally the same as for the mass transport equation [Eqs. (21a)–(21c)]. The solution is therefore also the same and we have

$$\tau_x/\rho v_0 = 0.332\nu(v_0/\nu x)^{1/2}; \quad \delta_v = 3.01(\nu x/v_0)^{1/2} \quad (85)$$

These are indeed the relationships demonstrated in the textbooks on hydrodynamics.⁽²¹⁾ In contrast to Eq. (82), a factor of the kind ν/D_B is missing

in Eq. (85). The reason is that the D_B of Eq. (13) is replaced by ν in Eq. (17a) so that ν/D_B turns into $\nu/\nu = 1$. δ_v is the equivalent thickness of the hydrodynamic boundary layer (Figure 5). A uniform presentation of momentum, mass, and heat transfer, pointing out the analogies between these phenomena, is to be found in particular textbooks.^(11,12,37)

4.3. Remarks on the Boundary Layers for Mass, Heat, and Momentum Transport

The thicknesses of the boundary layers given by Eqs. (82), (84), and (85) are the equivalent values, defined by assuming the concentration, temperature, or velocity profile to be a straight line up to the point where the value in the bulk solution is reached (Figure 5). In general, the three layers exist simultaneously near the electrode. This is the case in the electrolysis of Figure 2 (copper deposition in a cell with electrolyte flow). The occurrence of a diffusion layer is due to the removal of copper from the solution at the cathode, the temperature boundary layer is due to the necessity of evacuating the heat generated in the system[†] and the hydrodynamic boundary layer develops because of the loss of momentum at the electrode due to the friction forces. At the interface, there are fluxes of mass, heat, and momentum.[‡] The thicknesses of the three corresponding boundary layers [which, for the steady state, are given by Eqs. (82), (84), and (85)] depend in the same way on the relevant parameters. For example, in laminar flow the thickness of all boundary layers increases downstream for the reasons discussed in Section 1.1 (Figure 2). But the absolute values are different because the coefficients for molecular transport— D_B , a , and ν —are not the same. Let us elaborate somewhat on the relationship between δ , δ_T , and δ_v . For the sake of simplicity we consider first a convection-free nonsteady state. Such a situation is encountered at the beginning of electrolysis when the diffusion layer builds up (see Section 1.1) or when a hydrodynamic boundary layer develops at a plate suddenly set into motion. The time variation of the interfacial mass flux density has been derived in Chapter 2. For a constant interfacial concentration is given by Eq. (60) of Chapter 2:

$$N_{B,e} = -(c_{B,0} - c_{B,e})D_B^{1/2}\pi^{-1/2}t^{-1/2} \quad (86)$$

[†] The heat flux may go to the electrode or toward the solution. This depends on the relative amounts of the heat generated within the solution through ohmic effects and of the heat produced at the electrode solution interface due to the overpotential as well as on the relative ease with which the heat is transferred to the surroundings through the various boundaries of the cells (walls, electrodes, free surface of the solution) and, possibly, by the passage of the liquid through the cell. The evacuation of the heat may be of considerable importance in technical applications of electrochemistry.

[‡] In addition, there is a further flux at the interface; namely, that of charges which corresponds to the electrolysis current. Note that the flux of charges through the solution outside the diffusion layer obeys Ohm's law $\mathbf{j} \sim \kappa \nabla\Phi$, which is formally the same as Fick's law of diffusion or Fourier's law of heat conduction.

Combining with Eq. (1) we obtain

$$\delta = (\pi D_B t)^{1/2} \quad (87)$$

In the convection-free nonsteady state the diffusion layer grows in proportion to the square root of the diffusion coefficient D_B and of the time t .[†] Because of the analogy with heat and momentum transfer it can be expected (and it can be derived from the respective relationships) that similar relationships hold for δ_T and δ_v

$$\delta_T = (\pi a t)^{1/2}; \quad \delta_v = (\pi \nu t)^{1/2} \quad (88)$$

The ratio of the thicknesses reached by the boundary layers at a given time is equal to the ratio of the square roots of the respective coefficients, i.e., $\delta/\delta_v = (D_B/\nu)^{1/2}$, etc. This leads us to a further understanding of the physical meaning of the coefficients D_B , a , and ν : They are a measure of the rate at which a nonuniformity of concentration of temperature or of velocity, respectively, progresses into the fluid. The steady state is reached when this expansion is stopped by convective supply to the boundary layer which then equals the rate of removal at the interface, as discussed in Section 1.1. It is plausible that, as shown by Eqs. (82), (84), and (85), the depth of penetration of the nonuniformity into the fluid is larger the greater the coefficient D_B , a , or ν . Indeed, the rate of removal at the interface of mass, heat, and momentum increases with increasing D_B , a , and ν , respectively, whereas the rate of supply through convection of mass, heat, and momentum becomes larger with increasing distance BC in Figure 3. Therefore, δ , δ_T , and δ_v have to increase with increasing D_B , a , and ν , respectively. On the other hand, the rate of supply becomes greater with increasing bulk flow velocity v_0 so that δ , δ_T , and δ_v decrease with increasing v_0 .

4.4. Advantage of Using Dimensionless Groups in Analogy Considerations

The differential equations describing mass, heat, and momentum transport are formally the same, but they include quantities that have a different physical meaning. This difference disappears if one uses dimensionless correlations. For example, the relationship for the plate in laminar flow, Eq. (78c) is valid for both mass and heat transport. The *numerical values* of the variables are independent of the kind of transport considered. However, their meaning is not the same. In the case of mass transport, Sh is defined by Eq. (78b), whereas for heat transport it is equal to $q_e x / a \rho c_p (T_e - T_0)$ and is usually called the Nusselt number, Nu (x being again a characteristic length such as the

[†] It is interesting to note that this is also true for the case of a constant interfacial flux density. From Eq. (163) of Chapter 2 and Eq. (1) one obtains $\delta = 2(D_B t / \pi)^{1/2}$, which differs only slightly in the numerical coefficient from Eq. (87).

distance from the leading edge of the plate in the example of Section 2.3). Whereas Sh is the variable characteristic for the mass transfer rate, Nu is a kind of adimensional heat transfer rate. On the other hand, Sc represents in mass transport the ratio ν/D_B , but in heat transport ν/a and is then usually called the Prandtl number, Pr . In the electrolysis of aqueous solutions or molten salts ν/D_B is of the order of a few hundred to a few thousand, whereas for air Pr is about 1 and for water and various other common liquids it is of the order of 10. Therefore, the prediction of electrolytic mass transfer rates from heat transfer measurements with air or water (which are the most common ones) involves the difficulty that the Schmidt and Prandtl numbers are different, so that an extrapolation becomes necessary. This may not lead to a serious error (see Figure 17), but it is an element of uncertainty. Of course, if measurements or theoretical calculations at $Sc = Pr$ are available, the prediction of mass transfer from heat transfer or vice versa is a perfectly reliable one.

Very often the correlations for heat or mass transfer can be written with a fair approximation in the simple form

$$Sh = a Re_x^\alpha Sc^\beta \quad \text{with } a, \alpha, \beta = \text{numerical constants} \quad (89a)$$

$$Nu = a Re_x^\alpha Pr^\beta \quad \text{with } a, \alpha, \beta = \text{numerical constants} \quad (89b)$$

Now, Sh and Nu do not only represent *adimensionalized* transfer rates, they can also be regarded as normalized or adimensionalized boundary-layer thicknesses. Indeed, from Eq. (1) as well as from the definition of Nu given above or from Eq. (73) for Sh , it follows that

$$Sh = x/\delta; \quad Nu = x/\delta_T \quad (90)$$

Furthermore, applying Eqs. (89a) and (89b) we obtain

$$\frac{Sh}{Nu} = \frac{\delta_T}{\delta} = \left(\frac{Sc}{Pr}\right)^\beta = \left(\frac{a}{D_B}\right)^\beta \quad (91)$$

The ratio of the thicknesses of the boundary layers is equal to the ratio of the molecular transport coefficients raised to the power with which Sc or Pr appears in the correlation. Similarly, it can be shown that Sc^{-1} and Pr^{-1} (raised to some power) represent the ratio of the thicknesses of the diffusion and temperature boundary layer, respectively, to the thickness of the hydrodynamic boundary layer.

In the above discussion of the use of dimensionless groups in analogy considerations, we have referred explicitly to the mass and heat transport. In principle, quite similar remarks apply to momentum transport but the analogy involves in that case some peculiarities which we will discuss in the next section.

4.5. Considerations on Analogy with Momentum Transport

From Eqs. (5) and (78b) it is easily seen that Sh and Nu can be written in terms of the transfer coefficients k_d and k_c as

$$\text{Sh} = k_d x / D_B; \quad \text{Nu} = k_c x / a \quad (92)$$

In momentum transport the quantity analogous to k_d and k_c is $\tau_x / \rho v_0$. Therefore, the dimensionless group corresponding to Sh and Nu is

$$\text{Nu}' = \frac{\tau_x x}{\nu \rho v_0} \quad (93)$$

If we use (93) to rewrite Eq. (85) in dimensionless form we obtain

$$\text{Nu}' = 0.332 \text{Re}_x^{1/2} \quad (94)$$

If we compare this with Eq. (78c) we note that the multiplicative term corresponding to $\text{Sc}^{1/3}$ is missing. As was briefly mentioned, this is due to the fact that Pr is deduced from Sc by substituting a for D_B and if one does the corresponding substitution for momentum transport (i.e., ν for D_B) one obtains $\nu/\nu = 1$. The physical reason for this state of affairs is as follows. In Section 1.1 we realized that the steady state is established when the rate of removal at the interface through diffusion (which depends on D_B) is compensated by the rate of supply by convection (which depends on the thickness of the hydrodynamic boundary layer and thus on ν) (see Figure 3). Therefore, δ (and also Sh which is equal to x/δ) depends on both D_B and ν . In the case of shear stress, the supply of momentum to the boundary layer through convection again depends on the thickness of the hydrodynamic boundary layer and thus on ν , but so does the rate of removal of momentum at the interface through friction. The relevant coefficient happens to be the same here because the boundary layer governing the rate of the molecular transport process at the interface is now the same as the boundary layer which governs the supply by convection from the bulk. We may also express the result by saying that, in the case of momentum transfer at a wall, the dimensionless group corresponding to Sc and Pr is necessarily equal to one. Therefore, strictly speaking, prediction of mass or heat transfer rates from the shearing stress should be made only for Sc or Pr = 1.

Another peculiarity of momentum transport is due to custom. Traditionally in hydrodynamics, the shearing stress has not been made dimensionless by introducing Nu' given by Eq. (93) but by using the dimensionless friction coefficient $f/2$ defined as

$$\frac{f}{2} = \frac{\tau_x}{\rho v_0^2} \quad (95)$$

which characterizes the ratio of the viscous forces to the kinetic energy (or

inertia forces). The friction coefficient can also be written

$$\frac{\tau_x}{\rho v_0^2} = \frac{\tau_x x / \nu \rho v_0}{v_0 x / \nu} = \frac{\text{Nu}'}{\text{Re}_x} = \frac{f}{2} \quad (96)$$

We see that the dimensionless group commonly employed in hydrodynamics to describe the shearing stress does not correspond to Sh or Nu but to Sh/Re or Nu/Re. Therefore, if we want to predict mass or heat transfer rates from one of the numerous correlations of the form

$$f/2 = F(\text{Re}) \quad (97)$$

available in hydrodynamics, we must substitute Sh/Re or Nu/Re for $f/2$ in the above relationship. Of course, the conditions must be corresponding ones. This involves two difficulties.

First, as we have already pointed out, the dimensionless group corresponding to Sc and Pr is necessarily one in momentum transport, whereas in electrolytic systems Sc and Pr are large. To circumvent this difficulty, one often extrapolates to high Sc or Pr by assuming $\text{Sh} \sim \text{Sc}^{1/3}$ and $\text{Nu} \sim \text{Pr}^{1/3}$. This method was proposed by Chilton and Colburn in 1934⁽³⁸⁾ and is usually referred to today as the Chilton–Colburn analogy. One introduces the new dimensionless group

$$j_D = \frac{\text{Sh}}{\text{Re Sc}^{1/3}}, \quad j_H = \frac{\text{Nu}}{\text{Re Pr}^{1/3}} \quad (98)$$

According to the Chilton–Colburn analogy,⁽¹⁶⁾ one takes $f/2$ from correlation (97) and sets

$$j_D = j_H = f/2 \quad (99)$$

In principle, this allows us to predict limiting currents in electrolysis from friction-force measurements in hydrodynamics. The method has proved useful in a considerable number of cases, particularly for flat or streamlined surfaces. For many systems Sh and Nu are approximately proportional to $\text{Sc}^{1/3}$ or $\text{Pr}^{1/3}$. Moderate deviations from the exponent 1/3 are very damped in their effect on the value of the predicted heat or mass transfer rate because of the low value of the commonly encountered exponent (1/3).

However, there is another important complication which comes in addition to the problem of the Schmidt or Prandtl number. It is due to the occurrence of a form drag at curved surfaces (including rough ones). Let us consider as an example a liquid flowing past a stationary sphere. Especially in the turbulent region, the flowing fluid exerts on the front and rear side of the sphere pressures that are unequal and do not cancel. The result is a form drag in the flow direction which has no counterpart in mass or heat transfer. In the rear of the above sphere a turbulent wake develops which contributes to the degradation of mechanical energy to heat but causes very little mass

or heat transfer. The Chilton–Colburn analogy cannot be expected to hold in cases where the form drag is significant. This applies mainly to curved surfaces that are not streamlined. For a fluid flowing past a long cylinder perpendicularly to its axis, $f/2$ has been found to be 5–200 times larger than j_H .⁽¹¹⁾ A measure for the departure from the Chilton–Colburn analogy is the Le Goff number; L_f , defined as

$$L_f = \frac{j_D}{f/2} = \frac{j_H}{f/2} \quad (100)$$

When this analogy holds, L_f is equal to 1. When drag friction is significant, L_f may take values commonly ranging from 1 to 10^{-2} . The Chilton–Colburn analogy, and more generally the analogy between mass, heat, and momentum transport, has been recently reviewed by LeGoff.⁽³⁹⁾

The above complication of an $L_f \neq 1$ is linked with the fundamental fact that the amounts of mass (or substance) and of heat are scalar quantities, whereas the momentum is a vector. In Section 2.1 we have circumvented this difficulty by writing the fundamental differential equations in terms of the spatial components of the momentum, which are scalar quantities [Eqs. (17a), (17b), (17c)]. Each of these three equations is then formally identical with the equations for heat and mass transport. No difficulty arises in the use of the analogy as long as one has to solve only one of these equations, as it was in the case for the plate in laminar flow considered in Section 2.3. Indeed, in that case only the x component of momentum is transferred to the wall. However, with a curved surface one may have to consider the equation for the y component (and possibly even that for the z component) as well. The integration then yields two interfacial fluxes of momentum τ_x and τ_y (and possibly three), which represent two components of the stress that have to be added vectorially to yield the usually measured drag. This operation has no counterpart in mass and heat transport.

Recently Le Goff has presented a new view of the analogy between the transport phenomena based on an energy concept.⁽⁴⁰⁾

5. Mass Transport in Turbulent Flow

5.1. Fluctuating and Time-Averaged Quantities

Above a certain critical Reynolds number, characteristic for a given flow system, the nature of fluid flow changes drastically; it passes from laminar to turbulent motion. While in steady laminar flow the fluid particles follow definite streamlines, turbulent flow is characterized by a random chaotic motion of eddies superimposed on the main stream motion. Turbulent flow is unsteady in nature in the sense that at a given point the velocity, and, as a consequence, other properties such as pressure and composition, vary with

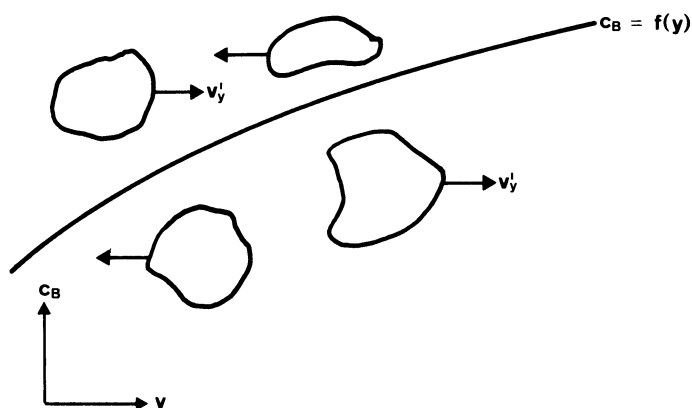


Figure 8. Motion of turbulent eddies (schematic).

respect to time. The eddies carry momentum and mass toward regions of lower concentration of these quantities: There is in turbulent flow an additional, very effective transport mechanism that can be visualized as follows. Macroscopic liquid volume elements (eddies) undergo a random movement, very roughly similar to the Brownian motion of molecules in a gas, except that the moving entity is larger by many orders of magnitude (Figure 8). The eddies carry momentum as well as the dissolved species with them. If eddies of different concentrations are exchanged against one another a fluctuation of concentration results. Note that, in the sense of Section 4, concentration may mean one of momentum or of a species. If one considers a sufficiently large number of eddies in a system with a gradient of concentration, say, in the $-y$ direction, the overall amount of momentum or of a species transported during a given time in the $+y$ and $-y$ directions do not cancel, and the result on the time average is a macroscopically observable flux of momentum or of a species in the $+y$ direction. There is a rough analogy with the fluxes due to friction or to diffusion, but the transport rates are much higher than for the molecular phenomena, because the moving entities are very much bigger. As a consequence *mass transport rates are considerably higher in turbulent flow than in a laminar regime.*

Turbulent flow plays an important role in industrial electrochemical processes. Since mass transport limits the rate of electrode reactions it is often of advantage to work under turbulent-flow conditions in order to realize the high mass transfer rates (i.e., current densities) which are necessary to keep the dimensions of the reactor at a reasonable size for a given production rate. However, turbulent flow has a disadvantage in that not only mass and heat but also momentum transfer is enhanced, which results in an increased resistance to flow. The gain achieved by reducing the size of the reactor is therefore partly counteracted by the larger pumping or stirring power required.

The optimization of the stirring of an electrochemical reactor will be discussed in Section 10.

The flow patterns in turbulent flow are extremely complex and there is no possibility to predict them completely even for the most simple flow geometry. Of course, the conservation equations remain valid in turbulent flow and are satisfied by the instantaneous values of the velocity components and of the concentration. However, they cannot be solved because of the random nature of the fluctuations. In the analysis of turbulent transport phenomena, one is usually not interested in the fluctuations but rather in mean quantities. To this end, the time average of the pertaining equations is taken and the properties are split up in a time-averaged mean part and a fluctuating part in the form

$$\begin{aligned} \mathbf{v} &= \bar{\mathbf{v}} + \mathbf{v}' \\ p &= \bar{p} + p' \\ c_B &= \bar{c}_B + c'_B \end{aligned} \quad (101)$$

where \mathbf{v} , p , and c_B are the instantaneous values, $\bar{\mathbf{v}}$, \bar{p} , and \bar{c}_B are the time-averaged values, and \mathbf{v}' , p' , and c'_B are the fluctuations. This representation of the properties is illustrated in Figure 9 for the case of the concentration. The time-averaged value of the concentration is defined as

$$\bar{c}_B = \frac{1}{\Delta t} \int_t^{t+\Delta t} c_B dt \quad (102)$$

where Δt is a time interval that is large compared to the period of the fluctuations. The mean values of the pressure and of the components of the velocity vector are defined in the same way.

The implications of this approach in the study of transport phenomena will be illustrated by considering the continuity equation, the equation of motion, and the equation of convective diffusion. The continuity equation for the instantaneous values of the velocity components is (incompressible fluid)

$$\nabla \cdot \mathbf{v} = 0 \quad (103)$$

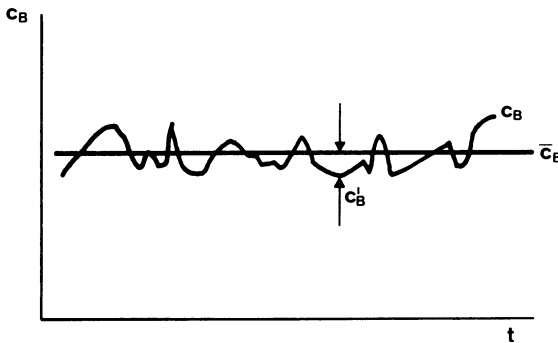


Figure 9. Fluctuation of the concentration in turbulent flow.

The x -momentum equation in terms of the instantaneous values of the velocity components and the pressure is written as (Newtonian fluid)

$$\frac{\partial(\rho v_x)}{\partial t} = -\nabla \cdot (\mathbf{v}v_x\rho) + \mu \nabla^2 v_x - \frac{\partial p}{\partial x} + \rho g_x \quad (104)$$

Neglecting the source term, we write the equation of convective diffusion for the instantaneous values of v_x , v_y , v_z , and c_B in the form

$$\frac{\partial(c_B)}{\partial t} = -\nabla \cdot (\mathbf{v}c_B) + D \nabla^2 c_B \quad (105)$$

The instantaneous values of the properties are then replaced by the sums of the mean and the fluctuating part [Eqs. (101)], and the time average of Eqs. (103), (104), and (105) are taken. We bear in mind that by virtue of the foregoing definitions, the time average of a fluctuation is zero:

$$\bar{v}' = \bar{p}' = \bar{c}'_B = 0 \quad (106a)$$

On the other hand, the fluctuations of the velocity components and of the concentrations are not independent, and therefore the time averages of products of fluctuations such as $\overline{v'_x v'_y}$ and $\overline{v'_x c'_B}$ may be different from zero. For example, one obtains for the product of c_B and v_x

$$c_B v_x = (\bar{c}_B + c'_B)(\bar{v}_x + v'_x) = \bar{c}_B \bar{v}_x + c'_B \bar{v}_x + \bar{c}_B v'_x + c'_B v'_x \quad (106b)$$

and upon averaging ($\bar{c}'_B \bar{v}_x = \bar{c}_B \bar{v}'_x = 0$),

$$\overline{c_B v_x} = \bar{c}_B \bar{v}_x + \overline{c'_B v'_x} \quad (106c)$$

Thus the time-averaged conservation equations become

$$\nabla \cdot \mathbf{v} = 0 \quad (\text{continuity}) \quad (107)$$

$$\frac{\partial(\rho \bar{v}_x)}{\partial t} = -\nabla \cdot (\bar{\mathbf{v}} \bar{v}_x \rho) + \mu \nabla^2 \bar{v}_x - \nabla \cdot (\overline{\mathbf{v}' v'_x \rho}) - \frac{\partial \bar{p}}{\partial x} + \rho g_x \quad (x \text{ momentum}) \quad (108)$$

$$\frac{\partial(\bar{c}_B)}{\partial t} = -\nabla \cdot (\bar{\mathbf{v}} \bar{c}_B) + D \nabla^2 \bar{c}_B - \nabla \cdot (\overline{\mathbf{v}' c'_B}) \quad (\text{convective diffusion}) \quad (109)$$

We note that the time-averaged velocity components satisfy the same continuity equation as for laminar flow.

A comparison of the time-averaged equations of motion and of convective diffusion with the corresponding equations for laminar flow reveals that they are the same except for an additional convective term [third term on the right-hand side of Eqs. (108) and (109)] containing the fluctuating components of the velocities and concentration. Note that quite generally, $c_B v$ is a convective flux (see Section 1) and therefore the $c'_B v'$ terms are the fluctuations of

that flux, as compared to the flux that one would have if a fluid with the concentration \bar{c}_B was moving at the velocity \bar{v} (i.e., at a velocity equal to the average value). An average $\overline{c'_B v'}$ of the fluctuating flux different from zero means that there is, on the average, a macroscopically observable flux due to the random fluctuations. Therefore, the additional convective terms of Eqs. (108) and (109) correspond to an additional transport brought about by the intense motion of the turbulent eddies.

In view of this situation the following notation is introduced:

$$\tau'_x = \overline{\rho v'_x v'} \quad (110)$$

$$\mathbf{N}'_B = \overline{c'_B \mathbf{v}'} \quad (111)$$

τ'_x is the turbulent flux of the x component of the momentum, also called turbulent shear stress or Reynolds stress. \mathbf{N}'_B is the turbulent mass flux. The total fluxes can thus be considered as the sum of a molecular and a turbulent term

$$\tau_x = \tau_x^m + \tau'_x = -\mu \nabla \bar{v}_x + \overline{\rho v'_x v'} \quad (112)$$

$$\mathbf{N}_B = \mathbf{N}_B^m + \mathbf{N}'_B = -D_B \nabla \bar{c}_B + \overline{c'_B \mathbf{v}'} \quad (113)$$

The conservation equations (108) and (109) then take the form

$$\frac{\partial(\rho \bar{v}_x)}{\partial \xi} = -\nabla \cdot (\bar{\mathbf{v}} v_x \rho) + \nabla \cdot \left(\mu \nabla \bar{v}_x - \overline{\mathbf{v}' v'_x \rho} \right) - \frac{\partial \bar{p}}{\partial x} + \rho g_x \quad (114)$$

and

$$\frac{\partial \bar{c}_B}{\partial t} = -\nabla \cdot (\bar{\mathbf{v}} c_B) + \nabla \cdot (D_B \nabla \bar{c}_B - \overline{\mathbf{v}' c'_B}) \quad (115)$$

The treatment so far illustrates the nature of the turbulent transport mechanisms but it provides no means to relate them in a quantitative way to known properties of the flow system. In fact, due to the complexity of the phenomenon of turbulence, there is no fundamental theory. The time-averaged conservation equations cannot be used for computational purposes unless relationships between the turbulent fluxes and mean quantities can be established.

5.2. Mass Transport Correlations

Many semiempirical models have been proposed to predict Reynolds stresses and turbulent heat and mass fluxes. In view of the qualitative model discussed in the first paragraph of Section 5.1 one can expect that there is such a flux (and thus average values of $\overline{c'_B v'}$, etc. different from zero) when there is a concentration gradient in the fluid. Furthermore, the analogy between the turbulent and molecular transport processes suggests that the

turbulent flux densities are proportional to the corresponding concentration gradients, which is a relationship commonly used today:

$$\tau'_x = \overline{\rho v'_x v'} = -\rho\varepsilon \nabla \bar{v}_x \quad (116)$$

$$\mathbf{N}'_B = \overline{c'_B \mathbf{v}'} = -\varepsilon_M \nabla \bar{c}_B \quad (117)$$

ε is called the eddy kinematic viscosity; ε_M is the turbulent or eddy diffusivity. The proposal to write the shear stress proportional to the velocity gradient was made as early as 1877 by Boussinesq.⁽⁴¹⁾ In contrast to the molecular viscosity and diffusivity, ε and ε_M are not characteristic properties of a fluid but depend on the intensity of the fluid motion. In general, they will therefore vary with position in a flow system. This variation is especially important in the neighborhood of solid walls where the motion of the fluid is slowed down by the friction forces. The eddies are gradually damped in the boundary layer and become inactive at the wall. In the bulk of a turbulent fluid $\rho\varepsilon$ and ε_M are very large compared to the molecular transport properties μ and D_B , but they decrease strongly when approaching the wall and become zero at the interface. When considering mass or momentum transfer to or from a solid wall, not only turbulent but also molecular diffusion has to be taken into account since both transport mechanisms are equally important in the region where $\rho\varepsilon$ and ε_M become comparable to μ and D_B , respectively. At the wall itself it is the molecular transport that predominates. The total fluxes near the interface are therefore given by

$$\tau_x = -(\mu + \rho\varepsilon)\nabla \bar{v}_x \quad (118)$$

$$\mathbf{N}_B = -(D_B + \varepsilon_M)\nabla \bar{c}_B \quad (119)$$

These equations do not allow us to calculate turbulent transfer rates a priori, but they are the starting point for the derivation of semiempirical equations for turbulent mass transport. In the following it shall be demonstrated how such a correlation can be obtained. We start from a one-dimensional form of Eq. (119); i.e., we consider mass transport in the direction y perpendicular to a solid wall (e.g., an electrode):

$$N_B = -(D_B + \varepsilon_M) \frac{d\bar{c}_B}{dy} \quad (120)$$

The integration of Eq. (120) between the limits $y = 0$ (interface) and $y = \infty$ (bulk of the fluid) yields the concentration difference between bulk and interface $c_{B,0} - c_{B,e}$ which is relevant for the mass flux toward the interface:

$$c_{B,0} - c_{B,e} = - \int_0^\infty \frac{N_B}{D_B + \varepsilon_M} dy \quad (121)$$

In developed turbulent mass transport the thickness of the boundary layer is virtually independent of location along a pipe or a plate. In contrast

to the situation in laminar flow (Figure 3), the influx of substance into the boundary layer parallel to the interface [which would correspond to $(N_{B,c})_1$ of Figure 3] is negligible. Therefore, the flux density of B perpendicular to the interface is virtually independent of y and equal to the interfacial flux density $N_{B,e}$.[†] Then, together with the definition of the mass transfer coefficient k_d given in Section 1.3, one obtains

$$k_d^{-1} = \int_0^{\infty} \frac{dy}{D_B + \varepsilon_M} \quad (122)$$

In order to determine how the eddy diffusivity of mass ε_M varies with the distance from the interface y , one assumes that it is equal to the eddy viscosity ε . In other words, the turbulent transport mechanisms for momentum and mass are considered to be the same.[‡] With this assumption it is possible to obtain $\varepsilon_M = \varepsilon$ from a known velocity profile.[§] In the numerous studies of turbulence near solid walls it has been found that the dependence of the tangential velocity \bar{v}_x on the distance y from the wall can be adequately described by a generalized correlation between two dimensionless variables defined as follows

$$v^+ = \bar{v}_x (\tau_e / \rho)^{-1/2} \quad (123a)$$

$$y^+ = y \nu^{-1} (\tau_e / \rho)^{1/2} \quad (123b)$$

The expression $(\tau_e / \rho)^{1/2} = v^*$ is called *shear stress velocity* and v^+ can be regarded as a velocity normalized with the shear stress velocity. From the one-dimensional form of Eq. (118) we derive

$$\varepsilon = \frac{|\tau_x|}{|\rho d\bar{v}_x/dy|} - \nu \quad (124)$$

As in the case of the mass flux, τ_x is constant in the layer adjacent to the wall and equal to its value τ_e at the interface. Introducing the substitutions (123a) and (123b) gives

$$\frac{\varepsilon}{\nu} = \left(\frac{dv^+}{dy^+} \right)^{-1} - 1 \quad (125)$$

Thus the turbulent exchange coefficient ε is given by the slope of the dimensionless velocity profile. Equation (125) is inserted into the expression for the mass transfer coefficient:

$$k_d^{-1} = \int_0^{\infty} \frac{dy}{\nu [D_B/\nu + (dv^+/dy^+)^{-1} - 1]} \quad (126)$$

[†] For the same reason the usual convective terms have been neglected in the expressions for the momentum and mass fluxes [Eqs. (118) and (119), respectively].

[‡] This idea seems plausible if one admits that there is a certain similarity between the motions of macroscopic eddies in turbulent flow and of the molecules in a gas. In the latter case, the kinetic theory of gases leads to the same values for the different transport properties of the gas.

[§] Certain authors have integrated (122) using correlations between ε and y^+ which were based on empirical knowledge or dimensional considerations.^(42,43)

or

$$k_d^{-1} = \left(\frac{\tau_e}{\rho}\right)^{-1/2} \int_0^\infty \frac{dy^+}{Sc^{-1} + (dv^+/dy^+)^{-1} - 1} \quad (127)$$

where $Sc = \nu/D_B$ is the dimensionless Schmidt number (see Section 3.4).

Many equations describing the generalized velocity profile can be found in the literature. Wasan and Wilke (44), for example, use the following correlations:

$$v^+ = y^+ - 1.04 \times 10^{-4}(y^+)^4 + 3.03 \times 10^{-6}(y^+)^5 \quad \text{for } y^+ < 20 \quad (128)$$

$$v^+ = 2.5 \ln y^+ + 5.5 \quad \text{for } y^+ > 20 \quad (129)$$

As in laminar flow, the concentration boundary layer is much thinner than the hydrodynamic boundary layer at the Schmidt numbers prevailing in aqueous solutions. Therefore, the integration of Eq. (127) is sufficiently accurate if we use only Eq. (128) for calculating ε/ν and take $y^+ = 20$ as an arbitrary upper integration limit. The result of the numerical integration of (127) between $y^+ = 0$ and 20 with dv^+/dy^+ derived from (128) can be expressed as

$$k_d^{-1} = 17.24(\tau_e/\rho)^{-1/2} Sc^{2/3} \quad (130)$$

This equation is valid at Schmidt numbers above about 100.

In general, all the derivations based on the analogy between momentum and mass transfer lead to the general result

$$k_d^{-1}(\tau_e/\rho)^{1/2} = f(Sc) \quad (131)$$

where $f(Sc)$ is usually a rather complicated function. At higher values of the Schmidt number, all these functions approach the form

$$f(Sc) \rightarrow \text{const} \times Sc^n \quad \text{for } Sc \gg 1 \quad (132)$$

where n has values between 0 and 1 depending on the amount of eddying assumed in the fluid layer adjacent to the wall; i.e., depending on the expression used for ε/ν in the integration of Eqs. (122) or (127). A value of $n = 2/3$, as in the case of the example given above, seems to correspond best to the experimental findings in turbulent mass transport studies, although measured values of $3/4$ are also encountered in the literature.

We solve Eq. (130) for the mass transport coefficient k_d and introduce the dimensionless friction factor f which is linked with the wall shear stress through

$$f = \frac{2\tau_e}{\rho v_0^2} \quad (133)$$

where v_0 is a characteristic velocity of the flow system. This leads to

$$k_d = 0.058 v_0 (f/2)^{1/2} Sc^{-2/3} \quad (134)$$

Finally, we can make Eq. (134) dimensionless by means of the Stanton number

$$St = k_d/v_0 \quad (135)$$

$$St = 0.058(f/2)^{1/2} Sc^{-2/3} \quad (136)$$

The derivation of this turbulent mass transport equation does not specify the flow system to which it can be applied. In fact the treatment is quite general, and its result should be valid for any type of boundary layer and pipe flow. The particular flow situation is taken into account by introducing an appropriate expression for the friction factor. For example, for developed turbulent pipe flow the latter is given by the Blasius equation

$$f = 0.079 Re^{-1/4} \quad (137)$$

and one obtains for turbulent mass transport to the walls of a pipe

$$St = 0.0115 Re^{-1/8} Sc^{-2/3} \quad (138)$$

or in terms of a Sherwood number ($Sh = St Re Sc$)

$$Sh = 0.0115 Re^{7/8} Sc^{1/3} \quad (139)$$

Similar correlations can be obtained for other flow systems by inserting the appropriate expression for the friction factor into Eq. (136). Correlations for turbulent mass transfer can be found in the textbooks on transport phenomena⁽¹¹⁻¹⁶⁾ which all contain more or less extensive treatments of turbulent transport. Flow systems of particular interest in electrochemical engineering are discussed in the book by Pickett⁽⁴⁵⁾ and also in the review article by Selman and Tobias.⁽⁴⁶⁾

5.3. General Remarks

Let us conclude this section with a few general remarks on the origin and occurrence of turbulence. If the laminar streamline flow pattern is disturbed, for example, by an obstacle (such as a protrusion on a wall) or by a vibration, this disturbance, in general, will be damped out by the viscous forces so that the flow remains laminar. However, if the kinetic energy of the streaming fluid is large compared to the friction forces, sufficient momentum is transferred from the main flow to the disturbances to sustain them: The flow loses its stability and becomes turbulent. Therefore, the relative magnitude of the kinetic energy (or, in other words, of the inertial forces) and of the viscous forces should be decisive for whether a disturbance is damped or not, i.e., for whether a flow is laminar or turbulent under given conditions. The ratio of these two quantities is the dimensionless Reynolds number

$Re = vl/\nu$. The higher the value of Re , the larger the ratio of inertial forces to viscous forces.

In fact, there is for each flow system a critical Reynolds number above which the flow may become turbulent. For pipe flow, the critical Reynolds number is 2300 (with the pipe diameter as the characteristic length). However, laminar flow can be observed at much higher values provided that possible disturbances are carefully excluded (perfectly straight tube, very smooth surface, etc.).⁽²¹⁾ Actually it is not possible to say above which Reynolds number the flow must become turbulent; one only knows that below about $Re = 2000$ the flow is always laminar no matter how large a disturbance is.

The so called transition flow (at Reynolds numbers not much higher than the critical value) may have an intermittent character in that there is a random succession of short laminar and turbulent periods.⁽²¹⁾ In this regime it is very difficult to describe the flow quantitatively and thus the mass transfer behavior is hardly predictable.

In turbulent flow the velocity profile is significantly different from that encountered in laminar flow. Figure 10(a) shows schematically the velocity profiles for laminar and turbulent flow in a tube. In laminar flow one has a parabolic distribution, whereas in turbulent flow it is much flatter due to the lateral exchange of momentum. In boundary-layer flow systems, such as the flow past a plate (Section 2.3), the flow becomes turbulent at a distance x from the leading edge which corresponds to the critical Reynolds number of about 3×10^5 for a smooth plate. One can thus have laminar and turbulent flow simultaneously on a plate. In the turbulent part the velocity profile is steeper at the wall and the hydrodynamic boundary-layer thickness is larger than in laminar flow, as is shown schematically in Figure 10(b). This enlargement of the boundary layer is characteristic for turbulent flow.

A somewhat different type of turbulence is encountered in systems where the overall Reynolds number is below its critical value, but where the flow near the wall is disturbed by obstacles such as a fixed bed of particles or cloths placed in the fluid flow. In the wake of an obstacle, eddies are formed which enhance mass transport to the wall. According to what has just been said about the stability of laminar flow, the eddies should be damped by viscosity at low Reynolds numbers. However, since the obstacles are closely packed, new eddies are produced continuously. The flow is not turbulent in the usual sense and therefore one speaks of flow systems with eddy promoters. Since the ratio of increase in mass transfer rate to increase in momentum transfer rate (= friction losses) is considerably larger with eddy promoters than in ordinary turbulence,⁽⁴⁷⁾ these systems are of interest in industrial electrochemical processes.⁽⁴⁸⁾

For further information on turbulence the reader is referred to textbooks on transport phenomena,⁽¹¹⁻¹⁶⁾ on hydrodynamics,⁽²¹⁾ and on turbulent flow.⁽⁴⁹⁻⁵¹⁾

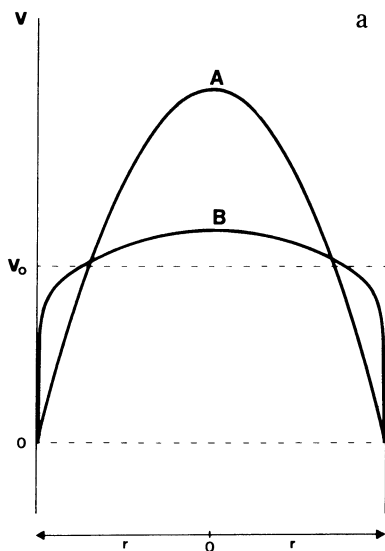
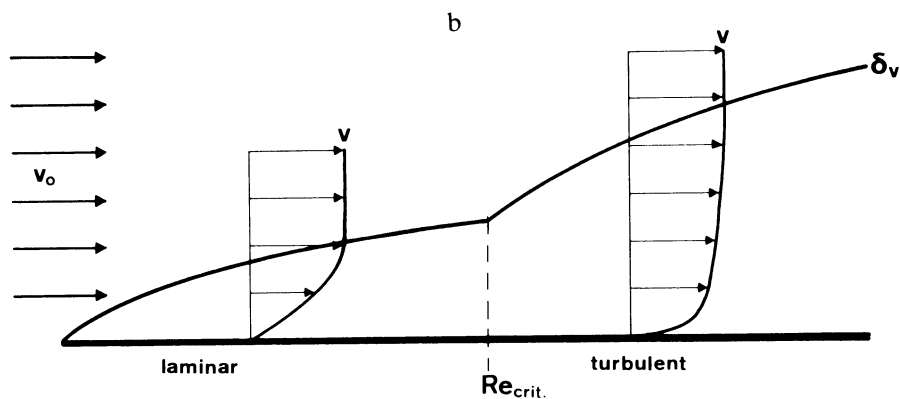


Figure 10. (a) Velocity distribution in a tube for laminar (curve A) and turbulent (curve B) flow. (b) Transition from laminar to turbulent flow on a plate.



6. Influence of Migration on Limiting Currents

6.1. Introduction

For the sake of simplicity, most of the considerations and discussions in this chapter are restricted to convective diffusion without migration. As a result, for the major part of the subjects treated here (e.g., the Nernst model, turbulent transport mechanism, and dimensional analysis), the argument is the same for electrolytic as well as for nonelectrolytic mass transport. Besides, we have seen that in electrolytic mass transport there are two limiting cases.

In one of them the contribution of migration to the overall mass transfer rate can be neglected (excess of supporting electrolyte), and in the other the contribution can be treated as if migration were absent (binary electrolyte). In Section 5 of Chapter 1 it has been shown that in these two cases the electric potential can be eliminated from the basic equations.

In the case of a binary electrolyte, the application of the electroneutrality condition leads to exactly the same form of the conservation equation as in nonelectrolytic mass transport, except for the diffusion coefficient for which the value of the neutral electrolyte has to be taken. In the equation for the electrode current density the influence of the electric field is expressed through the transport number and the use of the diffusion coefficient of the neutral electrolyte.

On the other hand, the addition of an excess of an indifferent electrolyte reduces the electric field to such an extent that it loses its influence on the transport of a minor ionic species in the solution, and diffusion and convection are the only transport mechanisms to be considered. Again we can apply the equations valid for nonelectrolytic mass transport or those for heat and momentum transport through the analogy. There are thus no specifically electrochemical phenomena in these two situations and the transport problems in these types of electrochemical systems can therefore be tackled with our knowledge from other domains in which transport processes play a role.

However, the problem becomes specifically "electrochemical" in the intermediate cases where a supporting electrolyte is present in a solution, but not in a large excess. There is also some practical interest in electrolyte solutions in which migration contributes to the overall current density. In fact, for practical applications binary electrolyte solutions are not very interesting because of their relatively low conductivity. The resulting ohmic potential drop can make limiting currents undetectable in analytical applications or in mass transport measurements (see Section 1.5). On the other hand in industrial applications the ohmic losses enhance the energy consumption of the process considerably so that the addition of an inert electrolyte is an economic necessity. Since in many cases the supporting electrolyte lowers the limiting current density and may have other disadvantages, one will probably avoid a large excess of it and instead make a compromise between maximum conductivity and maximum limiting current density.

In this section we will examine ionic mass transport in solutions with moderate concentration of supporting electrolyte, the theoretical treatment of which cannot be sufficiently approximated by considering one of the two limiting cases mentioned above.

We restrict our considerations to the case of the limiting current, i.e., the interfacial concentration $c_{\text{lim},e}$ of one of the species is zero. We call this species the limiting one and denote all quantities referring to it by the subscript *lim*. We further assume that the ions of the supporting electrolyte do not react at the electrode under the prevailing potential conditions.

6.2. Theoretical Approach

In principle, the theoretical approach is the same as for nonelectrolytic systems: The integration of the conservation equations, in which now the terms containing the electric potential are explicitly present together with the boundary conditions appropriate for the system under consideration, leads to the concentration and potential distributions from which one can calculate the interfacial flux densities of the reacting species and the electrode current density. For an ideal dilute electrolyte solution of arbitrary composition in which no chemical reactions take place, the conservation equation is [Eq. (21), Chapter 1]

$$\frac{\partial c_B}{\partial t} = D_B \nabla^2 c_B + F(RT)^{-1} z_B D_B \nabla \cdot (c_B \nabla \phi) - \mathbf{v} \cdot \nabla c_B \quad (140)$$

For each of the species present in the solution, Eq. (140) has to be solved together with the electroneutrality condition [Eq. (12), Chapter 1]

$$\sum_i z_i c_i = 0 \quad (141)$$

in order to obtain the solute concentrations and the potential.

This is a very complicated mathematical problem even for simple mass transport systems. It has been solved analytically by Eucken in 1907 for the simple case of three univalent ions in a stagnant Nernst diffusion layer.⁽⁵²⁾ Gordon *et al.*⁽⁵³⁾ gave a solution for the rotating disk electrode with the assumption of a constant electric field in the diffusion layer. A numerical solution exists for the case of a growing mercury drop.⁽⁵⁴⁾ The major contributions in this field are due to Newman who calculated the influence of migration on limiting currents by means of a numerical method for a number of cases.⁽⁵⁵⁻⁵⁷⁾ One of them is the rotating disk electrode which will illustrate the procedure. The problem of convective diffusion for this system is treated in more detail in a later volume. The axial flow velocity v_y depends only on the distance y normal to the disk and is, for a given y , constant over the disk. Therefore, the influx of substance from the bulk toward the interface is uniform over the disk and the thickness of the diffusion layer is constant; i.e., the concentration is a function of y only. On the other hand, the diffusion layer is very thin compared to the radius R of the disk (boundary-layer simplification) so that the potential gradient in the radial direction r , $\partial\phi/\partial r$, is negligible compared to $\partial\phi/\partial y$. Therefore, Eq. (140) reduces to

$$D_B \frac{d^2 c_B}{dy^2} - v_y \frac{dc_B}{dy} + F(RT)^{-1} z_B D_B \frac{d}{dy} \left(c_B \frac{d\phi}{dy} \right) = 0 \quad (142)$$

In addition, the velocity v_y can be approximated by the first term of its power series expansion, the diffusion layer being much thinner than the

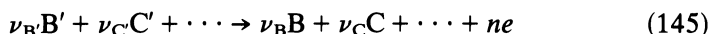
hydrodynamic boundary layer at the Schmidt numbers prevailing in electrolytic solutions:

$$v_y = -0.51(\omega^3/\nu)^{1/2}y^2 \quad (143)$$

Also we can state that the concentrations of all the species are constant and equal to their bulk values far from the electrode. This yields a first boundary condition:

$$c_B = c_{B,0} \quad \text{at } y = \infty \quad (144)$$

Except for the limiting species, the concentrations at the electrode solution interface are not known a priori. However, if one assumes that the reaction taking place at the electrode can be represented by [Eq. (30), Chapter 1]



one can relate the interfacial flux densities of the species to the electrode current density by means of Eq. (31) in Chapter 1:

$$N_{B,e} = j\nu_B(nF)^{-1} \quad (146)$$

While the electrode current density is not known in advance, the interfacial flux density of any of the species can be related to that of the limiting species. We can write

$$N_B = \frac{\nu_B}{\nu_{\text{lim}}} N_{\text{lim}} \quad \text{at } y = 0 \quad (147)$$

or, with the expressions for the flux densities [Eq. (19), Chapter 1],

$$\begin{aligned} D_B \frac{dc_B}{dy} + F(RT)^{-1} z_B D_{BC} \frac{d\phi}{dy} \\ = \frac{\nu_B}{\nu_{\text{lim}}} \left[D_{\text{lim}} \frac{dc_{\text{lim}}}{dy} + F(RT)^{-1} z_{\text{lim}} D_{\text{lim}} c_{\text{lim}} \frac{d\phi}{dy} \right] \quad \text{at } y = 0 \end{aligned} \quad (148)$$

This yields, together with the boundary condition for the limiting species

$$c_{\text{lim},e} = 0 \quad (149)$$

as many boundary conditions for the concentration as there are Eqs. (142).

In order to obtain a boundary condition concerning the electric potential one can set ϕ equal to zero at an arbitrary distance from the interface:

$$\phi = 0 \quad \text{at } y = y_{\text{max}} \quad (150)$$

With these boundary conditions the set of coupled ordinary differential equations (142) is solved numerically together with the electroneutrality equation.† After having calculated the concentration and potential profiles,

† The numerical method as well as the computer program used by Newman are described in reference 57.

the limiting current density can be evaluated from the interfacial flux density of the limiting species.

The result is represented in terms of a correction factor $I_{\text{lim},m}/I_{\text{lim}}$, where $I_{\text{lim},m}$ is the limiting current determined by diffusion *and* migration, and I_{lim} is the diffusion limiting current. Figure 11 shows the limiting-current correction factor for steady-state conditions as a function of the electrolyte composition for different cathodic reactions at a rotating disk electrode as calculated by Newman. The electrolyte composition is described by r , which is the ratio of the supporting electrolyte to the total electrolyte concentration (normality). The maximum enhancement of the limiting current density is found for $r = 0$, i.e., in the case of the binary salt. Under these conditions the correction factor for, say, the reduction of a cation is calculated from

$$(I_{\text{lim},m}/I_{\text{lim}})_{r=0} = (D/D_+)^{2/3}(1 - t_+)^{-1} \quad (151)$$

Equation (151) can be derived by dividing Eq. (4) by Eq. (1) (with $c_{\text{B},e} = 0$) and remembering that for the rotating disk electrode the diffusion-layer thickness is proportional to the one-third power of the diffusion coefficient. If the transport number is eliminated from (151) by combining Eqs. (44), (46), and (54) of Chapter 1, Eq. (151) can be written in an alternate form

$$\left(\frac{I_{\text{lim},m}}{I_{\text{lim}}}\right)_{r=0} = \left(1 - \frac{z_+}{z_-}\right)\left(\frac{D}{D_+}\right)^{-1/3} \quad (152)$$

For a symmetrical salt $z_- = -z_+$ and $I_{\text{lim},m}/I_{\text{lim}} = 2(D/D_+)^{-1/3}$. If the diffusion coefficient of the cation and the anion are not very different, the value of D/D_+ is close to unity [Eq. (54), Chapter 1], and the limiting current for the binary electrolyte will be about 2 times larger than in the case of the supported solution. In fact for the deposition of copper and silver, $I_{\text{lim},m}/I_{\text{lim}}$ at $r = 0$ is rather close to 2 (Figure 11). In both cases $D_+ < D_-$ and therefore $D/D_+ < 1$. As a consequence $(I_{\text{lim},m}/I_{\text{lim}})_{r=0} < 2$. However, for the discharge of hydrogen ions, the enhancement of the limiting current is larger due to the large value of the diffusivity of this ion compared to the diffusivities of the other ions present in the solution.

Migration does not necessarily enhance limiting currents. If an anion is reduced at a cathode, the electric field pushes the anion away from the electrode and migration thus counteracts diffusion. The "chemical force" driving the ions toward the electrode is still larger than the electric force, but the limiting current density is smaller than if there was an excess of indifferent electrolyte. An example for such a situation is the deposition of copper from a cyanide complex—mentioned in this context in Section 5.4 of Chapter 1. However, in this case the effect of migration is reduced by the cyanide ions that are liberated from the complex during the electrode reaction and that are accumulated in the diffusion layer. Their presence lowers the electric field in this region so that in a sense their action is that of an indifferent electrolyte.

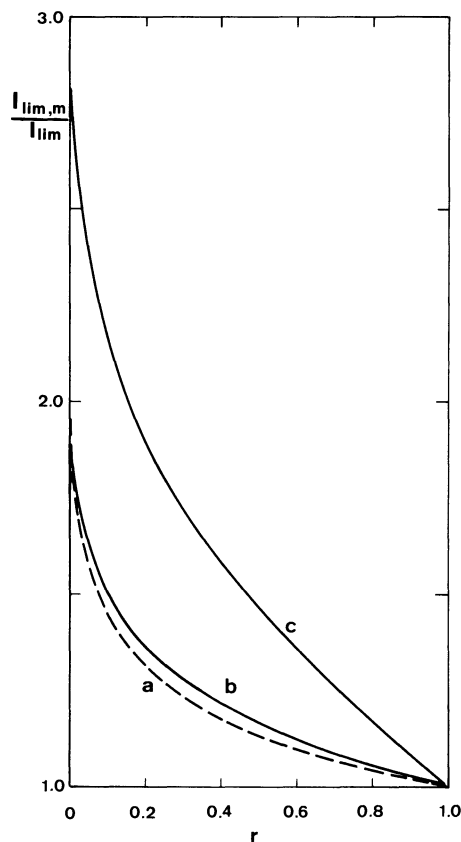


Figure 11. Limiting-current correction factor for different cathodic reactions at a rotating disk electrode.⁽⁵⁵⁾ Reduction of (a) Ag^+ from $\text{AgNO}_3\text{-HNO}_3$; (b) Cu^{+2} from $\text{CuSO}_4\text{-H}_2\text{SO}_4$; (c) H^+ from HCl-KCl .

It is not possible with such a system to realize the situation of a binary electrolyte with only one cation and one anion in solution. The same is true for redox reactions where the product species is always present in the vicinity of the electrode. Using the same method just described, Newman⁽⁵⁵⁾ calculated the effect of migration on the limiting currents for both the cathodic reduction of the ferricyanide ion and for the anodic oxidation of the ferrocyanide ion at a rotating disk electrode. Since the reacting species are anions in both cases, the limiting current is enhanced by migration in the anodic reaction while it is reduced in the cathodic process. The result is shown in Figure 12 for equimolar bulk concentrations of potassium ferricyanide and ferrocyanide in potassium hydroxide. Even in the complete absence of supporting electrolyte, the enhancement and reduction of the limiting currents are less than 10%. The maximum and minimum values for $I_{\text{lim},m}/I_{\text{lim}}$ are found when there is no supporting electrolyte and no product ion in the bulk solution. According to Newman the values for the rotating disk electrode are then $I_{\text{lim},m}/I_{\text{lim}} = 1.169$ and $I_{\text{lim},m}/I_{\text{lim}} = 0.886$ for the anodic and the cathodic reactions, respectively.

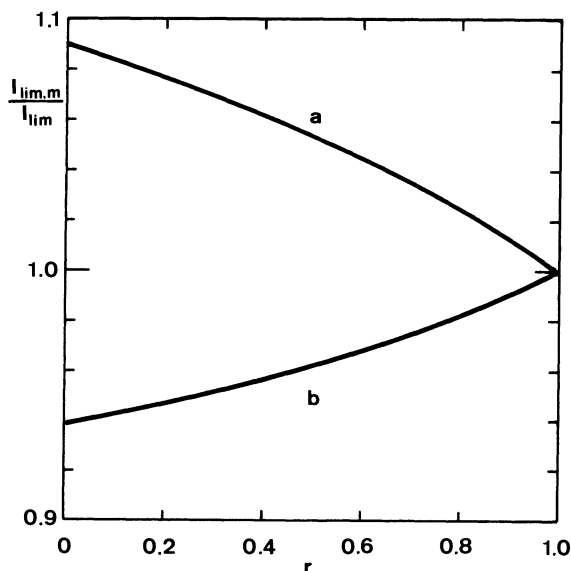


Figure 12. Limiting-current correction factor for ferri/ferrocyanide system at rotating disk electrode⁽⁵⁵⁾: (a) anodic reaction, (b) cathodic reaction.

A particular situation is encountered in solutions containing sulfate as anions and sulfuric acid as the supporting electrolyte. Such an electrolytic solution is used, for example, in copper refining as well as in copper and zinc electrowinning. Bisulfate ions do not dissociate completely except at low concentrations. In a solution with only partial dissociation, the concentration of hydrogen ions is smaller than in the case of total dissociation. Therefore, the conductivity is lower and as a consequence the electric field is reduced to a smaller extent than if all the sulfuric acid was dissociated into protons and sulfate ions. Hsueh and Newman⁽⁵⁸⁾ have calculated the effect of migration on limiting currents in the copper sulfate-sulfuric acid system for different degrees of dissociation. Figure 13 shows the result for the rotating disk electrode for the two extreme cases of no dissociation and of total dissociation.† One can see that the difference between the two situations is quite remarkable. The curve for a practical system will lie between these extreme cases depending on the dissociation constant of the bisulfate ion for which an equation correlating it to the ionic strength of the bulk solution is given in reference 58.

The considerations leading to Eqs. (151) and (152) are, in principle, the same for any hydrodynamic situation. It is easy to see that the correction terms for the limiting-current densities at $r = 0$ (single salt solution) should be the same for all flow systems which have the same dependence of the

† For the curve in Figure 11 total dissociation was assumed.

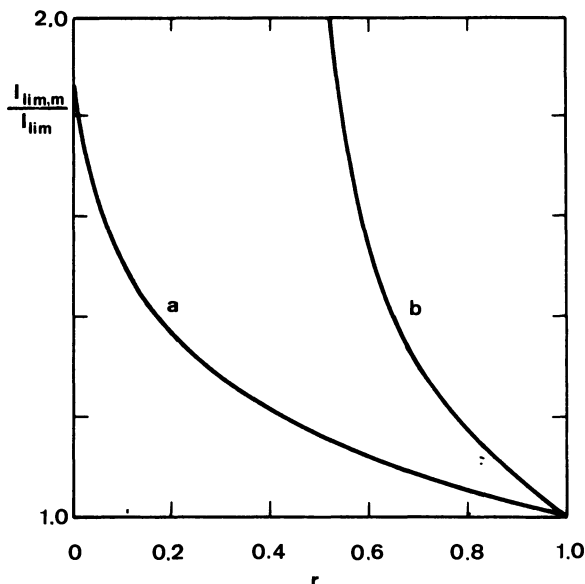


Figure 13. Limiting-current correction factor for deposition of copper from $\text{CuSO}_4\text{-H}_2\text{SO}_4$ solutions for (a) total and (b) no dissociation of bisulfate.⁽⁵⁸⁾

diffusion-layer thickness on the diffusion coefficient, provided that the components of the electrolytic solution are the same. In fact, Newman has shown⁽⁵⁹⁾ that the results obtained in the whole range $0 < r < 1$ for the rotating disk electrode can be directly applied to systems with arbitrary two-dimensional (e.g., flat plate) or axisymmetric (e.g., pipe flow) boundary layers.

Also, the correction factor shows the same dependence on the solution composition r for two unsteady diffusion systems: stagnant semi-infinite fluid and growing mercury drop. However, this correction factor is different from that applying to the aforementioned two-dimensional or axisymmetrical layers such as shown in Figures 11 and 12. But the difference is not large, except if the reacting ions have a very different mobility (as is the case for protons). It is remarkable and useful that the same or nearly the same correction can be used for a variety of hydrodynamic systems. It should be noted, however, that the integration which has to be performed numerically depends on the physical data of the system (diffusivities and mobilities of the species) and thus on the components of the solution.

Although the diffusion coefficients of most ionic species in aqueous solutions have similar values and the curves $I_{\text{lim},m}/I_{\text{lim}}$ do not differ much, there will be cases where it might be desirable, because of the peculiarity of the system or in order to achieve a better accuracy, to remake the whole calculation with the data pertinent to the system at hand. This can be readily done with the help of the detailed computer program given by Newman in his book.⁽⁵⁷⁾

A problem is the concentration dependence of the physical data. In the calculation leading to the numerical results of Figures 11 and 12 concentration-independent diffusivities were assumed, and values based on the ionic conductivities for infinite dilution were used. The correction factors presented in Figures 11 and 12 thus depend on the ratio r but not on the absolute values of the concentrations. In the case of concentrated solutions, one may prefer to employ values corresponding to the actual concentrations but the derivation sketched earlier in this section implies the use of the Nernst–Einstein relationship [Eq. (4.4) of, Chapter 1]

$$D_B = u_B^* RT = u_B RT (zF)^{-1} \quad (153)$$

which is valid only for infinite dilution.

6.3. Approximate Method

Before we complete this section let us briefly mention a simple approximation for the estimation of migration effects which has been widely used in the literature since it was employed by Wilke, Tobias and Eisenberg in 1953–1954 to describe electrolytic mass transport in natural convection and at rotating disks.^(6a,6b,60) One makes the overall mass balance for the whole diffusion layer, as we have considered it in the context of Figure 3. In the case of no migration the equation

$$N_{B,d} + (N_{B,c})_1 = (N_{B,c})_2 + (N_{B,c})_3$$

holds. If migration is not negligible the migration flux through plane AB of Figure 3 has to be taken into account in addition. For example, in the case of discharge of metallic cations of charge z_B and transport number t_B the migration flux density of these cations entering into the control volume $ABCD$ through plane AB , is $jt_B/z_B F$, where j is the current density.† On the other hand, the flux density of the cations leaving the control volume at the cathode (through plane CD) is $j/z_B F$. The mass balance yields

$$j(1 - t_B)/z_B F = (N_{B,c})_1 - (N_{B,c})_2 - (N_{B,c})_3 = (N_{B,d})_e \quad (154)$$

where it has been assumed that the algebraic sum of the convective fluxes of the cations $N_{B,c}$ remains the same, independent of whether there is migration

† This statement implies that the current density j is independent of y . This might seem at first sight surprising because in the control volume of Figure 3 the flux density of B by diffusion plus convection strongly varies with y . However, it must be remembered that the resultant of the convective fluxes $N_{B,c}$ of all species does not carry any current according to Eq. (23) of Chapter 1. Therefore no charges enter the control volume through BC when there is no diffusion flux.

or not. That is, it is assumed the equation

$$N_{B,d} + (N_{B,c})_1 = (N_{B,c})_2 + (N_{B,c})_3$$

remains valid. The diffusion flux density $(N_{B,d})_e$ is given by the usual mass transfer correlation applying to the hydrodynamic system considered. For example, for laminar flow along a plate it is given by Eq. (50). A question arises regarding the diffusion coefficients to be used. One can employ experimental values for the concentrations at hand (such as those given by Selman and Tobias for $\text{CuSO}_4 + \text{H}_2\text{SO}_4$ of various concentrations⁽⁴⁶⁾ or an average such as

$$D = D_1 + r(D_2 - D_1) \quad (155)$$

where D_1 and D_2 are the diffusion coefficients for $r = 0$ and $r = 1$, respectively (i.e., the values for the pure salt and for a great excess of indifferent electrolyte). For an ideal dilute solution, the correction factors $I_{\text{lim},m}/I_{\text{lim}}$ of Figures 11 and 12 can be compared to those calculated from Eqs. (154) and (155). In that case t_B is computed from Eq. (46) of Chapter 1 and D_1 and D_2 are taken for the ideal dilute solution. For a rotating disk the two values of $I_{\text{lim},m}/I_{\text{lim}}$ differ by a factor of 1–1.05 for $\text{CuSO}_4 + \text{H}_2\text{SO}_4$ and by a factor of 1–1.36 for $\text{HCl} + \text{KCl}$. In the case of concentrated solutions one can use in Eqs. (154) and (155) experimental values of t_B , D_1 , and D_2 for the solution at hand, whenever available. A comparison with the results of the integration of Eq. (142) is difficult in this case because, as has been already mentioned, the integration implies the validity of the Nernst–Einstein equation which is, in principle, valid only for infinite dilution. In any case an accurate treatment of concentrated solution is hardly possible at the present time. We will cover the tricky problem of electrolytic mass transport in concentrated systems in Section 9.

To conclude, let us note that in this section we have restricted ourselves to the influence of migration on limiting currents which is indeed the most important effect. However, migration also causes changes of concentration of the nonreacting species. For example, in the system $\text{CuSO}_4 + \text{Na}_2\text{SO}_4$ the Na^+ ions are drawn toward the cathode by the electric field and, since they are not discharged there, they accumulate until in the steady state the electric force is compensated by an osmotic or chemical force due to the concentration gradient acting in the opposite direction (see Section 4.7, Chapter 1). Such concentration changes can be of practical interest when, under special circumstances, they cause a noticeable change in pH near the interface, or when the concentration changes, through the concomitant variations of density, affect the hydrodynamic flow and thus indirectly the limiting current as in natural convection (see Section 7). The concentration changes of the supporting electrolyte have also been treated quantitatively by Newman. The reader is referred to his comprehensive work for further information.^(55–57)

7. Selected Systems of Interest to the Electrochemist

7.1. Introduction

The mass transfer behavior of a great number of flow systems has been investigated by electrochemical methods, but rather few of them are of practical interest in electrochemistry itself. Some specific flow systems are being used in electroanalysis and in methods for studying electrochemical reactions. In these applications one is interested in having a well-defined flow situation for which the mass transport correlation is known and/or in having a system that allows a variation of the mass transport rate in a large range. The latter aspect is especially important in studies of electrode kinetics when one wishes to distinguish between the contribution of different reaction steps to the overall kinetics of a process. Well-known flow systems for these purposes are the rotating disk, the rotating ring-disk, the rotating cylinder, the rotating wire, the wall-jet, and porous and thin-layer flow-through cells.

7.2. Industrial Processes

In industrial electrochemistry there are not many processes working under forced convection conditions. In some of them the concentrations of the reacting species are high, so that the actual working current densities are rather limited by energetic factors (ohmic drop) rather than by mass transfer. For example, this is the case in water and in chlorine electrolysis. In addition, the gas bubbles generated in a number of processes accelerate mass transport at the electrode where they are evolved (as well as at the counterelectrode) in a very efficient way. In chlorate electrolysis where one wants the electrolyte to circulate through the cell very rapidly, the ascending electrolytically formed gas bubbles act as an electrolyte pump in virtue of the gas-lift effect (see Chapter 3, Volume 2). A treatment of gas-evolving electrodes can be found in Chapter 7 of this volume.

7.3. Natural Convection

7.3.1. Vertical Electrodes with Laminar Flow: Theoretical Aspects

A very important kind of flow in certain industrial processes, especially in electrometallurgy, is natural convection. Natural or free-convection flow is caused by the density differences in a fluid which result from temperature or concentration gradients near an interface. For example, at a vertical electrode the concentration changes in the diffusion layer are usually accompanied by density changes in the horizontal direction. Depending on whether the electrolyte in the diffusion layer is heavier or lighter than in the bulk, a

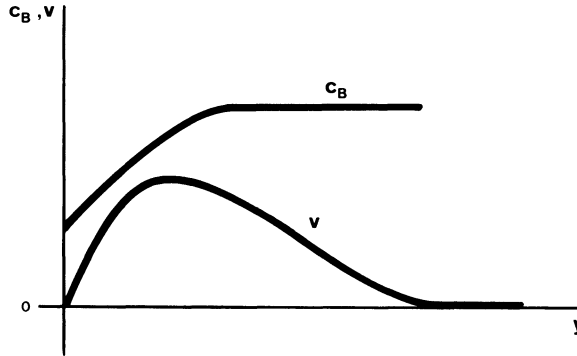


Figure 14. Velocity and concentration profiles in natural convection at a vertical electrode (schematic).

buoyancy force or a downward force acts on the diffusion layer and an upward or downward flow along the electrode results. In turn, the fluid flow influences the concentration profile and thus the mass flux at the wall. Eventually a steady state is established in which the mass and momentum transfer processes are closely linked. As in forced convection the main concentration and velocity changes occur in a narrow region near the electrode: The boundary-layer simplifications are applicable. Figure 14 shows schematically the velocity and concentration distributions in the boundary layer in natural convection at a vertical wall. A theoretical treatment of the coupled mass and momentum transport processes requires that the following set of equations be solved simultaneously:

$$\frac{\partial v_x}{\partial x} + \frac{\partial v_y}{\partial y} = 0 \quad (\text{continuity equation}) \quad (156)$$

$$v_x \frac{\partial v_x}{\partial x} + v_y \frac{\partial v_x}{\partial y} = \nu \frac{\partial^2 v_x}{\partial y^2} + \frac{g(\rho - \rho_0)}{\rho_0} \quad (\text{equation of motion}) \quad (157)$$

$$v_x \frac{\partial c_B}{\partial x} + v_y \frac{\partial c_B}{\partial y} = D_B \frac{\partial^2 c_B}{\partial y^2} \quad (\text{convective diffusion equation}) \quad (158)$$

y is the direction perpendicular to the wall, and x is the vertical direction. The last term in Eq. (157) represents the gravitational force acting on the fluid, ρ_0 being the density in the bulk. It is customary to express the density difference by a linear dependence on the concentrations of the species present in solution:

$$\frac{\rho - \rho_0}{\rho_0} = \sum_i \alpha_i (c_i - c_{i,0}) \quad (159)$$

α is the densification coefficient. Its meaning is comparable to that of the thermal expansion coefficient, which in natural convection heat transfer is the proportionality factor between the density and the temperature.

Early solutions of Eqs. (156)–(158) were obtained by the von Kármán–Pohlhausen integral method in which one refrains from fulfilling the fundamental differential equations for each volume element and instead requires a mass and momentum balance over the whole boundary layer, assuming arbitrary but plausible functions for the velocity and concentration profiles.^(5,60,61) Exact solutions of Eqs. (156)–(158) have been given by Ostrach,⁽⁶²⁾ Sparrow and Gregg,⁽⁶³⁾ and more recently by Selman and Newman.⁽⁵⁶⁾

For constant concentrations in the bulk and at the interface, the calculations lead to the following equation for mass transfer at the wall (laminar flow):

$$\bar{Sh} = C(Sc \bar{Gr})^{1/4} \quad (160)$$

The dimensionless coefficient C is a function of the Schmidt number. Its limiting value at high Schmidt numbers ($Sc > 10^3$) is 0.67 (for the average Sherwood number over an electrode of height L). Gr is the dimensionless Grashof number characteristic for natural convection:

$$\bar{Gr} = \frac{g(\rho_0 - \rho_e)L^3}{\rho_0\nu^2} \quad (161)$$

or, with (159)

$$\bar{Gr} = \frac{g \left[\sum_i \alpha_i (c_{i,0} - c_{i,e}) \right] L^3}{\nu^2} \quad (162)$$

The characteristic length L in \bar{Gr} and \bar{Sh} is the electrode height.

From Eq. (160) we can calculate the mass transfer coefficient \bar{k}_d . We obtain for the case of a binary electrolyte solution such as CuSO_4 (with deposition or dissolution of copper)

$$\bar{k}_d = 0.67 g^{1/4} \{ \alpha_{\text{CuSO}_4} [(c_{\text{CuSO}_4})_0 - (c_{\text{CuSO}_4})_e] \}^{1/4} D^{1/4} \nu^{-1/4} L^{-1/4} \quad (163)$$

The value $C = 0.67$ in (160) is used since in electrolyte solutions the Schmidt number is usually large. We have also taken into account that for a binary electrolyte the density term in the Grashof number reduces to

$$\frac{\rho_0 - \rho_e}{\rho_0} = \alpha_{\text{CuSO}_4} [(c_{\text{CuSO}_4})_0 - (c_{\text{CuSO}_4})_e] \quad (164)$$

where α_{CuSO_4} is the proportionality factor relating the concentration of the CuSO_4 solution to its density.† From the mass transfer coefficient we can calculate the current density in the same way as was done in Section 2.3. One

† In principle, two coefficients α are involved, $\alpha_{\text{Cu}^{2+}}$ and $\alpha_{\text{SO}_4^{2-}}$. However, because of electroneutrality $c_{\text{Cu}^{2+}}$ is everywhere equal to $c_{\text{SO}_4^{2-}}$ and the only measurable quantity is the overall proportionality factor α_{CuSO_4} .

obtains from Eq. (163) together with Eqs. (3), (4), and (6d) for the cathodic limiting current density [$(c_{\text{CuSO}_4})_e = (c_{\text{Cu}^{2+}})_e = 0$]

$$\bar{j}_{\text{lim}} = -0.67 z_B F (1 - t_B)^{-1} D^{3/4} (c_{\text{Cu}^{2+}})^{5/4} (g \alpha_{\text{CuSO}_4} / \nu L)^{1/4} \quad (165)$$

In contrast to the case of forced convection, \bar{j}_{lim} is not proportional to the concentration difference between bulk and interface but is proportional to the power 5/4 of this difference. The reason is that according to Eq. (163) \bar{k}_d (and thus δ) are not as usual independent of concentration, because the buoyancy force and thus the flow velocity depend on the density difference and therefore on the concentration difference between bulk and interface. Equation (165) is quite analogous to that applying to natural convection heat transfer.

In the case of a mixture of electrolytes the situation is more complicated because then the density difference $\rho_0 - \rho_e$ entering into the Grashof number not only depends on the concentration of the reacting species but also on that of the ions which do not react at the electrode. Let us consider a specific example, that of Cu deposition from a solution of $\text{CuSO}_4 + \text{H}_2\text{SO}_4$, as used in the industrially important refining and electrowinning of copper. The cathode potential is such that virtually no hydrogen is evolved. The H^+ ions migrate toward the cathode under the influence of the electric field, and since they are not discharged they accumulate there until a concentration develops such that, in the steady state, a diffusion (or osmotic) force balances the electric force (see Section 4.7 of chapter 1). Thus in the vicinity of the cathode there is an increase in acidity. Figure 15 shows schematically the concentration profiles of the H^+ and Cu^{2+} ions in the boundary layer. The concentration variation of the acid affects the density profile and thus the mass transport conditions. We see that in contrast to the case of forced convection the addition

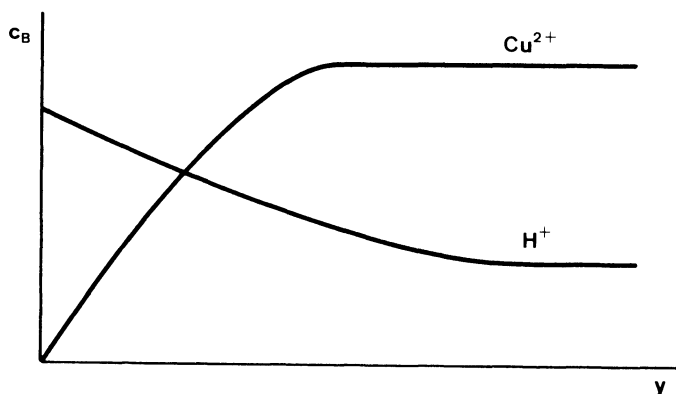


Figure 15. Concentration profiles of Cu^{2+} and H^+ ions in the deposition of copper from $\text{CuSO}_4\text{-H}_2\text{SO}_4$ solutions (schematic).

of a supporting electrolyte—although it eliminates the influence of migration—does not make the electrolytic natural convection problem fully similar to the nonelectrolytic situation.

First we treat the problem in a very simple generally applicable manner, which has been repeatedly used in the literature^(6a,64-67) and which is based essentially on the approximate procedure discussed at the end of Section 6 for the estimation of the migration effects in electrolytic mass transport.

Since the densification coefficients of the individual ionic species are unknown one uses the densification coefficients of the neutral electrolytes which are readily obtained from solution density data. Thus,

$$\sum_i \alpha_i (c_{i,0} - c_{i,e}) = \alpha_1 (c_{1,0} - c_{1,e}) + \alpha_2 (c_{2,0} - c_{2,e}) \quad (166)$$

where the subscripts 1 and 2 refer to CuSO_4 and H_2SO_4 , respectively. The concentrations of the neutral electrolytes are directly related to the concentrations of the ions: $c_1 = c_{\text{Cu}^{2+}}$; $c_2 = \frac{1}{2}c_{\text{H}^+}$ (total dissociation of the sulfuric acid being assumed). Thus, instead of (166) we can write

$$\sum_i \alpha_i (c_{i,0} - c_{i,e}) = \alpha_1 (c_{\text{Cu}^{2+},0} - c_{\text{Cu}^{2+},e}) + \alpha_2 \frac{1}{2} (c_{\text{H}^+,0} - c_{\text{H}^+,e}) \quad (167)$$

The concentration difference of the hydrogen ion can be related to that of the cupric ion. Applying the approximate method for the estimation of migration effects as discussed in Section 6, one obtains from Eq. (163) for the interfacial flux density of a species B

$$\bar{N}_{B,e} = \frac{\bar{j}_B}{z_B F} - 0.67 g^{1/4} \left[\sum_i \alpha_i (c_{i,0} - c_{i,e}) \right]^{1/4} D_B^{3/4} \nu^{-1/4} L^{-1/4} (c_{B,0} - c_{B,e}) \quad (168)$$

Equation (168) is written both for the cupric and hydrogen ion. Combination of these two equations, taking into account that for the nonreacting hydrogen ion $\bar{N}_{B,e} = 0$, yields (see p. 22 of Chapter 1)

$$(c_{\text{H}^+,0} - c_{\text{H}^+,e}) = (c_{\text{Cu}^{2+},0} - c_{\text{Cu}^{2+},e}) \left(\frac{2 t_{\text{H}^+}}{1 - t_{\text{Cu}^{2+}}} \right) \left(\frac{D_{\text{Cu}^{2+}}}{D_{\text{H}^+}} \right)^{3/4} \quad (169)$$

Thus, the densification can be expressed in terms of an overall densification coefficient α and the concentration difference of the reacting copper ion

$$\sum_i \alpha_i (c_{i,0} - c_{i,e}) = \alpha (c_{\text{Cu}^{2+},0} - c_{\text{Cu}^{2+},e}) \quad (170)$$

with†

$$\alpha = \alpha_1 - \alpha_2 \frac{t_{\text{H}^+}}{1 - t_{\text{Cu}^{2+}}} \left(\frac{D_{\text{Cu}^{2+}}}{D_{\text{H}^+}} \right)^{3/4} \quad (171)$$

† Note that the same problem, mentioned toward the end of Section 6, regarding the diffusion coefficients to be used arises here. Further discussion of this point is to be found in Section 9.

We now calculate the limiting current density for the copper deposition reaction by inserting (170) into (168), setting $c_{\text{Cu}^{2+},e} = 0$ and multiplying by $z_B F$

$$\bar{j}_{\text{lim}} = 0.67 z_B F (1 - t_{\text{Cu}^{2+}})^{-1} D_{\text{Cu}^{2+}}^{3/4} c_{\text{Cu}^{2+},0}^{5/4} (g\alpha/\nu L)^{1/4} \quad (172)$$

A more sophisticated treatment involving a numerical integration of the fundamental differential equation has been presented by Selman and Newman.⁽⁵⁶⁾ The approach method was similar to that outlined in the first part of Section 6. The result is represented in terms of a multiplicative correction factor ψ for the preexponential coefficient C in the dimensionless (nonelectrolytic) mass transport correlation [Eq. (160)] as a function of the solution composition in Figure 16. The correction factor has been calculated for both complete and no dissociation of the bisulfate ion. As in the example given in Section 6, the effect of migration is much more important with bisulfate than with sulfate. It is interesting to note that the limiting current correction factor does not approach unity for an excess of sulfuric acid as is the case in forced convection systems but is lower than one.

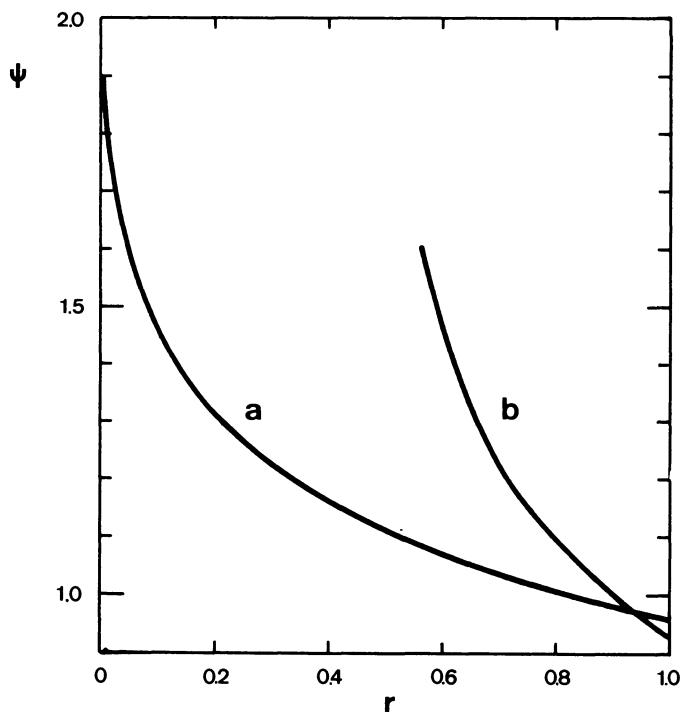


Figure 16. Correction factor for migration effect in copper deposition from $\text{CuSO}_4\text{-H}_2\text{SO}_4$ solutions under natural convection conditions: (a) total and (b) no dissociation of bisulfate.⁽⁵⁶⁾ Meaning of ψ given in Section 7.3.1.

There is, besides migration, an additional effect accounted for by the correction factor. It is due to the fact that the diffusion layer of H_2SO_4 is thicker than that of CuSO_4 (see Figure 15) because the hydrogen ion has a larger diffusion coefficient than the copper ion. As a result the density profile shows a minimum within the diffusion layer. This phenomenon, in turn, influences the velocity profile and thus the mass transfer rate in such a way that the limiting current is smaller than expected at an excess of sulfuric acid.

7.3.2. Vertical Electrodes with Laminar Flow: Experimental Results

Figure 17 shows experimental results, including measurements of limiting currents in metal deposition, nonelectrolytic dissolution of salts, and heat transfer data to air.^(8,33,60) In the electrolytic experiments, mixtures of electrolytes were used and the Grashof number was calculated by the approximate method of Eq. (171). All variables (L , c_0 , D , ν) were varied within a broad range. Nevertheless, all results fall neatly on the same line when they are represented in terms of the dimensionless numbers Sh , Gr , and Sc . This illustrates the advantage of using dimensionless groups. The figure also illustrates the fact that by and large electrolytic mass transport is only a special

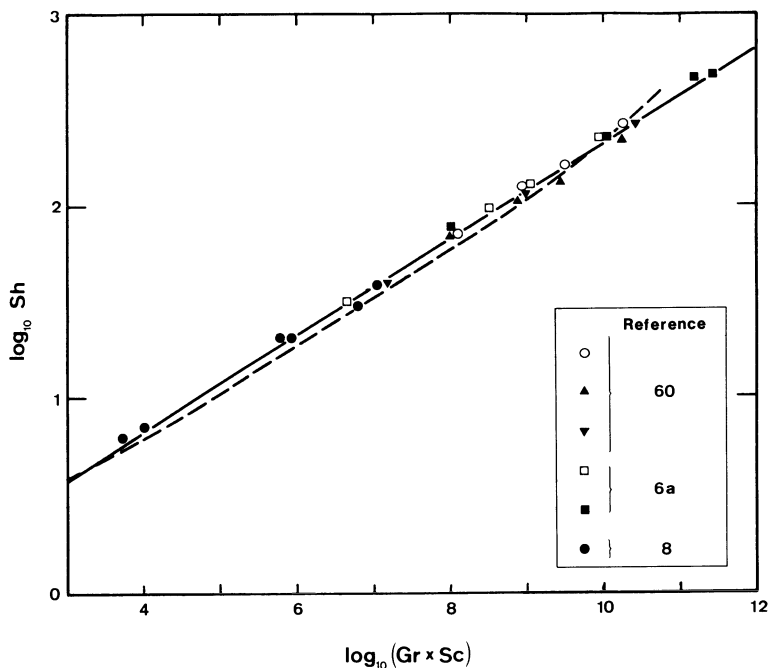


Figure 17. Natural convection at vertical plates. Experimental results. Points, mass transfer (○ and ▲ dissolution experiments, other points limiting-current measurements); broken line, heat transfer; solid line, Eq. (160) with $C = 0.67$.

case of transport phenomena in general and can be well predicted from other transport data. This appears to apply even to natural convection where the situation is less favorable than usual because, as discussed in Section 7.3.1, electric migration influences the hydrodynamic flow through its action on the concentrations within the diffusion layer, including those of nonreacting species. Note that the lines for heat and mass transfer are fairly close in spite of the fact that Pr was about 1 (air) whereas Sc ranged from 400 to 80,000. The exponent of $Sc Gr$ and the coefficient C agree well with theoretical expectations.

7.3.3. Vertical Electrodes with Turbulent Flow

At a certain height the natural convection becomes turbulent, in spite of the low flow velocities involved (typically a few mm s^{-1}). The critical value of $Sc \overline{Gr}$ is about 10^{12} . It seems to depend on Sc and is lower at low Sc values. In industrial processes, with stirring by natural convection, essentially (e.g., copper refining) vertical electrodes of a height of 1 m are used. Under these conditions, with concentrated solutions, the natural convection is turbulent, at least for a large part of the electrode. Limiting-current measurements with electrodes up to 1 m in height yielded the correlation

$$\overline{Sh} = c(Sc \overline{Gr})^a \quad (173)$$

with $a = 0.28$, $c = 0.31$,⁽⁶⁸⁾ and $a = 0.29$, $c = 0.15$.⁽⁶⁹⁾ The results pertain to systems where the flow probably was not turbulent over the whole electrode. For fully developed turbulence values of about 0.33 for the exponent a have been reported. The numerous studies of mass and heat transfer by laminar and turbulent natural convection are reviewed in references 70 and 71. A recent comprehensive discussion of the instability phenomena in natural convection is to be found in references 72.

7.3.4. Occurrence and Decay of Natural Convection: Case of Horizontal Plates

Natural convection, in principle, is always present in electrolytic systems with the electrodes arranged such that gravitational forces can cause a fluid flow. This is not the case at horizontal electrodes with the electrolyte density decreasing in the upward direction, since this is a hydrodynamically stable situation. Natural convection flow can also be suppressed by the viscous forces in systems with small dimensions. In a cell with vertical parallel electrodes, the flow is slowed down by friction more and more when the interelectrode distance decreases and eventually disappears completely. Böhm and Ibl⁽⁷³⁾ have shown that this transition occurs at electrode distances of about 0.5 mm and that with smaller gaps one has convection-free electrolysis, described in Chapter 2, in which the current is inversely proportional to the interelectrode

distance. Other systems in which natural convection flow is impeded by friction are porous electrodes.⁽⁷⁴⁾ Both cases are important in electrolytic cell design and especially in battery design where a large specific electrode area is one of the essential requirements.

At horizontal electrodes with the density decreasing in the downward direction, the situation is hydrodynamically unstable and a minor disturbance initiates a fluid flow. Experimental studies of mass transport at horizontal electrodes of different shapes have shown that in laminar flow the mass transport correlation is similar to that for the vertical plate

$$\overline{Sh} = c(\text{Sc } \overline{Gr})^{1/4} \quad (174)$$

with $c = 0.54$ (reference 75) and $c = 0.64$ (reference 76).

The characteristic length in (174) is the diameter of circular electrodes⁽⁷⁶⁾ or an equivalent diameter (surface area divided by surface perimeter) in the study using electrodes of different shapes.⁽⁷⁵⁾ The difference in the coefficient c may be due to the fact that the electrodes used in reference 76 were embedded in an insulating plate. At horizontal electrodes the flow becomes turbulent at much lower values of $\text{Sc } \overline{Gr}$ than at vertical plates. The critical value is about 10^7 . Above this limit experimental studies yielded for the mass transport correlation

$$\overline{Sh} = c(\text{Sc } \overline{Gr})^{1/3} \quad (175)$$

with $c = 0.15$ (reference 75), $c = 0.16$ (reference 76), and $c = 0.19$ (reference 77).

In reference 77 the distance between the electrode and a horizontal diaphragm placed above the electrode was used as the characteristic length. However, this distance had no influence on the mass transfer rate unless it was less than a few millimeters. The choice of a characteristic length is not very important here since the $(\text{Sc } \overline{Gr})^{1/3}$ dependence of \overline{Sh} demonstrates that the mass transfer rate does not depend on the dimensions of the electrodes. This is quite often the case with mass transport under fully developed turbulent flow conditions (see Section 7.4).

In the case of a mixture, the same difficulty regarding the evaluation of $\rho_0 - \rho_e$ is encountered as for vertical electrodes. The same approximate method as that explained on p. 196 has been used to take into account the influence of the concentration changes of an indifferent electrolyte. The use of this approximation may be one of the reasons for the abovementioned differences between the c values reported by various authors.

7.4. Channel Flow

Unless three-dimensional electrodes are used, the electrodes in electrolytic reactors commonly have the form of plates and are arranged in parallel. This configuration is suitable for accelerating the mass transport rate by

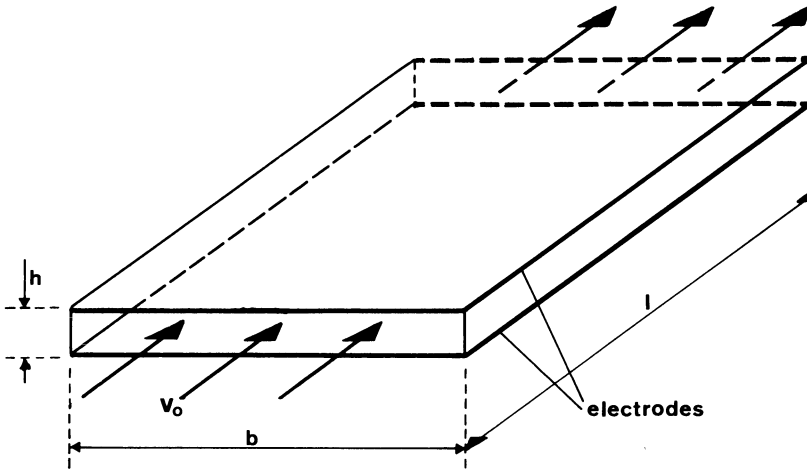


Figure 18. Schematic representation of channel cell.

stirring. This is achieved by pumping the electrolyte through the gap formed by the electrodes. We shall examine mass transfer in this flow system, usually referred to as channel flow, as a second example (Figure 18). The electrolyte is pumped through the cell with an average flow rate v_0 . The length of the plate electrodes in the flow direction is l , their width b . The distance between the electrodes is h . Channel flow has been studied extensively and a large number of mass transport correlations is available in the literature.⁽⁴⁶⁾ However, in order that an appropriate correlation can be chosen, the flow pattern has to be examined. The first question is whether the flow between the plates is laminar or turbulent. The same criterion applies as in circular tubes.⁽⁷⁸⁾ The critical Reynolds number is about 2300, where the hydraulic diameter (or equivalent) diameter d_h of the channel is used as the characteristic length in Re

$$Re = \frac{v_0 d_h}{\nu} \quad (176)$$

The hydraulic diameter is defined as 4 times the channel cross-sectional area divided by the wetted perimeter. For our channel it is

$$d_h = \frac{4bh}{2(b+h)} \quad (177)$$

If the width of the plates is large compared to the distance between them, as will probably be the case in an electrolytic reactor, the hydraulic diameter can be approximated by

$$d_h \approx 2h \quad (178)$$

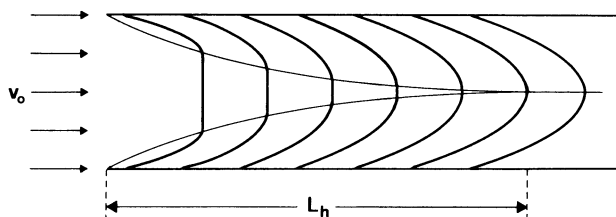


Figure 19. Developing velocity profile in a channel (not to scale).

Secondly, we have to check the extent to which the flow in the channel is developed. The flow pattern gradually changes until it reaches its final form. Let us consider the simplest case: at the entrance the velocity profile is practically uniform across the channel (see Figure 19). Due to the friction forces hydrodynamic boundary layers develop at the walls *A* and *B* (see Section 1) and increase in thickness until they reach the midplane of the channel and merge.† In this section of the channel the walls can be considered to behave as the plate treated in Section 2.3. Theoretically, an infinite distance from the entrance is required for the final flow pattern to be established, but in practice the flow is considered to be developed when the velocity in the midplane is within 1% of its final value. The hydrodynamic entrance length L_h for laminar flow in a thin channel is given by⁽⁷⁹⁾

$$L_h/d_h = 1.12 \times 10^{-2} \text{Re} \quad (179)$$

For turbulent flow the hydrodynamic entrance length L_h is independent of the Reynolds number:⁽²¹⁾

$$L_h/d_h = 50 \quad (180)$$

The question of whether or not the flow is developed is relevant to mass transport, since the latter is influenced by the hydrodynamic conditions. The thickness of the diffusion layer is closely related to that of the hydrodynamic boundary layer, as shown in Section 4.3.

Undeveloped flow conditions are encountered if the leading edge of the electrodes coincides with the entrance of the channel, whereas the flow is developed at an electrode located downstream (at a distance larger than L_h). One normally has to use different mass transport correlations for the two regions.

There is a third aspect to be considered when choosing a mass transport correlation. A diffusion layer builds up at the electrodes similar to the hydrodynamic boundary layers and, as for the flow, one speaks of developing or developed mass transfer conditions. A mass transfer entrance length L_M is defined in a way analogous as for L_h . If we combine all the possible conditions

† In principle, there are such boundary layers at each of the four walls of the channel, but since the gap is assumed to be narrow compared to b the velocity changes mainly in the direction perpendicular to the electrodes.

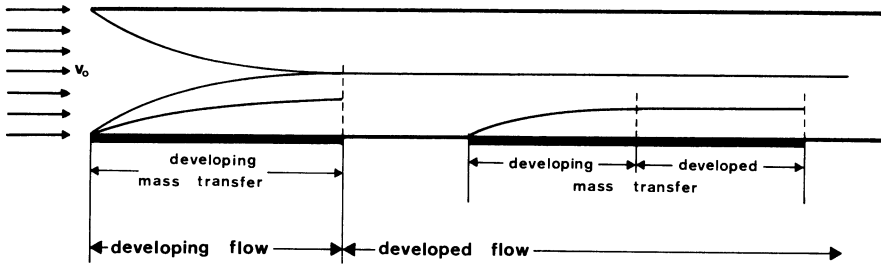


Figure 20. Schematic representation of the different flow and mass transfer regimes in a channel cell (not to scale).

listed above we find that there are three different situations each for laminar and turbulent flow (Figure 20) for each of which a different mass transport correlation applies. In the following the possible combinations shall be discussed briefly and mass transport correlations shall be given.

7.4.1. Developing Flow

As one can easily see in Figure 20, there can be no developed mass transport in this section of the channel. A diffusion layer and a hydrodynamic boundary layer are building up simultaneously from the leading edge of the channel wall. As already mentioned, this situation corresponds, in principle, to the plate electrode treated in Section 2.3. Therefore it should be possible to apply in *laminar flow* Eq. (50) derived for this system. Equation (50) is written in dimensionless form (see Section 3):

$$\bar{Sh} = 0.678 Sc^{1/3} Re^{1/2} \tag{78a}$$

with the plate length l as the characteristic length in \bar{Sh} and Re . However, the condition that the counterelectrode is located at an infinite distance from the electrode is not fulfilled in the channel and a slight influence of the hydraulic diameter on the mass transfer rate can be observed. Pickett and Ong⁽⁸⁰⁾ modified (78a) by introducing an empirical correction factor which takes the finite interelectrode distance into account:

$$\bar{Sh} = 0.96 \left(\frac{l}{d_h} \right)^{0,05} Sc^{1/3} Re^{1/2} \tag{181}$$

For *turbulent* conditions the same authors⁽⁸⁰⁾ found that there is no appreciable effect of the developing flow on the mass transfer rate and that the Chilton–Colburn analogy is suitable for this case.⁽⁴⁶⁾

7.4.2. Developed Flow

In *laminar flow* the mass transfer entrance length is extremely large, so that in practical systems developed mass transport conditions are usually not

realized (Ref. 12, p. 412). For undeveloped laminar mass transport in channels, an equation of the Levêque type used for circular tubes can be applied. Roušar *et al.*⁽⁸¹⁾ gave the following correlation:

$$\overline{\text{Sh}} = 1.85 \phi \left(\text{Re Sc} \frac{d_h}{l} \right)^{1/3} \quad (182)$$

Here the hydraulic diameter is used as the characteristic length in the dimensionless groups. ϕ is a correction factor taking into account the geometry of the flow channel. Values of ϕ are given in reference 79 for various ratios b/h and for cases where the electrode does not occupy the whole width of the channel wall. Note that in developing mass transport there are two characteristic lengths that play a role. d_h is relevant for the flow pattern and l takes into account the fact that the diffusion layer is developing. Thus an additional dimensionless group is required in the mass transfer equation (see Section 3.4.)

In *turbulent flow* the mass transport entrance length is very short due to the intense mixing by the turbulent eddies. From the experimental results of Van Shaw *et al.*⁽⁸²⁾ one can derive L_M as approximately given by

$$L_M/d_h = 10^4 \text{Re}^{-7/8} \quad (183)$$

For example, at a Reynolds number of 10^4 the entrance length is about 3 equivalent diameters. For this *entrance region* the same authors give an empirical mass transport correlation:

$$\overline{\text{Sh}} = 0.276 \text{Re}^{0.58} (\text{Sc } d_h/l)^{1/3} \quad (184)$$

As in laminar flow there are two characteristic lengths to be considered.

Unless the mass transfer entrance region is eliminated by the use of segmented electrodes, one cannot realize conditions with *fully developed* mass transfer. However, if the electrode is sufficiently long, the entrance effects become unimportant. This has the practical consequence that the mass transfer rate no longer depends on the length of the channel. In this case an equation such as Eq. (136), which has been derived on the basis of the analogy between momentum and mass transfer, can be used:

$$\overline{\text{Sh}} = \text{const} \times \text{Sc}^{1/3} (f/2)^{1/2} \text{Re} \quad (185)$$

For channels, the friction factor can be described with good accuracy by the Blasius equation (137) with the hydraulic diameter as the characteristic length.⁽⁷⁶⁾ The mass transport equation then takes the form:

$$\overline{\text{Sh}} = \text{const} \times \text{Sc}^{1/3} \text{Re}^{7/8} \quad (186)$$

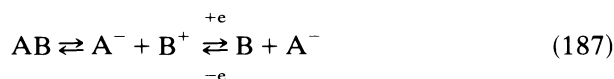
Empirical correlations differ very little from (186). The exponent of Re lies in the range 0.87–0.92. The constant in the equation is approximately 10^{-2} .

A number of correlations for developed mass transfer in turbulent flow can be found in reference 46.

It should be emphasized that the correlations given above are only typical examples for the respective conditions. For each of the situations discussed there are other—mostly empirical—correlations in the literature (see, e.g., reference 46). The differences between them are probably due in many cases to a slightly different experimental arrangement. It is therefore advisable to choose for one's own purposes a correlation that has been obtained under experimental conditions as close as possible to those of the flow system at hand. In many cases the choice will be somewhat arbitrary anyhow since the system cannot usually be accurately defined in terms of the general scheme outlined above. A variety of transition regimes is possible. For example, it may often be that only a part of the electrode lies in the region of developed flow or that the flow pattern is disturbed by construction elements of the cell.

8. Mass Transport Coupled with Chemical Reactions

Often the electrode reaction proper is preceded or followed by a homogeneous chemical reaction taking place in the solution, for example, according to the scheme:



The reaction $AB \rightleftharpoons A^- + B^+$ is a prereaction or a postreaction depending upon whether the electrode current is cathodic or anodic, respectively. The case of a homogeneous chemical reaction coupled with mass transport is discussed in Chapter 2 of this volume for convection free systems. It has been the object of many papers, especially in connection with polarography and with related methods. We will therefore restrict ourselves here to a brief discussion with a few general remarks.

If the chemical reaction is *slow*, it needs a large volume to run at a sufficient speed and takes place mainly in the bulk solution, outside of the diffusion layer. The amount of substance generated or consumed per unit time depends on the volume of the cell and, besides the current density, the current concentration (i.e., the current divided by the cell volume) is a relevant quantity for the operation of the system. This concept plays a role in chlorate electrolysis which is discussed in Chapter 3 of Volume 2.

If the chemical reaction is *fast*, it takes place close to the electrode: In the example of Eq. (187) the species B (which is involved in both the chemical and electrode reaction) is generated or consumed by the chemical reaction within the diffusion layer, in a region called the reaction layer. If the reaction

is very fast—and we will see more precisely what this means later—the reaction layer is thin and located in the inner part of the diffusion layer where convection is small or negligible. The fundamental differential equation (13) for the steady state ($dc_B/dt = 0$) takes the form

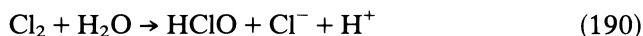
$$D_B \nabla^2 c_B = -\sum_r v_{Br}^* \quad (188)$$

In the absence of convection and a chemical reaction, the steady state at a plane electrode implies a linear concentration profile which can be realized only if the diffusion layer extends up to a counterwall (see p. 28 of Chapter 1 and p. 137 of this chapter). In contrast to this, in a reacting system a steady state with a nonlinear concentration profile can be established even in the absence of convection, as can be easily deduced from Eq. (188): The difference between the diffusion fluxes entering and leaving the infinitesimal control volume of Figure 3 in Chapter 1 is balanced by the generation or consumption of the considered species within the control volume.

Let us consider as an example the electrolytic generation of chlorine from a NaCl solution which is of considerable industrial importance (chlorine and chlorate electrolysis). The anode reaction is



Figure 21 shows schematically the main concentration profiles in the diffusion layer. The chlorine hydrolyzes in the aqueous solution according to



If the solution is not too acid (as is the case in chlorate electrolysis, see Section 2.3, of Chapter 3, of Volume 2), the equilibrium of reaction (190) lies sufficiently on the right-hand side and it proceeds according to an irreversible first-order reaction

$$\frac{dc_{\text{Cl}_2}}{dt} = -kc_{\text{Cl}_2} \quad (k = \text{reaction rate constant}) \quad (191)$$

At a plane electrode, (188) reduces to

$$D_{\text{Cl}_2} \frac{d^2 c_{\text{Cl}_2}}{dy^2} = kc_{\text{Cl}_2} \quad (192)$$

If the current density j generating Cl_2 according to Eq. (189) is given, our first boundary condition is†

$$D_{\text{Cl}_2} \left(\frac{dc_{\text{Cl}_2}}{dy} \right)_{y=0} = \frac{j}{2F} \quad (193)$$

† Note that in the case of chlorate electrolysis the current density generating Cl_2 is not equal to the total electrolysis current density j but rather to jt_1 because the fraction t_1 of the total current is used to make chlorate (see Chapter 3, Volume 2).

Since we have assumed a pH range in which the equilibrium of reaction (190) lies strongly on the right, our second boundary condition can be written

$$c_{\text{Cl}_2} = 0 \quad \text{for } y \rightarrow \infty \quad (194)$$

With these boundary conditions the solution of (192) is

$$c_{\text{Cl}_2} = (j/2FD_{\text{Cl}_2}a) \exp(-ay) \quad \text{with } a = (k/D_{\text{Cl}_2})^{1/2} \quad (195)$$

The concentration of chlorine at the interface is

$$(c_{\text{Cl}_2})_e = j/(2FD_{\text{Cl}_2}a) \quad (196)$$

If we define an equivalent thickness δ_R of the reaction layer in the same way as we defined the Nernst diffusion layer, we obtain from Eqs. (196) and (1)

$$\begin{aligned} \delta_R &= D_{\text{Cl}_2}[(c_{\text{Cl}_2})_e - (c_{\text{Cl}_2})_0]/(N_{\text{Cl}_2})_e \\ &= D_{\text{Cl}_2}(c_{\text{Cl}_2})_e/(N_{\text{Cl}_2})_e = a^{-1} = (D_{\text{Cl}_2}/k)^{1/2} \end{aligned} \quad (197)$$

This result can be generalized to any first-order homogeneous reaction. The thickness of the reaction layer is given by the square root of the ratio of the diffusion coefficient to the rate of the chemical reaction. We now can say more precisely what is meant by a fast reaction: It is a reaction which is fast *compared* to the rate of the diffusion process. δ_R increases with increasing diffusion coefficient and decreases with increasing reaction rate. For a very fast reaction, δ_R is extremely small, so that the homogeneous reaction virtually takes place at the interface, i.e., virtually turns into a heterogeneous reaction.

In the above example of chlorine hydrolysis a value of 6.3 s^{-1} can be taken for k at $13^\circ\text{C}^{(83)}$ and D_{Cl_2} is about $10^{-5} \text{ cm}^2 \text{ s}^{-1}$. This yields according to Eq. (197) a value of $1.2 \times 10^{-3} \text{ cm}$ for δ_R . According to Table 2 this is much less than the usual thickness δ of the diffusion layer for a moderately stirred solution or in free convection. We have thus verified a posteriori the assumption implied in the derivation of Eq. (195), namely, that the reaction takes place in a zone near the electrode where transport by convection is small compared to diffusion. However, it is seen that the validity of this statement depends on the hydrodynamic conditions. In the case at hand it is no longer true for a very strongly stirred solution where δ can drop somewhat below 10^{-3} cm .

As can be seen from Figure 21 the concentration which builds up at the interface at constant current density is proportional to δ_R . For small $(D/k)^{1/2}$ this buildup is more or less substantially reduced compared to what it would be in the absence of a chemical reaction. In a qualitative way this is easily understood: The substance is not removed from the diffusion layer by the mass transport alone, but additionally by the chemical reaction. In the electrolysis of NaCl solutions, it is thus possible by adjusting the pH for reaction (190) to run from left to right to decrease the interfacial concentration of chlorine in such a manner that a supersaturation sufficient for gas bubble

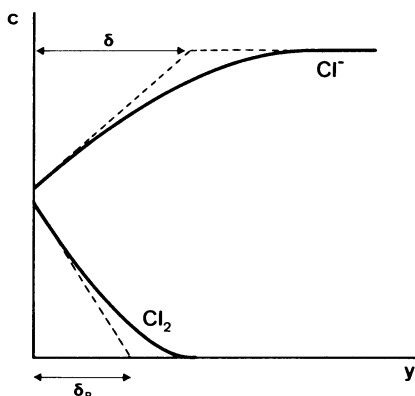


Figure 21. Concentration profiles near the anode in the electrolysis of a NaCl solution (schematic).

formation is not reached; i.e., there is no chlorine evolution even at relatively high current densities. This is the situation prevailing in chlorate electrolysis (in contrast to chlorine electrolysis). Of course, if the species considered is not generated but consumed at the electrode, it is the depletion in the diffusion layer that is decreased by the chemical reaction (provided there is a sufficient reservoir of the species feeding the prereaction).

9. Examples of Practical Calculations

9.1. Introduction

In this section an application example of convective mass transport theory to a practical electrochemical problem is presented. We will calculate the limiting-current densities of copper deposition from sulfate solutions with and without the addition of sulfuric acid. The concentrations considered are in the range used in copper electrorefining: 0.65 *m* CuSO₄ and 1.5 *m* H₂SO₄ at 60°C. The calculations are carried out for a channel flow cell and for natural convection.

Different problems, already discussed partly in Section 9 of Chapter 1 and in Section 6 of this chapter, arise due to the relatively high concentrations:

1. *Migration* is not negligible and has to be taken into account in an appropriate manner.
2. The solutions cannot be considered ideal. Note that in a 0.5 *m* CuSO₄ solution the activity coefficient has a value of about 0.06. One should therefore use *activities* rather than concentrations together with appropriate values of the diffusion coefficients.
3. We are not sure whether or not the *interfacial velocity* is negligible at these concentrations (Section 5.4, Chapter 1).
4. In contrast to ideal dilute solutions the *transport properties* (diffusivities and viscosities) are concentration dependent and will, in general, vary

across the diffusion layer. It is no longer possible, as for dilute solutions, to use their bulk values in the calculations.

For example, in Fick's equation for the interfacial flux density, written in its approximate form,

$$N_{B,e} = -D_B \frac{c_{B,0} - c_{B,e}}{\delta} \quad (1)$$

one has to take for D_B the value corresponding to the concentration at the interface—i.e., on the electrode side of the diffusion layer—since we calculate the flux density at this point. Especially at the limiting current, when $c_{B,e} \approx 0$, the interfacial diffusion coefficient may differ considerably from the bulk value, and therefore the interfacial flux density is also different from the value calculated with the bulk diffusivity. This effect is expected to be particularly pronounced in solutions of a single electrolyte the concentration of which varies from its bulk value to zero over the diffusion layer.

In the case of a mixture the diffusion coefficient not only depends on the concentration of the species considered but also on the overall concentration level (due to the influence of the latter on viscosity and interaction effects). In solutions with an excess of indifferent electrolyte the diffusion coefficient of a minor component will thus vary much less than in the case of a single electrolyte: (i) because the minor component is necessarily present in relatively small concentrations, and (ii) because the relative variation of the overall concentration (and thus of viscosity) is small. In addition, the accumulation or depletion of the reacting electrolyte in the diffusion layer is partly compensated by the concomitant depletion or accumulation, respectively, of the indifferent electrolyte (see Section 6.3).

The diffusion coefficient also has an influence on the interfacial flux density via the diffusion-layer thickness. For example, in mass transport at a plate in laminar flow one has $\delta \sim D_B^{1/3}$ [see Eq. (82)]. This diffusion coefficient can not be assumed to be equal to the bulk value.† Rather, it will lie between the bulk and the interfacial value. Since δ appears in the denominator of Eq. (1) it partly counteracts the effect of using the interfacial diffusivity as the proportionality factor in Eq. (1). For practical purposes it is certainly not convenient to deal with two different diffusion coefficients. However, it seems reasonable to use as an approximation mean values of the diffusion coefficient and also of the viscosity in order to take the variable transport properties into account.

All the complications listed above can be avoided in practical calculations if one disposes of experimental values of the transport properties which have been obtained under conditions as close as possible to those of the system under consideration (see Section 9.1, chapter 1 and Section 6.3 of this chapter).

† It is the diffusion coefficient appearing in the conservation equations (12) and (13). In solutions that cannot be considered very dilute, its variation with concentration should be taken into account in the integration of the conservation equations.

For example, a diffusion coefficient, calculated from limiting-current density measurements with the normal convective diffusion equation pertaining to the system being used, will include, in general, the additional effects mentioned above. Such experimental data thus represent integral, or effective properties, and are usually referred to a given bulk electrolyte composition. They can be used for other similar hydrodynamic systems, and one can assume that migration, variable transport properties, etc. are properly taken into account in this system also by the use of the integral diffusivity.

Newman and Hsueh have studied theoretically the influence of variable transport properties, nonzero interfacial velocity and a finite Schmidt number of the limiting-current density at a rotating disk electrode and expressed the results as a correction to the Levich equation.⁽⁸⁴⁾ The numerical calculation was confirmed by experimental results.⁽⁸⁵⁾ The variable transport properties were shown to be mainly responsible for the deviation from the dilute-solution equation. The authors point out that better agreement between the exact and constant-property equations can be obtained if the latter are used with averaged values of the transport properties. However, only very few computations like those of Newman and Hsueh are available today.

In the following calculations different methods that take into account the effect of migration and variable transport properties on the limiting currents of copper deposition are compared and possible deviations are discussed.

9.2. Copper Deposition in a Channel Cell

Copper is being deposited from the solution mentioned above in a channel cell of the type discussed in Section 7.4. The dimensions of the cell are $l = 1$ m, $b = 1$ m, $h = 0.02$ m, and $d_h = 0.039$ m. The deposition is assumed to take place under turbulent-flow conditions. According to Eq. (180) the hydrodynamic entrance length is 1.95 m, so that in our cell the flow is not developed. In this case the Chilton–Colburn analogy can be used to calculate the mass transfer rate to the channel wall (Section 7.4). From Eq. (98) and (99) we obtain

$$\overline{Sh} = (f/2) Sc^{1/3} Re \quad (198)$$

Assuming that the Blasius equation for the friction factor [Eq. (137)] is valid also for developing turbulent flow, we get

$$\overline{Sh} = 3.95 \times 10^{-2} Sc^{1/3} Re^{3/4} \quad (199)$$

Remembering the definitions of the dimensionless groups [Eq. (73)–(75)] we calculate the limiting interfacial flux density:

$$\tilde{N}_{B,\text{lim}} = -3.95 \times 10^{-2} c_{B,0} d_h^{-1/4} v_0^{3/4} v^{-5/12} D_B^{2/3} \quad (200)$$

For the numerical evaluation we assume a value of 0.5 m s^{-1} for the flow

velocity v_0 . Equation (200) then becomes

$$\bar{N}_{B,\text{lim}} = -34.35 \nu^{-5/12} D_B^{2/3} \quad (201)$$

With $z_B = 2$ for the cupric ion, the limiting current density of the deposition is

$$\bar{j}_{\text{lim}} = -6.63 \times 10^6 \nu^{-5/12} D_B^{2/3} \quad (202)$$

9.2.1. Deposition Without a Supporting Electrolyte

Let us first evaluate j_{lim} for a 0.65 *m* CuSO₄ solution containing no supporting electrolyte. In this case D_B in Eqs. (201) and (202) is to be replaced by the diffusion coefficient of the salt. Migration makes an important contribution to the flux of the cupric ions to the electrode. This can be taken into account in different ways.

9.2.1.1. Integral Diffusion Coefficients

Experimental integral diffusivities of CuSO₄ measured with the limiting-current method at a rotating disk electrode can be found in the literature.⁽⁸⁶⁾ If such values are inserted in Eq. (201) the resulting $\bar{N}_{B,\text{lim}}$ is also an integral flux density, containing convective diffusion and migration. Extrapolation of the diffusivity of CuSO₄ in a 0.65 *m* solution at 25°C–60°C with a temperature coefficient of 2.5% per degree[†] yields a value of $D = 2.5 \times 10^{-9} \text{ m}^2 \text{ s}^{-1}$. The viscosity can also be found in reference 86. The value given there for 25°C has been extrapolated to 60°C, with the temperature coefficient found experimentally for aqueous CuSO₄–H₂SO₄ solutions by Eisenberg *et al.*,⁽⁸⁷⁾ to yield $\nu = 5.4 \times 10^{-7} \text{ m}^2 \text{ s}^{-1}$. With these values, we obtain for the limiting-current density

$$\bar{j}_{\text{lim}} = -4992 \text{ A m}^{-2} \quad (203)$$

9.2.1.2. Method Using Transport Number

For a single electrolyte the influence of migration on the limiting-current density can be expressed by means of the transport number (Sections 1 and 2):

$$\bar{j}_{\text{lim}} = z_B F (1 - t_B)^{-1} \bar{N}_{B,\text{lim}} \quad (204)$$

$\bar{N}_{B,\text{lim}}$ represents the nonelectrolytic limiting flux density. If we replace it by Eq. (201)

$$\bar{j}_{\text{lim}} = -6.63 \times 10^6 \nu^{-5/12} D^{2/3} (1 - t_B)^{-1} \quad (205)$$

[†] In the following calculations all extrapolations of diffusion coefficients from ambient temperature to 60°C are carried out with this temperature coefficient. It is an average over the range of 2–3% per degree usually given for diffusivities (see, e.g., reference 57). If a temperature coefficient of 2% or 3% per degree were used, the resulting flux densities would in either case deviate by about 10% from the value obtained with 2.5% per degree.

D is the usual diffusion coefficient of the neutral CuSO_4 , in contrast to the one used above which included migration. In spite of a possible loss of accuracy (Section 9.1, Chapter 1) in the results, we will use diffusivities of CuSO_4 obtained with the diaphragm method.⁽⁸⁸⁾ In addition, we will use average values of ν , D , and t_B over the diffusion layer in order to take the variation of these properties with concentration into account. Arithmetic means are taken as an approximation of the properties of the solution in the bulk and at the interface. At the limiting current $c_{\text{CuSO}_4} \approx 0$ at the interface, and we can take, at the interface, the diffusivity of CuSO_4 , the transport number of Cu^{2+} corresponding to infinite dilution, and the viscosity of pure water. The averaged values at 60°C are $D_B = 1.27 \times 10^{-9} \text{ m}^2 \text{ s}^{-1}$ (reference 88); $\nu = 5.07 \times 10^{-7} \text{ m}^2 \text{ s}^{-1}$ (value for the bulk as above; value for water from physical tables); $t_B = 0.35$ ($t_B \approx 0.4$ at infinite dilution; $t_B \approx 0.3$ in 0.65 *m* CuSO_4 solution,⁽⁸⁹⁾ where t_B is assumed to be independent of temperature). If we evaluate Eq. (205) with these data we obtain

$$\bar{j}_{\text{lim}} = -5020 \text{ A m}^{-2} \quad (206)$$

The same calculation has also been carried out using the bulk values of D , ν , and t_B instead of averages. The resulting limiting-current density was then multiplied by a theoretical correction factor, accounting for nonzero interfacial velocity, finite Schmidt number, and variable transport properties, calculated by Newman and Hsueh⁽⁸⁴⁾ (see p. 210). Although the theoretical treatment was done for the rotating disk electrode, it is approximated here that the correction factor can also be used for other flow systems. In fact the limiting-current density obtained in this way was less than 1% higher than the value given in Eq. (206). We note that the transport number method leads to a result that is only about 0.6% higher than that obtained with an experimental integral diffusivity. The agreement is very good, and the use of diffusion coefficients measured with the diaphragm method does not affect the result of the calculation in this case.

For comparison, the limiting-current density was also evaluated with the exact method presented in Section 6.2. A nonelectrolytic limiting-current density was calculated with Eq. (202) using the diffusivity of the cupric ion at infinite dilution (from the limiting ionic conductivity⁽⁵⁷⁾) and the viscosity of pure water. The corresponding values at 60°C are $D_B = 1.7 \times 10^{-9} \text{ m}^2 \text{ s}^{-1}$; $\nu = 4.74 \times 10^{-7} \text{ m}^2 \text{ s}^{-1}$. The result was then multiplied by the limiting-current correction factor taken from reference 55 (see also Figure 11) for $r = 0$ (no supporting electrolyte). The value of the correction factor is 1.885. The limiting-current density then becomes

$$\bar{j}_{\text{lim}} = -7683 \text{ A m}^{-2} \quad (207)$$

This value is much higher than those calculated with other methods. This is due to the fact that the exact method in Section 6.2 pertains to ideal dilute solutions. There is no allowance made for viscosity and concentration effects.

The diffusivity and viscosity in ideal dilute solutions are much larger and lower, respectively, than in the relatively concentrated solution considered here, so that this method predicts a value of the limiting-current density that is too high.

9.2.2. Deposition with a Supporting Electrolyte

We now calculate the limiting-current density for the solution containing 0.65 *m* CuSO₄ and 1.5 *m* H₂SO₄. Migration and concentration effects can be expected to be less important due to the supporting electrolyte or to the high total electrolyte concentration. The same methods are used as above.

9.2.2.1. Integral Diffusion Coefficient

An integral diffusion coefficient for the cupric ion in the solution at hand, determined by the limiting-current method at a rotating disk electrode, can again be found in reference 86. Its value at 60°C extrapolated with the same temperature coefficient as above is $1.38 \times 10^{-9} \text{ m}^2 \text{ s}^{-1}$. The viscosity of the solution at 60°C, obtained by extrapolation of experimental data in reference 87, is $6.35 \times 10^{-7} \text{ m}^2 \text{ s}^{-1}$. With these values Eq. (202) yields

$$\bar{j}_{\text{lim}} = -3140 \text{ A m}^{-1} \quad (208)$$

We note that the addition of the supporting electrolyte lowers the limiting-current density by about 35% due to the partial suppression of migration and a decrease and increase of the diffusivity and of the viscosity, respectively.

9.2.2.2. Method Using Transport Number

Here we apply the approximate method outlined in Section 6.3. According to Eq. (154) the limiting-current density is linked with the limiting diffusion flux density in the following way:

$$\bar{j}_{\text{lim}} = z_{\text{B}}F(1 - t_{\text{B}})^{-1}\bar{N}_{\text{B,lim}} \quad (209)$$

or with Eq. (201)

$$\bar{j}_{\text{lim}} = -6.63 \times 10^6 (1 - t_{\text{B}})^{-1} \nu^{-5/12} D^{2/3} \quad (210)$$

For the diffusivity in this equation we take an average according to Eq. (155). D_2 is the diffusivity of the cupric ion in 1.5 *m* H₂SO₄ at a very low CuSO₄ concentration ($r \rightarrow 1$). From the data given in reference 86, we extrapolate a value of $D_2 = 1.26 \times 10^{-9} \text{ m}^2 \text{ s}^{-1}$ (60°C). D_1 is the diffusivity of CuSO₄ in an acid-free 0.65 *m* CuSO₄ solution ($r = 0$). Its value at 60°C is $1.11 \times 10^{-9} \text{ m}^2 \text{ s}^{-1}$.⁽⁸⁸⁾ With these values and a relative supporting electrolyte concentration of $r = 0.7$, the average diffusivity becomes $D = 1.21 \times 10^{-9} \text{ m}^2 \text{ s}^{-1}$.

For the viscosity we take the bulk value $\nu = 6.35 \times 10^{-7} \text{ m}^2 \text{ s}^{-1}$. The transport number of the Cu^{2+} ion as calculated by an empirical correlation given in reference 77 is $t_B = 0.072$. These values yield a limiting-current density of

$$\bar{j}_{\text{lim}} = -3108 \text{ A m}^{-2} \quad (211)$$

which is about 1% lower than the value calculated with the integral diffusivity.

Note that we have carried out the calculation with the bulk values of the transport properties and not with averages taken over the diffusion layer. Average values lead to a result that differs only by about 3% from that given in Eq. (211). The deviation is small because the transport properties vary much less across the diffusion layer than in an unsupported solution due to the relatively high electrolyte concentration. In view of the possible additional errors brought into the calculations by the averaging, the result based on the bulk properties is probably just as accurate and the evaluation of the interfacial properties not worth the effort.

Again the exact method described in Section 6.2 is applied for comparison. The nonelectrolytic limiting-current density is evaluated in this case with the transport properties pertaining to a 1.5 *m* sulfuric acid solution infinitely dilute with respect to CuSO_4 . The diffusivity of the cupric ion under these conditions at 60°C is $1.26 \times 10^{-9} \text{ m}^2 \text{ s}^{-1}$.⁽⁸⁶⁾ The viscosity is that of pure sulfuric acid: $\nu = 5.7 \times 10^{-7} \text{ m}^2 \text{ s}^{-1}$.⁽⁹⁰⁾ The limiting-current density correction factor is taken from reference 58. Its value for $r = 0.7$ is about 1.15 (assuming incomplete dissociation of bisulfate).^(58,86) We obtain for the limiting-current density

$$\bar{j}_{\text{lim}} = -3555 \text{ A m}^{-2} \quad (212)$$

The deviation from the limiting-current density calculated with the integral diffusivity is much smaller than in the case of the unsupported electrolyte solution for the reasons discussed at the beginning of this section. However, this improved agreement can be obtained only if the transport properties for infinitely dilute CuSO_4 in the supporting electrolyte solution, and not in water, are used. An even better agreement could probably be achieved by using mean values of the transport parameters.

9.3. Copper Deposition Under Natural Convection Conditions

We calculate the limiting-current density of the copper deposition reaction for the electrode configuration and size being used in copper electrometallurgy (see Chapter 6, Volume 2). The cells contain parallel vertical plates of approximately 1 m height and 1 m width. The electrolyte normally circulates through the tanks but at such a low flow rate that the influence of this flow on mass transfer to the electrodes can be neglected. The deposition proceeds essentially under natural convection conditions.

For our calculation the electrolyte composition and the working temperature are assumed to be the same as above (the calculation is carried out

only for the supported solution); the electrode height L , which is the only relevant length in the system (the interelectrode distance being a few centimeters), is 1 m. A preliminary calculation yields a $Sc \overline{Gr}$ product of about 10^{15} . This means that on a part of the electrode the flow is turbulent (Section 7.3.3). In this case, the mass transfer equation (173) with the empirical constants of Reference 68 can be applied

$$\overline{Sh} = 0.31(Sc \overline{Gr})^{0.28} \quad (213)$$

With the definitions of the dimensionless groups and with Eq. (170) we can calculate from (213) the limiting interfacial flux density

$$\overline{N}_{B,\text{lim}} = -0.31 c_{B,0}^{1.28} L^{-0.16} g^{0.28} \alpha^{0.28} \nu^{-0.28} D_B^{0.72} \quad (214)$$

We calculate the limiting-current density by the approximate method described in Section 7.3.1. For the diffusion coefficient and the viscosity we should see values averaged over the diffusion layer. However, as in the case of channel flow, the transport properties vary little across the diffusion layer in a solution containing a supporting electrolyte. Therefore, the use of their bulk values will not lead to an appreciable error. The overall densification coefficient is calculated with Eq. (171) with an exponent of the ratio of the diffusivities adapted to the mass transport correlation to be used here:

$$\alpha = \alpha_{\text{CuSO}_4} - \alpha_{\text{H}_2\text{SO}_4} \left(\frac{t_{\text{H}^+}}{1 - t_{\text{Cu}^{2+}}} \right) \left(\frac{D_{\text{Cu}^{2+}}}{D_{\text{H}^+}} \right)^{0.72} \quad (215)$$

The densification coefficients of the two electrolyte components can be obtained from density data in reference 91. Their values at 60°C are

$$\alpha_{\text{CuSO}_4} = 1.5 \times 10^{-4} \text{ m}^3 \text{ mol}^{-1}, \quad \alpha_{\text{H}_2\text{SO}_4} = 5.2 \times 10^{-5} \text{ m}^3 \text{ mol}^{-1}$$

The diffusivity of the cupric ion and the viscosity of the solution are the same as in channel flow [bulk values, diffusivity taken as an average according to Eq. (155)]: $\nu = 6.35 \times 10^{-7} \text{ m}^2 \text{ s}^{-1}$; $D_B = D_{\text{Cu}^{2+}} = 1.21 \times 10^{-9} \text{ m}^2 \text{ s}^{-1}$. For the diffusivity of the hydrogen ion in $\text{CuSO}_4\text{-H}_2\text{SO}_4$ solutions no values are available. We therefore take the value for sulfuric acid in $\text{H}_2\text{SO}_4\text{-H}_2\text{O}$ solutions. For a concentration corresponding approximately to the total electrolyte concentration in our solution, values of about $1.8 \times 10^{-9} \text{ m}^2 \text{ s}^{-1}$ at 25°C can be found in the literature.^(92,93) Extrapolation to 60°C with a temperature coefficient of 2.5% per degree yields a value of about $4.3 \times 10^{-9} \text{ m}^2 \text{ s}^{-1}$. Note that the diffusivity of H^+ does not have a significant influence on j_{lim} . A $\pm 50\%$ variation of D_{H^+} changes the limiting-current density by less than 1%. The transport numbers of Cu^{2+} and H^+ are calculated with the correlations given in reference 77. It is assumed that they are approximately the same at 60°C as at room temperature. We thus have $t_{\text{H}^+} = 0.6$, $t_{\text{Cu}^{2+}} = 0.072$. The overall densification coefficient is then: $\alpha = 1.37 \times 10^{-4} \text{ m}^3 \text{ mol}^{-1}$.

We can now calculate the interfacial flux density and, by multiplying with $z_B F(1 - t_B)^{-1}$, the limiting-current density and obtain

$$\bar{j}_{\text{lim}} = -833 \text{ A m}^{-2} \quad (216)$$

In this case it is difficult to compare the result of the approximate treatment with that of the exact calculation. The latter, briefly mentioned at the end of Section 7.3.1, has been carried out for laminar flow, i.e., for systems to which Eq. (160) applies.⁽⁵⁶⁾ However, we can tentatively assume that the limiting-current correction factor evaluated there can also be used as an approximation for the situation at hand. The nonelectrolytic limiting-current density, evaluated with the same α as here, but with the values for ν and D_B as in the exact calculation for channel flow, is multiplied with the correction factor of about 1.1 taken from reference 56. One calculates a limiting-current density of about 900 A m^{-2} . Again, the result is higher than that obtained with the approximate method, since the exact method is valid only for dilute solutions and does not take into account the effect of concentration variations.

9.4. Concluding Remarks

We have shown here how the main quantities of interest can be calculated for a practical system. The problems arising have already been mentioned at the beginning of this section, and we have seen in the course of the calculation that the transport properties, especially diffusivities, are probably the greatest problem. Even if we can find data in the literature extrapolations have to be made with respect to concentrations and temperature, and very often we have to do this in a somewhat arbitrary way.

A comparison of the limiting-current density calculated for natural convection in the preceding section with a value given in the literature⁽¹¹⁴⁾ for the same electrolyte at the same temperature illustrates the influence of the choice of transport properties and of the way of adapting them to the conditions at hand. Although the same transport correlation has been used, the result in Eq. (216) is 23% higher than the 675 A m^{-2} given in reference 114 due to differences in the values of $t_{\text{Cu}^{2+}}$, ν , α , and D_B . The respective terms in the mass transport correlation (214) differ by 2–9%, but unfortunately, in this case, they all act in the same direction. (One could imagine that in a favorable case they cancel each other at least partly so that the final results are closer.) The largest divergence comes from the diffusion coefficient for which an experimental value⁽¹¹⁴⁾ for CuSO_4 has been extrapolated to 60°C with a temperature coefficient of 2.4% per degree; in the present calculation, an average value according to Eq. (155) has been used. The averaging yields a diffusion coefficient about 9% higher than the one for CuSO_4 , and the slightly larger temperature coefficient used here (2.5% per degree) adds another 4%.

However, it is almost impossible to say which of the two diffusion coefficients is closer to reality. The problem with diffusivities is that at higher concentrations their definition becomes difficult. Depending on the method by which they have been determined, experimental values may include additional effects such as those mentioned at the beginning of Section 9. The application of such data in practical calculations may become doubtful if the experimenter is not completely aware of what the diffusion coefficient used really represents. The best and most reliable results can certainly be obtained with data determined in the same electrolyte, at the same temperature, in a similar flow system with a method corresponding to the situation being considered. For this reason the most reliable results in this section are the limiting-current densities calculated for channel flow with data determined also by the limiting-current technique in a flow system.

However, the good agreement of these results with those obtained with the approximate method indicates that the latter is also a useful method and that its accuracy is probably, in most cases, sufficient in view of the uncertainties regarding the transport parameters.

The problem of the accuracy of the diffusivities is perhaps not as important as it might seem. The deviation of the limiting current in the above systems is about $\pm 13\%$ for a variation of the diffusivity of $\pm 20\%$. If an uncertainty of $\pm 20\%$ for the limiting current is tolerated, the diffusivity may vary as much as $\pm 30\%$. Very often in engineering applications one has to be content with accuracies of this order of magnitude.

Likewise let us add a few remarks about the desired or required accuracy in the field of kinetics for the evaluation of mass transfer rates. In the study of electrode kinetics (i.e., of the charge-exchange reaction at the interface), the knowledge of the interfacial concentration of the reacting species is important. The difference between this concentration and that in the bulk depends on the mass transfer in the solution which is always present in an electrolysis. If one uses an experimental arrangement with convection it is important that the hydrodynamic conditions are accurately defined and the corresponding mass transport correlations well established. A classical system which fulfills this condition is the rotating disk. The problem which arises then is the uncertainty regarding the mass transport parameters. In practice, it is best to work under the condition that the concentration at the interface is virtually the same as that in the bulk. This will be the case if one accelerates the mass transport so much that it is very fast compared with the kinetics of the electrode reaction. If one only wishes to check whether this is true, an error of 20% in the mass transfer calculation is not relevant. If one cannot accelerate the mass transfer sufficiently, the case of mixed kinetics results. The evaluation of $c_0 - c_e$ is then more important but an accuracy of 10% may still be sufficient in view of the usual lack of reproducibility of kinetic measurements due to the variability of the electrode surface state and other conditions.

10. Evaluation of Interfacial Concentrations

In this chapter we have considered mass transfer at the limiting current, which is usually the most important case from the viewpoint of the electrochemist. However, sometimes it is of interest to evaluate, for a given electrolysis current, the concentration of the reacting species at the interface electrode solution (for current densities below the limiting one). In general, we can write (for the case in which migration need not be considered)

$$\frac{j\nu_B}{nF} = N_{B,e} = -k_d(c_{B,0} - c_{B,e}) \quad (217)$$

or

$$c_{B,e} = c_{B,0} + \frac{N_{B,e}}{k_d} = c_{B,0} + \frac{j\nu_B}{nFk_d}$$

which can be easily deduced from Eqs. (31) of Chapter 1 and (5) of this chapter.† A calculation of this sort has been carried out toward the end of Section 2.3 for a plate in laminar flow.

In the case where migration must be taken into account, one must use methods similar to those sketched in Section 6, either by integrating the fundamental equations with the migration term as has been done by Newman (see Section 6.2), or by applying the approximate procedure of Section 6.3; i.e., by using the equation

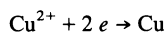
$$\frac{j}{F} \left(\frac{\nu_B}{n} - \frac{t_B}{z_B} \right) = N_{B,e} = -k_d(c_{B,0} - c_{B,e})$$

or

$$c_{B,e} = c_{B,0} + \frac{j}{k_d F} \left(\frac{\nu_B}{n} - \frac{t_B}{z_B} \right) \quad (218)$$

which is a generalized form of Eq. (154) and can be derived in the same manner as the latter. We have already noted that there are in the diffusion layer not only concentration changes with respect to the reacting species but also with respect to those not reacting (see Section 7.3.1, this chapter and Section 4.7, chapter 1). For example, in the electrolysis of a solution of $\text{CuSO}_4 + \text{Na}_2\text{SO}_4$, in broad potential range, the Na^+ ions do not react at the

† The meaning of the symbols ν_B and n is given in connection with Eq. (31) of Chapter 1. In the case of copper deposition,



from a solution of $\text{CuSO}_4 + \text{Na}_2\text{SO}$ (without concomitant hydrogen evolution), we have $\nu_{\text{Cu}^{2+}} = 1$, $z_{\text{Cu}^{2+}} = 2$, $\nu_{\text{Na}^+} = 1$; t_B denotes the transport number which for a dilute solution is given by Eq. [46] of Chapter 1.

cathode, but their concentration near the interface is increased and one may be interested in calculating the $c_{B,0} - c_{B,e}$ for the Na^+ ions. In such a case one cannot neglect the influence of migration since it is the cause of the accumulation of the Na^+ ions near the cathode. In the approximate method of evaluation the stoichiometric coefficient ν_B in Eq. (218) is zero, and we have

$$c_{B,e} = c_{B,0} + \frac{j t_B}{k_d z_B F} \quad (219)$$

The values of k_d in Eqs. (217)–(219) are taken from the mass transfer correlations valid for the hydrodynamic and geometric conditions considered. For example, for laminar flow at a plate one takes the correlation from k_d derived in Section 2.3. It should be kept in mind, however, that the k_d relationships usually employed in electrochemical problems are those obtained for the boundary condition of a constant interfacial concentration (limiting current, potentiostatic experiments). However, in the case considered here, i.e., where the current is given and is well below the limiting value, the interfacial concentration is not constant along the electrode and the boundary condition at the interface must be written in terms of the applied current. The simplest assumption is to regard the local current density as constant along the electrode.† The correlation for k_d at a plate in laminar flow has been derived for this boundary condition toward the end of Section 2.3. Further relationships for a constant mass or heat flux density can be found in the literature.

If no such correlation is available a reasonable approximation can probably be achieved by using the mass transfer correlation for a constant interfacial concentration. In the case of laminar natural convection at a vertical plate, the results for both boundary conditions differ by about 10%;⁽⁶³⁾ for forced laminar flow at a plate there is no difference (Section 2.3). It should be noted that in a controlled-current experiment only the *overall current* is fixed and the local current density may not be constant along the interface. The extent of this effect depends on the circumstances (see Chapter 4 on current distribution). If this effect is not negligible one cannot use nonelectrolytic correlations for the evaluation of interfacial concentrations and the integration of the fundamental equations has to be done, taking into account the transport of charges through the solutions due to the electric field. This can be done, in principle, by the method of Newman, along the lines sketched in Section 8 of Chapter 4.

Let us point out that even in the case of a local current density that is constant along the interface the interfacial concentration may vary. This is so

† Note that in a case such as that of copper deposition from $\text{CuSO}_4 + \text{Na}_2\text{SO}_4$ (see above), one may be interested in the interfacial concentration of the *nonreacting* species (e.g., Na^+) in a situation where the concentration of the *reacting species* is virtually zero at the interface (i.e., the species is reacting at the limiting current). Under these conditions the correlation for k_d at *constant interfacial concentration* should be used in Eqs. (217)–(219).

when the thickness of the diffusion layer changes. For example, in laminar flow the interfacial concentration will be constant for a rotating disk, but not at a plate with flow parallel to the electrode. Such concentration changes may cause occasionally relevant effects. An example will be given in Section 11.4 (Figure 26).

Several experimental methods have been developed for the investigation of the interfacial concentrations in connection with electroplating (e.g. pH determination). Let us mention the pinhole method of Read and Graham⁽¹²¹⁾ (in which the diffusion layer is sucked away through a pinhole) and the Brenner technique of freezing the diffusion layer.⁽¹²²⁾ Powerful procedures include the optical ones, in particular, interferometric.

11. Applications of Convective Mass Transport Theory

11.1. Generalities

Convective mass transport plays a considerable role in the study of electrochemical kinetics by methods such as the rotating disk or ring-disk electrode. It is also of importance in electroanalysis, for example, in classical polarography when a rotating Pt-wire anode is used instead of the mercury drop because the investigated species reacts at a too positive potential where mercury dissolves. Its theory forms the basis for the use of electrochemical systems as models for the study of convective mass or heat transport in general (see Section 11.2). Finally, it is omnipresent in technical electrolysis. Indeed, convection-free electrolysis is hardly ever encountered in industrial applications because the currents attainable are then much too small (Table 2) and the investment too high.

Thus, the theory of convective mass transport is one of the fundamentals of electrochemical engineering. It is involved in the analysis of technical electrochemical processes mainly in three ways: (i) mass transfer limits the rate of electrochemical reactions and is thus relevant to problems of optimization, (ii) it causes size effects and is thus relevant to problems of scale-up; (iii) it influences the current distribution at the limiting current and is thus relevant to cell design. We will consider the first two aspects in more detail in Sections 11.3 and 11.4. The third aspect will be treated in Chapter 4.

11.2. Electrochemical Systems as Models for Transport Measurements

11.2.1. Determination of Diffusion Coefficients

The rotating disk electrode is a convenient system for the determination of diffusion coefficients D . One measures the limiting current by recording

the current–voltage curve (see Section 1.5) for a solution of known concentration and viscosity and calculates D from the pertinent correlation for the limiting current. However, the application of the method requires that the current efficiency be 100% for the electrode reaction involved and that a current–voltage curve with an accurately measurable plateau be obtained. The complication of a high ohmic potential drop (see Section 1.5) can be avoided to a large extent by a procedure proposed by Newman.⁽⁸⁵⁾ Instead of determining the limiting current from the current–voltage curve, one measures, at a constant current, the electrode potential at decreasing rotation speed ω : The applied current becomes equal to the limiting current at a well-defined value of ω and the potential then rapidly changes. One thus obtains the limiting current without having recourse to a curve that is blurred by a variable ohmic drop ri (because j and therefore ri are maintained constant whereas j changes during the recording of the current–voltage curve of Figure 6).

11.2.2. Study of Convective Transport Phenomena

It has been pointed out several times that under certain conditions (low concentration of reacting species, high concentration of indifferent electrolyte) the relationships for electrolytic mass transport are the same as for mass transport at large, without electrolysis (see Section 5.1, chapter 1 and Section 2.1, this chapter). However, the electrochemical systems have one specific advantage: Because of the proportionality between interfacial flux density N_e and electrode current density j (Section 4.2, Chapter 1), the rate of mass exchange at the interface can be directly read off an ammeter. This provides a convenient means of measuring mass transport coefficients and studying transport phenomena in chemical engineering at large. This method was first used and proposed by Eisenberg, Tobias, Wilke,^(6,60) Ibl,⁽⁸⁾ and Grassmann.⁽⁹⁴⁾ Later, it was often used in particular by Grassmann's^(95–97) and Hanratty's groups.^(98,99) Through the use of a segmented electrode (with segments electrically insulated from each other), the method allows a comparatively simple measurement of local mass transport coefficients and the study of the distribution of the mass transport along an interface.⁽⁹⁴⁾ It also allows one to follow fast variations of the mass transport rate with time, as they occur on small areas in turbulent flow, and provides an interesting possibility for analyzing details of the turbulent phenomena.

The measurement is made by applying a potential to the working electrode, such that the indicator electrode reaction proceeds at the limiting current. The interfacial concentration of the reacting species is then zero and Eqs. (5) and (7) thus yield

$$N_{B,e} = k_d c_{B,0} = \frac{j_{\text{lim}}}{z_B F} \quad (220)$$

There is a simple proportionality between the measured limiting current and

the mass transfer coefficient k_d . Application of the method presupposes that the current efficiency for the indicator reaction is 100%. For accurate measurements the plateau of the current-voltage curve of Figure 6 should be truly horizontal and as long as possible (see Section 1.5). A system that fulfills this condition is a solution of ferrocyanide/ferricyanide + NaOH in excess with a nickel cathode. Iodine/iodide solutions also provide highly reversible electrode reactions. Another indicator reaction that has been used is the deposition of copper from an acid CuSO_4 solution. It has been mainly employed in natural convection where redox systems, such as the preceding ones, have density differences influenced by both the oxidized and reduced species (see Section 7.3). On the other hand, the CuSO_4 system has the disadvantage that at the limiting current metallic deposits become powdery after a while,^(100,101) and the electrode area is then ill defined, so that the determination of the limiting-current *density* from the measured *intensity* of the current becomes problematic. This pitfall and its avoidance have been discussed by Selman and Tobias.⁽⁴⁶⁾

Instead of the above potentiostatic measurements, more sophisticated methods have been developed recently by Epelboin and coworkers⁽¹⁰²⁻¹⁰⁴⁾ (see also Miller and Bruckenstein⁽¹⁰⁵⁾ and Tokuda *et al.*⁽¹⁰⁶⁾). They involve a sinusoidal or other modulation of the potential (or the current) or a modulation of the rotation speed of a disk, with a measurement of the electrochemical or electromechanical impedance. These methods allow a deeper insight into the mechanism of turbulence and are also used for the study of transport phenomena in non-Newtonian fluids.⁽¹⁰²⁾

Because of the analogy between mass, heat, and momentum transport (see Section 4), the electrochemical method of measurement of mass transport coefficients can also be used for the study of heat and momentum transport and the prediction of the heat transfer rate and shear stress. In the latter cases, the method has the disadvantage that the aqueous solutions used have Schmidt numbers of the order of 1000, whereas heat transfer in gases and liquids commonly involve Prandtl numbers on the order of 1-10. The application of electrochemical measurements to heat transport then involves an extrapolation with respect to the Prandtl number (Section 4.4). On the other hand, if one is interested in heat transfer at high Prandtl numbers, the classical methods are extremely difficult to apply. The electrochemical technique is then particularly valuable. In the application of the method to the measurement of the shear stress there is also the problem of the high Schmidt number and in addition there is the complication that the analogy between momentum and mass transport is less complete than that between heat and mass transport (see Section 4). However, reliable results are obtained inasmuch as the Chilton-Colburn analogy holds. The electrochemical technique has been used to obtain information about the shear stress by Epelboin's,^(102,107) Hanratty's,^(99,108) and Le Goff's groups.^(109,110)

The electrochemical technique has been reviewed in detail mainly from the viewpoint of its application to heat transfer and shear stress determinations by Mizushina.⁽¹¹¹⁾ Recently, the subject has been comprehensively reviewed more from the viewpoint of the electrochemist and from that of mass transport by Selman and Tobias.⁽⁴⁶⁾ The paper lists 200 correlations established or verified by the electrochemical method.

11.3. Limitation of Reaction Rate by Mass Transport: Optimization

The competitiveness of electrochemical processes compared to a chemical route is a matter of economics. The latter depends substantially on the capital investment for the electrolysis cell, which in turn is a function of current density. If this is high, the electrode area needed to produce a given amount in a prescribed time is small and the investment low. This is possible only if the mass transport is fast. However, one can increase the current density corresponding to a certain reaction only up to its limiting current density (see Section 1.4 and Chapter 1, Section 1). An increase of the total current density over this value does not, under given hydrodynamic conditions, result in any acceleration of the desired reaction and leads only to a drop in current efficiency, because a concomitant electrode reaction is now running.

Although from the standpoint of investment it would be desirable to operate industrial processes at the limiting current, one is in reality working more or less below it in most cases. There may be different reasons for this. Let us mention three important ones:

(a) In plating and electrometallurgy, the quality of the metal deposited at the limiting current is not that desired (see References 100, 101).

(b) An increase in current density lowers the investment but at the same time the voltage to be applied to an electrolytic cell becomes larger and so does the energy consumption. An increase of current density thus causes two effects that act in opposite directions. With some simplifying assumptions (linear dependence of investment cost and cell potential on current density, current efficiency independent of current density), one obtains a simple relationship for the optimum current density j_{op} ,^(31,112)

$$j_{op} = (a/bR)^{1/2} \quad (221)$$

where a is the specific investment cost per square meter of electrode area and per unit time of operation,† b the energy price (\$/kWh) and R the resistance of the electrolytic system for 1-m² electrode area. If j_{op} calculated

† It should be noted that a does not represent the cost of the initial investment but the amount to be paid per unit time (e.g., per year) for the amortization of and for the interest on the invested capital.

from Eq. (221) is smaller than the limiting current density there is no incentive to approach it since any increase of the current density above j_{op} leads to a more expensive process.

(c) If the electrode reaction is highly irreversible (large overpotential) the current efficiency drops drastically before the limiting current density of the desired reaction is reached and the cell must be operated well below the limiting current density.

Nevertheless, the calculation of the limiting current density remains important because it corresponds to the maximum utilization of a cell and thus yields the minimum investment cost for a given electrolytic solution and given hydrodynamic conditions. It represents the most favourable situation when one compares the electrochemical route with a chemical one. Therefore, a major aim of the electrochemical engineer is to overcome as much as possible the effects that impede operation close to the limiting current density; for example, in case (b) by increasing the optimum current density through a lowering of R in Eq. (221) (decrease of the activation overpotential, increase of the specific conductivity of the solution, smaller interelectrode distance), and in case (c) by accelerating the electrode kinetics through the use of a better electrode material. Once the electrochemist or electrochemical engineer has been successful in this endeavor the obstacle of the limitation of the reaction rate by the mass transport is faced and a major effort has to be devoted to accelerate the latter.

An acceleration of the mass transport can be achieved by stirring. However, this requires energy (which is dissipated into heat by the friction forces) and the cost of the process is increased. This cost has to be taken into account in the calculation of the optimum current density at which the overall cost is minimum. Let us consider as an example an electrolysis cell with channel flow discussed in Section 7. An increase of the flow rate increases the limiting current, but at the same time the energy required for the stirring also becomes larger. The resulting cost has to be balanced against the beneficial effect of the accelerated production (decrease of investment). There are thus two effects acting in opposite directions and the overall cost will be minimum at a certain flow rate.

An example of a simplified optimization of this kind is shown in Figure 22.^(112,113) Waste water from the plating industry containing small amounts of chromic acid is to be treated in an electrolytic tank (Figure 23), in which the solution is circulated by means of the propeller (a) and flows through the space between parallel vertical electrodes (channel flow). The curvers (b) decrease the friction losses due to the reversing of the flow direction.⁽¹²³⁾ The hexavalent chromium is reduced to trivalent, which is much less poisonous. The cathodic reduction can be carried out at the limiting current. The latter is small because the solution is dilute and a relatively large electrode area (i.e., high investment) is needed. In comparison to this the cost for the electric energy consumed in the electrolysis itself is negligible. The equation for the

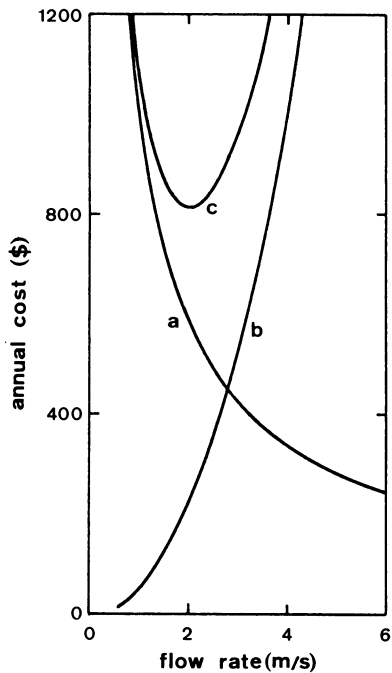


Figure 22. Optimization of stirring rate for electrolytic reduction of chromic acid in a flow cell. Curve a: Investment cost; curve b: stirring cost; curve c: total cost. Details of calculation in reference 112.

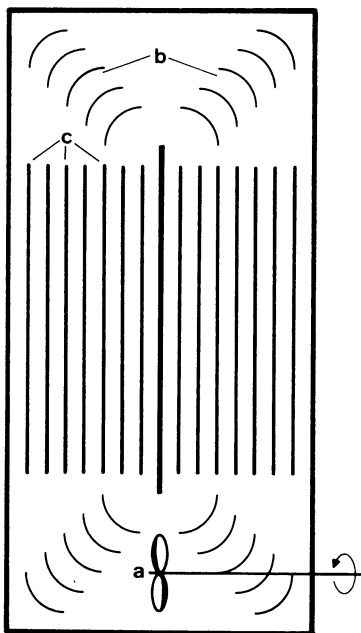


Figure 23. Hydrodynamic model for optimization of stirring rate. a, propeller; b, curvers; c, electrodes.

limiting interfacial flux density in channel flow (Eq. (200)] allows calculation of the electrode area (and thus the investment cost) needed for a given amount of solution to be treated per unit time. It decreases with increasing flow rate. The correlations for the friction losses in the hydrodynamic model of Figure 23 permit the computation of the cost of stirring (investment for pumps and energy consumed by them). It increases with flow rate. The total cost (investment for cells plus stirring cost) is plotted on the ordinate of Figure 22 as a function of flow rate. It goes through a minimum which corresponds to the optimum flow rate. Such optimization computation and evaluation of cost are typical for the feasibility studies popular in modern chemical engineering: The evaluation of the cost is often made as a preliminary step, in order to ascertain whether it is worthwhile to carry out an experimental investigation.

In the above example, after having optimized the rate of stirring, the next stage is comparison with modes of stirring other than that of Figure 23. For example, it may be that gas sparging would be a more economic way of accelerating the mass transfer. The value of the limiting current provides a criterion for an approximate comparison of the efficiency of various modes of stirring. Table 2 shows the limiting current density of the deposition of copper from a CuSO_4 solution for various hydrodynamic systems.

It is seen that natural convection, which is provided by nature virtually free of charge, is comparatively quite effective: The velocity of the fluid induced by the density differences at a vertical electrode is low (a few mm s^{-1}) but the liquid is flowing very near the interface, where its movement is most effective for the mass transport. In laminar flow at a plate (item 4) several cm s^{-1} are necessary to reach the same limiting current as in natural convection.

Table 2
Limiting-Current Densities for Various Hydrodynamic Systems

Hydrodynamic system	$j_{\text{lim}}(\text{A}/\text{m}^2)^a$	δ (mm) ^a
Convection-free electrolysis (after 2 h)	6.1	4.75
Natural convection at vertical electrode, height 0.1 m	144	0.2
Natural convection at horizontal electrode	365	0.08
Laminar flow along the plate electrode, $v_0 = 0.25 \text{ m s}^{-1}$, length 0.1 m	300	0.1
Turbulent channel flow, $v_0 = 25 \text{ m s}^{-1}$	36,500	0.0008
Rotating cylinder, 3 rps, $R = 0.05 \text{ m}$	810	0.036
Cathode with H_2 evolution, $2.2 \text{ liters m}^{-2} \text{ s}^{-1}$	7,200	0.004
Cathode with H_2 evolution, $0.17 \text{ liter m}^{-2} \text{ s}^{-1}$	1,940	0.015
Bubbling of gas through fritte $0.0017 \text{ liter s}^{-1}$	276	0.1
Bubbling of gas through fritte $0.28 \text{ liter s}^{-1}$	1,320	0.02
Wiping of electrode with net moving along interface	2,280	0.013
Ultrasound, $7 \times 10^{-4} \text{ W m}^{-2}$	5,000	0.006

^a The figures given refer to a 0.3 m solution of a univalent ion with a diffusivity of $10^{-9} \text{ m}^2 \text{ s}^{-1}$ and a kinematic viscosity of $10^{-6} \text{ m}^2 \text{ s}^{-1}$.^(115,119)

But this is the velocity in the core of the stream, which drops off near the wall and is much smaller in the region of the diffusion layer (see Figure 1). Table 2 also shows the limiting current at gas-evolving electrodes. Stirring through gas evolution (which can also be regarded as a natural convection) is most effective: It compresses the diffusion layer down to values that can otherwise only be attained by a most intensive mechanical stirring (items 7 and 8). At the other end of the spectrum we have the convection-free now stationary electrolysis (item 1) which can be realized, in the case of the system in Table 2, with a horizontal cathode facing downward: After 2 h the limiting current drops to a value which is some 50 times smaller than in natural convection and would be unacceptable in most industrial applications.†

The limiting currents shown in Table 2 give a general idea of the reaction rates attainable under various hydrodynamic conditions. However, from an engineering viewpoint a more relevant quantity is the stirring power needed to reach a certain value of the limiting-current density. Let us take as an example a solution used in copper refining ($0.65\text{ m CuSO}_4 + 1.5\text{ M H}_2\text{SO}_4$, 60°C) for which the limiting currents have been calculated in Section 9. We consider the hydrodynamic model of Figure 23 with channel flow. In the turbulent range the limiting current can be calculated from Eq. (200). The power P^* needed for the stirring is, per square meter of electrode area,⁽¹¹⁴⁾

$$P^* = 0.064 \rho v_0^3 h / l + 0.158 \rho v_0^3 h / d_h \text{Re}^{+1/4} \quad (222)$$

where the first term on the right-hand side corresponds to the friction losses at the curvers, and the second term to the losses at the electrodes. Combination of (222) with Eq. (200) yields the relationship between P^* and the limiting-current density j_{lim} . It is plotted in Figure 24. The stirring power increases quickly with the limiting current to be attained.

The above calculation is relevant to the optimization of copper refining which has been discussed by Ibl.⁽¹¹⁴⁾ The optimum current density calculated from Eq. (221) ranges from 600 to 1000 A m^{-2} , depending on the values selected for the amortization time and the rate of interest which determine the factor a in Eq. (221). Most refineries operate with vertical electrodes in natural convection at about 200 A m^{-2} . The cathodic limiting current for these conditions was calculated in Section 9.3 and amounts to 833 A m^{-2} . In principle, it would be possible to raise the operating current into the optimum range without having recourse to artificial stirring. However, one would then be at or very close to the limiting current where metallic deposits become powdery. To realize the optimum conditions it is thus necessary to stir.

Let us assume that in order to preserve the properties of the deposit one wishes to maintain the ratio of the operating to the limiting current at its present value, i.e., $200/833 \cong 1/4$. This means that we have to raise the

† There are some important practical systems (e.g., dry batteries) which operate virtually without convection. But the cell arrangement is a rather special one.

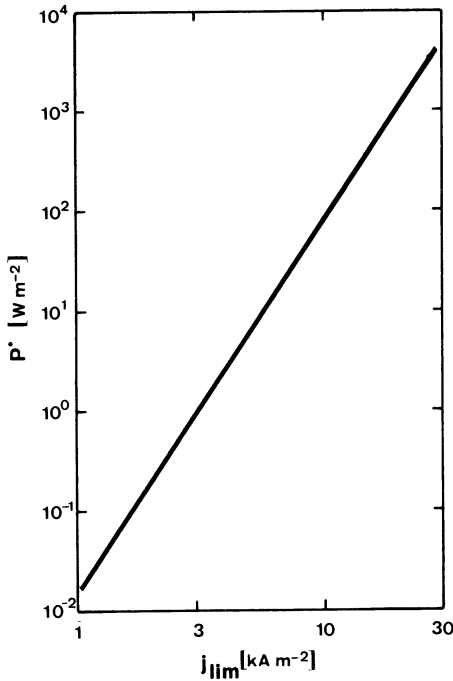


Figure 24. Specific stirring power as function of limiting current density. Solution: 0.65 *m* CuSO₄, 1.5 *m* H₂SO₄, 60°C. Cell dimensions as in the calculation in Section 9.2.

limiting current to 2.4–4 kA m⁻². With the hydrodynamic model of Figure 23 this would require a stirring power of 0.8–6 W m⁻² or 1–5 kWh ton⁻¹ of copper produced. This is much less than the power consumed for the electrolysis itself (50 W m⁻² at 200 A m⁻² and 600 W m⁻² at 800 A m⁻²). Ibl⁽¹¹⁴⁾ concluded that considerable savings could be achieved by carrying out the electrolytic refining of copper in a cell stirred through mechanical pumping or by gas sparging.

A similar conclusion applies to the electrowinning of copper, where the power needed for the electrolysis is much larger and the stirring power needed even relatively much less important than in copper refining. In copper refining, however, a complication would arise in a stirred system because of the sludge formation at the anode. This is probably one of the main reasons why such systems have not yet been used in industrial practice.

The above example illustrates the utility of the calculation of the stirring power P^* required to reach a given j_{lim} (or k_d). This quantity (or the ratio P_1^*/P_2^* for the two systems 1 and 2, taken at the same k_d or j_{lim}) can be used to compare the effectiveness of various modes of stirring.⁽¹¹⁵⁾ Such a comparison is presented in Figure 25 for channel flow, rotating disks, and cylinders. The quantity P^* has the advantage of being directly linked to the stirring cost. It may be noted that the ratio P_1^*/P_2^* at constant k_d (or j_{lim}) depends on the system and on the conditions. In fact, P^* is quite sensitive to inaccuracies

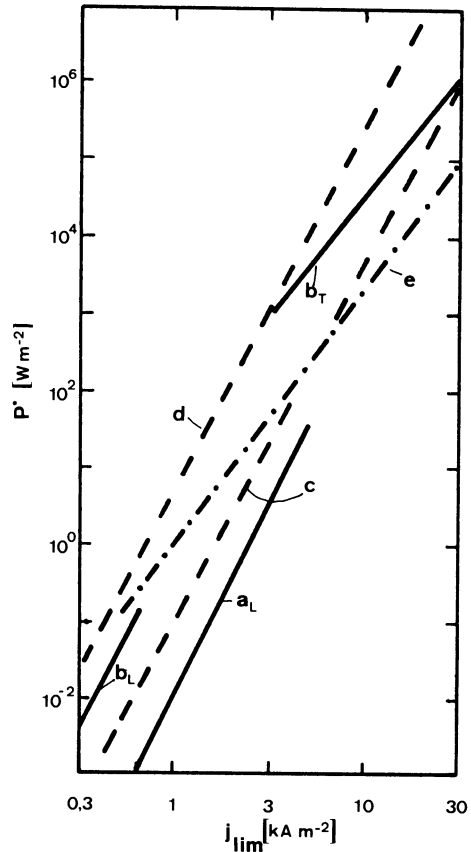


Figure 25. Comparison of specific stirring power for various hydrodynamic systems. a_L , laminar rotating disk, $R = 0.03\text{ m}$; b_L , laminar rotating disk, $R = 0.3\text{ m}$; b_T , turbulent rotating disk, $R = 0.3\text{ m}$; c , rotating cylinder, $R = 0.03\text{ m}$; d , rotating cylinder, $R = 0.3\text{ m}$; e , channel flow cell. Details of calculation in reference 120.

in the mass transfer correlations used or to changes in the conditions. For example, the curve in Figure 24 has been calculated for the temperature prevailing in industrial refineries, i.e., 60°C . If one assumes the temperature to be 20°C instead, the change in D_B and ν increases P^* by a factor of about 10.

The Le Goff number Lf has been proposed as a criterion for the efficiency of the stirring.⁽¹¹⁶⁾ It is the ratio of two dimensionless groups, namely, the Chilton–Colburn factor j_D and the friction coefficient $f/2$ (see Section 4.5):

$$Lf = \frac{j_D}{f/2} \quad (\text{Le Goff number}) \quad (223)$$

The choice of this criterion is related to the Chilton–Colburn analogy between mass and momentum transport, according to which Lf should be 1. This allows one to predict P^* at a given j_{lim} from $f/2$, as long as the Chilton–Colburn analogy holds. If this is not the case, Lf can be smaller or larger than 1. The second case is the more favorable one since then the limiting current for a given $f/2$ (and thus P^*) is larger than according to the Chilton–Colburn

analogy. To achieve an economic industrial process one should select a system with a Lf number as large as possible. However, it should be noted that Lf is not related in an univocal manner to P_1^*/P_2^* (which directly corresponds to the stirring cost): For a given Lf_1/Lf_2 the ratio P_1^*/P_2^* may be different depending on the conditions (e.g., in the case of channel flow, depending on the interelectrode distance).⁽¹¹⁷⁾

11.4. Scale-Up Effects

The development of an industrial process or device from a laboratory study usually involves a considerable increase in the size of the cells: This scale-up and the effects connected with it are a central problem of electrochemical engineering.

In general, a process can be more or less profoundly modified when the scale is changed. Let us list four important reasons:

1. Mass transport effects (see later).
2. Heat transport effects. Heat is usually generated in electrochemical systems through which a current flows. Sometimes heat is provided to the system in order to maintain a desired high temperature. In both cases heat is transferred from the system to the surroundings or vice versa. This heat transfer is affected by a change in size. Let us consider an electrolytic cell having the form of a cube of side a and containing equally spaced plate electrodes. The heat generated in such a cell is proportional to its volume, i.e., to a^3 , whereas the heat flux to the surroundings is proportional to the heat exchange area, i.e., to the area of the cell walls a^2 . Therefore, if one increases the cell size a , the amount of heat generated per unit time increases faster than the heat flux to the surroundings (for a given driving temperature difference between cell and surroundings). If no adequate measures are taken, a higher, undesired temperature may thus establish itself in the cell in scale-up.
3. Current distribution effects. In general, the current distribution tends to become less uniform when the electrode size is increased (see Chapter 4).
4. Impurity effects. Electrode reactions are affected considerably by adsorption phenomena. Important sources of adsorption are the impurities of the solution which at least in part may have their origin in the cell walls. Since the ratio of the wall area to cell volume decreases with increasing size, wash-out effects from the cell walls are relatively less important in a large cell than in a small one.†

† It should be noted that time effects also play an important role. Laboratory experiments usually last a few hours or less, industrial cells are running for months and years. There is enough time for the cell walls to be washed out and a steady state may establish itself, which, with respect to impurities, is quite different from that prevailing in laboratory experiments. In addition, over longer periods of time, corrosion of the electrodes and structural superficial modifications of their surface may take place, which affect the process considerably. Therefore, the transfer from the laboratory experiment to the industrial application not only involves a problem of scale-up in space but also of scale-up in time.

The current distribution will be treated in Chapter 4. In this section we will discuss the mass transport effects encountered in scale-up. As pointed out previously (Sections 1.1, 2.3, and 4.3) the thickness of the diffusion layer may vary along the interface. In metal deposition at a vertical cathode with laminar natural convection, the diffusion layer thickness increases with height; in laminar flow along a plate electrode, it increases with increasing distance from the leading edge. This has two consequences:

(a) Below the limiting current, when the local current density is approximately uniform along the electrode, the concentration difference between bulk and interface varies along the electrode. For example, for laminar flow along a plate this variation is given by Eq. (60). In metal deposition at a vertical cathode the depletion of metallic cations near the interface increases from bottom to top. If the electrode is large, such effects may become important. This is mainly the case when the variation of $c_{B,0} - c_{B,e}$ is such that $c_{B,e}$ is negligibly small in some parts of the electrode; i.e., some parts of the electrode work under limiting-current conditions while others do not. Figure 26 illustrates the influence of a variation of interfacial concentration. Copper is deposited at a cathode of 1 m height with natural convection. In general, metallic deposits are powdery when they are obtained at the limiting current.⁽¹¹⁸⁾ In the electrolysis of Figure 26 the average current density is such that (due to the increase of δ with height) the interfacial concentration $c_{B,e}$ is zero toward the top but not in the lower part of the cathode; i.e., the

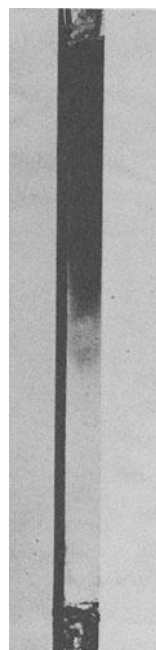


Figure 26. Influence of nonuniform mass transfer on metal deposition.

local current is the limiting one toward the top but not toward the bottom. The result is that the deposit is powdery and dark toward the top but adherent and bright in the lower part of the cathode.^(118,119) Such effects are more likely to be encountered in large cells than in small ones and the possibility of their occurrence should be taken into account in scale-up.

(b) At the limiting current, the interfacial concentration is zero and a variation of the thickness of the diffusion layer cannot cause a change of $c_{B,0} - c_{B,e}$ but does affect the local limiting-current density. This nonuniform current distribution will be discussed in Chapter 4. For example, in laminar flow along a plate the local limiting-current density decreases downstream according to Eq. (47). As a result of this, the average current density, given by Eq. (52) depends on the total electrode length l in the direction of the flow: It is inversely proportional to $l^{1/2}$. Therefore, if we apply the same average current density in two cells of different l it may happen that this current density is smaller than the average limiting-current density for the small cell but well above it for the large cell. In such a case the process would be more or less substantially modified in scale-up. If the limiting current is surpassed, the current efficiency for the desired reaction drops more or less severely in the large cell, and in a metal deposition the deposit becomes powdery and nonadherent although it may be smooth and compact in a smaller cell. Furthermore, if the average current density becomes larger than the average limiting-current density nonuniformity effects such as those shown in Figure 26 may appear in the industrial cell although they were not observed in the laboratory experiment. Another example of this kind is a nonuniform distribution of current efficiency along the electrode.

We may conclude that the possibility of mass transport effects should be envisaged in scale-up and that the current density has to be adjusted so that detrimental effects are avoided. The necessity, or extent, of such adjustments can be predicted from model experiments at constant values of the relevant dimensionless groups, as discussed in Section 4, or from a knowledge of the correlations such as Eq. (52) showing the influence of size on the limiting-current density.

Table 3 shows this influence for a number of selected hydrodynamic conditions. In general, the limiting current density decreases with increasing size under laminar flow conditions, whereas it depends very little, or virtually not at all, on size in the turbulent range. A notable exception is the rotating disk: In this case, the average limiting-current density is independent of the disk radius in laminar flow. This is linked with a uniform current distribution at the limiting current. One often refers to this feature—which is a great advantage of the rotating disk—by saying that it is equally accessible to mass transport over its whole surface. It should be noted, however, that this is no longer the case when the flow becomes turbulent. Above a certain rotation speed turbulence sets in toward the border of the disk. The flow is then in part laminar (toward the center), in part turbulent, and the local limiting-

Table 3
Influence of Electrode Size on the Average Limiting-Current Density^a

Hydrodynamic system	Average limiting-current density proportional to
Free convection at vertical electrodes, laminar flow	$L^{-1/4}$
Free convection at horizontal electrodes, turbulent flow	l^0
Laminar flow along plate	$l^{-1/2}$
Channel flow, laminar	$(ld_h)^{-1/3}$
Channel flow, turbulent	$d_h^{-1/4}$
Rotating disk, laminar flow	R^0
Rotating disk, turbulent flow	$R^{0.8}$
Rotating cylinder, laminar flow	$R^{0.4}$
Rotating cylinder, turbulent flow	$R^{0.2}$

^a See reference 115.

current density depends on location; i.e., the average limiting-current density depends on size. If the rotation speed is increased further, the flow eventually becomes turbulent over the whole electrode but the average limiting-current density still depends considerably on the size of the disk (item 7 of Table 3), in contrast to turbulent mass transport with most other geometries. Finally, let us note that the influence of size is also very small for gas-evolving electrodes.

In the foregoing discussion we considered the influence of a variation of the local-current density due to hydrodynamic effects at *constant bulk concentration*. However, in an industrial reactor the scale-up may also be influenced by a variation of the local current density which has nothing to do with hydrodynamics. Let us consider, for example, an electrochemical flow-through reactor corresponding to the channel flow cell discussed in Section 7.4, which operates at the limiting current. In the case where the limiting species is consumed in the electrode reaction the electrolyte is depleted downstream with respect to this species. The driving concentration difference between the bulk of the solution and the interface thus decreases and so does the local limiting-current density. A simple mass balance shows that in a channel cell with an interelectrode distance h the local limiting-current density varies exponentially with the distance x from the entry:

$$j_{\text{lim},x} = z_{\text{B}} F k_d c_{\text{B},\infty} \exp\left(-\frac{xk_d}{hv_0}\right) \quad (224)$$

where $c_{\text{B},\infty}$ is the concentration of the limiting species at the inlet, and k_d is the mass transfer coefficient in the channel. Equation (224) shows that the maximum utilization of a flow cell decreases downstream and that the overall efficiency becomes worse for longer reactors.

The above correlation corresponds to a plug flow reactor with continuous flow and would not be the same for a perfectly stirred tank. In practical systems the situation is somewhere in between. A more detailed discussion of the different types of electrochemical reactors and of their hydrodynamic characteristics is given by Pickett.⁽⁴⁵⁾

Auxiliary Notation

ψ correction factor (see Section 7.3.1 and Figure 16)

References

1. E. Brunner, *Z. Phys. Chem.* **47**, 56–102 (1904).
2. W. Nernst, *Z. Phys. Chem.* **47**, 52–55 (1904).
3. V. G. Levich, *Acta Physicochim. URSS* **17**, 252–307 (1942).
4. V. G. Levich, (a) *Zh. Fiz. Khim.* **22**, 575–585, 711–729 (1948). (b) *Physicochemical Hydrodynamics*, 1st and 2nd eds., State Publisher for Physico-mathematical Literature, Moscow (1952 and 1959) (in Russian); English translation: Prentice-Hall, Englewood Cliffs, NJ (1962).
5. C. Wagner, *J. Electrochem. Soc.* **95**, 161–173 (1949).
6. (a) C. R. Wilke, M. Eisenberg, and C. W. Tobias, *J. Electrochem. Soc.* **100**, 513–523 (1953). (b) M. Eisenberg, C. W. Tobias, and C. R. Wilke, *J. Electrochem. Soc.* **101**, 306–319 (1954).
7. J. N. Agar, *Discuss. Faraday Soc.* **1**, 26–37 (1947).
8. N. Ibl, *Chimia* **9**, 135–141 (1955).
9. N. Ibl, Y. Barrada, and G. Trümpler, *Helv. Chim. Acta* **37**, 583–597 (1954).
10. W. Vielstich, *Z. Elektrochemie* **57**, 646–655 (1953).
11. R. B. Bird, W. E. Stewart, and E. N. Lightfoot, *Transport Phenomena*, Wiley, New York (1960).
12. H. Brauer, *Stoffaustausch einschliesslich chemischer Reaktionen*, Sauerländer, Aarau and Frankfurt (1971).
13. J. C. Slattery, *Momentum, Energy and Mass Transfer in Continua*, McGraw-Hill, New York (1972).
14. A. H. P. Skelland, *Diffusional Mass Transfer*, Wiley, New York (1974).
15. T. K. Sherwood, R. L. Pigford, and C. R. Wilke, *Mass Transfer*, McGraw-Hill, New York (1975).
16. J. R. Welty, C. E. Wicks, and R. E. Wilson, *Fundamentals of Momentum, Heat and Mass Transfer*, 2nd ed., Wiley, New York (1976).
17. G. Wranglen and O. Nilsson, *Electrochim. Acta* **7**, 121–137 (1962).
18. H. Blasius, *Z. Math. Phys.* **56**, 1–37 (1908).
19. L. Howarth, *Proc. R. Soc. Lond. A* **164**, 547–579 (1938).
20. E. Eckert and O. Drewitz, *Forsch. Gebiete Ing. Wesen* **11**, 116–124 (1940).
21. H. Schlichting, *Boundary Layer Theory*, Chapter XII, 6th ed., McGraw-Hill, New York (1968).
22. H. Görtler, *Dimensionsanalyse*, Springer, Berlin (1975).
23. H. L. Langhaar, *Dimensional Analysis and Theory of Models*, 6.ed., Wiley, New York (1964).

24. W. J. Duncan, *Physical Similarity and Dimensional Analysis*, Edward Arnold, London (1953).
25. R. C. Pankhurst, *Dimensional Analysis and Scale Factors*, Chapman and Hall, London (1964).
26. P. W. Bridgman, *Dimensional Analysis*, rev. ed., 6th printing, Yale University Press, New Haven, CT (1949).
27. E. S. Taylor, *Dimensional Analysis for Engineers*, University Press, Winchester, MA (1974).
28. J. Zierep, *Similarity Laws and Modelling*, Marcel Dekker, New York (1977).
29. N. Ibl, *Electrochim. Acta* **1**, 117–129 (1959).
30. IUPAC Manual of Symbols and Terminology for Physicochemical Quantities and Units, *Pure Appl. Chem.* **51**, 1–41 (1979).
31. N. Ibl and P. M. Robertson, *Electrochim. Acta* **18**, 897–906 (1973).
32. H. S. Carslaw and J. C. Jaeger, *Conduction of Heat in Solids*, 2nd ed., Oxford University Press, Oxford (1959).
33. W. H. McAdams, *Heat Transmission*, McGraw-Hill, New York (1951).
34. J. P. Holman, *Heat Transfer*, 4th ed., McGraw-Hill, New York (1976).
35. M. N. Özışik, *Basic Heat Transfer*, McGraw-Hill, New York (1977).
36. B. Gebhart, *Heat Transfer*, 2nd ed., Tata-McGraw-Hill Ltd., Bombay and New Delhi (1971).
37. C. O. Bennett and J. E. Meyers, *Momentum, Heat and Mass Transfer*, McGraw-Hill, New York (1962).
38. T. H. Chilton and A. P. Colburn, *Ind. Eng. Chem.* **26**, 1183–1187 (1934).
39. P. Le Goff, *Chimie Indus.* **103**, 1805–1812, 1959–1966 (1970).
40. P. Le Goff, *Chem. Eng. J.* **20**, 197–209 (1980).
41. T. V. Boussinesq, *Mém. Prés. Acad. Sci. (Paris)* **XXIII**, 46 (1877).
42. C. S. Lin, R. W. Moulton, and G. L. Putman, *Ind. Eng. Chem.* **45**, 636–646 (1953).
43. R. G. Deissler, NACA—Report 1210 (1955).
44. D. T. Wasan and C. R. Wilke, *Int. J. Heat Mass Transfer* **7**, 87–94 (1964).
45. D. J. Pickett, *Electrochemical Reactor Design*, Elsevier, Amsterdam (1977).
46. J. R. Selman and C. W. Tobias, In: *Advances in Chemical Engineering*, T. B. Drew, G. R. Cokelet, J. W. Hoopes, Jr., and T. Vermeulen, eds., Vol. 10, pp. 211–318, Academic Press, New York (1978).
47. P. M. Robertson, F. Schwager, and N. Ibl, *J. Electroanal. Chem.* **65**, 883–900 (1975).
48. D. Hutin, A. Storck, and F. Coeuret, *Inform. Chimie* **189**, 227–235 (1979).
49. H. Tennekes and J. L. Lumley, *A First Course in Turbulence*, MIT Press, Cambridge, MA, and London (1972).
50. J. Rotta, *Turbulente Strömungen*, B. G. Teubner, Stuttgart (1972).
51. J. T. Davies, *Turbulence Phenomena*, Academic Press, New York and London (1972).
52. E. Eucken, *Z. Phys. Chem.* **59**, 72–117 (1907).
53. S. L. Gordon, J. S. Newman, and C. W. Tobias, *Ber. Bunsenges. Phys. Chem.* **70**, 414–420 (1966).
54. S. Okada, S. Yoshizawa, F. Hine, and K. Asada, *J. Electrochem. Soc. Jap.* **27**, E51–E52 (1959).
55. J. Newman, *Ind. Eng. Chem. Fund.* **5**, 525–529 (1966).
56. J. R. Selman and J. Newman, *J. Electrochem. Soc.* **118**, 1070–1078 (1971).
57. J. Newman, *Electrochemical Systems*, Prentice-Hall, Englewood Cliffs, NJ (1973).
58. L. Hsueh and J. Newman, *Ind. Eng. Chem. Fund.* **10**, 615–620 (1971).
59. J. Newman, *Int. J. Heat Mass Transfer* **10**, 983–997 (1967).
60. C. R. Wilke, C. W. Tobias, and M. Eisenberg, *Chem. Eng. Progr.* **49**, 663–674 (1953).
61. N. Ibl and R. H. Müller, *J. Electrochem. Soc.* **105**, 346–353 (1958).
62. S. Ostrach, NACA Technical Note 2635 (1952).
63. E. M. Sparrow and J. L. Gregg, *Trans. Am. Soc. Mech. Eng.* **78**, 435–440 (1956).

64. N. Ibl, *Electrochim. Acta* **1**, 3–17 (1959).
65. N. Ibl and U. Braun, *Chimia* **21**, 395–404 (1967).
66. E. Ravoo, J. W. Rotte, and F. W. Sevenstern, *Chem. Eng. Sci.* **25**, 1637–1652 (1970).
67. A. F. J. Smith and A. A. Wragg, *J. Appl. Electrochem.* **4**, 219–228 (1974).
68. M. G. Fouad and N. Ibl, *Electrochim. Acta* **3**, 233–243 (1960).
69. M. G. Fouad and T. Gouda, *Electrochim. Acta* **9**, 1071–1076 (1964).
70. F. A. Holland, R. M. Moores, F. A. Watson, and J. K. Wilkinson, *Heat Transfer*, Heinemann Books, London (1970).
71. G. D. Raithby and K. G. T. Hollands, *Adv. Heat Transfer* **11**, 295 (1975).
72. H. Gebhart, In: *Advances in Heat Transfer*, T. F. Irvine, J. P. Hartnett, eds., Vol. 9, pp. 273–348, Academic Press, New York and London (1973).
73. U. Böhm and N. Ibl, *Electrochim. Acta* **13**, 891–899 (1968).
74. R. Alkire and R. Plichta, *J. Electrochem. Soc.* **120**, 1060–1066 (1973).
75. J. R. Lloyd and W. R. Moran, *J. Heat Transfer* **96**, 443–447 (1974).
76. A. A. Wragg, *Electrochim. Acta* **13**, 2159–2165 (1968).
77. E. J. Fenech and C. W. Tobias, *Electrochim. Acta* **2**, 311–325 (1960).
78. H. Brauer, *Grundlagen der Einphasen- und Mehrphasenströmungen*, Sauerländer, Aarau and Frankfurt (1971).
79. K. Stephan, *Chem. Ing. Techn.* **31**, 773–778 (1959).
80. D. J. Pickett and L. L. Ong, *Electrochim. Acta* **19**, 875–882 (1974).
81. I. Roušar, J. Hostomský, V. Cezner, and B. Štverak, *J. Electrochem. Soc.* **118**, 881–884 (1971).
82. P. VanShaw, L. P. Reiss, and T. J. Hanratty, *A.I.Ch.E. J.* **9**, 362–364 (1963).
83. N. Ibl and D. Landolt, *J. Electrochem. Soc.* **115**, 713–720 (1968).
84. J. Newman and L. Hsueh, *Electrochim. Acta* **12**, 417–427 (1967).
85. L. Hsueh and J. Newman, *Electrochim. Acta* **12**, 429–438 (1967).
86. J. R. Selman, Measurement and Interpretation of Limiting Currents, Ph.D. thesis, University of California, Berkeley UCRL-20557 (1971).
87. M. Eisenberg, C. W. Tobias, and C. R. Wilkie, *J. Electrochem. Soc.* **103**, 413–416 (1956).
88. L. W. Öholm, *Soc. Sci. Fenn. Commentat. Phys. Math.* **12**, 1–8 (1942).
89. D. Dobos, *Electrochemical Data*, Elsevier, Amsterdam, Oxford, New York (1975).
90. *International Critical Tables*, Vol. V, 1st ed., McGraw-Hill, New York (1929).
91. *International Critical Tables*, Vol. III, 1st ed., pp. 56 and 67, McGraw-Hill, New York (1928).
92. A. R. Gordon, *J. Chem. Phys.* **8**, 423 (1940).
93. Landolt-Börnstein, *Phys. Chem. Tabelle*, Vol. II, Part 5a, p. 613, Springer, Berlin (1969).
94. P. Grassmann, N. Ibl, and J. Trueb, *Chem. Ing. Techn.* **33**, 529–533 (1961).
95. E. Weder, *Chem. Ing. Tech.* **39**, 914–918 (1967); *Wärme-Stoffübertragung* **1**, 10–14 (1968).
96. H. Bode, *Chem. Ing. Tech.* **43**, 293 (1971).
97. P. Grassmann and M. Tuma, *Ger. Chem. Eng.* **1**, 276–282 (1978).
98. L. P. Reiss and T. J. Hanratty, *A.I.Ch.E. J.* **8**, 245–247 (1962).
99. J. E. Mitchell and T. J. Hanratty, *J. Fluid Mech.* **26**, 199 (1966).
100. N. Ibl, *Proceedings of the International Conference on Protection Against Corrosion by Metal Finishing (Surface 66)*, Basel, Switzerland, p. 49, Forster, Zurich (1966).
101. N. Ibl and K. Schädegg, *J. Electrochem. Soc.* **114**, 54–58 (1967).
102. C. Deslouis, I. Epelboin, M. Keddam, L. Viet, O. Dossenbach, and N. Ibl, *Physicochemical Hydrodynamics: Proceedings of a Symposium*, V. G. Levich-Festschrift, D. B. Spalding, ed., 939–971, Advance Publications Ltd., London (1977).
103. D. Schuhmann, *C.R. Acad. Sci. Paris* **262**, 624–627 (1966).
104. G. Blanc, I. Epelboin, C. Gabrielli, and M. Keddam, *J. Electroanal. Chem. Interfacial Electrochem.* **62**, 59–94 (1975).
105. B. Miller and S. Bruckenstein, *Anal. Chem.* **46**, 2026–2033 (1974).

106. K. Tokuda, S. Bruckenstein, and B. Miller, *J. Electrochem. Soc.* **122**, 1316–1322 (1975).
107. C. Deslouis, I. Epelboin, B. Tribollet, and L. Viet, *Electrochim. Acta* **20**, 909–911 (1975).
108. L. P. Reiss and T. J. Hanratty, *A.I.Ch.E. J.* **9**, 154–160 (1963).
109. A. Storck and F. Coeuret, *Electrochim. Acta* **22**, 1155–1160 (1977).
110. D. Hutin and A. Storck, *J. Appl. Electrochem.* **9**, 351–359 (1979).
111. T. Mizushina, In: *Advances in Heat Transfer*, T. F. Irvine, ed., Vol. 7, pp. 87–161, Academic Press, New York (1971).
112. N. Ibl and E. Adam, *Chem. Ing. Tech.* **37**, 573–581 (1965).
113. N. Ibl and A. M. Frei, *Galvanotechnik Oberflächenschutz* **5**, 117–122 (1961).
114. N. Ibl, *Electrochim. Acta* **22**, 465–477 (1977).
115. N. Ibl, In: *14th International IUPAC Congress*, Hamburg, 1973, Vol. 5, pp. 31–48, Butterworth, London (1974).
116. J. M. Engasser and C. Horvath, *Ind. Eng. Chem. Fund.* **14**, 107–110 (1975).
117. F. Schwager, Dissertation ETH 6241, Zürich (1978).
118. N. Ibl, In: *Advances in Electrochemistry and Electrochemical Engineering*, C. W. Tobias and P. Delahay, eds. Vol. 2, pp. 49–143, Wiley, Interscience, New York and London (1962).
119. N. Ibl, *Chem. Ing. Tech.* **33**, 69–74 (1961).
120. N. Ibl, M. Braun, *Chem. Ing. Tech.* **45**, 182–188 (1973).
121. H. J. Read and K. Graham, *Trans. Electrochem. Soc.* **78**, 279 (1940); **80**, 329 (1941). See also *Proc. Am. Electroplaters Soc.* **1939**, 95 (1939).
122. A. Brenner, *Proc. Am. Electroplaters Soc.* **1940**, 95 (1940); **1941**, 28 (1941).
123. Ch. Fässler, Dissertation ETH 6560, Zürich (1980).

4

Current Distribution

N. IBL

1. Introduction : Practical Importance of Current and Potential Distribution

In general, the local current density j_x varies along an electrode. Similarly, the potential difference at the electrode–solution interface can depend on location. For example, the current density tends to be larger on the crests of an electrode with a serrated profile (Figure 8), or near the edges of an electrode that does not entirely fill the cross section of the electrolysis cell (Figures 3 and 10). This is due to the fact that, at these privileged spots, the cross section of the solution available for the passage of charges through the electrolyte increases with increasing distance from the electrode, so that the resistance for the current flow from the anode to the cathode is smaller at these spots than in other parts of the electrode.

The potential distribution, and even more the current distribution, are of great importance for the *technical applications* of electrochemistry. Let us give a few examples.

In *surface finishing*, the current distribution determines in electroplating the local variation in the thickness of the coating—a variation that one tries to minimize in order to avoid an accelerated corrosion (or wear) of the less well protected parts (see Chapter 7, Volume 2). The phenomena of leveling and electropolishing are due to current-distribution effects. The latter are also essential in electrochemical machining for the reproduction of the shape of

the matrix and for the smoothing of the treated surface. Likewise, the objects manufactured by electroforming can meet the required specifications only through an adequate current distribution.

In *electrometallurgy*, in the refining of copper, for example, the metallic layers deposited on the cathode are much thicker than in electroplating. A non uniform current distribution causes local surelevations—protuberances that may create short circuits with a counterelectrode. This imposes a lower limit to the interelectrode distance, which should be as small as possible in order to reduce the energetic losses through the Joule effect in the solution. Analogous phenomena occur at the anode. For example, in aluminium electrolysis the carbon anodes are consumed to form CO and CO₂, with a preferential attack on the edges: Depending on the importance of this effect, it is more or less difficult to maintain an optimum interelectrode distance. Even in the case of inert anodes, there is usually some corrosion, and this is often faster in the parts where the current density is higher.

The performance of certain kinds of *batteries* is considerably influenced by the distribution of the current within the spongy or granular layers (e.g., in the Pb or PbO₂ electrodes of the lead accumulator). Quite generally, the current and potential distributions play an essential role in the *three-dimensional electrodes*, such as porous, fixed or fluidized bed electrodes. These systems have a large active area compared to the volume of the electrolysis cell, thus reducing the investment cost (see Chapter 6, this volume). However, this advantage becomes a delusion when the current does not sufficiently penetrate into the interior of the body of the electrode. Furthermore, an unequal current distribution, in general, is accompanied by a local variation of the electrode potential. The result may be a change in the composition of the products of the electrochemical reactions, in particular, if the latter are very sensitive to the electrode potential, as is the case in some organic electrosyntheses.

Without dwelling any further on the technological aspects, we may conclude that the theory of current and potential distributions is one of the fundamentals of *electrochemical engineering*. In fact, it is also very relevant for *pure electrochemistry* and laboratory electrolysis, where, unfortunately, it has not received the attention it deserves. The well known maxima of the polarographic curves are due to a hydrodynamic flow, caused by a nonuniform distribution of current and potential due to the screening effect of the capillary on the upper parts of the mercury drop. In the galvanostatic technique (constant current) (see Chapter 2, Volume *Electrodics: experimental techniques*), the apparatus only keeps the overall current constant (i.e., the *average* current density). In reality a more or less marked local variation of the current density may occur, if the experiment is not designed to minimize the phenomenon. A similar difficulty arises with the potentiostatic method (constant electrode potential). One often controls the potential by measuring the

potential difference between the working electrode and a reference electrode which is connected with the working electrode by means of a Luggin capillary (Chapter 1, Volume 6). Depending on the distance of the interface from the tip of the capillary the latter shields the electrode to varying degrees. This modifies at the point of measurement the local current density, and thus the electrode potential, which are different there from their values over the major part of the electrode. As a result, the determination of the current–voltage relationship (which is most relevant in electrode kinetics studies) is vitiated since an average value of current density is measured rather than the local current density near the tip of the Luggin capillary. An additional error may arise if the tip of the capillary is located in an unfavorable section of the electrode, for example, near an edge where the local current density and thus the activation overpotential may be substantially larger than toward the middle of a plane electrode (see, e.g., Figures 15 and 21 and Section 6.3.6).

2. Experimental Methods

The current distribution can be determined experimentally with the help of segmented electrodes, by measuring the currents flowing through segments isolated from each other by a narrow inactive zone and maintained at the same potential.^(1–7,151) Instead of segments, microelectrodes embedded in the electrode have also been used.⁽¹⁶⁵⁾ Another possibility is the study of the variation, over an electrode, in the thickness of a metallic coating obtained with 100% current efficiency.^(8–11) Figure 1 shows the cross section through a deposit of copper on nickel. In agreement with what has been mentioned at the beginning of Section 1, it is seen that the coating is thicker on the crests of the serrated profile. Further techniques employed are autoradiography,^(12,13,143) atomic absorption,⁽¹⁴⁾ and measurements with rotating double probe electrodes.⁽¹⁴⁹⁾

The current distribution is closely linked to that of the potential. The latter distribution can be determined by measuring the local electric potential in the solution with the help of probes properly located in the interior of the cell or close to the electrode.^(15–20) One may thus obtain a potential map of the whole solution, or the variation with location of the potential difference over the electrode–solution interface.

The experimental methods are reviewed in a monograph by Rousselot⁽¹⁸⁾ as well as in a paper by Weiler and Zerweck⁽²¹⁾ (see also reference 174). These reviews also provide information on the semiquantitative and qualitative techniques used in electroplating. An experimental arrangement popular in this field is the Haring–Blum cell. We will discuss it in Sections 6.2 and 6.3.5 in connection with the concept of throwing power.

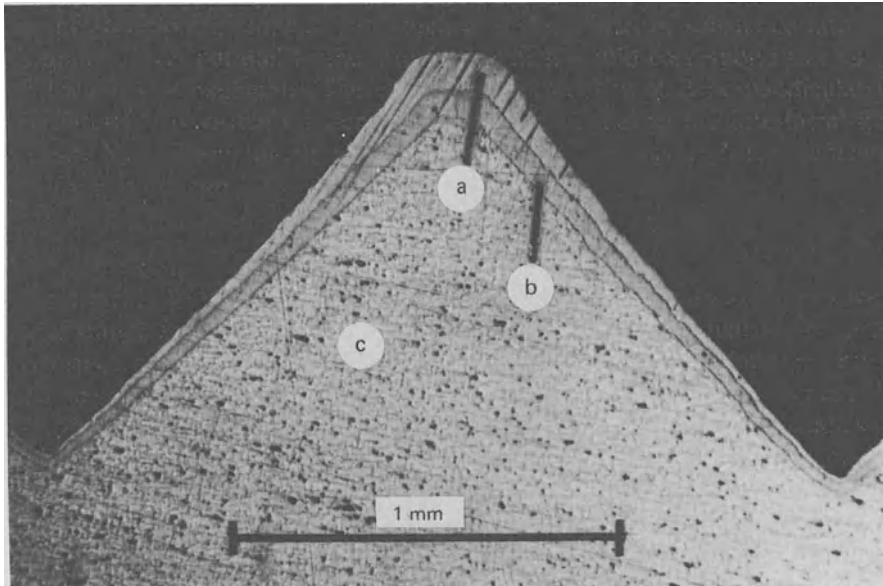


Figure 1. Copper coating on a serrated profile showing the increased thickness at the peak. a, protective layer; b, Cu deposit; c, substrate.

3. Main Types of Current and Potential Distributions

The main factors on which the current and potential distributions over an electrode depend are:

- (a) the geometry of the system;
- (b) the conductivity of the solution and electrodes;
- (c) the activation overpotential (which depends on the kinetics of the electrode reaction);
- (d) the transport overpotential (which is caused by the concentration differences between the electrode–solution interface and the bulk solution and controlled by the transport phenomena) (see Chapter 1, Section 7.2 on concentration overpotential).

Depending on the conditions, the influence of one or the other of these factors may be more or less neglected. Accordingly, one distinguishes three main types of current distributions.^(18,22,23,142)

Primary distribution (Section 5): This establishes itself when the influence of overpotential is negligible. The absence of transport overpotential implies that there are no appreciable concentration gradients in the solution, whereas

the absence of activation overpotential means that there is no influence of the kinetics of the electrode reaction.

Secondary distribution (Section 6): In this case, one takes into consideration the activation overpotential, but neglects the influence of the transport overpotential.

Tertiary distribution (Section 8): One takes into account the transport overpotential in addition to the activation overpotential.

4. Outline of Theory of Primary and Secondary Distribution

The most general theoretical approach to the problem of current and potential distribution starts from the integration of the fundamental equations of mass and charge transport [Eq. (21), Chapter 1]

$$\frac{\partial c_B}{\partial t} = D_B \nabla^2 c_B - F(RT)^{-1} z_B D_B \nabla \cdot (c_B \nabla \phi) - \mathbf{v} \cdot \nabla c_B + \sum_r v_{B,r}^* \quad (1)$$

In practice, more or less simplified versions of this equation are used (see also Chapters 1 and 3). The nature of the approximation made depends on the type of distribution considered (primary, secondary, or tertiary). In principle, the problem is similar to the theoretical treatment in Chapters 2 and 3 and the calculations of current and potential distributions can be regarded as particular cases of the theory of mass and charge transport. However, it has been customary to present the theoretical treatment of current and potential distributions separately from the discussion of mass transport as given in Chapters 2 and 3. This applies particularly to primary and secondary current distributions. Indeed, the simplifications of the basic equations are quite different here from those used in Chapters 2 and 3.

In primary and secondary distributions the influence of transport overpotential is neglected. This is justified at current densities that are low compared to the limiting current. The assumption implies that there are no concentration gradients in the solution; i.e., that the terms $D_B \nabla^2 c_B$ and $\mathbf{v} \cdot \nabla c_B$ in Eq. (1) can be dropped. Furthermore, we have $\nabla \cdot (c_B \nabla \phi) = \nabla c_B \cdot \nabla \phi + c_B \nabla^2 \phi = c_B \nabla^2 \phi$. Finally, if we multiply Eq. (1) by the ionic charge z_B and take the sum for all ionic species i in the solution, the terms $\sum_i z_i (\partial c_i / \partial t)$ and $\sum_i \sum_r z_B v_{B,r}^*$ are nil because of the electroneutrality condition $\sum_i z_i c_i = 0$. The sum of equations such as (1) (extended over all ionic species) thus reduces to

$$\nabla^2 \phi = \frac{\partial^2 \phi}{\partial x^2} + \frac{\partial^2 \phi}{\partial y^2} + \frac{\partial^2 \phi}{\partial z^2} = 0 \quad (2)$$

which is the Laplace equation. x , y , and z are the spatial coordinates and ϕ

is the electric potential at point x, y, z . The electroneutrality condition, which is implied in the validity of Eq. (2), means that this equation can be applied everywhere in the solution, except in the electric double layer at the electrode. Therefore, the boundary condition for the integration of Eq. (2) can be formulated as the value of the potential prevailing at the solution side limit of the electric double layer, which usually has a thickness of a few Å only.† The formulation of the above boundary condition is not the same for primary and secondary distributions (see Section 5.6). Furthermore, it depends upon whether or not the electrode has a conductivity that is virtually infinite compared to that of the solution. The first situation is that most commonly encountered in practice and in Sections 5 and 6, we will first restrict ourselves to this case. The case where the conductivity of the electrodes is not infinite will be treated in Section 7.

The integration of Eq. (2) yields the potential field in the solution

$$\phi = f(x, y, z) \quad (3)$$

In the absence of concentration gradients, the current density \mathbf{j} at any point in the solution is proportional to the gradient of the potential ϕ at that point and to the conductivity κ of the solution (Chapter 1, Section 4).

$$\mathbf{j} = -\kappa \nabla \phi \quad (4)$$

The current density \mathbf{j} is a vector (see also Section 4, Chapter 1). It is perpendicular to the equipotential surfaces and thus is the tangent to the current lines. The latter, which are shown as broken lines in Figure 3, indicate the direction in which the current flows and show the path followed by the electric charges. There is no transport of charges in a direction perpendicular to a current line.

The current density flowing through the electrode is a scalar quantity (see also Section 4, point 2 of Chapter 1). It is given, for a point of the electrode, by the component of the vector \mathbf{j} perpendicular to the interface for the point considered. Therefore, it can be obtained by applying Eq. (3) to the solution side of the double layer at the interface and by differentiating with respect to n , $\partial\phi/\partial n$, which is the direction perpendicular to the electrode. This yields the desired current and potential distributions over the electrode. In the following, in general, when we speak of current density we will mean the current density flowing through the electrode. Its local value will be denoted by j_x .‡

† The influence of departures from electroneutrality in the double layer has been discussed from the viewpoint of the mass transport equations in Section 6.1 of Chapter 1.

‡ Quite generally, for an electrode of arbitrary shape, the local current density is a function of these spatial coordinates and should be thus denoted by $j_{x,y,z}$. But most of the examples considered in this chapter are simple ones, where the local current density depends on one coordinate only.

An excellent discussion of the theory has been given in Chapter 18 of Newman's book *Electrochemical Systems*.⁽²²⁾ The current and potential distributions have been reviewed also by Rousselot⁽¹⁸⁾ in a monograph which is now somewhat outdated, however. More recently the subject has been reviewed by Ibl.⁽²³⁾ Surprisingly, it is almost never treated in the textbooks on electrochemistry. Noteworthy exceptions are the books by Gallone⁽²⁴⁾ and by Milazzo.^(25a)

It may also be noted that Eq. (2) is formally the same as the differential equation for steady-state heat conduction or mass diffusion (in the absence of convection and a source term). In fact, this type of equation corresponds to a classical problem of mathematical physics. Therefore, the solution obtained for the temperature field in heat conduction, or concentration field in diffusion, can be readily used to describe the potential field in electrolysis, provided that corresponding boundary conditions in the different types of problems are considered. The analogue of the current distribution over an electrode is the distribution of the interfacial flux density of heat or of mass over an interface. A good source of solutions for the case of heat conduction is the book by Carslaw and Jaeger.⁽¹²⁹⁾

The methods used for obtaining solutions of the Laplace equation in electrolytic systems can be divided in three categories: *analytical* techniques, *analogic procedures* and *numerical* methods. We will give examples and an outline of these methods in the next sections. Mathematically it may be interesting to subdivide the subject according to the three above mentioned techniques. However, we will follow the classical approach of distinguishing between primary and secondary distribution. It has the advantage of facilitating the illustrative, qualitative discussion of the subject. Also, the analytical solutions are very different for the two distributions. However, there is no substantial difference in the numerical methodology. The fundamental differential equations are the same for primary and secondary distribution and the modern computers are so powerful that the more complicated boundary condition involved in secondary distribution (see Section 6) can be handled with ease.

5. Primary Distribution

5.1. Boundary Conditions

In Sections 5 and 6 we assume an electrode conductivity that is infinite compared to the conductivity of the solution. This means that there are no potential differences within the electrode. Therefore, the metallic side of the electric double layer is an equipotential surface. Furthermore, since the influence of overpotential is negligible in primary current distribution, the potential difference across the double layer is constant over the electrode.

Therefore, the solution side of the double layer is an equipotential surface also, and we can take this as a boundary condition for the integration of Eq. (2).

However, the electrolyte is usually not only bounded by the electrodes but also by isolating surfaces (cell walls, free surface of the solution). Since no current flows through an isolating surface, $\partial\phi/\partial n$ must be zero at such a surface, and we can take this as a further boundary condition.

The boundary conditions for the integration of Eq. (2) can therefore be written

$$\phi = \text{const} \quad (\text{at the electrode surface}) \quad (5)$$

$$\frac{\partial\phi}{\partial n} = 0 \quad (\text{at an insulating surface}) \quad (6)$$

5.2. Kasper Method

Let us discuss first the method developed by Kasper in 1940.⁽²⁶⁾ Although he had some precursors (see Section 11) and based his treatment on previous work, it may be said that his papers gave the first lucid and detailed treatment that had an impact in electrochemistry. He used correct boundary conditions and distinguished adequately between primary and secondary distribution. He showed that few geometries yield a fully uniform current distribution (plane parallel electrodes filling completely the cross section of the cell, concentric cylinders, concentric spheres). Starting from the well-known laws of electrostatics and using the method of images, he calculated the potential lines and the current lines for simple geometries. Figure 2(a) shows the results for two parallel line sources, the picture representing a cross section perpendicular to the lines. From such a potential and current map, many distributions can be generated for a variety of electrolytic cells by the method of sectioning. Indeed, equipotential surfaces simulate electrodes [boundary condition (5)], and current lines simulate isolating walls, since no current flows perpendicular to a current line [boundary condition (6)]. Therefore, a volume bounded by current lines and by equipotential surfaces simulates an electrolytic cell. In Figure 2(a) the thick lines show a cross section through such a volume. The sections of the current lines contained in this volume give the current-density distribution on the equipotential surfaces *a* and *b*, i.e., on the electrodes.

Figure 2(b) shows the current distribution along *BB'* on a plane going through *BB'* and perpendicular to the plane of Figure 2(a). In view of the above argument this also represents the current distribution over a plane electrode, with a wire parallel to it as a counterelectrode (the figure showing the distribution in the direction perpendicular to the wire). The wire crosses the plane of Figure 2(a) at *O'*; the local current density is inversely proportional to a^3 , where *a* is the distance from *O'*.

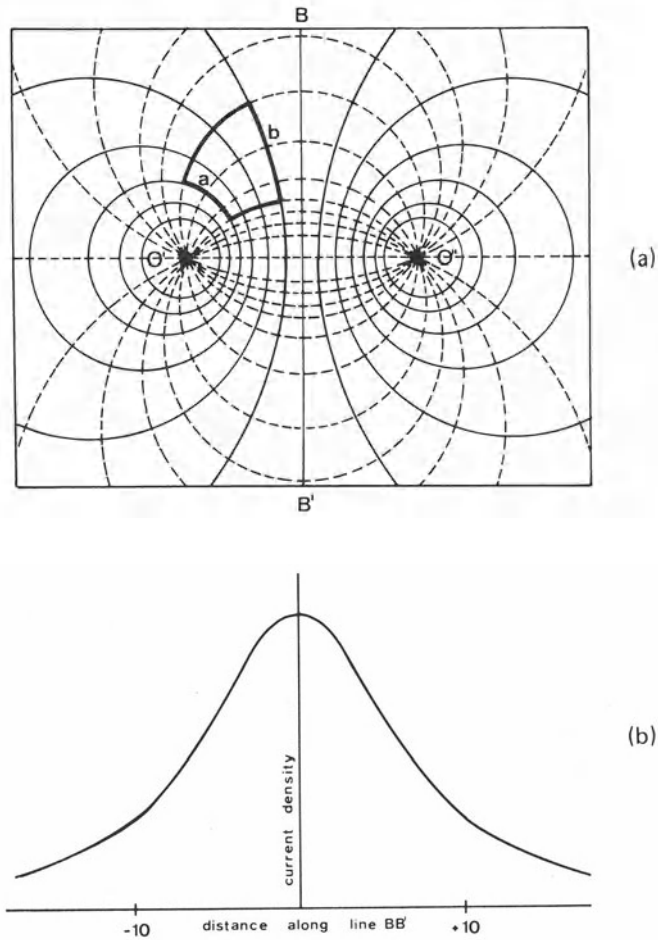


Figure 2. (a) Potential and current distribution between two parallel straight wires (source lines), illustrating the method of sectioning (the two wires are perpendicular to the plane of the figure, which they cross in O' and O''): ---, current lines; —, equipotential lines; —, boundaries of region sectioned out. (b) Current distribution along the BB' of part (a). (Points O' and O'' located 10 units away from the line BB' .)

5.3. Further Examples of Primary Distribution : Analytical Solutions for Plane Parallel and Disk Electrodes

Since Kasper, many authors have calculated the primary current distribution. Rousselot^(2,17,18,193) has described an analogic method in which one determines experimentally the potential field on conducting paper representing a model of the electrolytic system. The method has been extended to the study of secondary distribution by using paper stripes with prolongations at

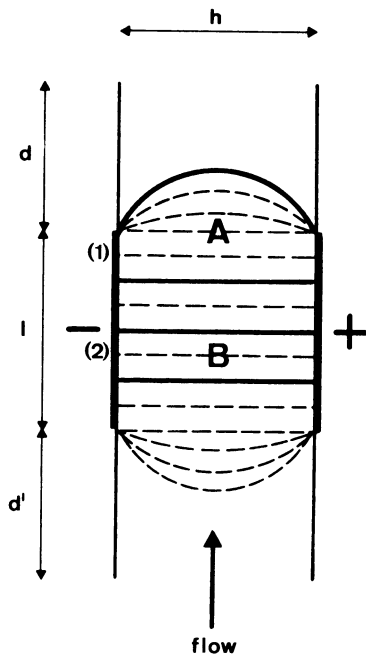


Figure 3. Electrolysis cell with plane parallel electrodes embedded in insulating walls: ---, current lines; ==, current tubes.

the electrode simulating the overpotential.⁽¹⁹³⁾ A number of authors used the method of conformal mapping,^(27-32,127) or Hankel transforms, the latter applied mainly to the case of the disk.⁽¹³⁰⁾

For simple geometries, analytical solutions can be given. Let us consider two cases of particular importance in electrochemistry. Our first system is the cell of Figure 3, containing two plane parallel electrodes embedded in insulating walls with d and $d' \gg l$. This is an example of the application of the conformal mapping method.⁽¹²⁷⁾ One obtains the following current distribution^(34,127):

$$\frac{j_x}{j} = \frac{\varepsilon \cosh \varepsilon / K \tanh^2 \varepsilon}{[\sinh^2 \varepsilon - \sinh^2 (2x'/l)]^{1/2}} \quad (7)$$

where $\varepsilon = \pi l / 2h$, h is the distance between the two electrodes, l the length of the electrode, and x' the distance from the center of the electrode. The function $K(m)$ (with $m = \tanh^2 \varepsilon$) is the first-order elliptic integral whose numerical values are given in tables.⁽³⁶⁾

It is seen that the current distribution depends on two characteristic dimensions, h and l , whereas in the case of the disk (which we will discuss in the next paragraph) there is only one such length, the radius r_0 . The distribution for $h = 2l$ is shown in Figure 4.

Let us now discuss the problem of current distribution at a disk electrode. An elegant solution has been given by Newman.^(35,127) A simple relationship is obtained if one considers an electrode embedded in an infinite insulating surface, the cell walls and the counterelectrode being located virtually at

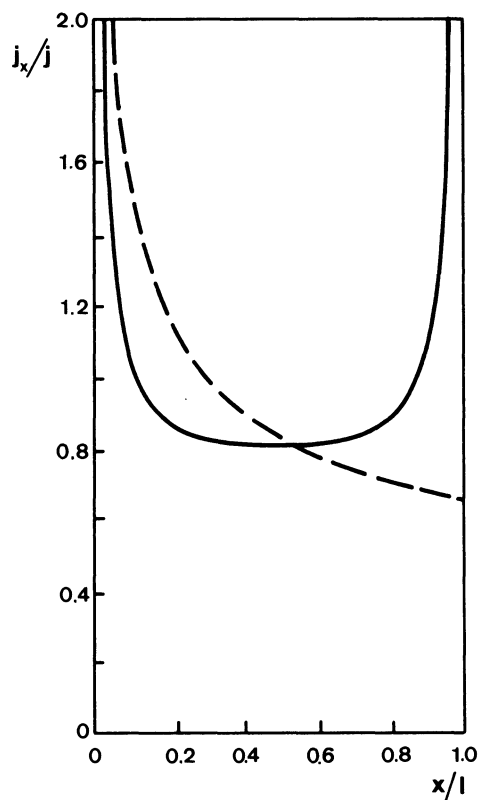


Figure 4. Current distribution in cell of Figure 3 with $l = 2h$; —, primary distribution calculated by integrating the Laplace equation; ---, limiting-current distribution (see Section 8.5).

infinity. The Laplace equation is transformed by introducing rotational elliptic coordinates ξ and η related to cylindrical coordinates by

$$z = r_0 \xi \eta \quad (8a)$$

$$r = r_0 [(1 + \xi^2)(1 - \eta^2)]^{1/2} \quad (8b)$$

where r_0 is the radius of the disk, z the normal distance from the disk, and r the distance from the axis of symmetry (which is perpendicular to the disk at its center). In this coordinate system Eq. (2) takes the form

$$\frac{\partial}{\partial \xi} \left[(1 + \xi^2) \frac{\partial \phi}{\partial \xi} \right] + \frac{\partial}{\partial \eta} \left[(1 - \eta^2) \frac{\partial \phi}{\partial \eta} \right] = 0 \quad (9)$$

The boundary conditions are

$$\phi = \phi_e \quad \text{at } \xi = 0 \text{ (on the disk electrode)} \quad (10a)$$

$$\frac{\partial \phi}{\partial \eta} = 0 \quad \text{at } \eta = 0 \text{ (on the insulating annulus)} \quad (10b)$$

$$\phi = 0 \quad \text{at } \xi = \infty \text{ (far from the disk)} \quad (10c)$$

The variables are separated by setting

$$\phi = P(\eta)M(\xi) \quad (11)$$

The differential equations for P and M are

$$\frac{d}{d\eta} \left[(1 - \eta^2) \frac{dP}{d\eta} \right] + p(p+1)P = 0 \quad (12)$$

$$\frac{d}{d\xi} \left[(1 + \xi^2) \frac{dM}{d\xi} \right] - p(p+1)M = 0 \quad (13a)$$

where $p(p+1) = k$ is the separation constant. If we set $x = i\xi (i = \sqrt{-1})$, Eq. (13a) takes the form

$$\frac{d}{dx} \left[(1 - x^2) \frac{dM}{dx} \right] + p(p+1)M = 0 \quad (13b)$$

Equations (12) and (13b) are Legendre differential equations.⁽¹³⁷⁾ In order to satisfy the boundary condition (10b), p must be an even integer $p = 2n$. The solution of Eq. (12) is thus a Legendre polynomial of order $2n$, P_{2n} . It remains finite at $\eta = 1$, which is a singular point located on the axis of symmetry.

Since the Laplace equation is linear, solutions can be superposed. Keeping this in mind, the solution of the transformed Laplace equation [Eq. (9)] can be expressed as a series,

$$\phi = \sum_{n=0}^{\infty} B_n P_{2n}(\eta) M_{2n}(\xi) \quad (14)$$

where $M_{2n}(\xi)$ is a Legendre function of imaginary argument which satisfies Eq. (13a) as well as the condition $M = 1$ at $\xi = 0$ and $M \rightarrow 0$ for $\xi \rightarrow \infty$. Therefore, the surface potential is given by

$$\phi_e = \sum_{n=0}^{\infty} B_n P_{2n}(\eta) \quad (15)$$

If ϕ_e is constant along the interface (independent of the local current density), the expression coefficients of the series are simply

$$B_0 = \phi_e, \quad B_n = 0 \quad \text{for } n = 1, 2$$

In this particular case the integration of Eq. (13a) is straightforward and yields

$$M_0 = 1 - \frac{2}{\pi} \tan^{-1} \xi \quad (16)$$

The potential distribution in the solutions is thus given by

$$\phi = B_0 P_0(\eta) M_0(\xi) = \phi_e \left(1 - \frac{2}{\pi} \tan^{-1} \xi \right) \quad (17)$$

Furthermore, the current density flowing through the electrode is

$$\frac{j_x}{\kappa} = \left(\frac{\partial \phi}{\partial z} \right)_{z=0} = \frac{-1}{r_0 \eta} \left(\frac{\partial \phi}{\partial \xi} \right)_{\xi=0} = \frac{-1}{r_0 \eta} \sum_{n=0}^{\infty} G_n P_{2n} M'_{2n}(0) \quad (18)$$

From Eq. (17) and an evaluation of the average current density j through integration over the surface of the disk, one finally obtains

$$\frac{j_x}{j} = \frac{0.5}{(1 - r^2/r_0^2)^{1/2}} \quad (19)$$

The primary current distribution for the important case of the ring disk electrode has also been calculated by Newman.^{(135)†}

The above method of approach belongs to the class of techniques involving integration by series. Before the computer era cosine and sine series were popular in the integration of equations similar to the Laplace equation, in particular, the integration of the diffusion equation.

5.4. Numerical Integration of the Laplace Equation

Equation (7) shows that even for relatively simple electrode configurations the calculation of the primary current distribution is a complex problem (see also Section 5.2) and obviously the difficulty increases further with increasing complication of the geometry. However, in the era of high-speed digital computers this is no longer a major obstacle since it is now possible to integrate the Laplace equation numerically. Today this is the most powerful procedure for the computation of the primary current distribution.

A finite-difference method for numerical computation has been described by Klingert *et al.*⁽³³⁾ for two-dimensional systems. The whole cross section of the electrolyte is covered by a network of square meshes of side s (the direction perpendicular to this plane being regarded as unimportant). Figure 5 shows a few of these meshes. A finite-difference form of the Laplace equation in place of the differential one is used. Instead of Eq. (2) we write

$$\frac{\Delta^2 \phi}{\Delta x^2} + \frac{\Delta^2 \phi}{\Delta y^2} = 0 \quad (20)$$

We have (Figure 5)

$$\frac{\Delta \phi}{\Delta x} = \frac{\Delta \phi}{s} = \frac{\phi_1 - \phi_0}{s} \quad (21a)$$

$$\frac{\Delta^2 \phi}{\Delta x^2} = \frac{\Delta(\Delta \phi)}{s^2} = \frac{(\phi_1 - \phi_0) - (\phi_0 - \phi_3)}{s^2} = \frac{\phi_1 + \phi_3 - 2\phi_0}{s^2} \quad (21b)$$

$$\frac{\Delta^2 \phi}{\Delta y^2} = \frac{\phi_2 + \phi_4 - 2\phi_0}{s^2} \quad (21c)$$

† The primary potential and current distribution around a bubble on an electrode has been computed by Sides and Tobias.⁽¹⁹⁹⁾

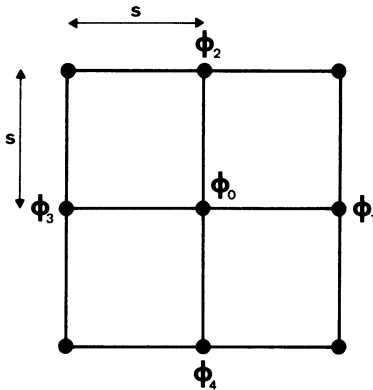


Figure 5. Network of meshes for numerical integration of the Laplace equation.

From (20), (21a), (21b), and (21c) one obtains the remarkably simple relationship

$$\phi_0 = \frac{1}{4}(\phi_1 + \phi_2 + \phi_3 + \phi_4) \quad (21d)$$

The boundary condition at the electrode is fulfilled by assigning the same potential to all points located at the electrode surface. The boundary condition at an insulating wall (where the normal flux must be zero) is taken care of by adding virtual mesh points on the other side of the boundary (outside of the electrolyte solution) and by assuming that the potential there is the same as for the symmetric point located on the electrolyte solution side of the boundary. Starting from these boundary conditions, one assigns some tentative plausible values to the potentials of the network and then refines them with the computer by an iterative procedure until the boundary conditions and Eq. (20) are fulfilled with a prescribed precision for any element of the network.

In selecting the network the grid interval chosen should be small in comparison to the distances over which a significant variation of flux occurs. Klingert *et al.*⁽³³⁾ used networks with a few hundred to a few thousand points. Figure 6 shows the potential map and the current lines calculated in this manner for a system consisting of a plane electrode facing one that has a corner. It is seen that the potential and current lines are strongly distorted near the corner.

Numerical methods other than the above mentioned finite-difference procedure have also been developed. In certain cases a superposition technique is more convenient. Since the Laplace equation (2) is linear, any solution of the equation may be added to any other solution and the result again will be a solution of Eq. (2). The superposition technique consists in adding up simple solutions of Eq. (2) until the prescribed boundary conditions are met. Pierini and Newman⁽¹²⁴⁾ have used this method to calculate primary current distribution at a disk more realistic than the idealized one considered earlier (Section 5.3) which had counterelectrode and cell walls located at infinity.

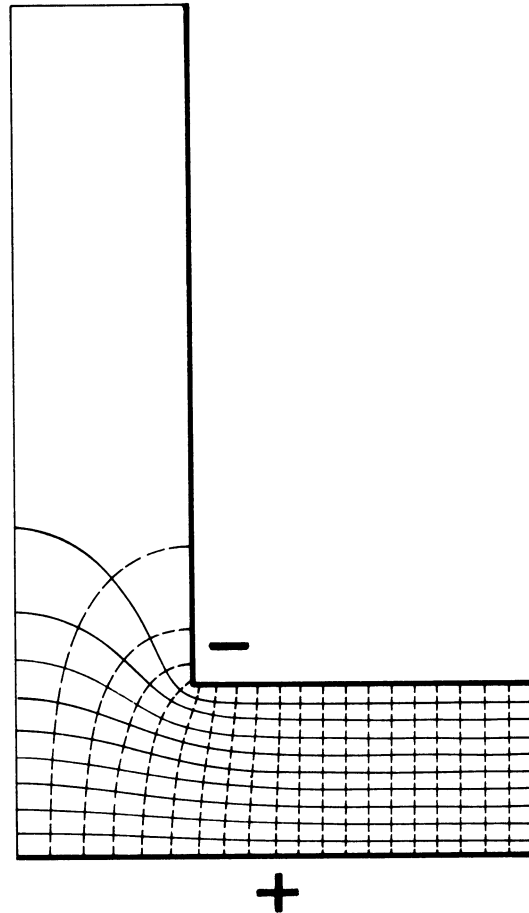


Figure 6. Potential map and current lines near a corner computed numerically by the difference method (primary distribution): —, potential lines; ---, current lines.

The superposition approach proved convenient to correct the infinity location problem with cell walls and counterelectrode at finite distances. The same coordinate transformation can be made by starting from the same general solutions. Also, advantage is taken of the similarity between the two distributions. An essential similarity in the above case is that j_x becomes infinite at the edge independent of whether the counterwalls are remote or not (see also Section 5.5). Fedkiw⁽¹⁷⁷⁾ applied a perturbation technique to the calculation of current distribution over a sinusoidal profile.

Finally, a variational method has been used recently by various authors.^(170,194,197,198) It consists in finding a function Φ that minimizes the energy density of the electric field in the region considered and satisfies the boundary conditions. For this function the total energy dissipation in the combined surface-volume system is a minimum, and it can be shown that the Laplace equation is satisfied. The two-dimensional region of interest

(inter-electrode space) is divided into a finite number of small elements, for example, triangles. Discrete linear potential functions are defined from each node (triangle peak). The unknown potential Φ is then obtained by solving numerically a system of linear equations, which can be represented in matrix formulation by

$$\mathbf{A}\Phi = \mathbf{b} \quad (22)$$

Φ is a vector (ϕ_1, ϕ_2), \mathbf{A} is a positive definite, symmetric matrix, the value of which depends on the triangulation employed, and \mathbf{b} is a vector depending only on boundary conditions. The system of linear equations is solved by over-relaxation, starting from a clever guess of the potential distribution within the region. The technique has also been called the finite-element method, as distinguished from the finite-difference procedure discussed at the beginning of the section.

The above variational technique is particularly suited to problems in which time variations are involved. Glarum⁽¹⁷⁰⁾ used it to calculate the current distribution for plating by periodic current reversal at a rotating disk electrode. Alkire *et al.*⁽¹⁹⁸⁾ computed, for a metal deposition, the evolution with time of the shape of an originally flat cathode near its edge. Sautebin *et al.*^(194,197) applied the variational technique to the theory of electrochemical machining. They predicted the leveling of a serrated anode during its dissolution and found a very good agreement with their experimental results.

5.5. Some General Aspects of Primary Distribution

Equations (7) and (19) show that the local current density becomes infinite at the edge of a disk or of a plane electrode as shown in Figure 3. Only when an electrode completely fills the cross section of the cell and is perpendicular to an insulating wall can one have a uniform primary current distribution. If the angle between the electrode and the insulating wall is sharp, the current density at the edge is zero; if the angle is obtuse, the current density is infinite (Figure 7). These extreme values taken by the local current density at certain privileged spots are characteristic of primary current distribution.

In reality, the local current density does not become infinite, for example, at the corner shown in Figure 6. There are two reasons for this: (a) In actual practice the angle is never perfectly sharp, i.e., the radius of curvature is small but finite. The distribution of Figure 6 has been calculated with the assumption of a radius of curvature equal to $h/20$, where h is the distance between the electrodes. (b) The overpotential opposes itself to a very strong variation of the current density, so that it cannot take extreme values as shown on Figure 7. We thus come to the problem of secondary current distribution.

Before we discuss this problem, let us note another interesting feature of primary distribution. The conductivity of the bath does not appear in the equations describing the primary distribution [e.g., in Eqs. (7) and (19)]. True,

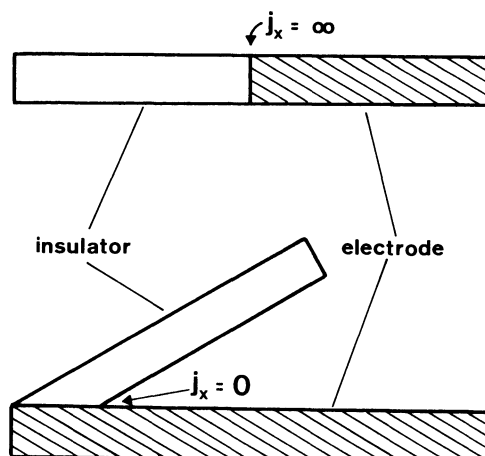


Figure 7. Current density at the junction between insulating and conducting wall.

the nonuniformity of distribution is due in fact to differences in the resistances of the current tubes [e.g., between the current tubes toward the edges (*A*) and toward the center (*B*) of the electrode of Figure 3]. But the ratio of these resistances is given by the geometry of the system only, and does not depend on the absolute value of the conductivity. Thus, it can be said that primary current distribution is that obtained when only geometric factors are taken into account (at least for systems in which the electrode resistance is negligible compared to that of the solution). In contrast to this, in the secondary distribution the value of the conductivity of the solution influences the repartition of the current and potential.

6. Secondary Distribution

6.1. Qualitative Considerations

In general, the secondary current distribution tends to be more uniform than the primary one. Near the edge of the electrode of Figure 3, the current density tends to be larger because the resistance of the current tube *A* is smaller than that of *B* (see section on primary current distribution). However, the larger current density near the edge⁽¹⁾ causes the overpotential to be higher there than toward the center.⁽²⁾ Therefore, the potential difference over the interface $\Delta\phi_1$ is larger than $\Delta\phi_2$. Since the potential difference between the interior of the metal of the cathode and that of the anode is constant everywhere ($\Delta\phi_m = \Delta\phi_1 + \Delta\phi_A = \Delta\phi_2 + \Delta\phi_B$), the larger value of $\Delta\phi_1$ has the consequence that the potential difference over the tube *A* ($\Delta\phi_A$) is *smaller* than that available for tube *B* ($\Delta\phi_B$). The result is that the current in tube *A* and therefore the current density at the edge is not as strongly

increased as it would be for the case of no equalizing action of the overpotential.

Another even more illustrative way to look at the problem is as follows. In secondary current distribution we consider only the influence of activation overpotential and disregard the effects of other types of overpotential. Now the derivative of the activation overpotential with respect to current density, $d\eta_a/dj$, is in fact a resistance per square meter of electrode area: we may call it the polarization resistance R_a . It represents the slowness of charge transfer across the interface and is therefore a quantity linked to the electrode kinetics. This resistance is in series with the resistance of the electrolyte R_e and with the polarization resistance of the counterelectrode R'_a (Figure 9). Now, if the activation overpotential is a linear function of the current density (as is the case in a first approximation over a limited range), the resistance R_a is a constant, independent of current density. If the kinetic properties of the interface are constant, R_a will also keep its value along the interface. For example, it will be the same at the crests and recesses of the serrated cathode profile of Figure 8. In this system the resistance R_p of the solution at a peak is smaller than the resistance R_r of the solution at a recess, for the reasons mentioned in the preceding paragraph. The result is

$$\frac{j_p}{j_r} = \frac{R_r}{R_p} > 1 \quad (23)$$

The current density is larger at the peak (j_p) than in the recess (j_r). However, if we add a constant resistance in series to R_p and R_r , the peak and recess will differ less with respect to the total resistance, i.e., the current distribution is rendered more uniform

$$\frac{j'_p}{j'_r} = \frac{R_a + R_r}{R_a + R_p} < \frac{R_r}{R_p}, \quad \frac{j'_p}{j'_r} < \frac{j_p}{j_r} \quad (24)$$

We have a very similar situation in the case of Figure 3: The resistance of tube A is smaller than that of tube B , but if we add the same polarization resistances in series to both R_A and R_B the difference between the currents

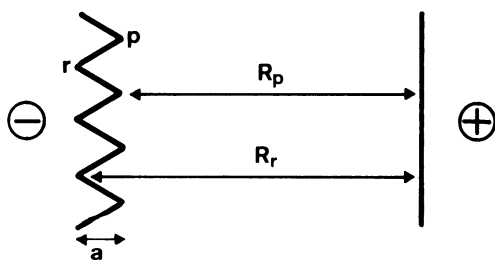


Figure 8. Serrated cathode profile (schematic).

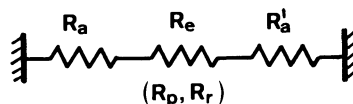


Figure 9. Representative model with resistances.

flowing through the two sets of resistances decreases. If the polarization resistance R_a is much larger than the electrolyte resistance R_e , we have a uniform current distribution even if the geometry is nonuniform and tends to cause a noneven distribution.

On the other hand, if R_a is zero, we have primary current distribution. We can also say that in the first case it is the transfer of charges through the interface which controls the current distribution; in the second case it is the transfer of charges through the solution. The slowest step, which is the controlling one, is where the high resistance occurs.

We may try to go a step further and introduce a quantity that characterizes more precisely the equalizing action of the overpotential. From what we have said, it appears that the equalizing action will be larger the greater the ratio R_a/R_e is. Now, R_e is the resistance of the solution per m^2 of cross-sectional area, and is given by the specific resistance times the distance between the two electrodes h . Or, expressed in terms of the specific conductivity κ , R_e is equal to h/κ . Remembering the definition of R_a , we obtain the following expression

$$Wa = \frac{d\eta_a}{dj} \frac{\kappa}{L} = \frac{R_a}{R_e} \quad (25)$$

where L is the characteristic length and is equal to h for the example in Figure 3. It is a dimensionless group called the *Wagner number*.⁽¹⁴²⁾ It represents the ratio of the polarization resistance to the solution resistance. The larger it is, the more even is the current distribution in spite of a nonuniform geometry. For $Wa = 0$ we have primary current distribution.

In the theoretical treatment given in the next sections we will see that it is indeed convenient to represent the results of the calculation by dimensionless groups in the form of the Wagner number. Note that the length L appearing in Eq. (25) may have various significances. In the case of Figure 3 it was the distance between the electrodes. But let us consider Figure 10. The cathode is very small and the distance to the counterelectrode is large. The resistance of the solution is almost entirely given by the layers of the solution close to the cathode where the cross section is small. This resistance is inversely proportional to the cross section, i.e., it is inversely proportional to the length l of the cathode. Therefore, R_e is given by l/κ and the Wagner number is given by $Wa = (d\eta_a/dj)\kappa/l$. A length characteristic of the system thus enters into the definition of the Wagner number. We will return to this question in Section 6.3.4.

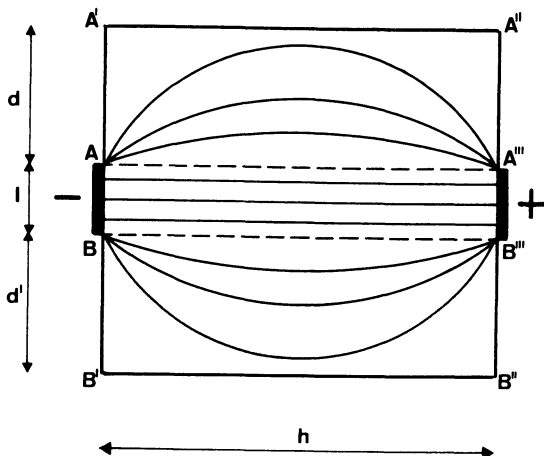


Figure 10. Cell with electrode length as controlling factor for solution resistance.

6.2. Semiquantitative Concepts and Tests Used in Electroplating

The distribution of the thickness of a metallic deposit is of particular importance in electroplating. A large number of papers deal with this subject. The approach is usually qualitative. The plater is interested in having a solution that yields a deposit thickness which is more uniform than would correspond to primary distribution. To characterize this property of a solution, the concept of the *throwing power* is often used in plating. The definition given by the International Standard Organisation (ISO) is “throwing power—the improvement of the coating (usually metal) distribution over the primary current distribution on an electrode (usually cathode in a given solution under specified conditions). The term may also be used for anodic processes for which the definition is analogous.”⁽¹²²⁾† This definition does not give a quantitative value to the throwing power. However, a quantification on an arbitrary scale can be obtained if one regards as representative the results of measurements made by a specific method. A popular test in electroplating is that of the *Haring-Blum cell* (Figure 11).^(11,120,121,128) It consists of two plane cathodes located at different distances a and b of a wire net anode. A number of variants to the arrangement of Figure 11 have also been proposed, for example, by Field.⁽¹⁸⁵⁾ His cell also consists of two cathodes placed at different distances from a common anode but they are located on the same side of the anode.

In the absence of overpotential, the ratio of the weights of metal deposited on the two cathodes of the Haring-Blum or of the Field cell should be inversely proportional to the distances to the anode. The departure from this ratio is

† In electroplating one distinguishes between throwing power and covering power. The latter is defined by ISO as “the ability of an electroplating solution under a given set of conditions to deposit metal on the surfaces of recesses or of deep holes.”⁽¹²²⁾

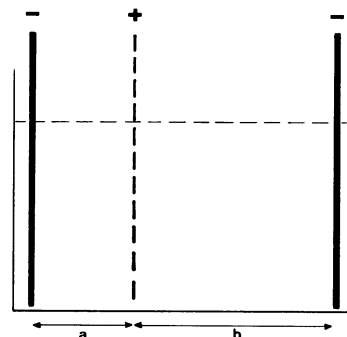


Figure 11. Haring-Blum cell for the determination of throwing power.

regarded as a measure of the throwing power which, following a proposal by Haring and Blum,⁽¹²⁸⁾ is defined according to

$$TP = \frac{A - (M_N/M_F)}{A} 100 [\%] \quad (26)$$

A is the ratio of the distance of the two cathodes to the anode and equals b/a (usually $A = 5$); M_N and M_F are the weights of metal deposited on the nearer and farther cathode, respectively.

A somewhat different definition is recommended by the British Standards Institution⁽¹¹⁾

$$TP = \frac{A - M_N/M_F}{A + M_N/M_F - 2} 100 [\%] \quad (27)$$

According to the latter definition, TP becomes 100% when the weights of the metal deposited on both cathodes are equal, i.e., when the throwing power is perfect.

The quantity defined by Eq. (26) or (27) is regarded as representative for the property of a solution to “throw the deposit from a crest into a recess;” i.e., for the ability of a solution to make the current distribution more uniform than would correspond to primary current distribution. In reality, this property is better characterized by the numerical value of the Wagner number. One major shortcoming of the throwing power index TP is that it does not take into account the influence of the geometry of the system in which a deposit is made (see Section 6.3.5). An improved definition and measurement of the throwing power has been proposed by Pierini and Newman⁽¹²³⁾ who suggested the use of the rotating ring disk electrode for that purpose (see Section 6.3.3.). Other authors^(45,174) have pointed out that the results obtained with a Haring-Blum cell could also be treated in terms of the polarization parameter instead of a calculation of TP. We will return to the problem of the measurements made with the Haring-Blum cell in Section 6.3.5.

Another “current distribution” device often used in the practice of electroplating is the *Hull cell* (Figure 12).^(5,11) The cathode is oblique with

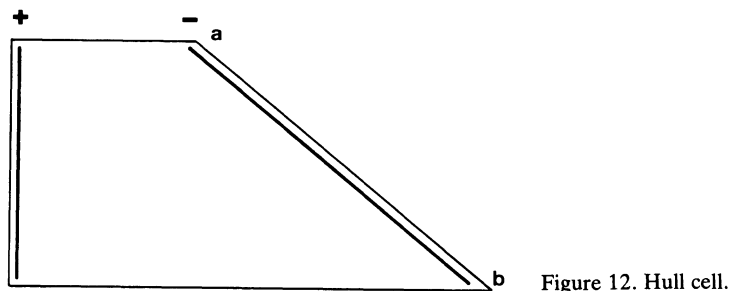


Figure 12. Hull cell.

respect to the anode so that the current density decreases continuously from a to b because of the increasing distance from the anode. The metal is therefore deposited at a variety of current densities and one observes metal stripes of different appearances because these stripes have been deposited at different current densities. The Hull cell is used for the purpose of determining, by a simple experiment, the current density range in which metal of a desired property is obtained. It is also employed to correct the composition of plating baths as they age.

The throwing power and the methods for its measurement in connection with electroplating have been reviewed by Rousselot,⁽¹⁸⁾ Weiler and Zerweck,⁽²¹⁾ and Raub and Müller.⁽¹⁸⁴⁾ These authors have also made extensive measurements of the throwing power for various plating baths.

In surface treatment, cathodic processes are more common than anodic ones. Nevertheless, the anodic throwing power is of importance for metal treatment techniques such as electrochemical machining or polishing. Anodic throwing power and its measurement has been reviewed recently by Zerweck.⁽¹⁷⁴⁾

6.3. Quantitative Treatment

6.3.1. Boundary Conditions

The principle of the quantitative evaluation of secondary current density distribution is essentially the same as for the primary distribution. One starts again from the Laplace equation [Eq. (2)]. The boundary condition pertaining to insulating surfaces [Eq. (6)] also remains the same. However, the boundary condition for the potential at the electrode surface is different from Eq. (5) because *we now take the influence of activation overpotential into account* and the potential difference $\Delta\phi$ over the electrode-solution interface is therefore dependent on the current density. Even if the metallic side of the interface is an equipotential surface ($\phi = \phi_m$) the solution side is not because, in general, the local current density varies along the interface. In the case of a single

electrode reaction, we now have instead of boundary condition (5)

$$\phi_e = \phi_m - \Delta\phi = f(j) \quad (28)$$

where ϕ_e is the potential at the solution side of the electrode–solution interface and ϕ_m is the constant value of the potential in the interior of the metal. $\Delta\phi$ is a function of current density which is determined by the kinetics of the electrode reaction.

The overpotential η is linked with $\Delta\phi$ by the relationship

$$\eta = \Delta\phi - \Delta\phi_{\text{eq}} \quad (29)$$

where $\Delta\phi_{\text{eq}}$ is the potential difference at the interface when the electrode reaction is at equilibrium ($j = 0$). $\Delta\phi_{\text{eq}}$ is independent of j . The new boundary condition (28) makes integration of the Laplace equation more difficult than in the case of primary distribution. However, the modern digital computers allow mastery of the problem.

To perform the calculation, an explicit form of the relationship

$$\Delta\phi = f(j) \quad (30)$$

must be used. The most commonly employed relationships are the linear approximation and Tafel's equation for the activation overpotential η_a .

(a) In the *linear approximation* we write

$$\Delta\phi = \Delta\phi_0 + Rj \quad (31)$$

where $\Delta\phi_0$ and R are constants. This approximation was particularly popular in the times before the era of the digital computers because it was felt that the linear Laplace equation was easier to integrate with a linear boundary condition. In fact, Eq. (31) is a reasonably good approximation over a limited range of current densities since it often prevails in a problem of current distribution. Note that $\Delta\phi_0$ is not the equilibrium potential difference over the interface, or the decomposition potential, but just the value of the potential difference $\Delta\phi$ extrapolated to $j = 0$ from the segment of the $\Delta\phi = f(j)$ curve lying in the region of current densities prevailing in the distribution problem at hand. The proportionality factor R to be used in the actual computation should be valid for the range of current densities prevailing in the problem at hand. Strictly speaking, R should be the activation polarization; i.e., we should have $R = R_a = d\eta_a/dj$. However, in the case of a macroprofile (see Section 8.3), R may possibly include some concentration overpotential (see footnote on p. 273).

(b) A more sophisticated boundary condition is the use of Tafel's equation

$$\eta_a = \chi + \beta \ln j \quad (32)$$

with $\beta = R^*T/\alpha zF$. α , β , and χ are coefficients which are independent of the current density. Tafel's equation is not valid close to equilibrium because then

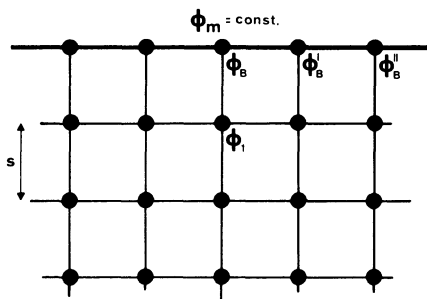


Figure 13. Network of meshes near boundary for numerical integration of the Laplace equation in secondary distribution.

one has to take into account both the forward and reverse current of the electrode reaction. In some treatments of current and potential distribution the somewhat more complete kinetic equation

$$j = j_0 \left[\exp \left(\frac{\alpha z F \eta_a}{R^* T} \right) - \exp \left(- \frac{(1 - \alpha) z F \eta_a}{R^* T} \right) \right] \quad (33)$$

has been used as boundary condition.

6.3.2. Outline of Integration

We will now discuss in more detail two of the techniques used for the calculation of secondary current distribution. We consider first the finite-difference technique.^(33,173) Its principle was outlined in Section 5.4 for the calculation of primary current distribution. The Laplace equation is replaced by the finite-difference equation (21d). The method is the same as in Section 5.4 except for the boundary condition at the electrodes.

Let us consider the segment of the network shown in Figure 13. The conducting boundary is at the top of the figure. The potential ϕ_m on the metallic side of the interface is constant but not the potentials ϕ_B, ϕ_B', \dots ($\phi_B \neq \phi_B', \dots$). In the case of secondary current distribution, the link between $\phi_m - \phi_B$ and the current density must be taken into account. The latter is proportional to the gradient of the potential in the direction perpendicular to the boundary and thus proportional to $(\phi_B - \phi_1)/s$. If the relationship between $\phi_m - \phi_B$ and j is linear [Eq. (31), where the zero of the potential scale has been chosen in such a way that $\Delta\phi_0 = 0$],

$$\phi_B = \phi_m - Rj_x \quad (31')$$

we thus have

$$\phi_B = \phi_m - \frac{R\kappa}{s}(\phi_B - \phi_1) = \frac{\phi_m + (R\kappa/s)\phi_1}{1 + (R\kappa/s)} \quad (34)$$

where κ is the conductivity of the solution.

Alternatively, if we assume the current–potential relationship to be described by Tafel’s equation [Eq. (32)] one obtains instead of (34)

$$\phi_B = \phi_m - \beta \ln \frac{(\phi_B - \phi_1)\kappa}{j_0 s} \quad (35)$$

where j_0 is the exchange current density. Estimation of the potential at the solution side of the interface in this case involves a trial and error procedure.

Otherwise the technique is similar to that sketched in Section 5.4 for primary distribution. One assigns plausible potential values to the points of the mesh, and by an iteration procedure fulfills exactly the difference (22) in such a way that the boundary condition (34) or (35) is satisfied.

Figure 14 shows the potential map and the current lines in secondary distribution at a corner electrode calculated by the above method, assuming a linear potential–current relationship with an R value of $1 \Omega \text{ cm}^2$. The conditions are similar to those of Figure 6 (in particular, regarding the assumed radius of curvature at the corner). The equalizing action of the overpotential is clearly seen from the figure. In Figure 14 the current lines penetrate much more into the region above the corner, toward the far end from the flat counterelectrode.

In certain problems there is an advantage to manipulating somewhat the fundamental differential equations before a calculation with the digital computer is performed. A good example is the disk electrode, which has been treated by Newman.^(35,127) We have already noted in Section 5.2 that the Laplace equation for the disk takes a very convenient symmetrical form if it is written in rotational elliptic coordinates [Eq. (9)]. A general solution is Eq. (14) (Section 5.3). The surface potential ϕ_e is given by

$$\phi_e = \sum_{n=0}^{\infty} B_n P_{2n}(\eta) \quad (15)$$

and the local current density at the disk is given by Eq. (18). So far the treatment is exactly the same as for the case of primary current distribution. The difference in secondary distribution is that ϕ_e in Eq. (15) can no longer be taken as constant and independent of local current density j_x . The relationship between j_x and the potential difference over the interface $\phi_m - \phi_e$ has to be taken into account [Eq. (28)]. Equation (18) thus becomes

$$\frac{f(\phi_m - \phi_e)}{\kappa} = -\frac{1}{r_0 \eta} \sum_{n=0}^{\infty} B_n P_{2n}(\eta) M'_{2n}(0) \quad (36)$$

The coefficients B_n in the expansion of the potential have to be so adjusted that the relationship between $\phi_m - \phi$ and j_x [Eq. (28)] is fulfilled. Multiplication by $\eta P_{2m}(\eta)$ and integration from $\eta = 0$ to $\eta = 1$ yields

$$B_m = -\frac{4m+1}{M'_{2m}(0)} \frac{r_0}{\kappa} \int_0^1 f(\phi_m - \phi_e) \eta P_{2m}(\eta) d\eta \quad (37)$$

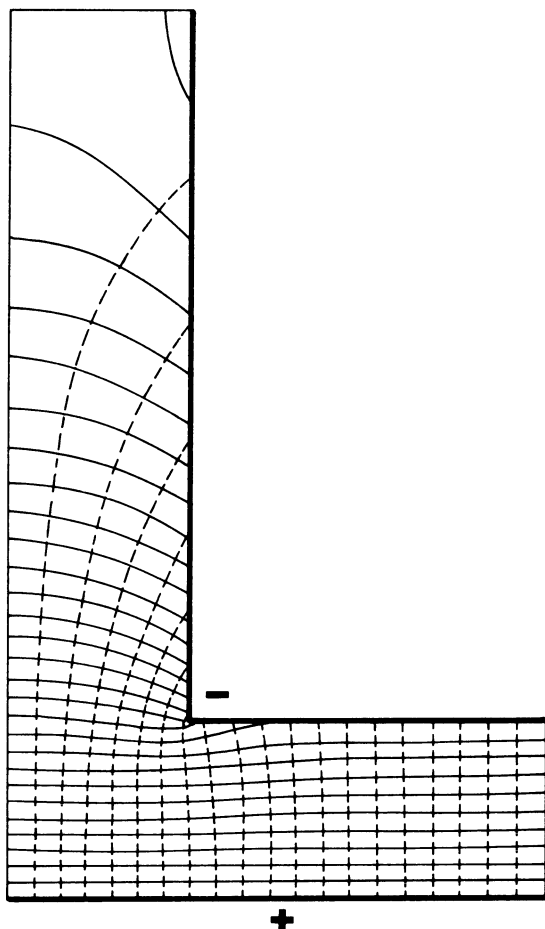


Figure 14. Potential map and current lines near a corner computed numerically by the difference method (secondary distribution): —, potential lines; ---, current lines.

For a given value of ϕ_m , this equation determines the coefficients B_m . This may involve a trial and error calculation, but the computer work is much less than if the finite-difference method was used. Two other methods involving digital computers that claim less computer work and more flexibility have been proposed recently. Alkire *et al.*,⁽¹⁹⁸⁾ and Sautebin *et al.*^(194,197) have used a variational approach (see also the end of Section 5.4) to determine the primary, secondary, and tertiary limiting-current distribution on a growing or receding electrode surface. Furthermore, Caban and Chapman⁽¹²⁶⁾ have calculated the tertiary distribution for the cell of Figure 1 with laminar flow by an orthogonal collocation technique.

6.3.3. Results of Distribution Calculation

The secondary current distribution has been calculated from the Laplace equation (2) for various systems such as plane parallel electrodes,^(38,41) a plane

electrode embedded in an isolating surface with a counterelectrode located at infinity,⁽⁴⁸⁾ tubular electrodes,^(26,40) the Hull cell,^(112,143) the slotted cell electrode,^(152,153) metal anodes in chlorine-caustic cells,^{(169)†} slot,^(27,173) disk,^(35,170) disk ring,^(47,123) serrated electrode (model of Figure 8),^(38,39) shape reproduction during cavity sinking in electrochemical machining,⁽¹⁶⁷⁾ evolution of cathode shape in metal deposition,⁽¹⁹⁸⁾ and of an anodic surface profile during dissolution as in electrochemical machining,^(194,197) a sinusoidal profile^(42,178) with variable $d\eta/dj$, i.e., variable Wagner number along the interface,⁽⁴⁹⁾ and local cells as encountered in corrosion.^{(15,50,114)‡}

The distribution at the ring and ring disk are of particular importance for electrochemical research. In the case of the ring disk, Newman has proposed taking the ratio of the average current at the disk and at the ring as a measure of the throwing power. This is expected to be a more representative figure than the throwing power derived from measurements with the Haring-Blum cell according to Eq. (27). The geometries of Figures 1 and 8 are of interest for technical applications.

Figures 15, 16, 17, and 18 show the current distribution for the disk, parallel plates, and a serrated electrode. The ordinate gives the ratio of the local current density j_x to the average current density j as a function of location (except for Figure 17 where the quantity plotted on the ordinate is $(j - j_\infty)/j_\infty$, j_∞ being the local current density at virtually infinite distance from the edge). The abscissas show in all the figures the normalized (or dimensionless) distance from a characteristic point (in the case of the disk, distance from the center; in the case of plane parallel electrode, distance from the edge; in the case of the serrated electrode, distance from the recess). In the case of Figure 15(a), 16, 17, and 18, the boundary condition (28) was expressed by a linear approximation, whereas in the case of Figure 15(b) the Tafel relationship was used.

Comparison of Figure 15(a) and 15(b) shows the difference between the two approximations. The calculated distribution is very similar in both cases. Larger differences may occur in regions where j_x varies strongly, as is the case near the edges of the electrode.

In Figure 18 the results of the Wagner calculation⁽³⁸⁾ for a serrated electrode are compared with the measurements of Mantzell.⁽⁵¹⁾ In these experiments the value of the Wagner number Wa was very small so that the curve shown in the figure corresponds virtually to primary distribution ($Wa \approx 0$).

† In this work, instead of integrating the Laplace equation, the cell was modeled with a three-dimensional network and Kirchhoff's law was applied. The calculation includes the case of expanded mesh titanium anodes of several characteristics.

‡ The potential distribution in a corroding hemispherical pit has been computed by Newman *et al.*⁽¹³⁹⁾ Further recent work on the theory and measurement of current and potential distributions in connection with corrosion is to be found in references 157-163 and 171.

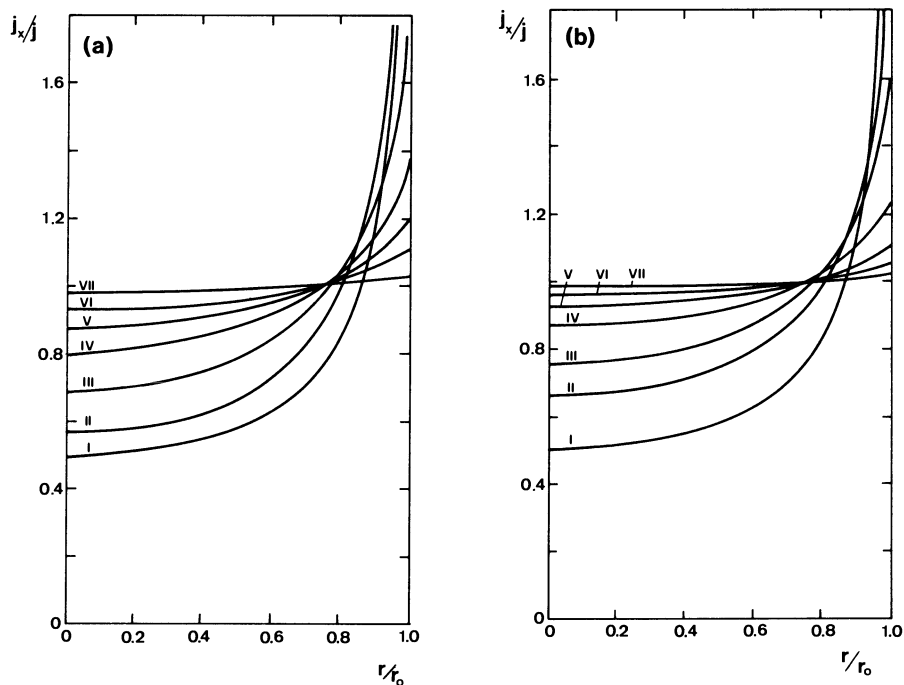


Figure 15. Secondary current distribution for a disk electrode of radius r_0 (reference 35): (a) linear approximation; (b) Tafel approximation. The curves correspond to various values of the parameter $Wa = \kappa(d\eta/dj)/r_0$. (a) curve I, $Wa = 0$ (primary distribution); II, $Wa = 0.05$; III, $Wa = 0.2$; IV, $Wa = 0.5$; V, $Wa = 1$; VI, $Wa = 2$; VII, $Wa = 10$. (b) curve I, $Wa = 0$ (primary distribution); II, $Wa = 0.13$; III, $Wa = 0.3$; IV, $Wa = 0.87$; V, $Wa = 1.86$; VI, $Wa = 3.85$; VII, $Wa = 9.9$.

6.3.4. Wagner Number, Characteristic Length

The various curves of Figures 15–17 correspond to different values of the Wagner number. In all cases it is seen that the current distribution is more uniform the larger the Wagner number is. For $Wa = 0$, we have primary distribution; for high values of Wa the distribution becomes more or less uniform. In Section 6.1, we have seen qualitatively that the reason for this is that the Wagner number is proportional to the ratio of the resistances to charge transport through the electric double layer and through the solution. Indeed, the theoretical treatment leads to the conclusion that it is convenient to present the results by lumping the variables together to dimensionless groups of the kind involving the Wagner number. The latter can also be regarded as a similarity variable analogous to those encountered in hydrodynamics.

In Figures 15–17 we have represented the current distribution by means of three dimensionless groups: j_x/j (which is a normalized local current density), x/a (which is a normalized distance), and the Wagner number. These

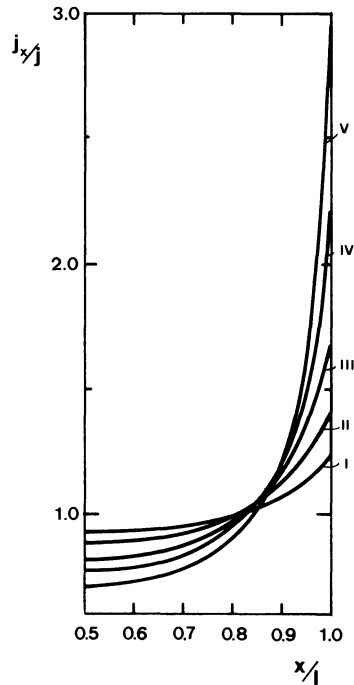


Figure 16. Secondary current distribution for the cell of Figure 3 with $h \gg l$ (Reference 38). The curves correspond to various values of the parameter $Wa = \kappa(d\eta/dj)/l$: curve I, $Wa = 0.8$; II, $Wa = 0.4$; III, $Wa = 0.2$; IV, $Wa = 0.1$; V, $Wa = 0$.

dimensionless groups play a role similar to that of the Sherwood or Reynolds number in mass transport. (Their introduction is in the domain of dimensional analysis.) Their use decreases the number of variables needed to describe the problem, facilitates the graphical representation of theoretical or experimental results, and strongly decreases the number of experiments needed to determine the function describing the current or potential distribution.

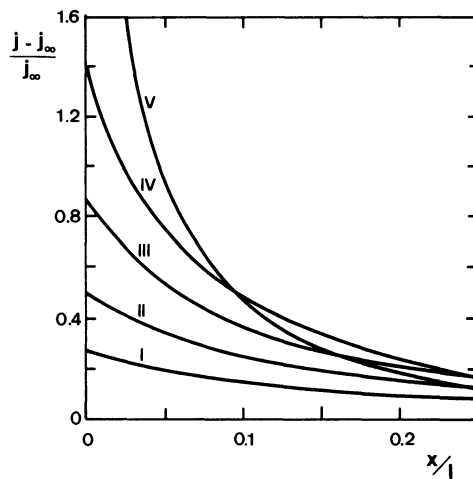


Figure 17. Secondary current distribution for the cell of Figure 3 with $l \gg h$ (Reference 38). The curves correspond to various values of the parameter $Wa = \kappa(d\eta/dj)/h$: curve I, $Wa = 0.63$; II, $Wa = 0.32$; III, $Wa = 0.16$; IV, $Wa = 0.08$; V, $Wa = 0.04$.

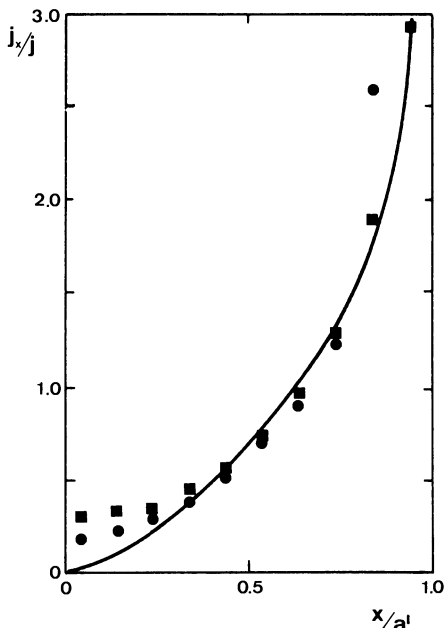


Figure 18. Current distribution for a serrated electrode (geometry of Figure 8). Curve calculated for $Wa \approx 0$ (Reference 38); ●, ■ measured points (Reference 51). ● Solution: 150 g/liter $ZnSO_4 \cdot 7H_2O + B(OH)_3$; $Wa = 0.006-0.0005$. ■ Solution: 150 g/liter $ZnSO_4 \cdot 7H_2O + 50 g (NH_4)_2SO_4 + 1000 g H_2O$; $Wa = 0.011-0.001$. a , distance between crest and recess; x , distance from the recess.

The minimum necessary number of dimensionless groups is governed by the rules of dimensional analysis (see Section 5, Chapter 3). In the case of Figures 15–17 we used three dimensionless groups. Depending on the circumstances, a larger number may be necessary to describe the problem completely. For example, it may be that the distribution *both* at the cathode and at the anode must be taken into consideration.† We may have two different resistances for charge transfer at the cathode and at the anode (i.e., two different slopes of the current–voltage curve, $d\eta_a/dj$). In that case two Wagner numbers are needed, one formed with the slope of the current–potential curve at the cathode, and the other with the slope of the current–potential curve at the anode.

Another example is the case of an electrode which has a resistance that is not negligible compared to that of the solution (Section 7). In that case there are two relevant conductivities—that of the electrode and that of the solution—and an additional dimensionless group is needed to describe the problem completely (see Section 7.1). An increase in the number of dimensionless groups may also be due to the geometry of the system. The length entering into the definition of the Wagner number is similar to the characteristic length which appears in the Sherwood or Reynolds number. For the system of Figures 16 and 17 we have only one relevant characteristic length: in the case of Figure 16 it is the distance between the electrodes, h ; in the case of Figure

† Note that the necessary number of dimensionless groups is also increased if the function $\Delta\phi = f(j)$ cannot be represented by the linear approximation, or by Tafel's equation. The problem is then most complex and has hardly been tackled in the literature except for the case of the disk.⁽³⁵⁾

17 it is the length of the electrode, l . This is because in the first case we have $l \gg h$; in the second case we have $h \gg l$. It is the smaller of the two lengths which is the controlling factor. However, if h and l are comparable, both of them influence the distribution and an additional dimensionless group has to be introduced. We can use either two groups of the form of the Wagner number (one of these numbers being formed with l as characteristic length, the second one being formed with h as characteristic length), or we can have one Wagner number (e.g., formed with h as characteristic length), and as second dimensionless group we may take the ratio h/l .

The fact that for $l \gg h$ (or $l \ll h$) only h (or only l) governs the current distribution can be qualitatively explained as follows. In the cell of Figure 1, for $l \gg h$, toward the center of the electrode a situation prevails which is essentially the same as for an electrode entirely filling the cross section of the cell, and the current distribution there is uniform. If the electrode length is increased, the central part with its uniform distribution becomes larger, but the distribution toward the edges is not affected. The latter depends on the extent to which the current lines grow out of the space formed by the two electrodes (curved current lines toward the top and bottom of Figure 1). The extent of this phenomenon is determined by the interelectrode distance h , which is thus the controlling characteristic length (whereas the size of l is not relevant).

The reason why l is the relevant length in the case $l \ll h$ (Figure 10) has already been discussed qualitatively in Section 6.1. Another way to reach the same conclusion is as follows. For a small l the current is short circuited through the solution along the electrode, over the distance l . The effectiveness of the resulting equalizing action on the current distribution is larger the smaller the l is. Therefore, l is the characteristic length which controls the current distribution, whereas the distance between the electrodes has virtually no influence. If h is large, the major part of the current flows from an electrode to the other through the spaces $AA'A''A'''$ and $BB'B''B'''$ (i.e., above and below the electrodes, see Figure 10). The concentration of the current lines at the edges of the electrode is hardly affected by the value of h , and the decrease of the "concentration" of current lines at the edges is governed only by the above mentioned short-circuiting effect.

In fact, in the case of a cell such as that of Figure 1 or 10, one would have to consider further lengths (in addition to h and l) to characterize completely and most generally the geometry of the system:

1. The depth l' of the electrode (dimension of the electrode in the direction perpendicular to the direction l)
2. The distances d and d' of the electrode edges to the insulating walls of the cells
3. The distances d'' and d''' of the upper and lower edges to the free surface of the solution and to the bottom of the cell, respectively (Figure 19).

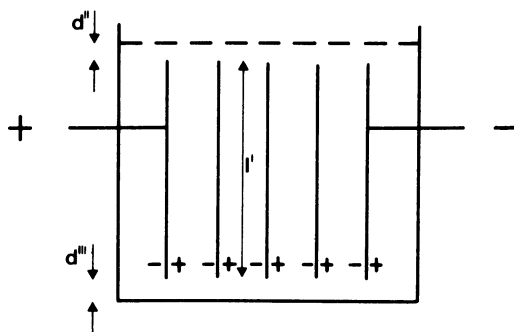


Figure 19. Electrolytic cell with bipolar electrodes.

In the most general case one would have to take into account all these lengths simultaneously. The problem would then be extremely complicated and has apparently never been considered quantitatively. In practice, the problem is often simpler. For example, in technical cells we may have $d = d' = d''' = 0$. The cases considered commonly in the literature are those that can be approximated by taking into account only the influence of h and/or l .

However, the distance d''' from the bottom of the cell plays an important role in *bipolar electrode* systems (Figure 19). In that case, only the terminal electrodes are connected with the external electric network; all the other electrodes act on one side as cathode and on the other side as anode.^(24,25) The current should flow from the anodic face of one electrode to the cathode side of the next one. However, part of the current goes directly from one terminal electrode to the other, through the open space below the electrodes, thus decreasing the current efficiency.

This problem has been treated by Roušar.^{(46)†} Note that the free space at the bottom of the cell may be necessary for various reasons (circulation of the electrolyte, conducting sludges that would otherwise cause shorts, as in electrolytic copper refining). Figure 19 is an example of systems with several electrodes in a cell. Such systems (bipolar or monopolar) are common in industrial applications. In addition to the current density variation over an electrode, the distribution of the current *between* the electrodes is of importance in that case. The influence of irregularities in this distribution on the current efficiency and power consumption in copper refining is discussed in a recent Russian paper.⁽¹⁵⁴⁾ Problems of distribution of this type in chlorine electrolysis have been the object of patents.^(155,156)

6.3.5. Trends of Secondary Current Distribution

In the cases where a complete calculation is not available (or would be very time consuming to perform), today's theory of current distribution allows us to predict at least certain trends. Indeed, as we have seen, the larger the Wagner number the more even the current distribution. From the structure

† The current distribution for bipolar rod electrodes over which the electrolyte flows in a thin film has been recently calculated by King and Wright.⁽¹⁷⁵⁾

of the Wagner number [Eq. (25)] we may then deduce the following general rules: The current distribution is *more uniform*

- (a) the smaller the characteristic length of the system;
- (b) the larger the conductivity κ of the solution;
- (c) the larger the slope of the activation overpotential–current curve ($\eta_a - j$ curve).

Some interesting conclusions may be drawn from this. For example, in general we may expect that the microscopic throwing power is better than the macroscopic throwing power. In the case of a cathode profile such as that shown in Figure 8, the secondary current distribution is more uniform if the “peaks” are small. For example, in copper deposition from a solution of 0.5 M CuSO₄ + 1 M H₂SO₄ at $j = 10 \text{ mA cm}^{-2}$ and $a = a'$ (Figure 29, Section 8.1) the distribution is virtually uniform for $a < 0.16 \text{ mm}$ but for peaks with $a > 1.6 \text{ mm}$ it is very uneven.⁽⁹⁰⁾

Another important result is that current distribution plays a role in the scale-up of electrolytic systems (i.e., in a change in size such as that which usually accompanies the industrial application of a process developed in the laboratory). An increase of the characteristic length makes the distribution less uniform. This is seen in Figure 20 which shows the variation of the thickness of an electrodeposited nickel coating over disks of various radii—the thickness being more uniform on the small disks.

Let us illustrate the above effect more quantitatively by a numerical example which will also give us a concrete idea of the magnitude of the Wagner number in practice. Consider a deposition from the above CuSO₄ solution having a conductivity of $0.4 \Omega^{-1} \text{ cm}^{-1}$ and a slope $d\eta_a/dj$ of the potential–current curve of $1.28 \text{ V A}^{-1} \text{ cm}^2$ [obtained from Tafel’s equation Eq. (32) for $j = 20 \text{ mA cm}^{-2}$, $\alpha = 0.5$, $z = 2$, and $T = 298 \text{ K}$]. From Eq. (25) we thus obtain for the Wagner number $Wa = 5$ if the characteristic length is 0.1 cm and $Wa = 0.05$ for $L = 10 \text{ cm}$. The first case corresponds approximately to curve VI of Figure 15(b). On a disk of radius 1 mm, the distribution of current is virtually uniform. But for a radius of 10 cm, $Wa = 0.05$, and the distribution lies between curves I and II of Figure 15(b)—the distribution being nearly the primary one, which would correspond to $Wa = 0$. Quite generally, for electrodes of large dimensions the distribution tends to be the primary one.

Besides the influence of size, another interesting consequence which we may easily deduce from the structure of the Wagner number is the role of the level of the average current density. The latter has no influence on the current distribution if we can sufficiently approximate the potential–current relationship by a straight line [Eq. (31)], because $d\eta_a/dj$ and thus Wa are then independent of current density. However, if Tafel’s equation is to be applied, the derivation of Eq. (32) yields

$$\frac{d\eta_a}{dj} = \frac{\beta}{j} \quad (38)$$

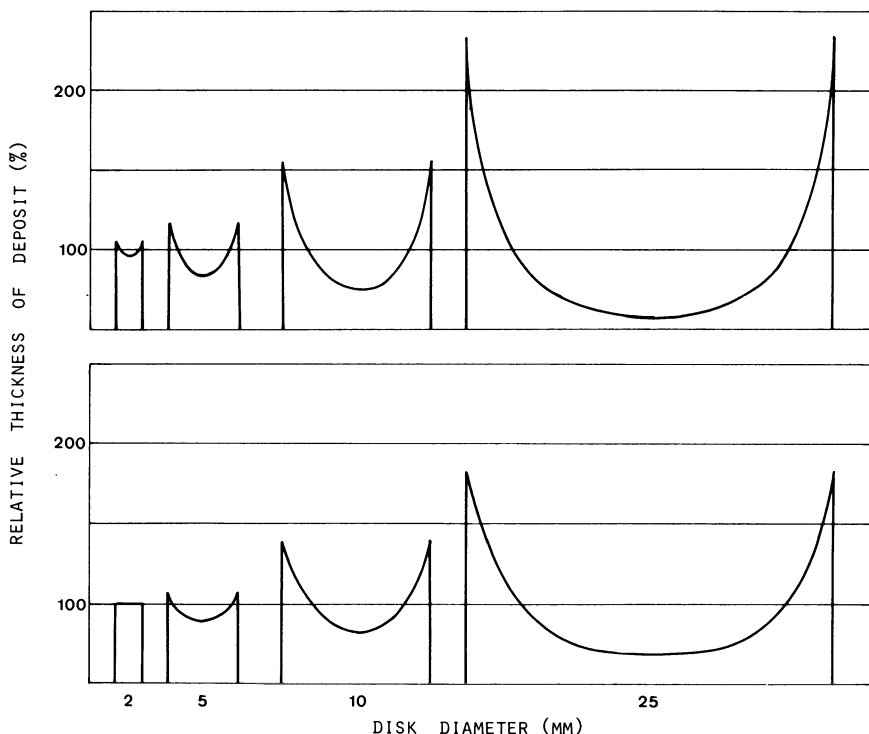


Figure 20. Variation of thickness of electrodeposited nickel over disk electrodes of various diameter (References 120 and 184). Upper graph: deposition from a bright nickel bath. Lower graph: deposition from a Watt's nickel bath.

that is, the Wagner number decreases with increasing average current density.† Therefore, the current and potential distributions tend to become less uniform at high current densities.

The trends mentioned under (b) and (c) at the beginning of this section show that, in addition to the geometry and operating conditions (current density), the current distribution depends on the nature of the electrochemical system (electrolytic solution and electrode material). For example, addition of a supporting electrolyte, which increases the conductivity κ , or of an organic additive, which increases $d\eta_a/dj$ will make Wa larger and thus improve the uniformity of current distribution. In electroplating one often characterizes with the throwing power the ability of a bath to render the current distribution more even (as compared to primary distribution). We have already introduced this concept in Section 6.2 but postponed the discussion of its adequacy. The throwing power TP is usually quantified by means of Eq. (26) or (27) which

† Note that the variation of $d\eta_a/dj$ with current density raises the question of the value to use in forming Wagner number according to Eq. (25). The Wagner numbers shown on Figure 15(b) have been calculated with the average current density flowing through the electrode.

permits the calculation of TP from measurements made with the Haring–Blum cell (Figure 11).

From the discussion given in Sections 6.3.3 and 6.3.4, it is apparent that the Wagner number is a more useful parameter for the description of current distribution than the throwing power as defined by Eq. (26) or (27). Firstly, the numerical values of TP thus obtained depend on the ratio b/a of the distance of the two cathodes to the common anode (Figure 11) as well as on the value of one of the two distances; i.e., the TP values depend on a standardization of the Haring–Blum cell. Secondly, TP does not allow predictions of the influence of size on the current distribution. Take, for example the system considered above ($\kappa = 0.4 \Omega^{-1} \text{cm}^{-1}$, $d\eta_a/dj = 1.28 \text{ V A}^{-1} \text{cm}^2$). For this system the Haring–Blum experiment will yield a TP of 9.3% if one uses Eq. (27), if the distance ratio of the Haring–Blum cell has the usual value of 5, and the distance a is 2.5 cm. We have seen that for this solution on a disk electrode we may have a distribution given by curve VI or curve I–II in Figure 15(b), depending on the radius. That is, for one and the same throwing power one may have two very different equalizing actions of overpotential.

Now, let us compare the behavior of two solutions; one (A) with $d\eta_a/dj = 1 \text{ V A}^{-1} \text{cm}^2$ and $\kappa = 0.4 \Omega^{-1} \text{cm}^{-1}$; and the second (B) with $d\eta_a/dj = 1.28 \text{ V A}^{-1} \text{cm}^2$ and $\kappa = 0.8 \Omega^{-1} \text{cm}^{-1}$. With the same Haring–Blum cell as before we would measure with solution A a TP of 7.4% and with solution B a TP of 17.0%. It can be easily shown that for a disk of radius 1 mm one would have for solutions A and B the distributions given by curves VI and VII, respectively, whereas for $r_0 = 1 \text{ cm}$ one would have the curves III and IV of Figure 15(b), respectively.

For the large radius, the solution with a high TP value equalizes the current distribution substantially better than solution A, but for the small radius both solutions lead to a virtually uniform deposit. This illustrates that TP as defined by Eq. (26) or (27) characterizes only poorly a given solution from the viewpoint of current distribution. The Wagner number is a more directly relevant quantity. It can be determined experimentally by measuring the conductivity of the solution and the potential–current curve.† Its recording

† In principle, the quantity entering into the definition of the Wagner number is the activation overpotential η_a , whereas the usual potential–current curve yields the total overpotential η . A subtraction of η_c is possible under well-defined hydrodynamic conditions. Otherwise, η_c should be negligible; i.e., the ratio j/j_m of the current in the range of interest to the limiting current should be small. This ratio can be decreased by vigorous stirring. Note that in the case of a macroprofile (see Section 8.3) η_c acts on the current distribution at least in the same direction as η_a . In certain cases (mainly in turbulent flow) j_c and $d\eta_c/dj$ vary only little along the interfaces for small values of j/j_{lim} . In an approximate treatment one may then lump together η_a and η_c and form the Wagner number with $d(\eta_a + \eta_c)/dj$ instead of with $d\eta_a/dj$. Tafel's law is not applicable under these conditions but the linear approximation may still be a reasonably good one over a limited range of current densities. The proportionality factor R in Eq. (31) is then $R = d(\eta_a + \eta_c)/dj$, and may possibly include other kinds of overpotentials, provided they can be approximated by a linear relationship, with a proportionality factor which remains the same over the whole electrode.

is more complicated if there are two concomitant electrode reactions because then the partial current–potential curve must be measured. However, the latter can also be determined by simple measurements made in the Haring–Blum cell, at least if we can accept as a sufficient approximation that the potential–current relationship is linear [Eq. (31)]. If we denote by V the potential difference applied to the cell of Figure 11 and by $\Delta\phi_0$ the constant of the linear potential relationship [Eq. (31)], we can write

$$\begin{aligned} V &= E_0 + \Delta\phi_0 + R_a j_N + \frac{a}{\kappa} j_N \\ &= E_0 + \Delta\phi_0 + R_a j_F + \frac{b}{\kappa} j_F \end{aligned} \quad (39)$$

where E_0 is a constant potential difference that includes the potential difference at the anode–solution interface, and j_N and j_F are the current densities flowing through the near and the far cathode, respectively. R is equal† to $d\eta_a/dj$. Noting that j_N/j_F is equal to the ratio of the weights of metal deposited, M_N/M_F , we can rewrite Eq. (39) as

$$B = \left(\frac{d\eta_a}{dj} \right) \kappa = a \frac{b/a - M_N/M_F}{M_N/M_F - 1} \quad (40)$$

The quantity B (which has been referred to as a polarization parameter in the literature^(174,184)) is thus obtained from the weights of the metal deposited at the rear end and at the far end cathode. It characterizes in a unique manner the current distribution properties of the solution studied, since in contrast to TP, it is independent of the dimensions of the Haring–Blum cell used, and represents in fact the conductivity of the solution times the slope of the potential–current curve. Division of B by the characteristic length yields the Wagner number for the system considered; for example, division by the radius yields the Wagner number for the disk.

6.3.6. Potential Distribution

To the variation of the local current density over the electrode, discussed in the preceding sections, corresponds a variation of the potential difference across the interface since $\Delta\phi$ and j_x are linked through an equation of the form (30). Figure 21 shows the secondary potential distribution on a disk for the same Wagner numbers as those of Figure 15(b). On the ordinate is the difference between the overpotential at distance r from the center and the overpotential corresponding to the average current density over the disk. This quantity is equal to the difference $\Delta\phi_r - \Delta\phi_j$ between the potential differences

† This implies that concentration overpotential is negligible. The current must therefore be much lower than the limiting current. That is, depending on the circumstances it may be necessary to stir vigorously the Haring–Blum cell (see also footnote on p. 273).

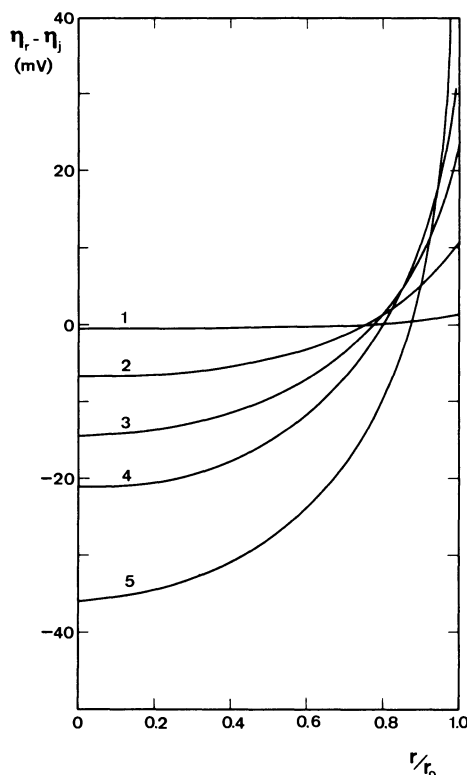


Figure 21. Potential distribution over the surface of a disk, as a function of the distance from the center r/r_0 . $\eta_r - \eta_j$ is the difference between the overpotential at distance r and the overpotential corresponding to the average current density. Curve 1, $Wa = 9.85$; curve 2, 0.87; curve 3, 0.30; curve 4, 0.13; curve 5, 0.

over the interface at r and for the average current density. It was calculated from the curves of Figure 15(b), assuming that the concentration overpotential is negligible and that the overpotential obeys Tafel's law (with $z = 1$, $\alpha = 0.5$, and $T = 298$ K). It is seen that, depending on the conditions, the variation of the electrode potential can be considerable. At first sight it might seem paradoxical that the largest variation in overpotential is observed for $Wa = 0$ (curve 5), i.e., for the primary current distribution defined as being the distribution which establishes itself for $\phi_e = \text{const.}$ (or $\Delta\phi = \text{const.}$). However, for $Wa = 0$, the current distribution (and thus the potential distribution in Figure 21) is more uneven than for any other value of Wa . At $Wa = 0$ the conditions are such that the variation of $\Delta\phi$ over the electrode does not affect the current distribution, which is virtually the same as for $\phi_e = \text{const.}$ The reason is that for $Wa = 0$ the variation of $\Delta\phi$ along the electrode is negligible compared to the total potential difference between cathode and anode.

The variation of potential along the electrode may have important practical consequences. The overpotential influences, for example, the *properties* of a deposited metal. At high overpotentials, more energy is available for the formation of new nuclei and a finer-grained deposit may result. Therefore, in electroplating an uneven distribution will not only cause variations of the

thickness of the metallic coating but may also lead to variations, along the electrode, in the structure of the electrodeposited metal.

On the other hand, if $\Delta\phi = \phi_m - \phi_e$ varies, it may in certain parts of the electrode reach values where a secondary reaction starts running. An uneven potential distribution may cause variations, along the electrode, of the *current efficiency* for the desired reaction. As we have seen, a change in size causes, in general, a change in the uniformity of current distribution. Therefore, in scale-up, the ratio of the products obtained in an electrosynthesis may be modified.

As a last example let us consider a *potentiostatic experiment*, of the kind very commonly carried out in the study of electrode kinetics, in electroanalytical chemistry, or in electrosynthesis. Usually, with the help of an appropriate electronic instrument, the potential difference $\phi_m - \phi_r$ between the metal of the working electrode and a reference electrode is maintained constant. Let us assume the reference electrode is connected (on the solution side) with the working electrode through a Luggin capillary, the tip of which is located close to the electrode at point M . Let us further assume that the ohmic potential drop between the tip of the capillary and the working electrode is negligible. Under such conditions, what the potentiostat maintains constant is the potential difference across the interface, $\Delta\phi = \phi_m - \phi_e$, at point M , but only at that point. It may be substantially different at other points of the electrode, depending on the nonuniformity of potential distribution. The extent to which such variations may occur is illustrated by Figure 21. Note that, as seen in Section 6.3.5, the nonuniformity of the distribution depends on the level of the average current density, if the overpotential obeys a relationship of the form of Tafel's equation. Therefore, the difference between the $\Delta\phi$ at M (which is maintained constant by the potentiostat) and the $\Delta\phi$ at other points depends, in general, on the applied average current density (or applied potential).

6.3.7. Experimental Results

Detailed experimental studies of current and potential distribution have been carried out in the case of disk electrodes.^(9,51-53,150) In general, the measurements were in good agreement with the theory (Figures 18 and 30). Without attempting to give an exhaustive bibliography, we will quote briefly some further experimental studies of distribution.† Many of them have been carried out in connection with electroplating. One, in particular, has measured

† The distribution reported in the literature and quoted here is based on experimental values and represents, in general, a secondary distribution since in practice there is always some overpotential. However, in most of the cases the value of the Wagner number is not indicated and the measured distribution may, in fact, approach more or less a primary distribution. Furthermore, concentration effects may not be negligible and one may have in reality to a certain extent a tertiary distribution.

the distribution of the current on triangular profiles and its penetration into a slot or cavities of various dimensions.^(10,11,54-61,174) Studies have been made of the improvement of current distribution through auxiliary aids (baffles, auxiliary bipolar electrodes)⁽¹⁶⁴⁾ or by a superimposed magnetic field.⁽¹⁷⁹⁾ The Hull cell (Figure 12) has been the object of a number of investigations.^(7,17,54,143-145,164) The current distribution measurements made by Watson⁽⁵⁷⁾ have been compared with calculated values by Cheh and Wan.⁽¹¹²⁾ Further various geometries have been studied experimentally by Rousselot⁽¹⁸⁾ and Steiner.^(3,4) Steiner has also considered the case of the superposition of an alternating current.^(61a) Andricacos *et al.*⁽¹³⁸⁾ have studied the current distribution in pulse plating (see also reference 192) and Shchigorev and Pisarev⁽¹⁸²⁾ the current distribution in electroplating with reverse current. The microthrowing power of baths with low metal content was investigated by Hasko and Bujtas.⁽¹⁸⁰⁾ Finally various authors^(19,62-66,188) have devoted their attention to the measurement of current distribution in cells with gas evolution, which is a frequently encountered case in industrial applications. A variation in the degree of gas bubble accumulation in the cell may be an important cause of nonuniform distribution. With vertical electrodes the degree of accumulation increases with increasing height.

7. Distribution with Finite Electrode Conductivity, Three-Dimensional Electrodes

7.1. Current Distribution

In the preceding sections we have restricted our attention to the case where the resistance of the electrode is negligible compared to that of the electrolytic solution. This is no longer true, for example, in the electroplating of thin wires, in the deposition of thin coatings on an insulating substrate, or for certain electrodes made of poorly conducting materials. If the current is fed to the ends of the electrode there is within the latter an ohmic potential drop, so that the metallic side of the electrode-solution interface is no longer an equipotential surface, and the boundary condition given by Eq. (5) or (28) must be modified accordingly for the integration of the Laplace equation. The current distribution along a wire or a resistant plate has been calculated by various authors:^(43,44,67-72) The treatment may be considerably simplified if one regards, as a first approximation, the current as unidirectional, i.e., either perpendicular or parallel to the electrode. In the first case, the electrode is monopolar, in the second case bipolar. Even if there is only one relevant characteristic length, the problem now depends on two dimensionless groups (in addition to j_x/j and x/l) because *both* the conductivity of the solution and that of the electrode must be taken into account. One finds again that the distribution is more uniform, the larger the $d\eta_a/dj$ is. Furthermore, it depends

on the ratio of the conductivity of the electrode to that of the solution. The distribution is more even, the larger this ratio is. Experimental studies have been carried out by several authors.^(146-148,183)

The electrode resistance can not be neglected for *porous electrodes*, as well as for electrodes with a *fixed* or *fluidized bed*. In these cases, the electrolytic solution penetrates into the pores or free space between the particles of the bed, so that the active interface extends itself into the body of the electrode. Hence the denomination *three-dimensional* electrodes, or particulate systems, is encountered in the literature. This special type of electrode has aroused much interest in recent years (see, e.g., reference 73). Indeed, the catalytic reactors of the chemical industry have a considerable advantage over the classical electrolytic cells: Their investment cost is relatively low because they have a large active area compared to their volume. The three-dimensional electrodes are in this respect analogous to the catalytic chemical reactors. As a consequence, considerable efforts are presently being devoted to their industrial realization, with the hope of decreasing the investment cost and making the electrochemical route more competitive. In fact, in certain batteries such as the lead accumulators, for example, spongy or granular structures, which are in essence three-dimensional electrodes, have been used for quite a long time. Various aspects of these three-dimensional electrodes are discussed in Chapter 6 of this volume as well as in other volumes of this treatise.

In heterogeneous catalysis, beds with porous grains are often employed. The reaction takes place virtually entirely on the surface of the pores, in the interior of the grains. However, if the reaction rate is large compared to that of diffusion, the reacting species is consumed mainly near the boundary of the grain and does not penetrate deeply into it. Therefore, if the latter is too large its central part is no longer utilized. A quite analogous problem exists for the three-dimensional electrodes. We will come back to this in Section 8.4.

The electrochemical system, in addition, has a complication of its own: the resistances of the electrode and electrolyte tend to prevent the penetration of the current into the three-dimensional structure even if the decrease of concentration of the electroactive species is negligible. The distributions of the current and potential play a particularly important role in three-dimensional electrodes and determine to a large extent their performance. It has been calculated and studied experimentally by various authors.^(13,43a,74-87,168) The distribution in various types of three-dimensional electrodes has been discussed in two review articles by de Levie⁽⁸⁸⁾ and by Newman and Tiedemann.⁽⁸⁹⁾

This section is restricted to the case of *secondary* current distribution, i.e., there are no concentration differences within the solution (no concentration overpotential). Let us consider the system shown schematically in Figure 22. It consists of a three-dimensional electrode D which may be a porous body or a bed of particles. The counterelectrode is in C; the current feeder

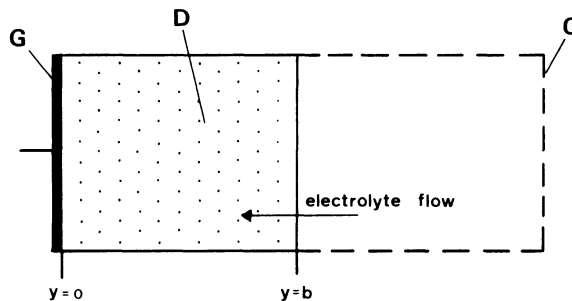


Figure 22. Three-dimensional electrode system (schematic).

to D is the grid G. The electrolytic solution flows through the system and fills the voids in the three-dimensional electrode. The electrochemical reaction takes place within the body of the electrode, at the solution–solid interface, the geometry of this is extremely complex.

An exact computation would have to start from a detailed description of this geometry which is in general not well known and the calculation would in any case be extremely complicated. We will use a macroscopic model which allows a much simpler approach.^(76,82) The three-dimensional structure is a labyrinth, with thin walls and narrow pores. Their dimension is small in comparison to the depth b of the electrode and they are distributed at random. In the above model the electrode is thus regarded as being made of two quasihomogeneous phases—one solid, the other liquid—which are interpenetrating each other; or we may also say they are superposed on each other. Each of them is regarded as a continuum and we may thus apply Eq. (4) for the calculation of the current in the two phases, provided that one uses an effective conductivity κ^* (i.e., corrected to take into account the average porosity and tortuosity, the pores not having the form of simple cylindrical straight tubes).

The potential ϕ depends mainly on the distance y from the current feeder G and we neglect the influence of the two other spatial coordinates. We thus have

$$j_l = -\kappa_l^* \frac{d\phi_l}{dy} \quad (41)$$

$$j_m = -\kappa_m^* \frac{d\phi_m}{dy} \quad (42)$$

where the subscripts l and m refer to the liquid and solid phase, respectively, j_l is an ionic current density, and j_m an electronic current density.

Since there is no accumulation of charges within the working electrode, the sum $j_l + j_m$ is independent of y . However, j_l and j_m vary with y : with increasing distance from G the current passes progressively from the solid

phase to the liquid phase. This transfer corresponds to the electrochemical reaction which takes place on the walls of the labyrinth. We have for a point $0 < y < b$

$$\frac{dj_l}{dy} = \frac{-dj_m}{dy} = j^* \quad (43)$$

The quantity j^* (expressed in A m^{-3}) is a transfer current which corresponds to the number of moles that react per unit volume and per unit time. Note that the current density j_l and j_m (A m^{-2}) corresponds not to the electroactive surface at the interior of the labyrinth but to a cross section perpendicular to the axis y . The quantity dj_l therefore corresponds to the number of moles that react, per square meter of electrode section, in the interval between y and $y + dy$, and dj_l/dy corresponds to the number of moles that react per unit volume and per unit time.

The current j^* is a function of the potential difference $\phi_m - \phi_l$ between the solid and liquid phases at the considered point y :

$$j^* = f(\phi_m - \phi_l) \quad (44)$$

The function f depends on the kinetics of the electrochemical reaction and on the area A of the active surface per unit volume. Euler and Nonnenmacher⁽⁷⁵⁾ have used a linear approximation, while Tobias, Newman, and Grens used both^(76,82) the linear approximation and the Tafel equation. In this latter case Eq. (44) may be written (for a cathodic reaction):

$$j^* = Akc \exp \left[-\frac{\alpha z F}{R^* T} (\phi_m - \phi_l) \right] \quad (45)$$

where k is a reaction rate constant, α the charge transfer coefficient, A the active electrode area per unit volume, and c the concentration of the reacting species. By combining this relationship with Eqs. (41) and (43) one obtains by differentiating Eq. (45) and eliminating ϕ_m , ϕ_l , and j_l

$$\beta \frac{d^2 j_m}{dy^2} = \frac{dj_m}{dy} \left[\frac{J}{\kappa_l^*} - j_m \left(\frac{1}{\kappa_l^*} + \frac{1}{\kappa_m^*} \right) \right] \quad (46)$$

with $\beta = R^* T / \alpha z F$. J is the overall current density:

$$J = j_l + j_m$$

The boundary conditions are

$$j_m = 0 \quad \text{for } y = b$$

$$j_m = J \quad \text{for } y = 0$$

By integration one obtains curves such as those represented in Figures 23 and 24.^(76,82) Figure 25 shows one curve (broken line) calculated with the

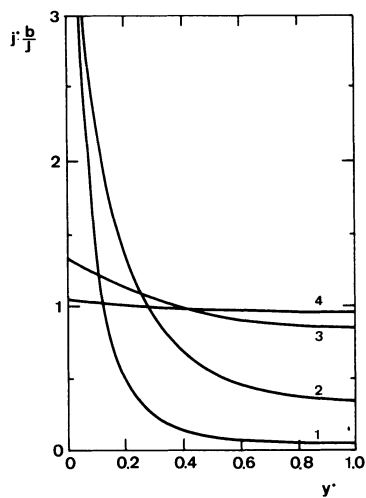


Figure 23. Secondary current distribution in a three-dimensional electrode for $Wa \rightarrow \infty$ (References 76 and 82). Curve 1, $Wa' = 0.01$; curve 2, 0.1; curve 3, 1; curve 4, 10.

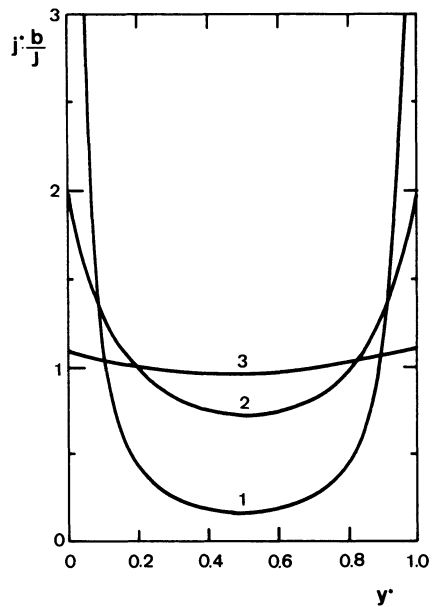


Figure 24. Secondary current distribution in a three-dimensional electrode for $Wa = 2 Wa'$ (References 76 and 82). Curve 1, $Wa' = 0.01$; curve 2, 0.1; curve 3, 1.

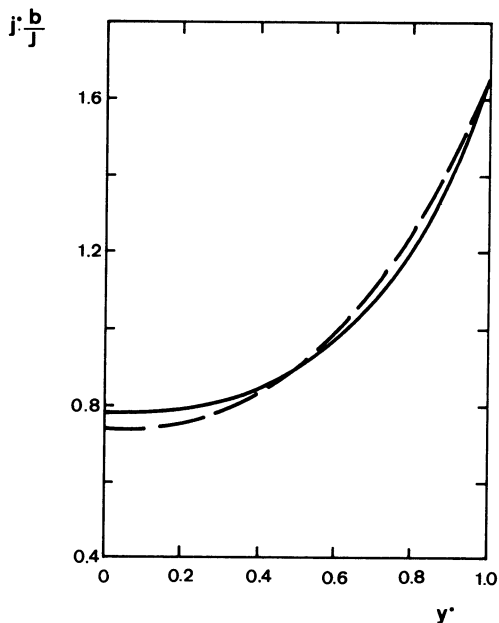


Figure 25. Secondary current distribution in a three-dimensional electrode: Comparison between Tafel approximation (—) and linear approximation (---) (Reference 76) for $Wa = 10$ and $Wa' = 0.5$.

linear approximation ($d\eta_a/dj = \text{const}$).[†] It is compared there with the result obtained with the Tafel approximation (full line).[‡]

The ratio $y^* = y/b$ (which is a normalized distance from the current feeder G) are plotted on the abscissa whereas the ordinate represents the quantity

$$j^* \left(\frac{b}{J} \right) = \frac{d(j_i/J)}{d(y/b)}$$

The curves show, in dimensionless form, the variation of the local value of the transfer current within the body of the electrode. They depend on *two* dimensionless groups, which is easily explained by the fact that in this case (as in that of the thin wire discussed at the beginning of this section but in contrast to the examples of Section 6) there are *two* conductivities in play—that of the liquid phase and that of the solid phase. For the Tafel approximation

[†] Note that the slope of the overpotential–current curve can be expressed in terms of *either* the current density j referred to the true active electrode area (i.e., the area of the pore walls), *or* the current density j_e, j_m, J referred to the area A^* of the electrode cross section perpendicular to y . The relationship between the two is obtained by writing $J = jAA^*b/A^* = jAb$, from which follows that $d\eta_a/dJ = \beta/J$ if $d\eta_a/dj = \beta/j$.

[‡] When Tafel's equation is applied $d\eta_a/dJ$ depends on J , and in comparison with the linear approximation the question arises as to which value of J one linearizes (i.e., for which J one sets $\beta/bJ = R_a$). In Figure 25 the linearization was made around the middle value between the extreme values of J in the bed (i.e., at $y^* = 0$ and $y^* = 1$).

these two dimensionless groups can be written in the form

$$Wa = \frac{\beta \kappa_l^*}{bJ} \quad (47a)$$

$$Wa' = \frac{\beta \kappa_l^* \kappa_m^*}{bJ(\kappa_l^* + \kappa_m^*)} \quad (48a)$$

Taking into account Eq. (38) we may rewrite these equations as

$$Wa = \frac{d\eta_a}{dJ} \frac{\kappa_l^*}{b} \quad (47b)$$

$$Wa' = \frac{(d\eta_a/dJ)\kappa_l^* \kappa_m^*}{b(\kappa_l^* + \kappa_m^*)} \quad (48b)$$

In this form the definitions of Wa and Wa' apply also to the case of the linear approximation (where $d\eta_a/dJ = R_a = \text{const}$). Combining the two equations we obtain

$$\frac{Wa}{Wa'} = 1 + \frac{\kappa_l^*}{\kappa_m^*} \quad (49)$$

The structure of Eq. (47b) is the same as that of Eq. (25) which defines the Wagner number Wa (Sections 6.1 and 6.3.4). Equations (48b) and (25) also have an analogous structure, with the difference, however, that Wa' depends on two conductivities instead of one.

The curves of Figures 23 and 24 correspond to various values of Wa' . We observe the same influence of the dimensionless Wagner number as in the examples of Section 6.3.3. The current distribution is *more uniform* the larger Wa' is; i.e., that

- (a) the *depth* of the electrode in the y direction *is smaller*;
- (b) the *slope* of the potential–current curve *is larger*;
- (c) the *conductivity* of the solid phase and (or) the liquid phase *is larger*.

The ratio of the conductivities of the liquid and solid phases affects the symmetry of the curves. Figure 24 corresponds to the case where $\kappa_l^* = \kappa_m^*$ ($Wa = 2 Wa'$). The curves are symmetric with respect to the middle of the electrode ($y^* = 0.5$). If the conductivity of the solution is much larger than that of the solid phase, the increase in current takes place mainly near the feeder grid. Figure 23 shows the limiting case where κ_m^* is negligible with respect to κ_l^* . ($\kappa_l^* \gg \kappa_m^*$, $Wa/Wa' \rightarrow \infty$ and $Wa' = \beta \kappa_m^*/bJ$ in the Tafel approximation.)

The form of the calculated curves is easily understood with the help of a simplified resistance model analogous to that used in Section 6.1 (Figure 9). In Figure 26(a), R_l and R_m are the resistances of the liquid and solid phases respectively, and R_a is the resistance to the passage of the current from one phase to the other. The value of R_a , which depends on the kinetics

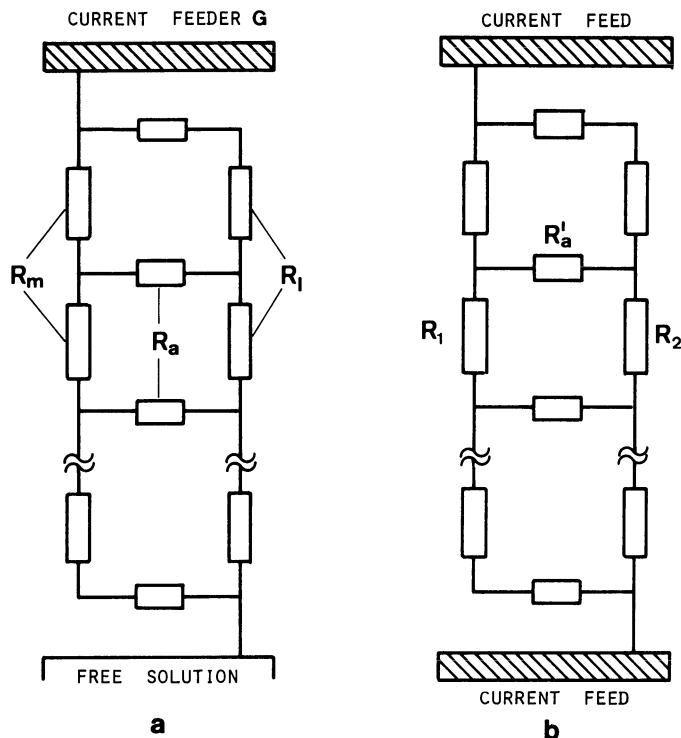


Figure 26. (a) Resistance model for current distribution in a three-dimensional electrode (fixed bed, porous electrode, etc.). (b) Resistance model for current distribution in Swiss-roll cell: $R'_a = R_l + (R_a)_{\text{cathode}} + (R_a)_{\text{anode}}$.

of the electrode reaction, is constant in the linear approximation but varies with y in the case of Tafel kinetics.

- (a) If R_a is negligible with respect to R_l and R_m , the transfer of the current from one phase to the other takes place only at the two ends of the electrode and the current distributes itself between the two phases according to the ratio of their conductivities:

$$j_l/j_m = \kappa_l^*/\kappa_m^*$$

The curve $Wa' = 0.01$ of Figure 24 corresponds to this case.

- (b) In contrast to this, a large resistance R_a opposes itself to the concentration of the transfer current at the ends. This current is thus distributed much more uniformly over the whole of the electrode. The curve $Wa' = 1$ of Figure 24 corresponds to this case.
- (c) Finally, if R_l is very small compared to R_m the ionic current penetrates very easily from the free electrolyte solution toward the interior of

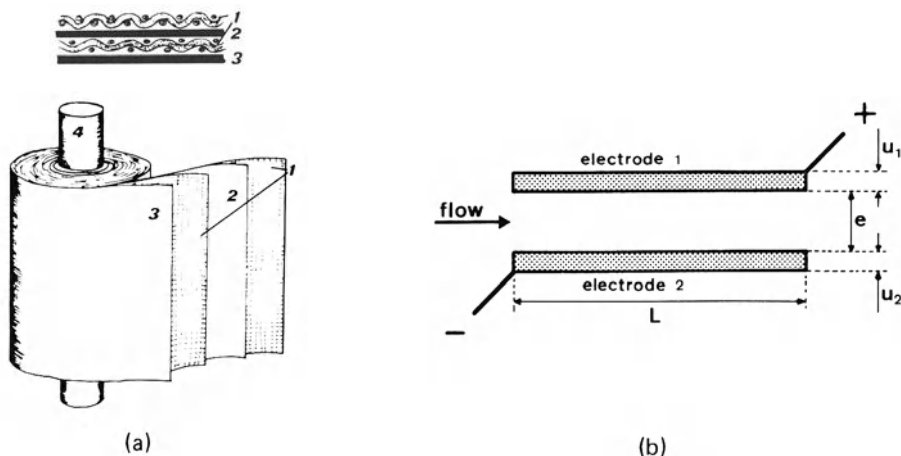


Figure 27. (a) Swiss-roll cell. Surface 1, cloth separators; surfaces 2 and 3, electrodes; 4, axis. (b) Model of electrode arrangement in Swiss-roll cell.

the liquid phase within the electrode. There is then no increase of the transfer current toward the end of the electrode adjacent to the free electrolyte and the electrochemical reaction takes place mainly at the other end of the electrode (Figure 23). Conversely, if R_m is very small the reaction takes place mainly toward the extremity of the electrode close to the free electrolyte.†

It is interesting to note that quite similar arguments can be developed for cells which at first sight do not seem to belong to the same family, such as the *Swiss-roll cell* [Figure 27(a)].⁽¹⁴⁰⁾ The cathode and the anode are thin foils rolled around a common axis. They are separated by a cloth to prevent short circuits. The solution flows through the system parallel to the axis. The purpose is a cell with a high active area per unit volume, as in the fluidized or fixed beds. The Swiss-roll cell is a three-dimensional system but we can also regard it as a cell with two very long parallel electrodes separated by a thin layer of electrolyte [Figure 27(b)]. Considered in this manner, the system is geometrically the same as that of Figure 1 or 10 (plane parallel electrodes). What makes it belong to the same general category (at least mathematically) as a three-dimensional electrode is the fact that the thin electrodes have resistances that may be non-negligible in comparison to that of the solution.

† Note that if one wishes to compare numerically R_a with R_m (or R_l), it is necessary to define these quantities more precisely. If we denote by r_m and r_l the specific resistance referred to a unit of volume of the three-dimensional electrodes we must likewise refer the transfer resistance to the same volume unit. We thus have

$$r_a = A^{-1}(d\eta_a/dj)$$

This quantity can then be numerically compared to r_m and r_e .

We can discuss qualitatively its behavior with a resistance model [Figure 26(b)] which is essentially the same as that for the fixed bed [Figure 26(a)]. R_1 and R_2 are the resistances of the cathode and anode, respectively, whereas in the case of Figure 26(a), R_m and R_l were the resistances of the solid matrix and solution within the electrode. The cross resistance R'_a of Figure 26(b) includes the resistance of the electrolyte and the resistances for the charge transfer at the cathode and anode [$R'_a = R_l + (R_a)_{\text{cathode}} + (R_a)_{\text{anode}}$], whereas in Figure 26(a) R_a represents only the resistance for the charge transfer $d\eta_a/dj$. But the structure of the resistance models of Figures 26(a) and 26(b) is the same. In the case of the linear approximation for the potential-current relationship (R_a and R'_a independent of y), the current distribution curves are the same for a conventional three-dimensional electrode and for the Swiss-roll cell, provided that one uses corresponding dimensionless groups, i.e.,

$$Wa = \frac{R'_a}{R_2} \quad (47c)$$

$$\frac{Wa}{Wa'} = 1 + \frac{R_1}{R_2} = 1 + \frac{\kappa_1}{\kappa_2} \quad (49b)$$

where

$$R_1 = L(\kappa_1 u_1)^{-1}, \quad R_2 = L(\kappa_2 u_2)^{-1}$$

$$R'_a = e(\kappa_l L)^{-1} + \frac{1}{L} \left(\frac{d\eta_a}{dj} \right)_{\text{anode}} + \frac{1}{L} \left(\frac{d\eta_a}{dj} \right)_{\text{cathode}}$$

For negligible polarization ($d\eta_a/dj \cong 0$), R'_a reduces to

$$e(\kappa_l L)^{-1} \quad \text{and} \quad Wa = L^2 \kappa_l / (\kappa_1 u_1 e)$$

In these equations R_1 , R_2 , and R'_a are the resistances per unit electrode width, u_1 and u_2 are the thicknesses of electrode foils 1 and 2, respectively, κ_1 and κ_2 their specific conductivity ($\Omega^{-1} \text{ cm}^{-1}$), e the interelectrode distance, L the electrode length [Figure 27(b)], and κ_l the specific conductivity of the electrolytic solution.

If Wa and Wa' as defined by Eqs. (47c) and (49b) are used for the Swiss-roll cell, the distribution shown by the broken line in Figure 25 (linear approximation) applies to both the Swiss-roll cell and an electrode of the type in Figure 22. For the conditions of Figure 25 ($Wa = 10$, $Wa' = 0.5$) the difference between the results obtained with the Tafel equation and the linear approximation is small. However, the difference becomes substantial for small values⁽⁷⁶⁾ of Wa' (i.e., when the distribution of the reaction rate is much less uniform).

The shape of the current distribution curves for the Swiss-roll cell can be understood in the same way as for Figure 26(a). If the resistances R_1 and R_2 are equal, the curves are symmetric around the point $L/2$ as in Figure 24.

If R'_a is large compared to R_1 and R_2 , the current distributes uniformly over the electrode. The current and potential distributions in the Swiss-roll cell have been discussed in more detail by Robertson⁽¹³²⁾ who has also calculated the distribution for the case of a Tafel polarization.

From the viewpoint of *technical application* the relevance of distribution curves such as those shown in Figures 23 and 24 lies in the fact that they represent the *variation of the reaction rate* within the body of the electrode or within the Swiss-roll cell. In the case of a distribution such as that on the curve $Wa' = 0.01$ in Figure 24, the central part of the electrode is poorly utilized. In order to increase Wa or Wa' one can for given values of κ_i^* and β decrease the electrode depth b . This is a problem of optimization of the thickness of the active layer similar to that encountered in the optimization of the size of the grains of a catalyst in diffusional kinetics. One may also envisage increasing κ_2 by utilizing a more porous system.

The value of κ_1 is much larger if a fluidized bed is used instead of a porous electrode or a fixed bed[†] (because the volume of the voids is much greater in the first case). It is true that in this case the conductivity of the solid phase κ_m (because of the poorer contact between the particles) becomes smaller and this tends to decrease Wa' . However, for very poorly conducting solutions the values of κ_i^* and κ_m^* become closer, and the distribution curves are more symmetric which means a tendency to better utilize the whole electrode. In the case of the Swiss-roll cell, within certain limits, one can adjust the thickness of the foils and thus their resistance in order to fit the value for the electrolyte and achieve a more uniform distribution. In fact, since the resistance of the foils is usually relatively small a substantially nonuniform distribution will occur only for very high values of L or very highly conducting solutions.[‡] Indeed, although the mathematical models for the three-dimensional electrodes and the Swiss-roll cell are one and the same, the characteristic parameter Wa contains the electrode resistivity for the Swiss-roll but the electrolyte resistivity for the three-dimensional electrode. Thus a high Wa number (and therefore good current distribution) is much more easily attainable with the Swiss-roll cell.

7.2. Variation of Potential

As we have seen in Section 6.3.6, in addition to the distribution of the current, the repartition of the potential is also relevant. It is particularly important in the case of three-dimensional systems because the variations can

[†] In a fluidized bed the contact between the particles is intermittent. Nevertheless, one can define an effective conductivity of the solid phase which represents a kind of time average.

[‡] The characteristic length in the case of the Swiss-roll cell may be the unwrapped length of the electrode rolls when the current is fed from the axis and container, or the width of the electrodes, for current feeders at the ends of the roll. This latter arrangement enables a shorter current path and therefore a better current distribution.

be quite large, and substantial changes in current efficiency may occur over the depth of the electrode. Figure 28(a) shows the case where one of the two phases has a much better conductivity than the other. The potential ϕ_m in the highly conducting phase remains constant, whereas that in the poorly conducting phase (ϕ_l) changes strongly, so that the driving force for the reaction may be quite different depending on the location within the three-dimensional structure. More favorable is the case where the two conductivities are comparable. Then we have the situation of Figure 28(b) where the lower curve represents the potential profile in the solid phase which is supposed to be connected with the negative pole. The upper line is the potential profile in the solution and the distance between the two lines represents the potential difference $\Delta\phi = \phi_m - \phi_l$ across the solid phase-solution interface, i.e., the driving force for the electrode reaction. This is seen to vary much less than in the case of Figure 28(a) because the potential changes markedly in a similar way in both phases.

However, the curves are not parallel. Their shape can be explained qualitatively as follows. The slope of the potential line for the liquid phase decreases with decreasing y because the current passes continuously from the liquid to the solid phase when one goes from right to left so that the voltage change per unit length $d\phi/dy$ decreases. On the other hand, the slope of the lower line increases from right to left because the current flowing through the solid phase increases with decreasing y . The potential difference $\Delta\phi$ at the interface thus changes with location even if the conductivities of the two phases were equal. In some cases $\Delta\phi$ may change so much that it drops below the equilibrium potential. For example, if one deposits copper on the solid particles of the bed it may happen that the bed is in reality bipolar, i.e., copper

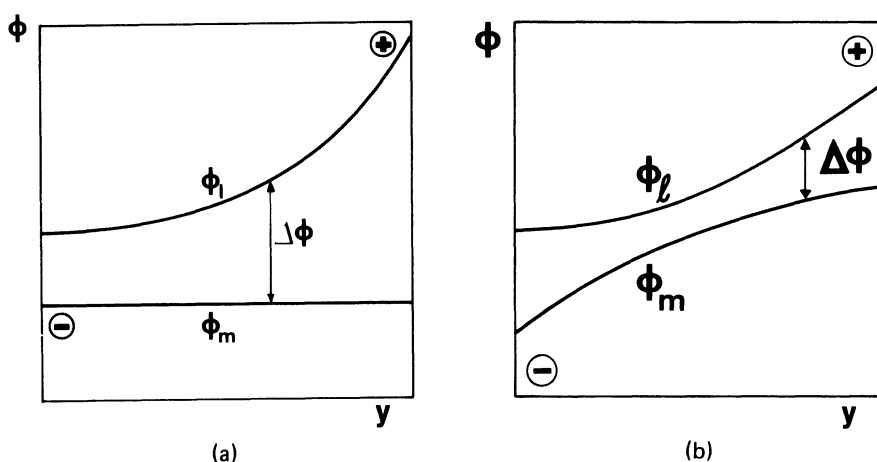


Figure 28. Potential profile in three-dimensional electrode (schematic) (a) One phase exhibits better conduction than the other. (b) Both phases with similar conductivities.

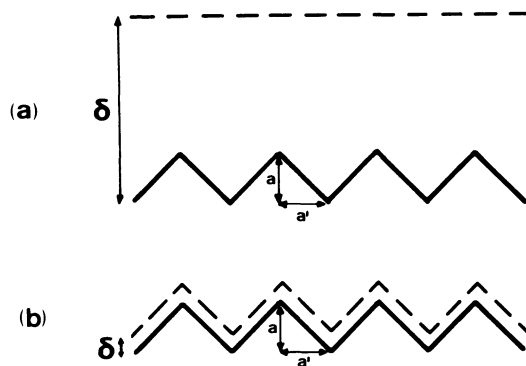


Figure 29. Serrated surface profile with diffusion layer, showing difference between (a) microprofile ($a \ll \delta$) and (b) macroprofile ($a \gg \delta$).

deposits only in certain parts which are cathodic whereas other parts of the bed are anodic so that dissolution of the metal takes place there. This phenomenon has been observed and studied by Hutin and Coeuret⁽¹⁸⁶⁾ and Germain and Goodridge.⁽¹⁸⁷⁾

8. Tertiary Distribution

8.1. General Remarks

The curves of Figures 23 and 24 were calculated under the assumption that the concentration is independent of y . This assumption is increasingly less fulfilled when the current density increases above a certain range. A similar remark applies to the systems considered in Section 6.3. We thus come to the tertiary distribution which will be discussed in this section.†

In this case one takes *concentration overpotential* into account. The effect exerted by the latter is qualitatively different from that of the activation overpotential. Its influence depends on the ratio of the characteristic length L to the thickness δ of the diffusion layer, discussed in Chapters 3 and 1 of this volume.

Let us consider, for example, a surface profile such as that shown in Figure 29 where we have indicated by a broken line the limit of the diffusion layer. For a given angle the characteristic dimension is the height a . We will distinguish two cases:^(37,90) $a \ll \delta$ (microprofile) and $a \gg \delta$ (macroprofile). In electroplating one distinguishes accordingly between a microscopic and a macroscopic throwing power (see Section 6.3.5) (micro-, macrothrowing

† In the literature one sometimes calls tertiary distribution the repartition when the current efficiency varies.^(11a) In this text the term tertiary distribution is used to denote the case where one has to take concentration overpotential into account. The sequence primary, secondary, tertiary distribution appears then more logical because it corresponds to the sequence no overpotential, activation overpotential, activation overpotential *and* concentration overpotential. This nomenclature is recommended by IUPAC.⁽¹⁴²⁾

power). Let us note that this distinction not only depends on the height of the profile considered but also on the thickness of the diffusion layer. The diffusion layer is thinner the more intensive the agitation of the solution. A given profile may therefore behave rather as a microprofile or rather as a macroprofile, depending on the hydrodynamic conditions. A number of plating baths have a good macro but a poor microthrowing power.

8.2. Distribution Over a Microprofile—Microscopic Throwing Power

The thickness δ of the diffusion layer is large with respect to the height a of the profile. The peaks are better accessible to diffusion than the recesses. This is because the free section for diffusion increases when one proceeds from the crest into the bulk of the solution. There is a peak effect analogous to that which exists in primary distribution. Under these conditions the depletion of the solution in a metal deposition, for example, is smaller on the crests: The concentration overpotential tends to be smaller there and thus acts in a direction opposite to that of the activation overpotential which is larger on the peaks. *The concentration overpotential therefore counteracts the equalizing action of the activation overpotential.*

The distribution over a microprofile has been discussed in more detail by Kardos and Gardner-Foulke⁽⁹⁾ (see also references 107, 176, 178). Recently, the repartition of diffusion-controlled metal deposition in a cylindrical pore was investigated by Popov *et al.*⁽¹⁸¹⁾ for potentiostatic and pulsating potential conditions. The current distribution over a microprofile is relevant for surface finishing in connection with certain specific applications involving metal deposition into small recesses. More generally it is of importance in electroplating because of its influence on the roughness and the appearance of the deposits. It is to be noted, however, that it is often more or less strongly modified by phenomena which we haven't yet taken into consideration; these phenomena supersede the effects we have already discussed.

The plating baths usually contain *organic additives* which, in spite of their small concentration in the solution, may play an important role because they are adsorbed at the electrode-solution interface and increase the overpotential for the metal deposition (see Chapter 7, Volume 2). In certain cases the degree of coverage of the surface by the adsorbed species varies along the profile and the same is then true for the activation overpotential η_a , which results in a modification of the current distribution.

Furthermore, the distribution is affected by phenomena linked with the *crystallization* of the metal. The incorporation of the discharged atoms into the lattice takes place preferentially on growth steps and thus there is an increase of current density at these privileged sites which are moving with time due to the crystallization. Finally, one must take into account nucleation. The formation of new nuclei requires a certain overpotential, which is part

of the crystallization overpotential, but once the nucleus is present the overpotential decreases and the current density on the newly formed small crystal increases.

We may envisage as an example the following situation which illustrates the role of crystallization phenomena. The major part of the surface, in particular, the growth steps, is blocked by adsorption. In the initial phase, the deposition will then take place mainly through formation of nuclei. If adsorption is slow, the freshly formed surfaces will be relatively free of adsorbed substances and the current density will be larger there than on the neighboring parts which are less active. One then observes mainly a growth of newly formed crystallites.

We see that crystallization phenomena may cause large local and time-dependent variations of current density. On the microscopic scale, a morphology of the deposit surface may finally develop which is quite different from that which would occur if there were only the influence of a concentration and activation overpotential which would be constant along the interface.

8.3. Distribution Over a Macroprofile—Macroscopic Throwing Power

The diffusion layer is thin compared to the height of the profile. This case includes that of plane electrodes. Here the diffusion layer follows a profile which is everywhere equally accessible to diffusion. Under these conditions in the case of a metal deposition, for example, the interfacial concentration of the metallic cations tends to be lower, and therefore the concentration overpotential higher, in parts of the electrode where for geometric reasons the local current density tends to be higher. This is the case on a macroscopic crest where the thickness of the diffusion layer is the same as in the recess [Figure 29(b)], but where the current density in secondary distribution would be higher over the crest. The increase of concentration overpotential on the crest opposes the increase in local current density there. In the case of a macroprofile, therefore, *the concentration overpotential acts in the same direction as the activation overpotential*; i.e., it tends to make current distribution more uniform and thus improve the throwing power on the macroscopic scale. It is to be noted, however, that the thickness of the diffusion layer δ may vary along a macroprofile for hydrodynamic reasons (as is the case along a plane electrode in laminar flow, see Section 2, Chapter 3), the result being that for one and the same local current density the concentration overpotential may be different on various parts of the electrode depending on the thickness of the diffusion layer. The influence of concentration overpotential is more complicated than that of activation overpotential which depends on the local current density only, and not on geometry as long as the properties of the surface remain constant. It is thus difficult to push further the qualitative discussion of the phenomena in tertiary current distribution.

The theoretical problem is also a tough one and has been solved only in the last ten years. The method of approach is as follows: In tertiary current distribution we must take into account the *concentration variations within the solution*. Therefore the Laplace equation [Eq. (2)] has to be replaced by Eq. (1). Furthermore, Eq. (4) for the current density within the solution is also no longer valid and has to be replaced by the equation

$$\mathbf{j} = -\frac{F^2}{R^*T} \nabla \phi \sum_k z_k^2 D_k c_k - F \sum_k z_k D_k \nabla c_k \quad (50)$$

A complete integration of these equations is hardly possible, at least in the presence of convection, as has been pointed out in Chapter 3. However, the problem can be solved approximately by the following arguments. The concentration gradients are essentially restricted to the diffusion layer, the thickness of which is small compared to the main dimensions of the system. One can thus proceed in a manner different for the bulk of the solution and for the diffusion layer. In the first region (where there are no concentration gradients), one applies the Laplace law. In the second case, one neglects the potential drop within the diffusion layer, and its influence on the concentration variations therein, which can be justified by the small thickness of the diffusion layer. One then calculates in two different manners the current flowing through the electrode: First, by integrating the Laplace equation down to the outer limit of the diffusion layer; i.e., virtually down to the electrode, and second, from the mass transport equations for a given interfacial concentration and a given distribution of the latter.

Since the two thus calculated currents must be equal, the interfacial concentration must be adjusted in such a manner that this condition is fulfilled. The equality of these two currents furnishes one of the boundary conditions for the integration of the Laplace equation. For the boundary condition on the electrodes (which requires knowledge of the potential difference across the interface) one takes into account activation overpotential, as well as concentration overpotential calculated from the interfacial concentration (see Section 7.2, Chapter 1). More details about the general theory are given in Newman's book⁽²²⁾ (see also references 81 and 127). In the following we will give an example.

Following a paper by Newman⁽³⁵⁾ (see also reference 92) let us sketch the quantitative argument for the case of the disk electrode, the theory of which we have already discussed in Sections 5.3 and 6.3.2, from the viewpoint of primary and secondary distribution. The concentration distribution of the reactant in the diffusion layer is determined from the equation.

$$v_r \frac{\partial c}{\partial r} + v_y \frac{\partial c}{\partial y} = D \frac{\partial^2 c}{\partial y^2} \quad (51)$$

or

$$ay\Omega(\Omega/\nu)^{1/2}\left(r\frac{\partial c}{\partial r}-y\frac{\partial c}{\partial y}\right)=D\frac{\partial c}{\partial y} \quad (52)$$

where only the dominant diffusion term $D(\partial^2 c/\partial y^2)$ needs to be included on the right-hand side because of the small thickness of the diffusion layer. The distance y normal to the disk is replaced by the variable

$$\zeta = y(a\nu/3D)^{1/3}\Omega/\nu \quad (53)$$

The solution of Eq. (52) is expressed in terms of this variable as a series

$$c = c_\infty \left[1 + \sum_{m=0}^{\infty} A_m \left(\frac{r}{r_0} \right)^{2m} \theta_m(\zeta) \right] \quad (54)$$

The concentration in the diffusion layer is thus represented by a power series of the radial coordinate, but only even powers are included because the concentration must be an even function of r .

$$c_0 = c_\infty \left[1 + \sum A_m \left(\frac{r}{r_0} \right)^{2m} \right] \quad (55)$$

The local current density flowing through the electrode is proportional to the derivative of the concentration normal to the interface (see Chapter 1, Section 5.4) and is given by

$$\frac{j}{nF} = \frac{D}{1-t} \left(\frac{\partial c}{\partial y} \right)_{y=0} = \frac{Dc_\infty}{1-t} \left(\frac{a\nu}{3D} \right)^{1/3} \frac{\Omega}{\nu} \sum_{m=0}^{\infty} A_m \left(\frac{r}{r_0} \right)^{2m} \theta'_m(0) \quad (56)$$

where t is the transference number of the reacting species.

The coefficients A_m in Eqs. (56) and (55) have yet to be determined. The potential distribution outside of the diffusion layer is calculated from the Laplace equation in the same way as in primary potential distribution (pp. 247–251). The local current density is thus linked to the potential through Eq. (18) which now applies to the outer border of the diffusion layer. In accordance with what was said on p. 292 the distribution of the current at this outer border is assumed to be the same as on the electrode surface (which is justified if the diffusion layer is very thin compared to the main dimension of the cell). One thus equates the local current densities given by Eqs. (56) and (18). This yields a relationship for the calculation of the coefficients A_m of Eqs. (55) and (56) and of B_n of Eq. (18). Furthermore, we have Eq. (15) which relates the electrode surface potential ϕ_e to the coefficients B_n . However, it has to be taken into account that the potential difference $\phi_m - \phi_e$ over the electrode–solution interface depends now on activation *and on concentration* overpotential. Both kinds of overpotential have been taken into account in the computation by Newman.⁽³⁵⁾ The concentration overpotential was calculated from the interfacial concentration c_e as given by Eq. (55). The activation

overpotential was calculated from the kinetic expression (33), where the exchange current density j_0 has been set proportional to $(c_e/c_0)^\gamma$ to take into account the change in concentration over the diffusion layer ($c_0 - c_e$). This yields

$$j = j_0^* \left(\frac{c_e}{c_0} \right)^\gamma \left\{ \exp \left(\frac{\alpha z F \eta_a}{R^* T} \right) - \exp \left[- \frac{(1 - \alpha) z F \eta_a}{R^* T} \right] \right\} \quad (57)$$

where j_0^* is the exchange current density at the bulk concentration c_0 and γ is a constant.

Newman has thus achieved a very complete and rather general calculation of the current distribution at a rotating disk electrode. The results are shown graphically in Figure 30 which also shows a comparison between theory and experiment. On the ordinate is the ratio j_x/j of the local current density to the average current density whereas the abscissa shows in dimensionless form the distance from the center of the disk. The three curves correspond to three different values of the ratio j/j_{lim} of the average current density to the *average limiting-current density*. With increasing value of this ratio the concentration differences over the diffusion layer and therefore the influence of concentration overpotential increases. The argument between the experimental points and the theoretical curves is satisfactory.

We may note that for $j/j_{lim} = 0.495$ the distribution is less uniform than for $j/j_{lim} = 0.194$. The reason is that at increasing current density $d\eta_a/dj$ decreases and the equalizing action of the activation overpotential thus becomes in general smaller (see Section 6.3.5). On the other hand at $j/j_{lim} = 0.69$ the distribution is approximately the same as for 0.495. This is due to

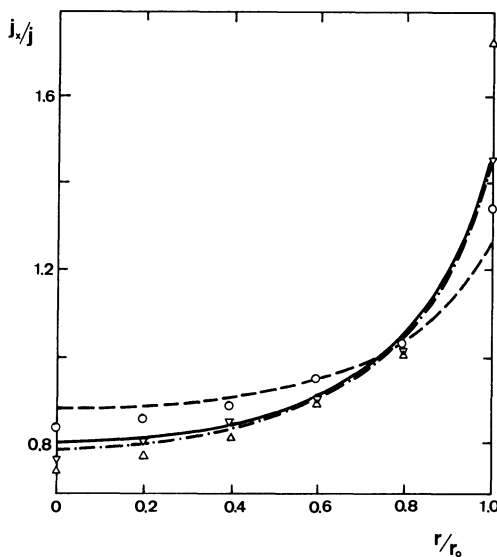


Figure 30. Tertiary current distribution at a rotating disk electrode in laminar flow. Comparison between theory and experiment (Reference 8): $j/j_{lim} = 0.194$, ---, calculated, \circ , experimental; $j/j_{lim} = 0.495$, —, calculated, Δ , experimental; $j/j_{lim} = 0.69$, - · - · - calculated, ∇ , experimental.

the fact that the decrease of the equalizing action of η_a at increasing j is compensated here by the influence of η_c which becomes significant since we are approaching the limiting current. It is now the concentration overpotential which tends to make the distribution more uniform since the thickness of the diffusion layer is constant over a rotating disk in laminar flow and the distribution of the current is uniform at the limiting current.

Further systems for which a tertiary current distribution has been calculated are plane⁽⁴¹⁾ or tubular electrodes^(40,134) in laminar flow, vertical electrodes with natural convection,^(93,165) a plane electrode below a rotating disk,⁽¹⁷²⁾ moving sheet electrodes,⁽¹³¹⁾ and moving resistive wire electrodes.⁽¹³⁶⁾ The results presented (like those of Figure 30) apply to a steady state, i.e., the current is independent of time (see Chapter 3).

Figure 31 shows the tertiary distribution calculated by Parrish and Newman⁽⁴¹⁾ for the cell of Figure 3 with laminar flow of the fluid parallel to the electrode. The overpotential was calculated according to the Tafel equation [Eq. (32)]. The various curves correspond to different values of the ratio h/l (distance between/length of electrodes) and to different values of the ratio j/j_{lim} of the average current to the limiting current. The ordinate shows the ratio of the local current density j_x to the limiting current density j_{lim} , as a function of the distance x from the leading edge of the electrode (normalized with a total electrode length l). One observes an asymmetry of the distribution curves, j_x/j_{lim} being larger toward the upstream end than at the downstream

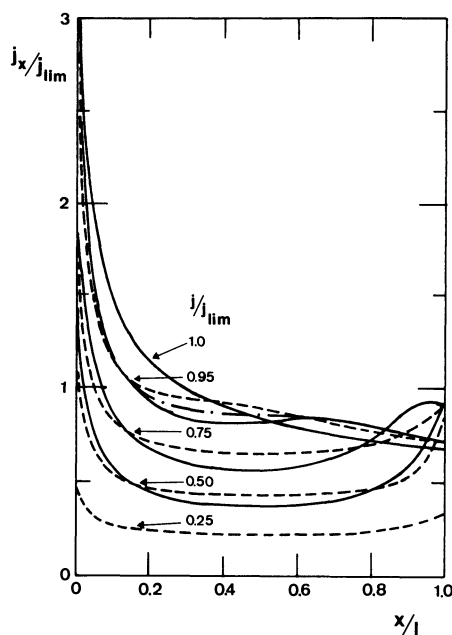


Figure 31. Tertiary current distribution (Reference 41) in the cell of Figure 3 with laminar flow of the fluid along the electrode: $h/l = 0.5$, ---; $h/l = 1.0$, - · - · -; $h/l = \infty$, —.

end of the electrode. This is due to the variation of the thickness of the diffusion layer δ which increases downstream with increasing x , as we have seen in Sections 1 and 5 of Chapter 3. The mass transport toward the electrode is less effective downstream, the result being that the concentration overpotential tends to decrease and the local current density increases toward the leading edge. This phenomenon is superimposed on the edge effects of the primary distribution and causes an asymmetry of the curve for the distribution of the current density. This asymmetry is more marked the larger the average current density is and the closer it is to the limiting current. It is remarkable that the distribution curve already exhibits a noticeable asymmetry even for an average current equal to a quarter of j_{lim} only.

The two preceding examples refer to systems with *forced convection* (in the case of Figure 30, rotation of the disk; in the case of Figure 31, pumping of the solution through the cell). To conclude this section let us briefly consider as a third example the case of a plane vertical cathode with *natural convection* (due to the density differences present in the electrolyte solutions; see Section 9, Chapter 3). In metal deposition the thickness of the diffusion layer δ increases with height. The result is an asymmetry of the current distribution similar to that exhibited by the curve of Figure 31. The local current density tends to increase toward the bottom of the cathode, especially at current densities close to the limiting one. This prediction of the theory has been confirmed by experiment.^(94,165)

8.4. Case of Three-Dimensional Electrodes

In Section 7.1 we discussed the secondary current distribution in a three-dimensional electrode, the concentration within the electrode structure being assumed uniform. In reality, the electrochemical reaction causes a diminution (or an increase) of the concentration of the reacting species, the effect being more or less pronounced depending on the current density. The result is a concentration overpotential that modifies the potential distribution (see also Chapter 6 in this volume).

Let us take as an example the system treated by Newman and Tobias⁽⁷⁶⁾ which is the one that we discussed in Section 7.1 (see Figure 22). We consider the case where the flow velocity through the porous electrode is zero. Furthermore, we assume that the concentration and potential depend only on the coordinate y . We take into account the concentration variations by making a mass balance. The transfer current j^* represents the number of moles that react per unit time and per unit volume. This quantity corresponds to the source term of Eq. (13) of Chapter 3. In a steady state for a given point y , this quantity must be equal to the variation of the flux density of diffusion ($dN_a/dy = dj_i/nF dy$) at that point. Denoting by D_{eff} an effective diffusion coefficient that takes into account porosity and tortuosity we can therefore

write the relationship [which is a particular case of Eq. (13) of Chapter 3]

$$D_{\text{eff}} \frac{d^2 c}{dy^2} = \frac{j^*}{nF} = \frac{1}{nF} \frac{dj_l}{dy} \quad (58)$$

The boundary conditions are taken as $c = c_0$ at $y = b$ and $dc/dy = 0$ at $y = 0$. The first condition expresses the fact that the solution is considered well stirred and therefore no substantial diffusion layer develops in the free solution on the front side of the porous electrode. The second condition expresses the fact that there is no flux of the reacting species through the feeder plate G.

The transfer current j^* is related to the potential through (45) where the concentration c is not variable. The potentials ϕ_m and ϕ_l are related to the current densities j_m and j_l through Eqs. (41) and (42), as in the problem of Section 7.1. The combination of these equations yields a differential equation that must be solved simultaneously with Eq. (58). This simultaneous integration gives the variation of the concentration and potential as a function of y from which one obtains the distribution of the transfer current $j^* = f(y)$.

The results are shown in Figure 32 in dimensionless form for $Wa = 10$ and $Wa' = 0.5$. It shows on the one hand the ratio $\xi = c/c_0$ of the concentration at point y^* to that in the free solution, and on the other hand the quantity j^*b/J which has already been considered in Section 7.1 and which is a normalized (dimensionless) transfer current. The curves correspond to various

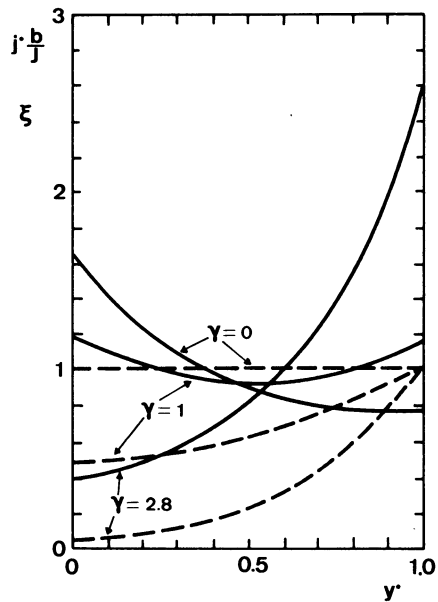


Figure 32. Tertiary distribution of the transfer current j^*b/J (—) and of the concentration ξ (---) in a three-dimensional electrode with $Wa = 10$ and $Wa' = 0.5$ (Reference 76).

values of the dimensionless parameter γ defined by

$$\gamma = \frac{Jb}{nFD_{\text{eff}}c_0} \quad (59)$$

The parameter γ characterizes the total current density J flowing through the porous electrode (see Section 7.1). The curve $\gamma = 0$ corresponds to the secondary distribution. It is seen that with increasing current density the distribution becomes first more uniform and then again more asymmetric but in the opposite direction: The transfer current increases toward the end of the electrode facing the free solution, instead of the opposite end. This can be qualitatively explained as follows. For Figure 32 $Wa/Wa' = 20$, i.e., the resistance of the liquid phase R_l is small compared to R_m [Figure 25(a)]. In the secondary distribution the ionic current penetrates deeply into the electrode and the reaction takes place mainly near the feeder plate at $y = 0$ (curve $\gamma = 0$). Inasmuch as J increases, the solution within the electrode is depleted more and more with respect to the consumed species, and this tends to prevent the ionic current from penetrating into the body of the electrode. At $\gamma = 2.8$, the reaction occurs mainly in the vicinity of the free electrolyte, not because the resistance of the liquid phase is large, but because in the region close to the feeder plate there is not enough substance available for the reaction.

The curves of Figure 32 have been calculated with certain simplifying assumptions. The application of Eq. (41) implies that the conductivity of the solution is constant in spite of the concentration variation. This condition is realized when the solution contains, in addition to the reacting species, a supporting electrolyte in much larger concentration. It has also been postulated that the liquid completely fills the voids of the electrode and does not flow through it.

Other cases have also been treated in the literature. Coeuret⁽⁹⁵⁾ and Gaunand *et al.*⁽⁹⁶⁾ as well as Alkire and Gracon⁽⁹⁷⁾ (see also reference 132) have recently discussed electrodes in which the solution flows through the porous structure. Electrodes with pores partially filled with gas are utilized in fuel cells where one of the reacting species is a gas (for a more detailed discussion of this type of electrode, see references 88 and 98 and Chapter 5 of this volume). Grens and Tobias⁽⁸²⁾ have calculated the current distribution during the transient state which precedes (at the beginning of electrolysis) the establishment of a steady state (see also references 88 and 166). Euler^(99,100) and Bonnemay with coworkers⁽¹⁰¹⁾ have considered the case where the porous system is anisotropic, i.e., the effective conductivity and diffusion coefficient depend on direction. For further information about mass transport in a three-dimensional electrode the reader is referred to Chapters 5 and 6 of this volume.

8.5. Particular Case of Limiting Current—Mass Transport Control

8.5.1. General Remarks

The general case where one takes into account both concentration and activation overpotentials is a most complex one. In this section we will consider an extreme case—that of the limiting current—where the concentration at the electrode–solution interface is virtually zero for a species consumed at the electrode. The general theory of the limiting current is treated in Chapters 2 and 3. Here we will deal with the special aspect of current distribution only which can be deduced, however, from the fundamentals discussed in Chapters 2 and 3.

At the limiting current the concentration overpotential η_c and its derivative with respect to current density, $d\eta_c/dj$, tend toward infinity. Their influence is then completely predominant compared to that of activation overpotential, and the current distribution is *controlled by the transport phenomena* (diffusion, convection). The mass transport imposes the current distribution, which is its own. Thus, one has a situation that is quite different from the one considered in Sections 4–7. The conductivity of the bath and the activation overpotential no longer have any influence on the distribution. The geometry of the system has an effect only inasmuch as it acts on the mass transport. The Wagner number, defined with the total overpotential $d\eta/dj$, becomes infinite.

Let us again distinguish between the two cases which we have considered in Sections 8.2 and 8.3 (microprofile, macroprofile, Figure 29).

8.5.2. Distribution Over a Microprofile

8.5.2.1. General Effects

If the height of the microprofile a is very small compared to the thickness of the diffusion layer δ , and if there are no crystallographic effects, the current distribution over the microprofile is governed, at the limiting current, by diffusion, because the hydrodynamic flow is virtually zero in the immediate vicinity of the cathode due to the friction forces (unstirred Nernst diffusion layer, see Section 1, Chapter 3). Convection controls the transport of the reacting species toward the outer parts of the diffusion layer, but the further, finer distribution of the transport flux over the serrated surface is determined by diffusion. The crests are favored from the viewpoint of diffusion; they are better accessible to diffusion than the recesses and the local current density is larger there. In fact, in this steady state the current distribution at the limiting current is the same as the primary distribution because Fick's second

law for the steady state,

$$\nabla^2 c = 0 \quad (60)$$

is formally identical with the Laplace law, and the boundary conditions are also the same ($c_e = 0 = \text{const}$ at the limiting current; $\phi_e = \text{const}$ in primary distribution). A more detailed discussion of this approach has been given by Kardos and Gardner-Foulke^(9,104) (see also the review paper on distribution over microprofiles by Despič and Popov⁽¹¹³⁾). In the following we will discuss some practical consequences of the mass transport control of electrochemical reactions on microprofiles.

8.5.2.2. Formation of Metallic Powders at the Limiting Current

In Section 8.2 we noted that, on the microscopic scale, crystallographic effects may play an important role. However, at the limiting current, where the concentration overpotential η_c becomes infinite, its influence is very strong compared to those of other effects. Thus, there is a marked tendency to deposit more rapidly metal on a crest than in a recess; i.e., there is a strong tendency to amplify small excrescences initially present, or formed later on, due to the heterogeneities of the surface. Metallic deposits obtained electrolytically at the limiting current are therefore extremely rough or powdery. This is a very general rule verified for many systems.^(90,102,113)

At the end of Section 8.1 we have mentioned that a profile with a given height may, depending on the thickness of the diffusion layer, behave like a microprofile or like a macroprofile. We have made use of this fact for a verification of the hypothesis of the diffusion-current distribution mechanism of powder formation at the limiting current.⁽¹⁰³⁾ Copper and silver have been deposited by current pulses of very short duration, of the order of a microsecond. Under these circumstances, the thickness of the diffusion layer has little time to increase and remains very small during the whole pulse. In our experiments δ was of the order of $0.1 \mu\text{m}$, i.e. 100–1000 times smaller than under the usual conditions. One should then expect a strong diminution of the amplification of roughness through the tertiary current distribution. Indeed we have found that no metallic powders were formed and that the roughness of the deposits was very small at very high pulse-current densities ($150\text{--}250 \text{ A cm}^{-2}$), although the interfacial concentration drops rapidly to zero after the beginning of the pulse, so that during the major part of the pulse one has limiting-current conditions.^(103,192)

8.5.2.3. Cathodic Levelling

When the electrolyzed solution contains certain organic additives (e.g., thiourea), the deposition of a metal below the limiting current takes place preferentially in the recesses, resulting in a leveling of the surface. This phenomenon plays an important role in electroplating (see Chapter 7, Volume 2). The influence of leveling additives can be explained in the following

manner. These substances are codeposited with the metal (or decompose on the interface) at a rate controlled by their transport toward the interface. Since the crests are privileged from the viewpoint of diffusion, they are preferentially covered by the additive or its decomposition products. This creates a situation quite different from that which we have hitherto considered; namely, the current-potential relationship is no longer constant along the interface. If the additive is an inhibitor, i.e., if it increases the overpotential, the latter will be larger, and the local current density therefore tends to be smaller at the peaks than in the recesses. The resulting leveling is as if it were the inverse phenomenon of the powder formation at the limiting current. The mass transport control of deposition of the metal amplifies the roughness, whereas the control of the codeposition of an additive decreases it. This mechanism of leveling has been discussed in more detail in review articles by Kardos and Gardner-Foulke.^(9,104)

It has been shown by Osterwald⁽¹⁹⁰⁾ that, in addition to the above type of cathodic leveling, this phenomenon can also take place through another mechanism. Certain additives act catalytically during metal deposition, i.e., lower the overpotential. By accumulating in the recesses for geometric reasons, they enhance the metal deposition there and thus level the deposit.

8.5.2.4. Anodic Leveling—Electropolishing

Under certain conditions the anodic dissolution of a metal is controlled by mass transport. The local current density is then larger on protruding parts, which are thus preferentially dissolved. This results in a leveling of the surface.⁽¹⁰⁷⁾ At first sight one would be tempted to say that the transport process controlling the dissolution is diffusion of the cations formed at the anode toward the bulk of the bath. In reality, one has rather (in general) a diffusion toward the interface of cation acceptors (i.e., of complexing or, more generally, solvating substances), without which the passage of the metal into the solution could not take place. In the concentrated systems utilized in electropolishing, this acceptor can be, for example, water, the concentration of which in the diffusion layer is strongly decreased.^(105,106)

Another mechanism which may be involved in certain cases is the precipitation of a salt in the recesses, where the solution becomes oversaturated due to the slower diffusion. The recesses would thus be blocked for the dissolution of the metal.^(195,196)† In one way or the other, the control of the current distribution by diffusion plays an essential role in the mechanism of electropolishing (see, e.g., references 106, 107, and 108). This mechanism is discussed in more detail in a review article by Epelboin.⁽¹⁰⁶⁾ For further information about electropolishing the reader is referred to Chapter 8 of Volume 2.

† According to a recent work⁽¹⁹⁷⁾ the precipitation of a salt is mainly involved in the mechanism of anodic brightening (smoothing on the scale of the wavelength of light), as distinguished from leveling (smoothing on a larger scale in the range of tens of μm).

8.5.3. Distribution Over a Macroprofile

In this case, the height a of the profile is very large compared to the thickness of the diffusion layer δ . In convection-free diffusion, δ is then independent of location, except for a zone near a free edge of the electrode, the extent of which is of the order of magnitude of δ . However, hydrodynamic effects can cause long-range variations of δ , as is the case for a plate in laminar flow (Section 8.3 and Chapter 3, Section 2.3). At a macroprofile, the limiting-current distribution is essentially determined by hydrodynamic factors. The distribution can be uniform, but only if the hydrodynamics are uniform, as is the case for a rotating disk in laminar flow. In that case, the macroscopic throwing power is extremely good ($Wa \rightarrow \infty$), in contrast to the microscopic throwing power, which as seen in Section 8.5.2 is extremely poor.

Let us now consider the influence of hydrodynamics on δ .^(23,109) Table 1 shows the variation of δ and of the local limiting-current density j_{lim} along the electrode for a few typical systems. For certain situations the distribution of the limiting current is virtually uniform, for others it is not. However, even when there is a variation of the local current density, the exponent p of x in the relationship $j_{lim} \approx x^{-p}$ is small, i.e., the variation of j_{lim} with the distance x is rather slow.

Nevertheless, the departure from a uniform distribution of the limiting current may be considerable, as illustrated by the broken line of Figure 4 which applies to the geometry of Figure 3, with laminar flow of the fluid parallel to the electrodes. The characteristic feature of the tertiary distribution, which has been mentioned already in Section 8.3, is now even more marked than in Figure 31. The curve is disymmetric, with an increase of the current toward the upstream end, in contrast to the primary distribution shown by the full line, where there is no difference between the two ends of the electrodes.

Table 1
Variation with Location of the Diffusion Layer Thickness (δ) and of the Limiting Current for Some Hydrodynamic Regimes

	δ	j_{lim}
Natural convection		
Vertical electrode	$\approx x^{1/4}$	$\approx x^{-1/4}$
Horizontal electrode	independent of x	independent of x
Forced convection		
Plate in laminar flow	$\approx x^{1/2}$	$\approx x^{-1/2}$
Plate in turbulent flow	independent of x	independent of x
Rotating disk (laminar flow)	independent of r	independent of r
Rotating disk (turbulent flow)	$\approx r^{-0.8}$	$\approx r^{0.8}$
Electrode with gas evolution	probably often independent of x	probably often independent of x

x , distance from the end of the cathode
 r , distance from the center

An interesting case is that of gas-evolving electrodes, commonly encountered in industrial electrolytic processes. We consider the limiting current of, say, copper deposition, or of the reduction of ferric ions to ferrous ions, which is controlled by the transport toward the cathode of the consumed species, this mass transport being accelerated through the concomitant gas evolution. We do not have exact information about the distribution of such a limiting current (or of the corresponding equivalent thickness of the diffusion layer δ) along the gas-evolving electrode. Janssen and Hoogland⁽¹¹⁰⁾ have found for a vertical electrode a weak variation of δ with the height ($\delta \approx x^{0.13}$). In an earlier work⁽¹¹¹⁾ we have observed no influence of the height x . In general, the variation of δ is probably often small, or nonexistent, for gas-evolving electrodes.† For further information about mass transfer at gas-evolving electrodes the reader is referred to Chapter 7 of this volume.

9. Influence of a Few Other Kinds of Overpotentials

We will conclude our discussion of the influence of overpotential on the current distribution by a few remarks on the existence and influence of some types of overpotential other than those already considered. In our treatment of the role of concentration overpotential in Section 8 we have tacitly assumed that it is solely governed by the transport phenomena (diffusion, convection, migration). However, one can also have the case, frequent in organic electrochemistry, that the species consumed at the electrode is regenerated through a homogeneous preceding reaction which takes place in the diffusion layer^(25a) (see Section 8, Chapter 3). Thus, one has a reaction layer in which the diffusion is coupled with a chemical reaction. The interfacial concentration, and therefore the overpotential calculated from the latter, depend on the rate of the chemical reaction. The influence of this kind of overpotential (called reaction overpotential) on the current distribution does not seem to have drawn much attention so far. Qualitatively, this overpotential acts probably in the same direction as the pure concentration overpotential (i.e., as if there were no preceding reaction). Let us note, however, that the thickness of the reaction layer is smaller the faster the preceding reaction is. It may be much smaller than that of the diffusion layer which would establish itself under the

† Since there is a concomitant gas evolution, we have here, in reality, the case of a distribution with two simultaneous electrode reactions, which will be discussed more fully in Section 10. However, since we are considering here only the limiting current of, say, the reduction of ferric ions, this limiting current and its distribution are not affected by the potential distribution within the solution, but only by the stirring effect of the gas evolution. The situation is essentially the same as if this stirring were achieved in another manner (e.g., by rotating a disk), without simultaneous second electrode reaction. However, any nonuniformity of the gas-evolution reaction will cause a nonuniformity of its stirring effect and thus a variation of the local limiting-current density.

same hydrodynamic conditions, in the absence of a preceding reaction. Therefore under certain conditions a surface profile of a given height can behave as a macroprofile from the viewpoint of pure concentration overpotential, but as a microprofile from the viewpoint of reaction overpotential.

Another possible effect is that the electrode is covered by a solid layer, which is thin but has a high resistance (such as an oxide film). This case is encountered mainly in anodic reactions. One then has an additional resistance in series with the resistance due to the activation overpotential ($d\eta_a/di$) and with that of the electrolyte. This resistance acts in the same direction as the activation resistance: If it is uniform along the interface, it tends to render the current distribution more homogeneous. An interesting case is that of the manufacture of electrolytic condensers with aluminum or tantalum oxide. They have a three-dimensional porous structure (pellets) and are of the same type as the electrode discussed in Section 7. The oxide, which constitutes the dielectric, is produced electrolytically on the walls of the pores. We may apply the model of Figure 26(a), where R_a is to be replaced by the resistance of the oxide, which is the main resistance for the passage of the charges from the solid to the liquid phase. Since this resistance is very high compared to R_m and R_b , the current penetrates easily into the interior of the porous structure.

Finally, let us remark that in the problems of current distribution, one usually assumes that the current is faradaic; i.e., it corresponds to an electrochemical reaction that takes place at the interface. However, immediately after switching on the electrolysis current, during a lapse of time of the order of a millisecond, the current is used mainly to charge or discharge the electrochemical double layer at the interface (capacitive current). The distribution of the capacitive current over a rough surface, or within a porous electrode, has been treated by de Levie.⁽⁸⁸⁾ This kind of current distribution plays a role in alternating current or in pulsed current. It is shown that the penetration of the capacitive current into a recess, slot, or porous structure depends on frequency.

10. Current Distribution in the Case of Simultaneous Electrode Reactions

In the preceding sections we have assumed that a single reaction takes place at the electrode. However, we have already noted in Section 6.3.6 that due to the variation of the interfacial potential difference the current efficiency may not be 100%, at least in some parts of the electrode. In fact, in actual practice, simultaneous electrode reactions are very common. In the literature, however, this case has received very little attention in contrast to the current distribution for a single electrode reaction.

Let us assume that two species 1 and 2 can be consumed in a cathode reaction. If 1 reacts at a much less negative potential than 2 and is present in not too large concentration, one will easily have a situation where the reaction consuming species 1 takes place at the limiting current. The distribution of that reaction rate along the electrode can then be calculated from mass transfer considerations without taking species 2 or the potential distribution in the solution into account, especially if there is an excess of indifferent electrolyte. An example is the electrowinning of copper from a solution containing a small amount of Ag^+ ions. The rate of deposition of the silver (but not that of the copper) is controlled by the mass transport and the silver content of the deposit varies along the electrode according to the variation of the mass transport rate. In the electrolytic production of copper (where δ decreases from bottom to top along the vertical cathode because of the stirring of the solution by the oxygen at the anode), one indeed observes a corresponding variation of the silver content of the deposit.⁽¹⁴⁾ Similar effects may be important in the electrolytic formation of alloys: When one of the metals is much more noble than the others and is deposited at its limiting rate, the composition of the alloy changes locally according to the variation of the mass transport rate.

If the cathode potential is sufficiently negative, the two reactions (which we have envisaged above) will both take place at their limiting currents: this is the simplest situation for which the partial currents of the *two* reactions can be calculated from the general rules of mass transport. In principle, Table 1 applies. Matsuda⁽¹⁴¹⁾ has treated the mass transport controlled current distribution at a number of electrode configurations for a variety of multiple reaction sequences.

Another situation, which is in fact frequent, is that neither of the two reactions is running at its limiting rate. Let $1j_x$ and $2j_x$ be the partial local current densities for reactions 1 and 2. They depend on the potential which varies along the electrode. The current efficiency for reaction 1 is $1j_x/(1j_x + 2j_x)$. If $1j_x$ and $2j_x$ vary differently with the potential, the variation of the latter along the interface will result in a change in the current efficiency along the electrode. A common example of two simultaneous reactions running below the cathodic limiting current is metal deposition and hydrogen evolution. This situation is frequently encountered in electroplating and electrometallurgy. An industrially important example is the deposition of zinc from acid zinc sulfate solutions. The overpotential for the concomitant hydrogen evolution increases much faster with current density than the overpotential for the metal deposition, the result being an improvement of the current efficiency for metal deposition with increasing overall current density. Therefore, the current efficiency for metal deposition is larger in the parts of the electrode which carry a higher overall current density. The nonuniformity of the distribution is thus reinforced: The distribution of the thickness of the metal is less uniform than the distribution of the overall current density.

In electroplating, in the case of simultaneous hydrogen evolution, one sometimes speaks of metal distribution instead of current distribution in order to take into account the above mentioned fact that in the case of several reactions the distribution of the partial current density may be different from that of the overall current density. Sometimes one also finds in the literature the term tertiary current distribution referring to a situation where several reactions occur simultaneously. (In the present text, however, we have reserved this name for the case where concentration overpotential, in addition to activation overpotential, influences the current distribution; see Section 8.1.)

A quantitative approach is as follows. The partial current densities for reactions 1 and 2 are functions of the potential difference $\Delta\phi$ over the interface

$$\begin{aligned} {}_1j_x &= f_1(\Delta\phi) \\ {}_2j_x &= f_2(\Delta\phi) \end{aligned} \quad (61)$$

The functions f_1 and f_2 can be taken as being in the form of Eq. (33). The overall current density j is given by the sum of these two functions

$$j = {}_1j_x + {}_2j_x = f_1(\Delta\phi) + f_2(\Delta\phi) \quad (62)$$

In the linear approximation mentioned in Section 6.3.1, we have

$$\Delta\phi = R_1{}_1j_x + (\Delta\phi_0)_1 = R_2{}_2j_x + (\Delta\phi_0)_2 \quad (63)$$

with $R_1, R_2, (\Delta\phi_0)_1, (\Delta\phi_0)_2 = \text{const}$ or

$$j = \Delta\phi(1/R_1 + 1/R_2) - (\Delta\phi_0)_1/R_1 - (\Delta\phi_0)_2/R_2 \quad (64)$$

and

$$\frac{d\Delta\phi}{dj} = (1/R_1 + 1/R_2)^{-1} \quad (65)$$

The secondary distribution can be calculated by integrating the Laplace equation [Eq. (2)]. The boundary condition for the insulating surfaces is the same as before [Eq. (6)]. For the second boundary condition, Eq. (30) has to be replaced by the relationship which is the inverse of Eq. (62):

$$\Delta\phi = f'({}_1j_x + {}_2j_x) \quad (66)$$

In the case of the linear approximation this takes the form

$$\Delta\phi = j(1/R_1 + 1/R_2)^{-1} = \frac{[R_2(\Delta\phi_0)_1 + R_1(\Delta\phi_0)_2](R_1 + R_2)}{R_1R_2}$$

The integration of the Laplace equation yields the repartition of the potential within the solution as well as along the electrode surface (ϕ_e). From this repartition one obtains, with the help of the equation,

$$-\left(\frac{\partial\phi}{\partial n}\right)_e = j = f_1(\Delta\phi) + f_2(\Delta\phi) \quad (67)$$

the distribution of the global current. The distribution of the partial currents and of the current efficiency is obtained from Eq. (61).

The problem of current distribution with simultaneous electrode reactions has been solved numerically by Alkire and Mirarefi⁽¹³⁵⁾ for simplified conditions. They considered simultaneous deposition of copper and reduction of ferric to ferrous ions from a solution of $\text{CuSO}_4 + \text{H}_2\text{SO}_4 + \text{FeSO}_4 + \text{Fe}_2(\text{SO}_4)_3$. The cell arrangement is shown in Figure 33. In this model the cathode is tubular with a radius r_0 small compared to the length L so that the potential distribution perpendicular to the wall of the tube need not be considered. That is, one can regard the potential ϕ as being constant within a cross section of the tube located at a distance x from the leading edge. The potential distribution is thus assumed to be essentially one-dimensional and it is described by the equation

$${}_1j_x + {}_2j_x = \frac{r_0 \kappa}{2} \frac{d^2 \phi}{dx^2} \quad (68)$$

The equation expresses the result of a charge balance for an infinitesimal volume of length dx , ${}_1j_x$ and ${}_2j_x$ being pseudohomogeneous source terms since they correspond to the rate at which charges are provided to the infinitesimal volume.

The counterelectrode is placed outside of the tube (Figure 33). The solution is flowing through the tube in laminar flow, the mass transfer behavior being constrained to the entrance (Levêque) region. A first relationship between the interfacial concentration c_e and the reaction rate (and thus the partial local current density j_x) is obtained for each species by integrating for that species the equation of convective diffusion according to the Levêque approximation

$$\frac{4Q}{\pi r_0^3} y \frac{\partial c_i}{\partial x} = D_i \frac{\partial^2 c_i}{\partial y^2} \quad (69)$$

where Q is the volumetric flow rate. A further relationship between the partial

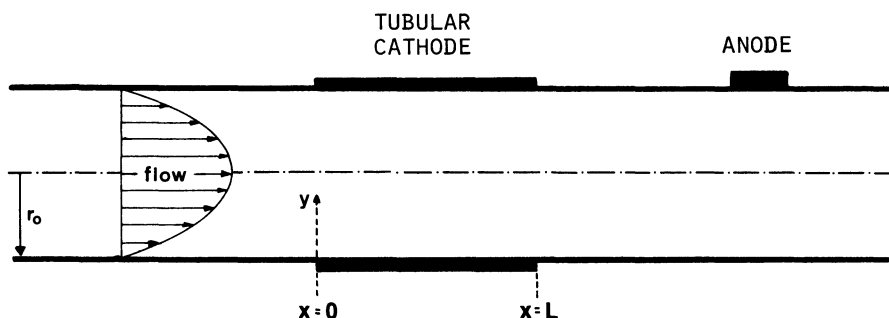


Figure 33. Tubular electrode model for calculation of current distribution for the case of two simultaneous electrode reactions.

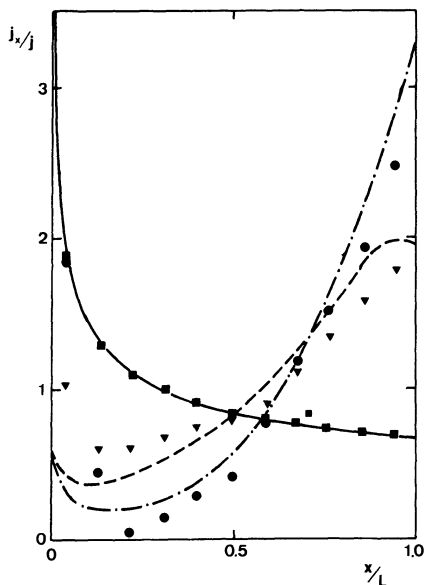


Figure 34. Experimental and calculated tertiary current distribution in a two reaction system ($\text{Cu}^{2+} \rightarrow \text{Cu}$, $\text{Fe}^{3+} \rightarrow \text{Fe}^{2+}$): ϕ_m 50 mV, - · - · - calculated curve, ●, experimental point; $\phi_m = 250$ mV, --- calculated, ▼, experimental; $\phi_m =$ limiting current, — calculated, ■, experimental.

current densities, the interfacial concentration, and the potential at the electrode is provided by equations of the form of Eq. (57) for each species.

The calculation of Alkire and Mirarefi therefore takes into account both concentration and potential distribution as well as activation overpotential. The numerical integration of the above equations involves an iterative procedure starting from a trial potential distribution which was assumed to be linear between $x = 1$ and $x = L$. This assumed potential distribution yields a trial interfacial concentration and current distribution which is used to make a new guess for the potential distribution. The authors finally obtained a complete solution of the problem including the distribution of the partial local current as well as that of the total current. They also made an extended experimental study of the system using a sectioned electrode. Figure 34 shows some of the experimental results and the results of the computation for the purpose of comparison. On the ordinate is plotted the ratio of the total current density on a section to the average total current density. The different curves correspond to various values of the applied potential ϕ_m . For further experimental details the reader is referred to the original literature. The agreement between experiment and theory is fair. This paper illustrates the immense progress recently made in the treatment of the most complex current-distribution problems.

11. Historical Note

The first recorded observations of an uneven current distribution in electrolysis date back to the experiment of Nobili in 1834. He used a strongly

alkaline solution of lead oxide, the anode was a horizontal sheet of gold or platinum, and the cathode consisted of a platinum wire the tip of which dipped into the solution.⁽¹¹⁵⁾ Upon electrolysis, concentric rings appear, centered on the projection of the cathode wire on the anode. They are due to interference effects caused by lead peroxide deposits of various thicknesses. The phenomenon was interpreted theoretically eleven years after Nobili's publication by Edmond Becquerel,⁽¹¹⁶⁾ who was the father of the famous discoverer of radioactivity, Henry Becquerel. He did not find the right equation for the current distribution, however. The phenomenon, which in the meantime had become known as Nobili's rings, was reexamined later by various authors, in particular, by E. Dubois-Raymond⁽¹¹⁷⁾ and by Bernhard Riemann⁽¹¹⁸⁾ (the one who introduced the concept of Riemann spaces).

Although the possible role of overpotential in current distribution was already mentioned by Dubois-Raymond in 1847, it was Weber who for the first time in 1873 gave mathematical considerations to the influence of overpotential on current distribution. Weber⁽¹¹⁹⁾ enunciated what he called the second boundary-value problem of potential theory, which incorporates a linear polarization, in contrast to the first boundary-value problem in which polarization takes no part. In later decades the problem of current and potential distribution were treated mainly by mathematicians and physicists in the context of general potential theory, rather than in connection with electrochemistry. It was only in 1940–42 that Kasper⁽²⁶⁾ presented a thorough theoretical treatment from the viewpoint of electrolysis, especially electroplating. His method was discussed in the section on primary current distribution (Section 5.2). Kasper also gave the solution for a simple case of secondary current distribution.

Although electrochemistry was a well-established technology by the end of the 19th century, the theory of current distribution was astonishingly undeveloped until very recently. In 1950 Kronsbein⁽⁷⁸⁾ in his excellent review of earlier literature writes: "This historical review shows that existing mathematics is not capable of solving any but the most simple problem of current distribution, and those usually only by disregarding polarization of the electrodes." It is only in the last 20 years that practical problems of current distribution of some complexity could be solved, with the help of electronic computers. Their availability marked a turning point. In the last decades rapid progress was made thanks mainly to scientists representing the Berkeley school of electrochemical engineering (Tobias, Newman, Alkire, and others). In Russia it is mainly Poddubnyi^(32,39,48,152) and Levich and in France, Rousselot^(2,17) who mainly contributed to the recent advance of the field.

It should be noted, however, that many early qualitative papers have been written over the years in connection with electroplating. The applications of electroplating became significant soon after 1840, when improved current sources became available. The expansion of plating into mass production created a strong economic urge demanding more knowledge of the practical

operations of the various plating processes including metal distribution. The numerous papers dealing with current distribution from the practical viewpoint of the plater in the period 1910–1940 have been quoted in the review paper by Kronsbein. Except for the already mentioned work by Kasper, the publications of that period connected with plating were nonmathematical and dealt either with experimental results on metal distribution, or with the introduction of test methods, such as Pan's cavity scale⁽¹⁸⁹⁾ and the bent cathode test,^(11,157) or devices such as the Haring–Blum, Field, and the Hull cells (see Sections 6.2 and 6.3.5) which were designed to characterize the throwing power—a qualitative concept introduced during that time and which has been discussed in Sections 6.2 and 6.3.5. Although Hoar and Agar⁽⁴⁵⁾ presented as early as 1947 a lucid discussion of the combined influence of geometry, conductivity, and overpotential on current distribution, and recognized the importance of the Wagner number, this concept found little application in plating until now. The recent sophisticated theoretical papers have their roots in the general advance of electrochemical engineering rather than in the development of the fundamentals of electroplating.

Auxiliary Notation

a	height of crest (Figure 29) (m)
a'	distance crest–recess (Figure 29) (m)
b	depth of three-dimensional electrode (m)
d, d', d'', d'''	distances from electrode to isolating walls (Figures 1, 10, and 19) (m)
e	distance between electrodes [Figure 27(b)] (m)
l'	electrode height (m)
u	electrode thickness [Figure 27(b)] (m)
A	active area per unit volume (m^{-1})

References

1. E. Mantzell, *Z. Elektrochem. Ber. Deutsch. Bunsenges.* **41**, 10 (1935).
2. R. H. Rousselot, In: *Proceedings of the International Conference on Protection against Corrosion by Metal Finishing*, Basel, 1966, p. 39, Forster Verlag, Zurich (1966).
3. J. Steiner, *Z. Phys. Chem.* **196**, 235 (1950); *Arch. Tech. ATM Blatt* **8227**, 2 (1950); see also *Z. Phys. Chem.* **200**, 53 (1952).
4. J. Steiner and K. Schery, *Metalloberfläche* **3**, B129 (1951); **4**, B113 (1952).
5. W. Nohse, *Die Untersuchung galvanischer Bäder in der Hull-Zelle*, Leuze Verlag, Saalgau/Württemberg, Germany (1965).
6. N. Ibl, W. Rüegg, and G. Trümpler, *Helv. Chim. Acta* **36**, 1624 (1953).
7. T. Bolch and G. G. Weiler, *Metalloberfläche* **29**, 386 (1975).
8. V. Marathe and J. Newman, *J. Electrochem. Soc.* **116**, 1704 (1969).
9. O. Kardos and D. Gardner-Foulke, *Advances in Electrochemistry and Electrochemical Engineering*, Vol. 2, p. 145, P. Delahay and C. W. Tobias, Eds. Wiley, New York and London (1962).

10. D. Gardner-Foulke and O. Kardos, *Proc. Am. Electroplaters Soc.* **43**, 172 (1956).
11. W. Rüegg, *Oberflächenbehandlung von Zinkdruckguss*, Juris Verlag, Zürich (1970).
12. B. Stverak, I. Roušar, J. Hostomsky, V. Cezner, and M. Sob, *Radioisotopy* **13**, 151 (1972); *Chem. Abstr.* **77**, 13125j (1972).
13. H. Bode and J. Euler, *Electrochim. Acta* **11**, 1211, 1221, 1231 (1966).
14. V. A. Ettel, B. V. Tilak, and A. S. Gendron, *J. Electrochem. Soc.* **121**, 867 (1974).
15. P. Neufeld and D. V. Patel, *Trans. Inst. Metal Finishing* **52**, 71 (1974).
16. J. J. Christie and J. D. Thomas, *Plating* **52**, 855 (1965).
17. R. H. Rousselot, *Ingénieurs Automobile* **33** Oct. (1960).
18. R. H. Rousselot, *Répartition du potentiel et du courant dans les électrolytes*, Dunod, Paris (1959).
19. C. W. Tobias, *J. Electrochem. Soc.* **106**, 833 (1959).
20. G. G. Weiler and Th. Bolch, *Galvanotechnik* **66**, 785 (1975).
21. G. G. Weiler and K. Zerweck, *Metalloberfläche* **29**, 111 (1975).
22. J. Newman, *Electrochemical Systems*, Prentice-Hall, Englewood Cliffs, NJ (1973).
23. N. Ibl, *Tech. Ingénieur* **12**, D-902 (1976).
24. P. Gallone, *Principi dei Processi Elettrochimici*, Tamburini Ed., Milano (1970).
25. G. Milazzo, (a) *Electrochimie*, Vol. 1, p. 188, Dunod, Paris (1969); (b) *Elektrochemie*, Vol. 1, pp. 343–354, Birkhäuser Verlag, Basel (1980).
26. C. Kasper, *Trans. Electrochem. Soc.* **77**, 353 (1940); **78**, 131 (1940); **82**, 153 (1942).
27. C. Wagner, *Plating* **48**, 997 (1961).
28. F. Hine, S. Yoshizawa, and S. Okada, *J. Electrochem. Soc.* **103**, 186 (1956).
29. S. Okada, S. Yoshizawa, and F. Hine, *Mem. Fac. Eng. (Kyoto Univ.)* **14**, 63 (1952).
30. E. Weber, *Bull. A.S.E.* **51**, 1011 (1960).
31. H. F. Moulton, *Proc. Lond. Math. Soc. (Ser. 2)* **3**, 104 (1905).
32. A. I. Maslii, N. P. Poddubnyi, and B. Ya. Pirogov, *Elektrokhimiya* **6**, 70 (1970).
33. J. A. Klingert, S. Lynn, and C. W. Tobias, *Electrochim. Acta* **9**, 297 (1964).
34. J. Newman, *Ind. Eng. Chem.* **60**, 12 (1968).
35. J. Newman, *J. Electrochem. Soc.* **113**, 501, 1235 (1966).
36. M. Abramowitz and I. A. Stegun, *Handbook of Mathematical Functions*, p. 608, National Bureau of Standards Washington, D.C. (1964).
37. N. Ibl, *Oberfläche-Surface* **16**, 23 (1975).
38. C. Wagner, *J. Electrochem. Soc.* **98**, 116 (1951).
39. N. P. Poddubnyi and E. I. Rudenko, *Elektrokhimiya* **4**, 943 (1968).
40. R. Alkire and A. A. Mirarefi, *J. Electrochem. Soc.* **120**, 1507 (1973).
41. W. R. Parrish and J. Newman, *J. Electrochem. Soc.* **117**, 43 (1970).
42. V. T. Ivanov and G. A. Kandrat'eva, *Elektrokhimiya*, **10**, 1395 (1974).
43. R. Alkire and R. Varjian, *J. Electrochem. Soc.* **121**, 622 (1974). (a) R. Alkire, *J. Electrochem. Soc.* **120**, 900 (1973).
44. C. W. Tobias and R. Wijsman, *J. Electrochem. Soc.* **100**, 459 (1953).
45. T. P. Hoar and J. N. Agar, *Discuss. Faraday Soc.* **1**, 162 (1947).
46. I. Roušar, *J. Electrochem. Soc.* **116**, 676 (1969).
47. V. I. Ivanov and A. I. Shafeev, *Elektrokhimiya* **9**, 1191 (1972).
48. N. P. Gnusin, N. P. Poddubnyi, E. N. Rudenko, and A. G. Fomin, *Elektrokhimiya* **1**, 452 (1965).
49. C. Wagner, *Electrochim. Acta* **12**, 131 (1967).
50. C. Wagner, *J. Electrochem. Soc.* **107**, 445 (1960).
51. E. Mantzell, *Z. Elektrochem.* **42**, 303 (1936). (a) B. Miller and M. I. Bellavance, *J. Electrochem. Soc.* **120**, 42 (1973).
52. S. Bruckenstein and B. Miller, *J. Electrochem. Soc.* **117**, 1044 (1970).
53. W. H. Smyrl and J. Newman, *J. Electrochem. Soc.* **119**, 208, 212 (1972).
54. E. Raub, *Metalloberfläche* **12**, 353 (1958); **13**, 304 (1959); *Plating* **45**, 486 (1958).

55. J. D. Thomas, *Proc. Am. Electroplaters Soc.* **43**, 60 (1956).
56. J. Elze, *Metall.* **15**, 542 (1961).
57. S. A. Watson, *Trans. Inst. Met. Finishing* **37**, 28, 144 (1960).
58. G. E. Gardam, *J. Electrodepositors Tech. Soc.* **22**, 155 (1974).
59. S. A. Watson and J. Edwards, *Trans. Inst. Met. Finishing* **34**, 167 (1957).
60. L. B. Garmon and H. Leidheiser, Jr., *Plating* **48**, 1003 (1961); *Proc. Am. Electroplaters Soc.* **46**, 50 (1959).
61. R. H. Rousselot, *Trans. Inst. Met. Finishing* **41**, 40 (1964). (a) J. Steiner, *Z. Phys. Chem.* **201**, 161 (1952).
62. I. Roušar, A. Regner, and V. Cezner, *Collect. Czech. Chem. Commun.* **31**, 4139 (1966).
63. I. Roušar and V. Cezner, *Collect. Czech. Chem. Commun.* **32**, 1137 (1967).
64. I. Roušar, V. Cezner, and J. Hostomsky, *Collect. Czech. Chem. Commun.* **33**, 808 (1968).
65. Z. Nagy, *J. Appl. Electrochem.* **6**, 171 (1976).
66. J. E. Funk and J. F. Thorpe, *J. Electrochem. Soc.* **116**, 48 (1969).
67. B. E. Conway, E. Gileadi, and H. Oswin, *Can. J. Chem.* **41**, 2447 (1963).
68. S. K. Rangarajan, M. J. Dignam, and B. E. Conway, *Can. J. Chem.* **45**, 422 (1967).
69. J. Wojtowicz, L. Laliberté, and B. E. Conway, *Electrochim. Acta* **13**, 361 (1968).
70. A. Böhnlein, *Metalloberfläche* **24**, 210 (1970).
71. S. Ishizaka, H. Matsuda, and Y. Wada, *J. Electrochem. Soc. Jap.* **22**, 420 (1954).
72. R. Alkire and A. Tvarusko, *J. Electrochem. Soc.* **119**, 340 (1972).
73. F. Goodridge and C. J. H. King, *Technique of Electroorganic Synthesis*, Chapter II, N. L. Weinberg, Ed., Wiley, New York (1974).
74. J. Euler, *Electrochim. Acta* **13**, 1533 (1968); **18**, 385 (1973).
75. K. J. Euler and W. Nonnenmacher, *Electrochim. Acta* **2**, 268 (1960).
76. J. S. Newman and C. W. Tobias, *J. Electrochem. Soc.* **109**, 1183 (1962).
77. R. Alkire and P. K. Ng, *J. Electrochem. Soc.* **121**, 95 (1974).
78. J. Kronsbein, *Plating* **37**, 851 (1950).
79. R. E. Sioda, *Electrochim. Acta* **16**, 1569 (1971).
80. A. Winsel, *Z. Elektrochem.* **66**, 287 (1962).
81. R. Buvet, N. Guillou, and B. Warszawski, *Electrochim. Acta* **6**, 113 (1962).
82. E. A. Grens and C. W. Tobias, *Ber. Bunsenges.* **68**, 236 (1964).
83. K. J. Euler, *Electrochim. Acta* **8**, 409 (1963).
84. M. Fleischmann, J. W. Oldfield, and L. Tennakoon, *J. Appl. Electrochem.* **1**, 103 (1971).
85. J. N. Hiddleston and A. F. Douglas, *Electrochim. Acta* **15**, 431 (1970).
86. O. S. Kreuzhek and V. V. Stender, *Dokl. Akad. Nauk. SSSR* **106**, 487 (1956); **107**, 280 (1956).
87. V. S. Daniel-Bekh, *Zh. Fiz. Khim.* **22**, 697 (1948). (a) P. Bro and H. Y. Kang, *J. Electrochem. Soc.* **118**, 519 (1971). (b) Z. Nagy and J. O'M. Bockris, *J. Electrochem. Soc.* **119**, 1129 (1972).
88. R. de Levie, *Advances in Electrochemistry and Electrochemical Engineering*, P. Delahay and C. W. Tobias, Eds. Vol. 6, p. 329, Wiley, New York and London (1967).
89. J. Newman and W. Tiedemann, *A.I.Ch.E. J.* **21**, 25 (1975).
90. N. Ibl, In: *Proceedings of the International Conference Protection against Corrosion by Metal Finishing*, Basel, 1966, p. 48, Forster Verlag, Zurich (1966).
91. J. Newman, *Int. J. Heat Mass Transfer* **10**, 983 (1967).
92. P. Pierini, P. Appel, and J. Newman, *J. Electrochem. Soc.* **123**, 366 (1976).
93. K. Asada, F. Hine, S. Yoshizawa, and S. Okada, *J. Electrochem. Soc.* **107**, 242 (1960).
94. C. Wagner, *Trans. Electrochem. Soc.* **95**, 161 (1949).
95. F. Coeuret, *Electrochim. Acta* **21**, 203 (1976).
96. A. Gaunand, D. Hutin, and F. Coeuret, *Electrochim. Acta* **22**, 93 (1977).
97. R. Alkire and B. Gracon, *J. Electrochem. Soc.* **122**, 1594 (1975).
98. N. D. Bennion and C. W. Tobias, *J. Electrochem. Soc.* **113**, 589, 593 (1966).
99. K. J. Euler, *Metalloberfläche* **27**, 87 (1973).

100. K. J. Euler, *Electrochim. Acta* **18**, 385 (1973).
101. M. Bonnemay, G. Bronoël, E. Levart, and A. A. Pilla, *J. Electroanal. Chem.* **13**, 58 (1967).
102. N. Ibl, In: *Advances in Electrochemistry and Electrochemical Engineering*, C. W. Tobias and P. Delahay, Eds. Vol. 2, p. 49, Wiley, New York and London (1962).
103. N. Ibl and M. Braun, *Chem. Ing. Tech.* **45**, 182 (1973); *Oberfläche Surface* **14**, 49 (1973).
104. O. Kardos, *Plating* **61**, 129, 229, 316 (1974).
105. E. Darmois, I. Epelboin, and D. Amine, *C.R. Acad. Sci.* **230**, 386 (1950).
106. I. Epelboin, In: *Proceedings of the International Conference Protection against Corrosion by Metal Finishing*, Basel, 1966, p. 69, Forster Verlag, Zurich (1966).
107. C. Wagner, *J. Electrochem. Soc.* **101**, 225 (1954).
108. M. Daguinet, M. Froment, and M. Keddami, *J. Microscopie* **5**, 569 (1966).
109. N. Ibl, *Chem. Ing. Tech.* **33**, 69 (1961).
110. L. J. J. Janssen and J. G. Hoogland, *Electrochim. Acta* **15**, 1013 (1970).
111. N. Ibl and J. Venzel, *Metalloberfläche* **24**, 365 (1970).
112. H. Y. Cheh and C. C. Wan, *J. Appl. Electrochem.* **3**, 113 (1973).
113. A. R. Despič and K. I. Popov, *Modern Aspects Electrochem.* **7**, 199 (1972).
114. R. Alkire and G. Nicolaidis, *J. Electrochem. Soc.* **122**, 25 (1975).
115. Nobili, *Mem. Osservazioni Ed. Erudite (Florence)* **1**, 56 (1834).
116. E. Becquerel, *Ann. Chim. Phys. Ser. 3* **13**, 216 (1845).
117. E. du Bois-Reymond and W. Beetz, *Ann. Phys. Chem. (Poggendorff)* **71**, 71 (1847).
118. B. Riemann, *Ann. Phys. Chem. (Poggendorff)* **95**, 130 (1855).
119. H. Weber, *J. Reine Ange. Math. (Crelle)* **75**, 75 (1872); **76**, 1 (1873).
120. Dettner/Elze, *Handbuch der Galvanotechnik*, Vol. I/1, Carl Hanser Verlag, München (1963).
121. D. G. Foule, in F. H. Reid and W. Goldie, *Gold Plating Technology*, p. 67, Electrochemical Publications Limited, London (1974).
122. International Standard, ISO 2080-1973, definition 235 and 654.
123. P. Pierini and J. Newman, *J. Electrochem. Soc.* **124**, 701 (1977); **125**, 79 (1978).
124. P. Pierini and J. Newman, *J. Electrochem. Soc.* **126**, 1348 (1979).
125. J. J. Miksis and J. Newman, *J. Electrochem. Soc.* **123**, 1030 (1976).
126. R. Caban and T. W. Chapman, *J. Electrochem. Soc.* **123**, 1036 (1976).
127. J. Newman, *Electroanalytical Chemistry*, A. J. Bard, Ed., Vol. 6, (a) pp. 309–313; (b) pp. 313–338, Marcel Dekker, New York (1973).
128. H. E. Haring and N. Blum, *Trans. Electrochem. Soc.* **44**, 313 (1923).
129. H. S. Carslaw and J. C. Jaeger, *Conduction of Heat in Solids*, Clarendon Press, Oxford (1959).
130. L. Nanis and W. Kesselman, *J. Electrochem. Soc.* **118**, 454 (1971).
131. K. Viswanathan and D. T. Chin, *J. Electrochem. Soc.* **124**, 709 (1977).
132. P. M. Robertson, *Electrochim. Acta* **22**, 411 (1977).
133. R. Alkire and P. K. Ng, *J. Electrochem. Soc.* **124**, 1220 (1977).
134. R. Alkire and A. A. Mirarefi, *J. Electrochem. Soc.* **124**, 1043 (1977).
135. R. Alkire and A. A. Mirarefi, *J. Electrochem. Soc.* **124**, 1214 (1977).
136. R. Alkire and R. Varjian, *J. Electrochem. Soc.* **124**, 388 (1977).
137. H. Margenau and G. M. Murphy, *The Mathematics of Physics and Chemistry*, Van Nostrand, New York (1955).
138. P. C. Andricacos, H. Y. Cheh, and H. B. Linford, *Plating and Surf. Finishing* **64**, 42 (July 1977); **64**, 44 (Sept. 1977).
139. J. Newman, D. N. Hansson, and K. Vetter, *Electrochim. Acta* **22**, 829 (1977).
140. P. M. Robertson, F. Schwager, and N. Ibl, *J. Electroanal. Chem.* **65**, 883 (1975).
141. H. Matsuda, *J. Electroanal. Chem.* **15**, 109, 325 (1967); **21**, 433 (1969); **22**, 413 (1969); **25**, 461 (1970); **35**, 77 (1972); **38**, 159 (1972); **44**, 199 (1973).
142. N. Ibl, IUPAC Information Bulletin, No. 59 (July 1977).

143. B. Stverak, M. Srb, L. Vrobel, and I. Rousar, *Radioisotopy* **18**, 207 (1977); *Chem. Abstr.* **88**, 56411u (1978).
144. I. Susuma, U. Yasuo, and I. Toru, *Kinzoku Hyomen Gijutsu* **30**, 17, 22 (1979); *Chem. Abstr.* **90**, 194592w, 212136g (1979).
145. T. Ryuichi and N. Hideo, *Kinzoku Hyomen Gijutsu* **27**, 676 (1976); *Chem. Abstr.* **87**, 13376y (1977).
146. A. S. Gorbachev, E. G. Chekunov, I. A. Popova, and E. V. Vtyurina, *Zashch. Met.* **11**, 392 (1975); *Chem. Abstr.* **83**, 105315y (1975).
147. K. Madry, J. Przulski, and M. Kozlowski, *Chem. Stosow.* **22**, 389 (1978); *Chem. Abstr.* **90**, 194608f (1979).
148. A. Tvarusko, *Plating* **61**, 846 (1974).
149. O. Takeji and U. Nobuyuki, *Nippon Kagaku Kaishi* **1**, 33 (1979); *Chem. Abstr.* **90**, 129466u (1979).
150. R. A. Pavlovskii, *Elektrokhim.* **14**, 257 (1978); *Chem. Abstr.* **89**, 13898 (1978).
151. L. I. Kadaner, Z. I. Mikvabiya, and A. I. Korobka, *Zh. Vses. Khim. O-va* **22**, 470 (1977); *Chem. Abstr.* **87**, 174732b (1977).
152. A. A. Davydenko and N. P. Poddubnyi, *Elektrokhim.* **14**, 1728 (1978); *Chem. Abstr.* **90**, 63484q (1979).
153. V. T. Ivanov, G. I. Kharitonov, and G. A. Kondrat'eva, *Elektrokhim.* **11**, 1857 (1975); *Chem. Abstr.* **84**, 97118q (1976).
154. S. I. Korisheh and A. V. Pomosov, *Tsvetn. Met.* **23**, (Aug. 1978); *Chem. Abstr.* **89**, 223014w (1978).
155. A. G. Hoechst, *Neth. Appl.* **78**, 05, 205 (1979); *Chem. Abstr.* **90**, 159156k (1979).
156. A. Gerhard, Ger. Offen. 2,342,372 (24 April 1975); *Chem. Abstr.* **83**, 87423a (1975).
157. W. L. Pinner and E. M. Baker, *Trans. Electrochem. Soc.* **55**, 315 (1929).
158. E. A. Svyadoshch, Yu. Ya. Iossel, G. E. Klenov, and A. M. Vishnevskii, *Elektrokhim.* **14**, 219 (1978); *Chem. Abstr.* **88**, 128146m (1978).
159. E. McCafferty, *Corros. Sci.* **16**, 183 (1976); *J. Electrochem. Soc.* **124**, 1869 (1977); *Chem. Abstr.* **85**, 132640y (1976).
160. G. E. Klenov and A. M. Vishnevskii, *Zashch. Met.* **11**, 80 (1975); *Chem. Abstr.* **82**, 177042j (1975).
161. J. Newman, *Int. Corros. Conf. Ser.* **45** (1971); *Chem. Abstr.* **84**, 186483x (1976).
162. E. McCafferty, *Chem. Abstr.* **83**, 87123c (1975).
163. J. T. Waber, *J. Electrochem. Soc.* **101**, 271 (1954); **102**, 240 (1955).
164. W. Engelmaier, Th. Kessler, and R. Alkire, *J. Electrochem. Soc.* **125**, 209 (1978).
165. Y. Awakura, A. Ebata, and Y. Kondo, *J. Electrochem. Soc.* **126**, 23 (1979).
166. H. Gu and D. N. Bennion, *J. Electrochem. Soc.* **126**, 965 (1979).
167. J. Riggs, Ph.D. Thesis, University of California, Berkeley (1977).
168. K. J. Euler and B. Sein, *J. Appl. Electrochem.* **8**, 49 (1978).
169. L. E. Vaaler, *J. Appl. Electrochem.* **9**, 21 (1979).
170. S. H. Glarum, *J. Electrochem. Soc.* **124**, 518 (1977).
171. W. H. Smyrl and J. Newman, *J. Electrochem. Soc.* **123**, 1423 (1976).
172. R. V. Homsy and J. Newman, *J. Electrochem. Soc.* **121**, 1448 (1974).
173. G. G. Weiler, *Metalloberfläche* **30**, 26 (1976).
174. K. Zerweck, *Metalloberfläche* **30**, 212 (1976).
175. C. J. H. King and A. R. Wright, *Electrochim. Acta* **22**, 1135 (1977).
176. V. I. Belokon, B. B. Chernov and N. Y. Kovarski, *Elektrokhim.* **11**, 1655 (1975); *Chem. Abstr.* **84**, 157119c (1976).
177. P. Fedkiw, *J. Electrochem. Soc.* **127**, 1304 (1980).
178. A. N. Barabotkin, V. T. Ivanov, and G. A. Kondrat'eva, *Elektrokhim.* **11**, 800 (1975).
179. P. Csokan, *Trans. Inst. Met. Finishing* **54**, Pt. 1, 49 (1976); *Chem. Abstr.* **85**, 84612s (1976).
180. D. F. Hasko and P. Bujtas, *Trans. Inst. Met. Finishing* **54** Pt. 1, 35 (1976); *Chem. Abstr.* **85**, 84611r (1976).

181. K. I. Popov, B. J. Lazarevic, D. N. Keca, M. V. Vojnovic, and D. S. Dojcinovic, *Glas. Hem. Drus. Beograd* **40**, 379 (1975); *Chem. Abstr.* **85**, 84609w, 84610q (1976).
182. I. G. Shchigorev and V. I. Pisarev, *Zashch. Met.* **12**, 484 (1976).
183. L. I. Kadaner and Z. I. Mikvabiya, *Elektrokhim.* **13**, 573 (1977).
184. E. Raub and K. Müller, *Metalloberfläche* **15**, 261, 293 (1961).
185. S. Field, *Metal Ind. Lond.* **40**, 403 (1932); **44**, 614 (1934).
186. D. Hutin and F. Coeuret, *J. Appl. Electrochem.* **7**, 463 (1977).
187. S. Germain and F. Goodridge, *Electrochim. Acta* **21**, 545 (1976).
188. R. Alkire and Po-Yen Lu, *J. Electrochem. Soc.* **126**, 2118 (1979).
189. L. C. Pan, *Metal Ind. New York* **28**, 271 (1930).
190. J. Osterwald, *Oberfläche-Surf.* **17**, 89 (1976).
191. R. N. Fleck, M.S. Thesis, University of California (Sept. 1964) (UCRL-11612).
192. N. Ibl, *Surf. Tech.* **10**, 81 (1980).
193. R. H. Rousselot, *J. Rech. CNRS* **47**, 141 (1959).
194. R. Sautebin, H. Froidevaux, and D. Landolt, *J. Electrochem. Soc.* **127**, 1096 (1980).
195. M. Datta and D. Landolt, *J. Electrochem. Soc.* **122**, 1466 (1975).
196. D. Landolt, R. H. Muller, and C. W. Tobias, *J. Electrochem. Soc.* **116**, 1384 (1969).
197. R. Sautebin, Thesis, Ecole Polytechnique Fédérale Lausanne, Switzerland (1980).
198. R. Alkire, T. Bergh, and R. L. Sani, *J. Electrochem. Soc.* **125**, 1981 (1978).
199. P. J. Sides and C. W. Tobias, *J. Electrochem. Soc.* **127**, 288 (1980).

5

Porous Electrodes

YU. A. CHIZMADZHEV and YU. G. CHIRKOV

1. Introduction

The porous electrode problem is not new in electrochemistry. Nevertheless in the 1960s in connection with an intensive development of the fuel cell investigations, the knowledge in this field has undergone considerable transformation. Earlier, the porous electrodes were only emphasized to be systems with distributed parameters. The effective transfer coefficients were considered as constants to be determined from experiments. Three-phase systems containing both gas and liquid in a porous catalyst had not been studied yet.

The new applied problems have stimulated more profound development of macrokinetics for electrochemical processes in porous electrodes. It was the theory of chemical catalysis, taking into account the porous structure and hydrodynamic features, that has been a starting point in these studies. In addition, three-phase systems were to be considered and the significance of the potential distribution in electrochemical systems was to be taken in account. The 1960s were marked by a furious activity in this field. Because of this the present exposition is based on literature that appeared during that period. The most important results obtained through the 1970s will also be reviewed.

This chapter begins with a brief survey of the processes in porous electrodes. In addition, the classification of well-known porous electrode types is given. The effectiveness of porous electrodes and the regime in which they work depends on the distribution of liquid and gaseous reagents, rate of transport processes, and the local kinetics of the electrochemical reactions. All these factors are determined by catalytic potentialities and media structural organization. The main characteristics of porous media and experimental procedures for their determination are discussed in Section 2. Then in Section 3, the principal facts and theories concerning capillary equilibrium are given. The mechanism of operation of three-phase systems and gas porous electrodes, in particular, can be understood only on the basis of these results. Section 3 begins with an analysis of different models of porous media, with special attention given to branching capillaries theory and lattice models. The extent of pore filling by gas and liquid in different regimes is determined. A comparison with experiments reveals the degree of correlation between models and real porous structures. The theory of capillary equilibrium corrects results obtained by mercury porosimetry and therefore is of special significance. Section 4 is dedicated to transport processes in liquid and gas phases, the complex structure of porous media being taken into consideration. The effective diffusion and electrical conductivity coefficients are calculated and empirical formulas and experimental facts are listed. On the basis of these results from previous sections, a quantitative study of the electrochemical activity of porous electrodes is presented in Section 5.

At first the results concerning liquid (two-phase) electrodes are stated. Then the mechanisms of gas electrodes including hydrophobized ones are analyzed in detail. The theoretical ideas and calculations are compared with experimental data. Knowledge of the conditions of current generation enables one to find ways of optimizing the porous electrodes, i.e., the methods of augmenting the electrical activity of the electrodes, heightening the extent of catalyst exploitation, choosing judiciously the electrode thickness, and so on.

1.1. Porous Electrode

The porous electrode has found wide application in various branches of applied electrochemistry where the slow electrochemical processes are being utilized. To illustrate this, one can mention chemical sources of current, fuel cells, electrolyzers, installations for electrosynthesis, and so on. The idea underlying the use of the porous electrode is extremely simple. In order to demonstrate the underlying principle, let us consider a smooth electrode operating under kinetic conditions. It is obvious that the process going on at the electrode may be considerably intensified by developing the surface of the electrode. If the smooth electrode is replaced by a porous layer of thickness d and specific inner surface S_0 , one can readily estimate the upper limit for

the current density per unit apparent surface, j :

$$j = IS_0d, \quad (1)$$

where I is the local current density. This formula has been derived on the assumption that the porous electrode operates under kinetic conditions, i.e., neither concentration nor ohmic difficulties are involved. As the thickness d increases, these factors inevitably come into play; the system is no longer equally accessible, and the electrochemical process penetrates only to a limited depth in the layer. In spite of the constraints linked with the mass and charge transfer processes, the use of the porous electrodes with highly developed inner surfaces makes it possible to achieve the values of electrochemical activity which are sufficient for technological applications.

The study of the mechanism of current generation in the porous electrode involves great difficulties. This is because the total current collected from the porous electrode is the result of the superposition of a variety of processes, such as the local kinetics of the electrochemical reaction, diffusion, and convection. When a smooth electrode operates under the conditions of mixed kinetics, all the above processes produce a chain of successive events, so that, in principle, it is possible to isolate one stage or another. With the porous electrode, the situation is different. In this case, because of the effect of unequal accessibility, the process is not local, as it is on the smooth electrode, but rather has a distributed character. The process character may change, as the process penetrates from the outer surface of the electrode deep into the porous medium. Furthermore, one can no longer separate the diffusional, ohmic, activation, and other limitations to determine the one limiting stage. The situation is further complicated by the fact that all these phenomena take place in a porous medium which has an intricate configuration. In the porous gas electrodes, one should take into consideration the peculiarities of the gas-electrolyte distribution in the porous medium of the electrode, because its activity depends heavily on this factor.

The main problem in the theory of porous electrodes is to calculate the total current, to determine the distribution of the process into the depth of the electrode, and to establish the principal factors influencing the above characteristics. The method of describing the processes operating in the porous electrodes consists in assuming an equivalent homogeneous isotropic medium characterized by certain effective coefficients. These coefficients are expressed in terms of the structural, transport, and microkinetic characteristics of the system. To find these effective coefficients is the most difficult problem, which cannot be solved without employing the methods of modern theoretical physics. The last stage reduces to solving a set of differential equations describing the distributions of the potential and concentration of the reactants, the reaction products, and the ions into the depth of the electrode. This stage presents no difficulties, especially if the modern computational technique is employed.

1.2. Types of Porous Electrodes

Before we proceed with the presentation of the main results, however, we shall briefly discuss the question of the functional classification of porous electrodes. All the necessary details, a complete bibliography, and the history of the problem may be found in monographs.⁽¹⁻³⁾

Many types of porous electrodes exist. For example, there are electrodes on which the reactions proceed involving only substances dissolved in a solution and electrodes where the solid phase, i.e., the material of which they are fabricated, takes part in the reaction. In the former case, it is natural to call the electrode *inert*, whereas in the latter the electrode may be referred to as *reacting*. As an example of the reacting electrode, one can mention the positive electrodes of lead-acid accumulators. The distinguishing feature of reacting electrodes is that their structural parameters, such as the porosity and specific surface, may vary.

As soon as the active material is spent, the reacting electrode becomes idle, whereas the working life of the inert electrode may, in principle, be unlimited provided that there is a continuous supply of the reactant and removal of the reaction products. In practice, the service life of such electrodes is not, of course, unlimited. This is due, however, to other factors (e.g., to catalyst poisoning).

It is customary to distinguish between *the two-phase electrodes* and *the three-phase electrodes*. In the two-phase electrodes, the porous space is completely saturated with a mixture of an electrolyte solution and a reactant which is well soluble in the electrolyte. If the reactant (usually a gas) is poorly soluble in the aqueous solution of the electrolyte, the porous space of the electrode must contain both the liquid and gaseous phases. Thus the system turns out to be three-phase. Such an electrode is capable of functioning successfully only in the case when it is possible to develop an electrolyte-reactant-catalyst interface in the porous medium. The application of a porous catalyst enables one to overcome the outer-diffusion difficulties and to shift the current generation into the inner-diffusion or inner-kinetic conditions. The solubility of typical gas reagents, for example, hydrogen and oxygen, is low in the commonly used solutions ($c_{B,0} \sim 10^{-6} \text{ mol cm}^{-3}$). Therefore, under the natural convection conditions, the outer-diffusion current on the fully immersed or flooded electrode will be

$$j \approx nFDc_{B,0}/\delta \sim 10^{-4} \text{ A cm}^{-2}, \quad (2)$$

whereas, given a sufficiently large pressure drop and moderate polarization, $j \geq 10^{-1} \text{ A cm}^{-2}$ is collected from a porous gas electrode. Thus the elimination of the outer-diffusion constraints and the development of the three-phase interfacial boundary increases the electrochemical activity of the electrode by three orders of magnitude. These results and those of direct experiments on the pressure-drop dependence of the current indicate that the character of

the filling of the porous matrix with the liquid and gas is of paramount importance.

In the last decade, wide acceptance has been gained by the *hydrophobic electrodes*, first advanced by Niedrach and Alford.⁽⁴⁾ In these electrodes, a developed electrode–electrolyte–gas interfacial boundary is created by introducing into the system a hydrophobic substance (usually Teflon). The use of highly dispersed catalysts, based on the platinum group metals and mixed with a hydrophobic agent, has made it possible to raise significantly the electrochemical activity of the three-phase electrodes in fuel cells. Another important advantage of the hydrophobic systems is that there is no necessity for maintaining an excess pressure in the gas relative to the electrolyte, as is the case with hydrophilic porous gas-fed electrodes.

The hydrophobic electrodes may be utilized for an efficient burning of not only the gaseous fuels, but also the liquid fuels which are sparingly soluble in the electrolyte (e.g., gasoline). In similar systems it is also possible to bring about the inverse process, namely, electrosynthesis.⁽⁵⁾

One may point out other types of porous electrodes. Thus, in recent years, several investigations have been carried out on the liquid electrodes, which operate using, for example, hydrazine and in which the gas is produced as a byproduct of the electrochemical reaction. These electrodes have been called the *liquid–gas electrodes*.⁽⁶⁾ The gas thus produced may lower the electrical conductivity of the system, giving rise to liquid convection and screening some of the operating surface of the electrode.

In this chapter, the primary emphasis is placed on the analysis of the two-phase and three-phase low-temperature inert porous electrodes, the theory of which is currently best developed. These electrodes find wide application in sources of current. The need for producing high-efficiency fuel cells has given a powerful impetus to a detailed study of such systems.

2. Porous Media

2.1. Properties of Porous Media

By the *porous medium*, one usually means a solid called the *matrix*, which contains a sufficiently large number of cavities whose dimensions are small compared with the characteristic dimensions of the whole body. These cavities are called *pores* irrespective of their shape.

Pores in a porous medium may be either linked (*communicating pores*) or isolated. The communicating pores make up the so-called *effective pore space*. Only there do the physicochemical processes discussed in this chapter take place. Accordingly, in what follows, we shall be referring to the effective pore space alone. The properties of porous media have been studied extensively in the literature. Complete bibliographics are available in monographs.^(7,8)

The chief integral characteristics of a porous medium are the porosity and the specific inner surface. Porosity is defined as the ratio of the volume of the porous space to the entire volume of the medium. This quantity is dimensionless. The specific inner surface S_0 is the ratio of the inner surface of the solid phase to the total volume of the medium. This quantity has the dimension of reciprocal length. The value of the specific inner surface determine, in particular, the activity of porous catalysts. A correct determination of its value is therefore of substantial importance.

The simplest model of a porous medium is that of packed spheres. In such a model, the matrix of the porous medium consists of spherical grains of the same radius r packed (or arrayed) in a rigorous order. In this model, the magnitude of porosity is determined entirely by the closeness of the packed spheres to one another. The closeness of the arrangement is determined, in turn, by the angle ψ (Figure 1). Therefore, the porosity

$$g = 1 - \pi/[6(1 - \cos \psi)(1 + 2 \cos \psi)^{1/2}] \quad (3)$$

is independent of the sphere radius, assuming its minimum value, $g = 0.259$, in the case of hexagonal packing of spheres [Figure 1(a), $\psi = 60^\circ$] and its maximum value, $g = 0.476$, in the case of cubic packing [Figure 1(b), $\psi = 90^\circ$]. One can readily estimate the value of the specific surface by making use of the packed sphere model. Thus, for the cubic packing of spheres, $S_0 = \pi/2r$.

Unfortunately, one can hardly suppose that the grains constituting a real porous medium are of a regular geometrical shape and of the same dimensions. This takes place only in specially designed laboratory tests. A real picture is shown in Figure 2, from which one can see that the matrices differ from one another both in shape and in size.

Let us suppose that an examination of grains making up a porous medium has revealed that the grains have a nearly spherical shape (i.e., they may be characterized by only one parameter, the grain radius r). Sampling the grains randomly before the preparation of a porous medium, one may determine the distribution of the grains in size. Let us assume that the histogram thus

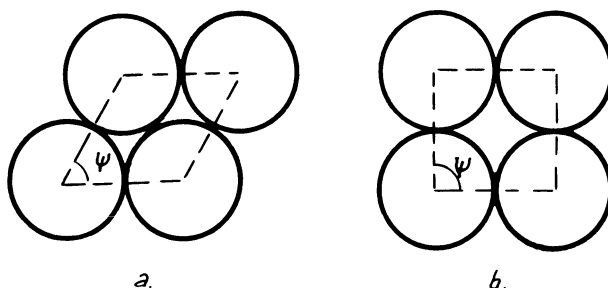


Figure 1. Models of packed spheres: (a) hexagonal packing; (b) cubic packing.

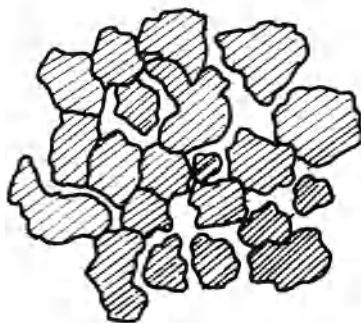


Figure 2. Actual distribution of particles in size and shape in a porous medium.

constructed may well be approximated by the following gamma-distribution.

$$F(r) = \frac{\beta^\alpha}{\Gamma(\alpha)} r^{\alpha-1} \exp(-\beta r) \quad (4)$$

where β is a constant.

Then, taking advantage of the density distribution (4), one may determine the average grain radius \bar{r} . With its help, one can estimate the order of magnitude of the specific inner surface: $S_0 \sim \bar{r}^{-1}$. Using similar methods, it is possible to determine also other averaged characteristics of the porous medium under study; for example, the average coordination number (the number of nearest neighbors of a grain) and the porosity. The characteristics of a porous space may be estimated from those of the grains of the matrix only in certain exceptional cases, namely, if the porous medium is purposefully composed of spherical particles and if the manner of its preparation does not distort significantly the original shape of the grains. In the fabrication of the porous electrodes, however, grains are usually sintered, pressed, and so on. Therefore, as a result of moulding, heat treatment, and adhesive force action, the shape and size of the constituent grains may change radically. Sometimes, the porous medium is molded by mixing particles of two different substances, one of them forming the matrix of the porous medium and the other serving as the pore former. The latter is subsequently removed from the medium. Thus, in the fabrication of the *hydrophilic porous electrodes*, the active layer of the electrode is constituted by a mixture of the catalyst (nickel, silver) and the pore former (usually ammonium bicarbonate NH_4HCO_3). By varying the number and size of the grains of the pore former, it is possible to produce a wide variety of structures of the active layer of the electrode. The arguments just presented show that it is appropriate to describe porous media using the characteristics of pores themselves, which we do not relate to the size of the original grains.

The sizes and shapes of pores are extremely varied. In order to elucidate their properties and role in the various physical and chemical processes, some authors have attempted to classify pores proceeding from various characteristics. In some classifications, pores are divided into groups depending on the

role they play in the hydrodynamical phenomena. In others, detailed correlation has been established between the shapes of pores and the sorption processes. These examples show that one cannot reasonably hope to give an exact description of a porous medium, which may be described sufficiently well, it appears, by the statistical method alone.

A prolonged discussion in the literature has been initiated by posing the question of what should be understood by the *pore size*, because cavities of highly intricate configurations cannot, of course, be characterized by a single quantity. An interesting definition has been proposed in reference (7). At each point of a porous space, the pore radius may be defined as that of the largest sphere containing this point and remaining entirely within the pore. This definition, unfortunately, is of little use in practical applications.

The concept of pore size has a clear-cut meaning only within the framework of the model adopted. The most widely recognized model is the capillary model, in which the pore size is represented by the radius of a circular tube simulating a pore. Of course, it would be naive to think that in real porous media there are such tubes, i.e., pores of regular geometrical shape. Therefore, in shifting from a real porous medium to a model, one should define the pore radius in such a way that the circular tube assumed in the model is equivalent to its original in some respect, i.e., its volume, capillary adsorption, or other property.

In the capillary model, the pore radius distribution has a simple meaning. The distribution density $f(r)$ is defined in such a manner that the product $f(r) dr$ yields the relative number of pores whose radius ranges from r to $r + dr$.

If the number of pore mouths per unit area of some arbitrary cross section is denoted by N , then in the capillary model the porosity may be expressed by the following formula

$$g = \beta N \pi \int_0^{\infty} r^2 f(r) dr \quad (5)$$

Here β represents the tortuosity factor or simply tortuosity. This latter quantity has given rise to a prolonged discussion in the literature. Initially, it was introduced to characterize the difference between the length traversed by a liquid flow in a porous medium and the thickness of the medium. Its very name suggests that tortuosity is a purely geometrical factor. Nevertheless, no exact geometrical definition of tortuosity has been given so far. Therefore, there is nothing surprising in the fact that different authors give entirely different values for this factor. Furthermore, in the literature, one sometimes encounters the concept of *electrical tortuosity*, which characterizes the contour passed by the electrical current through the liquid phase. We shall return to the electrical tortuosity in Section 4 where the transport phenomena in porous media are discussed. Here we deal with a purely geometrical notion of tortuosity.

By tortuosity we mean the ratio of the true length of a pore to its projection upon some chosen axis which is averaged over some cross-sectional area

$$\beta = \overline{dl/dx} \tag{6}$$

Let the pore axis be a line, the direction of which at each point is that of a random vector determined by the angles θ and φ in spherical coordinates. These angles are confined within the following limits: $0 \leq \theta \leq \pi/2$, $0 \leq \varphi \leq 2\pi$. Since $dl = dx/\cos \theta$, we have $\overline{dl} = dx(\overline{1/\cos \theta})$ and

$$\beta = \overline{1/\cos \theta} \tag{7}$$

If all the pore directions in a volume are assumed to be equally probable, then the two-dimensional density of the distribution of the random quantities θ and φ in the volume will be written as $\sin \theta/2\pi$. In order to calculate the tortuosity, however, one should know the law of pore distribution along directions drawn across some cross section. This law is readily obtained from that for the three-dimensional case if we take into account the fact that the probability of a pore passing through some area, making an angle θ with the normal to this area, is proportional to $\cos \theta$. This means that the three-dimensional law should contain a factor proportional to $\cos \theta$. Taking account of normalization, the required density of the distribution of the random quantities θ and φ for the pores passing through some cross section will take on the form $(\sin \theta \cos \theta)/\pi$. Calculating with such a distribution, we get for the average value of the reciprocal of the cosine,

$$\overline{1/\cos \theta} = \int_0^{2\pi} \int_0^{\pi/2} \frac{1}{\cos \theta} \frac{\sin \theta \cos \theta}{\pi} d\theta d\varphi = 2 \tag{8}$$

Thus the geometrical tortuosity entering into formula (5) turns out to equal 2. In such a representation, the tortuosity is independent of the pore radius.

It remains to be shown how the specific inner surface is calculated within the framework of the capillary model. If pores are represented by circular tubes of constant radius, we obtain

$$S_0 = 2N\pi\beta \int_0^\infty rf(r) dr \tag{9}$$

2.2. Experimental Methods for Determining Characteristics of Porous Media

The principal method of studying the porous structure is the mercury penetration technique suggested by Ritter and Drake.⁽⁹⁾ In their method, a liquid that does not wet a solid may be introduced into its capillaries (pores) only at some elevated pressure, whose value is given by the Laplace relation

$$P = \sigma \cos \theta (1/r_1 + 1/r_2) \tag{10}$$

where P is the mercury pressure and r_1 and r_2 are the principal radii of curvature of the surface of the mercury meniscus in a pore (in a cylindrical pore of radius r , obviously, $r_1 = r_2 = r$). Thus to each value of the equilibrium pressure (P), there corresponds a certain value of the radius (r) of pores filled with mercury. After a preliminary pumping to pressures of 10^{-3} – 10^{-4} mm Hg, a sample held in vacuum is filled with mercury, whereupon the volume of mercury is measured that penetrates the pores as the pressure is gradually increased to atmospheric value. Then a dilatometer containing the sample is transferred to a high-pressure vessel where the measurements are carried out to pressures between 1000 and 1500 atm. Making use of the procedure just described, it is possible to measure the pores with radii from several tens of microns down to 100 \AA .

As an illustration, Figure 3(a) shows the integrated distribution curve representing the dependence of the volume of mercury having penetrated a sample on $\log r$ for the active layer of an electrode prepared by introducing the pore former NH_4HCO_3 (see Reference 10). As one can see, such a process of electrode manufacturing makes it possible to produce the porous structure with two types of pores to which the two inflection points of the V – $\log r$ curve correspond. Larger pores are produced during volatilization of ammonium bicarbonate, whereas narrow pores correspond to gaps between the catalyst particles. For a dispersed agglomerated catalyst, one may expect a third inflection point corresponding to micropores in the catalyst grains. The ratio of the total volume of penetrated mercury to the sample volumes gives the total porosity of the sample (g). When all the pores are filled with mercury, its value must be the same as that found by the weight measurements:

$$g = (d_1 - d_2)/d_1 \quad (11)$$

where d_1 and d_2 are the true and apparent specific gravities of the sample, respectively.

Differentiating the V – r curve enables one to obtain the curve $(dV/dr) - \log r$, on which there are maxima corresponding to different groups of pores of similar radii [see Figure 3(b)]. An important characteristic of porous structure is the dependence of the pore surface on the pore radius. This

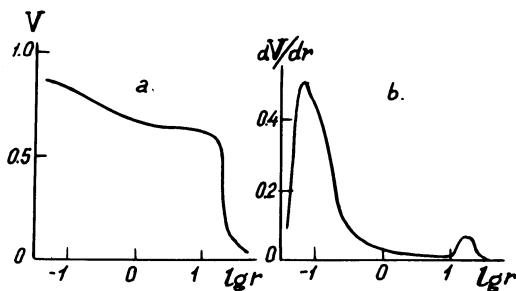


Figure 3. Characteristic curves for the porous structure of a silver electrode with a pore former (20% NH_4HCO_3), according to the mercury porosimetry data⁽¹⁰⁾: (a) integral curve; (b) differential curve.

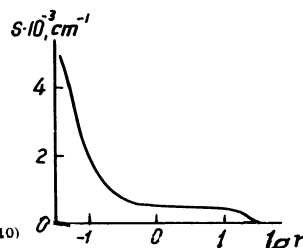


Figure 4. Specific inner surface of pores as a function of $\log r$ (10)

dependence may be found by graphical integration of the curve shown in Figure 3(a), according to the equation:

$$S_0 = \int_{\infty}^r \frac{2}{r} dV \tag{12}$$

An example of such a calculation is illustrated in Figure 4 from which it follows that the surface of narrow pores is much greater than that of wide pores.

Up to this point, it has been assumed that the pores have circular cross sections whose diameters remain constant along the pore length. A real porous structure, however, is characterized by the presence of "corrugated" pores, the study of which calls for measuring not only the forward run of the $V-r$ curve (P increases), but also its backward run (P decreases). The mercury penetration technique does not always suit this purpose, because in the course of long measurements on porous metallic bodies (such as silver and nickel) partial amalgamation may occur. Therefore, the method of studying the porous structure by allowing the wetting liquid to flow directly from the active layer of the porous electrode is highly useful. This procedure has a number of advantages over the mercury porosimetry technique. Using the liquid penetration method, one can study the phenomenon of capillary hysteresis carrying out measurements directly under working conditions (including the case when the system is energized).

An essential supplement to the method of porosimetry is the capillary condensation technique. According to capillary condensation theory, the vapor being adsorbed in a medium may condense in pores at a pressure much lower than that of saturated vapor (P_s), provided that there is a concave liquid meniscus. The relations between the radius of curvature of a spherical liquid meniscus (r_m) and the equilibrium vapor upon the meniscus is given by

$$r_m = 2\sigma V/[RT \ln (P_s/P)] \tag{13}$$

where σ is the surface tension of the liquid, and V is its molecular volume.

It can be readily seen that, by measuring the amount of condensed vapor as a function of the P_s/P ratio, it is possible to construct the curves $V-r$ and $(dV/dr)-r$. Taking advantage of this technique, one succeeds in studying the pores with radii from 15 or 20 to several hundred angstroms, which is especially important in the case of highly dispersed catalysts having specific surfaces

between 20 and 50 m² g⁻¹ or even higher and characterized by a developed microporosity.⁽¹¹⁾

The most important characteristic of the porous media of the two-phase electrodes is their specific surface, which may be found by the method proposed by Brunauer, Emmet, and Teller (BET).⁽¹²⁾ The BET technique is based on measuring (in moles) the amount of an adsorbed substance a_m covering the surface S_0 as a monomolecular layer. In this case,

$$S_0 = a_m N_A s_0 \quad (14)$$

where N_A is the Avogadro number and s_0 is the area covered by a single molecule of the adsorbate, which is usually represented by nitrogen at its boiling temperature.

The value of a_m is determined from a graph corresponding to the equation of polymolecular vapor adsorption

$$\frac{P/P_s}{a(1 - P/P_s)} = \frac{1}{a_m C} + \frac{C - 1}{a_m C} \cdot \frac{P}{P_s} \quad (15)$$

Here a is the value of adsorption at the relative pressure P/P_s and C is a constant.

It should be kept in mind that the BET method allows only the total surface of adsorbents to be measured. Meanwhile, in the fuel cell electrodes, highly dispersed carriers (coal, metal carbides) activated by small amounts of noble metals are sometimes used. In such cases, there arises the problem of measuring separately the surfaces of the carrier and of the catalyst, which may be solved by carrying out selective adsorption.

For metals that adsorb hydrogen or oxygen well in electrolyte solutions, an essential supplement to the BET technique is the method of charging curves. Using these curves, one may determine the amount of chemisorbed, electrochemically active gas and then, from its coverage at a given potential, the catalyst surface.⁽¹³⁾ An important advantage of this method is the possibility of carrying out measurements directly on the electrode without the necessity of destroying it and also determining the part of its surface accessible to the electrochemical process. The surface of a solid may be measured also by the x-ray diffraction technique (assuming that the particles constituting the porous solid are individual grains), by electron microscopy, and by other methods. However, they are not versatile, which accounts for the fact that they are employed relatively seldom.

The brief review of the methods of studying the porous media leads one to conclude that more than one method is necessary to obtain even the approximate characteristics of the porous structure. This statement is especially true when we study such complicated systems as the porous hydrophobic electrodes.

The hydrophobic electrode represents a sintered mixture of the particles of a hydrophobizer (usually Teflon) and a hydrophilic catalyst (e.g., platinum

black). The particles of Teflon and platinum are present in the system as agglomerates of definite sizes and porosities. The distribution of pores in radii, as found by the mercury porosimetry technique, is alone insufficient to characterize fully the structure of a hydrophobic electrode. Such an electrode contains purely hydrophilic pores in the catalyst grains, purely hydrophobic pores in the Teflon grains, and also pores with hydrophilic-hydrophobic walls. Apart from the pore-radius distribution, one should have at least an idea of the average dimensions of the agglomerates of Teflon and platinum and of their porosities. At the present time, there is practically no method which would enable one to formulate clearly a model of the structure of the hydrophilic-hydrophobic porous media, although several attempts have been made to develop such a method. Thus, Tarasevich *et al.*⁽¹⁴⁾ have allowed mercury to penetrate into samples whose hydrophilic pores were initially filled with water, which was subsequently frozen in order to fix it in the pores. The mercury porosimetry method has made it possible, therefore, to find the radial distribution of the hydrophobic pores that remained unfilled. The radial distribution of gas pores is shown by the second curve in Figure 5. Note especially the presence of the fraction of minute pores which appear to permeate the agglomerates of fluoroplastic particles. In what follows, it will be shown that these tiny pores play the dominant role in the processes of current generation in hydrophobic electrodes.

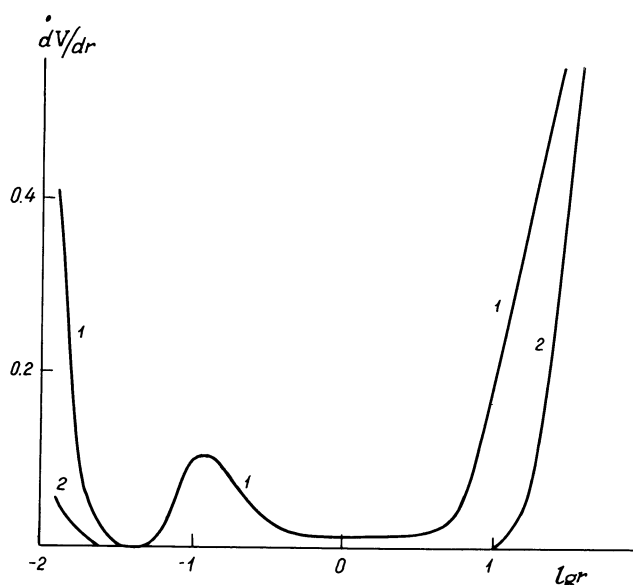


Figure 5. Pore-radius distribution in a hydrophobic electrode⁽¹⁴⁾: Curve 1, mercury porosimetry; Curve 2, gas pores.

One more approach toward the problem of establishing the structure of hydrophobic electrodes has been suggested by Abidor *et al.*⁽¹⁵⁾ Their method may be called the double porosimetry technique. In the first stage of their procedure, the mercury porosimetry method is applied and, in the second stage, water or some alkali is pressed into the hydrophobic porous electrode. These liquids wet the hydrophilic pore walls and, for this reason, the porosimetric curve for (say) water is entirely different from that for mercury. The comparison and analysis of these curves yields information about the dimensions of hydrophobic and hydrophilic pores in the electrode.

It was not our intent to give a comprehensive treatment of all the methods developed so far. We have therefore briefly discussed only those methods that find application in studies of the porous electrode structure. The reader interested in details is referred to special monographs and reviews.^(12,16a-c)

3. Capillary Equilibrium

The calculation of capillary equilibrium may turn out to be useful in many fields: in underground hydrodynamics and gas dynamics, in studying capillary condensation, processes of drying, impregnation, and so on. The theory of capillary equilibrium also provides a basis for calculating the electrochemical activity of the porous gas electrodes.

If a porous media is filled with two different phases, for example, with two immiscible liquids or with liquid and gas, a capillary pressure will arise at the phase boundary. The equilibrium between phases can be maintained only by external pressure, compensating the capillary one. An extremely complex problem of pressure dependence of phase space distribution in porous media arises during a study of capillary equilibrium. Three main models—serial, branching capillary, and lattice—will be discussed. The random processes theory allows us to determine both the degree of pore filling by different phases and spatial distribution of these phases. In the last section the experimental data and their correlation with theory are discussed.

The simplest formulation of the problem of capillary equilibrium is as follows. Let some unwetting liquid be in contact with a semi-infinite porous medium. Under the pressure from the outside, the liquid penetrates into the medium and the liquid menisci arise in pores where the capillary pressure is equal to the external pressure. Much the same situation is observed when the wetting liquid that fills the porous medium is expelled from it by a gas. The problem of the spatial distribution of phases in the porous medium may be solved only when it is known in what pores may appear a liquid meniscus at each specified pressure, i.e., if the medium is represented by a sufficiently simple model. The problem of the meniscus position in an individual pore can be solved most simply if such a pore is visualized as a variable-radius capillary. We shall consider the penetration of some unwetting liquid (e.g.,

mercury) into the porous medium. Before the mercury penetration takes place, the porous medium is freed from the gas.

If the mercury pressure is P , a meniscus forms in pores of radius [see Eq. (10)]

$$r_* = 2\sigma|\cos \theta|/P \quad (16)$$

Here σ is the surface tension and θ is the wetting angle. Cosine is taken modulo, because for a nonwetting liquid, $90^\circ < \theta < 180^\circ$.

The pores that satisfy condition (16) will be referred to as critical. The pores of a smaller radius (subcritical) must then be empty. As the pressure from the outside increases, so does the amount of mercury penetrating the medium, because the mercury begins to penetrate into increasingly smaller pores.

The chief characteristic of a porous space is the pore-radius distribution density, $f(r)$. Making use of this function, one may, for example, determine the fraction of supercritical pores in an electrode:

$$\gamma = \int_{r_*}^{\infty} f(r) dr \quad (17)$$

Then, obviously, the fraction of the subcritical pores will be $1 - \gamma$. It is not sufficient, however, to assign the values of the external pressure P and of the function $f(r)$ to characterize fully the process of filling of the porous medium with the nonwetting liquid. One should also know something about the order of alternation of the elements of which the medium is composed. If, in a statistical description of the porous medium, the profile of a pore is considered to be the realization of an accidental process, one should indicate the category of the process assumed in the calculations (i.e., whether it is a Markovian process, a steady-state process, or something else). In what follows, unless specified otherwise, we shall make the simplest assumption that the radius variation along the pore is purely random (i.e., we have a process with independent tests). This means that, no matter what the pore radius was in the cross section with the coordinate x , in the nearest cross section with the coordinate $x + dx$ the pore radius may assume any possible value with the probability density $f(r)$. It will be emphasized once again that only in the model of independent tests does the assignment of the distribution $f(r)$ characterize unambiguously a porous medium. The employment of other types of random processes will require a knowledge of the correlation functions and other characteristics.

This, however, does not exhaust the formulation of a model of the porous medium. One should also take into consideration the specific character of the problem of capillary equilibrium. On the surface separating the porous body from the nonwetting liquid, every supercritical pore will be filled with the liquid; narrow subcritical pores will remain, at a specific (fixed) pressure, free of the liquid. With the further penetration of the liquid front into the porous

body, not every supercritical pore can be filled with the liquid at the specified pressure, because a subcritical pore [see Figure 6(a)] may block the supercritical pore behind it, thus separating the larger pore from the liquid. Only if branching of supercritical pores takes place can the liquid penetrate further into the porous medium [Figure 6(b)].

The main problem in capillary equilibrium theory is how to calculate the probability that any supercritical pore, which is located at a distance x from the surface of a body, may be filled with a liquid. Let us call the process of the transition of a supercritical pore into a subcritical one "the death of the supercritical pore." A model of the porous medium is called a "serial model" if the process leading to the supercritical pore death takes place, yet the pores cannot branch. Clearly, the serial model suggests that a liquid can penetrate into a porous body only to some finite depth.

A more general model of the porous medium is the model of bifurcating (or branching) capillaries. This model involves the competition between two processes; namely, as the liquid penetrates into the porous medium, a pore, which is supercritical near its surface, may either "perish" (the pore death process) or move further into the medium by way of bifurcation. If the bifurcation probability is higher than the death probability, then obviously the liquid can penetrate infinitely into the porous medium. This phenomenon will be referred to as the porous medium breakthrough.

However, the processes of pore death and bifurcation do not exhaust all the essential effects accompanying the filling of the porous medium with the nonwetting liquid. Bifurcation is most effective only in the case when the resulting branches [see Figure 6(b)] independently favor the penetration of the liquid front into the porous medium, i.e., provided there form no closed

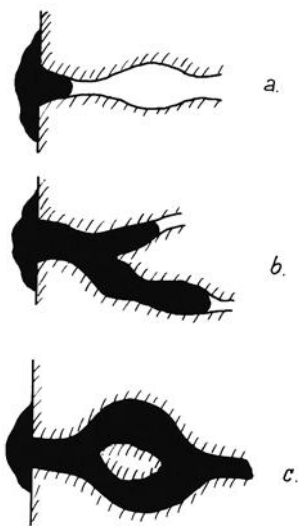


Figure 6. Principal effects arising when a porous medium is filled with mercury: (a) pore death; (b) branching; (c) looping.

contours or loops [see Figure 6(c)]. To assume that there are no loops would obviously be artificial. As will be shown later, the disregard of the loops may considerably distort the actual character of filling of the porous medium with a liquid. The role played by loops may be consistently taken into account only in the lattice models, which are the most comprehensive models in the problem of capillary equilibrium.

It should also be emphasized that in what follows we shall analyze the three models of the porous medium outlined above, but we shall not discuss the dynamics of the filling of a porous medium with a liquid. We shall be concerned only with the statics of the phenomenon, i.e., with the equilibrium configuration of the gas-liquid-solid interfacial boundary that will form after all the transient saturation processes in the porous body have been finished.

3.1. Branching Processes

The problem of capillary equilibrium in the model of intersecting pores of variable cross section and with no loops has first been solved by Markin.⁽¹⁷⁾ Serial model calculations have been carried out by Chernenko and Chizmadzhev.⁽¹⁸⁾ In this chapter, the above problems are treated using the formalism of the theory of random branching processes which makes possible a very substantial reduction in numerical work.

As each supercritical pore located on the body surface moves along a "path" of length x , it may "generate" s supercritical pores independently of the other pores, the generation probability being $p_s(x)$. We introduce the generating function

$$F(x, z) = \sum_{s=0}^{\infty} p_s(x) z^s, \quad 0 \leq z \leq 1, \quad (18)$$

containing all information concerning the distribution of the probabilities $p_s(x)$. It is known⁽¹⁹⁾ that the function $F(x, z)$ is defined as the solution to the inverse Kolmogoroff equation

$$\frac{d}{dx} F(x, z) = \sum_{s=0}^{\infty} \lambda_s F^s(x, z) \quad (19)$$

with the initial condition

$$F(0, z) = z \quad (20)$$

because the process of pore generation is started by a single supercritical pore located on the body surface. In Eq. (19), λ_s are the densities of the probabilities of transition of one supercritical pore into s supercritical pores. These quantities are defined in such a way that

$$\sum_{s=0}^{\infty} \lambda_s = 0 \quad (21)$$

Performing integration in Eq. (19), we obtain

$$x = \int_z^{F(x,z)} \frac{du}{\varphi(u)}, \quad \varphi(u) = \sum_{s=0}^{\infty} \lambda_s u^s \quad (22)$$

which is the solution to the problem.

3.1.1. Serial Model

The serial model takes account only of the effect of pore corrugation, i.e., the possibility of the pore death. Let λ denote the pore death probability density. Then, we have

$$\lambda_0 = \lambda, \quad \lambda_1 = -\lambda, \quad \lambda_k = 0, \quad k \geq 2 \quad (23)$$

and from Eq. (22) it follows that

$$F(x, z) = 1 - (1 - z) \exp(-\lambda x) \quad (24)$$

Keeping in mind the definition of the generating function (18), we shall find what interests us in the first place, namely, the probability that a pore, which is supercritical on the surface of the body, will remain supercritical at some distance x

$$P(x) = \exp(-\lambda x) \quad (25)$$

Let us now determine the average depth of penetration of the liquid front in a porous body and also its dispersion. Since

$$\int (n) = \int_0^{\infty} x^n \exp(-\lambda x) dx = \frac{n!}{\lambda^{n+1}} \quad (26)$$

the average thickness of the "liquid" layer at the surface will be

$$\langle x \rangle = \int (1) / \int (0) = \lambda^{-1} \quad (27)$$

and its dispersion:

$$(\langle x^2 \rangle - \langle x \rangle^2)^{1/2} = \lambda^{-1} \quad (28)$$

That is, the dispersion turns out to be of the order of the average depth of penetration. Thus even in the serial model there is no sharp boundary to separate the region thoroughly wetted by the liquid from that free of the liquid.

3.1.2. Branching

Let λ again be the supercritical pore death probability density and ν the probability of dichotomic branching (or bifurcation). For simplicity, we assume that at $k \geq 3$ all $\lambda_k = 0$. Then,

$$\varphi(u) = \lambda - (\lambda + \nu)u + \nu u^2 = (u - 1)(\nu u - \lambda) \quad (29)$$

Integrating Eq. (22), we obtain

$$F(x, z) = \begin{cases} \frac{\lambda - \nu z - \lambda(1-z) \exp[-(\lambda - \nu)x]}{\lambda - \nu z - \nu(1-z) \exp[-(\lambda - \nu)x]}, & \lambda \neq \nu \\ 1 - (1-z)/[1 + \lambda(1-z)x], & \lambda = \nu \end{cases} \quad (30)$$

The character of liquid penetration into the porous medium depends critically on the relative values of the probabilities of pore death and branching. It follows from Eq. (30), at $\lambda \geq \nu$, that the probability $p_0(x) = F(x, 0)$ of the pore supercritical at the surface perishing tends to unity as $x \rightarrow \infty$. This means that if the death probability is higher than the branching probability, the liquid may penetrate into the porous medium only to some finite depth. For $\lambda < \nu$, the situation is different. Now $p_0(x)_{x \rightarrow \infty} = \lambda/\nu$. Therefore, the probability that the liquid will penetrate into the porous medium over an arbitrarily large distance is $1 - \lambda/\nu$; i.e., the breakthrough phenomenon takes place.

Let us now estimate the degree of filling of the porous medium with a liquid when $x \rightarrow \infty$. We designate this quantity as P_∞ . At some depth in the porous medium, a randomly sampled supercritical pore may independently reach the boundary between the liquid and porous body from one of the two possible directions. Taking one by one all possibilities, we may write the symbolic equations

$$P_\infty = P(\text{O}—\text{O}) + P(\text{O}—\text{⊗}) + P(\text{⊗}—\text{O}) \quad (31)$$

$$P(\text{O}—\text{O}) = P^2(\text{—O}), \quad P(\text{O}—\text{⊗}) = P(\text{—O})P(\text{—⊗})$$

where the symbol —O means that the supercritical pore is linked, at the end indicated, with a single system of supercritical pores. The fact that a pore is not linked with such a system is denoted by the symbol —⊗. From the preceding calculations it follows that the respective probabilities will be

$$P(\text{—O}) = 1 - \lambda/\nu, \quad (P - \text{⊗}) = \lambda/\nu \quad (32)$$

Substituting (32) into (31), we finally obtain

$$P_\infty = 1 - (\lambda/\nu)^2 \quad (33)$$

Thus the model of branching capillaries, which is more realistic than the serial model, clearly indicates the possibility of the breakthrough phenomenon. The theory enables one to estimate the degree of filling of an electrode with the gas and with the electrolyte, provided the dependences of the constants λ and ν on the pressure difference, as well as the functions of the pore-radius distribution, are known.

3.2. Lattice Models

Let us assume that pores are arranged in a regular lattice (a square grid in the two-dimensional case). The lattice constant may have, for example, the

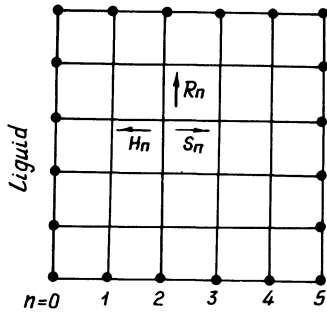


Figure 7. Porous medium as approximated by a square lattice.

meaning of the average diameter of the matrix grains making up the porous medium. The links connecting the lattice sites are characterized by their minimum radius. According to this characteristic, the lattice links may be divided into permeable and impermeable. (The probability that a link is permeable is denoted by γ .)

Let the surface of a two-dimensional semi-infinite porous medium coincide with one of the generating lines of a square lattice. Let it be denoted by number 0 (Figure 7). The succeeding lines, which are parallel to the surface, are numerated by the natural numbers. The volume of the porous space is assumed to be completely confined within the lattice sites. It is necessary to determine the degree of filling of the medium with a liquid. An exact solution to this problem will be given somewhat later. Now we shall demonstrate an approximate solution which yields a qualitatively correct picture of the phenomena involved.

Let us consider an arbitrary lattice site located on the line n . From this site, four links extend. We assume that a liquid may penetrate through each of these links (pores) independently. Thereby we in fact refuse at the moment to take into account the presence of loops in the lattice. Let R_n denote the probability that the surface of a porous body will be reached by starting from a lattice site located on the n th line of sites and going through one of the pores extending parallel to the body surface, moving all the while through supercritical pores only and not returning to the original site. A similar probability, but for the case when the pore through which some fluid departs from the original site extends toward the body surface, will be denoted by H_n ; and that for the pore running away from the surface, by S_n (Figure 7). For the probabilities defined in Figure 7, we have the following set of equations

$$S_n = \gamma[1 - (1 - S_{n+1})(1 - R_{n+1})^2] \quad (34)$$

$$R_n = \gamma[1 - (1 - R_n)(1 - H_n)(1 - S_n)] \quad (35)$$

$$H_n = \gamma[1 - (1 - H_{n-1})(1 - R_{n-1})^2] \quad (36)$$

with the boundary condition $H_{n=1} = \gamma$, which implies that on the surface of

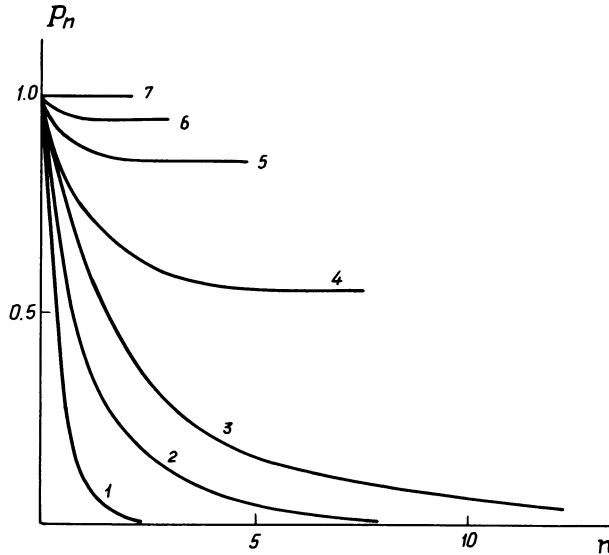


Figure 8. Extent of the filling of the sites of a square lattice with a liquid: curve 1, $\gamma = 0.1$; 2, $\gamma = 0.3$; 3, $\gamma = 1/3$ (breakthrough point); 4, $\gamma = 0.4$; 5, $\gamma = 0.5$; 6, $\gamma = 0.6$; 7, $\gamma = 0.8$.

the body each supercritical pore is filled with the liquid. The probability, P_n , that a lattice site is filled with the liquid is evidently

$$P_n = 1 - (1 - H_n)(1 - R_n)^2(1 - S_n) \tag{37}$$

The results of solving the set of equations (34)–(37), which have been obtained in a computer-aided calculation, are presented in Figure 8. The figure shows that at $\gamma < \frac{1}{3}$ the liquid penetrates into the porous medium only to a finite depth. With increasing γ , the thickness of the liquid layer increases, reaching its maximum value (of the order of 10 times the value of the lattice constant) at the breakthrough point. The small thickness of the region of nonuniform filling of pores with the liquid is due to the fact that the possible correlation between the neighboring links penetrable to liquid was neglected in the calculation. At $\gamma > \frac{1}{3}$, the liquid penetrates arbitrarily far into the porous body and, behind the layer of nonuniform filling, the porous medium is filled with the liquid uniformly.

The probability P_∞ may be estimated analytically. Obviously, a supercritical pore removed from the surface infinitely deep into the porous medium does not “remember” from whence it “came”. An analysis of simultaneous equations (34)–(37) indicates that, when $n \rightarrow \infty$, $H_n = R_n = S_n = T$, where the quantity T satisfies the equation

$$T = \gamma[1 - (1 - T)^3] \tag{38}$$

Solving Eq. (38), we find, apart from the trivial solution $T \equiv 0$, that

$$T = 1.5 - (1/\gamma - 0.75)^{1/2}, \quad P_\infty = 1 - (1 - T)^4 \quad (39)$$

From Eq. (39) it follows that the breakthrough occurs at $\gamma_* = \frac{1}{3}$.

Basically, the problem of capillary equilibrium is a version of the general problem concerning the origin of a single coherent system of elements of definite type, which has been named the *percolation problem*. Solving this problem is of interest in the study of the behavior of diluted ferromagnetics and the metal–semiconductor transitions in disordered systems, in the theories of polymers, automatic control, neuron networks, and in calculating the effective electrical conductivities of porous media partly filled with a gas (see Section 4). The percolation problem was formulated for the first time by Broadbent and Hammersley⁽²⁰⁾; comprehensive reviews of the related questions are available.^(21,22)

Up to now, relatively few exact analytical results have been obtained in solving the percolation problem. Only the values of percolation threshold (breakthrough points) for a number of two-dimensional lattices have been found analytically, whereas the percolation probabilities [quantities of the type of P_∞ in relation (33)] are found numerically using the Monte-Carlo technique. The fundamental idea of the analytical methods consists in considering clusters, which represent coherent assemblies of links of one type. In the square lattice shown in Figure 9 some examples of the simplest clusters are illustrated, with the links filled with liquid denoted by the solid lines and those impermeable to liquid by the dashed lines. By introducing the probabilities of occurrence of clusters of each type and by summing over all cluster realizations with appropriate statistical weights, one can represent the average radius of a cluster in the form of an infinite series diverging at the breakthrough point. Hence one derives the equation from which the breakthrough point may be found. For the square lattice, $\gamma_* = \frac{1}{2}$, whereas for the triangular lattice $\gamma_* = 2 \sin(\pi/18) \approx 0.3473$.⁽²³⁾ In recent years, some approaches have been developed⁽²⁴⁾ which make it possible to obtain analytical results consistent with those of Monte-Carlo calculations. The main idea of these analytical

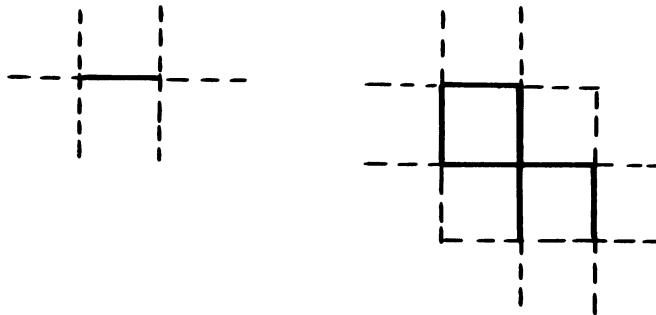


Figure 9. Examples of clusters.

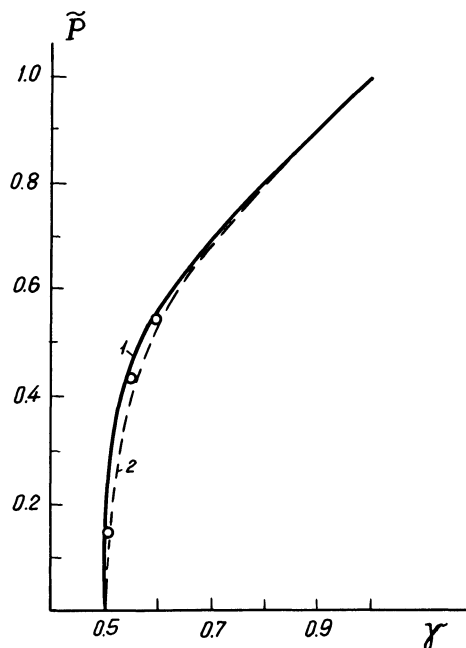


Figure 10. Percolation probability as a function of the fraction of links permeable to a liquid.

methods consists in introducing equivalent pseudolattices having a treelike structure with a variable coordination number. The problem of calculating the percolation probability can be solved quite simply in this approximation, because, in analogy with Eq. (38), we have for a “tree” with coordination number $cn = \sigma + 1$

$$P = \gamma[1 - (1 - P)^\sigma] \tag{40}$$

3.2.2. Square Lattice

In order to illustrate the intent of the above approaches, we shall consider a square lattice. The percolation probability for the square lattice, which has been calculated by using the Monte-Carlo technique,⁽²⁵⁾ is shown in Figure 10 by solid curve 1. The breakthrough takes place at $\gamma_* = 0.5$, whereupon the curve $\tilde{P} = \gamma P$ steeply rises, and at $\gamma \approx 0.7$ the percolation probability P already approaches unity (i.e., practically all the lattice sites are filled with liquid). In Section 3.2., a different value for the breakthrough point ($\gamma_* = \frac{1}{3}$) was obtained. In that section, the lattice was approximated by a tree with coordination number $cn = 4$. Thus, disregard of loops leads to significant distortions in the actual picture of capillary equilibrium. In lattices, breakthrough comes later than in pseudolattices, because in lattices a liquid escaping through the links adjoining the original link [see Figures 6(b) and (c)] comes back to the original link by way of loops. Let us now try to understand why, in the square lattice, breakthrough occurs exactly at the point $\gamma_* = \frac{1}{2}$.

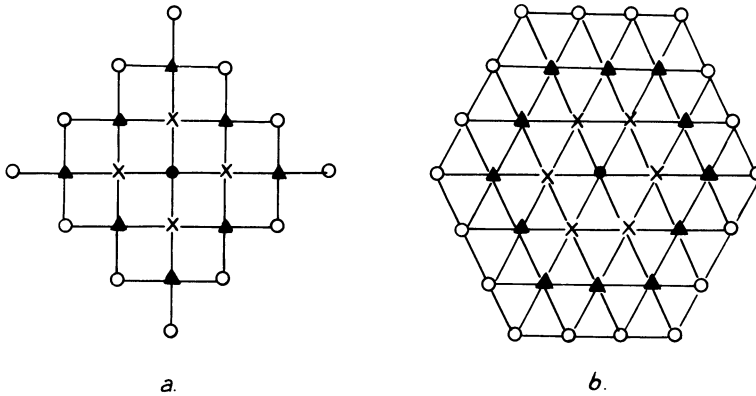


Figure 11. Calculation of the percolation probability in regular lattices.

We consider a square lattice in which some arbitrarily chosen site is fixed and labeled with a circle [Figure 11(a)]. Let some liquid be supplied through this site. The liquid can percolate further through the four links issuing from the original site, thereby penetrating into the first layer of sites, which comprises four sites labeled with crosses in Figure 11(a). From this moment on, the liquid can flow through twelve links leading to the next layer of sites, which is labeled with triangles. Naturally, the slower the quantity ξ (i.e., the increase in the number of links issuing from a single site in a given layer of sites) decreases in each new layer of sites, the easier it will be for the liquid to penetrate infinitely far into the medium. Let us calculate the value of ξ . In the zero site, $\xi = 4$. In the layers of sites with $m \geq 1$, the numbers of sites (S) and of links (B) and the number ξ are given by the following equations:

$$S = 4m, \quad B = 8m + 4, \quad \xi = B/S = 2 + 1/m \quad (41)$$

Thus, it follows from relations (41) that the process of percolation of a liquid from the source site, which is represented by any site of an infinite lattice, proceeds similarly to the percolation process in a semi-infinite porous medium (see Figure 8). Namely, in the immediate vicinity of a point source of liquid, there is a region of nonuniform filling, but further from the source the percolation process becomes uniform [see Figure 11(a)].

It can readily be seen that percolation is most difficult when $m \rightarrow \infty$ and $\xi \rightarrow \xi_\infty = 2$. It is this region of uniform percolation (large m) that determines the moment of breakthrough. Indeed, at large m , the liquid that has reached any site in the m layer of sites [Figure 12a)] may percolate to the $m + 1$ layer only through the two links connecting the original site with sites 1 and 2 in the $(m + 1)$ layer. At the moment of breakthrough, the fraction of links penetrable to liquid is still so small that simultaneous percolation to sites 1 and 2 is, on average, impossible. Assuming the probabilities of percolation to sites 1 and 2 to be independent of each other and the liquid percolation

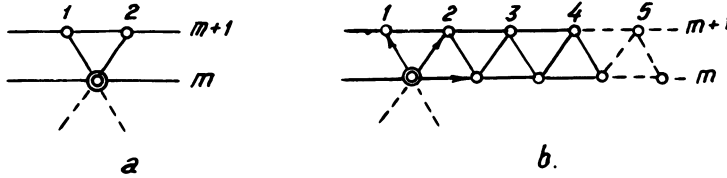


Figure 12. Calculation of the percolation threshold in regular lattices.

from the m layer to the $(m + 1)$ layer to be certain, we have

$$2\gamma_* = 1, \quad \gamma_* = \frac{1}{2} \tag{42}$$

Thus we have found the exact value of the percolation threshold. In order to make certain that the suggested approach to the evaluation of the breakthrough threshold in lattices is correct, we shall consider one more example. For the triangular lattice of links, we have [see Figure 11(b)]

$$S = 6m, \quad B = 18m + 6, \quad \xi = 3 + 1/m \tag{43}$$

3.2.3. Triangular Lattice

Let us now examine the conditions of asymptotic percolation in the triangular lattice. As relations (43) indicate, at $m \rightarrow \infty$, $\xi \rightarrow \xi_\infty = 3$, i.e., on average, each site in the m layer may be continued by three links connecting the m layer with the $(m + 1)$ layer. These links are indicated by arrows in Figure 12(b). When $\gamma = \gamma_*$, the conditions of percolation are such that from the original site in the m layer the liquid may penetrate to only one site in the $(m + 1)$ layer [sites 1, 2, 3, . . . , in Figure 12(b)]. The reason is that nonlinear effects at the percolation threshold are impossible (to be more exact, at $\gamma \rightarrow \gamma_*$ their probability tends to zero). Therefore, summing over all probabilities of possible transition from the original site to those of the $(m + 1)$ layer and equating the obtained sum to unity, we obtain

$$\gamma + (\gamma + \gamma^2 - \gamma^3) \sum_{s=1}^{\infty} \gamma^{s-1} = \frac{\gamma(2 - \gamma^2)}{(1 - \gamma)} = 1 \tag{44}$$

Or, in another form,

$$\gamma^3 - 3\gamma + 1 = 0 \tag{45}$$

The only real root of this equation found within the interval $(0, 1)$ is $\gamma = 2 \sin(\pi/18)$. The same result is obtained by the method of clusters.⁽²³⁾

Figures 11(a) and 12(a) show that at points sufficiently distant from the site which is a source of liquid, the square lattice of links may be approximated by tree with coordination number $cn = 3$. According to relation (40), the breakthrough occurs then at $\gamma_* = \frac{1}{2}$.

In the region of nonuniform filling (in the neighbourhood of the source site), the approximation of the lattice by trees should have a different character. Let us examine again Figure 11(a). It shows that in the zero site the lattice

resembles a tree with coordination number $cn = 5$, because $5 - 1 = 4$ links emanate from this site. In the next layer of sites [formulas (41)], exactly four links emanate from each site; therefore, the lattice there resembles a tree with $cn = 4$. In the subsequent layers of sites, there takes place the transition from trees with $cn = 4$ to a tree with $cn = 3$. Therefore, a complicated tree arranged in the way suggested by relations (41) should provide a good approximation for the quantity \tilde{P} . It is not known *a priori* how many branchings with $cn = 4$ should be taken in going from the branching with $cn = 4$ to the asymptotic branching with $cn = 3$ in order to obtain a reasonably exact approximation of the function \tilde{P} . Denoting this unknown parameter by n , we find the function \tilde{P}_n approximating the function \tilde{P} for the square lattice by solving successively the simultaneous equations

$$\tilde{P}_n = \gamma[1 - (1 - T_n)^4], \quad T_n = \gamma[1 - (1 - T_{n-1})^3] \quad (46)$$

Here we take, as a zero-order approximation (T_0), the function defined by relation (40), in which $\sigma = 2$ (a tree with coordination number $cn = 3$). Then, for \tilde{P}_n , the breakthrough point will be located at $\gamma = 0.5$.

Equations (46) are constructed analogously to Eq. (40), but they take account of the fact that the coordination number varies from point to point. Setting $n = 1, 2$, etc. and comparing the values of \tilde{P}_n calculated by formulas (46) with those of curve 1 in Figure 10 calculated by the Monte-Carlo method, we obtain, at $n = 1$, dashed curve 2. A still better approximation is attained at $n = 2$ (crosses above curve 2 shown in Figure 10). The calculation shows that the best approximation is reached at $n = 3$. In this case, the explicit expression for the percolation probability $\tilde{P}_{n=3}(\gamma)$ has the form

$$\tilde{P}_{n=3} = \gamma[1 - (1 - \gamma\{1 - [1 - \gamma(1 - \{1 - \gamma[1 - (1/\gamma - 1)^3]\}^3]\}^3)]^4 \quad (47)$$

3.3. Experimental Facts

A direct experimental verification of the theoretical conclusions drawn in calculating the capillary equilibrium in hydrophilic porous media has been made in works by Ksenzhek *et al.*⁽²⁶⁾ and by Pshenichnikov and Zhuravleva.⁽²⁷⁾ In these studies, the wetting liquid was expelled from porous media by gases. As mentioned previously, this problem is equivalent to that of mercury penetration into an empty porous medium.

Figure 13 illustrates the degree of filling the medium with a gas as a function of pressure.⁽²⁶⁾ The experiment has been performed with five plates of different thicknesses. The numbers on the curves indicate the thicknesses of the plates in millimeters. All samples were prepared by sintering powder with the particle size of $205 \pm 25 \mu\text{m}$, the porosity of the samples being 0.47.

The shape of the curves suggests that, at one and the same pressure, the thinner samples show a higher degree of filling with gas. This is indicative of the fact that a greater amount of gas is contained near the surface than in the depths of the sample.

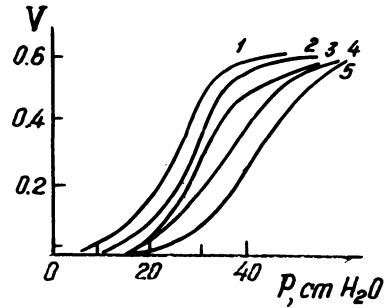


Figure 13. Pressure dependence of the filling of a porous medium with a gas.⁽²⁶⁾ Thickness of specimens (mm): Curve 1, 1.55; 2, 2.55; 3, 4.3; 4, 5.65; 5, 8.25.

In order to clarify the character of filling of the samples in depth, it is more convenient to use the graph shown in Figure 14, which illustrates the dependence of the total volume of gas in a porous plate on its thickness. The numbers on the curves indicate the gas pressures in centimeters of water column. The character of the curves exhibits most vividly the nonuniformity of filling of the porous medium with gas. The curves corresponding to pressures of 20 and 30 cm H₂O finally reach plateaus, which means that the amount of gas in the medium no longer changes with the increasing thickness. Here a damping regime of filling is realized (see curves 1 and 2 in Figure 8). The curves corresponding to pressures of 40, 50, and 60 cm H₂O continues to rise steadily. In this case, the breakthrough conditions appear to be realized (curves 4, 5, etc. in Figure 8).

The theory of capillary equilibrium in the model of intersecting pores of variable cross section, which has been developed previously, shows in a different light the method of studying the distribution of pores according to their radii by using the mercury penetration technique suggested by Ritter and Drake (see Section 2.1). This method offers the possibility of determining the distribution of pore volumes in radii, $\alpha(r)$. This distribution is found as follows: the product of the probability density $\alpha(r)$ and dr yields the relative fraction of the volume of pores whose radii range from r to $r + dr$. Were it

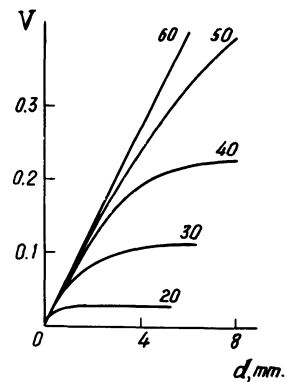


Figure 14. Amount of gas in a porous medium as a function of the specimen thickness (numbers at curves indicate the gas pressure in cm Hg).⁽²⁶⁾

not for the effect of blocking of the larger pores by the smaller ones, the distribution $\alpha(r)$ would make it possible to determine also the distribution of pores in radii, $f(r)$, according to the formula

$$f(r) = \alpha(r)/r^2 \int_0^{\infty} \frac{\alpha(t)}{t^2} dt \quad (48)$$

It is well known, however, that the results one obtains using the mercury porosimetry technique are subject to strong distortions, because at the pressures indicated not all supercritical pores are filled with mercury. Nevertheless, most of the results of measurements of the distribution of the pore volumes according to their dimensions still remain uncorrected.

On the basis of the obtained solution to the problem of capillary equilibrium, methods of correcting the experimental curves for capillary equilibrium measured according to Ritter and Drake have been proposed.^(28,29) In order to visualize the character of distortion of the true distribution of pores in radii, let us examine the simpler inverse problem. We assume that the pore radius distribution is already known. Let it be the uniform distribution shown by curve 1 in Figure 15. We shall now calculate the capillary equilibrium in the medium using the methods outlined in this section for arbitrary regular lattices, leaving loops out of account. Having found the degree of filling of the pore volume with mercury, $\alpha(r)$, we then determine $f(r)$ by formula (48). Carrying out this procedure⁽³⁰⁾ has yielded the result shown in Figure 15 (curves 2 and 3). It can be seen that the mercury porosimetry underestimates the number of wide pores in a sample and overestimates the number of narrow pores. This can be accounted for by the fact that mercury begins to break through a porous medium only when the number of wide supercritical pores is sufficiently large for the probability of supercritical pore branching to become equal to the probability of supercritical pore death. It is evident that as the mercury pressure increases, the number of subcritical pores decreases; therefore, the parameter ν increases, while the parameter λ decreases.

Figure 15 also shows that the distortion of the actual distribution becomes greater as the coherence of the porous space, which is characterized by the

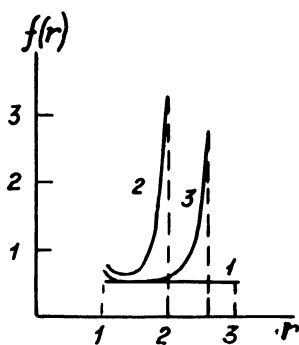


Figure 15. Actual pore-radius distribution, curve 1, and the apparent pore-radius distribution determined by the mercury porosimetry technique: Curve 2, honeycomb lattice; curve 3, cubic lattice.⁽³⁰⁾

coordination number of the lattice, decreases. The larger the coordination number cn , the earlier comes the moment when the liquid begins to penetrate into the porous sample to arbitrarily large depths. For this reason, the number of "unmeasured" wide pores decreases with increasing coordination number. Naturally, at $cn = \infty$ (an ideal case when there is no pore death), the experimental and theoretical curves must coincide.

In this section, we have confined our discussion to capillary models. In the literature, one can also find data regarding equilibrium in the model of packed spheres.^(31,32) The results obtained in these approaches are in qualitative agreement.

4. Transport Processes

The transport processes, such as flow, diffusion, heat transfer, and passage of electrical current, may severely limit the magnitude of the electrochemical activity of the porous electrode. Therefore, the more completely the transport limitations are removed, the more effective is the shift from the smooth electrode to the porous electrode. In this section, the stages of transport processes, which are of the greatest importance for the porous electrodes, will be investigated independently from one another. In the porous electrode, however, they are interrelated, as will be discussed in the following section. At this point, the complexity of the structure of a porous medium makes it necessary to describe porous media as homogeneous by introducing some effective coefficients. A more detailed description of transport processes in porous media is available in the literature.^(33,34)

4.1. Convective Diffusion

Let us consider the diffusion of a reactant dissolved in some immobile electrolyte filling the porous matrix. The quantity \tilde{D} is defined in such a manner that the diffusion flux through a homogeneous medium is identical to the flux through a real porous medium, the other factors being equal. Let us consider a porous layer of thickness d . If the concentration difference in this layer amounts to $c_1 - c_2$, the diffusion flux per unit surface will be $\tilde{D}(c_1 - c_2)/d$. The flux in a real porous medium is dependent on its structure. Let the pores be represented by cylinders of constant cross sections s and with tortuosity β . This means that the actual length of each pore encountered in the layer of thickness d is equal to βd . If there are N pores per unit area of the outer surface, then the volume of the porous space confined within the layer and referred to the unit area of the outer surface is $s\beta dN$. Consequently, the porosity of the layer is given by

$$g = s\beta dN/d = s\beta N \quad (49)$$

The diffusion flux through each pore is $D(c_1 - c_2)s/\beta d$ and the flux through all the pores confined within the unit area of the outer surface is $DsN(c_1 - c_2)/\beta d$. Comparing this expression with that for the flux in a homogeneous medium, we find the expression for the effective diffusion coefficient

$$\tilde{D} = Dg/\beta^2 \quad (50)$$

In the above arguments, the pore tortuosity alone has been taken into consideration, but not the shape of the pores nor their character of "corrugation." Unfortunately, these factors significantly affect the kinetic parameters of porous media; therefore, no quantitative agreement with experiment can be expected unless these factors are taken into account. Sometimes, the following procedure is adopted: The effect of corrugation is included in the tortuosity factor β . Of course, the tortuosity factor then loses its physical meaning, becoming merely a fitting parameter.

One often has to consider the diffusion of a gas in a porous medium partly filled with a liquid. According to Ksenzhek *et al.*,⁽³⁵⁾ the effective diffusion coefficient may then be represented by the following empirical formula:

$$\tilde{D} = Dg^{3.5}(1 - g_l/g)^{3.5} \quad (51)$$

where g_l is the "liquid porosity," i.e., the ratio of the volume of the liquid to the total volume of the porous medium.

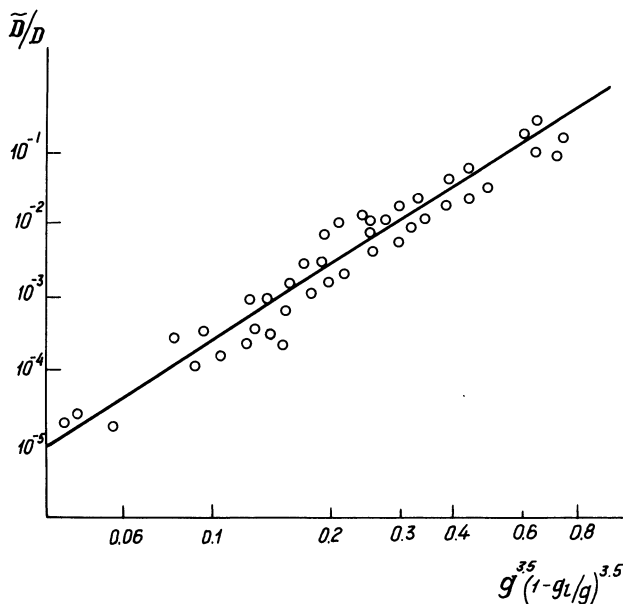


Figure 16. Effective diffusion coefficient in a three-phase system.⁽³⁵⁾

The relationship between the results calculated from the dependence (51) and the experimental data is shown in Figure 16. It can be seen that the data points lie fairly close to the calculated curve. Nevertheless, expression (51) is physically unsubstantiated. Moreover, this formula contains only one parameter of the medium, namely, its porosity. But the kinetic coefficients cannot be expressed in terms of the porosity alone. As already mentioned, a more detailed consideration of the medium structure is necessary. Therefore, such formulas as (51) are not universal, i.e., they are not suitable for the description of any medium, although sometimes such formulas may turn out to be very helpful.

The supply of the reactant to a porous two-phase electrode can be brought about by pumping through the electrode some liquid in which the reactant is dissolved. In such a case, one has to solve the problem of convective diffusion in porous media. In order to avoid the necessity of considering again and again the structure of the porous medium in its whole complexity, one usually proceeds once more to describe it in terms of a homogeneous medium characterized by the effective kinetic coefficients. These coefficients are chosen so that the solution of the problem of fluxes in the homogeneous medium coincides with the real fluxes in porous media.

Let us first consider the regularities governing the flow of liquids and gases through porous media. This problem has been dealt with extensively in the literature.^(7,8) We therefore confine ourselves to giving some general information concerning the problem under consideration. The chief parameter characterizing the motion of a continuous medium is the Reynolds number, $Re = \rho v l / \mu$, where ρ is the density, v the rate of flow, μ the viscosity, and l the characteristic length. When flow in a porous medium is considered, the average size of pores or the diameter of grains constituting the matrix of the medium are usually taken as the parameter l . If the Reynolds number does not exceed several units, the liquid flow is said to be laminar. As the Reynolds number increases from 1 to 10, laminar flow gradually changes into turbulent flow.

The laminar flow of liquids and gases in porous media obeys Darcy's law which relates the volume flow rate q to the pressure difference $P_1 - P_2$:

$$q = K(P_1 - P_2)s/\mu d \quad (52)$$

Here s denotes the cross-sectional area of the medium and d is the length over which the pressure difference is measured. The proportionality coefficient K is referred to as permeability. It characterizes the ability of a porous medium to be permeated by a liquid or a gas under a pressure gradient.

The permeability K is often regarded as an empirical parameter. The physics of the phenomenon under study, however, may be understood only if we establish a relationship between the permeability and some structural characteristics of the medium. Permeability may be calculated by assuming a certain model of the porous medium. For example, the Kozeny formula

derived for the capillary model has found wide use

$$K = \frac{Cg^3}{S_0^2} \quad (53)$$

Here, as usual, g is the porosity and S_0 is the specific surface. The coefficient C is called the Kozeny constant. It depends solely on the shape of the cross section of the capillaries. For the circular cross section, $C = 0.5$; for the square cross section, $C = 0.5619$, and for the regular triangle, $C = 0.5974$. Another important relationship involved is the dependence of permeability on pore radius. In the case of straight circular capillaries of one and the same radius r , we have

$$K = gr^2/8 \quad (54)$$

This formula may be of use for a rough estimation of the pore dimensions.

The main shortcoming of formula (53) is that it has been derived for a regular-structure model, whereas a real porous medium is far from regular. It should be emphasized that, in order to find the permeability of a medium, one should know the microscopic properties of flow. By choosing a definite structure of the medium, we in fact specify the local characteristics of the flow. The regular models, which have been used to find permeability, have been based upon the exact solutions of the Navier–Stokes equation obtainable for a separate structural unit of the model, for example, for a cylindrical capillary of constant radius. In reality, the porous space is irregular, the pore radius varying from point to point. Accordingly, even at low Reynolds numbers the motion of a liquid in the porous medium has much in common with turbulent flow. The fluctuations of velocity in the porous medium are analogous to the pulsation velocity of the turbulent flux. The statistical approach to the calculation of permeability has been developed in a number of works and summarized in a monograph.⁽⁷⁾ One should mention that the determination of the pulsation velocity distribution is very important when solving diffusion problems.

We shall now consider convective diffusion in a porous medium. Let a liquid flowing through a porous medium contain some substance of concentration c . The flux of the dissolved substance is then equal to qc . If, however, the substance concentration in the medium varies from point to point, then there will be an additional contribution to the flux of the substance equal to $\tilde{D}\nabla c$. The role of this term is especially prominent under nonsteady-state conditions. The coefficient \tilde{D} is related not only to the structure of the porous space discussed in the previous section, but also to the properties of the flow of a liquid through the medium. This is the convective diffusion coefficient, which is also referred to as the dispersion coefficient.

In studying the dispersion coefficient, the usually adopted procedure is as follows. A small amount of dynamically neutral admixture is introduced at some point (or cross section) into the liquid flow. This means that the

admixture does not alter the properties of the flow. Such an admixture is called the *label*. The next step is to observe the diffusion of the label. The rate of this diffusion determines the dispersion coefficient.

Dispersion takes place in ordinary laminar flow of liquid through a cylindrical tube. If a label is introduced into the liquid flowing through the tube at the entrance, the label will be dispersed along the tube together with the liquid, at the same time spreading through it. The reason for this spreading (or diffusion) is as follows. Separate layers of liquid move at different velocities. The molecules of the label which diffuse across the flow of the liquid find their way into these layers. The molecules that happened to penetrate into the central layers of the flow are carried away with the liquid faster than those that worked their way closer to the wall of the tube. As a result, the label originally concentrated in a single cross section spreads throughout an increasingly larger volume. According to Taylor,⁽³⁶⁾ the dispersion coefficient is then given by

$$\check{D} = D + \delta r^2 u^2 / D \quad (55)$$

Here, as before, D is the molecular diffusion coefficient, r is the radius of the tube, u is the average velocity of flow, and δ is the factor that takes into account the shape of the cross section of the tube. For a circular cross section $\delta = 1/48$.

Comparison with experiment, however, has revealed that convective diffusion in porous media cannot be described by formula (55). This is due to the fact that the so-called regular models fail to take proper account of the lack of order in real media and the ensuing complexity of the local velocity distribution. Attempts have been made repeatedly to treat the problem statistically. For example, Saman⁽³⁷⁾ and Nikolaevskii⁽³⁸⁾ represented a porous medium as an assembly of capillaries, which can be characterized by a certain distribution in radii. In the models adopted, the dispersion coefficient was calculated.

When one considers a whole assembly of pores, rather than a single pore, the main property of convective diffusion becomes strikingly prominent. Namely, flow through a porous medium displays very similar characteristics under both laminar and turbulent conditions. It is easily understandable, because the velocity of liquid in each pore depends on the pore dimensions, which vary randomly from point to point. The velocity of flow is therefore a random function of coordinates. This is virtually the same situation observed in ordinary turbulent flow. Accordingly, the spreading of a neutral admixture obeys a law similar to that governing diffusion in a turbulent flow.

The random character of flow through porous media may be described⁽³⁹⁾ by a random tensor T_{ij} , which relates the components of the true velocity v_i to those of the average velocity of flow u_j

$$v_i = \sum_j T_{ij} u_j \quad (56)$$

Further analysis indicates that the dispersion coefficient should be proportional to the product of the average velocity u by some length l characteristic of a given medium:

$$\tilde{D} = ul \quad (57)$$

It is impossible to obtain more specific results at this stage. In order to proceed further, one should adopt some model of the porous medium. Here the model of cells of perfect mixing⁽⁴⁰⁾ has turned out to be very useful in the relevant calculations over a wide interval of Reynolds numbers, especially at their large values.

In porous media consisting of packed or sintered particles, the porous space is represented by individual cells linked with one another by narrow passages. At sufficiently high Reynolds numbers, the motion in a separate cell becomes turbulent. This process is assisted by the fact that in each cell there enter several currents coming from various directions and having different velocities. Thus it may be assumed that within a single cell, a liquid (or a gas) is well mixed and that the concentration of the substance introduced is uniform throughout the cell. This provides the physical basis for the model of cells of perfect mixing. A porous medium is modeled as a row of cells through which a three-dimensional flow of liquid, q , passes. For brevity, we shall discuss only the flow of a liquid, although all the arguments to be presented are equally valid for the flow of gas. If the volume of a cell is denoted by V and its length by l , the average velocity of flow is given by

$$u = ql/V \quad (58)$$

In order to find the dispersion coefficient, let us suppose that a label in the form of a certain number, m , of dynamically neutral particles is introduced into the flow entering the first cell. Since the flow going out of the cell is q , each of these particles may leave the cell in a unit time with the probability q/V . This means that the time during which a particle stays in a cell is a random variable with the distribution density $f(t) = q \exp(-qt/V)/V$. In this case, the average time during which the particle stays in the cell and the mean-square deviation from it are given by

$$\bar{t} = V/q, \quad \sigma^2 = \overline{(t - \bar{t})^2} = V^2/q^2 \quad (59)$$

The total time in which a particle passes through n cells is the sum of n independent random variables having the same distribution density.

As follows from the central limit theorem in probability theory, the above sum (the total time T) tends to the normal (Gaussian) distribution as n tends to infinity:

$$\bar{T} = n\bar{t} = nV/q, \quad \overline{(T - \bar{T})^2} = n\sigma^2 = nV^2/q^2 \quad (60)$$

This means that the concentration of the label particles in the flow going out

of the n th cell varies with time according to the law

$$c(n, T) = \frac{m/V}{(2\pi n\sigma^2)^{1/2}} \exp \left[-\frac{(T - \bar{T})^2}{2n\sigma^2} \right] \quad (61)$$

The ratio m/V is the initial concentration of the label in the first cell.

For ordinary diffusion of a substance in a continuous flow, the spreading of a label introduced at a single point is also determined by the normal distribution. For one-dimensional diffusion, the label concentration measured after a time T at some distance d from the point at which the label has been introduced is described by the function

$$c(d, T) = \frac{B}{(4\pi\tilde{D}T)^{1/2}} \exp \left[-\frac{(d - uT)^2}{4\tilde{D}T} \right], \quad (62)$$

where B is a constant.

If a sufficiently large distance d is chosen, namely, if $d \gg \tilde{D}/u$, the most essential dependence of the label concentration on time is determined by the numerator of the exponent. In all the remaining cases, T may be replaced quite harmlessly by d/u . As a result, formula (62) will assume the form

$$c(d, T) = \frac{B}{(4\pi\tilde{D}d/u)^{1/2}} \exp \left[-\frac{(T - d/u)^2}{4\tilde{D}d/u^3} \right] \quad (63)$$

The formal coincidence of expressions (61) and (63) enables one to turn to a homogeneous description of the porous medium and to introduce the effective coefficient of convective diffusion or dispersion, \tilde{D} . A comparison of these formulas makes it possible to establish the relationship between the parameters characterizing these problems. Specifically, for the dispersion coefficient, we get

$$\tilde{D} = ul/2 \quad (64)$$

For the description of a porous medium in terms of diffusion to be valid, it is necessary that sufficient time elapses to allow the normal concentration distribution to set in. To achieve this, a large number of cells is required:

$$n \gg 1, \quad (65)$$

i.e., the medium should be sufficiently extensive. The greater n , the more exact is the description in terms of diffusion.

In expression (64), the length of an elementary cell is taken as the characteristic length l . For a rhombohedral close packing of spheres, it amounts to 0.815 of the diameter of a sphere. For a random packing, l may be considered to be equal to the diameter. The value of the dispersion coefficient thus found has been confirmed experimentally.

As the rate of flow decreases, the dispersion coefficient may become different from that given by Eq. (64). One of the reasons for such a deviation

is that the hydrodynamical mixing in cells deteriorates. A part of the total cell volume is occupied by the so-called "stagnant zones," which do not participate in the mixing. The stagnant zones serve as traps for the diffusing matter, thus increasing dispersion. Especially pronounced are the stagnant effects in the neighborhood of contact points between solid particles. These regions are equivalent to deep, narrow channels. Turbulent pulsations do not penetrate into them, the true local velocity of flow is close to zero there, and the transport of substance is brought about only by a slow process of molecular diffusion.

We shall now investigate the dispersion coefficient in the case when there are stagnant zones in the medium.^(41,42) Let the porous medium represent a succession of identical cells, each having volume V and length l . A part of this volume, equal to αV , is occupied by a stagnant zone, the rest of the volume, $(1 - \alpha)V$, being taken up by a zone of perfect mixing. There is an exchange of substance (liquid or gas) between these two zones, which proceeds at a rate p .

The mechanism of exchange between the stagnant zone and the zone of perfect mixing may be both convective and diffusional. We shall not describe it here in detail. An exact theoretical calculation of the rate of exchange is hardly possible, because of the complexity of porous structure. But the exchange rate can be estimated easily. For example, if the diffusional exchange mechanism is assumed, then, from the dimensional analysis, it follows that the exchange rate should be proportional to the product of the molecular diffusion coefficient by a certain parameter having the dimension of length. This parameter may be represented by the square root of the value of the boundary separating the two zones. This value may be estimated from hydrodynamical considerations. Clearly, the boundary between the zones will diminish with increasing rate of flow. Consequently, the parameter p is a decreasing function of the flow rate.

Evaluation of parameter p shows the essential difference between a liquid and a gas. For the former, the stagnant zones play a more significant role than for the latter, because the molecular diffusion coefficient for liquids is much smaller than that for gases. The dimensional analysis enables one to find the order of magnitude of the rate of exchange, provided that its mechanism is known. One should, however, bear in mind that the exchange mechanism can be extremely complicated and that there may be several exchange mechanisms operating concurrently.

Omitting mathematical manipulations,⁽⁴³⁾ we present the net result of the calculation for the model of cells of perfect mixing containing stagnant zones. The expression for the effective diffusion coefficient has the form

$$\tilde{D} = ul/2 + ul\alpha^2 q/p, \quad (66)$$

where $l = d/n$ is the length of a cell and $u = ql/V$ is the average velocity of flow.

If a system does not contain stagnant zones, in other words, if $\alpha = 0$, it is known^(41,43) that the diffusion coefficient has the form of $ul/2$. Formula (66) also takes into account the dispersion associated with the mixing in the "running" zone and with the exchange of a particle between the running and stagnant zones. It is of interest to note that the first term in Eq. (66) coincides with the diffusion coefficient in the case when a cell is free of stagnant zones, i.e., the cell is entirely a "running" one. In reality, a part of the cell is occupied by a stagnant zone. Therefore, one should not think that in formula (66) there are two additive terms, each of which is responsible for a definite mechanism of mixing.

The presence of the second term on the right-hand side of Eq. (66) may make the diffusion coefficient very large and this, in turn, may place a very severe restriction upon the value of d [characterizing the extension (length) of a porous medium] which is necessary for the normal distribution to set in. As a result, in an experimental determination of the dispersion coefficient, the chosen length of the porous medium may be insufficient to allow a valid description in terms of diffusion. In practice, this is apparent in the fact that at the system termination the concentration distribution exhibits a very long and stable temporal "tail," whereas the approximation of the experimental dependence by an appropriate normal distribution results in a strongly underestimated value of the dispersion coefficient.

4.2. Diffusion in Gases

The character of gas diffusion in the porous space of electrodes is largely determined by the relationship between the average pore radius r and the mean free path λ . If the latter is expressed in centimeters and the gas pressure in atmospheres, the mean free path is roughly given by⁽⁴⁴⁾

$$\lambda = 10^{-5}/P \quad (67)$$

Formula (67) shows that at $P = 1$ atm, $\lambda = 10^{-5}$ cm. When $\lambda \ll r$, a gas may be treated as a continuous viscous medium; at $\lambda \gg r$, one deals with the molecular (Knudsen) gas flow.

In porous bodies, the pore diameters are small; therefore, a Knudsen gas may exist even at atmospheric pressure. Here, the rigorous criteria are as follows. At Knudsen numbers $\text{Kn} = \lambda/r \geq 10$, we have a Knudsen region of gas flow; at $10 \geq \text{Kn} \geq 10^{-1}$, the region will be transient and at $\text{Kn} \leq 10^{-1}$, the gas may be regarded as a continuous medium. Thus at $P = 1$ atm, in porous electrodes with the pore radius $r \leq 10^{-6}$ cm, we have a Knudsen gas flow, but for the pore radius $r \geq 10^{-4}$ cm, the flow becomes viscous.

If the mean free path of the gas molecules is considerably smaller than the pore diameter and if the concentration of the diffusing admixture is small in comparison with the total gas concentration, the flux of the substance

transported is given by

$$N = -D \nabla c, \quad (68)$$

where D is the diffusion coefficient and c is the concentration of the diffusing admixture. Resistance to transport arises then due to collisions of the gas molecules with each other. In the Knudsen gas, the dominant role is played by the collisions of the molecules with the pore walls, while the presence of other gases does not affect the diffusion of the chief component. However, if there is a one-component gas in the pores, one should speak of the flow of the gas and not of its diffusion.

We shall consider next several examples of gas transport through an individual pore. Let a pore contain a mixture of two gases with molar concentrations c_1 and c_2 . The molar fluxes of these two substances per unit area are denoted by N_1 and N_2 , respectively. The total molar flux is $N = N_1 + N_2$. For the flux of component 1, the following equation is valid

$$N_1 = -D_{12} \frac{dc_1}{dx} + c_1 \bar{N}/c, \quad (69)$$

where D_{12} is the binary diffusion coefficient, c is the total gas concentration equal to $c = c_1 + c_2$. This equation may be integrated if the ratio of fluxes N_1/N_2 is known.

Of particular interest is the case when one of the components is represented by the reactant consumed in the reaction and where the other component is inert. Ordinary air supplied to the oxygen electrode may furnish an example. In such a system the flux of the inert gas, N_2 is zero, while the total flux is equal to the reactant flux:

$$N = N_1 \quad (70)$$

Substituting this equation into Eq. (69) and solving for N_1 , we find

$$N_1 = -D_{12} \frac{dc_1}{dx} / \left(1 - \frac{c_1}{c}\right) \quad (71)$$

If the gas pressure varies very little along a pore, the total gas concentration c will be constant. This facilitates the integration of Eq. (71). Let the component concentration at the pore entrance be denoted by c_{10} and c_{20} ; the reaction takes place at some distance d from the entrance, the reactant concentration at this point being c_1 . The expression for the flux is given by

$$N_1 = (D_{12}c/d) \ln \frac{c - c_1}{c_{20}} \quad (72)$$

This formula makes it possible to determine the maximum possible value of the flux, which can be reached when $c_1 = 0$. In electrical units, the limiting current will be

$$j_{\text{lim}} = (nFD_{12}c/d) \ln c/c_{20} \quad (73)$$

Table 1
Dependence of the Coefficient f on the c_{10}/c Ratio

c_{10}/c	0	0.3	0.6	0.9
f	1	1.189	1.527	2.558

where n is the number of electrons taking part in the reaction of a single molecule and F is the Faraday number.

Equation (73) can be rearranged to take the form convenient for comparison with the usual Fick's law of diffusion

$$j_{\text{lim}} = fnFD_{12}c_{10}/d, \quad (74)$$

where

$$f = (c/c_{10}) \ln (c/c_{20}) \quad (75)$$

If the coefficient f is unity, we have a purely Fick-type diffusion. Therefore, this quantity gives the deviation from the ordinary law. It depends on the portion of the reacting gas in the mixture. This is illustrated in Table 1, which lists the values of the coefficient f at different molar fractions of the reacting gas. One concludes that, if the reactant content is not too high, the coefficient f is close to unity and the transport of gas is satisfactorily described by Fick's law.

Formula (74) describes the limiting diffusion current per unit area of the pore cross section. Let us now estimate the limiting current per unit area of the apparent surface of an electrode. If the porosity of the electrode is g , then the part of the apparent surface of the electrode confined within the pore mouths will also be g . If all the pores were represented by parallel cylinders of length d , the limiting diffusion current per unit area of the electrode's apparent surface could be obtained from formula (74) by multiplying it by the porosity g :

$$j_{\text{lim}} = nFD_{12}gc_{10}f/d \quad (76)$$

Let us estimate this quantity numerically. Putting $n = 4$, $D = 10^{-1} \text{ cm}^2 \text{ s}^{-1}$, $d \sim 10^{-1} \text{ cm}$, $g \sim 0.5$, $c_{10}/c \sim 0.5$, and $P = 1 \text{ atm}$, we obtain $f = 1.38$ and the current $j \sim 6 \text{ A cm}^{-2}$. Such a small value of the limiting current has been obtained because in integrating Eq. (71), we have assumed that the gas pressure along the pore remains unchanged. This is true only in the case when the fraction of the diffusing component is very small. Thus the obtained results are applicable only when the relative concentrations of the reacting gas are low. In the opposite case, the gas pressure changes along the pore and it becomes necessary to consider the flow of the gas under the influence of the pressure gradient. For simplicity, we shall consider a single-component gas.

The flow of a gas in a circular cylindrical capillary is governed by Poiseuille's law provided that the capillary radius is sufficiently large. In a narrow capillary, it obeys Knudsen's law. An interpolation formula has been derived⁽⁷⁾ which covers both the extreme cases, as well as the case of the transition zone between them. The molar flux flowing through a tube of radius r and length d is given by

$$Q = (\pi r^2 \Delta P / d) [r^2 \bar{P} / 8 \mu R T + A \frac{4}{3} r (2 / \pi R T M)^{1/2}] \quad (77)$$

Here ΔP is the pressure difference between the ends of the tube, \bar{P} is the average value of pressure in the tube, μ is the viscosity, R is the gas constant, T is the absolute temperature, and M is the molecular weight. The quantity designated as A is called the Adzumi constant; for a single-component gas it is equal to 0.9, whereas for a mixture of gases it is about 0.66.

The first term in formula (77) describes the Poiseuille flow, while the second term gives the effect of Knudsen flow. The relative role of these terms depends on the tube radius. The first term contains the squared radius and plays the main role in wide capillaries, whereas in narrow capillaries the second term takes over.

If, again, we represent an electrode as an assembly of parallel capillaries of constant radius r , the diffusion current per unit area of the apparent surface will (in electrical units) be

$$j = n F N Q \quad (78)$$

where N is the number of pore mouths per unit area of the electrode's apparent surface. This number is given by the expression $N = g / \pi r^2$, g being the porosity. Let us now find the limiting value of the diffusion current per unit area of the apparent surface. This value is reached if, at the end of a pore where the reaction takes place, the pressure is zero. If the pressure is P at the pore entrance, then $\Delta P = P$ and $\bar{P} = P/2$. Substituting this into Eq. (79), we obtain

$$j_{\text{lim}} = [(n F g P) / d] [r^2 P / 16 \mu R T + A \frac{4}{3} r (2 / \pi R T M)^{1/2}] \quad (79)$$

Let us now estimate the limiting value of diffusion current at room temperature and atmospheric pressure. Let $g = 0.5$, $d = 10^{-1}$ cm, $r = 10^{-4}$ cm, and $\mu = 10^{-4}$ poise. To be specific, let us consider oxygen; in this case, $n = 4$ and $M = 32$. Substituting this into Eq. (79), we find that $j_{\text{lim}} = 700$ A cm⁻².

We have thus obtained a much higher value for the limiting diffusion current than that previously obtained by formula (76). It should be noted that in the latter case a more exact physical picture of gas transport has been assumed. The value of the limiting current just obtained by formula (79) is also considerably higher than those of currents usually collected from electrodes in practice. Therefore, there are practically no difficulties involved in the gas supply by diffusion in the electrode. The rate of current generation is determined by the other stages of the process.

A detailed treatment of the theory of kinetic phenomena in liquids and gases can be found in monographs^(45-47a) and papers.^(47b-47e)

4.3. Effective Electrical Conductivity

The calculation of the effective electrical conductivity of porous media is of great importance not only for the theory and practice of operation of porous electrodes, but also for a number of other problems; for example, electric logging, evaluation of oil-bearing capacity of geological strata, and so on.

4.3.1. Two-Phase Systems

We shall first consider the passage of electrical current through the electrolyte solution saturating completely a porous medium. It will be assumed that the current does not pass through the matrix of the medium. In this case, the problem becomes analogous to that arising in the study of laminar flow or molecular diffusion in a porous space. For the current I passing through a porous layer of thickness d and area S_0 under the influence of the potential difference $\Delta\phi$, one may write a relationship similar to Darcy's law

$$j = \tilde{\kappa} S_0 \Delta\phi / d \quad (80)$$

This relationship serves in fact as the definition of effective electrical conductivity $\tilde{\kappa}$, which is dependent upon the electrical conductivity of the electrolyte κ and upon the structure of the porous medium. If the pores were represented by cylinders of constant cross sections with the tortuosity factor β , then by direct analogy with formula (50), one would be able to write

$$\tilde{\kappa} = \kappa g / \beta^2 \quad (81)$$

If the pores are distributed according to their radii, assuming that the radii remain constant along single pores, then relationship (81) remains valid. If, however, the pore radius varies from point to point, i.e., the pore is corrugated, the effective electrical conductivity is no longer given by formula (81). One can readily demonstrate⁽²⁸⁾ that in the serial model the change in Eq. (81) reduces to the appearance of an additional factor multiplying β^2 , which is the product of the average square of the pore radius and the reciprocal average square of the pore radius, i.e., $\overline{r^2} \cdot \overline{r^{-2}}$. From general considerations it follows that this product should be greater than unity, so that the electrical conductivity of the corrugated pores is lower than that of the pores of constant cross section. This fact has been repeatedly mentioned in experimental studies. It is quite evident that the pore intersections must significantly influence the effective electrical conductivity, as does their corrugated nature. This question has not yet been treated theoretically. Because of the absence of a reliable theory, attempts have been made to include the effect of the

complexity of the porous structure into the tortuosity factor β (as is sometimes done in solving the diffusion problem), while retaining formula (81). In such a case, the factor β loses its original physical meaning, becoming simply a fitting parameter. In studying the effective electrical conductivity experimentally, the structural details of the porous medium are disregarded and empirical formulas are found, which express the electrical conductivity in terms of the porosity alone. For example, in the literature one often encounters the following empirical formula

$$\tilde{\kappa} = \kappa g^m, \quad (82)$$

where m ranges from 1.3 to 3.0 in different media.

4.3.2. Three-Phase Systems

In experiments, one often has to deal with a medium only partially filled with electrolyte. In this case, another empirical formula is employed

$$\tilde{\kappa} = \kappa g^m (g_l/g)^n, \quad (83)$$

where g is the total porosity, g_l is the liquid porosity, m and n are constants characterizing the medium, n being approximately equal to 2. The accuracy and range of application of this formula are not great. In the literature, one can also encounter other empirical relationships of the same type as formula (83). However, we shall not discuss them because of their lack of generality and physical meaning.

Turning to the calculation of the effective electrical conductivity, it is natural to start with the case when the nonconducting phase of the medium, for example, a gas, is represented by inclusions present in the medium in a small concentration. The calculations of the effective electrical conductivity of such systems with inclusions of the insulating or poorly conducting phases have long been attempted. As an illustration, we present the formula⁽⁴⁸⁾

$$\tilde{\kappa} = \kappa_1 [1 + 3(\kappa_2 - \kappa_1)\theta / (\kappa_2 + 2\kappa_1)] \quad (84)$$

where θ is the concentration of spherical particles of conductivity κ_2 ($0 \leq \theta \leq 1$) and where κ_1 is the electrolyte conductivity. Naturally, this formula is applicable only at small concentrations of the inclusions. This can be seen from Figure 17 borrowed from a work⁽⁴⁹⁾ in which the electrical conductivity of mixtures of metal powders with insulators ($\kappa_2 = 0$) has been measured. In recent years, attempts have been made^(25,49) to extend formulas of the type of (84) to cover the range of the higher concentrations θ . However, the accuracy attained with these formulas becomes markedly poorer as the breakthrough point is approached. One can see already from Figure 17 that the effective electrical conductivity becomes nonzero only after a certain threshold concentration of conducting inclusions has been reached, i.e., as soon as these inclusions have formed a single coherent system. Thus the problem of calcula-

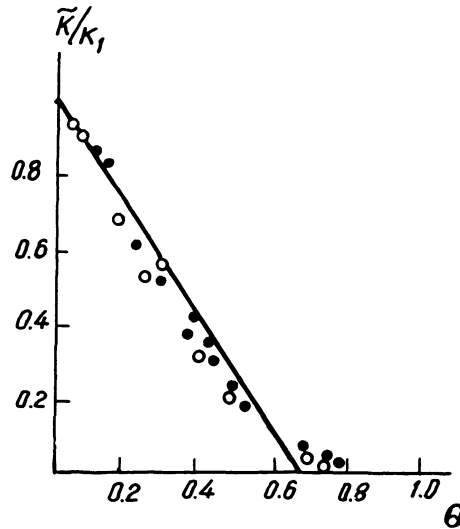


Figure 17. Effective electrical conductivity in a binary mixture.⁽⁴⁹⁾

tion of the effective electrical conductivity reduces, to a certain extent, to the percolation problem. It would be therefore natural to rest (e.g., in lattice models) upon the theory of capillary equilibrium as outlined in Section 3.

Figure 18 shows the results of the Monte-Carlo calculations⁽²⁵⁾ of the dependence of the percolation probability (solid curve) and the effective electrical conductivity (points of that curve are denoted by triangles) upon the fraction, γ , of links of a cubic lattice permeable to the electrolyte. In such a cubic lattice of links, the breakthrough occurs at $\gamma_* = \frac{1}{4}$. At the same moment, the effective electrical conductivity first becomes nonzero. The dashed curve corresponds to the calculation based on self-consistent field theory. As can be seen from the figure, at $\gamma \rightarrow \gamma_*$ this curve does not coincide with that obtained by the Monte-Carlo method.

The question of the disagreement between the curves for \tilde{P} and $\bar{\kappa} = \tilde{\kappa}/\kappa$ shown in Figure 18 is worth mentioning. Everywhere in a porous medium with the exception of the narrow breakthrough zone, $\gamma \sim \frac{1}{4}$, the quantity \tilde{P} has the meaning of the fraction of links permeable to electrolyte, which adjoin, at least at one of their two ends, an infinite, single system of links of the cubic lattice filled with electrolyte. The fact that the curve $(\bar{\kappa}, \gamma)$ lies below the curve (\tilde{P}, γ) has a simple physical explanation.^(50,51) In porous media partly filled with electrolyte, all the electrolyte-filled pores may be divided into two categories: “blind” pores which are filled with electrolyte at one end only and “through-going” pores which are filled with electrolyte at both ends. It is clear that only the through-going pores can contribute to the electrical conductivity of the medium. In the vicinity of the breakthrough point, the through-going pores are still few; therefore the value of $\bar{\kappa}$ is close to zero. The number of through-going pores is primarily determined by the structure

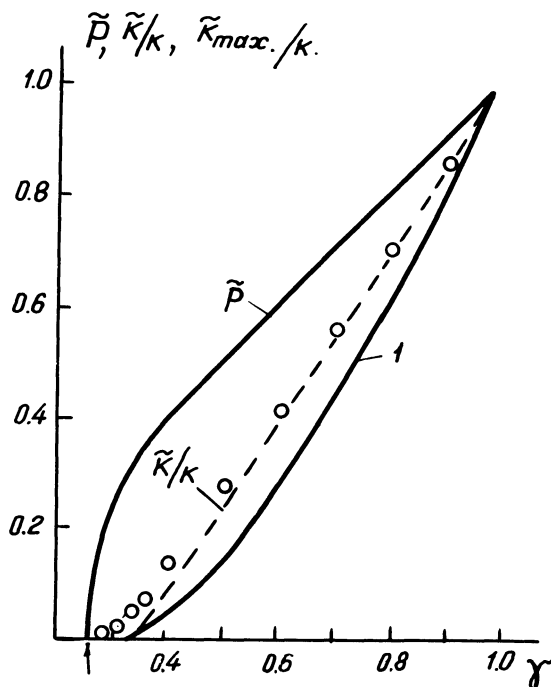


Figure 18. Percolation probability⁽²⁵⁾ and the effective electrical conductivity^(25,51) in lattices. Curve 1 has been calculated according to references 39 and 85.

of the porous space in the electrode. Thus there arises a tempting possibility of evaluating the structure of one porous electrode or another from the behavior of the $(\tilde{\kappa}, g_l)$ curve.

In order to establish the relationship between this function and electrode structure, we shall turn to model representations. Let us estimate the upper limit of the effective electrical conductivity in lattices of links.⁽⁵¹⁾ If all the through-going links are arranged in rows parallel to the direction of the electric field, $\tilde{\kappa}$ will evidently assume its maximum value. Let Z be the probability that a link is filled with electrolyte from one of the sides (which one is preliminary specified). Then $\tilde{Z} = Z^2$ is the probability that the link will be a through-going one. And the number of through-going links determines the value of $\tilde{\kappa}_{\max}$:

$$\tilde{\kappa}_{\max} = \kappa g \tilde{Z} = \kappa g Z^2, \quad (85)$$

where g is the total porosity of the lattice of links. The dependence of $\tilde{\kappa}_{\max}$ on γ , which has been calculated according to formula (39), is presented in Figure 18, curve 1. The liquid porosity of the lattice of links is given by

$$g_l = g[1 - (1 - Z)^2] \quad (86)$$

Therefore, eliminating Z from Eqs. (85) and (86), we find the relationship

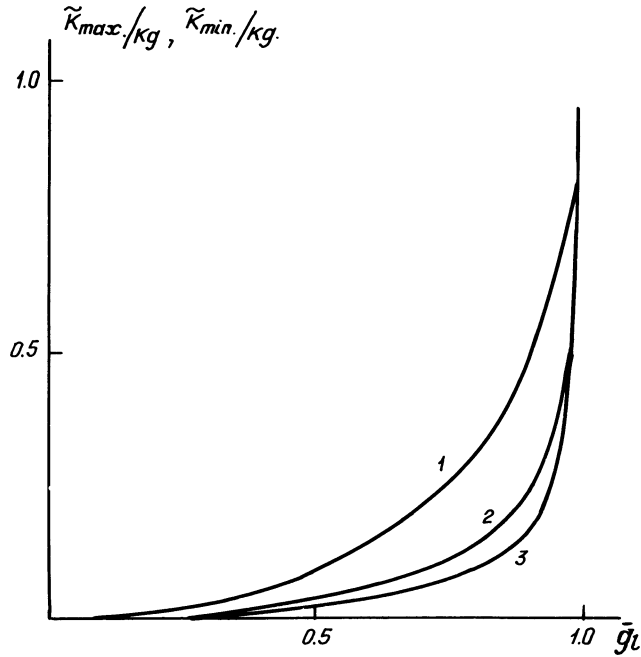


Figure 19. Reduced electrical conductivities of link lattices. (See text for explanation.)

between $\tilde{\kappa}_{max}$ and the liquid porosity

$$\tilde{\kappa}_{max} = \kappa g / [1 - (1 - \bar{g}_l)^{1/2}]^2, \tag{87}$$

where $\bar{g}_l = g_l/g$ is the reduced liquid porosity. The dependence of $\tilde{\kappa}_{max} = \tilde{\kappa}_{max}/\kappa g$ upon \bar{g}_l is shown in Figure 19, curve 1. From this dependence it follows that the “blind-pore” effect makes it possible to explain the difference between the curves for $\tilde{\kappa}(\gamma)$ and for $\tilde{P}(\gamma)$. It is also of interest to note that the effect just indicated appears to underlie the quadratic dependence of $\tilde{\kappa}(g_l)$ in formula (83). One should emphasize that the curve obtained has a universal character, because the derivation of formula (87) is independent of the coordination number of the lattice.

The lower limit for the electrical conductivity of the lattice of links, $\tilde{\kappa}_{min}$, will be obtained if all rows made up by the through-going links are assumed to have the maximum tortuosity, but the pore intersections are neglected (i.e., in intersecting pores, the electrical current will take the shortest possible routes, which will result in an increase in electrical conductivity). Then, for the square and cubic lattices of links, we obtain

$$\tilde{\kappa}_{min, cn=4} = \frac{\kappa g}{2} \left[1 + 3 \left(\frac{1}{Z} - 1 \right) \right]^{-1}, \quad \tilde{\kappa}_{min, cn=6} = \frac{\kappa g}{3} \frac{Z^{1/2}}{[1 + 7(Z^{-1/2} - 1)]} \tag{88}$$

The relationship between these quantities and the liquid porosity is presented in Figure 19, curves 2 and 3.

Apart from the evaluation of $\tilde{\kappa}_{\max}$ and $\tilde{\kappa}_{\min}$ for lattices of links and sites, a procedure has been developed which makes it possible to calculate, to any desired degree of accuracy, the effective electrical conductivity of regular lattices of links filled either partly or completely with electrolyte.⁽⁵²⁾

5. Electrochemical Activity of Electrodes

5.1. Two-Phase Electrodes

In two-phase systems, a porous electrode is completely filled with an electrolyte, in which the reactants and the reaction products are dissolved. A multitude of reactants may be involved in an electrochemical process but, in almost every case, it is possible to isolate one substance, usually present in the solution at a low concentration, whose relative change in concentration is great and whose concentration in a definite zone of the electrode may drop to zero, whereas the concentrations of the other reactants involved in the electrochemical process change but little. Such a substance is commonly referred to as the limiting (or key) reactant of the process. For simplicity, in the subsequent analysis we shall be discussing only the key reactant, disregarding completely the process of removal of the reaction products.

The process of electrical current generation in two-phase electrodes comprises a number of stages. In the first stage, the reactants are transported through a solution to the outer surface of a porous electrode. This stage, which is called the external diffusion stage, depends first of all on the conditions of mixing. If there is some indifferent electrolyte in the solution, then, in order to estimate the reaction rate at this stage, one may resort to relationship (2), where $C_{B,0}$ is the reactant concentration in the solution volume and δ is the diffusion layer thickness.

The next stage is the transport of the reactants through the porous space of the catalyst filled with the electrolyte. Finally, there take place adsorption, the electrochemical reaction, and the generation of ionic current. The electrochemical reaction proceeds both on the outer and inner surfaces of the electrode. If the electrode material is highly active, so that the exchange current exceeds the limiting current of external diffusion, then at sufficiently high potentials the reactant concentration at the outer surface tends to zero. As a result, the reactants do not penetrate into the porous electrode and the electrical current is largely generated at the outer surface. Under such a relationship between the constants of the electrochemical reaction and those of external diffusion, the application of porous electrodes is, as a rule, impractical, because the increase in current obtained by developing the electrode's surface is negligible. However, there exist devices (e.g., conversion units in electrochemical transducers), where the use of a porous membrane made of

an active material is dictated by other considerations. Namely, in order to retain the linear characteristics of such a device, it is necessary to attain total consumption of the reactant, which is just what the porous membrane is intended to achieve.

In most of the applications, a porous electrode is efficient in those cases when kinetic conditions are achieved on its outer surface and the reactant concentration is close to the bulk one. In such cases, the process of current generation may be intensified considerably by developing the inner surface of the electrode.

When an electrical current passes through a porous electrode, the current distribution in the latter is not equipotential. We mean, of course, the potential in the solution filling the pores of the electrode. The current passing through the pores gradually shunts into the electrode's matrix as a result of the electrochemical reaction. The presence of the ohmic, activational, and concentrational resistances in the electrode changes the potential distribution in it in such a way that, in practice, the electrochemical reaction penetrates only to a limited depth.

The quantitative treatment of such systems is based upon the following procedure suggested by Zel'dovich.⁽⁵³⁾ A porous medium is treated as a homogeneous one in which the volume reactions described by some effective parameters take place, whereas the transport processes are characterized by effective coefficients determined by the true coefficients and structural factors. Such a description is sufficiently exact provided that the grain dimensions are small in comparison with the characteristic lengths of the processes involved.

The last question has been considered in detail by Frumkin,⁽⁵⁴⁾ who investigated the problem of current distribution in a semi-infinite tube of radius r filled with an electrolyte solution, with a specified value of the potential at the entrance to the tube. The conductivity of the tube material was assumed to be infinitely high, with the reactant concentration remaining constant. The electrochemical reaction proceeds on the walls of the tube. An analysis of the solution to this essentially two-dimensional problem has revealed that, in those cases in which the parameter $(r/l)^2 \ll 1$, where l is the characteristic length of the process, the problem may be treated as one-dimensional.

Let us now return to the analysis of the two-phase electrodes. If there are n components in a liquid, of which m components take part in the electrochemical reaction, the equation for the parameters averaged over some cross section will be written in the form^(55,56)

$$\begin{aligned} \operatorname{div} \mathbf{j}_k &= -S_0 I(\eta, c_k), & k \leq m \\ \operatorname{div} \mathbf{j}_i &= 0, & l \leq n - m \\ \sum z_i c_i &= 0, \end{aligned} \tag{89}$$

where the subscript k refers to the discharging components and i to those substances which do not participate in the reaction, S_0 is the specific inner

surface of the medium under consideration, and $I(\eta, c_k)$ is the polarization curve for a smooth electrode.

It is assumed, as usual, that the system is electrically neutral. In the general case, the flux of any component must evidently include three terms: the diffusion, migration, and convection fluxes, i.e.,

$$\mathbf{j}/zF = -\tilde{D}\nabla c - \tilde{u}c\frac{|z|}{z}\nabla\eta + \mathbf{v}c \quad (90)$$

where \mathbf{v} is the velocity of the liquid flow, \tilde{u} is the effective mobility, z is the charge number, and \tilde{D} is the effective diffusion coefficient. Here and in what follows, it is assumed that the solution is dilute. The extension to the case of concentrated solutions is discussed at length in Chapter 6 of the present volume; we therefore shall not consider this question, especially because it does not help to elucidate the specific character of porous media.

It presents no difficulty to supplement the set of equations (89) to include the potential drop in the matrix.⁽⁵⁷⁾ This set of equations is sufficiently complicated so it is best to consider a number of particular cases.

5.1.1. Ohmic-Activation Conditions

These are achieved when there are no concentrational difficulties in the system. The input polarization in the system is assumed to be specified and equal to η_0 . Let us denote by η the mean polarization. In accord with Eq. (90), the current density should have the form

$$\mathbf{j} = -\tilde{\kappa}\nabla\eta \quad (91)$$

where $\tilde{\kappa}$ is the effective electrical conductivity (see Section 4.3). The equation of continuity then assumes the form

$$\tilde{\kappa}\frac{d^2\eta}{dx^2} = S_0I(\eta) \quad (92)$$

In the derivation of this equation, it has been assumed that the potential changes insignificantly across each capillary. It should further be assumed that at a given x the actual potential values in any two channels are close to each other.

If the polarization characteristic is linear, i.e., if $I = \chi\eta$, the solution to Eq. (92) has, in the case of a semi-infinite electrode, an especially simple form

$$\eta = \eta_0 \exp(-x/l) \quad (93)$$

where

$$l = (\tilde{\kappa}/\chi S_0)^{1/2}, \quad \eta_{x=0} = \eta_0 \quad (94)$$

Thus the electrochemical process falls off exponentially as it penetrates deeper into the electrode.

This reaction proceeds intensely only in that region of the electrode of which thickness is of the order of l , so that it is not expedient to make electrodes of greater thickness. The electrochemical activity, j , of a porous electrode turns out to be proportional to the constants characterizing the rate of the process⁽⁵⁸⁾

$$j \sim (\tilde{\kappa}\chi S_0)^{1/2} \quad (95)$$

One can readily derive the expression for the current–voltage characteristic of a porous electrode in the nonlinear case when

$$I = \chi b \sinh(\eta/b), \quad b = 2RT/F \quad (96)$$

We have

$$j = 2b(\chi\tilde{\kappa}S_0)^{1/2} \sinh(\eta_0/2b) \quad (97)$$

Comparing (96) with (97), one can see that a porous electrode is characterized by the effective reaction-rate constant $\tilde{\chi} = 2(\chi S_0\tilde{\kappa})^{1/2}$ and by the activation energy which is twice as low. The solution of such a problem for a thin porous electrode presents no difficulties.

5.1.2. Diffusion Conditions

These occur when, aside from electrochemically active substances, there is an excess of some extraneous (background) electrolyte. Such a system may be treated as equipotential so that the process is determined by the active component concentration distribution, which is described by the equation

$$\tilde{D} \frac{d^2c}{dx^2} = S_0 I(\eta, c) \quad (98)$$

where c is the average reactant concentration. In some cases, at sufficiently high potentials, the polarization characteristic has the form

$$I = \tau c \exp(\eta/b) \quad (99)$$

so that

$$\frac{d^2c}{dx^2} = (\tau S_0 / \tilde{D} n F) \exp(\eta/b), \quad (100)$$

where polarization is treated as a parameter. The solution to this equation is as follows⁽⁵⁹⁾:

$$\begin{aligned} c &= c_0 \exp(-x/l_a), \\ j &= (nF\tilde{D}S_0\tau)^{1/2} c_0 \exp(\eta/2b) \end{aligned} \quad (101)$$

where $l_a = (nF\tilde{D}/S_0\tau)^{1/2} \exp(-\eta/2b)$ is the characteristic length.

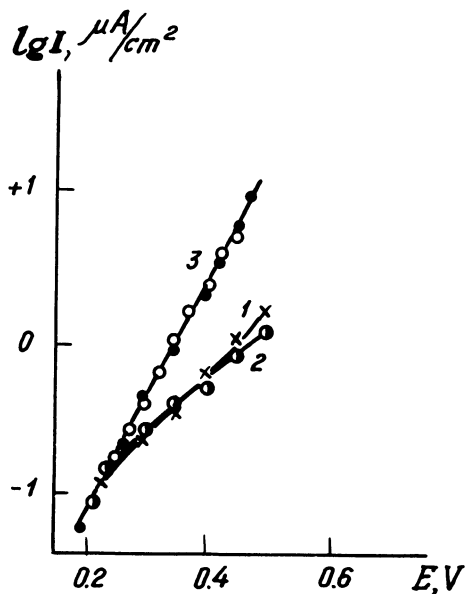


Figure 20. Polarization curves for methanol electrooxidation.⁽⁶⁰⁾

Formula (101) may be thought as giving the polarization characteristic of a porous electrode. It is of interest to compare it with the polarization characteristic of a smooth electrode (99). The comparison shows that the porous electrode is characterized by the effective reaction-rate constant $\tilde{\tau} = (nFS_0\check{D}/\tau)^{1/2}$ and by half the activation energy necessary for the smooth electrode. The efficiency of the porous electrode is given by the relation

$$\tilde{\tau}/\tau = (nFS_0\check{D}/\tau)^{1/2} \quad (102)$$

i.e., it increases with the increasing specific surface and the decreasing rate of the electrode process.

To illustrate this, we present the polarization curves⁽⁶⁰⁾ for methanol electrooxidation on platinum porous electrodes of different structures in 1 *N* of KOH (see Figure 20). In the figure, curve 3 corresponds to the internal kinetic conditions of current generation, while curves 1 and 2 constructed for electrodes of another structure enable one to observe at $E_0 \sim 0.25$ V the shift from the internal-kinetic to ohmic-diffusion conditions of the electrode operation.

5.1.3. Capillary Models

The outlined methods of describing the processes taking place in an electrode are characterized by the fact that they all proceed from the averaged equations with effective coefficients. It is natural to call the theories of this class phenomenological. At the first stage, at which the equations are derived,

a phenomenological theory ignores the details of the structure of a porous medium; such a theory does not require that one or another medium model be assigned. In phenomenological theories, the structure of the porous medium is “hidden” in the effective coefficients. But the calculation of the latter requires the adoption of some model of the porous medium so that it is impossible to avoid models altogether.

Along with the phenomenological theories, the model approach is used. In the model theories, the reasoning runs as follows. First of all, a model for the porous medium is adopted. For the two-phase porous electrodes, the most frequently used model is the capillary one, in which pores are represented by a system of parallel capillaries. Usually, these are cylindrical capillaries of constant radius. Then the polarization characteristic of a separate pore is calculated. By summing the currents in all pores, the total electrochemical activity of the electrode is found.

The shortcomings of the capillary model are obvious. Real pores are corrugated and have a distribution of radii (see Sections 2 and 3); they also intersect. Moreover, the capillary radius and distribution per unit area of the outer electrode surface are defined ambiguously in the capillary model. Nevertheless, this model of two-phase electrodes has been studied in a large number of works, yielding qualitatively the same results as those obtained in the phenomenological approach with effective coefficients.

In the capillary models, different limiting cases have been analyzed, such as ohmic-activation control⁽⁶¹⁻⁷¹⁾ and diffusion control.⁽⁵⁵⁾ Also, the ohmic losses in the electrode matrix have been taken into account, and the more general cases of current distribution in a porous electrode have been analyzed in which both the change in concentration and the ohmic-activation losses are considered.^(59,72-75)

5.1.4. Convective Conditions

In order to overcome the difficulties associated with diffusion, different methods of forced convection of the electrolyte together with the reactant dissolved in it are employed. Such a treatment results in a change in the conditions of supply of the reactant into the pores of the electrode: molecular diffusion gives way to convective diffusion. Regarding convective transport as the principal mechanism and neglecting the diffusion term in relationship (90), as has been done in other works,^(60,76) we obtain

$$c_B z_B \tilde{D}_B \frac{F}{RT} \frac{d\eta}{dx} + v c_B = v_B j_B / nF \quad (103)$$

Multiplying both sides of Eq. (103) by z_B and summing over all components, yields

$$\frac{d\eta}{dx} = \frac{RTj}{F^2 \sum \tilde{D}_B c_B z_B^2} = \tilde{\rho} j \quad (104)$$

Substituting (104) into (103), we obtain for the flux of the j th component the following expression

$$N_B = \tilde{v}_B c_B \quad (105)$$

where

$$\tilde{v}_B = v [1 - n c_B z_B \tilde{D}_B / \nu_B \sum c_B z_B^2 D_B]^{-1}$$

The current per unit cross sectional area, j , is related to the local current density, I , by the obvious expression

$$j(x) = S_0 \int_x^d I(x) dx \quad (106)$$

From Eqs. (105) and (106) we derive one of the fundamental equations

$$\frac{dc}{dx} = \frac{\nu S_0 I(\eta, c)}{\tilde{v}_B n F} \quad (107)$$

In conjunction with Eq. (92), this basic equation gives a full description of electrode performance under convective conditions provided that definite boundary conditions depending upon a particular scheme of reactant supply and reaction product removal are formulated. The characteristics of such electrodes are usually calculated with the aid of a computer.

5.2. Three-Phase Hydrophilic Electrodes

Let us now turn to consideration of the three-phase systems. At first, we shall consider hydrophilic electrodes. In Section 1, it has been pointed out that, by increasing the pressure difference between the gas and the electrolyte, it is possible to reduce significantly the external diffusion limitations on the supply to the catalyst of the reactant dissolved in the electrolyte. Therefore, the calculation of capillary equilibrium is extremely important for the optimization of the performance of three-phase hydrophilic electrodes.

In the early stages of the development of the theory of porous electrodes, it was believed that the liquid and the gas filling an electrode were separated by a sharp boundary, which penetrated deeper and deeper into the porous medium as the pressure was increased. This belief prompted the development of the capillary models.^(3,77-80) In such models, an electrode is approximated by an assemblage of cylindrical pores, each of which is partly filled with a gas and partly with an electrolyte. In the gaseous phase, the pore surface is covered by the film of the electrolyte. Pore intersections are evidently disregarded in such an approach.

Within the framework of the capillary model, it is difficult to explain the experimental dependence of the electrochemical activity of a hydrophilic electrode on the gas–electrolyte pressure difference (Figure 21), which has been obtained in many studies.^(81,82) Moreover, in a constant-radius cylindrical

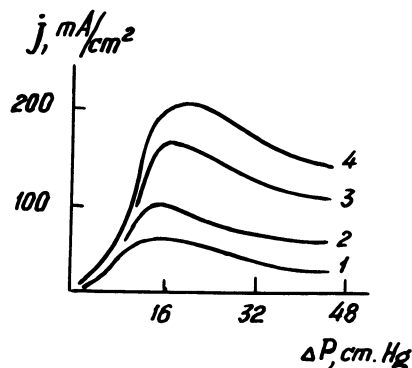


Figure 21. Electrochemical activity of the hydrophilic electrode as a function of the pressure drop at the various polarizations (η in mB): Curve 1, $\eta = 50$; 2, $\eta = 100$; 3, $\eta = 200$; 4, $\eta = 300$.⁽⁸²⁾

pore, the liquid meniscus is unstable. For this reason, the physical meaning of such capillary-model parameters as the length of the liquid and gaseous regions of a pore, the pore radius, etc. is obscure. However, the study of capillary models has permitted formulation of a number of important questions related to the performance of hydrophilic electrodes. Of these, the most important is the question about the principal mechanism of current generation in an individual pore; in other words, about the localization of the current generation process. Generally speaking, several possible mechanisms of current generation may operate:

1. A gas dissolves in the electrolyte film, diffuses through it, is adsorbed on the surface of the gaseous part of the pore, diffuses across this surface into the liquid region of the pore where its electrochemical burning⁽³⁾ takes place.
2. The generation of current may also proceed beneath the electrolyte film. However, this film is thin and therefore, due to high ohmic losses, only a short band of the film bordering on the meniscus is actually capable of operating.
3. The gas diffuses through the liquid meniscus and is burned in the liquid region of the pore.

It is conceivable that there may be other means of current generation in a pore, but it is already clear that, depending upon the relative values of the parameters characterizing the process, such as the pore radius, film thickness, meniscus dimensions, exchange current, electrode polarization, electrolyte concentration, and temperature, one or another mechanism of current generation will be dominant.

This problem has initiated a great number of investigations in which both theoretical^(83,84) and experimental^(85,86) solutions have been sought. In the experimental studies, attempts have been made to simulate the process occurring in an individual pore with the help of electrodes partly immersed in the

electrolyte solution.^(85,86) Such a procedure had the disadvantage that the dimensions of the half-immersed electrodes (measured in centimeters) were greatly different from those of real pores (measured in microns). Only in some of the experiments^(80,87,88,89) were model pores of appropriate dimensions utilized. In such modeling, however, there arises a new difficulty, namely, the experimenter deals with a regular structure of pores, whereas the real porous electrodes are statistical systems.

The methods of quantitative description of the electrochemical activity of three-phase porous electrodes lack the versatility inherent in the theory of two-phase systems. The characteristics of the porous gas electrodes are usually calculated for specific models. The choice of the model is dependent upon the dominant mechanism of current generation, which in turn depends on the numerous parameters listed above, including the pressure difference.

5.2.1. Model of Intersecting Capillaries

Calculations carried out within the framework of this model⁽²⁸⁾ are based on the assumption that the current generation process is localized in the neighborhood of intersections of liquid pores with gaseous ones. In this case, the equation for the potential distribution is written in the form

$$\kappa \frac{d^2 \eta}{dx^2} = \iint N(r_i, r_k) I(\eta, r_i, r_k) dr_i dr_k \quad (108)$$

where $N(r_i, r_k)$ is the number of intersections between the gaseous pores of radius r_i and the liquid pores of radius r_k in a unit volume of the electrode, and $I(\eta, r_i, r_k)$ is the current generated by a single intersection. The function N is found from simple probabilistic considerations, while the function I is calculated separately for each mechanism of current generation. Having done this, one can readily perform the integration in Eq. (108).

As an illustration, we present the expression for the electrochemical activity of an electrode at low polarization values, which has been derived for the case of the diffusion mechanism of current generation in the neighborhood of each intersection

$$j = E_0 (g_l^2 g_g / r_2 r_1^{1/2})^{1/2} [(2Fk/RT\beta^2)(DFc_0 j_0 / 2)^{1/2}]^{1/2} \quad (109)$$

where r_1 and r_2 are the average radii of the liquid and gaseous pores, respectively. For $j_0 = 10^{-4}$ A cm⁻², $r_1 = 1$ μm, $r_2 = 10$ μm, $\eta_0 = 100$ mV, we obtain $j \sim 150$ mA cm⁻².

Yet another characteristic of the electrochemical process—the characteristic length determining the optimum value of the electrode thickness—is of interest. It is given by

$$l = [kr_2 r_1^{1/2} RT / 2^{1/2} \beta^2 F g_g (DFc_0 j_0)^{1/2}]^{1/2} \quad (110)$$

Table 2
Dependence of the Activity of a Hydrophilic Electrode on the Average Radius of Gaseous Pores^a

$r_2(\mu\text{m})$	$j \text{ (mA cm}^{-2}\text{)}$	$\Delta P \text{ (mm Hg)}$	$d \text{ (mm)}$
10	119	60	12.7
1	375	600	4

^a In calculating the data tabulated above it has been assumed that $2\sigma \cos \theta = 600 \mu\text{m} \cdot \text{mm Hg}$, $i_0 = 10^{-5} \text{ A cm}^{-2}$, $\eta_0 = 180 \text{ mV}$.

From this relationship certain conclusions may be drawn regarding the dependence of the electrochemical activity on the structural characteristics of electrodes. With this purpose, we rewrite Eq. (109) in a simplified form, isolating the structural factors:

$$j \sim (g_g g_l^2 / \beta^2 r_2 r_1^{1/2})^{1/2} \tag{111}$$

Since $g_l \sim g$ and $g_g \sim g$, we have $j \sim g^{3/2}$; i.e., the electrochemical activity is proportional to the porosity factor raised to the power 3/2. At a specified porosity and average radii of the liquid and gaseous pores, the electrochemical activity is maximum if the following relationships hold:

$$g_l = \frac{2}{3}g, \quad g_g = \frac{1}{3}g \tag{112}$$

The total current is inversely proportional to the square root of the average radius of gaseous pores, i.e., $j \sim r_2^{-1/2}$. It should be mentioned that the parameter r_2 determines also the order of magnitude of the working pressure, namely, $r_2 \sim 1/\Delta P$. In order to illustrate this dependence, we have tabulated the values of the parameters r_2 , j , ΔP , and d calculated using the data of reference 90 (see Table 2). It can be seen that the square-root dependence of j on ΔP is confirmed experimentally.⁽⁹⁰⁾

5.2.2. Biporous Capillary Model

In the approach just discussed, it is assumed that the process of current generation is localized in the neighborhood of intersections of gaseous pores with liquid ones. The characteristic dimensions of this region should not exceed the average distance, r_g , between the neighboring intersections (see Figure 22). However, estimates show that the above condition is satisfied only either for highly active catalysts or for high electrode polarizations. Usually, the reverse requirement is fulfilled. Therefore, for the description of a hydrophilic electrode, the model of cylindrical gaseous pores, which is also called the biporous model,⁽⁹¹⁾ is preferable. This model is illustrated in Figure 23 and is a further development of the original model of cylindrical capillaries.

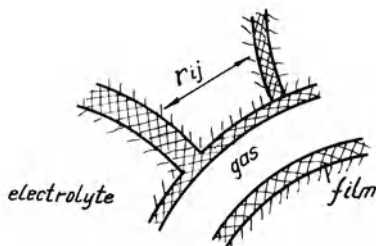


Figure 22. Intersecting pore model.

The biporous model has been realized by the process of manufacturing of the hydrophilic electrodes, which are usually prepared by sintering a mixture of catalyst and pore former, the latter being removed from the system at a certain stage. The measurements of pores by the mercury porosimetry technique show that two types of pores arise from such a manufacturing process: wide pores of average radius r_2 and narrow pores of average radius r_1 . The wide pores represent rows of connected cavities left over upon the removal of coarse grains (the pore former), whereas the small (narrow) pores are the gaps between the catalyst particles which are considerably finer than those making up the pore former. The operating gas pressure difference is chosen so that the wide pores are largely filled with the gas. To prevent gas bubbling into the electrolyte chamber, the electrode is covered on this side with a finely porous stopping layer, which is completely filled with the electrolyte (see Figure 23).

The biporous model incorporates the results of capillary equilibrium theory. According to the concepts of this model, an electrode operates under the conditions of capillary breakthrough so that it is almost uniformly filled with the gas and the liquid. In the biporous model, small pores play a twofold role. First, they determine the ohmic conductivity in the electrolyte, and second, they provide a contribution to current generation, because their surfaces are well developed. In the biporous model, one encounters no difficulty in accounting for the experimentally observed dependences of current on the pressure difference.

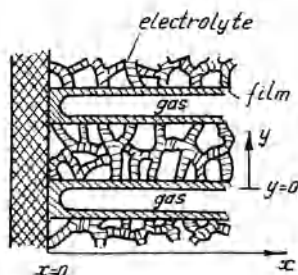


Figure 23. Hydrophilic electrode: the biporous model.

It will be helpful to trace all the stages preceding the electrochemical burning of the gaseous reactant. The reactant is transported by the Poiseuille flow through a gaseous pore deep into the porous electrode. This stage is not a limiting one for the process of current generation, because the gas diffusion coefficient is very high ($D_g \sim 10^{-1} \text{ cm}^2 \text{ s}^{-1}$), exceeding by several orders of magnitude the liquid diffusion coefficient. Therefore, in regard to the supply of gases, the three-phase electrodes may be treated as equally accessible systems. An exception is the air electrode, utilizing for its operation oxygen extracted from ambient air. Nitrogen, the inert component of air, hampers the supply of oxygen by diffusion into the electrode. Accordingly, in air electrodes a peculiar process takes place—the so-called Stefanian diffusion of oxygen (see Section 4.2).

The great mobility of gases and aqueous vapors determines also the small value of the electrolyte concentration gradient in the gas electrodes. The initial nonuniform distribution of electrolyte concentration across the electrode thickness, which arises, for example, when an electrochemical source of current is turned on, quickly becomes uniform under the influence of flows of aqueous vapor.^(92,93) Therefore, to a first approximation, the electrolyte concentration in a porous gas electrode may be assumed to be constant. The next stage of the process is the diffusion of the gas reactant through a thin ($\sim 10^{-4} \text{ cm}$) film of the electrolyte. A typical diffusion current (about $10^{-2} \text{ A cm}^{-2}$) is usually much higher than the exchange current characteristic of the electrochemical stage. For this reason, the diffusion of a gas through the electrolyte film almost never restricts the process of current generation.

The electrochemical burning of a gas may occur both on the outer surface of gaseous pores, under the electrolyte film, and on the inner surfaces of small “liquid” pores. The specific surface of small (liquid) pores significantly exceeds that of wide (gaseous) pores. Consequently, in spite of the limitations associated with diffusion taking place during the supply of a gas to small pores, the electrochemical process must proceed mainly on the surface of liquid pores. These qualitative considerations have been borne out by numerical computations.^(28,94,95)

In what follows, we confine our consideration to the process of diffusion of the gas dissolved in the electrolyte into the small pores, while omitting a number of stages which could in certain cases complicate the process of current generation. By these stages, we mean the processes of adsorption and desorption, passivation of the catalyst surface, bulk and surface migration of gases (e.g., hydrogen in palladium), and other processes.

In order to estimate the upper limit on the electrochemical activity of a hydrophilic electrode, we first assume that the limitations due to internal diffusion are negligible. The polarization distribution across the electrode thickness is then described by Eq. (92). In this equation, we set

$$I = j_0[\exp(\bar{\eta}) - \exp(-\bar{\eta})] = 2j_0 \sinh \bar{\eta} \quad (113)$$

Then, instead of Eq. (92), we have

$$\frac{d^2 \bar{\eta}}{d\bar{x}^2} = \sinh \bar{\eta}, \quad \bar{\eta}|_{x=0} = \bar{\eta}_0, \quad \left. \frac{d\bar{\eta}}{dx} \right|_{x=d} = 0 \quad (114)$$

where $\bar{x} = x/l$, $l = (RT\bar{\kappa}/2\alpha Fj_0 S_0)^{1/2}$ is the characteristic ohmic length, and η_0 is the electrode polarization in the plane where the active layer of the electrode borders on the fine-grained blocking layer (see Figure 23). This plane is called the "face side" of an electrode. If the electrode is sufficiently thin ($d \ll l$), its inner surface may be considered as equally accessible for the electrochemical process. Accordingly, the expression for the electrochemical activity has the following simple form:

$$j = S_0 dI = 2S_0 d j_0 \sinh \bar{\eta}_0 \sim \exp(\bar{\eta}_0) \quad (115)$$

But with the increasing electrode thickness, the ohmic difficulties also become greater: polarization on the back side of the electrode $\bar{\eta}_d$ (at $x = d$) becomes less than the electrode polarization on the face side $\bar{\eta}_0$. As a result, the conditions of current generation change from purely kinetic to ohmic-kinetic. Integrating Eq. (114) once, we find the electrochemical activity of the electrode

$$j_d = -\bar{\kappa} \left. \frac{d\eta}{dx} \right|_{x=0} = 2(j_0 \bar{\kappa} R T S_0 / \alpha F)^{1/2} (\cosh \bar{\eta}_0 - \cosh \bar{\eta}_d)^{1/2} \sim \exp(\bar{\eta}_0/2) \quad (116)$$

Expression (116) contains an unknown parameter $\bar{\eta}_d$, the electrode's back-side polarization. To determine this parameter, we again perform an integration for Eq. (114). As a result, we obtain the following expression, which relates the quantities $\bar{\eta}_0$, $\bar{\eta}_d$, and d :

$$\begin{aligned} d/l = 2 \exp(\bar{\eta}_d/2) & \left[F(\exp(-\bar{\eta}_d), \pi/2) \right. \\ & \left. - F\left(\exp(-\bar{\eta}_d), \arcsin \left[\exp\left(-\frac{\bar{\eta}_0 - \bar{\eta}_d}{2}\right)\right]\right) \right] \end{aligned} \quad (117)$$

where $F(\kappa, \alpha)$ are the elliptic integrals of the first kind.

In sufficiently thick electrodes, the electrochemical equilibrium is established on the back sides. Therefore, in Eq. (116), we may set $\bar{\eta}_d = 0$. We thereby determine the electrochemical activity of a thick electrode, j_∞ . Calculated by formulas (112) and (117), the dependence of the ratio j_d/j_∞ on the ratio d/l ⁽⁵⁵⁾ is illustrated in Figure 24. Clearly, at $d \gg l$, we have $j_d \rightarrow j_\infty$. The curves shown in Figure 24 differ in their values of electrode polarization $\bar{\eta}_0$. As the parameter $\bar{\eta}_0$ increases, the thickness of the region of current generation drastically decreases. The thickness of the current-generation zone may be defined, for example, as the distance from the electrode surface over which 90% of the current collected from an infinitely thick electrode is generated.

At small values of the d/l ratio, the curves in Figure 24 display a linear section. In this region, electrodes may be considered as thin, their electrochemical activity being determined by formula (115).

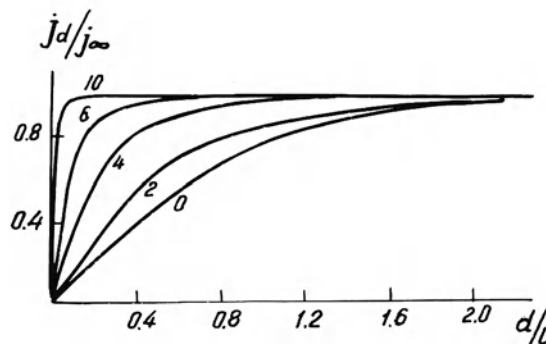


Figure 24. Distribution of the current generation process across the hydrophilic electrode thickness at various polarizations increasing with the number at the curves.⁽⁵⁵⁾

From a comparison between formulas (115) and (116), there follows the important conclusion that the nonequal accessibility of the electrochemical process across the electrode thickness halves the slope of the polarization curve $\ln j - \bar{\eta}_0$. It will be shown below that, when the internal-diffusion limitations are taken into account, the slope of the polarization curve is again reduced to half its value, because $j \sim \exp(\bar{\eta}_0/4)$.

Formula (116) allows evaluation of the order of magnitude of the electrochemical activity of hydrophilic electrodes. Given the parameter values, $\bar{\eta}_0 \sim 1$, $j_0 = 10^{-5} \text{ A cm}^{-2}$, $\tilde{\kappa} = 0.1 \text{ ohm}^{-1} \text{ cm}^{-1}$, $RT/\alpha F = 50 \text{ mV}$ ($\alpha = 1/2$), and $S_0 = 10^4 \text{ cm}^{-1}$, we have $j \sim 0.1 \text{ A cm}^{-2}$, which by the order of its magnitude coincides with the values obtained experimentally (see Figure 21).

Until now, it has been assumed that in the electrode there exists an optimum relationship between the gas and the electrolyte, so that the limitations associated with internal diffusion are negligible. Unfortunately, this can be achieved only at low electrode polarizations.

Let us consider this question quantitatively. In an electrode, gaseous pores are separated by the average distance of $L = 2R$ (see Figure 25). Let the number of these pores per unit area of the apparent surface of the electrode be N . In this case, if the gaseous pores are visualized in a zero approximation as straight circular tubes (the model of cylindrical gaseous pores, see Figure

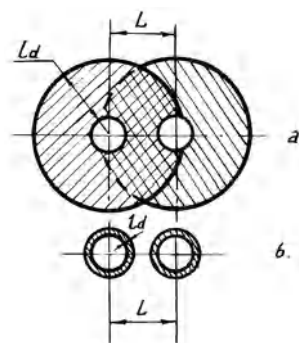


Figure 25. Possible types of localization of the current generation process in the neighborhood of gaseous pores.

23), the gas porosity of the electrode and the surface of the gaseous pores are given, respectively, by

$$g_g = \pi r_2^2 N, \quad S_g = 2\pi r_2 N, \quad (118)$$

where r_2 is the average radius of the gaseous pores. Making use of Eq. (118) and the model shown in Figure 23, it can be demonstrated that

$$R = 1/2N^{1/2} = (\pi g_g)^{1/2}/S_g \quad (119)$$

The quantity R should be compared with the depth of penetration of the electrochemical process into small liquid pores (in Figure 23, the direction is along the y axis). This process is characterized by the length l_d introduced by relationship (101). Let us estimate the ratio of l_d to R , assuming that $\bar{D} \sim 10^{-5} \text{ cm}^2 \text{ s}^{-1}$, $n = 1$, $c_0 \sim 10^{-7} \text{ mole cm}^{-3}$, $j_0 \sim 10^{-7} \text{ A cm}^{-2}$ (oxygen silver electrode in alkaline electrolyte⁽¹⁰⁾), $S_0 \sim 1/r_1$, r_1 being the liquid pore radius, $2b = 50 \text{ mV}$, $g_g = 0.25$, and $S_g \sim 1/r_2$. Finally, we get

$$l_d/R \sim (r_1^{1/2}/r_2) \exp(-\eta/50) \quad (120)$$

Since usually $r_1 \sim 10^{-4} \text{ cm}$ and $r_2 \sim 10^{-3} \text{ cm}$, it is clear that at small polarizations ($\eta \leq 50 \text{ mV}$) the average distance between the neighboring gaseous pores turns out to be much shorter than the characteristic length of diffusion. This implies that the diffusion of a gas into liquid pores does not place limitations on the process of gas burning. Thus in three-phase electrodes with gas reactants it is possible, at low electrode polarizations, to remove almost completely the limitations associated with diffusion.

With the increasing polarization, however, the depth of penetration of the electrochemical process into the three-phase electrode radically (exponentially) decreases in the radial direction from a gaseous pore. This follows (at high polarizations, $R \gg l_d$) from formula (120). Thus the conditions of current generation in an electrode will be those of ohmic activation, provided that the inequally

$$l_d \geq R \quad (121)$$

holds. If the reaction zones of two neighboring gaseous pores overlap, the liquid pores generate electrical current under the kinetic conditions (Figure 25). If, however, $l_d < R$, the internal diffusion conditions of current generation take place, i.e., the process of current generation is localized at the surface of gas pore (Figure 25), whereas the catalyst contributes only partially to the electrochemical process—the degree of its utilization being relatively small.

In principle, the polarization characteristics of porous gas electrodes may be calculated exactly. The problem is solved in two stages. First, a layer of thickness Δx is isolated in an arbitrary cross section x parallel to the frontal plane of the electrode. The process of current generation is to some degree localized near each gaseous pore. Since any cross section x on average, is equipotential, the magnitude of current generated over some interval near

the gaseous pore is determined by gas diffusion into the small pores. Solving the problem of gas diffusion in the radial direction, one can find the quasi-local current-voltage characteristic. If, however, the regions of current generation of the neighboring gaseous pores do not overlap, their effect will be additive. The next stage consists in solving the equation of the type (114) for the polarization as a function of x , whose right-hand side contains the already determined quasilocal polarization characteristics. In the next section, we shall give an example of such a calculation for the hydrophobic electrodes. The resultant expressions are rather tedious so we omit them, presenting only some graphs. Figure 26 shows representative polarization characteristics for the hydrogen electrodes.⁽⁷⁸⁾ These characteristics have been calculated on the basis of a model similar to that described above, but somewhat simplified in that the contribution of small pores into the total reaction surface is taken into account by the roughness factor f of gaseous pores. At large values of f , such a description becomes too crude, because it neglects the limitations associated with diffusion, which may significantly reduce the surface of small pores actually taking part in the reaction. Two pairs of curves designated in Figure 26 as 1 and 2 refer to the cases of $f = 3$ and $f = 60$, respectively. The dashed curves represent the calculated results, while the solid curves correspond to the experimental data. As the roughness factor increases, the curves exhibit a purely diffusional character, the inflection point vanishing from them. Such behavior of polarization curves is in good agreement with the data of many authors. Sometimes, the change in electrolyte concentration across the electrode thickness is also taken into account.^(59,95,96)

In order to include more correctly the contribution from small pores, it is necessary to consider the diffusion of a dissolved gas. The relevant calculations and measurements have been made, for example, for the oxygen electrode, the active layer of which was prepared from a mixture of powders of the silver catalyst and the pore former.⁽¹⁰⁾ Electrodes of various structures have been fabricated by changing the amount and dispersion of ammonium

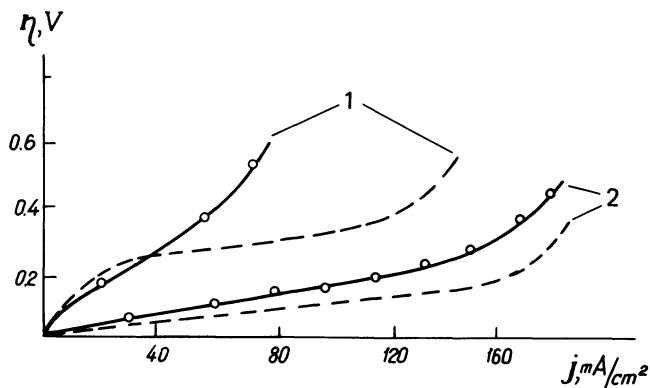


Figure 26. Representative polarization characteristics of hydrogen electrodes.

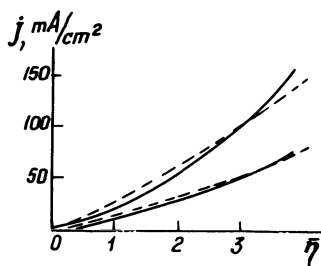


Figure 27. Experimental (solid curves) and calculated (dashed curves) polarization characteristics for oxygen electrodes of different structure.⁽¹⁰⁾

bicarbonate. A combined study of the structural and electrochemical characteristics of the electrodes has made it possible to elucidate in great detail the dominant mechanisms of current generation. Figure 27 presents the experimental and calculated polarization curves for two different structures. A great amount of information can be gained from the dependence of current on the pressure difference, which is shown in Figure 28 for one out of ten structures explored. In the region of low pressures (about 0.1 atm), the internal diffusion mechanism is dominant, whereas at the higher pressures (about 0.9 atm) the kinetic mechanisms prevails. In the same figure, curve 3 illustrates the contribution to the total electrode activity from the film wetting of the gaseous pores. Even at $P \sim 0.8$ atm, the film mechanism contribution to the current amounts to only 13%.

5.3. Hydrophobic Electrodes

To understand the mechanism of operation of one or another porous electrode, it is necessary to know, first of all, the dominant channels through which the gas and electrolyte are supplied into the depth of the electrode's porous medium and to understand the nature of these channels. All the remaining problems (such as the determination of current generation conditions in the electrode, values of the effective coefficients, etc.) cannot be solved satisfactorily if the electrode structure, and gas and electrolyte supply channels are unknown.

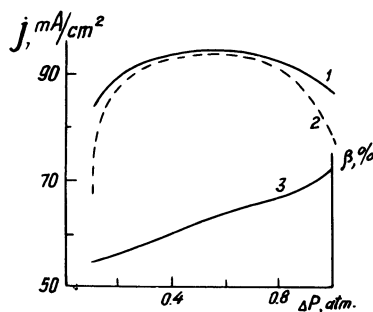


Figure 28. Behavior of the quantity $j(\Delta p)$: Curve 1, experimental; curve 2, calculated; curve 3, fraction of current generated by gaseous pores (the film mechanism).

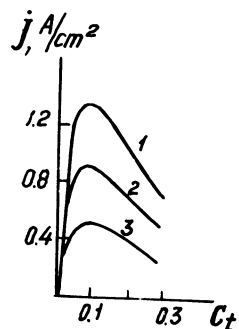


Figure 29. Dependence of the electrochemical activity of the hydrophobic electrode made of platinum and fluoroplastic on the concentration of fluoroplastic in the layer [Experimental curves⁽⁹⁷⁾ at the various polarizations (η in mV): Curve 1, $\eta = 750$; 2, $\eta = 800$; 3, $\eta = 850$.]

In order to solve these basic problems for the hydrophobic electrodes, it is necessary to determine the pore distribution not only in radii, but also in values of the effective angle of wetting by the electrolyte of the hydrophilic-hydrophobic pore walls. The activity of hydrophobic electrodes is determined not only by the pressure difference, but by the hydrophobizer concentration, c_t . Typical (j, c_t) curves⁽⁹⁷⁾ are shown in Figure 29. The presence of a maximum on each of these curves can be easily explained. To the left of the maximum, at small values of c_t , the electrode activity is low, because the number of gaseous pores is small. On the right-hand branch of such a curve, at large values of c_t , the amount of the hydrophilic catalyst is insignificant; therefore, the electrode contains an insufficient amount of the electrolyte.

In recent years, the mechanism of operation of two-component hydrophobic electrodes made of platinum (catalyst) and fluoroplastic (hydrophobizer and adhesive) has received the most study.^(4,98-104) In the range of optimum fluoroplastic concentrations, a model⁽¹⁰⁵⁾ for this structure is schematically shown in Figure 30, where the average size of fluoroplastic grains, which is equal to several microns, exceeds by about an order of magnitude that of catalyst grains.

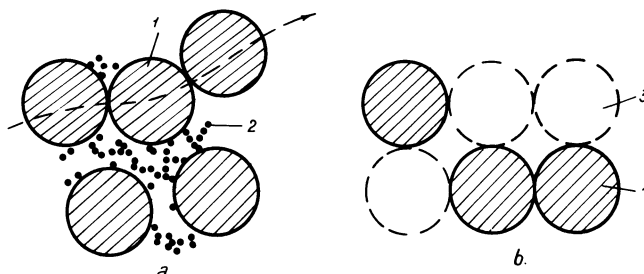


Figure 30. Models for the structure of the hydrophobic electrode made of platinum and fluoroplastic: (a) random arrangement of fluoroplastic; (b) regular arrangement of fluoroplastic grains; 1, fluoroplastic grains; 2, catalyst grains; 3, vacancies which may be occupied by fluoroplastic grains.

In a hydrophobic electrode, there are channels for gas supply which are formed by pores with the hydrophilic–hydrophobic walls, and also purely hydrophobic pores in chains of connected agglomerates of fluoroplastic particles (see Figure 5). In order to clarify the relative role of these channels, it is necessary to solve the problem of capillary equilibrium in such a system. Since the method of calculation is analogous to that described in Section 3, we present only the principal results,⁽¹⁰⁶⁾ which reduce to the fact that the breakthrough phenomenon in purely hydrophobic pores occurs at considerably lower fluoroplastic concentrations than it does in hydrophilic–hydrophobic pores. Accordingly, the purely hydrophobic gas-supply channel may be regarded as dominant. Such a conclusion makes it possible to explain why the electrode activity is practically independent of the pressure difference and also why the maxima on (j, c_t) curves shown in Figure 29 are so localized. To illustrate this highly important conclusion, we shall give one example. Figure 31(a) presents the experimental dependences⁽⁹⁷⁾ of the total (g) gas (g_g) and liquid (g_l) porosities on the weight concentration of the hydrophobizer in a hydrophobic electrode made of platinum black and fluoroplastic. Straightforward calculations⁽¹⁰⁷⁾ have made it possible to estimate the specific volume occupied by the grains of fluoroplastic [V_t , Figure 31(b)] and the porosity (g_t) of these grains. The fact that in Figure 31(a) and (b) the product $g_t V_t$ roughly coincides with the g_g suggests that in such an electrode the gas is largely contained in fluoroplastic grains and that there are practically no pores with the hydrophilic–hydrophobic walls.

The concepts of the active-layer structure of a hydrophobic electrode presented above provide a basis for polarization characteristic calculations, which differ very little from those made in hydrophilic electrode theory. Here, the gaseous pores formed by fluoroplastic grains are represented as straight

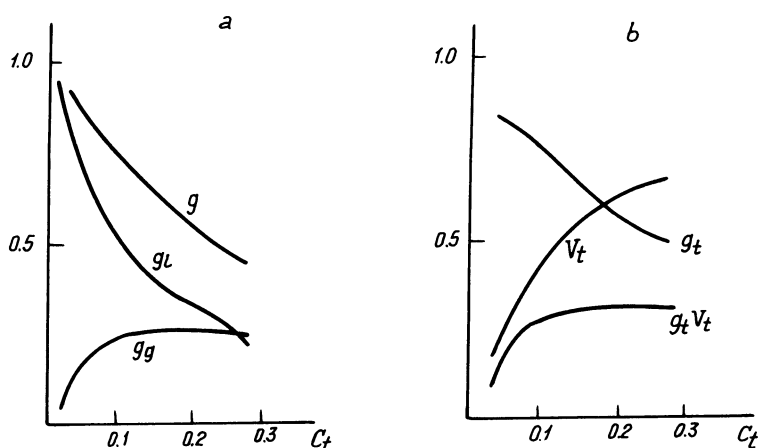


Figure 31. Electrolyte–gas distribution in the hydrophobic electrode: (a) experiment⁽⁹⁷⁾; (b) calculation.⁽¹⁰⁷⁾

circular cylinders of constant radius r_i (the average size of fluoroplastic grains), which are arrayed regularly. The gas diffuses into the region adjoining a gaseous pore which contains the electrolyte-saturated catalyst-fluoroplastic mixture. In order to calculate the electrode activity, one should estimate the number of equivalent gaseous pore per unit area of the electrode. Bear in mind that not all fluoroplastic grains belong to a single system of gaseous pores. To make such a calculation, it is convenient to shift from the model of random arrangement of fluoroplastic grains [Figure 30(a)] to the regular-array model [Figure 30(b)]. Let θ be the probability that the grains of fluoroplastic occupy only the centers of a cubic lattice, the remaining space in the lattice being filled with the catalyst. Taking advantage of the theory of capillary equilibrium for this model, one may calculate the probability Y that a grain of fluoroplastic belongs to a single system of gaseous pores. The average distance between the neighboring gaseous pores, R , is then found from simple geometrical considerations

$$R = r_i / [(1 - \theta) Y]^{1/2} \quad (122)$$

Let us now find the current density per unit area of the surface of gaseous pores. The equation describing the concentration of oxygen dissolved in the electrolyte, $\bar{c} = c/c_0$ (c_0 being the oxygen solubility) in the vicinity of a gaseous pore has a form

$$\frac{1}{\bar{\rho}} \frac{d}{d\bar{\rho}} \left(\bar{\rho} \frac{d\bar{c}}{d\bar{\rho}} \right) = \bar{c} - e^{-\bar{\eta}}, \quad \bar{c} \Big|_{\rho=r_i} = 1, \quad \frac{d\bar{c}}{d\rho} \Big|_{\rho=R} = 0 \quad (123)$$

where $\bar{\rho} = \rho/l_d$ is the reduced polar radius, l_d is the characteristic diffusion length, $\bar{\eta} = \alpha F \eta / RT$ is the electrode polarization, and $2R$ is the average distance between the gaseous pores. In the derivation of Eq. (119) we have described the electrochemical kinetics by the equation $I = i_0(\bar{c}e^{\bar{\eta}} - 1)$, which is valid when $\bar{\eta} > 1$ and which leads to a qualitative agreement when $\bar{\eta} \rightarrow 0$. Solving Eq. (123), we shall find the desired current density per unit area of the gaseous pore surface:

$$j = \frac{nFDc_0}{l_d} [1 - \exp(-\bar{\eta})] \Psi \quad (124)$$

$$\Psi = \frac{I_1\left(\frac{R}{l_d}\right) K_1\left(\frac{r_i}{l_d}\right) - I_1\left(\frac{r_i}{l_d}\right) K_1\left(\frac{R}{l_d}\right)}{I_1\left(\frac{R}{l_d}\right) K_0\left(\frac{r_i}{l_d}\right) + I_0\left(\frac{r_i}{l_d}\right) K_1\left(\frac{R}{l_d}\right)},$$

where $I_0, I_1, K_0,$ and K_1 are the Bessel functions of purely imaginary argument.

That the conditions are nearly kinetic can conveniently be characterized by the parameter

$$\chi = 2(r_i/l_d)\Psi / [(R/l_d)^2 - (r_i/l_d)^2] \quad (125)$$

which is the ratio of the current generated in the neighborhood of an individual gaseous pore to the current generated under purely kinetic conditions.

Let us now proceed to determine the polarization characteristics of a hydrophobic electrode. The polarization distribution in such an electrode is described by the equation

$$\frac{d^2 \bar{\eta}}{d\bar{x}^2} = \exp(\bar{\eta}/2)[1 - \exp(-\bar{\eta})]\Psi(\bar{\eta}),$$

$$\bar{\eta}|_{x=0} = \bar{\eta}_0, \quad \left. \frac{d\bar{\eta}}{dx} \right|_{x=d} = 0$$
(16)

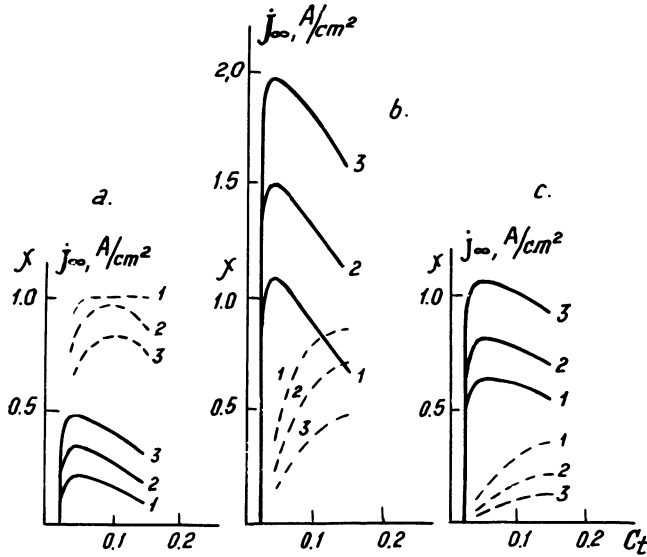
where $\bar{x} = x/l$ is the reduced coordinate, l is the characteristic length, and d is the electrode thickness. For the platinum-fluoroplastic electrodes several hundred microns thick and at potentials, E_0 , between 750 and 850 mV (Figure 29), the electrochemical activity of the electrode practically no longer depends on its thickness. The relationship between j_∞ and c_t is given by

$$j_\infty = \left(\frac{\tilde{\kappa}RT}{\alpha F} \frac{1}{r_t} \frac{2\pi\theta Y}{(1 - \frac{1}{6}\pi\theta Y)} \{Dc_0 F j_0 \tilde{S} d_c (\pi/6) g_l (1 - g_c) \right. \\ \left. \times [1 - \frac{1}{6}\pi\theta(1 - Y)] \right)^{1/2} \left(\int_0^{\eta_0} \exp(x/2)(1 - e^{-x})\Psi(x) dx \right)^{1/2} \quad (127)$$

where d_c is the specific gravity of platinum. In calculating the current by formula (127) it is assumed that $\tilde{\kappa} = \kappa g_l$ and $\tilde{D} = D g_l$; the parameters θ , g_c , and Y are determined from a calculation employing the measured values of g_b , g_g , and S_c [see Figure 31(a)]. The average radius of fluoroplastic particles, r_t , is not measured directly. Estimates show that it amounts to several microns.^(105,108)

Let us now investigate the dependence of the electrode activity on the kinetic and structural parameters. For $r_t = 1 \mu\text{m}$ and $t = 25^\circ\text{C}$, we have $D = 6 \times 10^{-6} \text{ cm}^2 \text{ s}^{-1}$, $j_0 = 2 \times 10^{-8} \text{ A cm}^{-2}$, $c_0 = 2 \times 10^{-7} \text{ mol cm}^{-3}$. The dependence of j_∞ and χ on c_t calculated by formulas (125) and (127) are presented in Figure 32. A comparison between Figures 29 and 32 shows that the calculated (j_∞, c_t) curves reproduce correctly all essential features of the experimental curves, having, however, different absolute values. This difference can be accounted for by the fact that at currents about 1 A cm^{-2} , the electrodes are heated and their temperature becomes higher than room temperature. Setting now $r_t = 1 \mu\text{m}$ and $t = 80^\circ\text{C}$, we obtain $\kappa = 1.3 \text{ ohm}^{-1} \text{ cm}^{-1}$, $D = 10^{-5} \text{ cm}^2 \text{ s}^{-1}$, $c_0 = 5.5 \times 10^{-8} \text{ mol cm}^{-3}$, and $j_0 = 5 \times 10^{-7} \text{ A cm}^{-2}$. The calculated values of current are now higher than the experimental ones. A more satisfactory agreement can be reached if we put $r_t = 4 \mu\text{m}$ [see Figure 32(c)].

The heavy dependence of current generation conditions (and consequently, the degree of catalyst utilization) on the absolute dimensions of fluoroplastic grains is illustrated in Figure 33, where the concentration profiles



32. Electrochemical activity and the extent of catalyst utilization in the hydrophobized platinum-fluoroplastic electrode as functions of the fluoroplastic concentration in the active layer (calculated curves): solid curves, j_{∞} ; dashed curves, χ ; (a) $t = 25^{\circ}\text{C}$, $r_t = 1 \mu\text{m}$; (b) $t = 80^{\circ}\text{C}$, $r_t = 1 \mu\text{m}$; (c) $t = 80^{\circ}\text{C}$, $r_t = 4 \mu\text{m}$; (η in mV): Curve 1, $\eta = 850$; 2, $\eta = 800$; 3, $\eta = 750$.

for oxygen dissolved in the electrolyte at the surface of a gas pore are presented, as calculated from Eq. (123). As the value of r_t increases, the kinetic conditions of current generation soon give way to the internal diffusion conditions.

Thus the electrochemical activity of platinum-fluoroplastic electrodes significantly depends both on the r_t parameter and the temperature. It will also be noted that, as can be seen from Figure 32, the optimum electrochemical activity of an electrode and the optimum degree of utilization of its catalyst (the quantity χ) cannot be achieved simultaneously. An increase in the electrode activity may therefore be attained only at the expense of the lower degree of catalyst utilization.

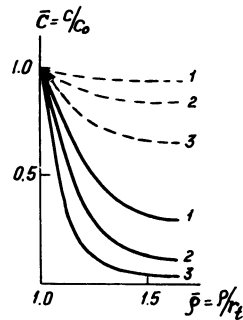


Figure 33. Concentration of oxygen dissolved in the electrolyte as distributed between the neighboring gaseous pores (at the frontal surface of the platinum-fluoroplastic electrode) (η in mV): Curve 1, $\eta = 850$; 2, $\eta = 800$; 3, $\eta = 750$. Dashed line, $r_t = 1 \mu\text{m}$; solid curve, $r_t = 5 \mu\text{m}$; $t = 25^{\circ}\text{C}$, $c_t = 0.04$.

As one can see from Figure 32(c), the current generation conditions in platinum-fluoroplastic electrodes approach the conditions of internal diffusion (the degree of platinum utilization is low). The same situation is observed in multicomponent hydrophobic systems. In a number of studies,^(4,109) it has been shown that as platinum is added into carbon Teflon-bonded electrodes their characteristics increase only to a certain critical content of platinum in the active layer.

Similar approaches to the calculation of the electrochemical activity of the hydrophobic electrode have been developed elsewhere.⁽¹¹⁰⁻¹¹²⁾ In this section, the difference in the operating mechanism between the hydrophilic and hydrophobic electrodes, as well as the influence of structure upon the electrochemical activity of hydrophobic electrodes, have been discussed only in broad outline. The details of interest to the reader can be found in other works.⁽¹¹³⁻¹¹⁵⁾

6. Conclusion

The problem of manufacturing efficient porous electrodes naturally falls into three major parts. The first includes the task of selecting the most suitable electrode materials and studying the local electrochemical kinetics involving all practically important reactants. The second part of the problem reduces to the study of the macrokinetics of the processes operating in porous media, which should take into account the transport stages and the known microkinetics. Finally, the third part of the problem comprises the relevant technological developments, design calculations, and construction of systems utilizing the porous electrodes. The present chapter has been devoted to the discussion of problems of the macrokinetics of processes occurring in porous electrodes. It is precisely the macrokinetic data that provide the basis for design calculations.

The theory of the macrokinetic processes in porous media is now at a sufficiently high level of development. It enables one to calculate, with a reasonable accuracy, the electrochemical activity of porous electrodes, to determine the process distribution across the electrode thickness, to choose the optimum structure of the porous space, and to evaluate the degree of catalyst exploitation. The presence in the theory of a large number of parameters, not all of which have been reliably established for each particular system, often hampers design calculations. The qualitative predictions made by the theory, however, remain indispensable in designing industrial installations, electrochemical generators, and other devices.

The existing theory of porous electrodes is based upon a formal transition from a real porous medium to an equivalent homogeneous system containing the volume sources. The expressions for fluxes in this case retain the same form as those employed in the theory of electrolyte solutions, but with the

effective coefficients dependent upon the structural characteristics of the porous medium being substituted for the usual kinetic coefficients. Another distinction is that in the differential transport equations, the terms containing sources, which are as a rule nonlinear with respect to the electric potential, are introduced. Today, solving such equations with the aid of a computer is not difficult. Accordingly, the main point of the problem distinctly shifts toward the more rigorous calculation of the effective transport coefficients and the better substantiated derivation of the fundamental equations by averaging the initial relationships valid for individual pores. At this point, electrochemical theory is intimately related to the hydrodynamics of porous media and also to one of the fundamental problems of statistical physics called the "percolation problem." In several sections of this chapter, it has been demonstrated how the methods and concepts of these related branches of science can be fruitfully employed in the theory of porous electrodes. In our opinion, it is along this route that new advances can be expected.

Auxiliary Notation

A	Adzumi constant	γ	fraction of supercritical pores
C	Cozeni constant	γ_*	percolation threshold or breakthrough points
L	Average distance between gas pores	γ	probability density for supercritical pore bifurcation
N	pore density per unit surface	λ	probability density for the supercritical pore death
p	rate of exchange in mixing cells	ρ	radius in polar coordinates
P	percolation probability	σ	surface tension; dispersion
Q	molecular flux	θ	impurity fraction in a mixture; wetting angle
u	average flow velocity	Ψ	angle characterizing grain packing
\sim	sign over a symbol denotes effective parameter in the context of porous media: e.g. \tilde{D} is the effective diffusion coefficient	ϕ	inner potential of a phase
α	parameter characterizing Stagnant zones	χ, τ	proportionality constants associated with local polarization characteristics
$\alpha(r)$	density of pore volume distribution		
β	tortuosity factor		

References

1. W. Vielstich, *Brennstoffelemente*, Verlag Chemie, GmbH. Weinheim/Bergstr. (1965).
2. E. Justi, M. Pilkuhn, W. Scheibe, and A. Winsel, *Hochbelastbare Wasserstoff-Diffusion-Elektroden für Betrieb bei Umgebungstemperatur und Niederdruck*, Verlag der Akademie der Wissenschaften und der Literatur in Mainz, Wiesbaden (1960).
3. J. O'M. Bockris and S. Srinivasan, *Fuel Cells: Their Electrochemistry*, McGraw-Hill, New York (1969).
4. L. W. Niedrach and H. R. Alford, A new high-performance fuel cell employing conducting-porous-Teflon electrodes and liquid electrolytes, *J. Electrochem. Soc.* **112**, 117-124 (1965).

5. (a) Yu. G. Chirkov, I. A. Kedrinsky, and V. L. Kornienko, In: *Itogi Nauki i Tekhniki, Seriya Elektrokimiya*, Yu. M. Polukarov, Ed., Vol. 11, pp. 176–220 VINITI Publishers, Moscow (1976). (b) V. G. Danilov, I. A. Kedrinsky, and Yu. G. Chirkov, Carrying out of reaction products during octane oxidation on hydrophobized electrodes, *Elektrokhim.* **14**, 492 (1978). (c) V. G. Danilov, I. A. Kedrinsky, and Yu. G. Chirkov, Low-temperature octane oxidation on hydrophobized electrodes, *Elektrokhim.* **14**, 1257–1260 (1978). (d) V. G. Danilov, I. A. Kedrinsky, Yu. G. Chirkov, F. R. Yuppertz, and G. L. Reznikov, Low-temperature electrochemical petrol B-70 oxidation on hydrophobized electrodes, *Elektrokhim.* **14**, 1567–1570 (1978). (e) V. G. Danilov, I. A. Kedrinsky, and Yu. G. Chirkov, On amount of pores filling in hydrophobized electrodes by electrolyte and liquid reagent (octane), *Elektrokhim.* **15**, 328–332 (1979). (f) V. G. Danilov, I. A. Kedrinsky, and Yu. G. Chirkov, An maximum origin study at $I_c\delta$ curves in hydrophobized electrodes with liquid reagent (octane), *Elektrokhim.* **15**, 1296–1301 (1979).
6. N. V. Korovin, *Electrochemical Generators* (In Russian), Energiya Publishers, Moscow (1974).
7. A. E. Scheidegger, *The Physics of Flow Through Porous Media*, Macmillan, New York (1961).
8. R. E. Collins, *Flow of Fluids Through Porous Materials*, Reinhold, New York (1961).
9. H. L. Ritter and L. C. Drake, Pore-size distribution in porous materials, *Ind. Eng. Chem. Anal. Ed.* **17**, 782–786 (1945).
10. R. Kh. Burshtein, V. A. Vakhonin, M. R. Tarasevich, E. I. Khrushcheva, Yu. A. Chizmadzhev, and Yu. G. Chirkov, Oxygen production on the silver porous electrode, *Elektrokhim.* **6**, 939–948 (1970).
11. E. Y. Weisman, Structural studies of porous electrodes, *J. Electrochem. Soc.* **114**, 658–665 (1967).
12. S. Brunauer, *The Adsorption of Gases and Vapors*, Vol. I, Oxford University Press, Oxford (1944).
13. R. Kh. Burshtein, M. R. Tarasevich, and V. S. Vilinskaya, A study of hydrogen and oxygen adsorption on dispersed palladium, *Elektrokhim.* **3**, 349–355 (1967).
14. M. R. Tarasevich, A. V. Dribinsky, and R. Kh. Burshtein, A study of the liquid–gas distribution in the porous catalyst–hydrophobizer system, *Elektrokhim.* **7**, 1144–1148 (1971).
15. I. G. Abidor, Ya. B. Shimshelovich, and V. S. Bagotskii, A study of the properties of hydrophobic porous bodies by the penetration technique. I. One-component porous bodies, *Elektrokhim.* **9**, 186–189 (1973).
16. (a) S. Gregg and K. Sing, *Adsorption, Surface Area and Porosity*, Academic Press, London and New York (1967). (b) S. W. Sing Kenneth, The characterization of porous solids by gas adsorption, *Ber. Bunsenges. Phys. Chem.* **79**(9), 724–730 (1975). (c) Halász István and Martin Kornél, Bestimmung der porenverteilung (10–4000 Å) von Festkörpern mit der methode der ausschluß-chromatographie, *Ber. Bunsenges. Phys. Chem.* **79**(9), 731–732 (1975).
17. V. S. Markin, Capillary equilibrium in porous media, report. I. Statement of the problem and the derivation of equations, *Izv. Akad. Nauk SSR Ser. Khim.* **9**, 1523–1530 (1965).
18. A. A. Chernenko and Yu. A. Chizmadzhev, Concerning the theory of capillary equilibrium in a porous body, *Dokl. Akad. Nauk SSSR* **151**, 392–395 (1963). (b) Yu. G. Chirkov and A. A. Chernenko, Capillary equilibrium calculation in random walk model, *Elektrokhim.* **13**, 1850–1853 (1977). (c) Yu. G. Chirkov and A. A. Chernenko, Capillary equilibrium near porous substance surface, *Elektrokhim.* **14**, 529–534 (1978). (d) A. A. Chernenko and Yu. G. Chirkov, On capillary equilibrium theory in porous media, *Elektrokhim.* **14**, 1013–1018 (1978). (e) A. A. Chernenko and Yu. G. Chirkov, Structure of division border gas/porous media in approximate serial model with autocorrelation of pore radius, *Elektrokhim.* **14**, 1202–1204 (1978).

19. W. Feller, *An Introduction to Probability Theory and Its Applications*, 3d ed., Vol. 1, Wiley, New York (1968).
20. S. R. Broadbent and J. M. Hammersley, Percolation Processes, *Proc. Cambridge Phil. Soc.* **53**, 629–645 (1957).
21. V. K. S. Shant and S. Kirkpatrick, An introduction to percolation theory, *Adv. Phys.* **20**, 325–357 (1971).
22. J. W. Essam, In: *Phase Transitions and Critical Phenomena*, Vol. 2, C. Domb and M. S. Green, Eds., pp. 197–270, Academic Press, London and New York (1972).
23. M. F. Sykes and J. W. Essam, Exact critical percolation probabilities for site and bond problems in two dimensions, *J. Math. Phys.* **5**, 1117–1127 (1964).
24. (a) Yu. G. Chirkov and V. S. Markin, Calculation in the percolation problem. III. The percolation probability, *Elektrokhim.* **12**, 1019–1024 (1976). (b) Yu. G. Chirkov, On percolation problem. IV. Asymptotical method of estimate of percolation threshold, *Elektrokhim.* **13**, 1026–1031 (1977). (c) Yu. G. Chirkov, On percolation problem. VI. A semi-infinite porous media, *Elektrokhim.* **13**, 1304–1310 (1977). (d) Yu. G. Chirkov, Porous electrodes and percolation, *Elektrokhim.* **14**, 903–906 (1978).
25. S. Kirkpatrick, Percolation and conduction, *Rev. Mod. Phys.* **45**, 574–588 (1973).
26. O. S. Ksenzhek, E. A. Kalinovskii, and L. P. Tsyganok, Capillary Equilibrium in Porous media with intersecting pores. II. Substitution of gases for liquids in porous media, *Zh. Fiz. Chim.* **38**, 2587–2593 (1964).
27. A. G. Pshenichnikov and V. N. Zhuravleva, Concerning the structure of porous gas electrodes, *Elektrokhim.* **6**, 998–1002 (1970).
28. Yu. A. Chizmadzhev, V. S. Markin, M. R. Tarasevich, and Yu. G. Chirkov, *Macrokinetics of Processes in Porous Media*, Nauka Publishers, Moscow (1971).
29. S. S. Bartenev, The filtration coefficient and the pore size distribution within underformable porous materials. I. Methods of determining the pore size distribution, *Zh. Fiz. Chim.* **49**, 1472–1475 (1975).
30. Yu. G. Chirkov, Capillary equilibrium in hydrophilic-hydrophobic Media. II. Filling of Homogeneous Irregular Lattices with Liquids, *Elektrokhim.* **7**, 1212–1215 (1971).
31. R. P. Mayer and R. A. Stowe, Mercury porosimetry—breakthrough pressure for penetration between packed spheres, *J. Colloid Sci.* **20**, 893–911 (1965).
32. (a) R. P. Iczkowski, Breakthrough pressure for random sphere packings, *Ind. Eng. Chem. Fund.* **6**, 263–265 (1967). (b) Yu. G. Chirkov and A. A. Chernenko, On interpretation of mercury porometry data, *Elektrokhim.* **15**, 697–700 (1979).
33. E. E. Petersen, *Chemical Reaction Analysis*, Prentice-Hall, Englewood Cliffs, NJ (1965).
34. R. Aris, *Introduction to the Analysis of Chemical Reactors*, Englewood Cliffs, NJ (1965).
35. O. S. Ksenzhek, E. A. Kalinovskii, and V. P. Tsyachnyi, Diffusion and flow of gases through the nickel porous electrodes *Zh. Prikladn. Khim.* **37**, 2619–2624 (1964).
36. G. Taylor, Dispersion of soluble matter in solvent flowing slowly through a tube, *Proc. R. Soc. Lond. A* **219**, 186–203 (1953).
37. P. G. Saman, A theory of dispersion in a porous medium, *J. Fluid Mech.* **6**, 321–349 (1959).
38. V. N. Nikolaevskii, A capillary model of diffusion in porous media, *Izv. Akad. Nauk SSSR Mekh. Mashinost.* **4**, 146–149 (1959).
39. V. N. Nikolaevskii, Convective diffusion in porous media, *Prikl. Mat. Mekh.* **23**, 1042–1050 (1959).
40. H. Kramers and G. Alberda, Frequency response analysis of continuous flow systems, *Chem. Eng. Sci.* **2**, 173–181 (1953).
41. H. A. Dean, A mathematical model for dispersion in the direction of flow in porous media, *Soc. Petr. Eng. J.* **3**, 49–52 (1953).
42. V. G. Levich, V. S. Markin, and Yu. A. Chizmadzhev, On hydrodynamic mixing in a model of a porous medium with stagnant zones, *Chem. Eng. Sci.* **22**, 1357–1367 (1967).

43. G. A. Turner, Dispersion in flow through pipes and paced beds, *Br. Chem. Eng.* **9**, 376–383 (1964).
44. J. O. Hirschfelder, Ch. F. Curtis and R. B. Bird, *Molecular Theory of Gases and Liquids*, Wiley, New York, and Chapman and Hall, London (1954).
45. L. D. Landau and E. M. Lifshitz, *Mechanics of Continuous Media*, GITTL, Moscow (1950).
46. V. G. Levich, *Physical and Chemical Hydrodynamics*, Fizmatgiz, Moscow (1959).
47. (a) D. A. Frank-Kamenetskii, *Diffusion and Heat Transfer in Chemical Kinetics*, Nauka Publishers, Moscow (1968). (b) P. Hugo, Gastransport im Übergangsgebiet zwischen Knudsenbereich und laminarströmung, *Ber. Bunsenges. Phys. Chem.* **79**(9), 748–758 (1975). (c) M. Kotter, P. Lovera, and L. Riekert, Zur bestimmung effektiver diffusions-koeffizienten in porösen katalysatoren, *Ber. Bunsenges. Phys. Chem.* **79**(9), 807–808 (1975). (d) E. Schütt and K. Will, Experimentelle untersuchung der diffusion von gasen in porösen feststoffen mit unterschiedlichen porenpektren, *Ber. Bunsenges. Phys. Chem.* **79**(9), 763–765 (1975). (e) U. Wiesmsnn, Einige bemerkungen zur auswertung stationärer messunger bei der diffusion von gasen in porösen feststoffen mit unterschiedlichen poredurchmessern, *Ber. Bunsenges. Phys. Chem.* **79**(9), 765–767 (1975).
48. L. D. Landau and E. M. Lifshitz, *Electrodynamics of Continuous Media*, GITTL, Moscow (1959).
49. V. V. Skorokhod, On the electrical conductivity of dispersed mixtures of conductors with insulators, *Inzh. Fiz. Zh.* **2**(8), 51–58 (1959).
50. B. J. Last and D. J. Thouless, Percolation theory and electrical conductivity, *Phys. Rev. Lett.* **27**, 1719–1721 (1971).
51. Yu. G. Chirkov, A theory of electrical conductivity of porous media. I. Limiting electrical conductivity of regular lattices partly filled with electrolyte, *Elektrokhim.* **7**, 1512–1515 (1971).
52. Yu. G. Chirkov, A theory of electrical conductivity of porous media completely filled with electrolyte. II. The method of successive approximations, *Elektrokhim.* **8**, 1187–1191 (1972).
53. Ya. B. Zel'dovich, Concerning the theory of reaction on a porous or powdery material, *Zh. Fiz. Khim.* **13**, 163–169 (1939).
54. A. N. Frumkin, On the distribution of the corrosion process over the length of a tube, *Zh. Fiz. Khim.* **23**, 1477–1482 (1949).
55. O. S. Ksenzhek, Diffusion conditions of operation of the porous electrodes, *Zh. Fiz. Khim.* **36**, 243–248 (1962).
56. K. Micka, Zur theory der porösen elektroden. I. Grundgleichungen, *Coll. Czech. Chem. Commun.* **29**, 1998–2007 (1964).
57. V. S. Daniel'-Bek, Concerning the polarization of porous electrodes. I. On the distribution of current and potential inside an electrode, *Zh. Fiz. Khim.* **22**, 697–710 (1948).
58. O. S. Ksenzhek, Macrokinetics of processes on porous electrodes, *Electrochim. Acta* **9**, 629–637 (1964).
59. L. Austin and H. Lerner, The mode of operation of porous diffusion electrodes. I. Simple redox systems, *Electrochim. Acta* **9**, 1469–1481 (1964).
60. I. G. Gurevich, Yu. M. Volkovich, and V. S. Bagotskii, *Liquid Porous Electrodes*, Nauka i Tekhnika Publishers, Minsk (1974).
61. O. S. Ksenzhek and V. V. Stender, On the Distribution of Current in a Porous Electrode, *Dokl. Akad. Nauk SSSR* **107**, 280–283 (1956).
62. J. Euler and W. Nonnenmacher, Stromverteilung in porösen elektroden, *Electrochim. Acta* **2**, 268–286 (1960).
63. J. S. Newman and C. W. Tobias, Theoretical analysis of current distribution in porous electrodes, *J. Electrochem. Soc.* **109**, 1183–1191 (1962).
64. S. Srinivasan, H. D. Hurwitz, and J. O'M. Bockris, Fundamental equations of electrochemical kinetics at porous gas-diffusion electrodes, *J. Chem. Phys.* **46**, 3108–3122 (1967).

65. R. de Levie, In: *Advances in Electrochemistry and Electrochemical Engineering*, P. Delahay, Ed., Vol. 6, pp. 329–397, Wiley, New York and London (1967).
66. J. J. Coleman, Distribution of current in porous electrodes, *J. Electrochem. Soc.* **98**, 26–30 (1951).
67. J. Euler, The variation of the current distribution in porous manganese dioxide electrodes during discharge, *Electrochim. Acta* **7**, 205–223 (1962).
68. K. Micka, In: *Fuel Cell Systems*, Advances in Chemistry, Series 47, R. F. Gould, Ed., pp. 73–82, American Chemical Society, Washington, D.C. (1965).
69. V. S. Daniel'-Bek, Concerning the polarization of porous electrodes. III. Operation of a porous electrode in the region of low polarization, *Elektrokhim.* **1**, 1319–1324 (1965).
70. A. Winsel, Current distribution in porous electrodes, *Z. Electrochem.* **66**, 287–304 (1962).
71. F. A. Posey, Methods for the calculation of polarization in porous electrodes, *J. Electrochem. Soc.* **111**, 1173–1181 (1964).
72. A. S. Chudinov and N. V. Korovin, Computer-aided analysis of porous electrode operation. I. A liquid porous electrode with diffusion rear-wall supply of the reactants, *Elektrokhim.* **3**, 311–315 (1976).
73. I. G. Gurevich and V. S. Bagotsky, Porous electrodes with liquid reactants under steady-state operating conditions, *Electrochim. Acta* **9**, 1151–1176 (1964).
74. I. G. Gurevich and V. S. Bagotsky, Steady-state operation of a porous electrode polarized from one side with diffusion supply of liquid reactants from both sides, *Electrochim. Acta* **12**, 593–614 (1967).
75. L. Austin, Tafel slopes for flooded diffusion electrodes, *Trans. Faraday Soc.* **60**, 1319–1324 (1964).
76. I. A. Zaidenman and R. M. Perskaya, On the liquid diffusion electrodes (original slope of polarization curves), *Zh. Fiz. Khim.* **33**, 50–57 (1959).
77. A. Borucka and J. N. Agar, An electrical analogue for meniscus gas electrodes, *Electrochim. Acta* **11**, 603–621 (1966).
78. R. Iczkovsky, Polarization characteristics of the hydrogen gas diffusion electrodes, *J. Electrochem. Soc.* **111**, 605–609 (1964).
79. S. Srinivasan and H. D. Hurwitz, Theory of a thin-film model of porous gas diffusion electrodes, *Electrochim. Acta* **12**, 495–512 (1967).
80. (a) J. O'M. Bockris and E. D. Cahan, Effect of a finite-contact-angle meniscus on kinetics in porous electrode systems, *J. Chem. Phys.* **50**, 1307–1324 (1969). (b) A. Winsel, Transportvorgänge in porösen Elektroden, *Ber. Bunsenges. Phys. Chem.* **79**(9), 827–836 (1975).
81. R. Kh. Burshtein, A. G. Pshenichnikov, and N. A. Shumilova, Concerning the mechanism of operation of the diffusion electrodes, *Dokl. Akad. Nauk SSSR* **143**, 1409–1412 (1962).
82. O. S. Ksenzhek, In: *Fuel Cells, Some Problems of Their Theory*, pp. 5–17, Nauka, Moscow (1964).
83. Yu. G. Chirkov and Yu. A. Chizmadzhev, On the mechanism of current generation in a porous gas electrode, a report. I. Diffusion in the σ -phase, *Izv. Akad. Nauk SSSR Ser. Khim.*, pp. 225–234 (1964).
84. Yu. A. Chizmadzhev, Some problems of the theory of porous gas electrodes, *Elektrokhim.* **2**, 3–43 (1966).
85. F. G. Will, Electrochemical oxidation of hydrogen on partially immersed platinum electrodes. II. Theoretical treatment, *J. Electrochem. Soc.* **110**, 152–160 (1963).
86. M. B. Knaster and M. I. Temkin, Rate of hydrogen ionization on active electrodes, *Dokl. Akad. Nauk SSSR* **152**, 658–661 (1963).
87. R. de Levie, On porous electrodes in electrolyte solutions, *Electrochim. Acta* **8**, 751–780 (1963).
88. E. Justi and H. Kleinschmager, Geometrically arranged gas diffusion electrodes, *Z. Naturforsch. A* **20**, 1725–1727 (1965).
89. (a) H. Thiele and A. Wiechen, Elektroden mit Isoporen für Brennstoffzellen, *Z. Naturforsch. A* **22**, 1571–1574 (1967). (b) H. Grüne, Modellbetrachtungen zum Gas-Elektrolyt-Haushalt

- von gestützten gasdiffusionselektroden für brennstoffzellen, *Siemens Forsch. Entwickl.-Ber.* **6**(6), 364–370 (1977).
90. R. Kh. Burshtein, V. S. Markin, A. G. Pshenichnikov, Yu. A. Chizmadzhev, and Yu. G. Chirkov, The relationship between structure and electrochemical properties of porous gas electrodes, *Electrochim. Acta* **9**, 733–787 (1964).
 91. A. G. Pshenichnikov, Some problems of the theory of porous electrodes, *Dokl. Akad. Nauk* **148**, 1121–1124 (1963).
 92. N. S. Lidorenko and V. A. Onishchuk, Concerning the effect of mass transfer in the gaseous phase upon the operation of a fuel cell, *Dokl. Akad. Nauk SSSR* **201**, 1389–1392 (1971).
 93. L. M. Pis'men and S. I. Kuchanov, The effect of large-scale transport processes on the steady-state conditions of operation of the gas-liquid cells, *Dokl. Akad. Nauk SSSR* **203**, 163–166 (1972).
 94. E. A. Grens, R. M. Turner, and T. Katan, A model for analysis of porous gas electrodes, *Adv. Energy Conversion* **4**, 109–119 (1964).
 95. E. Grens, Analysis, of operation of porous gas electrodes with two superimposed scales of pore structure, *Indust. Eng. Chem. Fund.* **5**, 542–547 (1966).
 96. R. Brown and J. Rockett, Theory of the performance of porous fuel cell electrodes, *J. Electrochem. Soc.* **113**, 207–213 (1966).
 97. A. P. Baranov, G. V. Shteinberg, and V. S. Bagotskii, A study of the hydrophobized active layer of the gas-diffusion electrode, *Elektrokhim.* **7**, 387–390 (1971).
 98. L. G. Austin and S. Almaula, An experimental study of the mode of operation of porous gas-diffusion electrodes with hydrogen fuel, *J. Electrochem. Soc.* **114**, 927–933 (1967).
 99. R. G. Halderman, W. P. Coleman, S. H. Langer, and W. A. Barber, *Adv. Chem. Ser.* **47**, 106 (1965).
 100. G. V. Elmore and H. A. Tanner, Intermediate temperature fuel cells, *J. Electrochem. Soc.* **108**, 669–671 (1961).
 101. W. T. Grubb and C. J. Michalske, A simple gas structure for the evaluation of catalysts (electrocatalysts) in working fuel cells, *J. Electrochem. Soc.* **111**, 477–478 (1964).
 102. C. Bianchi, Improved porous electrode for studying electrocatalytic actions of gases and vapors, *J. Electrochem. Soc.* **112**, 233–235 (1965).
 103. V. S. Bagotskii, G. V. Shteinberg, N. A. Urisson, L. N. Mokrousov, I. I. Astakhov, Z. I. Kudryavtseva, and A. P. Baranov, Concerning the structure of the hydrophobized layer of a catalyst, *Elektrokhim.* **6**, 1045–1048 (1970).
 104. R. Kh. Burshtein, A. V. Dribinskii, Yu. I. Kryukov, A. G. Pshenichnikov, and M. R. Tarasevich, A study of the structure of a fluoroplastic-catalyst porous system, *Elektrokhim.* **6**, 1356–1359 (1970).
 105. G. V. Shteinberg, Yu. G. Chirkov, A. P. Baranov, and V. S. Bagotskii, A model of the hydrophobized electrode structure, *Elektrokhim.* **8**, 1044–1047 (1972).
 106. Yu. G. Chirkov, Capillary equilibrium in hydrophobized electrode. I. A model of packed spheres of constant radius, *Elektrokhim.* **7**, 1341–1345 (1971).
 107. Yu. G. Chirkov, On the mechanism of filling the hydrophobized electrodes with gas, *Elektrokhim.* **8**, 1661–1665 (1975).
 108. I. G. Abidor, V. S. Bagotskii, and Yu. M. Vol'fkovich, The effect of the structure of the hydrophobized electrode on its electrochemical characteristics, *Elektrokhim.* **10**, 1628–1634 (1974).
 109. H. J. Zeligler, Fuel cell performance as a function of catalyst surface area, *J. Electrochem. Soc.* **114**, 144–145 (1967).
 110. F. G. Will and D. J. Ben Daniel, Significance of electrolyte films for performance porous hydrogen electrodes. I. Film model, *J. Electrochem. Soc.* **116**, 933–937 (1969).
 111. J. Giner and C. Hunter, The mechanism of operation of the Teflon-bonded gas diffusion electrode: A mathematical model, *J. Electrochem. Soc.* **116**, 1124–1130 (1969).
 112. P. Ruetschi and J. B. Ockerman, Polarization of partly wetted porous electrodes, *J. Electrochem. Soc.* **116**, 1222–1227 (1969).

113. Yu. G. Chirkov and Yu. A. Chizmadzhev, In: *Itogi Nauki i Tekhniki, Seriya Elektrokimiya*, Yu. M. Polukarov, Ed., Vol. 9, pp. 5–45, VINITI Publishers, Moscow (1974).
114. Yu. G. Chirkov, Distinction between the hydrophobized and hydrophilic electrodes. V. The role of the electrode structure, *Elektrokhim.* **11**, 544–551 (1975).
115. Yu. G. Chirkov, The relationship between the activity of the hydrophobized electrode and its structure. II. Multicomponent systems, *Elektrokhim.* **11**, 403–409 (1975).

6

Porous Flow-Through and Fluidized-Bed Electrodes

F. GOODRIDGE and A. R. WRIGHT

1. Introduction

1.1. Aims and Treatment of the Chapter

This chapter presents a coherent picture of this relatively recently opened field, rather than giving a review of the latest published work. The aim is to introduce scientists and engineers to the field of three-dimensional electrodes without sacrificing a sound approach for the sake of simplicity. Since these types of electrodes are essentially for industrial application, emphasis is placed on aspects which might affect scale-up and costs. The basic properties of these electrodes are considered in a quantitative manner in the hope of understanding their behavior and, if only in part, predicting their performance.

The chapter is divided into two major sections dealing with monopolar and bipolar arrangements as defined in Section 1.2. As will be seen, bipolar three-dimensional electrodes are in their infancy as far as industrial development is concerned. We have deliberately omitted two types of electrodes from our discussion. The first are porous fuel cell electrodes, where the charge transfer occurs at a three-phase boundary and which do not fall within our definition of porous flow-through electrodes. The second are slurry electrodes,

F. GOODRIDGE and A. R. WRIGHT • Department of Chemical Engineering, Merz Court, Claremont Road, University of Newcastle upon Tyne, Newcastle upon Tyne NE1 7RU, England.

which come within our definition but cannot be treated systematically until more information is available.

Finally, it must be pointed out that in common with most classifications, the division between two- and three-dimensional electrodes is not a sharp one. However, this fact does not produce any serious obstacles to our treatment of the field.

1.2. General Considerations

Good cell design is an essential feature of any industrial electrolytic process, particularly if it has to compete with alternative technologies. It is possible to define three parameters which enable us to judge quantitatively the success of a particular cell design; these are Y_C , the chemical yield, Y_{ST} the space-time yield, and Y_E , the energy yield.

The first can be defined as

$$Y_C = \frac{\text{actual amount of product obtained}}{\text{maximum amount of product obtainable for given conversion}} \quad (1)$$

This parameter is of particular importance under two conditions. Firstly, when we are dealing with a very costly feedstock and secondly, when removal of by-products requires an expensive separation train. The former condition will affect operating and capital related costs, the latter mainly capital related costs.

Space-time yield is defined as the quantity of product obtained per unit volume of cell in unit time and is given by

$$Y_{ST} = ajQ_E C_E \quad (2)$$

where a is the superficial geometrical electrode area per unit volume of cell, j the current density, Q_E the amount of product per unit charge if the current efficiency, C_E , is 100%. The parameter Y_{ST} is a direct guide to cell costs. It is important to note, however, that in many cases these constitute only a small part of the overall plant costs.

The energy yield is defined as the amount of product per unit electrical energy and therefore affects operating costs. It incorporates both cell voltage, V^c , and current efficiency, C_E , in the form

$$Y_E = 0.036 C_E / n V^c \quad (3)$$

where Y_E is in kmol/kWh and n is the number of electrons transferred per molecule. It is often more convenient to use the inverse of Y_E , namely, the energy consumption, E_c .

Table 1 indicates how these three parameters are linked to features of cell design. A detailed discussion of these relationships can be found elsewhere.⁽¹⁾

If one looks at Eq. (2), it is clear that in order to improve space time yields, either the specific electrode area, a , or the current density, j , must be

Table 1
Relationship between Design Features and Parameters

Desirable design features	Parameters affected		
High electrode area per unit cell volume	Y_{ST}		Y_E
Uniform electrode potential	Y_{ST}	Y_C	Y_E
Low internal ohmic resistance			Y_E
Good heat and mass transfer	Y_{ST}	Y_C	
Ability to act as flow cell	Y_{ST}	Y_C	
Simplicity of construction and ease of electrode renewal			
Ability to cope with gases			Y_E
Ability to operate at elevated pressure	Y_{ST}		

increased. The latter procedure can lead to lower current efficiencies (and possibly lower chemical yields) thereby defeating the original objective. Additionally, for metal deposition too high a current density can result in powdery deposits and prohibitive electricity costs. One must therefore consider the alternative option, namely, increasing the electrode area per unit volume of cell.

Conventional cell design employs electrodes in the shape of plates, rods, or gauzes. These are termed *two-dimensional electrodes* since electrode potential and current distribution have to be considered in two dimensions, y and z only (see Figure 1). Using this type of electrode, there is naturally a limit to the value of a , however ingenious the design. A way of overcoming this limitation is to use what are termed *three-dimensional electrodes*, which can take the following forms:

- (i) Continuous electron-conducting porous structures, with electrolyte flow through the pores.
- (ii) Individual electron-conducting particles in the form of a fixed bed (see Section 2.1.2) with electrolyte flow through the free volume.

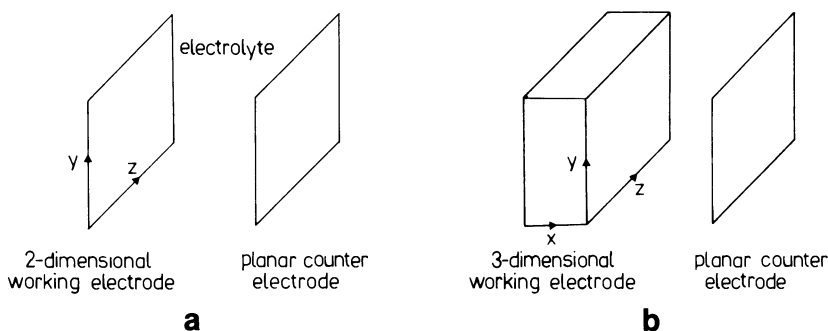


Figure 1. Classification of two- and three-dimensional electrodes.

- (iii) Individual electron-conducting particles fluidised by the flow of electrolyte (FBE).
- (iv) Individual electron-conducting particles circulated as a slurry.

Categories (i) and (ii) are called porous flow-through electrodes (PFTE), while (ii), (iii), and (iv) are termed particulate electrodes. The concept three-dimensional arises from the fact that one now has to consider potential and current distribution along an additional dimension x (see Figure 1).

Apart from their high specific area, there can be other incentives for the use of three-dimensional electrodes. These can occur in a continuous process when the working electrode itself is modified by the reaction, for example, in the continuous replenishment of the anode in the Nalco process^(2,3) and the deposition of metal in an effluent treatment.⁽⁴⁾ In addition, the employment of bipolar fluidized-bed electrodes (see below and Section 4.2.2) can be indicated when there is a danger of electrode passivation and a self-cleaning electrode could solve this problem.

Similar to their two-dimensional counterparts, three-dimensional electrodes can be linked in either a monopolar [Figure 2(a)] or a bipolar [Figure 2(b)] mode. Additionally, particulate electrodes can be operated in such a way as to make an individual electron-conducting particle completely cathodic [Figure 3(c)] or anodic, i.e., monopolar. Alternatively, we can produce bipolar particles [Figure 3(b)] where one side is cathodic, the other anodic. It is the state of the individual particles that gives rise to the definition of monopolar and bipolar structures used in the present chapter. For this reason continuous structures as classed under category (i) will be regarded as monopolar only. We return to a more detailed discussion of bipolarity in Section 4.

Cells incorporating three-dimensional electrodes can be constructed in a number of geometries. Figure 4 illustrates three typical arrangements. In each case the counterelectrode is shown in two-dimensional form. The electrode shown in Figure 4(a) has a cylindrical geometry with planar symmetry. As we shall see in Section 3, it is this geometry where current and electrolyte

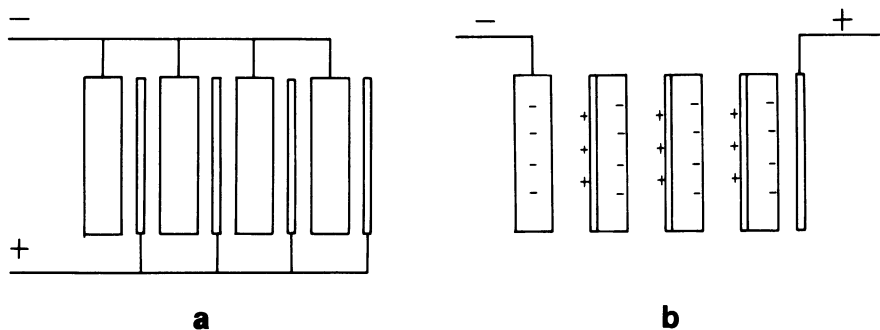


Figure 2. Monopolar and bipolar arrangements for a given number of three-dimensional electrodes: (a) monopolar; (b) bipolar.

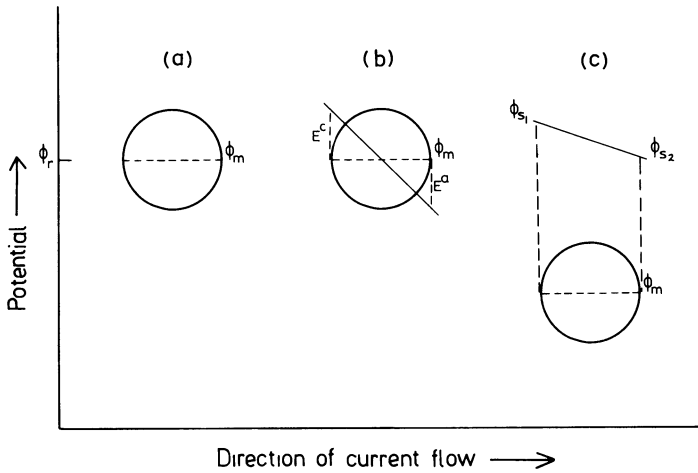


Figure 3. Monopolar and bipolar nature of individual particles: (a) particle in the absence of a voltage gradient; (b) uncharged bipolar particle; (c) charged monopolar particle.

flow in parallel that has been modeled most extensively. This geometry has proven convenient when investigating fundamental aspects of particulate electrodes, since the length of the current path can easily be changed during an experiment. Geometries shown in Figure 4(b) and 4(c) are more suitable for industrial development since the length of current and electrolyte paths in these *flow-by* arrangements (current and electrolyte flow at right angles) can be varied independently of each other. Figure 4(b) has a rectangular geometry with planar symmetry and 4(c) cylindrical geometry and symmetry.

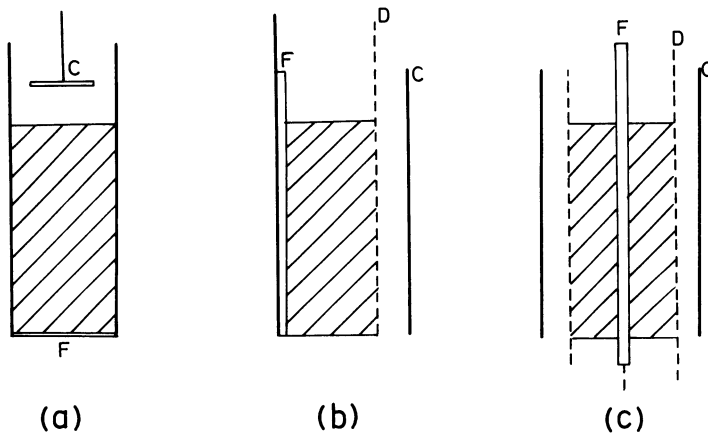


Figure 4. Geometries of three-dimensional electrodes: (a) cylindrical three-dimensional electrode with planar symmetry; (b) rectangular three-dimensional electrode with planar symmetry; (c) cylindrical three-dimensional electrode with cylindrical symmetry. C, counter-electrode; D, diaphragm; and F, current feeder.

2. Hydrodynamic and Mass Transfer Aspects of Three-Dimensional Electrodes

2.1. Hydrodynamic Aspects

2.1.1. Introduction

In this section we consider some of the characteristics of PFTEs and FBEs and obtain expressions for parameters such as characteristic electrolyte velocities and pressure losses, which are important in the design of these electrodes. It is unfortunate that some of the topics considered here have in our opinion not been adequately treated in standard texts. For this reason our discussion is possibly more detailed than one might normally expect.

Before entering the complexity of PFTEs and FBEs, consider the behavior of a single particle which forms the basic unit of these structures. For simplicity, consider a single sphere moving with a relative velocity v through a liquid (see Figure 5). Due to its motion, the sphere experiences a retarding force, F' , which opposes the relative velocity v . The magnitude of the force, F' , is given by

$$F' = \frac{1}{2} C_D A_s \rho_s v^s \quad (4)$$

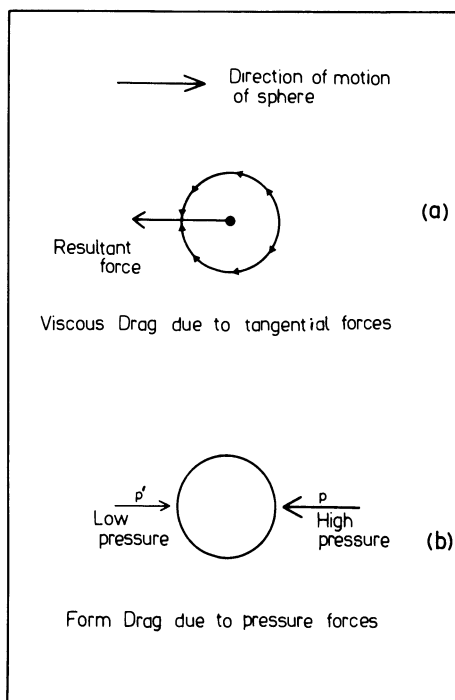


Figure 5. Viscous and form drag on a single sphere.

where C_D is the drag coefficient, A_s the projected area of the sphere of diameter d , ($\pi d^2/4$), and ρ_s the liquid density.

The constant C_D is found to be dependent on the Reynolds number Re_p , defined as

$$Re_p = dv \rho_s / \eta \quad (5)$$

where η is the viscosity of the liquid. For example, in the laminar region where $Re_p < 1$, $C_D = 24/Re_p$. In the turbulent regime ($Re_p > 1000$), C_D becomes reasonably constant. For further information consult reference 5.

The force F' is made up of two components. The first is the resultant of the viscous forces [see Figure 5(a)] which act tangentially around the sphere and is termed the viscous drag, F_v . The second is caused by a pressure variation around the sphere, whereby a high-pressure region, p , forms around the front and a low-pressure region, p' , around the tail [see Figure 5(b)], giving rise to a resultant force, F_f , called the form drag. Thus,

$$F' = F_v + F_f \quad (6)$$

Under laminar conditions the drag is almost entirely due to viscous drag:

$$F' \approx F_v = a'' \eta v \quad (7)$$

where a'' is a function of particle geometry. Under highly turbulent conditions, one is mainly dealing with form drag:

$$F' \approx F_f = b'' \rho_s v^2 \quad (8)$$

where the value of b'' again depends on the geometry of the particle. Combining Eqs. (7) and (8) one arrives at an alternative expression for F' :

$$F' = a'' \eta v + b'' \rho_s v^2 \quad (9)$$

which finds use later in this section within the context of fixed beds.

2.1.2. Flow of Electrolyte Through a Particulate Electrode

Consider now a large number of particles contained in a vessel and supported on a grid or liquid distributor which retains the particles but allows passage of liquid. An arrangement of this nature was implied in Section 1.2 when we defined the term particulate electrode and is known as a bed; liquid being able to pass through it in upward and downward flow. Let us consider the latter first.

2.1.2.1. Downward Flow

If one determines the pressure loss, ΔP , and bed height, h , as a function of the superficial velocity, v , one gets the sort of relationship shown in Figure 6. The variation in ΔP indicates two regions [Figure 6(b)]. At low velocities (region I), ΔP increases linearly with v , while at higher velocities (region II),

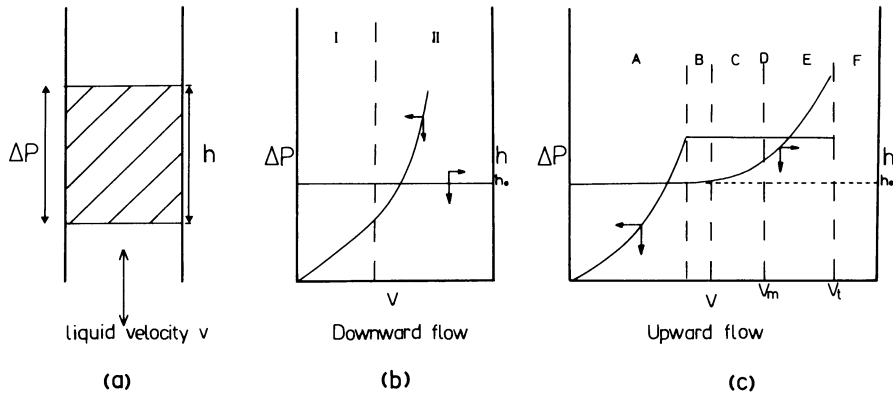


Figure 6. Flow regimes of particulate electrodes.

ΔP increases more rapidly. Throughout the velocity range one should note that the particles remain motionless, each retaining its original position. This is reflected in the constancy of h , and such a bed is termed a fixed bed as defined under category (ii) in Section 1.2. Clearly the behavior exemplified by Figure 6(b) will apply also to category (i), the continuous matrix.

2.1.2.2. Upward Flow

If one again measures ΔP and h as a function of v [Figure 6(c)], results will differ considerably from the case for downward flow. Visually one would observe particles to be stationary in regions (A) to (C) and mobile in regions (D) to (F). Consider now the behavior of the bed in these various regions in greater detail.

Region A. Fixed-bed behavior: At low velocities the flow is that through a fixed bed, the particles remaining stationary. The situation is identical with that described for downward flow in Section 2.1.2.1.

Region B. Fixed-bed behavior with realignment: As the flow velocity is raised, the drag force on the particles increases until a point is reached where the total drag force is equal to the weight of the bed. Any further increase in the drag due to a higher liquid velocity would lift the bed bodily out of its container. The particles prevent this by realigning themselves so that they offer resistance to the liquid flow. Internal changes of this nature cause little or no change in the bed volume.

Region C. Fixed-bed behavior with increased voidage: When the particles are all aligned so that they present the minimum resistance to flow, a further increase in flow rate is accommodated by a rearrangement of the particles to a more open structure resulting in an increase of the voidage, ϵ , the free volume per unit total volume of bed. This, in turn, reduces the true velocity

of the liquid through the bed and prevents an increase in liquid drag. An increase in voidage naturally requires an increase in the overall volume (i.e., expansion) of the bed and this is readily observed. Thus, although the bed is still fixed, it has a greater height than it had at the outset.

Region D. Incipient fluidization: As the flow rate is raised further there comes a point where an increase in the voidage can only be achieved by the particles losing touch with one another. Unimpeded by its neighbors, each particle now becomes free to move about in a random manner, its weight being balanced by the liquid drag force it experiences. The bed is said to be fluidized and the onset of fluidization is referred to as incipient or minimum fluidization.

Region E. Fluidization: The bed remains in a fluidized state over a range of flow rates beyond that required for incipient fluidization, but each increment in the flow rate causes regular and progressive expansion of the bed. If the distribution of voidage and particles remains uniform, then this type of fluidization is called homogeneous. Alternatively, the terms particulate, quiescent, or dispersive are used. Figure 7(a) and (b) show examples of this type of fluidization. As long as the voidage remains uniform, beds are still termed homogeneous even though definite particle circulation patterns [Figure 7(b)] may exist. Figure 7(c) gives an example of a bed where voidage is no longer uniform. Here a narrow layer of particles in a more expanded state moves rapidly upward, while a wider band of particles in a more condensed state descends slowly. As will be seen later, this spouting bed regime combines some of the properties of a moving fixed bed⁽⁶⁾ with those of a fluidized one.

Region F. Entrainment: If we continue increasing the flow rate we will reach a situation where the velocity of the liquid is equal to the terminal velocity of the particles, which are then entrained by the liquid stream. Eventually, transport of all the solid will occur and a slurry formed. Returning to Figure 6(c), we can now define v_M as the minimum fluidization velocity, v_t as the entrainment velocity, and $(h - h_0)/h_0$ as the relative bed expansion.

Up to this point we have been concerned with a qualitative examination of PFTEs and FBEs. We now obtain quantitative expressions for some of the key hydrodynamic parameters involved in the use and performance of these electrodes, i.e., pressure loss, minimum fluidization, and entrainment velocity.

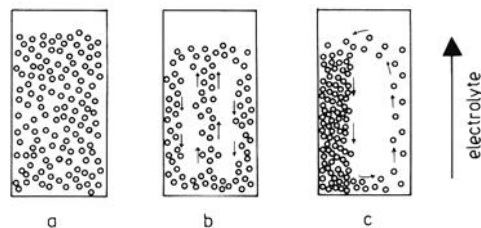


Figure 7. Particle motion in fluidized-bed electrodes: (a) homogeneous fluidization; (b) homogeneous fluidization with particle circulation; (c) spouting bed.

2.1.3. Pressure Loss

The observed dependence of pressure loss on the liquid velocity shown in Figure 6(b) is very similar to that found for the flow of liquid through a pipe. In the latter case, the initial linear region corresponds to laminar flow and, therefore, it seems reasonable to suppose that the same holds good for region I in Figure 6(b). Similarly one can assume that in both cases departure from linearity occurs with the onset of turbulence. Following the usual practice we shall at first consider laminar flow separately from turbulent flow, since the former is amenable to a theoretical approach.

By using a simple analogue of a PFTE in terms of an array of parallel cylindrical channels of length h' , and starting with the Hagen–Poiseuille equation for capillary flow,^(7a) one obtains an expression for the superficial velocity, v , of electrolyte:

$$v = \frac{1}{2} \frac{\varepsilon^3}{(1 - \varepsilon)^2} \frac{1}{S_0^2} \frac{\Delta P}{\eta h'} \quad (10)$$

where η is the liquid viscosity, ε the voidage, S_0 the surface area per unit volume of solid, and ΔP the pressure loss in the analogue. It might be argued that any similarity between a block with regular cylindrical holes and a PFTE containing a complex network of sinuous, interconnected passages of varying diameters is too remote to be of quantitative use. Even so, it is interesting to pursue the analogy to see how far this approach matches experimental observations. If we assume that h' , the effective length of our flow passages, is proportional to h , the length of our electrode in the direction of electrolyte flow, we obtain the Carman–Kozeny equation^(7b):

$$\frac{\Delta P}{h} = R' \frac{(1 - \varepsilon)^2}{\varepsilon^3} S_0^2 \eta v \quad (11)$$

As a justification of our approach, a value of the constant R' of 4.2 is found to describe the pressure loss in a PFTE under laminar conditions to an accuracy of $\pm 10\%$.

In looking for an expression for ΔP applicable not only to laminar but also to transitional and turbulent conditions, it is unfortunate that the latter two do not lend themselves to a treatment analogous to the laminar case. We must therefore resort to an empirical approach. Confining our attention first to particulate systems, it is evident that the pressure loss is due to the interaction between the particles and the liquid electrolyte. It would therefore seem reasonable to look for a lead in the behavior of a liquid flowing over a single particle as discussed in Section 2.1.1. Assuming that F_E , the drag force in the electrode, is roughly composed of the summation of events around its individual particles, we can write from Eq. (9)

$$F_E = \sum_1^{n'} F' = \sum_1^{n'} a'' \eta v + \sum_1^{n'} b'' \rho_s v^2 = a' \eta v + b' \rho_s v^2 \quad (12)$$

where n' is the number of particles making up the electrode. In addition, we can state that the drag force, F_E , exerted by the fluid on the electrode, is equal to the drag force, F_F , exerted by the electrode on the fluid. Furthermore, F_F is the direct cause of the pressure loss in the electrode, ΔP . Thus we have

$$\Delta P = a_0 \eta v + b_0 \rho_s v^2 \quad (13)$$

where in line with the dependence of a'' and b'' , we would expect a_0 and b_0 to be a function of the geometry of the particle shape. From Eq. (11) we can write

$$a_0 = 4.2h \frac{(1 - \epsilon)^2}{\epsilon^3} S_0^2 \quad (14)$$

From experimental evidence, Ergun⁽⁸⁾ has shown that b_0 may be correlated by

$$b_0 = \beta' h \frac{(1 - \epsilon)}{\epsilon^3} S_0 \quad (15)$$

where the value of β' depends on the shape of the particles making up the electrode structure and lies between 0.1 and 0.9 (0.3 for spherical particles). We therefore arrive at a universal equation for pressure loss through a particulate system:

$$\Delta P = 4.2h \frac{(1 - \epsilon)^2}{\epsilon^3} S_0^2 \eta v + \beta' h \frac{(1 - \epsilon)}{\epsilon^3} S_0 \rho_s v^2 \quad (16)$$

We may note that regarding the terms on the right-hand side of the equation: (a) when $Re_p < 20$, flow is laminar and the first term is much greater than second term; (b) when $Re_p > 1000$, flow is fully turbulent and the first term is much less than second term. Although Eq. (16) is strictly applicable to a particulate electrode only, it is reasonable to expect an equation of similar form for a porous matrix.

2.1.4. Minimum Fluidization Velocity

At the point of incipient fluidization we may regard the bed as just entering the fluidized state or just departing from the fixed state. Taking the latter view, the pressure loss will be given by Eq. (16). Assuming spherical particles,

$$\frac{\Delta P_M}{h} = 4.2 \frac{(1 - \epsilon_M)^2}{\epsilon_M^3} S_0^2 \eta v_M + 0.3 \frac{(1 - \epsilon_M)}{\epsilon_M^3} S_0 \rho_s v_M^2 \quad (17)$$

where the suffix M refers to minimum fluidization. From Figure 6 we see that the point of incipient fluidization lies in the region of constant pressure loss and we may, therefore, also write

$$\Delta P_M = \frac{\text{apparent weight of bed}}{\text{cross-sectional area of bed}} = h(1 - \epsilon_M)(\rho_m - \rho_s)g \quad (18)$$

Equating Eqs. (17) and (18) and simplifying, we obtain a quadratic equation for v_M :

$$\frac{0.3S_0\rho_s v_M^2}{\varepsilon_M^3} + 4.2 \frac{(1 - \varepsilon_M)}{\varepsilon_M^3} S_0^2 \eta v_M - (\rho_m - \rho_s)g = 0 \quad (19)$$

Experimental values of ε_M are usually employed in solving Eq. (19).

2.1.5. Entrainment Velocity

As expansion increases in a liquid fluidized bed, particles will eventually be so far apart that

- (a) The true velocity and superficial velocity will be identical.
- (b) The drag force on each particle will be virtually unaffected by its neighbors.

Under these conditions, the drag force on each particle, F' , can be evaluated from Eq. (4) and the point of entrainment can be equated with the apparent weight of the particle.

2.2. Mass Transfer Aspects

2.2.1. Introduction

So far in this section we have implied that there would be no difference between the behavior of a continuous porous structure defined under category (i) in Section 1.2, and a fixed bed of particles, category (ii). This is correct up to a point, but before considering mass transfer in these structures, possible differences must be made clear. A considerable amount of published work on the experimental behavior of PFTes has used continuous structures with an average pore size as low as 1 μm , which one can term *microporous electrodes*. This small pore size, and the associated low electrolyte velocity, has an important bearing on two parameters; h'' , the length of electrode required to establish a fully developed laminar flow, and H , the length required to achieve a fully developed concentration profile of the diffusing reactant. These two lengths are usually referred to as entrance effects. As pointed out by Ateya and Austin,⁽⁹⁾ Levich gives these two quantities for flow in a pipe as

$$h'' \approx 0.1r \text{ Re} \quad (20)$$

and

$$H \approx vr^2/D_B \quad (21)$$

where r is the radius of the pipe, Re the Reynolds number based on it, v the flow velocity of the electrolyte, and D_B the diffusivity of the solute. It has

already been mentioned in Section 2.1.3 that the complex network of small pores in an actual electrode is far removed from the idealized model envisaged as a set of parallel pipes. Fortunately, typical values of Re are of the order of 10^{-3} and hence we can safely regard the flow as being laminar in nature, even though Re as used in Eq. (20) applies strictly to flow in a pipe. Using $r = 10^{-4}$ cm, $Re = 10^{-3}$, $v = 0.1$ cm s $^{-1}$ and $D_B = 10^{-5}$ cm 2 s $^{-1}$ we obtain values for h'' and H of 10^{-8} cm and 10^{-4} cm, respectively. Clearly, entrance effects will be absent from even the smallest experimental microporous electrode.

The situation could be quite different for a particulate electrode. Here individual particles can be large in size and therefore a characteristic length of the latter must be used when calculating values of Re . For a particle diameter of 0.5 cm and $v = 1$ cm s $^{-1}$, Re is now 50 and the electrolyte flow will be turbulent in nature. Great care is therefore necessary to make sure that entrance effects do not cause misleading experimental results. For example, in the case of a fluidized bed electrode with a mean particle size of 500 μ m it was found⁽¹⁰⁾ that entrance effects existed over a distance of several centimeters above the electrolyte diffuser.

2.2.2. Mass Transfer Coefficients

As we shall see when discussing models of three-dimensional electrodes near, or under, limiting-current conditions, in order to compute the performance of the electrode, values of mass transfer coefficients must be known. The literature on mass transfer uses a variety of symbols and for definitions and a basic treatment the reader is referred to standard texts.^(11,12) Here we briefly consider k_d , a liquid-phase mass transfer coefficient and its values in PFTEs and FBES.

One way of defining k_d in an electrochemical context is to write for a single reaction

$$j_{lim} = nFk_d c_B \quad (22)$$

where j_{lim} is the limiting current, nF the number of Faradays per g-mol and c_B the bulk concentration of the reacting species B in g-mol per unit volume. It follows from Eq. (22) that k_d has the dimensions of velocity.

2.2.2.1. k_d in Porous Flow-through Electrodes

Mass transfer coefficients for PFTEs are usually expressed in the dimensionless form:

$$(k_d d)/D_B = \text{const} \times Re_p^m \times Sc^{1/3} \quad (23)$$

where d is a characteristic length of the particles making up the structure, D_B the diffusivity of the reactant in the electrolyte, Re_p the Reynolds number based on particle size, and Sc the dimensionless Schmidt number $\eta/\rho_s D$, η

and ρ_s being the viscosity and density of the electrolyte, respectively. The exponent m is found to be strongly dependent on the internal structure of the PFTE and to some extent on Re itself. Equation (23) is an empirically simplified form of a relationship based on an analogy between momentum and mass transfer.⁽¹³⁾ Although the original expression only held for Sc in the region of unity, Eq. (23) can be used for a range of values. Conservatively, Eq. (23) can be regarded as valid for range $0.6 < Sc < 2500$. It should be realized that k_d for the case of a fixed bed represents the average value of as large a number as possible of random dumpings of particles. Results of mass transfer to a single particle located in a bed cannot be extrapolated to the behavior of the whole bed unless experimentation takes account of this consideration. Even then there is considerable uncertainty if the single active particle is surrounded by others which do not take part in the mass transfer process. This situation is quite different from that when all particles are active. Probably the most convenient method of determining k_d experimentally is to use a limiting-current technique.⁽¹⁴⁾

Looking now at actual correlations, Bennion and Newman⁽¹⁵⁾ for very low Reynolds numbers use an equation based on the work of Bird *et al.*⁽¹⁶⁾

$$\frac{k_d}{aD_B} = 0.91 \left(\frac{\rho_s v}{a\eta\psi_1} \right)^{0.49} \psi_1^2 Sc^{1/3} \quad (24)$$

where a is a characteristic dimension in terms of area per unit volume of bed, v the superficial velocity of electrolyte, and ψ_1 a shape factor. It should be pointed out that Bird *et al.* use this correlation for the gas phase and, remembering our previous discussion, care must be exercised extrapolating it to liquids. Miyauchi and Nomura⁽¹⁷⁾ have measured coefficients for mass transfer to an array of a small number of spheres, again for low Reynolds numbers, but as stated before, there is the uncertainty of applying these results to a situation where all the spheres are active. The considerable variations in the correlations listed by Karabelas *et al.*⁽¹⁸⁾ emphasize the uncertainty in the values of mass transfer coefficients. For higher Reynolds numbers ($35 < Re_p < 140$) Jolls and Hanratty⁽¹⁹⁾ have produced the correlation

$$(k_d d)/D_B = 1.44 Re_p^{0.58} Sc^{1/3} \quad (25)$$

For still higher values of Re_p the authors suggest a constant of 1.59 and the index $m = 0.56$. Again there is the uncertainty of applying these values derived from a single sphere to an active bed.

2.2.2.2. k_d in Fluidized-Bed Electrodes

No direct information is available for estimating mass transfer coefficients to particles making up a liquid fluidized bed.⁽²⁰⁾ Correlations are available for transport to a current feeder immersed in a fluidized bed of nonconducting particles.⁽²¹⁾ The difficulty is the measurement of mass transfer rates between

a moving particle and the liquid electrolyte.⁽²²⁾ The best one can do therefore is to employ a correlation of the type described by Pickett⁽²³⁾:

$$(k_d d)/D_B = 1.0 \frac{(1 - \varepsilon)^{1/2}}{\varepsilon} \text{Re}_p^{1/2} \text{Sc}^{1/3} \quad (26)$$

where ε is the bed voidage. The constant in Eq. (26) is determined from experimentally measured currents. Values of mass transfer coefficients calculated from this expression must be viewed with caution since the derivation involves two doubtful assumptions, namely, a uniform mass transfer coefficient and limiting-current operation throughout the bed. Furthermore, the experimental data on which the equation is based were obtained using a very small FBE.

3. Monopolar Three-Dimensional Electrodes

In this section models are derived for monopolar electrodes and predictions compared with experimental findings. Finally these electrodes will be considered from the point of view of industrial development. Although there are important mechanistic differences between PFTes and FBEs in the way charge is transferred through the solid phase, the models that have gained acceptance produce a common mathematical treatment which is used here. Only if a bipolar mode of charge transfer is assumed (see Section 3.1.4) will the models described in this section not apply to a FBE. Although the models discussed here will in general account for the behavior of batteries and fuel cells, these are outside the scope of the present chapter.

3.1. Mathematical Models

As shown in Table 1 electrode potential distribution can affect the space-time, chemical, and energy yields of a three-dimensional electrode. If the potential distribution in one of these structures is highly nonuniform, a number of serious consequences may result. Thus a lack of selectivity and limited penetration depth by the current may outweigh any advantages over two-dimensional electrodes. It is therefore important, both from a fundamental and practical point of view, to attempt a prediction of potential, and hence current, distributions in these three-dimensional electrodes.

Models often consider one of two extreme situations, namely, activation-controlled or mass-transfer-controlled currents. With activation control, the potential and current distributions are determined by the ohmic drop in the two phases and the local overpotential. For a two-dimensional electrode, provided certain conditions are met,⁽²⁴⁾ one can in principle obtain these current distributions from the Laplace equation in conjunction with a rate expression. For three-dimensional electrodes the inability to define the

problem on a microscopic scale makes this impossible. One therefore has to use a macroscopic^(25,26) approach in which it is assumed that Ohm's law applies to both phases and that there is an overall conservation of charge. In applying Ohm's law, effective values of conductivities are used which implies that the two phases are treated as coincidental continua. Exchange of current between the two phases is determined by an average value of the electrode area as well as that of the local electrode potential. It is postulated that the latter will be related to the potential difference between the two phases derived by the use of Ohm's law. Sometimes analytical solutions are possible, but often numerical methods are required. With mass transfer control the analytical solutions, again based on a macroscopic approach, are on the whole much simpler in form. A difficulty arises in using them, however, since values of some of the averaged parameters, such as specific surface area and mass transfer coefficients, are unreliable. In addition, it is difficult to account quantitatively for departures from plug flow or fully mixed conditions.

In the present treatment the simplified approach of assuming either activation or mass transfer control has been emphasized because it leads to analytical solutions, which in turn provide a general understanding of electrode behavior. In Section 3.1.3 reference is briefly made to solutions of the more general situation where both activation and mass transfer have to be considered simultaneously. It must be emphasized that the technique of setting up equations for these more complex situations is identical with that used for the simplified cases, but usually numerical solutions are required.

As soon as concentration differences in the reactor, whether in the bulk of the electrolyte or near the electrode, become significant, hydrodynamic conditions in the electrode will assume increasing importance. For this reason models are considered under two headings, depending on whether current and electrolyte flow in parallel [Figure 4(a)] or at right angles to each other [Figure 4(b) and (c)]. As we shall see, L , the length or thickness of an electrode in the direction of current flow is of crucial importance in determining performance. One advantage of the flow-by electrode is that it makes it possible to optimize current distribution and hydrodynamic conditions independently of each other. This is reflected by the fact that most industrial developments use flow-by electrodes. Nevertheless, it is important when comparing the performance of the two arrangements to do this for identical values of L , since otherwise the parallel case could be at a disadvantage right from the start.

3.1.1. Models for Activation-Controlled Conditions

3.1.1.1. Electrolyte and Current Flow in Parallel with Each Other

Models for this case have been proposed by a number of authors. To outline the type of approach used we shall present a treatment that follows closely that by Newman and Tobias.⁽²⁷⁾ Differences between models are in

the main concerned with the type of kinetic expression used. Whenever we derive equations for a model, we shall use the boundary conditions given by the author whose treatment we are following. In order to make the mathematics reasonably tractable, a number of assumptions have to be made in addition to those implicit in the macroscopic approach. In the present example they can be listed as follows:

1. Only a one-dimensional treatment is used.
2. Steady-state conditions apply and no structural changes occur within the electrode.
3. The composition of the liquid phase is uniform.
4. The effective conductivity of the solid is uniform.
5. Ohm's law can be applied to the liquid and the solid.
6. Only a single first-order electrochemical reaction occurs.
7. There is sufficient supporting electrolyte to ignore ionic migration for the transport of reactant.
8. A Tafel or linear approximation is used for the polarization curve.

Consider Figure 8. Electrolyte flows in the direction x through a three-dimensional electrode extending from $x = 0$ to $x = L$ where a wide-mesh current feeder is situated. j_m and j_s are current densities in the solid and solution phases respectively, expressed in terms of the projected cross-sectional area of the electrode rather than the actual surface areas of the individual phases. ϕ_m and ϕ_s are then the corresponding potentials of the solid and solution phase, respectively, expressed with respect to a reference potential ϕ^0 , arbitrarily taken as zero.

Since there is no generation of charge, we can write

$$j_m + j_s = j \tag{27}$$

or

$$\frac{dj_m}{dx} + \frac{dj_s}{dx} = 0 \tag{28}$$

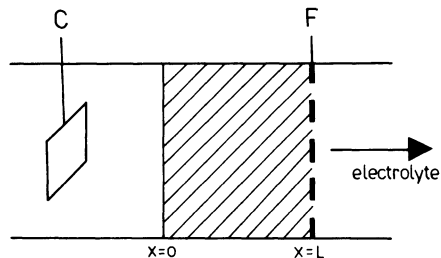


Figure 8. Schematic arrangement of cell with three-dimensional electrode as a basis for model calculation: C, counterelectrode; F, current feeder.

As boundary conditions we shall use (see Figure 8)

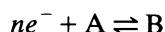
$$j_m = 0, \quad \phi_s = 0, \quad \text{at } x = 0 \quad (29)$$

$$j_m = j, \quad \text{at } x = L \quad (30)$$

As mentioned before we will also need an expression for the rate of electrochemical reaction, dj_m/dx , of the form

$$\frac{dj_m}{dx} = af(\phi_m - \phi_s, c) \quad (31)$$

where a is the specific area of the electrode, and c are concentration terms. The function $f(\phi_m - \phi_s, c)$ is in general complex, but for a first-order reaction



is commonly written in the form

$$\frac{dj_m}{dx} = aj_0 \left\{ \frac{c_A}{c_{A,0}} \exp - \left[\frac{\alpha nF}{RT} (\phi_m - \phi_s) \right] - \frac{c_B}{c_{B,0}} \exp \left[\frac{(1 - \alpha)nF}{RT} (\phi_m - \phi_s) \right] \right\} \quad (32)$$

where j_0 is the exchange current density, c_A and c_B are the concentrations of A and B, respectively, the subscript 0 denoting the concentration for which j_0 is defined and the reduction current has been considered as positive. In Eq. (32), the first term on the right-hand side refers to the cathodic, the second to the anodic reaction. Some further approximations can be made to Eq. (32). Firstly, we will assume for the moment that the ratios of concentration reduce to unity. Secondly, at very high values of $\phi_m - \phi_s$, usually $\phi_m - \phi_s \gg 0.06$ V, one of the terms on the right-hand side will disappear. Thus for a cathodic reaction this Tafel approximation will give

$$\frac{dj_m}{dx} = aj_0 \left\{ \exp - \left[\frac{\alpha nF}{RT} (\phi_m - \phi_s) \right] \right\} \quad (33)$$

Alternatively for very low values of $\phi_m - \phi_s$, in the range $0 < \phi_m - \phi_s \leq 0.06$ V 32 can be linearised to:

$$-\frac{dj_m}{dx} = \frac{aj_0 nF}{RT} (\phi_m - \phi_s) \quad (34)$$

We shall use Eq. (33) in the first case.

Finally we apply Ohm's law to the solid and liquid phases:

$$j_m = -K_m \frac{d\phi_m}{dx} \quad (35)$$

$$j_s = -K_s \frac{d\phi_s}{dx} \quad (36)$$

Differentiating (33), substituting (35) and (36) into the resulting expression, and eliminating j_s by means of (27) we obtain

$$\frac{d^2 j_m}{dx^2} = \beta \frac{dj_m}{dx} \left[j_m \left(\frac{1}{K_s} + \frac{1}{K_m} \right) - \frac{j}{K_s} \right] \quad (37)$$

where $\beta = \alpha nF/RT$. Transforming (37) into a dimensionless form results in

$$\frac{d^2 j_d}{dy^2} = \frac{dj_d}{dy} (\delta j_d - \epsilon') \quad (38)$$

where

$$j_d = j_m/j \quad (39)$$

$$y = x/L \quad (40)$$

$$\delta = Lj\beta \left[\frac{1}{K_s} + \frac{1}{K_m} \right] \quad (41)$$

and

$$\epsilon' = \frac{Lj\beta}{K_s} \quad (42)$$

Boundary conditions (29) and (30) now become

$$j_d = 0, \quad \text{at } y = 0 \quad (43)$$

$$j_d = 1, \quad \text{at } y = 1 \quad (44)$$

For the anodic case, Eq. (38) is unchanged but $|j|$ replaces j and β is $(1 - \alpha)nF/RT$ in Eqs. (37), (41), and (42). The solution of (38) is given by

$$j_d = \frac{2\theta}{\delta} \tan(\theta y - \psi) + \frac{\epsilon'}{\delta} \quad (45)$$

where

$$\tan \theta = \frac{2\delta\theta}{4\theta^2 - \epsilon'(\delta - \epsilon')} \quad (46)$$

and

$$\tan \psi = \frac{\epsilon'}{2\theta} \quad (47)$$

Integration constants θ and ψ are found by a trial-and-error procedure. Differentiating (45) we obtain an expression for the current distribution through the electrode:

$$\frac{dj_d}{dy} = \frac{2\theta^2}{\delta} \sec^2(\theta y - \psi) \quad (48)$$

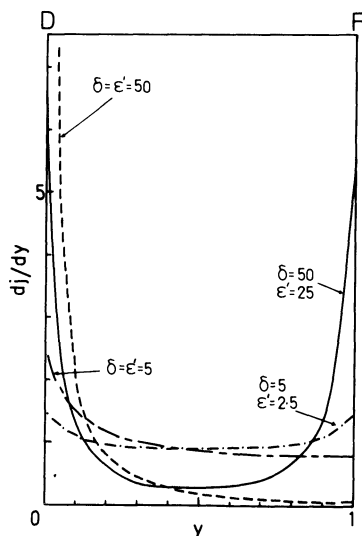


Figure 9. Plot of dj_a/dy calculated as a function of δ and ϵ' .

We have already mentioned the importance of uniform current distribution in three-dimensional electrodes. Equation (48) in conjunction with dimensionless groups δ and ϵ' enable us to make a quantitative estimate of dj_a/dy ; δ can be regarded as a ratio of the competing effects between ohmic resistance and the rate of chemical reaction. Low values of δ (i.e., a thin electrode, low current density, or high conductivities) will lead to a relatively uniform current distribution (see Figure 9). High values of δ have the opposite effect. A second important parameter influencing the degree of uniformity of current distribution is the ratio of K_m to K_s . For the majority of flow-through electrodes the value of K_m is very nearly that for the pure electronic conductor making up the solid phase and hence $K_m \gg K_s$. This corresponds to the situation when $\epsilon' = \delta$. Most of the activity in the electrode (see Figure 9) then occurs near the counterelectrode. In fluidized-bed electrodes, K_m is a complex function of collision frequency, charge capacity, nature of solid surface, etc., and K_m is therefore very much lower than the electronic conductivity of the parent material. In fact, $K_m = K_s$ is a reasonable relationship. Under these circumstances $\epsilon' = \delta/2$ and, as shown in Figure 9, current distribution is more uniform than for the previous case, maximum activity appearing near both boundaries of the three-dimensional electrode. The complex problem of charge transfer in fluidized-bed electrodes is discussed in Section 3.1.4.

Complementary deductions on current distribution can be made from a study of potential distribution, $\phi_m - \phi_s = \phi$, through the electrode. Figure 10 shows potential distributions for a Tafel approximation when $K_m \gg K_s$ and $K_m = K_s$, for two values of δ . Clearly ϕ is more uniform in the second case since changes in ϕ_s are compensated to a certain extent by changes in ϕ_m , which remains constant when $K_m \gg K_s$.

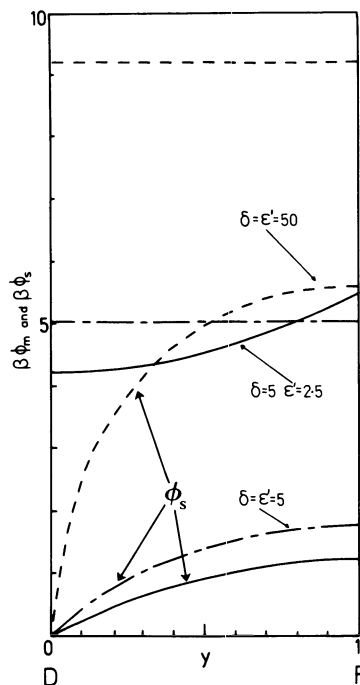


Figure 10. Plot of potential distribution calculated as a function of δ and ϵ' : D, diaphragm; F, current feeder.

Using Eq. (34) instead of (33) gives the current distribution dj_d/dy as^(27a)

$$\frac{dj_d}{dy} = \frac{K_s \nu}{K_s + K_s \sinh \nu} \left[\frac{K_m}{K_s} \cosh \nu(1 - y) + \cosh \nu y \right] \quad (49)$$

where

$$\nu = L \left[\frac{aj_0 n F}{RT} \left(\frac{1}{K_s} + \frac{1}{K_m} \right) \right]^{1/2} \quad (50)$$

Here we see that ν is an expression analogous to δ in indicating the degree of nonuniformity of current distribution, but ν is more applicable to low values of ϕ .

It is possible to regard the quantities L/δ and L/ν as characteristic penetration depths leading to the concept of an effectiveness factor along lines used by workers in the field of catalysis. Coeuret and coworkers⁽²⁸⁾ have interpreted their results in this way for an infinitely large conductivity of the solid. Bearing this in mind, some of their expressions can be equated to L/ν .

At this point we should mention an empirical, but nevertheless useful, concept of effective bed thickness, L_{eff} , which Kreysa and Heitz⁽²⁹⁾ have applied to fixed- and fluidized-bed electrodes. Figure 11 shows that, for the reduction of $10^{-4} M$ solution of benzoquinone in a fluidized bed of silver spheres, current density remains unchanged when increasing the dimension

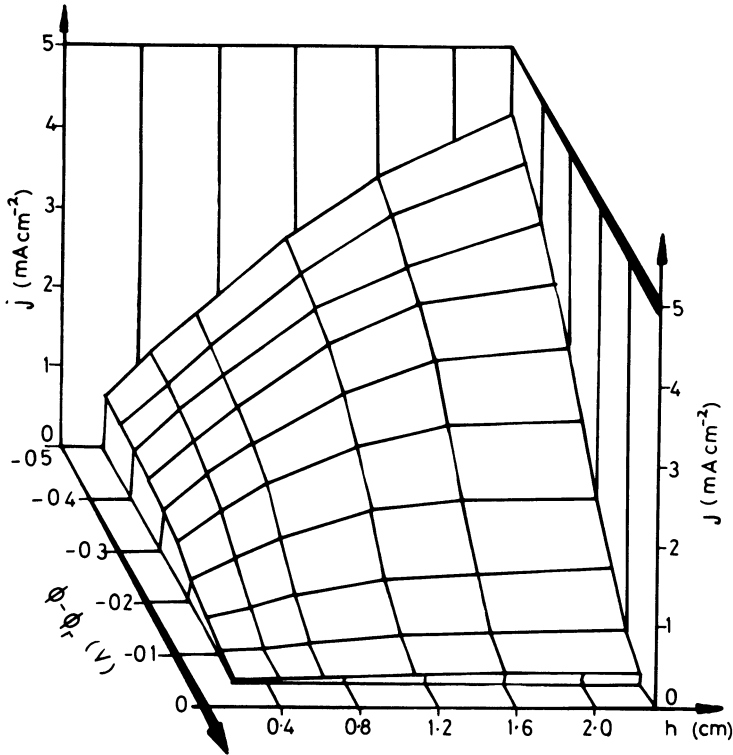


Figure 11. Three-dimensional plot of current density as a function of bed height and electrode potential.

of the bed in the direction of current flow beyond a given value, L_{eff} . The cell used had the configuration and symmetry depicted in Figure 4(a), and some caution must be exercised about the absolute values of the current density since in view of the small bed heights used, entrance effects cannot be ruled out. For a fixed bed, Kreysa and Heitz derive a value for L_{eff} based on considerations of similarity and a linear approximation to the polarization curve for the bed electrode⁽³⁰⁾:

$$L_{\text{eff}}/(K_s \Delta \phi / \Delta j) = 0.36 \quad (51)$$

where j is the cross-sectional current density for the bed electrode.

Turning again to FBES, Fleischmann and Oldfield⁽³¹⁾ used essentially the Newman and Tobias approach described previously to obtain model equations for these systems. In the context of PFTEs, Coeuret and collaborators⁽²⁸⁾ use an empirical polarization expression of the form

$$j = \text{const} \times (\phi_m - \phi_s)^m \quad (52)$$

where $0 < m < 1$, whilst Goodridge and coworkers⁽³²⁾ compute potential and

current distributions in FBEs using experimentally determined polarization curves.

In our derivations so far, it has been assumed that any concentration changes in the electrolyte as it flowed through the cell could be considered as negligible. Although that is a reasonable assumption in a large number of situations, let us see what would happen if a significant concentration change, from $c_{A,0}$ to c_A , occurred. Following again Newman and Tobias,⁽²⁷⁾ Eq. (33) would now be

$$\frac{dj_m}{dx} = aj_0 \frac{c_A}{c_{A,0}} \exp \left[-\frac{\alpha nF}{RT} (\phi_m - \phi_s) \right] \quad (53)$$

Ignoring ionic migration in the presence of excess supporting electrolyte (K_s will also remain constant) and in the absence of any convective component, the flux of reactant A, N_A , will be given by

$$N_A = -D_B \frac{dc_A}{dx} \quad (54)$$

and a mass balance of species A gives

$$\frac{dj_m}{dx} = nFD_B \frac{d^2c_A}{dx^2} \quad (55)$$

Equations (27), (35), and (36) will remain as before. Boundary conditions are now

$$j_m = 0, \quad \phi_s = 0, \quad c_A = c_{A,0}, \quad \text{at } x = 0 \quad (56)$$

$$j_m = j, \quad \frac{dc_A}{dx} = 0, \quad \text{at } x = L \quad (57)$$

Integrating Eq. (55), differentiating (53), eliminating j_s , ϕ_s , ϕ_m , and making the resulting equation dimensionless [cf. (37)] we obtain

$$\frac{d^2j_d}{dy^2} = \frac{dj_d}{dy} \left[\delta j_d - \varepsilon' + \frac{\gamma(j_d - 1)}{\lambda} \right] \quad (58)$$

where

$$\lambda = \frac{c_A}{c_{A,0}} \quad (59)$$

and

$$\gamma = \frac{jL}{nFD_{BCA,0}} \quad (60)$$

For an anodic reaction j in (60) will have to be replaced by $|j|$. Boundary

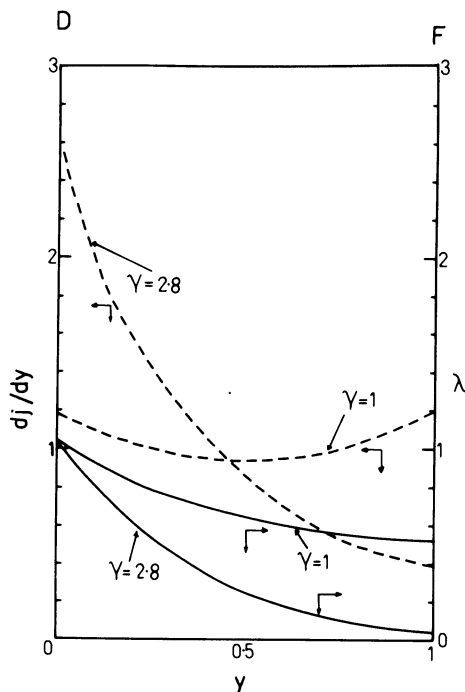


Figure 12. Plot dj_d/dy calculated as a function of γ and λ : D, diaphragm; F, current feeder.

conditions in a dimensionless form are

$$j_d = 0, \quad \lambda = 1, \quad \text{at } y = 0 \quad (61)$$

$$j_d = 1, \quad \text{at } y = 1 \quad (62)$$

Newman has solved Eq. (58) by a series of approximations. Figure 12 shows his plots⁽²⁷⁾ of current distribution dj_d/dy and concentration profiles λ as a function of γ . It is apparent that the depletion effect shifts activity away from the feeder toward the electrode-solution interface.

3.1.1.2. Electrolyte and Current Flow at Right Angles to Each Other

It has been shown⁽²⁷⁾ that unless δ and ν are below a given value, potential and current distributions are significantly nonuniform. From an industrial point of view, the geometries to be discussed now [Figure 4(b) and (c)] are preferable to that of Figure 4(a), since in the former two cases dispersion can be minimized because it is possible to keep L (or Δr) small while preserving a long electrolyte flow-path. An alternative way of looking at this advantage is to realize that residence times can be arranged independently of the length of current path. So far only Alkire and Ng⁽³³⁾ have modeled a flow-by situation and taken account of concentration differences. Their analysis applies to reactor geometry Figure 4(c). One difficulty of treating a flow-by cell is that a two-dimensional model is required and hence numerical methods have to be used.

3.1.2. Models for Mass-Transfer-Controlled Conditions

3.1.2.1. Electrolyte and Current Flow in Parallel with Each Other

Steady-state treatments of PFTEs working under limiting-current conditions have been presented by a number of workers.^(15,26,34,35) Fleischmann and Oldfield⁽³¹⁾ have derived expressions for a FBE also operating under a limiting-current regime. It is not surprising that some of their equations are identical with those derived by Bennion and Newman,⁽¹⁵⁾ and it is this latter treatment that is used here.

In the following derivations we adopt the simplifying assumptions used in Section 3.2.1 and, in addition, postulate that the electrolyte inside the pores of the electrode moves in plug flow. Consider again Figure 8. From a mass balance over a differential element of volume dx we have for a reaction $A \rightarrow B$

$$v \frac{dc_A}{dx} = -ak_d c_A \quad (63)$$

where v is the superficial velocity of the electrolyte and c_A the concentration of reactant per unit volume of electrolyte. Some authors have defined the concentration of reactant in the pores of the electrode as ϵc_A . While in principle there is nothing wrong with this procedure, it does lead to an undesirable definition of mass transfer coefficients based on varying voidage. k_d in Eq. (63) is therefore the conventional mass transfer coefficient considered in Section 2.2.2. We can relate the concentration gradient to dj_s/dx , the activity of the electrode, by the use of Faraday's law:

$$\frac{dj_s}{dx} = nFv \frac{dc_A}{dx} \quad (64)$$

Finally Eq. (36) gives the potential distribution:

$$j_s = -K_s \frac{d\phi_s}{dx} \quad (65)$$

Our boundary conditions will be

$$c_A = c_{A,0}, \quad \phi_s = 0, \quad \text{at } x = 0 \quad (66)$$

$$c_A = c_{A,L}, \quad j_s = 0, \quad \text{at } x = L \quad (67)$$

Solutions of (63), (64), and (65) yield expressions for the concentration of reactant, the current density, and the potential in the electrolyte—all as a function of the distance in the direction of current flow:

$$c_A = c_{A,0} \exp(-\alpha'x) \quad (68)$$

$$j_s = vnF[c_{A,0} \exp(-\alpha'x) - c_{A,L}] \quad (69)$$

and

$$j = vnF(c_{A,0} - c_{A,L}) \quad (70)$$

$$\phi_s = \frac{v^2 nF}{K_s a k_d} [c_{A,0} \exp(-\alpha'x) + \alpha' c_{A,L} x - c_{A,0}] \quad (71)$$

where

$$\alpha' = (ak_d)/v \quad (72)$$

From Eq. (68) we can define a useful criterion of performance, namely, a collection efficiency, given by

$$(c_{A,0} - c_{A,L})/c_{A,0} = 1 - \exp(-\alpha'L) \quad (73)$$

Chu *et al.*⁽³⁶⁾ have extended the model described so far to a nonsteady-state situation and confirmed their predictions by the use of copper deposition as a test reaction.

3.1.2.2. Electrolyte and Current Flow at Right Angles to Each Other

Again only Alkire and his coworkers have considered flow-by electrodes under limiting-current conditions. Alkire and Ng⁽³⁷⁾ developed a model for the present situation by means of an extension of their previous treatment of the activation-controlled case,⁽³³⁾ but this time the PFTE is in the annulus formed by two concentric cylinders. Again their dimensionless equations have to be solved numerically. It is interesting to note that one of their dimensionless parameters, ζ , defined by

$$\zeta = \frac{(\Delta r)^2 a j_0 nF}{RT} \frac{1}{K_s} \quad (74)$$

where Δr is the width of the annulus in the direction of current flow, is identical to ν^2 from Eq. (50), provided $K_m \rightarrow \infty$.

If the entire electrode works under limiting-current conditions then concentrations of reactant at the solid electrode surface will essentially be zero and hence liquid concentrations in a radial direction (the direction of current flow) will be uniform. Concentrations in an axial direction (direction of electrolyte flow) will be given by Eq. (68) and the volumetric reaction rate will be the same as for the situation described in Section 3.1.2.1, the corresponding current density j being given by Eq. (70).

3.1.3. More General Models

Even with as wide a limiting-current plateau as for the ferro/ferricyanide system, in many instances only part of the three-dimensional electrode works under a mass-transfer-controlled regime.⁽³⁸⁾ A number of authors have attempted to deal with this situation, as well as including in their models more complex reaction schemes. Here we cannot attempt detailed coverage but

will refer the reader to some of the original publications. As we have indicated before, most of the solutions employ numerical methods. Thus Sioda⁽³⁹⁾ considers the case of a PFTE ($K_m \rightarrow \infty$) operating below the limiting current for a reversible reaction obeying the Nernst equation but includes the effect of mass transport. Later work⁽³⁵⁾ considers the effect of an ECE sequence. Alkire and Gracon⁽³⁴⁾ have produced a very general analysis for a single-electrode reaction, capable of predicting PFTE behavior over a wide range of operating conditions which include charge transfer resistance and axial diffusion. Alkire and Gould⁽⁴⁰⁾ have extended this work to multiple reaction sequences, including ECE, and the deposition of several metals. More recently, Trainham and Newman⁽⁴¹⁾ have presented a model for a PFTE operating above and below limiting current, which considers the effect of axial diffusion and dispersion and includes a simultaneous side reaction in the reaction scheme. Finally, models derived by Ateya and Austin also take into account axial dispersion and diffusion, first for a single reversible reaction⁽⁹⁾ and later for irreversible one-electron and consecutive two-electron reactions.⁽⁴²⁾

3.1.4. *Experimental Investigations of Potential and Current Distributions*

It is of course rather difficult to insert potential probes into a continuous matrix and indeed point current densities are usually determined for these structures by obtaining values for the relative amounts of material either deposited or dissolved; alternatively, the current flow into isolated segments of the electrode has been measured. Examples of these methods together with their relative merits and limitations have been discussed by Newman and Tiedeman.⁽²⁶⁾ Early work on potential profiles in fixed- and fluidized-bed electrodes, reported by Goodridge and coworkers,^(10,32,38) used fixed and movable composite probes comprised of an insulated metal wire exposed at the end of a Luggin capillary. Thus potential measurements of ϕ_m (with respect to the feeder) and of ϕ_s (with respect to a reference electrode) could be made. This technique was refined by attaching the movable probe to a micrometer, thereby gaining in positional accuracy. A further development is concerned with a probe (see Figure 13) which, by the addition of an insulated wire, measures ϕ_m with respect to the local rest potential instead of that of the feeder electrode.

Most of the results discussed in this section have been obtained in cells with a flow-by configuration. A recent design of such a cell used in the authors' laboratories and suitable both for fixed- and fluidized-bed electrodes is shown in Figure 14. For the sake of simplicity the potential measuring probes are not shown. For fixed beds these are inserted through the current feeder while for fluidized beds a single vertical probe is found to be more convenient. The cell body is made from polypropylene with cylindrical TPX windows set in the side.

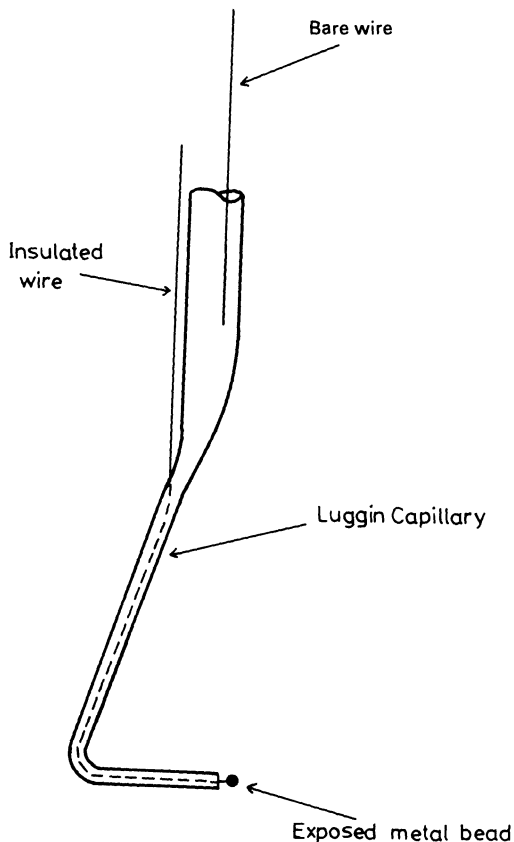


Figure 13. Sketch of a probe for the measurement of local overpotentials.

Consider first results obtained for the reduction of *m*-nitrobenzene sulfonic acid to metanilic acid, using a fixed-bed⁽⁴³⁾ and fluidized-bed electrodes.⁽³²⁾ In each case the electrodes consisted of copper-coated glass beads (in later work the tendency has been to use solid metal particles whenever possible), 500 μm in diameter and had the cylindrical geometry and symmetry shown in Figure 4(c). Figure 15 records a plot of experimental values of ϕ_m and ϕ_s as a function of $r/\Delta r$, the dimensionless bed thickness in the direction of current flow. For the fixed bed one gets the profile predicted by Figure 10 for $\varepsilon' \approx \delta$; thus ϕ_m is constant and ϕ_s increases sharply as the diaphragm is approached. For the fluidized bed the shape of the curves is again as predicted for the case $\varepsilon' \approx \delta/2$. Not surprisingly the same agreement holds between experiment (Figure 16) and model (Figure 9), when expressing results in terms of current distribution, dj_a/dy . It should be pointed out, however, that the shapes of the experimental curves are modified by the fact that in a cylindrical geometry the cross-sectional area increases as one moves from the central feeder to the circumference of the bed.

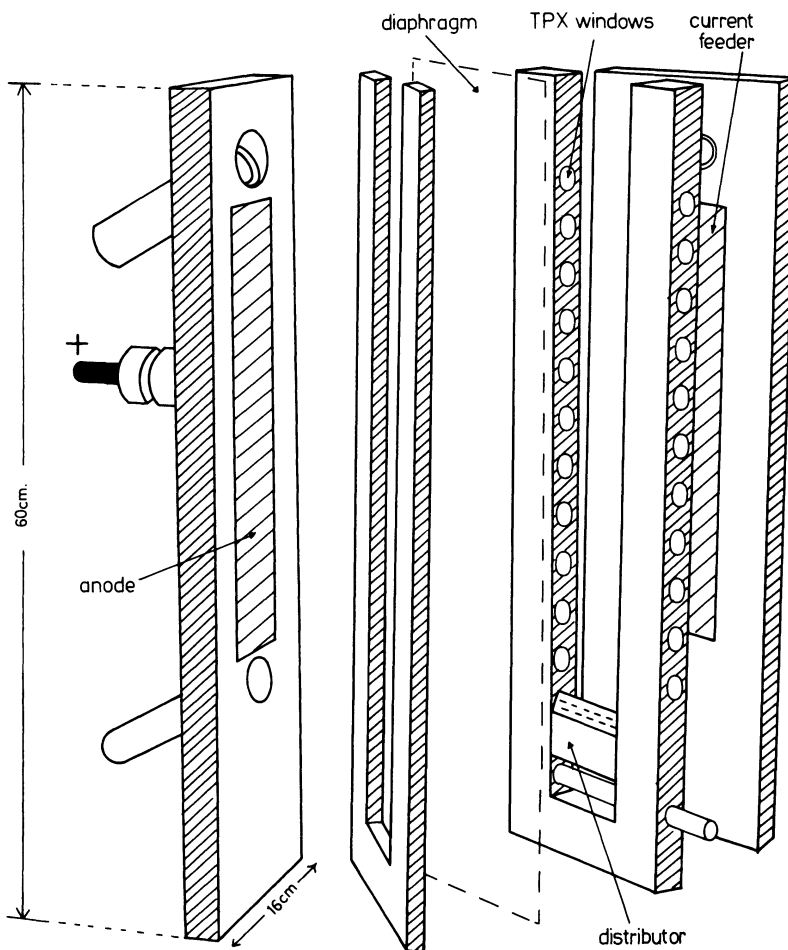


Figure 14. Expanded view of a cell suitable for fixed-bed or fluidized-bed electrodes.

The qualitative correctness of Eq. (45) is again demonstrated (Figure 17) when considering the effect of expansion of a FBE on j_d , during copper deposition⁽⁴⁴⁾ under activation control ($j = 1400 \text{ A m}^{-2}$). At 20% expansion it can be seen that the major activity is confined to a region near the diaphragm corresponding to the situation noted previously for a fixed bed, where $\epsilon' \approx \delta$. This contrasts with the case for the organic reaction (Figure 16), presumably because of the cleanliness of a continuously renewed metal surface giving high values of K_m . Only at higher expansions do we get back to the situation more characteristic for a FBE, where $\epsilon' \approx \delta/2$ and activity occurs at either extremes of the bed.

At first sight it is surprising that the results in Figures 15–17 can satisfactorily be interpreted by a simple one-dimensional model and yet were obtained

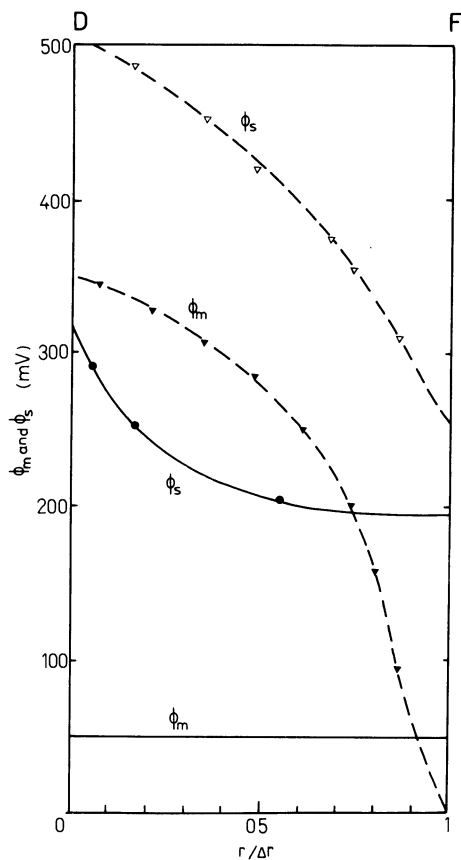


Figure 15. Plot of experimentally determined potential distributions for fixed-bed and fluidized-bed electrodes during an organic reaction: D, diaphragm; F, current feeder; —, fixed bed; ---, fluidized bed.

in cells with flow-by configuration. The explanation is that experimental conditions were such that concentration changes in the direction of current and electrolyte flow could be ignored.

So far, it has been demonstrated that on the whole qualitative agreement between model predictions and experimental findings is satisfactory. As soon as one attempts an assessment of quantitative predictions, one immediately meets the problem of obtaining reliable values of parameters to be inserted in the equations. Uncertainties in the value of k_d , the mass transfer coefficient, have already been discussed in Section 2.2.2. Again, estimates of a , the specific electrode area, are in the case of a porous matrix often in considerable doubt.^(41,45) Values of a have been obtained by double-layer charging⁽⁴⁶⁾ or the use of geometrical variables.⁽⁴⁷⁾ For fixed-bed and fluidized-bed electrodes the specific area may be estimated from the particle size, but there is evidence⁽³⁸⁾ that not all the geometrical area is electrochemically active. For particles of regular shape this could be due to shielding,⁽³⁸⁾ while for irregularly shaped particles actual contact⁽⁴⁵⁾ could in part be responsible. The effective

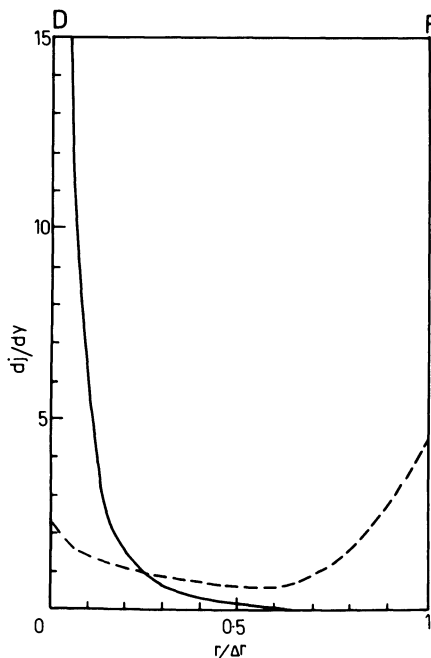


Figure 16. Plot of experimentally determined $d_{j,d}/dy$ for fixed-bed and fluidized-bed electrodes during an organic reaction: D, diaphragm; F, current feeder; —, fixed bed; ---, fluidized bed.

electrolyte conductivity, K_s , can readily be determined by experiment or estimation,⁽⁴⁸⁾ but values of exchange current densities for many reactions are not known accurately. Therefore, due to all these uncertainties it can frequently become necessary to adjust parameters^(34,37,41) in order to obtain agreement between experimental and calculated results. Bearing these limitations in mind, authors with few exceptions^(9,34) appear to be able to account for the behavior of PFTes.

In contrast, charge transfer in the particulate phase of FBEs is a process of considerable complexity. It has already been seen that values of K_m can be dependent on the nature of the reaction taking place. In addition values of K_m in the vicinity of the electrolyte distributor appear to be higher⁽¹⁰⁾ than in the main body of the bed, the effect extending over several centimeters. In fact, this is one of the few occasions where it is possible to determine directly the extent of an entrance effect mentioned in Section 2.2.1. Fleischmann and Oldfield,⁽⁴⁹⁾ on the basis of collisions between individual particles in a FBE, have obtained an analytical expression for K_m involving a collision frequency, ν' , the double-layer capacity, C_d , the contact time during collisions, t_c , and the RC time constant for charge sharing during a collision, τ . Beenackers and colleagues⁽⁵⁰⁾ actually determined these quantities experimentally in order to test an expression for K_m very similar to that obtained by Fleischmann and Oldfield. It was found that values calculated in this way were on the average three orders of magnitude lower than those obtained from experimentally determined potential profiles. It would appear therefore

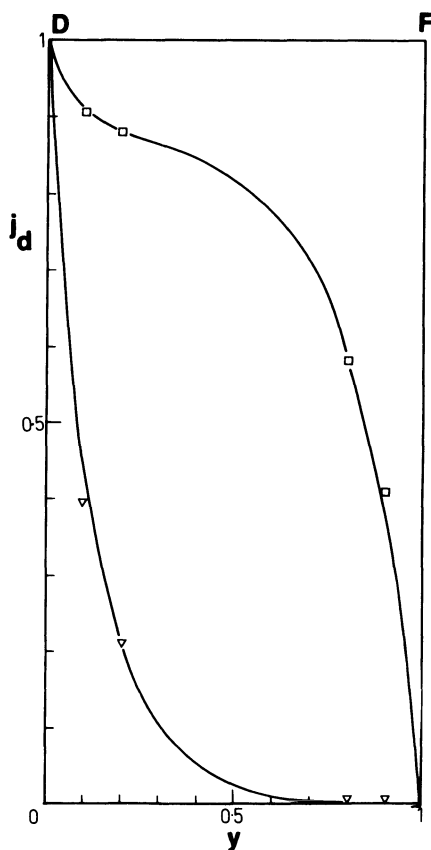


Figure 17. Plot of experimentally determined current distributions as a function of bed expansion for a fluidized-bed electrode during copper deposition: D, diaphragm; F, current feeder; ∇ , 20% expansion; \square , 50% expansion.

that expressions based on collisions between individual particles cannot produce reasonable values for K_m . Beenackers and coworkers⁽⁵⁰⁾ have produced a tentative model based on charge transfer between aggregates of particles, but unfortunately the resulting expression contains some parameters which are still unknown.

Until now any argument on charge transfer in FBEs has been based on the kind of potential profile shown in Figure 15, representing averaged values of ϕ_m . Many workers when determining particle potentials in FBEs have observed rapid fluctuations in the potentials of the fluidized particles, frequencies of these variations being of the order of 10^3 Hz. A statistical analysis of local overpotentials by Fleischmann and Kelsall⁽⁵¹⁾ ascribes these fluctuations to the random charge-sharing process in the particulate phase coupled with the loss of charge due to the electrochemical reaction. Further work⁽⁵²⁾ shows that the potential values of these fluctuations range from cathodic to anodic over a large portion of the bed. This phenomenon has been interpreted by Plimley and Wright⁽⁵²⁾ in terms of a bipolar charge transfer mechanism of particle aggregates.

3.2. Industrial Aspects

3.2.1. Porous Flow-through Electrodes

The only large scale process so far, using PFTEs in the form of a fixed bed, is that developed by Nalco for the production of tetra alkyl lead. The cell and its construction, as well as the process as a whole, has received considerable attention in the literature and for details the reader is referred to a selection of publications.^(2,3,53,54) The anode consists of lead pellets, which are consumed by the reaction and subject to mass transfer control. This, as we have seen in Section 3.1.2, should lead to a reasonably uniform current distribution and avoid an uneven decrease in pellet diameters.

On a development scale, one of the few other organic reactions performed in a fixed bed has already been mentioned in Section 3.1.3, namely, the production of metanilic acid.⁽⁴³⁾ Most of the other applications contemplated for PFTEs involve the deposition of metals from dilute effluent streams. Examples investigated include copper,^(15,28,34,36,41,45) antimony,⁽⁵⁵⁾ lead,⁽⁵⁶⁾ and mercury.⁽⁵⁷⁾ Figure 18 illustrates the principle of a cell described by Wenger and Bennion⁽⁴⁵⁾ based on a previous design.⁽¹⁵⁾ In essence, catholyte and anolyte (in the ratio of 99:1, respectively) flow through the cylindrical PFTEs. Maximum catholyte flow rate is governed by the need to avoid hydrogen evolution. After a given period, the polarity and flow ratios are reversed and the deposited copper is redissolved from the graphite bed.

3.2.2. Fluidized-Bed Electrodes

Although early experiments were more concerned with organic electrosynthesis,⁽⁵⁸⁾ industrial developments have been mainly in the field of metal winning and effluent treatment. Initial work concerned the deposition of zinc from an alkaline medium,⁽⁵⁹⁾ followed by that of Flett,^(60,61) Fleischmann and coworkers,⁽⁶²⁾ and Surfleet and Crowle,⁽⁶³⁾ who all showed that copper could be deposited satisfactorily in FBEs, both from leach liquors and very dilute

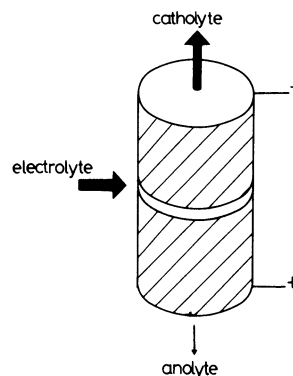


Figure 18. Schematic diagram of the Wenger-Bennion cell for the removal of copper from dilute solutions.

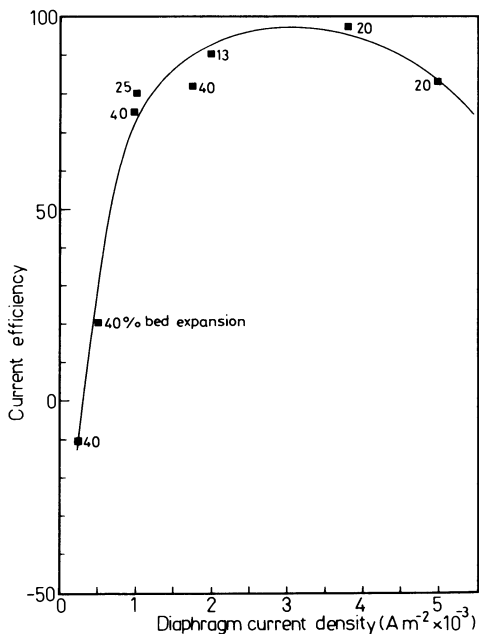


Figure 19. Current efficiencies for copper deposition using a fluidized-bed electrode pilot plant cell.

effluents. Wilkinson and Haines⁽⁶⁴⁾ working on a considerably larger scale, with beds mainly $0.12\ m^2$ in cross section, demonstrated that copper winning still resulted in satisfactory current efficiencies. This was confirmed by Goodridge and coworkers⁽⁶⁵⁾ who also used a pilot plant unit with a cell having a rectangular geometry and a cross-sectional area of $0.25\ m^2$. Figure 19 shows some of their typical current efficiencies as a function of current density; starting concentrations were about $5\ g\ liter^{-1}$ of copper, a typical composition for a leach liquor.

One of the drawbacks of using a uniformly fluidized-bed electrode [Figure 7(a) and (b)] is that some deposition of metal will occur on the feeder electrode, although this can be minimized by a suitable choice of feeder electrodes and operating conditions. Models predict an increase in the rate of deposition on the feeder with increase in metal concentration, i.e., metal winning compared to effluent treatment. For an industrial metal winning electrolysis, lasting thousands of hours, it is imperative to avoid this deposition altogether. By the simple expedient of inclining the cell away from the vertical, one can impose the circulation pattern depicted in Figure 7(c) and described in Section 2.1.2. When using this technique for metal deposition,⁽⁶⁶⁾ one finds that the condensed falling phase acts in the manner of a fixed bed. As expected from Eq. (48), activity at the feeder electrode is at a minimum, deposition occurring near the boundary between the falling and rising layer, and in the latter itself. This view is confirmed by potential profiles obtained for the deposition of zinc from acid solutions⁽⁶⁶⁾ and the more extensive data shown in Figure 20

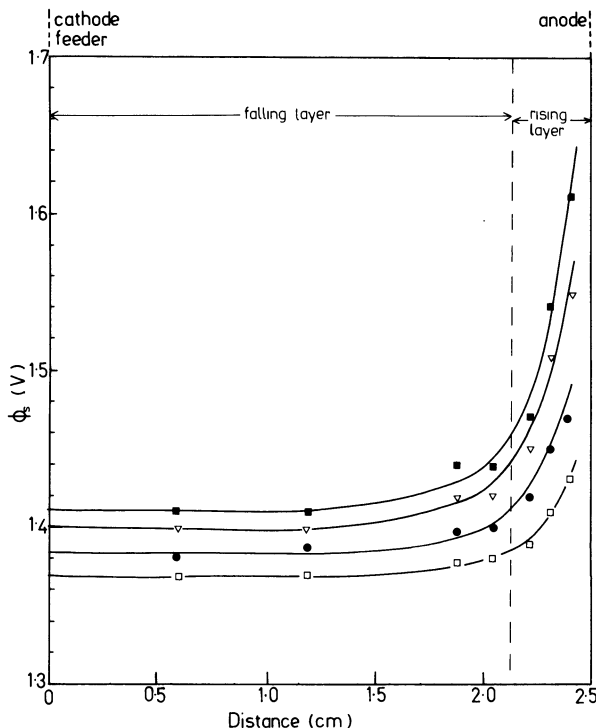


Figure 20. Experimentally determined values of ϕ_s with respect to the feeder for zinc deposition in an undivided spouting bed cell: \blacksquare , 5500 A m^{-2} ; ∇ , 4400 A m^{-2} ; \bullet , 2800 A m^{-2} ; \square , 1100 A m^{-2} .

for zinc deposition from alkaline media.⁽⁶⁷⁾ Inserting a metal probe into the falling layer in the vicinity of the current feeder confirms the absence of deposition. As a further advantage of the use of this flow regime, agglomeration of particles, which under certain conditions can be a problem with more concentrated solutions, is also avoided.

Raats and coworkers⁽⁴⁾ have used a pilot plant scale FBE for the removal of metals from dilute effluent streams. Processes investigated include the removal and simultaneous separation of copper and cadmium from a concentrated zinc stream, the removal of copper from a stream of chlorinated hydrocarbons, that of mercury from a stream of brine, and that of copper from nickel and arsenic effluents, respectively. The configuration of their cell is shown in Figure 21. An interesting feature is the multiplicity of current feeders and corresponding anodes in the wide cylindrical envelope. Again, as in all the examples considered in Section 3.3.2, current and electrolyte flow at right angles to each other.

It is instructive to compare the space-time yields of the PFTE of Bennion *et al.*^(15,45) with that of the FBE described above. Using the performance

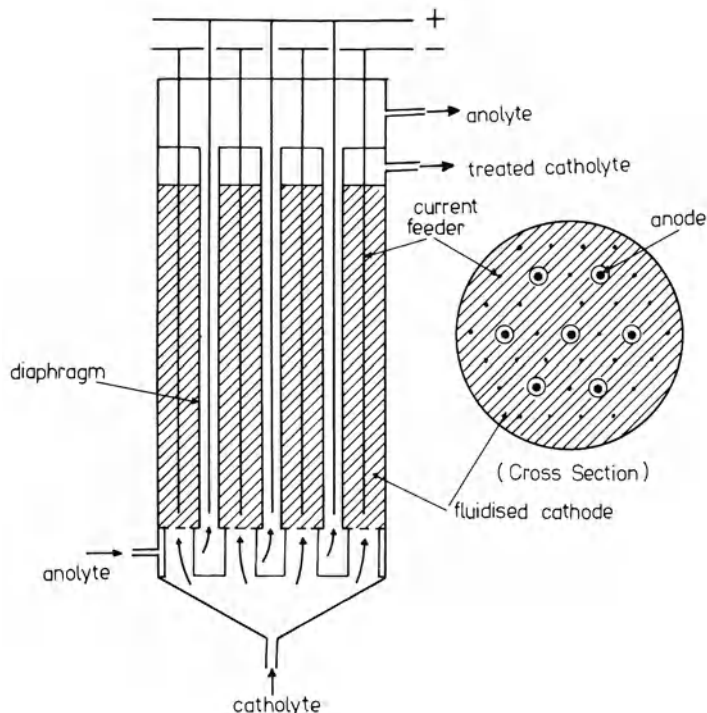


Figure 21. Diagrammatic arrangement of a fluidized-bed electrode cell for the removal of metals from effluent streams.

figures given in the respective publications for the removal of copper from an initial concentration of $800 \text{ mg liter}^{-1}$ to less than 1 mg liter^{-1} and choosing a flow rate $200 \text{ m}^3 \text{ h}^{-1}$ (quoted in reference 4 for the zinc stream), we arrive at a cell volume of $80\text{--}200 \text{ m}^3$ for the PFTE compared to $2\text{--}8 \text{ m}^3$ for the FBE. As Bennion and Newman⁽¹⁵⁾ have shown, capital costs are a major consideration in the removal of copper from an effluent stream, and the PFTE involves an additional dissolution step. It appears that in this type of application the FBE system described above has an advantage over the PFTE.

So far, it has been tacitly implied that diaphragms are always a necessity when using a FBE. It is possible, however, to avoid shorting a cathodic bed in the absence of a diaphragm by the choice of a suitable anode material. Thus with a lead dioxide anode it is possible, for example, to deposit copper from a molar sulfuric acid solution⁽⁶⁸⁾ at a cross-sectional current density of $10,000 \text{ A m}^{-2}$ at the surprisingly low cell voltage of 3.45 V. For a concentration change of 3.5 to 0.5 g liter^{-1} , current efficiencies ranged from 87% to 81%, respectively. The cell used had a rectangular geometry and an active feeder area of 0.01 m^2 .

Finally, one must ask to what extent models can aid in the design of industrial cells. It is hoped that the treatment so far has convinced the reader

that modeling can lead to a deeper understanding of the behavior of PFTEs and FBEs. Furthermore, it can be instructive to calculate actual electrode dimensions on the basis of some of the models discussed. For example, Wenger and Bennion⁽⁴⁵⁾ in the context of copper deposition from dilute solutions have calculated a maximum electrode thickness in the direction of current flow on the basis of avoiding hydrogen evolution in a PFTE. However, it is not possible at present to predict with confidence the performance of a large unit from that of a laboratory cell. Therefore, there is no substitute for investigating experimentally the performance of a full-sized module.

4. Bipolar Three-Dimensional Electrodes

The use of bipolar two-dimensional electrodes in industrial cells, particularly in those of a filter press-type construction, is now commonplace. Advantages of this arrangement, apart from lighter electrodes, in terms of minimization of expensive external bus-bars and the use of high-voltage, low-current power sources are considerable. Yet the development of bipolar three-dimensional electrodes is in a relatively early stage.

As already stated briefly in Section 1.2, an electrode is considered bipolar when each unit making up the three-dimensional electrode acts as a complete bipole. It follows that individual units have to be electronically isolated from their neighbors, either mechanically⁽⁶⁹⁾ or by fluidization.⁽⁷⁰⁾ Clearly this is only possible with particulate electrodes and hence the bipolar porous electrode modeled by Alkire⁽⁷¹⁾ does not fall within our definition.

Let us now discuss in some detail how an individual electron-conducting particle becomes a bipole. Consider such a unit immersed in an electrolyte. In the absence of any current flow [Figure 3(a)] the particle assumes a reversible potential (or alternatively a rest potential) ϕ_r with respect to the particular electrolyte given by

$$\phi_r = \phi_m - \phi_s \quad (75)$$

the subscripts m and s referring to the particle and electrolyte, respectively. For the sake of simplicity we assume $\phi_s = 0$. When current flows through the electrolyte [Figure 3(b)], a potential gradient will be set up in the liquid. Since the potential of the particle itself is still at rest and can be considered uniform, part of its surface will now exhibit an electrode potential such that $\phi_m - \phi_{s_1} < \phi_r$, i.e., cathodically polarized, while at its opposite end $\phi_m - \phi_{s_2} > \phi_r$, i.e., anodically polarized. If E^c and E^a are the minimum electrode potentials required for the respective cathodic and anodic reactions of the system, current will flow in and out of the particle when $-(\phi_m - \phi_{s_1}) \geq E^c$ and $\phi_m - \phi_{s_2} \geq E^a$. The amounts of faradaic current sustained by the particle and of nonfaradaic current (termed by-pass current) going through the electrolyte will depend on the relative resistances of the solid and liquid paths. In contrast to this

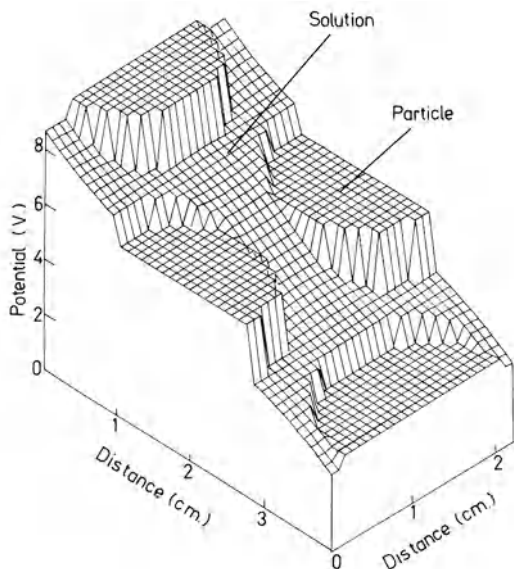


Figure 22. Computer-generated isometric projection of potential distribution for a two-dimensional array of bipolar cylinders.

bipolar particle, consider again the situation shown in Figure 3(c). Here the solid potential, ϕ_m , is strongly cathodic with respect to ϕ_r and hence $\phi_{s_1} - \phi_{s_2} \ll \phi$. The particle will therefore be monopolar.

Lloyd and coworkers⁽⁷²⁾ have demonstrated the essential soundness of the picture presented so far by probing potentials at intervals of 1 mm in a two-dimensional array of cylinders. Figure 22 shows a computer-generated isometric projection of some typical results. We can see that particles are equipotential, with faradaic activity at each end. It is also clear that by-pass current is flowing around the particles.

4.1. Mathematical Models

Relatively little work has been done on modeling bipolar particulate electrodes compared with the effort that has gone into their monopolar counterparts. Although, as we shall see later, scale-up of bipolar structures is easier than scale-up of monopolar ones, a rigorous solution in order to obtain potential and current distributions is extremely difficult. To illustrate this, consider an array of conducting cylinders, infinite in length, immersed in an electrolyte [Figure 23(a)]. Note that already we have simplified the attack by reducing the problem to a two-dimensional one. The system is enclosed in an insulated container, current entering and leaving uniformly at opposite sides as indicated. As a further simplification, assume that the threshold voltages, E^c and E^a , are numerically equal and hence the problem is reduced to determining potential and current distributions over the element $ABCD$. In order to remove any doubt about some of the boundary conditions

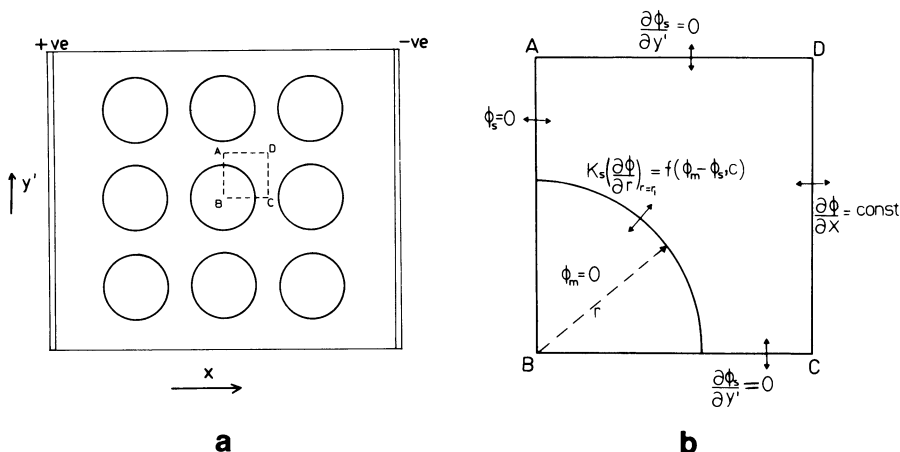


Figure 23. (a) Two-dimensional representation of an array of bipolar cylinders. (b) Boundary conditions for a single bipolar cylinder.

let us consider a single cylinder instead of the array in Figure 23(a). We still assume the solid to have a uniform potential, ϕ_m , which is arbitrarily taken as zero. The appropriate boundary conditions are indicated in Figure 23(b). At the particle surface the current leaves orthogonally and represents the rate of the faradaic process, i.e.,

$$K_s \frac{\partial \phi_s}{\partial r} = f(\phi_m - \phi_s, c) \tag{76}$$

An expression such as Eq. (32) or one of its simplified forms may be used for this boundary condition. Alternatively, an experimental polarization curve could be employed. Solution of the two-dimensional Laplace equation,

$$\frac{\partial^2 \phi}{\partial x^2} + \frac{\partial^2 \phi}{\partial y^2} = 0 \tag{77}$$

in conjunction with the boundary conditions mentioned, would give the potential and current distributions in the system.

The only approach along these lines has been made by Hartland and Spencer⁽⁷³⁾ who obtained an analytical solution of Eq. (77) for a single infinite cylinder of radius r . Their assumption, which made solution possible, was that the electrode potential over the active regions of the cylinder surface was constant, i.e.,

$$\phi^c = E^c \quad \text{and} \quad \phi^a = E^a \tag{78}$$

where c and a refer to the cathodic and anodic area, respectively. It is implied in the solution that the two potentials are numerically equal. Assumptions (78) are equivalent to saying that the polarization curve approximates that

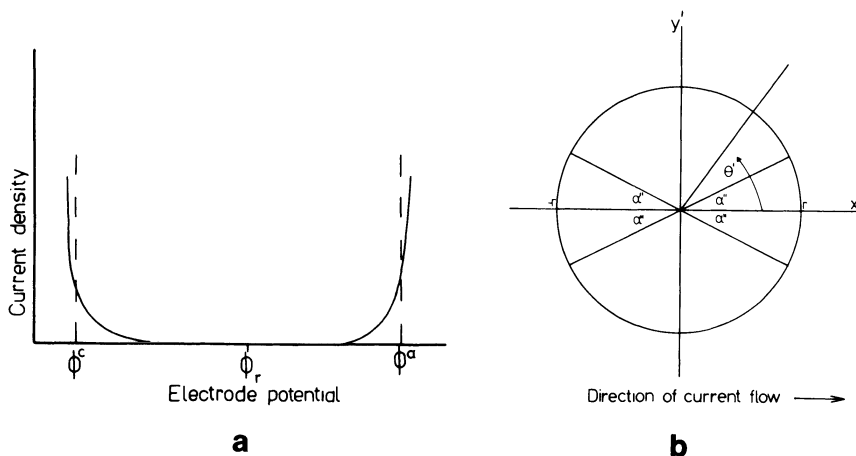


Figure 24. Polarization curve (a) and active area (b) for a bipolar cylinder of infinite length.

shown in Figure 24(a). It is further assumed that at large distances from the cylinder the potential drop through the electrolyte is V_0/r and the current density in the free electrolyte would therefore be $(K_s V_0)/r$. Looking at Figure 24(b), since the configuration is symmetrical about the x and y axis, current flows into the cylinder over the part for which $\pi - \alpha'' < \theta' < \pi + \alpha''$ and out of it for $-\alpha'' < \theta' < \alpha''$, there being no flow over the remainder of the surface. The authors derive an expression for j , the current density for flow out of the cylinder ($-\alpha'' < \theta' < \alpha''$), as

$$j = \frac{-2K_s V_0}{r} (\sin^2 \alpha'' - \sin^2 \theta')^{1/2} \quad (79)$$

and hence the total current I through the cylinder per unit length in the z direction is

$$I = -2r \int_0^{\alpha''} j d\theta' = 4K_s V_0 \int_0^{\alpha''} (\sin^2 \alpha'' - \sin^2 \theta')^{1/2} d\theta' \quad (80)$$

In Figure 25(a), $I/2K_s V_0$ is shown as a function of α'' and $2V_0/(E^a - E^c)$. As we increase the potential gradient through the electrolyte for a given threshold voltage, the current through the solid increases rapidly. This is in accordance with experimental observations discussed later. It is also of interest to consider the situation just before current flow occurs, i.e., $I = 0$. From Figure 25(a) we find that for $I = 0$,

$$2V_0/(E^a - E^c) = 0.5 \quad (81)$$

i.e., $E^a - E^c = 4V_0$. Since current will only start flowing through the solid once this condition is met, it follows that the potential drop in the electrolyte across the cylinder must be twice that in the electrolyte well removed from

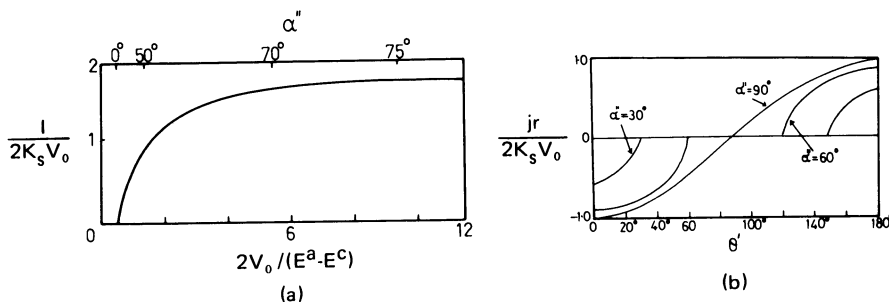


Figure 25. Calculated current distribution on a bipolar cylinder of infinite length.

it. A very simple experiment using conductivity paper in which a circular hole has been cut proves this finding to be correct. Another of their important plots is that of the current density j as a function of θ' , for different values of α'' , shown in Figure 25(b).

A relatively simple model first proposed by Fleischmann and coworkers⁽⁷⁴⁾ relates the active area of a bipolar particle to the applied voltage gradient and some reaction and cell parameters. Essentially this is a model applicable to an array of closely packed solids and was first used to predict the behavior of an intimate mixture of conducting and nonconducting beads. Here the simplifying assumption made was that the reaction was mass-transfer-controlled and hence current density was constant over the active area. Goodridge and coworkers⁽⁶⁹⁾ applied the model to a packed bed of conducting cylinders (Figure 26) and it is this treatment that will be discussed here. An interesting point that should be mentioned is that under conditions where the reaction was not mass-transfer-controlled, experiments using a sectioned cylinder⁽⁶⁹⁾ showed a relatively uniform current distribution over the active particle area.

Consider now a cylinder of radius r and length l as shown in Figure 27. If a voltage gradient V' is applied to the cell, then, just as in the previous model, at a threshold voltage V_t (note that $V_t = E^a - E^c$) the cylinder begins

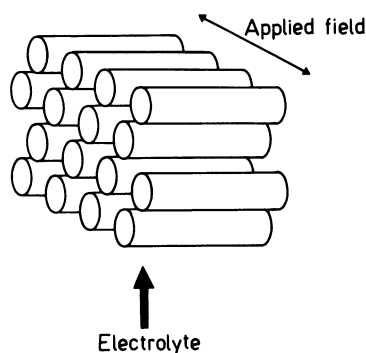


Figure 26. Diagrammatic representation of a bipolar fixed bed of conducting cylinders isolated from each other by nonconducting spacers (not shown).

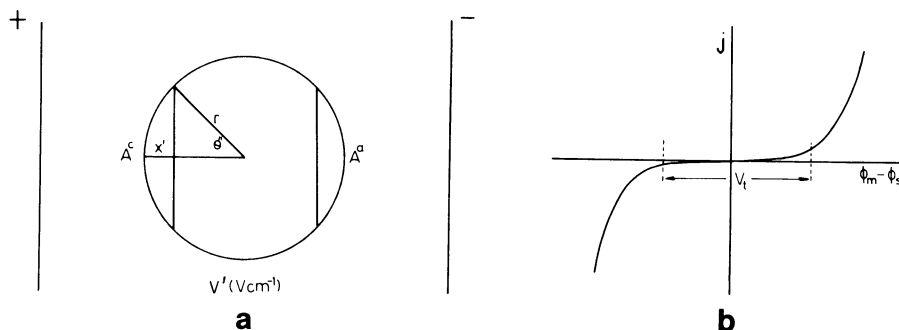


Figure 27. Active area (a) and threshold voltage (b) for a reaction on a bipolar particle.

to function as a bipolar electrode. The active area A , where it is assumed that $A = A^c = A^a$, is given by

$$A = 2rl\theta'' = 2rl \cos^{-1} (1 - x'/r) \quad (82)$$

Since from Figure 27

$$x' = r - V_i/2V' \quad (83)$$

we have

$$A = 2rl \cos^{-1} (V_i/2rV') \quad (84)$$

N , the number of cylinders per unit volume of cell, is given by

$$N = (1 - \varepsilon)/\pi r^2 l \quad (85)$$

and therefore S , the active area per unit volume of cell, will be

$$S = NA = \frac{2(1 - \varepsilon)}{\pi r} \cos^{-1} (V_i/2rV') \quad (86)$$

In order to achieve the same performance by means of planar bipolar cells, we would need S of them per unit length, each having an equivalent cell voltage, V_c , given by

$$V_c = V'/S = \pi r V' / [2(1 - \varepsilon) \cos^{-1} (V_i/2rV')] \quad (87)$$

For an n electron change and 100% current efficiency, E_c , the energy required to produce 1 kmol of product at a cell voltage V_c is given by

$$E_c = 14nV_c = 14n\pi r V' / [(1 - \varepsilon) \cos^{-1} (V_i/2rV')] \quad (88)$$

Differentiating (88) with respect to V' and equating the result to zero gives the voltage gradient V'_{\min} for which E_c is a minimum:

$$V'_{\min} = 0.77 V_i/r \quad (89)$$

and hence $E_{c,\min}$ from Eq. (88) is

$$E_{c,\min} = 39nV_i/(1 - \varepsilon) \quad (90)$$

These simple equations were tested⁽⁶⁹⁾ using bromine generation as the reaction. The plot of energy consumption, E_c , against the applied field, V' , (see Figure 29) gave the shape predicted by Eq. (88) but experimental values of E_c were consistently higher than the calculated ones, since the model does not take into account any by-pass currents. Equation (89) was obeyed by the experimental results, values for the calculated and experimental slopes being surprisingly close. On the whole, the model seems to predict the behavior of the bipolar system better than one would anticipate from the relative crudeness of the assumptions.

As has been indicated, Eqs. (82)–(90) assume that all the current passes through the array of cylinders. In practice, it has been found that for a given electrode material, cell geometry, and electrolyte composition, the fraction of nonfaradaic current is a function of applied voltage. In order to be able to calculate the relative amounts of faradaic and nonfaradaic current from potential measurements King and Wright⁽⁷⁵⁾ have developed a simple resistance analogue. This has been applied most extensively to a form of falling film cell in the shape of electrolyte flowing down a vertical series of rods,⁽⁷⁶⁾ the test reaction being again the generation of bromine from an aqueous solution of sodium bromide. Figure 28 demonstrates the good agreement between direct measurement and calculated values. It is also interesting to

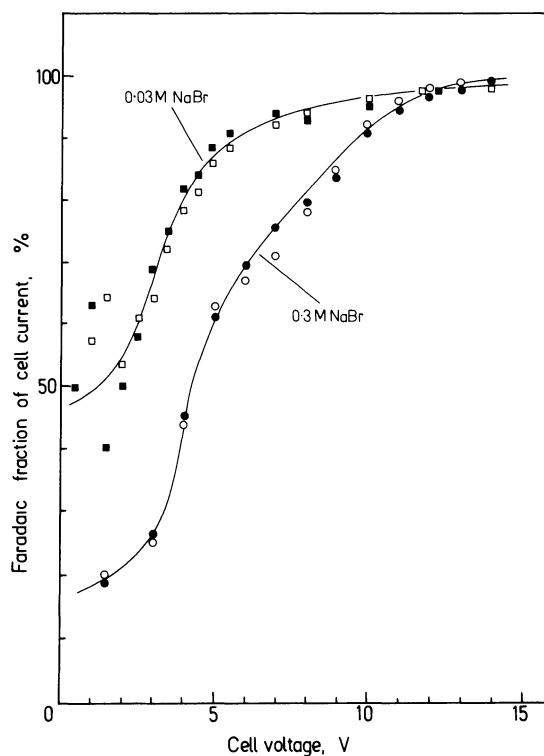


Figure 28. Faradaic current on a falling film cell: \square , \circ , calculated; \blacksquare , \bullet , experimental.

note that, as implied in the plot of total current against applied voltage [Figure 25(a)] based on the model by Hartland and Spencer,⁷³ by-pass current falls off quickly with applied voltage. Another important finding demonstrated by Figure 28 is that at high current densities the fraction of by-pass current becomes independent of the concentration of sodium bromide, since the faradaic resistance decreases rapidly with an increase in current density. It follows that, provided conditions are chosen correctly, these bipolar particulate electrodes are not restricted to poorly conducting solutions.

Finally, Eardly and coworkers⁽⁷⁷⁾ use a semiempirical network made up of combined faradaic and nonfaradaic resistances which are derived from experimental results with an array of stacked copper cylinders⁽⁷⁷⁾ and a fluidized bed of copper particles.⁽⁷⁸⁾ It is claimed that this technique permits the calculation of conductivities and currents under a wide range of conditions.

4.2. Experimental Aspects

Since bipolar three-dimensional electrodes require that the individual particles are isolated from one another, it follows that they can only fall into classes (ii)–(iv) (see Section 1.2), namely, particulate electrodes, and that class (i) is excluded. It is expected that, in these particulate electrodes, current passes consecutively through the particles and the intervening electrolyte. Any current which by-passes the particles represents an energy loss and careful consideration must therefore be given to minimize this effect by a combination of lowering the voidage of the bed, reducing the faradaic resistance of the electrode process (high current density and reactant concentration), and decreasing the conductivity of the electrolyte. However, the energy consumption passes, as predicted by Eq. (88), through a minimum with an increase in the applied voltage. In order to achieve a required space-time yield there comes a point, therefore, when it will be more advantageous to decrease particle size rather than increase the applied field.

There are other characteristics of bipolar particulate electrodes which should be noted. Firstly, by their very nature they can only exist in an undivided cell and hence reactions where intimate mixing of anolyte and catholyte is deleterious to the required product are unsuitable for these systems. Secondly, electrode potential can presumably be nonuniform over a single active area even though some experimental evidence⁽⁶⁹⁾ for uniform activity has been found in a particular system. Thirdly, they present the practical difficulty of requiring an electrode material that is equally suitable for both anodic and cathodic conditions.

4.2.1. Fixed-Bed Electrodes

Early work on these systems was done using mixtures of conducting and nonconducting beads.^(74,79) The difficulty of obtaining mixtures of uniform

composition together with the disadvantage of relatively low active areas due to the presence of nonconducting beads resulted in unsatisfactory performance figures. Much improved results were obtained with a system of packed graphite rods, isolated from each other by thin O rings (Figure 26). This system has been used for a number of reactions such as the production of bromine and the epoxidation of styrene,⁽⁶⁹⁾ when for large rod diameters energy consumptions of about 250 kWh kmol⁻¹ were observed. Rods isolated from each other by positive location in two parallel polypropylene plates have been employed by the authors in a small pilot plant at elevated pressures up to 6 atm, for the epoxidation of propylene to propylene oxide. Typical energy consumptions for bromine generation in this pilot plant are shown in Figure 29. It is interesting to note that the model still holds on scale-up.

Electrodes described so far have been operating under what might be termed flooded conditions. The design mentioned next consists of stacked layers of conducting particles, e.g., graphite Raschig rings,⁽⁸⁰⁾ adjacent layers being isolated from one another by the insertion of thin porous insulating sheets. Electrolyte runs down the packing in a thin film. An advantage of this arrangement is its ability to act simultaneously as a gas absorption tower when dealing with a gaseous reactant, as in the production of propylene oxide. Reported energy consumption for this reaction, using a laboratory-sized cell,

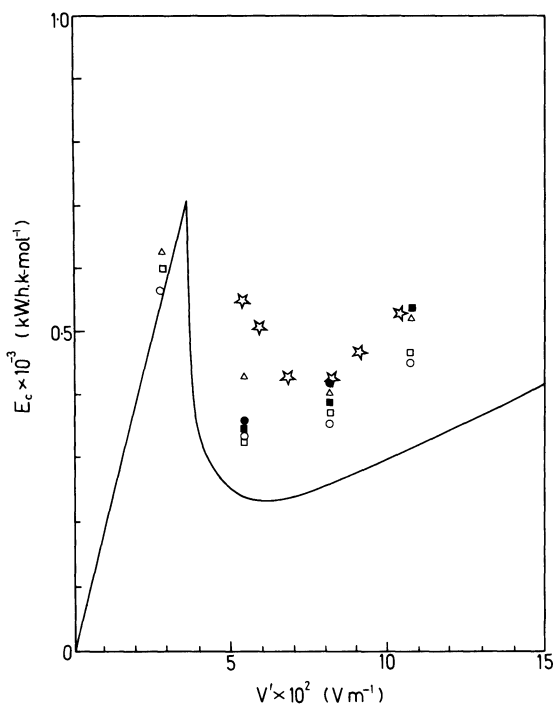


Figure 29. Calculated and experimental energy consumptions for bipolar fixed-bed electrodes with varying bromide concentrations: —, calculated; ●, 10⁻² M, ■, 5 × 10⁻² M; ○, 10⁻¹ M; △, 2 × 10⁻¹ M; □, 5 × 10⁻¹ M; ☆, 10⁻¹ M (pilot plant).

is about the same as for the packed rod cell, namely, 220 kWh kmol⁻¹. The methoxylation of *N*-acetyl- α -alanine in methyl alcohol has been described by Mitzlaff⁽⁸¹⁾ in a cell identical in concept with the falling film cell described previously. An interesting comparison arises between results obtained by Mitzlaff with a cell having concentric two-dimensional electrodes and those from his falling film cell. As pointed out by Gallone⁽⁸²⁾ space-time yields of the three-dimensional electrode are two orders of magnitude higher than those of the two-dimensional one.

4.2.2. Fluidized-Bed Electrodes

Cells discussed so far have used mechanical means of separating the bipolar particles. A different approach is to fluidize the bed. This is a recent development⁽⁷⁰⁾ and the system offers some novel properties. Apart from its great simplicity, the particles due to their rotation undergo automatic reversal of polarity which can result in a self-cleaning action. Additionally, the electrode can conveniently be scaled-up with particles of a smaller size than would be practicable for a fixed bed; it being capable therefore of higher space-time yields. On the debit side, energy consumption would normally be higher than for the fixed-bed system, in part due to a significantly greater proportion of by-pass current, unless expansion is very low.

Reactions studied so far with this electrode⁽⁷⁰⁾ are the production of hypobromite, the electrolysis of seawater, and the formation of dimethyl sebacate. For hypohalite production, the FBE compares particularly poorly with the fixed-bed system, since apart from the increased by-pass currents emphasized by high expansions, back-reduction of the hypobromite occurs due to the particle rotation. It is interesting to note in this context that for the highly irreversible Kolbé reaction the FBE performs slightly better than the falling film cell⁽⁷⁶⁾ mentioned in Section 4.1.

4.3. Industrial Aspects

A considerable advantage that bipolar particulate electrodes have over monopolar ones is the fact that scale-up in the direction of current flow is not limited. This will result in cells of far simpler construction than monopolar ones. We have already seen in Section 4.2 that in terms of space-time yields, particulate bipolar electrodes compare very favorably with two-dimensional ones.

Yet from an industrial point of view, bipolar particulate electrodes are in a very early stage of development. One of the few known applications is that by Resource Control Inc.^(88,84) for effluent treatment. The bed consists of low-conductivity carbonaceous pellets which can be agitated by a flow of air to prevent agglomeration.

Auxiliary Notation

Units are based on the SI system. If different units are used in the text, these have been specified.

a	electrode area per unit volume of electrode (m^{-1})	E_c	energy consumption ($kWh\ kmol^{-1}$)
a'	factor in Eq. (12) (m)	$E_{c,min}$	minimum energy consumption ($kWh\ kmol^{-1}$)
a''	factor in Eq. (7) (m)	F	faraday (C g-equiv. ⁻¹)
a_0	factor in Eq. (13) (m^{-1})	F'	drag force (N)
b'	factor in Eq. (12) (m^2)	F_E	drag force in electrode (N)
b''	factor in Eq. (8) (m^2)	F_F	drag force exerted by the electrode on the fluid (N)
b_0	factor in Eq. (13) (dimensionless)	F_f	form drag (N)
c_A, c_B	concentration of A and B, respectively ($kmol\ m^{-3}$)	$F_{p}, F_{p'}$	drag defined by Figure 5(b) (N)
c_0	concentration for which j_0 is defined ($kmol\ m^{-3}$)	F_v	viscous drag (N)
d	diameter of pipe or characteristic length of particle (m)	H	concentration entrance region (m)
h	bed height (m)	I	current (A)
h'	length of channel (m)	R	universal gas constant ($J/kmol^{-1}\ K^{-1}$)
h''	hydrodynamic entrance region (m)	S_0	surface area per unit volume of solid (m^{-1})
h_0	initial bed height (m)	α	transfer coefficient (dimensionless)
j	current density (Am^{-2})	α'	ak_d/v (m^{-1})
j_d	current density = j_m/j (dimensionless)	α''	angle defining active area on bipolar particle in Figure 25 (rad)
j_0	exchange current density (Am^{-2})	β	factor in Eq. (37) (V^{-1})
k_d	mass transfer coefficient (ms^{-1})	β'	factor in Eq. (15) (dimensionless)
l	length of cylinder (m)	γ	defined by Eq. (60) (dimensionless)
n	number of electrons per molecule (molecule ⁻¹)	δ	defined by Eq. (41) (dimensionless)
n'	number of particles making up electrode structure (dimensionless)	ϵ	voidage (dimensionless)
r	radius (m)	ϵ'	defined by Eq. (42) (dimensionless)
Δr	radius of annulus (m)	ϵ_M	voidage at incipient fluidization (dimensionless)
t_c	contact time during particle collision (s)	ζ	defined by Eq. (74) (dimensionless)
v_M	minimum fluidization velocity (ms^{-1})	η	viscosity (Nsm^{-2})
v_t	entrainment velocity (ms^{-1})	θ	defined by Eq. (46) (dimensionless)
x	distance in the direction of current flow (m)	θ'	angle defining area on a bipolar particle in Figure 25 (rad)
x'	distance defined in Figure 27 (m)	θ''	angle defining area on a bipolar particle in Figure 27 (rad)
y	distance in the direction of current flow = x/L (dimensionless)	λ	defined by Eq. (59) (dimensionless)
y'	dimension (m)	ν	defined by Eq. (50) (dimensionless)
A	active bipolar area (m^2)	ν'	collision frequency (Hz)
A_s	projected area of sphere (m^2)	ρ	density ($kg\ m^{-3}$)
C_D	drag coefficient (dimensionless)	τ	time constant for charge sharing during collision between two particles (s)
C_d	double layer capacity ($F\ m^{-2}$)	ψ	defined by Eq. (47) (dimensionless)
C_E	current efficiency (dimensionless)	ψ_1	shape factor (dimensionless)
D_B	molecular diffusivity ($m^2\ s^{-1}$)	ϕ	electrode potential (V)
E, ϕ	electrode potential	ϕ^0	reference potential (V)

ϕ_m, ϕ_s	potential (V)	Sc	Schmidt number = $\frac{n}{\rho_s D_B}$
ϕ_r	rest potential (V)		(dimensionless)
K_m	effective conductivity of solid phase ($\Omega - m^{-1}$)	V'	voltage gradient ($V m^{-1}$)
K_s	effective conductivity of electrolyte ($\Omega - m^{-1}$)	V^c	cell voltage (V)
L	length or depth of three-dimensional electrode in the direction of current flow (m)	V'_{min}	voltage gradient for minimum energy consumption ($V m^{-1}$)
L_{eff}	effective bed height (m)	V_c	voltage defined by Eq. (87) (V)
N	Number of cylinders per unit volume of bipolar cell (m^{-3})	V_0	applied voltage (V)
ΔP	pressure loss ($N m^{-2}$)	V_t	threshold voltage = $E^a - E^c$ (V)
ΔP_M	pressure loss at minimum fluidization ($N m^{-2}$)	Y_C	chemical yield (dimensionless)
Q_E	electrochemical equivalent ($kmol C^{-1}$)	Y_E	energy yield ($kmol kWh^{-1}$)
R'	factor in Eq. (11) (dimensionless)	Y_{ST}	space-time yield ($kmol m^{-3} s^{-1}$)
Re	Reynolds number based on pipe diameter (dimensionless)	<i>Superscripts</i>	
Re _p	Reynolds number based on particle dimension (dimensionless)	a	anode
S	active area per unit volume of bipolar cell (m^{-1})	c	cathode
		<i>Subscripts</i>	
		m	solid phase
		s	solution phase

References

1. F. Goodridge and C. J. H. King, In: *Technique of Electroorganic Synthesis*, N. L. Weinberg, Ed., Part I, Chap. 2, pp. 123–127, Wiley, New York (1974).
2. D. G. Braithwaite, U.S. Patents 3,007,857; 3,256,161; 3,287,248 (Nalco Chem. Co.).
3. L. L. Bott, U.S. Patent 3,479,274 (Nalco Chem. Co.).
4. C. M. S. Raats, H. F. Boon, and G. van der Heiden, Fluidized bed electrolysis for the removal or recovery of metals from dilute solutions. International Symposium on Chloride Hydrometallurgy, Brussels, 26–28 September (1977).
5. R. N. Olson, *Essentials of Engineering Fluid Mechanics*, pp. 280–287, Intertext Books, London (1966).
6. C. Orr Jr., *Particulate Technology*, pp. 192–197, MacMillan, New York (1966).
7. (a) J. M. Coulson and J. F. Richardson, *Chemical Engineering*, Vol. I, p. 52, Pergamon Press Ltd., London (1977). (b) *ibid.*, Vol. II, p. 129 (1978).
8. M. Leva, *Fluidization*, p. 52, McGraw Hill, New York (1959).
9. B. G. Ateya and L. G. Austin, Steady-state polarization at PFTE with small pore diameter I. Reversible kinetics, *J. Electrochem. Soc.* **124**, 83–89 (1977).
10. F. Goodridge, D. I. Holden, H. D. Murray, and R. E. Plimley, FBES. II. Nonuniform behavior of the hydrodynamic entrance region, *Trans. Inst. Chem. Eng.* **49**, 137–141 (1971).
11. R. E. Treyball, *Mass Transfer Operations*, McGraw-Hill, New York (1968).
12. R. B. Bird, W. E. Stewart, and E. N. Lightfoot, *Transport Phenomena*, Wiley, New York (1960).
13. T. K. Sherwood, R. L. Pigford, and C. R. Wilke, pp. 159–171, *Mass Transfer*, McGraw-Hill, New York (1975).

14. A. A. Wragg, Application of the limiting diffusion current technique in chemical engineering, *The Chem. Eng.* 39–44, 49 (1977).
15. D. N. Bennion and J. Newman, Electrochemical removal of copper ions from very dilute solutions, *J. Appl. Electrochem.* **2**, 113–122 (1972).
16. Reference 12, pp. 411 and 679.
17. T. Miyauchi and T. Nomura, Liquid-film mass-transfer coefficient for packed beds in the low Reynolds number region, *Int. Chem. Eng.* **12**, 360–366 (1972).
18. A. J. Karabelas, T. H. Wegner, and T. J. Hanratty, Use of asymptotic relations to correlate mass transfer rates in packed beds, *Chem. Eng. Sci.* **26**, 1581–1589 (1971).
19. K. R. Jolls and T. J. Hanratty, Use of electrochemical techniques to study mass transfer rates and local skin friction to a sphere in a dumped bed, *AIChE J.* **15**, 199–205 (1969).
20. W. J. Beek, In: *Fluidisation*, J. F. Davidson and D. Harrison, Eds., Chap. 9, pp. 431–470, Academic Press, London (1971).
21. A. Storck, F. Vergnes, and P. Le Goff, Transfert de matière entre un électrolyte et une paroi cylindrique immergée dans un lit fixe ou fluidisé de grains isolants, *Powder Technol.* **12**, 215–223 (1975).
22. F. Goodridge and D. V. Nassif, unpublished work.
23. D. J. Pickett, *Electrochemical Reactor Design*, p. 162, Elsevier, Oxford (1977).
24. C. Wagner, Theoretical analysis of the current density distribution in electrolytic cells, *J. Electrochem. Soc.* **98**, 116–128 (1951).
25. E. A. Grens II, On the assumptions underlying theoretical models for flooded porous electrodes, *Electrochim. Acta* **15**, 1047–1057 (1970).
26. J. Newman and W. Tiedemann, Porous-electrode theory with battery applications, *AIChE J.* **21**, 25–41 (1975).
27. J. S. Newman and C. W. Tobias, Theoretical analysis of current distribution in porous electrodes, *J. Electrochem. Soc.* **109**, 1183–1191 (1962). (a) J. Euler and W. Nonnemacher, Stromverteilung in Porösen Elektroden, *Electrochim. Acta* **2**, 268–286 (1960).
28. M. Paulin, D. Hutin, and F. Coeuret, Theoretical and experimental study of flow-through porous electrodes, *J. Electrochem. Soc.* **124**, 180–188 (1977).
29. G. Kreysa and E. Heitz, Reaktions- und verfahrenstechnische Aspekte elektrochemischer Fest- und Wirbelbett-Zellen, *Chem.-Ing.-Tech.* **48**, 852–860 (1976).
30. G. Kreysa and E. Heitz, The similarity law of effective height of packed bed electrodes, *Electrochim. Acta* **20**, 919–921 (1975).
31. M. Fleischmann and J. W. Oldfield, FBEs. I. Polarization predicted by simplified models, *J. Electroanal. Chem.* **29**, 211–230 (1971).
32. F. Goodridge, D. I. Holden, H. D. Murray, and R. E. Plimley, FBE. I. A mathematical model of the FBE, *Trans. Inst. Chem. Eng.* **49**, 128–136 (1971).
33. R. Alkire and P. K. Ng, Two-dimensional current distribution within a packed-bed electrochemical flow reactor, *J. Electrochem. Soc.* **121**, 95–103 (1974).
34. R. Alkire and B. Gracon, Flow-through porous electrodes, *J. Electrochem. Soc.* **122**, 1594–1601 (1975).
35. R. E. Sioda, The ECE mechanism in flow electrolysis in porous electrodes under conditions of limiting current, *Electrochim. Acta* **20**, 457–461 (1975).
36. A. K. P. Chu, M. Fleischmann, and G. J. Hills, Packed-bed electrodes. I. The electrochemical extraction of copper ions from dilute aqueous solutions, *J. Appl. Electrochem.* **4**, 323–330 (1974).
37. R. Alkire and P. K. Ng, Studies on flow-by porous electrodes having perpendicular directions of current and electrolyte flow, *J. Electrochem. Soc.* **124**, 1220–1227 (1977).
38. F. Goodridge and B. M. Ismail, The anodic behavior of packed and fluidised bed electrodes, *Inst. Chem. Eng. Symp. Ser.* **37**, 1.29–1.52 (1971).
39. R. E. Sioda, Current–potential dependence in the flow electrolysis on a porous electrode, *J. Electroanal. Chem.* **34**, 399–409 (1972).

40. R. Alkire and R. Gould, Analysis of multiple reaction sequences in flow-through porous electrodes, *J. Electrochem. Soc.* **123**, 1842–1849 (1976).
41. J. A. Trainham and J. Newman, A flow-through porous electrode model: Application to metal-ion removal from dilute streams, *J. Electrochem. Soc.* **124**, 1528–1540 (1977).
42. B. G. Ateya and L. G. Austin, Steady-state polarization at PFTE with small pore diameter. II. Irreversible kinetics for one-electron and consecutive two-electron transfer reactions, *J. Electrochem. Soc.* **124**, 1540–1548 (1977).
43. P. J. Ayre and F. Goodridge, unpublished work.
44. S. Germain and F. Goodridge, Copper deposition in a fluidized bed cell, *Electrochim. Acta* **21**, 545–550 (1976).
45. R. S. Wenger and D. N. Bennion, Electrochemical concentrating and purifying from dilute copper solutions, *J. Appl. Electrochem.* **6**, 385–396 (1976).
46. W. Tiedemann and J. Newman, Double-layer capacity determination of porous electrodes, *J. Electrochem. Soc.* **122**, 70–74 (1975).
47. T. Katan and H. F. Bauman, Relating structural variables of porous electrodes, *J. Electrochem. Soc.* **122**, 77–80 (1975).
48. R. E. Meredith and C. W. Tobias, In: *Advances in Electrochemistry and Electrochemical Engineering*, C. W. Tobias, Ed., Vol. 2, pp. 15–47 (1962).
49. M. Fleischmann and J. W. Oldfield, FBEs. II. The effective resistivity of the discontinuous metal phase, *J. Electroanal. Chem.* **29**, 231–240 (1971).
50. A. A. C. M. Beenackers, W. P. M. van Swaaij, and A. Welmers, Mechanism of charge transfer in the discontinuous metal phase of a FBE, *Electrochim. Acta* **22**, 1277–1281 (1977).
51. M. Fleischmann and G. H. Kelsall, An investigation of the local behaviour of a copper FBE, *Chem. and Ind.*, 329–330 (1975).
52. R. E. Plimey and A. R. Wright, unpublished work.
53. Reference 1, pp. 135–137.
54. L. L. Bott, How Nalco makes lead alkyls, *Hydrocarbon Process. Petrol. Refiner* **44**, 115–118 (1965).
55. R. W. Houghton and A. T. Kuhn, Antimony removal from dilute solutions using a restrained bed electrochemical reactor, *J. Appl. Electrochem.* **4**, 69–73 (1974).
56. J. A. Trainham and J. Newman, A thermodynamic estimation of the minimum concentration attainable in a flow-through porous electrode reactor, *J. Appl. Electrochem.* **7**, 287–297 (1977).
57. G. A. Carlson, U.S. Patent 3,647,653 (PPG Industries).
58. J. R. Backhurst, J. M. Coulson, F. Goodridge, R. E. Plimley, and M. Fleischmann, Preliminary investigation of FBE, *J. Electrochem. Soc.* **116**, 1600–1607 (1969).
59. J. R. Backhurst, F. Goodridge, R. E. Plimley, and M. Fleischmann, Some aspects of a fluidized Zn/oxygen electrode system, *Nature* **211**, 55–57 (1969).
60. D. S. Flett, The electrowinning of copper from dilute copper sulfate solutions with a FBE, *Chem. and Ind.* 300–302 (1971).
61. D. S. Flett, The FBE in extractive metallurgy, *Chem. and Ind.* 983–988 (1972).
62. M. Fleischmann, J. W. Oldfield, and L. Tennakoon, FBEs. IV. Electrodeposition of copper in a fluidised bed of copper-coated spheres, *J. Appl. Electrochem.* **1**, 103–112 (1971).
63. B. Surfleet and V. A. Crowle, Quantitative recovery of metals from dilute copper sulphate solutions, *Trans. Inst. Met. Finish* **50**, 227–232 (1972).
64. J. A. E. Wilkinson and K. P. Haines, Feasibility study on the electrowinning of copper with FBEs, *Trans. Inst. Min. Met.* **81**, C157–162 (1972).
65. F. Goodridge and C. J. Vance, Copper deposition in a pilot-plant-scale fluidized-bed cell, *Electrochim. Acta* **24**, 1237–1242 (1979).
66. F. Goodridge and C. J. Vance, The electrowinning of zinc using a circulating bed electrode, *Electrochim. Acta* **22**, 1073–1076 (1977).
67. F. Goodridge and K. Scott, unpublished work.

68. M. Fleischmann, F. Goodridge, and C. J. Vance, Patent Application 41622/75.
69. F. Goodridge, C. J. H. King, and A. R. Wright, The behavior of bipolar packed-bed electrodes, *Electrochim. Acta* **22**, 347–352 (1977).
70. F. Goodridge, C. J. H. King, and A. R. Wright, Performance studies on a bipolar FBE, *Electrochim. Acta* **22**, 1087–1091 (1977).
71. R. Alkire, A theoretical study of bipolar porous electrodes, *J. Electrochem. Soc.* **120**, 900–905 (1973).
72. J. L. Lloyd, C. J. H. King, and A. R. Wright, unpublished work.
73. S. Hartland and A. J. M. Spencer, Electrolytic dissolution in a potential gradient, *Trans. Inst. Chem. Eng.* **41**, 328–335 (1963).
74. M. Fleischmann, J. W. Oldfield, and C. L. K. Tennakoon, The electrochemical bipolar particulate cell, *Inst. Chem. Eng. Symp. Ser.* **37**, 1.53–1.69 (1971).
75. C. J. H. King and A. R. Wright, Current distribution in a thin film bipolar electrode system, *Electrochim. Acta* **22**, 1135–1139 (1977).
76. C. J. H. King, K. Lister, and R. E. Plimley, A novel bipolar electrolytic flow cell for synthesis, *Trans. Inst. Chem. Eng.* **53**, 20–25 (1975).
77. D. C. Eardly, D. Handley, and S. P. S. Andrew, Bipolar electrolysis with intraphase conduction in two phase media, *Electrochim. Acta* **18**, 839–848 (1973).
78. D. Handley and D. C. Eardly, Bipolar electrolysis with intraphase conduction in fluidized beds, *Chem. and Ind.* 330–332 (1975).
79. O. B. Osifade, The production of propylene oxide by an electrochemical method using a bipolar packed bed cell, Ph.D. thesis, University of Newcastle upon Tyne, England (1972).
80. A. V. Bousoulengas, Bipolar trickle-bed reactors, Ph.D. thesis, University of Southampton, England (1976).
81. M. Mitzlaff, DOS 23 37 016. (Farbwerke Hoechst AG.).
82. P. Gallone, Achievements and tasks of electrochemical engineering, *Electrochim. Acta* **22**, 913–920 (1977).
83. J. H. Shockor, U.S. Patent 3,692,661 (Resource Control Inc.).
84. Anonymous, Electrolysis speeds up waste treatment, *Environ. Sci. Technol.* **4**, 201 (1970).

7

Gas-Evolving Electrodes

HELMUT VOGT

In a large number of relevant industrial processes, gases are generated by electrochemical reactions. Processes linked to the evolution of gas exhibit some characteristics which are not typical of electrode processes in general. Gas bubbles develop at bubble nuclei, grow in size, finally break off, and rise in the liquid, thus providing a locally nonsteady-state condition. A detailed knowledge of the events at gas-evolving electrodes is necessary for a quantitative treatment of mass transfer and, closely connected with it, of heat transfer. On the other hand, charge transport within bubble-filled electrolytes is of considerable practical interest. These three aspects form the main subject matter of this chapter.

1. Characterization of Gas-Evolving Electrodes

The mode of action of gas-evolving electrodes is twofold: First, the electrode acts as an instrument by which, as a consequence of an electrochemical reaction, a substance is generated which appears to be dissolved in the adjacent liquid. In this respect, the gas-evolving electrode does not differ from other electrodes, the product of which occurs in dissolved form in the electrolyte. Second, the electrode acts as an instrument that by a physical process liberates the dissolved substance from the liquid with formation of a

gaseous phase. In this respect, the electrode does not differ from other solid surfaces which evolve gas as a consequence of further supersaturation of the liquid with gas due to a decrease of pressure or to an increase of temperature.

The combined action of both functions characterizes the gas-evolving electrode. Both functions, the electrochemical and the physical one, are quantitatively interconnected in the overall steady-state condition, if some prerequisites are satisfied, such as:

1. Consecutive homogeneous reactions (or heterogeneous reactions inside the electrolyte) do not occur.
2. Gas does not diffuse through and is not absorbed by the electrode material, as may occur in considerable amounts with hydrogen at various materials, such as palladium or tantalum.^(1,2)
3. Gas is not evolved at other solid surfaces apart from the electrode.

2. Regimes in Gas Evolution

Whether or not the substance generated at the electrode is transferred into the gaseous phase depends on the controlling conditions. If the current density of the gas-generating reaction is very low, the dissolved gas is removed from the electrode in the direction of liquid bulk by molecular diffusion and usually by superposed liquid convection without any formation of a gas phase. This occurs even at higher current densities if the dissolved gas tends to react homogeneously and quickly enough, as chlorine in electrochemical chlorate synthesis, for example.^(3,4) Such conditions do not prevail at gas-evolving electrodes and will not be mentioned again.

If the current density is sufficiently high, gas bubbles form at predestined nucleation sites located at the electrode surface. The prerequisite is a sufficient supersaturation of the liquid adjacent to the electrode, only occurring (in steady state) at current densities that are not too low. The bubble adhering to the surface grows subsequently by supply of dissolved gas from the surrounding liquid. The bubble departs and rises when it finally reaches a size at which the buoyancy forces together with shear forces caused by a moving liquid exceed the adhesion forces resulting from the interfacial tension. After a waiting time, a consecutive bubble forms at the same nucleation site. Mass and heat transfer increase with the current density, although the bubbles cover an increasing part of the electrode surface. These phenomena are typical of nucleate gas evolution.

A further increase of the current density results in a higher supersaturation. As a consequence, additional nucleation sites are activated, and the number of simultaneously adhering bubbles increases. The bubbles interact and finally touch each other to cover the whole electrode surface, forming an

unstable gas film which incessantly collapses and reforms. Under certain conditions, the gas film transforms into a stable one. This is the regime of film gas evolution and the reason for the anode effect, a phenomenon well known in alumina electrolysis.⁽⁵⁻⁷⁾

3. Analogy with Boiling

It has been stated repeatedly that the processes at gas-evolving electrodes are analogous to boiling.⁽⁸⁾ Vapor bubbles are formed out of sufficiently superheated liquids at nucleation sites on heated surfaces and grow by thermal conduction from the surrounding liquid (and from a liquid microlayer at the base of the bubble⁽⁹⁾) until the departure size is reached and the bubble breaks off. The consecutive bubble forms at the same nucleation site. This regime is called *nucleate boiling*.⁽¹⁰⁻¹²⁾ Heat transfer increases with superheating until a vapor film builds up, which cuts heat transfer down. The factors involved in a second increase of heat transfer at even higher heat flux are related to thermal conduction and radiation in the gas film. There is no analogous situation at gas-evolving electrodes due to the high electrical resistance of the gas.

Boiling processes have been investigated for decades and are better known and interpreted today than the analogous processes at gas-evolving electrodes. For quantitative use of the analogy some differences must be pointed out, mainly concerning the rate of bubble growth and the existence of the above mentioned microlayer. Nevertheless, the knowledge of the boiling process is the basis for comprehension of the process at gas-evolving electrodes. This applies to nucleate boiling as well as to film boiling.

4. Nucleate Gas Evolution

4.1. Nucleation

According to homogeneous nucleation theory,⁽¹³⁾ the spontaneous formation of a bubble in a liquid occurs when a thermodynamic fluctuation of sufficient magnitude occurs to form a bubble of at least the critical radius, given by the Laplace equation, written for multicomponent solutes⁽¹⁴⁾ as

$$R_c = \frac{2\gamma_{LG}}{p_G - p_L} = \frac{2\gamma_{LG}}{p_v + p_L \sum (x_{iL}/x_{iL,s}) - p_L} \quad (1)$$

where γ_{LG} is the liquid/gas interfacial tension, x_{iL} denotes the equilibrium mole fraction of gas in the liquid contacting the bubble of radius R_c , and $x_{iL,s}$ is the equilibrium mole fraction of gas at a flat interface. The pressure p_G of the gaseous phase forming the bubble is composed of the vapor pressure p_v

of the pure solvent and the gas pressure of the solute (i.e., of the dissolved gas). A radius $R > r_c$ must be attained in order to achieve bubble growth, otherwise the bubble dissolves again.⁽¹⁷³⁾ Considering only a single solute and introducing the Henry coefficient $H = p_{iG}/x_{iL}$, we find the relation between the supersaturation of the dissolved gas in the immediate vicinity of the bubble and the excess pressure inside the bubble to be:

$$x_{2L} - x_{2L,s} = \Delta x_{2L} = \frac{p_G - p_L}{H - p_v} \quad (2)$$

Hence, the critical bubble radius R_c is governed by the liquid supersaturation and by properties of the solution⁽¹⁵⁾:

$$R_c = \frac{2\gamma_{LG}}{\Delta x_{2L}(H - p_v)} \approx \frac{2\gamma_{LG}}{\Delta x_{2L}H} \quad (3)$$

This consideration fundamentally also applies to heterogeneous nucleation occurring at gas-evolving electrodes. Real surfaces contain pits, scratches, and grooves of various sizes and are never perfectly wetted by the liquid. These cavities contain entrapped gas. The conditions for entrapment as a function of the geometry of the groove and the contact angle were studied by Bankoff⁽¹⁶⁾ and Cole.⁽¹⁷⁾ Since nucleation occurs from a preexisting gas phase, under certain conditions the residual gas may act as a bubble initiator or nucleus. If at a given supersaturation the radius of the interface is smaller than R_c , the nucleation site remains inactive. If, on the other hand, the real radius of the cavity under consideration exceeds R_c , the residual gas grows by a supply of dissolved gas from the surrounding solution. After the departure of the bubble, some residual gas is left over and serves as a nucleus for the successive bubble (Figure 1).

The concentration of dissolved gas reaches its maximum value in the liquid adjacent to the electrode (due to impediment of mass transfer in the direction of the bulk). Since nuclei are situated at the solid surface, bubbles

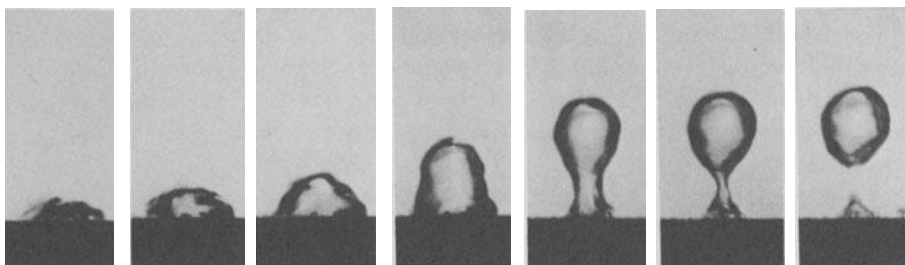


Figure 1. Bubble departure at a planar horizontal platinum electrode according to high-speed photos by Piontelli *et al.*⁽¹⁸⁾ Chlorine evolved out of 2 N HCl at 20°C. Average current density, 35,000 A m⁻². Profile view at 3000 frames/second. (Courtesy of Dr. B. Mazza, Milano.)

are preferably formed at the electrode. The surface then acts as a gas-evolving electrode.

The process and the conditions of nucleation correspond to those in nucleate boiling. These were comprehensively reported by Cole and Stralen.^(17,19) Cheh⁽²⁰⁾ conducted a theoretical and numerical analysis of the nucleation events at gas-evolving electrodes.

Supersaturation in the immediate vicinity of hydrogen- and oxygen-evolving electrodes has been measured by Shibata.^(21,22) It was found that the supersaturation attained a limiting value at current densities of about 1000 A m^{-2} and were 20–160 times larger than the solubilities at 1 bar, depending, in particular, on the surface condition of the electrode.⁽²³⁾ Shibata's results agree quantitatively with values obtained by Bon and Tobias⁽²⁴⁾ under comparable conditions.⁽²⁵⁾ It was pointed out that the supersaturation of the liquid governing the nucleation (i.e., the liquid contacting gas-evolving electrodes) must be strictly distinguished from the supersaturation governing bubble growth.⁽²⁶⁾ The latter appears in the vicinity of macroscopic bubbles adhering at gas-evolving electrodes and exhibits substantially lower values.

It is obvious that the number of active nucleation sites on a given area depends not only on the supersaturation but also on the total number of available nucleation sites whose geometry allows activation. To find an absolute standard for the quality of the solid surface is difficult. With relative success the surface roughness was predicted in nucleate boiling.^(12,27,28) This roughness is not completely representative, however, since it is not generally equivalent to the number of nucleation sites. Not only cavities but also spherical protrusions and sharp, jagged peaks on the surface may act as nuclei, as is known from boiling.⁽²⁹⁾ Therefore, an increase in surface roughness need not necessarily be accompanied by an acceleration of mass transfer (which results from an increase in the number of nuclei) as is supported by experiments of Kind and coworkers.^(30,31) Another phenomenon well known from boiling is the aging of nucleation sites, which results in a loss of activity in the course of time,⁽¹²⁾ and which also occurs at gas-evolving electrodes.⁽³²⁾ Secondary chemical or physical reactions, which under certain conditions reform the surface structure, as observed in nucleate boiling,⁽³³⁾ may also change the number of available sites.

4.2. Bubble Growth

From the energy equation, the growth of a spherical bubble of initial radius R_c (surrounded by an infinite nonviscous and incompressible liquid) is described by the Rayleigh equation of motion⁽³⁴⁾:

$$\frac{\rho_L}{2} \int_{R_c}^{\infty} 4\pi r^2 \left(\frac{R^2}{r^2} \frac{dR}{dt} \right)^2 dr = \frac{4}{3} \pi (R^3 - R_c^3) \Delta p$$

resulting in a growth law

$$\frac{dR}{dt} = \left\{ \frac{2}{3} \frac{\Delta p}{\rho_L} \left[1 - \left(\frac{R_c}{R} \right)^3 \right] \right\}^{0.5} \quad (4)$$

It is seen that a bubble of critical radius R_c remains in a metastable equilibrium.

When the bubble begins to grow, the growth behavior depends strongly on viscous, inertia, and interfacial forces. With increasing diameter, the rate of mass transfer of dissolved gas from the liquid becomes prevailing, and other forces can soon be neglected. Equation (4) indicates that the initial growth of very small bubbles is slow. As experimentally shown by Glas and Westwater,⁽³⁵⁾ the transition from this slow initial growth to the asymptotic growth occurs in an immeasurably short time. Therefore, it is the asymptotic bubble growth that attracts practical interest.

The asymptotic bubble growth can satisfactorily be described by solutions of the diffusion equation. Epstein and Plesset⁽³⁶⁾ assumed an initially uniformly supersaturated solution surrounding the growing gas bubble and considered any convective influence negligible, and they arrived at a solution that can be derived easily from the previous calculations by Langmuir.⁽³⁷⁾ Birkhoff *et al.*⁽³⁸⁾ also started from an initially uniform concentration field and found an exact solution that may be generally written

$$Fo' = \frac{C_1}{Ja'^n} \quad (5)$$

where the Fourier number of mass transfer

$$Fo' = \frac{D_2 t}{R^2} \quad (6)$$

reflects the growth behavior depending on the concentration difference. This difference is expressed as the Jakob number of mass transfer

$$Ja' = \frac{M_G}{\rho_G} \frac{\rho_L}{M_L} \Delta x_2 = \frac{M_G}{\rho_G} \Delta c_2 \quad (7)$$

Δx_2 or Δc_2 is the driving force of bubble growth and is approximated by the supersaturation of the liquid with dissolved gas in the vicinity of the growing bubble. For the limiting case of infinitely small supersaturation, $Ja' \rightarrow 0$, one must use

$$C_1 = 0.5 \quad \text{and} \quad n = 1$$

whereas for the opposite case of infinite supersaturation, $Ja' \rightarrow \infty$, one must apply⁽³⁸⁾

$$C_1 = \pi/12 \quad \text{and} \quad n = 2, \quad \text{if } (\rho_L - \rho_G)/\rho_L \rightarrow 1$$

The theory was extended by Scriven,⁽³⁹⁾ who also tabulated the function $Fo' = Fo'(Ja')$. A growth law for a spherical bubble tangent to a wall with a

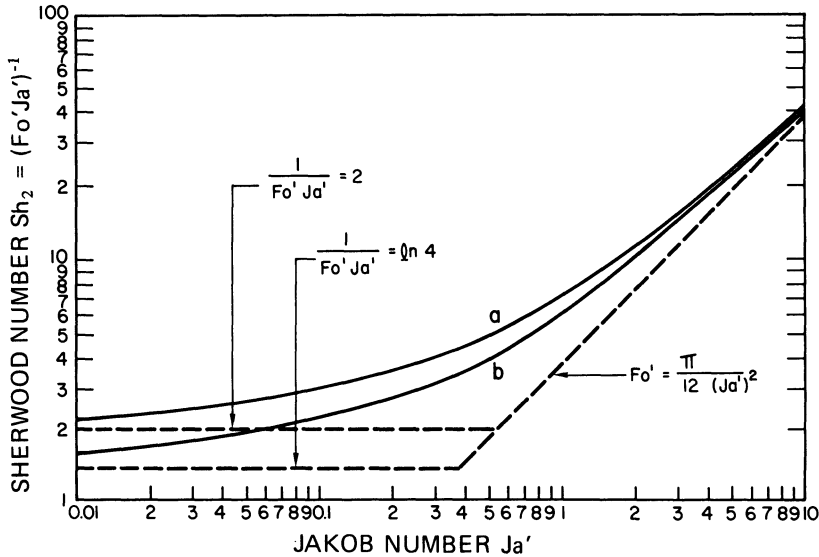


Figure 2. Bubble growth law $Fo' = C_1 (Ja')^{-n}$ for $\rho_G/\rho_L \rightarrow 0$: Curve a, hemispherical bubble⁽³⁹⁾; curve b, tangent spherical bubble.⁽⁴⁶⁾

contact angle $\vartheta = 0$ was developed by Buehl and Westwater⁽⁴⁰⁾ and does not differ essentially from the case of an isolated bubble or a hemispheric bubble.^(38,39) The growth laws are shown in Figure 2.

Introducing the general mass transfer equation of dissolved gas to the bubble surface

$$\frac{\dot{n}_2}{A} = k_d \Delta c_2$$

and a growth relation of the bubble radius R

$$\frac{dR}{dt} = \frac{\dot{n}_2}{A} \frac{M_G}{\rho_G}$$

and combining them with Eqs. (6) and (7) shows that the function $(Fo'Ja')^{-1}$, used as the ordinate in Figure 2, is equal to the Sherwood number of the dissolved gas⁽⁴¹⁾:

$$Sh_2 = \frac{2Rk_d}{D_2} = \frac{1}{Fo'Ja'} \tag{8}$$

Note that the limiting case of $Fo = (\pi/12) Ja'^{-2}$ applies to the growth of vapor bubbles in superheated liquids, caused by heat conduction instead of diffusion. In this case, thermal quantities have to be introduced into the Fourier and Jakob number instead of mass transfer quantities as used here.

Various solutions of the heat conduction equation were presented^(42,43) in the corresponding field of nucleate boiling. An excellent summary of available theories was published by van Stralen⁽⁴⁴⁾; another more recent survey was done by Afgan.⁽⁴⁵⁾

Gas bubbles generated by electrolysis at common current densities grow at medium values of the Jakob number ($Ja' \approx 10^{-2} - 10^0$). This was shown experimentally by high-speed motion picture photography through a microscope, carried out by Westwater and coworkers.^(35,46) The fact that the growth law of gas bubbles differs from that of vapor bubbles is evident from Figure 2. None of the limiting conditions mentioned above is adequate for gas bubble growth.

The growth law (5) only applies to uniform initial concentration of gas in the electrolyte surrounding the bubble. In fact, as the dissolved gas is generated at the electrode and moved into the growing bubble as well as toward the liquid bulk, the real initial concentration field is nonuniform. Special solutions of a general integrodifferential growth equation for a spherical symmetric concentration field and an axisymmetric one were presented by Cheh and Tobias.⁽⁴⁷⁾ In these cases, the radius of the bubble is no longer proportional to $(D_2t)^{0.5}$ as the conditions depart from those of constant Fourier number, this being typical of initially uniform concentration.

The experimental investigation of bubble growth has shown fairly constant Fourier numbers during the total growth period,^(35,48) a behavior which can be considered typical of moderate current densities, but need not necessarily reflect the conditions at high current densities. Darby and Haque⁽⁴⁹⁾ observed a growth behavior $R \sim t^{1/3}$ at 10^4 A m^{-2} and concluded that at high current densities some mechanism other than mass transfer of dissolved gas may be rate determining.

As a general principle, the validity of all growth laws is restricted to cases where the adhering bubbles do not mutually interfere, i.e., a restriction to moderate current densities. At current densities above $\sim 1000 \text{ A m}^{-2}$ various anomalies occur as studied by Westerheide and Westwater.⁽⁴⁶⁾ Bubbles growing at active nucleation sites located close to each other interfere in growth behavior, since the movement of electrolyte, induced by the increase in bubble diameter, effects the concentration field. Bubble growth is speeded up, but under certain conditions which are not understood a slowdown is observed.⁽⁴⁶⁾

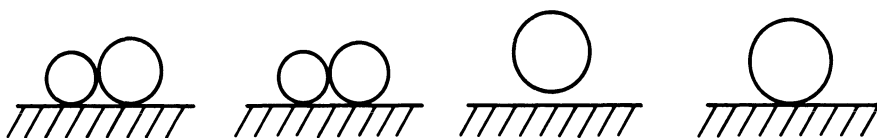


Figure 3. Coalescence of two neighboring bubbles according to high-speed photos by Westerheide and Westwater.⁽⁴⁶⁾ Profile view at 1450 frames/second.

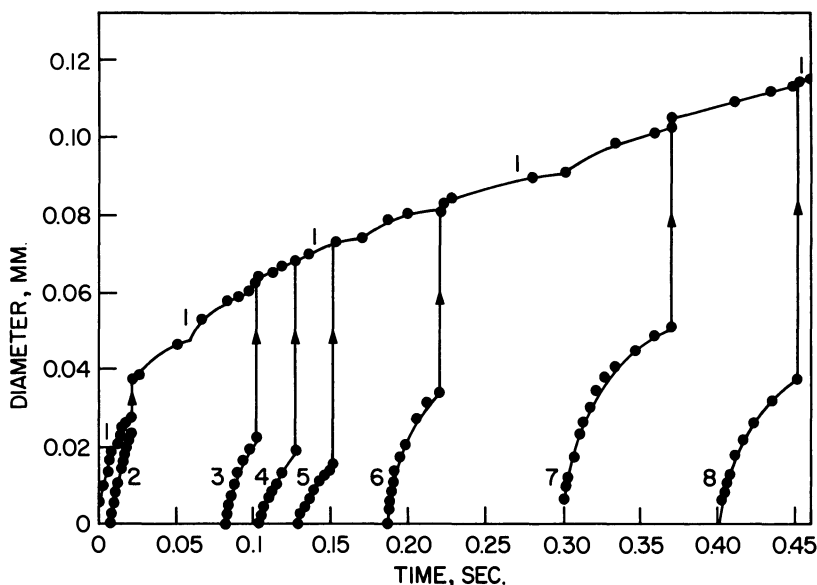


Figure 4. Growth of eight consecutive coalescing bubbles.⁽⁴⁶⁾

A very important anomaly is the coalescence of bubbles on the electrode surface. As soon as singular bubbles touch each other while growing coalescence may occur. Small bubbles are swallowed by large ones. A peculiar phenomenon is the jump-off of two bubbles of nearly equal size in coalescence, characterized by a departure of the resulting bubble from the electrode followed by an immediate return to the electrode where the bubble remains attached⁽⁴⁶⁾ (Figure 3). Another reason for coalescence is the sliding of big bubbles upward along the electrode while embodying small bubbles in a kind of scavenging effect.^(51,52) It seems that this effect is favored by conditions influenced by the polarity of the electrode.⁽⁵³⁾ Coalescence occurs within short times $\sim 10^{-4}$ s.⁽⁴⁶⁾

Growth of bubbles undergoing step-wise increases in size by coalescence does not fit the theory since the concentration field in the vicinity of the new bubble has been disturbed by the event of coalescence (Figure 4). Furthermore, large bubbles formed by coalescence need not detach from the electrode but, at least under certain conditions, adhere to the electrode while smaller bubbles depart.⁽⁵²⁾

4.3. Bubble Departure

The growing bubble remains attached to the electrode surface until a sufficient size is attained. The departure volume is governed by the dynamics

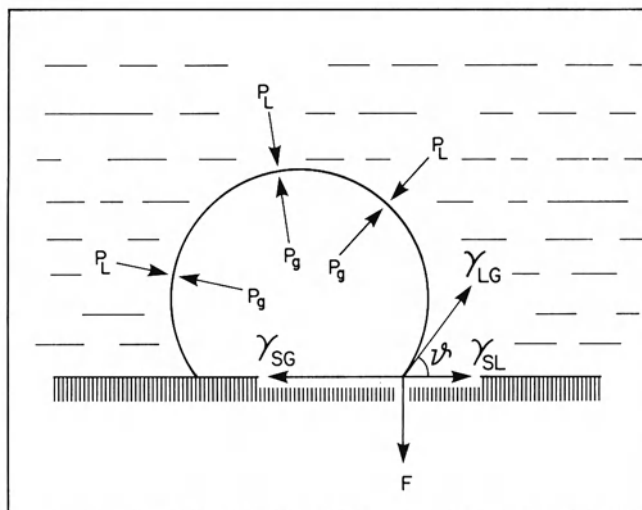


Figure 5. Balance of static forces acting on the idealized adhering bubble.⁽⁵⁷⁾ (From Ibl and Venczel,⁽⁵⁸⁾ p. 4.)

of the surrounding liquid as well as by the buoyancy, pressure, and adhesion forces⁽⁵⁴⁻⁵⁷⁾ (Figure 5).

Considering a bubble adhering to a horizontal plane facing upward and assuming static equilibrium, Fritz and Ende^(59,60) found a relationship

$$\frac{[(\pi/6)d^3]^{1/3}}{[2\gamma/g(\rho_L - \rho_G)]^{0.5}} = f(\vartheta) \quad (8)$$

where d is the diameter of a sphere which equals the volume of the real bubble of usually irregular shape. Based on the calculations of Bashforth and Adams⁽⁶¹⁾ and of Wark⁽⁵⁴⁾ for the shape of an adhering bubble, the function $f(\vartheta)$ can be tabulated⁽⁵⁹⁾ and can easily be approximated by

$$d = 1.18 \vartheta \left[\frac{\gamma}{g(\rho_L - \rho_G)} \right]^{0.5} \quad (9)$$

to give an expression for the bubble departure diameter, depending on physical properties only. For boiling conditions, Eq. (9) was repeatedly confirmed by experiments under various operating conditions and is widely accepted. However, for gas-evolving electrodes, bubble departure diameters predicted from Eq. (9) were found to be in agreement with observed values only for extremely low gas rates.⁽⁶²⁾ For common operating conditions, this equation is useful for qualitative predictions only, as is evident from the departure diameters of carbon dioxide bubbles evolved in cryolite-alumina melts: Big bubbles are formed in melts with small alumina contents whereas fine frothy

bubbles are typical with high alumina contents.⁽⁶³⁾ This behavior is accompanied by a significant change in contact angle, varying between 120° in alumina-free melts and values near 10° for high alumina concentrations.^(5,64) Absolute departure diameters given by Eq. (9) are not generally valid for various reasons.

The interfacial tension at the electrode–electrolyte interface depends to a large extent on the electric potential as first shown by Lippmann.⁽⁶⁵⁾ Since the interfacial tensions at the solid–gas and the gas–liquid interface remain practically constant, the contact angle itself changes with the electric potential. This was experimentally supported by Möller.^(66,67) Even after introducing the real contact angles^(5,40) into Eq. (9), the predicted departure diameters disagree with those determined by experiments. One of the reasons might be the interaction between bubbles and the fluid dynamics of the liquid. It is noteworthy that an increase of bubble diameter with increasing current density was observed^(18,53,68,69) (probably due to bubble coalescence,⁽⁵⁶⁾ which was thoroughly discussed by Piontelli *et al.*⁽¹⁸⁾ whereas Venczel and Ibl^(70–72) reported a remarkable decrease of bubble diameter. A maximum in bubble diameter as a function of current density was found by Coehn and Neumann.⁽⁷³⁾

Our present knowledge is still unsatisfactory in predicting the size of departure diameters. At metal or graphite electrodes, faced horizontally upward or vertical, d is of the order of 50 μm ,^(30,48,53,74–79) depending on the polarity of the electrode^(53,56,80) and the nature of the electrolyte solution^(80,81) and its concentration at the electrode⁽⁸⁰⁾ which in turn is influenced by the current density^(30,75) and the liquid bulk flow velocity.⁽⁸²⁾ Poorly wettable surfaces as PTFE-coated electrodes⁽⁷⁷⁾ or electrodes facing downward⁽⁷⁰⁾ show much larger diameters.

Salt melts exhibit a different behavior compared to aqueous solutions. Several observations seem to prove that departure diameters are considerably larger, being of the order of 1 mm.^(83,84)

Experimentally determined size distributions of bubbles evolved in aqueous solutions^(30,74,75,79,85) and in molten salts^(52,83) are known and show that the real diameter varies widely.

5. Mass Transfer

If in a liquid a concentration difference of a species (ion or neutral molecule) occurs between the interface at the electrode and the liquid bulk, mass transfer takes place. Diffusion may be superimposed by mass flow, denoting the regime of convective mass transfer. If (with or without the convection) bubbles are formed at the electrode, the processes connected with the formation and the detachment of the bubbles are able to influence considerably mass transfer rates and may be predominant.

The greater technical interest lies in nucleate gas evolution. Out of a number of influential quantities, some (position,^(53,74,86) polarity,^(53,74) roughness of the electrode,^(30,87) temperature,^(30,77) pressure,⁽⁷⁷⁾ gas evolution rate, nature of gas^(30,74,86)) have been quantitatively investigated; others can only be guessed.⁽³⁰⁾ The available mass transfer theories are all imperfect and need further improvement. Experimental and theoretical investigations in the field were initiated by Ibl not more than twenty years ago and continue on a wide range.

5.1. Empirical Correlations

It is known that mass transfer at gas-evolving electrodes is strongly influenced by the volume flux \dot{V}_G/A of gas evolved at the electrode, understood as the volume flow rate referred to the geometrical area of the electrode. Consequently, correlations of the type⁽⁸⁸⁾

$$k_d = \text{const} \left(\frac{\dot{V}_G}{A} \right)^m \quad (10)$$

were tried, where k_d is the mean mass transfer coefficient defined by

$$k_d = \frac{1}{A \Delta c_1} \frac{dn_1}{dt} \quad (11)$$

The factor in Eq. (10) was considered approximately constant and adapted to the experimental conditions. Values for the exponent m from various workers are compiled in Table 1. Sometimes the correlation was proposed as

$$\delta = \text{const} \left(\frac{\dot{V}_G}{A} \right)^{-m} \quad (12)$$

Since by definition, $\delta \equiv D_1/k_d$, the extent of the influence of the diffusion coefficient D_1 of the transferred species is left undecided.

Ibl and coworkers⁽⁵⁶⁾ presented the relationship

$$k_d = \text{const} \left(\frac{\dot{V}_G}{A} \right)^m D_1^{0.5} \quad (13)$$

which correlated experimental results with varying diffusion coefficients.

5.2. Theoretical Approaches

Mass transfer at gas-evolving electrodes is essentially influenced by the following effects:

1. *Penetration effect*⁽⁵⁶⁾: A bubble having reached the departure diameter and being detached from the electrode rises upward, transferring momentum

Table 1
Exponent m in Eq. (10) According to Various Experimental Investigations

Gas	Electrolyte	m	Publication
H ₂	alkaline	0.43	Green and Robinson ⁽⁸⁹⁾
		0.29	Vondrák and Balej ⁽⁹⁰⁾
		0.36	Janssen and Hoogland ⁽⁵³⁾
		0.25	Fouad and Sedahmed ⁽⁸⁶⁾
		0.65	Roušar <i>et al.</i> ⁽⁷⁶⁾
		0.17–0.30	Janssen ⁽⁷⁷⁾
H ₂	acid	0.5(0.59)	Roald and Beck ⁽⁹¹⁾
		0.525	Venczel ⁽⁷⁰⁾
		0.47	Janssen and Hoogland ⁽⁷⁴⁾
		0.62 (Pt)	Janssen and Hoogland ⁽⁵³⁾
		0.36 (Hg)	Janssen and Hoogland ⁽⁵³⁾
		0.45	Kind ⁽³⁰⁾
O ₂	alkaline	0.87/0.33	Janssen and Hoogland ⁽⁵³⁾
		0.4	Fouad and Sedahmed ⁽⁸⁶⁾
O ₂	acid	0.5	Beck ⁽⁸⁸⁾
		0.4	Janssen and Hoogland ⁽⁷⁴⁾
		0.6	Ibl ⁽⁵⁶⁾
		0.57	Janssen and Hoogland ⁽⁵³⁾
		0.66	Kind ⁽³⁰⁾
Cl ₂	acid	0.71	Janssen and Hoogland ⁽⁷⁴⁾

to the surrounding liquid. As a result, a flow wake develops, causing an essentially centripetal flow pattern. Liquid from the outer edge of the concentration boundary layer or from outside is entrained to the electrode surface. As a consequence, it is supposed that the concentration of the liquid adjacent to the electrode is periodically replaced.

2. *Microconvection effect*⁽¹⁵⁾: During the growth time of the bubble adhering to the electrode surface, liquid is pushed past the electrode in centrifugal directions. A microconvective flow regime develops in the vicinity of the bubble. The impact diminishes with increasing distance from the bubble center.

3. *Hydrodynamic or macroconvection effect*⁽⁷⁴⁾: The swarm of bubbles which rises near the electrode causes a convective liquid flow that is not directly related to the individual bubble phenomena as described above. This two-phase flow can result in considerable flow velocities which can interfere with the other effects.

Each effect acts on mass transfer. Various models were developed, which considered one or the other of the effects as the most influential. The results will be presented in terms of the mass transfer coefficient, which has been discussed in Chapter 3.

The *penetration model* was developed by Ibl.^(56,70,71,92) It is assumed that after the bubble has separated from the electrode, a solution having the

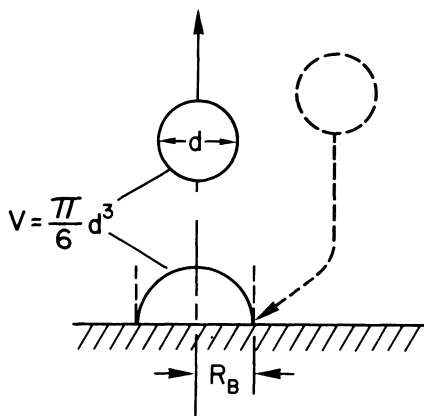


Figure 6. Schematic representation of the penetration model.

concentration of the bulk of liquid reaches the active nucleation center area of the electrode (Figure 6) and the electroactive species then diffuses toward the electrode until the next bubble starts growing at the same nucleation site. This happens after a waiting time t_w . The theory assumes that during the waiting time mass transfer is governed predominantly by nonsteady-state diffusion in a quiescent liquid. The mass transfer coefficient k_d is thus calculated for the condition of constant interfacial concentration⁽⁹³⁾ by integrating the Cottrell equation⁽⁹⁴⁾ over the waiting time t_w and taking the time average.

$$k_d = t_w^{-1} \int_0^{t_w} \left(\frac{D_1}{\pi t} \right)^{0.5} dt \quad (14)$$

To evaluate t_w , Ibl divides the volume flux \dot{V}_G/A of the evolved gas and the area πR_B^2 covered by the bubble, assumed to be hemispherical, by the average volume $\pi d^3/6$ of a departing bubble, where R_B denotes the radius of the adhering bubble immediately before departure. This yields the number of bubbles evolved at a site per unit time, the inverse of which is equated with the waiting time,

$$t_w = \frac{\pi d^3/6}{\pi R_B^2} \frac{A}{\dot{V}_G} \quad (15)$$

This assumes that the whole electrode area is active and that the bubbles grow infinitely fast. If they do not, one must take into account that, on the average, the fraction θ of the electrode area is covered by bubbles attached to it. The electrode is thus on the average blocked during a fraction θ of the time available, and the upper integration limit in Eq. (14) is now $t_w - t_w\theta$ (the time over which one averages remains, however, equal to t_w). Ibl^(56,70,71) thus obtains from Eqs. (14) and (15)

$$k_d = \left[\frac{6D_1\dot{V}_G(1-\theta)}{\pi R_B A} \right]^{0.5} \quad (16)$$

To consider various shapes of the departing bubbles of shape factor C_2

$$d = C_2^{1/3} R_B \quad (17)$$

is introduced, e.g., $C_2 = 8$ for the spherical bubble and $C_2 = 4$ for the hemispherical bubble, to render Eq. (16) independent of bubble shape:

$$k_d = 2 \left[\frac{6}{\pi C_2} \frac{\dot{V}_G D_1 (1 - \theta)}{A R_B} \right]^{0.5} \quad (18)$$

where θ equals the fraction of the electrode area covered by adhering bubbles. Eq. (18) may be written in a dimensionless form. Introducing

$$\text{Sh} = \frac{k_d d}{D_1} \quad (\text{Sherwood number}) \quad (19)$$

$$\text{Re} = \frac{\dot{V}_G d}{A \nu} \quad (\text{Reynolds number}) \quad (20)$$

$$\text{Sc} = \frac{\nu}{D_1} \quad (\text{Schmidt number}) \quad (21)$$

and inserting d from Eq. (17) yields

$$\text{Sh} = \left(\frac{24}{\pi} \right)^{0.5} C_2^{-1/3} (\text{Re Sc})^{0.5} (1 - \theta)^{0.5} \quad (22)$$

Departure diameters d are known.^(53,70,76) The fractional surface coverage θ was experimentally determined by Venczel⁽⁷⁰⁾ for special conditions; his results may be roughly approximated by

$$\theta = 0.5 \text{Re}^{0.18} \quad (23)$$

A more extended range was tentatively described by Vogt⁽²⁶⁾ using experimental data from various sources.

A variation of Ibl's theory was presented by Roušar and Cezner.⁽⁹⁵⁾ They adopted from Ibl two assumptions: that after bubble departure, the liquid with the bulk concentration reaches the electrode surface, and that mass transfer occurs exclusively by nonsteady-state diffusion in quiescent liquid. Essentially, they introduced two new assumptions related to the mass transfer area and time of exposure: one takes into account that, in view of the discrete number z_A of nucleation sites, a part of the electrode surface may remain permanently inactive. If the area uncovered by the departing bubble is again on the average πR_B^2 , the area with no mass transfer is equal to $(Az_A^{-1} - \pi R_B^2)$. The second new assumption is that almost immediately after the bubble with radius R_B breaks off, the next bubble begins to grow at the same nucleation site. The duration of mass transfer by diffusion is considered equal to the residence time t_B , to be understood as the time from the start of growth of a bubble adhering to the electrode surface up to its

departure. Hence, the mass transfer coefficient may be written

$$k_d = \frac{\pi R_B^2}{Az_A^{-1}} \frac{1}{t_B} \int_0^{t_B} \left(\frac{D_1}{\pi t} \right)^{0.5} dt \quad (24)$$

instead of Eq. (14). The gas volume flux is given by

$$\frac{\dot{V}_G}{A} = \frac{\pi d^3/6}{Az_A^{-1}(t_B + t_w)} \quad (25)$$

Using again the assumption of zero waiting time, $t_w/t_B = 0$, the mass transfer coefficient becomes

$$k_d = \frac{12}{C_2} \left(\frac{D_1 t_B}{\pi} \right)^{0.5} \frac{\dot{V}_G}{AR_B} \quad (26)$$

Considering only spherical bubbles, $C_2 = 8$, gives

$$k_d = \frac{1.5 D_1^{0.5}}{\pi^{0.5}} \frac{\dot{V}_G}{A} \frac{t_B^{0.5}}{R_B} \quad (27)$$

For two limiting cases of the fractional surface coverage, $\theta \rightarrow 0$ and $\theta \rightarrow 1$, Roušar and Cezner eliminated the quotient $(t_B^{0.5}/R_B)$ using an empirical relationship which was taken from the experimental results of Glas and Westwater.⁽³⁵⁾

It is possible to develop Roušar's model in another way. Eliminating the unknown residence time t_B in Eq. (26) by means of an expression relating the gas volume flux to the number z_B of bubbles adhering simultaneously at the total electrode area A ,

$$\frac{\dot{V}_G}{A} = \frac{\pi d^3/6}{Az_B^{-1} t_B} \quad (28)$$

results in

$$k_d = \frac{24^{0.5}}{C_2 R_B} \left(\frac{\dot{V}_G d^3 D_1}{A^2 z_B^{-1}} \right)^{0.5} \quad (29)$$

Introducing the fractional electrode coverage θ defined by

$$\theta = \frac{t_B^{-1} \int_0^{t_B} \pi R^2 dt}{Az_B^{-1}} \quad (30)$$

which together with $R \sim t^{0.5}$ (see Section 4.2) gives

$$\theta = \frac{\pi}{2} \frac{R_B^2}{Az_B^{-1}} \quad (31)$$

Then, considering Eq. (17), Roušar's model yields:

$$\text{Sh} = \left(\frac{48}{\pi}\right)^{0.5} C_2^{-1/3} (\text{Re Sc})^{0.5} \theta^{0.5} \quad (32)$$

It is seen that Eq. (32) differs from the Ibl's model, Eq. (22), mainly with respect to view of the influence of the fractional coverage θ which, however, is of moderate effect in mean values of θ .

Another application of the penetration model to those electrodes where bubble coalescence occurs frequently was made by Janssen and van Stralen.⁽⁹⁶⁾ It was assumed that each bubble departing with the radius R_C is formed by coalescence of two adhering bubbles of nearly equal size and that solution having the bulk concentration penetrates to the electrode at a surface area $\pi f R_C^2$ which is a part of the total surface area A/z_C pertinent in average to each bubble formed by coalescence. Integration of the Cottrell equation over the time t_C between two coalescences at the same place:

$$k_d = \frac{\pi f R_C^2}{A z_C^{-1} t_C} \int_0^{t_C} \left(\frac{D_1}{\pi t}\right)^{0.5} dt \quad (33)$$

after combination with

$$\frac{\dot{V}_G}{A} = \frac{4\pi R_C^3}{3A z_C^{-1} t_C} \quad (34)$$

yields

$$k_d = \frac{D_1}{\delta_N} = \left(3 \frac{\dot{V}_G}{A} \frac{z_C R_C}{A} D_1\right)^{0.5} f \quad (35)$$

An analogous relation for heat transfer in nuclear boiling can be deduced from van Stralen's relaxation microlayer model.⁽¹⁹⁾ Values of $z_C R_C/A$ were reported in Reference 96 based on interesting experiments with transparent nickel electrodes in gas evolution.

The *microconvection model*^(15,97) differs from the penetration model mainly in that it assumes convective mass transfer to be active alone. Diffusion in quiescent liquid is disregarded. The growing bubble induces a liquid flow past the electrode surface, the velocity of which is considered decisive for the rate of mass transfer (Figure 7). The mass transfer area under consideration equals $A z_B^{-1} - \pi R^2$ and varies with time as $R(t)$. The mass transfer coefficient is the mean value in the residence time t_B of the bubble and the area pertinent to each adhering bubble:

$$k_d = \frac{1}{t_B A z_B^{-1}} \int_0^{t_B} \int_{R(t)}^{(A/\pi z_B)^{0.5}} 2\pi r k_{xt} dr dt \quad (36)$$

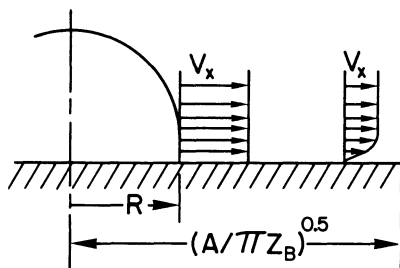


Figure 7. Schematic representation of the micro-convection model.

Local and temporal mass transfer coefficient k_{xt} is estimated from

$$k_{xt} = C_3 \left(\frac{D_1 v_x}{x} \right)^{0.5} \quad (37)$$

where the factor C_3 varies between $\pi^{-0.5}$ (valid for the mass transfer equation for laminar plug flow parallel to a planar surface,⁽⁹⁸⁾ applied to the liquid adjacent to the bubble) and $f(Sc)/Sc^{1/6}$ (for the Polhausen–Levich equation^(99,100) for developed laminar boundary layer flow, applied to the outer edge of the area Az_B^{-1}). Assuming that the velocity distribution at the bubble-liquid interface is of plug flow type and develops steadily into a boundary layer flow as the distance from the bubble increases, integration of Eq. (36) under consideration of $R \sim t^{0.5}$ and Eq. (28) results in⁽⁹⁷⁾

$$\begin{aligned} Sh = 1.562(Re Sc)^{0.5} \left(1 + \frac{0.29}{Sc^{1/6}} + 0.0047 Sc^{0.053} \right) \\ \times \theta^{0.25} (1 - \theta^{0.5})^{0.5} \end{aligned} \quad (38)$$

which could be approximated for practical use by^(15,97)

$$Sh = 0.93 Re^{0.5} Sc^{0.487} \quad (39)$$

The numerical results of the penetration and the microconvection model, Eqs. (22) and (39), do not differ essentially, except for extremely small fractional surface coverages (Figure 8). The mass transfer equations are also capable of describing experimental data satisfactorily, as shown by a compilation,^(15,97) although the scatter is considerable due to the simplicity of the models used and to the difficulties in performance of the experiments and evaluation of the data. All models imply an insufficiency inasmuch as they assume that after departure of a bubble, liquid with the bulk concentration is present over part or all of the electrode surface. On the basis of direct observation, Ibl and Venczel^(71,72) have discussed the possibility of an influence caused by a remaining thin liquid film adjacent to the electrode, so that the bulk concentration may only exist at a finite distance from the wall. The authors concluded, however, that under common conditions the influence may be negligible.

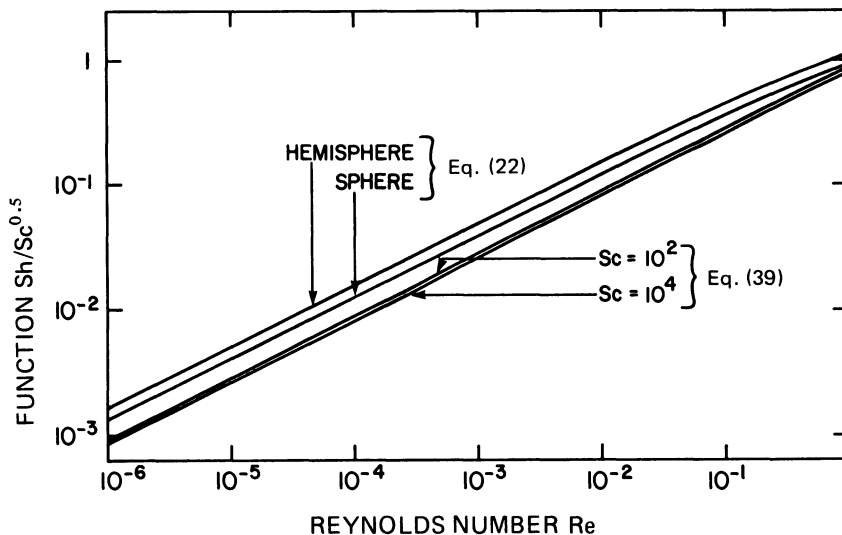


Figure 8. Comparison of the mass transfer correlations of Ibl and coworkers^(56,70,71,92) and of Vogt.^(15,97)

The third model was first proposed by Janssen and Hoogland^(53,74) and was discussed by Ibl.⁽⁵⁶⁾ This *hydrodynamic model* considers the electrolyte flow caused by the lift effect of the ascending bubbles to be the governing quantity in mass transfer at gas-evolving electrodes. The velocity distribution of the liquid boundary layer depends on the cell dimensions, the volumetric flux of evolved gas, the velocity of rise of the bubbles, and the liquid viscosity. The model claims to be applicable in cases where coalescence of adhering bubbles does not occur,⁽⁷⁷⁾ and was quantitatively described by Janssen and Barendrecht.⁽¹⁰¹⁾ It is based on the mass transfer equation for natural turbulent convection at plane walls:

$$\text{Sh}_1 = \frac{k_d L}{D_1} = \text{const} (\text{Gr Sc})^{1/3} \quad (40)$$

where the Grashof number is given by

$$\text{Gr} = \frac{gL^3}{\nu^2} \frac{\rho_o - \rho_e}{\rho_e} \quad (41)$$

The numerical constant in Eq. (40) is in the range 0.15–0.19. ρ_e denotes the mean density immediately at the electrode/electrolyte interface and ρ_o the bulk density. Setting for bubble-filled electrolytes $\rho_o = \rho_L$ and $\rho_e = (1 - \chi_e)\rho_L + \chi_e\rho_G \approx (1 - \chi_e)\rho_L$, one obtains for the Grashof number:

$$\text{Gr} = \frac{gL^3}{\nu^2} \frac{\chi_e}{1 - \chi_e} \quad (42)$$

The authors assumed a ratio of the terminal rising velocity v_r of an isolated spherical bubble to the volumetric gas flux according to

$$\frac{v_r}{\dot{V}_G/A} = \frac{1 - \varphi_e}{\varphi_e} \quad (43)$$

and introduced a drag coefficient Z into the Grashof number. Inserting v_r from Eq. (68) (see Section 8.2) and taking into account that $\rho_G \ll \rho_L$ results in

$$\text{Sh} = \frac{k_d d}{D_1} = \text{const} (Z \text{Re Sc})^{1/3} \quad (44)$$

Note that contrary to the other models, the mass transfer here coefficient depends on the rate of gas evolved according to $k_d \sim (\dot{V}_G/A)^{1/3}$ if the drag coefficient Z is a constant. Inserting Eq. (25) into Eq. (44) results in ⁽¹⁰¹⁾

$$\delta = \text{const} \left[\frac{D_1 A (t_B + t_w)}{Z dz_B} \right]^{1/3} \quad (45)$$

Eq. (45) is closely related to an analogous heat transfer equation derived by Zuber ⁽¹⁰²⁾ for nucleate boiling.

Eq. (40) mainly differs from the other mass transfer equations presented here in that the model does not refer to microeffects occurring in the vicinity of bubbles departing from the electrode (penetration model) or of bubbles growing while adhering to the electrode (microconvection model) but takes into account flow effects induced by bubbles rising near the electrode. Insofar the effect exhibits no difference in gas-evolving and in gas sparged electrodes without gas evolution. It is, therefore, plausible that Ibl *et al.* ^(103,104) could use Eq. (40) to correlate experimental mass transfer data obtained at vertical gas bubble-sparged electrodes and could generally apply the same equation to mass transfer in two-phase flow of gas bubbles and liquid past an electrode ⁽¹⁰⁵⁾ at gas-evolving electrodes, as well as at gas-sparged ones.

5.3. Mass Transfer with Superposition of Liquid Bulk Flow

In all cell arrangements with gas-evolving electrodes, a liquid bulk flow (or macroconvection) occurs in addition to the microconvection caused by the bubbles adhering to the electrode surface. The macroconvection is due to the momentum transferred to the liquid by the rising bubbles. Often, additional mechanical pumping is applied in order to remove the bubbles quickly from the interelectrode space in order to keep the ohmic voltage drop low, or in order to remove unstable intermediate products from the electrodes without delay to prevent further reaction.

Such a macroconvection brings an additional influence to bear on mass and heat transfer. This influence is large when the Reynolds number associated

with the gas evolution rate, Eq. (20), is small compared to the Reynolds number

$$\text{Re} = \frac{vL_h}{\nu} \quad (46)$$

associated with the mean liquid flow velocity v . L_h is a characteristic length of the channel. Experiments by Fouad and Sedahmed⁽¹⁰⁶⁾ strikingly show how the geometry of the channel may influence mass transfer at gas-evolving electrodes. As a consequence, bulk liquid flow must not generally be disregarded but has to be considered together with the mass transfer as already discussed.

Beck⁽⁸⁸⁾ proposed calculating the combined mass transfer coefficient \bar{k}_d by addition of the coefficients calculated separately and independently of each other for both processes:

$$\bar{k}_d = k_d + k_d^h \quad (47)$$

(For prediction of the mass transfer coefficient k_d^h for hydrodynamic flow without phase change, see Chapter 3.) Beck's proposal was accepted by Birkett and Kuhn⁽¹⁰⁷⁾ on the basis of an analysis of experimental data. With regard to the influence of bulk flow on the departure diameter and with reference to the results obtained in the field of nucleate boiling, Vogt⁽⁵⁰⁾ tested and proposed the correlation

$$\bar{k}_d = k_d \left[1 + \left(\frac{k_d^h}{k_d} \right)^2 \right]^{0.5} \quad (48)$$

based on the corresponding heat transfer equation by Kutateladze.⁽¹⁰⁸⁾

6. Heat Transfer

Heat transfer at gas-evolving electrodes has received less research than mass transfer. Nevertheless, there are cases where a correlation for prediction of heat transfer is needed, especially in the simultaneous use of gas-evolving electrodes as cooling surfaces in industrial electrolysis cells⁽⁹⁵⁾ and in the estimation of surface temperatures of electrodes as used in electrochemical machining, where temperatures near the boiling point are possible.⁽¹⁰⁹⁾

Because of the analogy between nucleate gas evolution and nucleate boiling, it is appropriate to refer to a correlation developed by Zuber⁽¹⁰²⁾ for heat transfer in nucleate boiling and based on the leading idea that heat transfer is governed by natural convection. As the temperature of the liquid boundary layer increases, its density usually decreases, whereby buoyancy forces induce a flow. The evolved gas (or vapor) further reduces the density of the gas-liquid mixture. Both effects act simultaneously and are equivalent.

Convective heat transfer is expressed by

$$\text{Nu} = \frac{hd}{k} = \text{const} \times (\text{Gr Pr})^{1/3} \quad (49)$$

for values of $(\text{Gr Pr}) > 2 \times 10^7$,⁽¹⁷¹⁾ where the Grashof number

$$\text{Gr} = \frac{qd^3}{\nu^2} \left[B(T_e - T_0) + \varphi \frac{\rho_{L,e} - \rho_G}{\rho_{L,0}} \right] \quad (50)$$

and the Prandtl number

$$\text{Pr} = \frac{\nu}{a} \quad (51)$$

The volume fraction of gas

$$\varphi = \frac{V_G}{V_G + V_L} \quad (52)$$

in the liquid boundary layer may be calculated with use of the velocity of rise of the bubbles.⁽¹⁰²⁾ Magrini⁽⁵⁸⁾ successfully applied Eqs. (49) and (50) to heat transfer at gas-evolving electrodes.

Another possibility consists in making use of the analogy between heat and mass transfer and refers to available mass transfer correlations.⁽¹¹⁰⁾ Formal exchange of the corresponding dimensionless groups in Ibl's correlation (22) leads to

$$\text{Nu} = \frac{2.76}{C_2^{1/3}} (\text{Re Pr})^{0.5} (1 - \theta)^{0.5} \quad (53)$$

Correspondingly, it follows from Eq. (39) that

$$\text{Nu} = 0.93 \text{Re}^{0.5} \text{Pr}^{0.487} \quad (54)$$

It stands to reason that, if necessary, bulk liquid flow has to be taken into account as discussed in Section 5.3 for mass transfer.

7. Film Gas Evolution

As the current density of the gas-generating reaction is increased, the supersaturation of the dissolved gas in the vicinity of the electrode increases too. As a consequence, the gas bubbles grow more rapidly but also the simultaneously adhering bubbles become more numerous because the number of active nucleation sites grows. Bubbles are positioned closer and finally

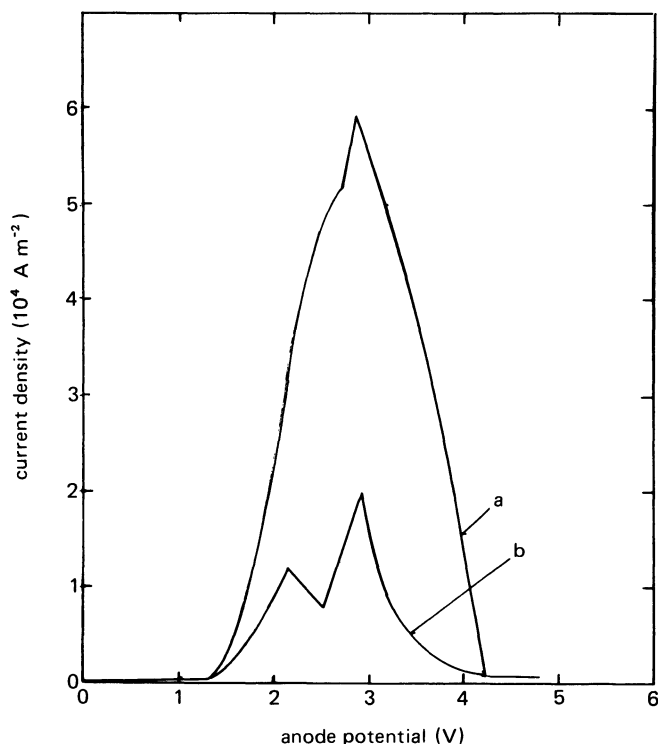


Figure 9. Potential-sweep diagram for a graphite anode vs. an aluminum reference electrode in a cryolite melt with 2 wt.% Al_2O_3 (curve a) and 0.4 wt.% Al_2O_3 (curve b) at 1020°C. (From Thonstad *et al.*⁽¹¹¹⁾)

interfere with each other and impede the liquid contact with the electrode. Throughout the whole range of nucleate gas evolution, an increase in electrode potential is followed by an increase of the gas volume flux. This behavior, however, occurs only until a critical current density (of the gas-generating reaction) is attained.

As the current density exceeds the critical value, gas volume flux goes down considerably (Figure 9). The system behaves electrically unstable since no definite potential can be coordinated to the current density, depending on whether a potentiostatic or galvanostatic or other arrangement has been chosen.⁽¹¹²⁾ At the critical current density, the morphology of gas evolution changes significantly. At lower current densities, gas bubbles are evolved at active nucleation sites, and an unstable gas film blankets the electrode at current densities beyond the critical one. Nucleation sites are no longer effective and the surface roughness has lost its influence.⁽¹¹³⁾ The gas film is irregular and in violent motion (Figure 10).

Finally a condition is reached where the configuration of gas evolution changes once more with the formation of a stable gas film. Further increases

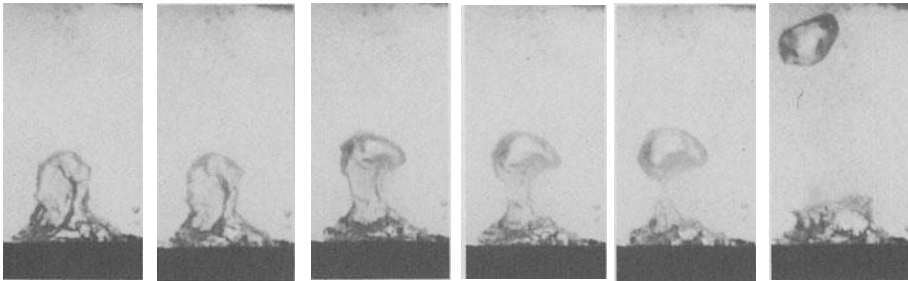


Figure 10. Bubble departure in film gas evolution. Hydrogen evolved out of 2 N NaOH at 20°C, platinum cathode. Average current density, 130,000 A m⁻². Profile view at 3000 frames/second. (Courtesy of Dr. B. Mazza and Dr. P. Pedferri, Milano.)

in the potential do not affect the gas flux, but sparks penetrate the gas film. At much higher potentials a renewed increase of the current density results, accompanied and produced by sparks, and finally a stable arc develops.^(111,113)

This phenomenon is known from alumina electrolysis and has attracted special interest. As in applied electrolysis the cell voltage further increases when the critical current density has been reached. The stable film configuration with the accompanying effects forms soon after the range of the unstable film gas evolution has been passed. This behavior is known as the *anode effect*. Nevertheless, it is not restricted to the alumina electrolysis nor is it observed at anodes only. It also occurs in other systems⁽¹¹³⁾ and at cathodes⁽¹⁸⁾ whenever the gas flux has reached sufficiently high values.

The formation of an unstable gas film followed by a transformation into a stable one, is well known in boiling and is called *burnout effect*. This analogous phenomenon has been more thoroughly investigated and was convincingly interpreted and experimentally proven as a consequence of hydrodynamic instabilities. These instabilities have also been applied to the corresponding phenomena at gas-evolving electrodes by Mazza *et al.*⁽⁵⁵⁾ which appears feasible at least if the contact angles are sufficiently small. The morphologic correspondence of the phenomena is also supported by the instructive high-speed photographs for boiling⁽¹¹⁴⁾ and for gas-evolving electrodes.^(18,115)

The lower critical volume flux marking the incipience of the stable gas film, usually associated with the anode effect, may be estimated by the application of an analysis by Zuber.⁽¹¹⁶⁾ A horizontal electrode, facing upward and covered by an unstable gas film, may be considered (Figure 11). The gas film below the liquid can subsist only if an interface of wavy form between the two fluids exists and if the surface tension energy exceeds the sum of kinetic and potential energies of the wave.⁽¹¹⁷⁾ The critical wavelength is⁽¹¹⁸⁾

$$\lambda = 2\pi \left[\frac{C_3 \gamma}{g(\rho_L - \rho_G)} \right]^{0.5} \quad (55)$$

where the factor C_3 varies due to disturbances within the range⁽¹¹⁶⁾ $1 \leq C_3 \leq 3$.

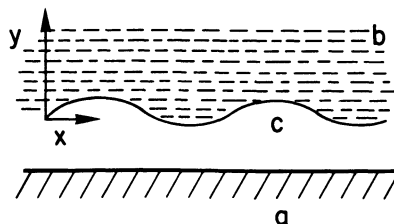


Figure 11. The electrode being covered by a stable gas film. a, solid electrode; b, electrolyte; c, gas.

If the wavelength is smaller than the critical value, the gas film is stable. On the other hand, the speed c' of propagation of a small disturbance for a given configuration of quiescent liquids^(119a) is

$$c'^2 = \left(\frac{\lambda}{\tau}\right)^2 = \frac{2\pi}{\lambda} \frac{\gamma}{\rho_L + \rho_G} \tag{56}$$

if gravity is not taken into account. Combining Eqs. (55) and (56) results in

$$\frac{\lambda}{\tau} = \left[\frac{\gamma g (\rho_L - \rho_G)}{C_3 (\rho_L + \rho_G)^2} \right]^{0.25} \tag{57}$$

Making use of the Taylor instability,⁽¹²⁰⁾ Zuber^(116,121) interpreted the wavelength as the distance between two neighboring active nucleation sites and as directly proportional to the departure diameter. This can be seen from a comparison of Eqs. (55) and (9). The lower critical volume flux results in

$$\begin{aligned} \left(\frac{\dot{V}_G}{A}\right)'_c &= \frac{\pi}{24} \frac{(2\pi C_3)^{0.5}}{3} \left[\frac{\gamma g (\rho_L - \rho_G)}{C_3 \rho_L^2} \right]^{0.25} \left(\frac{\rho_L}{\rho_L + \rho_G}\right)^{0.5} \\ &\approx 0.11 C_3^{0.25} \left(\frac{\gamma g}{\rho_L}\right)^{0.25} \end{aligned} \tag{58}$$

A similar consideration can be applied to the critical peak volume flux which divides nucleate and unstable film gas evolution. This phenomenon can be analyzed by means of the criteria of the Helmholtz instability^(122,123) and the Taylor instability. Two immiscible fluids, flowing relative to each other, may represent the outgoing gas and the incoming liquid (Figure 12). A relative

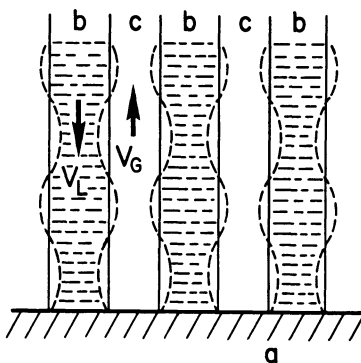


Figure 12. Column-wise gas-liquid configuration: a, solid electrode; b, electrolyte; c, gas.

velocity ($v_L + v_G$) exists above which a small disturbance at the interface will amplify and upset the flow. Equation (56) must be extended by a velocity term^(119b) whereas gravity influence will again be disregarded:

$$c'^2 = \frac{2\pi}{\lambda} \frac{\gamma}{(\rho_L + \rho_G)} - \frac{\rho_L \rho_G}{(\rho_L + \rho_G)^2} (v_L + v_G)^2 \quad (59)$$

The condition for stability of the given configuration is that c be real, hence

$$(v_L + v_G)^2 = \frac{2\pi}{\lambda} \frac{\delta'}{\rho_G} \frac{\rho_L + \rho_G}{\rho_L} \quad (60)$$

Inserting the critical wavelength from Eq. (55) yields

$$v_G \approx \left[\frac{\gamma g (\rho_L - \rho_G)}{C_3 \rho_G^2} \right]^{0.25} \quad (61)$$

irrespective of whether the liquid velocity v_L is set equal to zero or whether v_L (as for pure substances) is replaced using the continuity $\rho_L v_L = \rho_G v_G$. Zuber⁽¹¹⁶⁾ equated $v_G = \lambda/\tau$ and used the interpretations as mentioned above, which results in the peak volume flux⁽¹²¹⁾

$$\left(\frac{\dot{V}_G}{A} \right)_c = \frac{\pi}{24} \frac{3}{(2\pi)^{0.5}} \left[\frac{\gamma g (\rho_L - \rho_G)}{C_3 \rho_G^2} \right]^{0.25} \quad (62)$$

Equation (62) was shown⁽¹¹⁶⁾ to fit various experimental boiling data fairly well. According to Borishanskiy (see Reference 11, p. 385) the numerical factor is about 0.18 and depends slightly on the Archimedes number. A stability criterion similar to Eq. (62) had been developed by Kutateladze⁽¹²⁴⁾ by means of dimensional analysis. All these applications refer to boiling. For gas-evolving electrodes Eq. (62) was modified by Mazza *et al.*⁽⁵⁵⁾ In their papers^(18,55,125) extensive experimental data and observations for the critical phenomena at gas-evolving electrodes can be found.

The transition from nucleate to film region does not seem to be merely a hydrodynamic problem. Katz⁽¹²⁶⁾ proposed considering the solid-liquid interfacial tension γ_{SL} in addition to the liquid-gas interfacial tension γ . In fact, in cases where the contact angle increases considerably (as a result of an influence of changing γ_{SL}), the critical volume flux shifts to lower values. This phenomenon is of utmost interest in alumina electrolysis. If the alumina content in the melt decreases in the course of operation, the anode effect occurs and is considered an indication for trouble-free operation of the cell in industrial practice. Correlation between the occurrence of the anode effect and the contact angle (which increases up to 115°) was clearly shown by Belyaev.⁽⁵⁾ The corresponding behavior was also observed in melts of NaF-AlF₃ as the content of aluminum fluoride decreases. The reasons for the change of the contact angle are still under controversial discussion; a recent review on it is given by Mazza *et al.*⁽¹²⁷⁾

8. Bubble-Filled Electrolytes

After the bubbles have detached themselves from the electrode, they remain dispersed in the electrolyte for a certain time in the interelectrode space, where they affect cell operation by increasing ohmic voltage drop. As the electric conductivity of gas is practically equal to zero, the current-conducting sectional area is restricted to the liquid. Therefore, efforts are made to maintain the volume fraction of gas in electrolyte at low values in the bulk of the liquid-gas mixture. The decrease of the conductivity can be estimated with reasonable success and limited by appropriate design and operation of the cell. However, bubbles may cause a considerable voltage drop when they accumulate in the electrolyte layer in the vicinity of the electrode, especially at electrodes of unfavorable design and horizontal surfaces facing downward. Such a layer, extremely enriched in gas bubbles, has a thickness of a few millimeters⁽¹²⁸⁾ and may be a major cause of the overall voltage drop. This phenomenon of a locally strongly obstructed gas removal is known as *bubble curtain effect*. Its extent is controlled by the electrode geometry and the hydrodynamic flow conditions.

Conductivity of a gas-liquid mixture, its effect on the cell operation conditions, and arrangements for cell design will now be discussed.

8.1. Effective Conductivity

Numerous investigations have been done to evaluate the influence of a dispersed phase of various sizes on the properties of a heterogenous system. The effective conductivity of an electrolyte uniformly filled with gas bubbles stands as a special case.

Maxwell⁽¹²⁹⁾ studied a single sphere of conductivity κ_G surrounded by an extended continuum of conductivity κ_L and derived the classical result for the effective conductivity κ of the mixture:

$$\frac{\kappa}{\kappa_L} = 1 - \frac{3}{\frac{2 + \kappa_G/\kappa_L}{1 - \kappa_G/\kappa_L}} \quad (63)$$

φ denotes the volume fraction of gas as defined by Eq. (52). As shown by Hashin and Shtrikman,⁽¹³⁰⁾ the Maxwell relationship is an upper bound.

Rayleigh⁽¹³¹⁾ treated the case of spheres of uniform size arranged in cubical lattice positions, where the field is perpendicular to a side of the cube, and arrived at

$$\frac{\kappa}{\kappa_L} = 1 - \frac{3}{\frac{2 + \kappa_G/\kappa_L}{1 - \kappa_G/\kappa_L} + \varphi - 0.522\varphi^{10/3} \frac{1 - \kappa_G/\kappa_L}{4/3 + \kappa_G/\kappa_L}} \quad (64)$$

written with consideration of a correction by Runge.⁽¹³²⁾ A modified derivation of Eq. (64) for the conductivity of a cubical array of spheres in a continuum was given by Meredith and Tobias,⁽¹³³⁾

$$\frac{\kappa}{\kappa_L} = 1 - \frac{3\varphi}{\frac{2 + \kappa_G/\kappa_L}{1 - \kappa_G/\kappa_L} + \varphi - 1.315\varphi^{10/3} / \left(\frac{4/3 + \kappa_G/\kappa_L}{1 - \kappa_G/\kappa_L} + 0.409\varphi^{7/3} \right)} \quad (65)$$

showing an improvement for high values of φ over the classical equations.

Bruggeman⁽¹³⁴⁾ assumed that in mixtures with high fractions of the dispersed component the conductivity of the medium surrounding a particle will be more accurately expressed by the conductivity of the mixture as a whole. Based on Maxwell's result, he obtained from Eq. (63) for spheres

$$1 - \varphi = \frac{\kappa_G - \kappa}{\kappa_G - \kappa_L} \left(\frac{\kappa_L}{\kappa} \right)^{1/3} \quad (66)$$

Various other equations were presented in the valuable review by Meredith and Tobias.⁽¹³⁵⁾

The equations simplify considerably for nonconducting spheres as applies for gas bubbles. For the special case, $\kappa_G/\kappa_L = 0$, Eq. (63) results in

$$\frac{\kappa}{\kappa_L} = 1 - \frac{3}{2/\varphi + 1} \quad (63a)$$

and the Bruggeman equation (66) takes the simple form

$$\frac{\kappa}{\kappa_L} = (1 - \varphi)^{3/2} \quad (66a)$$

As may be seen from a comparison of Eq. (63a) with a series extension of Eq. (66a), both equations coincide for small values of the gas fraction φ . A simplified expression⁽¹³⁶⁾

$$\frac{\kappa}{\kappa_L} = 1 - 1.5\varphi \quad (63b)$$

is useful for $\varphi < 0.1$.

Eqs. (63) and (66) are shown in Figure 13. It is not easy to decide which is the most adequate of the theoretical equations, since the differences between them are rather small and the experimental findings diverge. Tobias and coworkers^(135,137) compared the equations with various experimental data and found Eq. (63) superior for low fractions of gas ($\varphi < 0.1$), whereas for larger volume fractions and various sizes of the dispersed spheres Eq. (66) was found to fit the experimental data. In contrast, Turner⁽¹³⁸⁾ considered the Maxwell equation (63) to hold very well in comparison to experimental results for large volume fractions also. It appears doubtful—at least where the conductivity of gas-bubble-filled electrolytes is concerned—whether repeated efforts

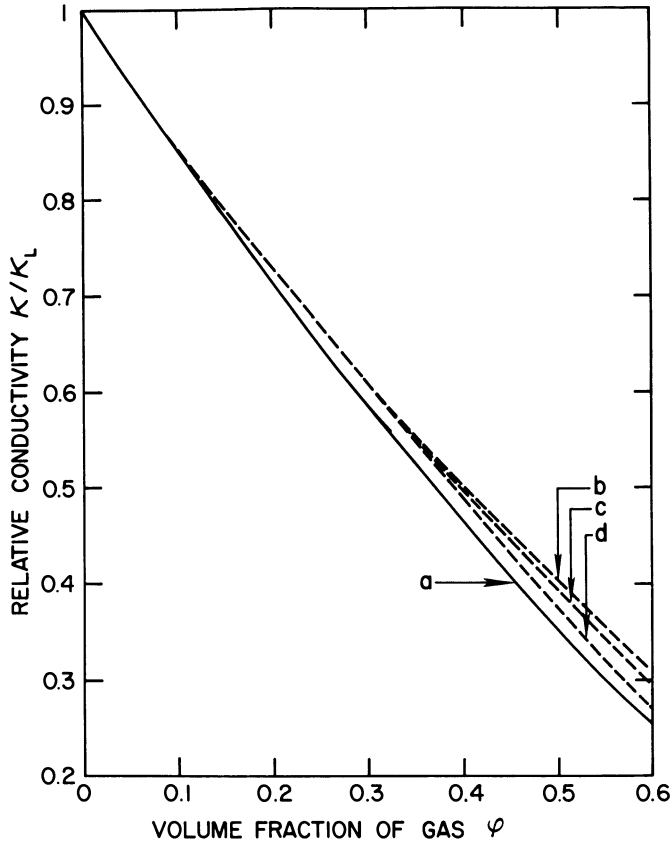


Figure 13. Effective conductivity of a bubble-filled electrolyte depending on the volumetric gas fraction: Curve a, Eq. (66a); b, Eq. (63a); c, Eq. (64); d, Eq. (65).

to improve the simple classical relationships by more sophisticated ones are justifiable. Additional references related to the problem are listed by Jeffrey⁽¹³⁹⁾ and Turner.⁽¹³⁸⁾

Purely empirical equations have been collected and compared by Meredith and Tobias⁽¹³⁵⁾ and were found inferior to the best theoretical ones.

8.2. Rising Velocity of Gas Bubbles

In a quiescent electrolyte, the gas bubbles move with the rising velocity. Steady-state rising velocity v_r of a single gas bubble relative to an infinitely extended liquid can be predicted from

$$v_r = \left[\frac{4}{3} \frac{gd}{\zeta} \left(1 - \frac{\rho_G}{\rho_L} \right) \right]^{0.5} \quad (67)$$

For bubbles with very small diameters d , having a spherical shape, the Stokes law is valid. The friction factor:

$$\zeta = \frac{24\nu_L}{v_r d} = \frac{24}{\text{Re}}$$

applies to the case where the gas-liquid interface is rigid as with solid spheres. Recent investigations have shown that this behavior is restricted to bubbles in liquids with surface active agents.⁽¹⁰⁰⁾ In common electrolytes, a circulation inside the bubble develops,⁽¹⁴⁰⁾ see Figure 14. The interface is shifted and consequently the resistance decreases compared to solid spheres. Mobility of the interface depends on the ratio of the dynamic viscosities of the two phases and was taken into account by Hadamard⁽¹⁴²⁾ and Rybczyński.⁽¹⁴³⁾ For gas bubbles in liquids, the coefficient is reduced to $\zeta = 16/\text{Re}$ as long as inertia forces are negligible; i.e., for Reynolds numbers $\text{Re} < 1.4$.⁽¹⁴¹⁾ Equation (67) reduces to^(100,144)

$$v_r = \frac{gd^2}{12\nu_L} \left(1 - \frac{\rho_G}{\rho_L} \right) \quad (68)$$

which usually applies to bubbles from gas-evolving electrodes. A more extended range for spherical bubbles is described by⁽¹⁴¹⁾

$$\zeta = \frac{16}{\text{Re}} + \frac{14.9}{\text{Re}^{0.78}(1 + 10 \text{Re}^{-0.6})} \quad (69)$$

valid for Reynolds numbers

$$\text{Re} = \frac{v_r d}{\nu_L} < 2.3 \left(\frac{\gamma^3}{g\nu_L^4 \rho_L^3} \right)^{0.209} \quad (70)$$

Higher Reynolds numbers lead to deformation of spherical bubbles.

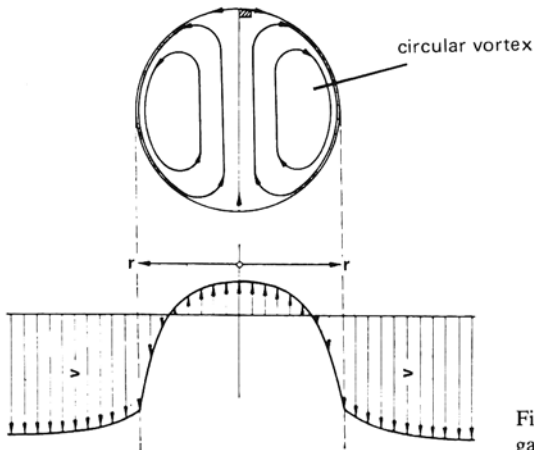


Figure 14. Circulation flow inside moving gas bubbles.⁽¹⁴¹⁾

Steady-state rising velocity is attained asymptotically after bubble departure from the electrode. For partial estimation of a nonsteady-state distance an arbitrary distance $y_{0.95}$ is useful, being the vertical distance of accelerated rise of a bubble which starts with the velocity $v = 0$. It must be taken into account that apart from the mass of gas a certain mass of liquid must be accelerated. Assuming that this liquid mass may correspond to half the bubble volume, the distance is

$$y_{0.95} = 2.05 \frac{v_r^2}{g} \frac{0.5 + \rho_G/\rho_L}{1 - \rho_G/\rho_L} \approx \frac{v_r^2}{g} \quad (71)$$

For example, a bubble of diameter $d = 50 \mu\text{m}$ rises in a usual aqueous electrolyte solution with a relative rising velocity of about 2 mm s^{-1} . If the fact that the real bubble deforms during detachment from the electrode is disregarded, it is found that the bubble attains 95% of the steady-state rising velocity within a distance of less than $1 \mu\text{m}$.

The terminal rising velocity of bubbles in a swarm may differ substantially from the velocity of a single bubble in an infinitely extended liquid as discussed so far. If the bubbles form a cluster at low gas fractions, the velocity distributions around the bubbles interact in such a way that the drag is lowered and the rising velocity increases in comparison to a single bubble. The maximum effect is attained at gas fractions of about $\varphi = 1\text{--}2\%$. As the gas fraction increases further, the rising velocity decreases for all bubble arrangements due to other effects: In a closed system, bubbles in a swarm rising relative to the surrounding liquid cause a counterflow to satisfy the continuity condition so that the velocity with respect to a fixed horizontal plane is decreased. Furthermore, the liquid between the bubbles exhibits velocity gradients varying with time and space and induces an enlarged momentum transfer which also results in an increased drag—an effect which is attributed to swarm turbulence. Both effects simultaneously gain in influence as the gas fraction increases. They are shown separately in the theoretical treatment of Kaskas⁽¹⁴⁴⁾ which gives for dispersions of uniformly sized, spherical, solid particles in liquids⁽¹⁴⁵⁾

$$\frac{v_{rs}}{v_r} = \frac{1}{1 + \frac{\varphi}{(1 - \varphi)^2}} \cdot \frac{1 - \varphi}{1 + \frac{1.05}{[1 + (\pi/12\varphi)^2]^{0.5} - 0.5}} \quad (72)$$

where v_{rs} is the rising velocity of bubbles in a swarm and v_r is the rising velocity of an isolated bubble. Equation (72) is in satisfactory agreement with the experimental data of Richardson and Zaki⁽¹⁴⁶⁾ expressed by

$$\frac{v_{rs}}{v_r} = (1 - \varphi)^{4.65} \quad (73)$$

In an open system a counterflow of liquid does not develop. Impediment of the bubble rising velocity is solely caused by swarm turbulence. The first

term of the right-hand side of Eq. (72) must be set equal to unity, and the rising velocity results in⁽¹⁴⁵⁾

$$\frac{v_{rs}}{v_r} = \frac{1 - \varphi}{1 + \frac{1.05}{(1 + 0.0685/\varphi^2)^{0.5} - 0.5}} \quad (74)$$

or, in a rough approximation restricted to $\varphi < 0.3$,

$$\frac{v_{rs}}{v_r} = (1 - \varphi)^4 \quad (75)$$

8.3. Current Distribution and Ohmic Resistance

Knowledge of the local effective resistance of the bubble-filled electrolyte and the resulting distribution of the current density over the electrode surface is of great relevance in industrial cell design and operation. Experiments with cells operated under technical conditions have been conducted to determine the local gas fraction^(147,148) and the relative resistivity of bubble-filled electrolytes,^(149,150) and valuable results are available. However, measurements are difficult and the data obtained are restricted to special geometries and arrangements. A general prediction of the current distribution and the effective ohmic resistance is not less difficult since they depend on the local values of gas fraction, bubble rising velocity (and therefore on the mean bubble diameter), on the electrolyte flow velocity, the cell geometry, and other parameters. Nevertheless, some practical results based on and restricted to simplifying approximations can be given.

For gas bubbles escaping from the interelectrode space only through the top sectional area and with uniform distribution over the sectional area, the problem can be analyzed using a simple model introduced by Tobias⁽¹⁵¹⁾ (Figure 15). Gas bubbles rise in the interelectrode space. The volume fraction of gas in electrolyte varies with the level x . Hence, the effective conductivity of the mixture and the current density depend on the level also. A volume element of the interelectrode space, located at the distance x from the bottom of the cell as shown in Figure 15, is considered. Its volume fraction of gas in electrolyte at the length x is defined by

$$\varphi_x = \frac{dV_{G,x}}{ws dx} \quad (76)$$

Introducing an absolute gas velocity at x , $v_{G,x} = dx/dt$, the gas flow rate may be written

$$\frac{dV_{G,x}}{dt} = \dot{V}_{G,x} = \varphi_x w s v_{G,x} \quad (77)$$

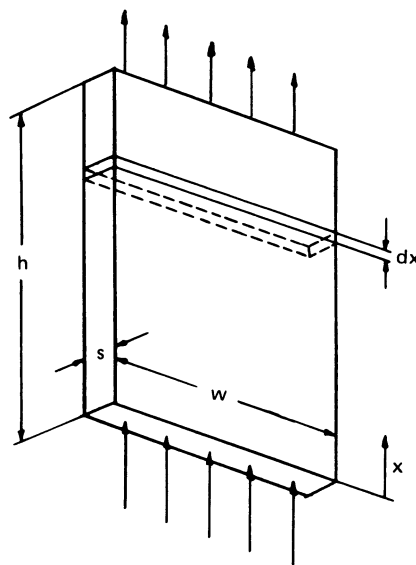


Figure 15. Model of gas-evolving cell.

and equals the total flow rate of gas evolved at the electrode area below x :

$$\dot{V}_{G,x} = wC_4 \int_0^x j dx \quad (78)$$

where

$$C_4 = \frac{RT\varepsilon}{pFn} \quad (79)$$

or—for the case of both electrodes evolving gas and elevated temperatures where it might be necessary to consider the vapor pressure p_v of the solvent—

$$C_4 = \frac{RT}{(p - p_v)F} \left[\left(\frac{\varepsilon}{n} \right)_A + \left(\frac{\varepsilon}{n} \right)_C \right] \quad (79)$$

The gas velocity $v_{G,x}$ with respect to the cell is composed of the mean rising velocity of the bubble swarm and the flow velocity of the liquid entraining the swarm and is, therefore, a function of x :

$$v_{G,x} = v_r(1 - \varphi_x)^4 + \frac{\dot{V}_L}{sw(1 - \varphi_x)} \quad (80)$$

The current-dependent portion of the potential drop between the electrodes at a local current density j , governed by the effective resistivity of the gas in electrolyte dispersion and by the overpotentials, is written in a nondimensional form

$$\left(\frac{\Delta\phi}{j} \right)_x \frac{\kappa_L}{s} = \frac{\kappa_L}{\kappa} + \text{Wa} \quad (81)$$

where the Wagner number[†] Wa —formed with the interelectrode distance and the conductivity of the bubble free electrolyte—

$$Wa = \frac{d\eta \kappa_L}{dj s} \quad (82)$$

is approximately taken as independent of the current density; i.e., the polarization is linear.

If, in agreement with the treatment of Tobias,⁽¹⁵¹⁾ a stagnant electrolyte is considered ($\dot{V}_L = 0$) and the relative gas bubble rising velocity is taken as independent of x , $v_{G,x} = v_G = \text{const}$ [e.g., setting a mean value from Eq. (75)], Eq. (77) in combination with (78) reduces to

$$d\varphi_x = \frac{d\dot{V}_{G,x}}{swv_G} = \frac{C_4}{sv_G} j dx \quad (83)$$

Furthermore, if the electrodes are assumed equipotential and the influence of the overpotential on the current distribution is disregarded, the local current density from Eq. (81) together with Eq. (66) is

$$j = \frac{\Delta\phi\kappa_L}{s}(1 - \varphi_x)^{1.5} \quad (84)$$

and Eq. (83) can easily be integrated. The local gas fraction results in⁽¹⁵¹⁾

$$\varphi_x = 1 - \left(1 + C_5 \frac{x}{h}\right)^{-2} \quad (85)$$

where the dimensionless parameter is

$$C_5 = \frac{\Delta\phi\kappa_L h C_4}{2v_G s^2} \quad (86)$$

The local current density distribution follows by combination of Eqs. (84), (85), and (66):

$$j = \frac{\Delta\phi\kappa_L}{s(1 + C_5 x/h)^3} \quad (87)$$

The mean relative resistivity of the bubble-filled electrolyte results from Eq. (87) by integration over the total height of cell:

$$\frac{\Delta\phi A \kappa_L (1 + C_5)^2}{Is \quad 1 + C_5/2} \quad (88)$$

Equations (85)–(88) are valuable since they allow estimation of the voltage drop and current distribution in industrial cells. However, it must not be overlooked that the model used is based on some assumptions which

[†] See Chapter 4, Section 6.1.

involve substantial deviations from reality. For one of them, the disregard of overpotential influence was estimated by an approximation of Tobias⁽¹⁵¹⁾ showing under unfavorable conditions a noticeable leveling of the current distribution and substantial deviation from the equations given. Another assumption taking the gas fraction as constant over the whole sectional area at each position x is at least questionable since in real cells an enlarged gas concentration in the vicinity of the gas-evolving electrode would be encountered. Furthermore, it is evident that neglecting the electrolyte flow is a condition which is not representative of most industrial cells where swift removal of gas is a major object in cell operation. In industrial cells it is common to have a rapidly moving electrolyte, the velocity of which is greater than the relative bubble rise velocity by some orders of magnitude. Indeed, as experimentally confirmed by Thorpe and coworkers^(79,152) at a water electrolysis cell, the slip ratio of gas bubbles and surrounding liquid is for practical purposes equal to unity. It would thus appear an adequate simplification to completely disregard the rising velocity v_r instead of \dot{V}_L .

Roušar and coworkers carried out a detailed analysis of flowing electrolyte in cells with bipolar⁽¹⁵³⁻¹⁵⁶⁾ and unipolar electrodes.⁽¹⁵⁷⁾ The basis of the work is discussed in the following, disregarding here the effect of potential drop in the electrodes and the bubble separator channels. Combining the absolute liquid flow rate

$$\dot{V}_L = (1 - \varphi_x)wsv_{L,x} \quad (89)$$

with the corresponding equation for the gas flow rate, Eq. (77), results in

$$\frac{\dot{V}_{G,x}}{\dot{V}_L} = \frac{\varphi_x v_{G,x}}{1 - \varphi_x v_{L,x}} \quad (90)$$

where the velocity ratio may be set equal to unity if the relative bubble rise velocity v_r is considered negligible.† Introducing Eq. (76) together with the Maxwell equation (63a) into Eq. (81), instead of (66a) to consider the influence of the gas fraction on the effective conductivity, results in

$$\left(\frac{\Delta\phi}{j}\right)_x \frac{\kappa_L}{s} = 1 + 1.5 \frac{\dot{V}_G A}{\dot{V}_L Ih} \int_0^x j dx + Wa \quad (91)$$

\dot{V}_G is the total gas flow rate evolved in the flow channel of the cell, and h denotes the total length of the electrode in flow direction, not necessarily the height. Assuming equipotential electrodes, the mean relative resistivity of the bubble-filled electrolyte compared to a bubble-free one results in

$$\frac{\overline{\Delta\phi A \kappa_L}}{Is} = 1 + 0.75 \frac{\dot{V}_G}{\dot{V}_L} \quad (92)$$

† In Rousar's original treatment v_r is taken into account by using $\dot{V}_G/[\dot{V}_L + v_r ws(1 - \varphi_{x=L})^{4.5}]$ instead of \dot{V}_G/\dot{V}_L in Equation (91).

where $\overline{\Delta\phi}$ denotes the mean ohmic potential drop across the electrolyte. The current distribution results in

$$\frac{j}{I/A} = \frac{1 + C_6}{[4(x/L)(1 + C_6) + C_6^2]^{0.5}} \quad (93)$$

where

$$C_6 = \frac{4}{3} \frac{\dot{V}_L}{\dot{V}_G} (1 + \text{Wa}) \quad (94)$$

A further rather rough analysis in context with a problem in organic electrosynthesis was presented by Beck.⁽¹⁵⁸⁾ Nagy⁽¹⁵⁹⁾ calculated the current distribution under the influence of gas bubbles for the special geometry of a diaphragm cell, using the Bruggeman equation (66a) and considering the overpotential, but for a stagnant electrolyte only.

Equation (88) is useful in optimizing electrode spacing with respect to the ohmic voltage drop in the gas-filled electrolyte. Optimizations of system parameters for cells with stagnant electrolyte were conducted by Tobias,^(151,159) by Kurgan and Fioshin,⁽¹⁶⁰⁾ and by Nagy.⁽¹⁵⁹⁾

All theoretical contributions mentioned so far are based on the assumption of a uniform distribution of bubbles at each sectional area perpendicular to the flow direction of gas bubbles. Two models taking into account a nonuniform bubble distribution were suggested by MacMullin (see Reference 149) but were found to disagree strongly with experimental data. Hine *et al.*⁽¹⁴⁹⁾ pointed out that the total ohmic resistance may be affected by a "fixed layer" thus taking into account the well-known fact that near the electrodes a layer of accumulated bubbles or a "bubble curtain" exists with enlarged resistivity and by the remaining bulk layer containing bubbles, too. Based on this idea, a hydrodynamic model for the ohmic interelectrode resistance was developed recently.⁽¹⁶¹⁾

8.4. Influence of Temperature and Pressure

The volume of gas contained in the interelectrode space depends not only on cell flow conditions but also on temperature and pressure of the electrolyte and, hence, of the gas. At elevated temperatures it is not always satisfactory to set the volume of the gaseous phase equal to the volume of gas evolved at the electrodes as was done in the previous section. One must keep in mind that, due to evaporation of electrolyte components corresponding to their vapor pressure at a given temperature and concentration, the real volume of the gaseous phase is larger than the volume V_G evolved at the

electrode. In the extension of Eq. (38) the volume fraction of gas plus vapor is then

$$\varphi = \frac{1}{1 + \frac{V_L (p - p_v)}{V_G p}} \quad (95)$$

where p_v is the vapor pressure of the solvent (water) and p is the total pressure (gas + solvent) in the bubble. At electrolyte temperatures near the boiling point the vapor pressure of aqueous electrolytes may essentially contribute to the total gas-vapor volume and generally prevents cell operation at high temperature—as otherwise desired with respect to gas-free electrolyte conductivity. Moreover, desorption of homogeneously reacting gases by the gas bubbles from the counterelectrode† may additionally contribute to an increase of the total volume and has to be considered in technical cells.

The fact that increasing pressure decreases the gas volume is profitably utilized in pressure electrolysis of water.‡ The phenomenon of a decrease in cell potential as pressure increases has been known for some time and was convincingly interpreted as a result of diminution of gas bubble diameter in bulk liquid and in the pores of the diaphragm.⁽¹⁶²⁾

8.5. Electrode Geometry and Flow Conditions

It is obvious that an undelayed removal of gas out of the interelectrode space is an essential demand in designing industrial cells with gas evolution in order to decrease the fraction of gas in the electrolyte and to lower the voltage drop. High electrolyte velocities are sought. Some cells use centrifugal pumps; others make use of the buoyancy forces developed by the liquid-gas mixture of reduced density and operate a closed-loop system which, if carefully designed, makes a mechanical pumping superfluous.⁽¹⁶³⁾§

Vertical electrodes are preferred from this viewpoint, since the bubble curtain effect is less marked. Perforations of an electrode easily allow a partial gas removal of gas-containing electrolyte out of the interelectrode space (Figure 16). Utmost care is necessary for an unhindered gas removal with horizontal electrodes, especially at large current densities. In addition to the foam layer below the electrode, the area above the lower side of the electrode will be covered by adhering bubbles which may grow to an excessive size and blanket a considerable portion of the electrode surface⁽⁷⁰⁾ if no special arrangements are made. To minimize both effects, vertical bores and slits are used

† For example, chlorine desorption by hydrogen in electrosynthesis of chlorate (see Vol. 2, Chapter 3).

‡ See Volume 2, Chapter 1.

§ See Volume 2, Chapter 3.

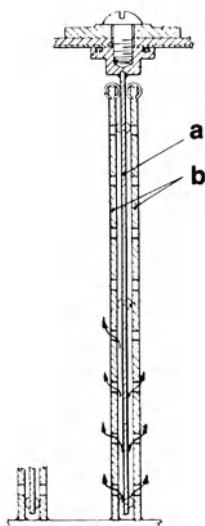


Figure 16. Removal of bubble-containing electrolyte from the interelectrode space through perforations of the cathode⁽¹⁶⁴⁾: a, anode; b, cathode.

on graphite electrodes.^(165–167) Metal electrodes are preferably formed by rods arranged parallel^(168,169) or by nets or screens made of extended metal^(128,168). Recently, even at horizontal electrodes, inclined channels⁽¹⁷⁰⁾ were successfully applied to make use of the self-convection of the bubble-filled electrolyte (Figure 17).

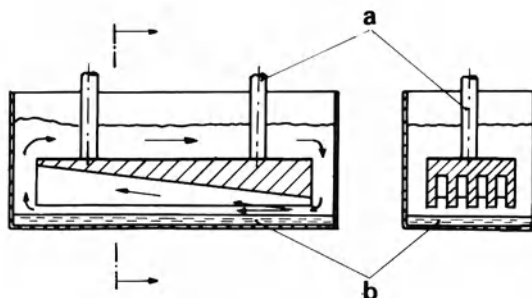


Figure 17. Improved gas removal at horizontal electrodes for alkalichloride electrolyzers according to Müller.⁽¹⁷⁰⁾

References

1. A. Coehn, Eine Wirkung der elektrostatischen Ladung elektrolytisch entwickelter Gasblasen, *Z. Elektrochem.* **29**, 306–308 (1923).
2. M. C. Witherspoon, R. C. Johnston, and F. A. Lewis, The steady-state hydrogen content of catalytically active noble metal cathodes during hydrogen bubble evolution at high current densities, *Electrochim. Acta* **20**, 519–521 (1975).

3. N. Ibl and D. Landolt, Zur Kinetik der Chlorat-Bildung bei der NaCl-Elektrolyse, *Chem. Ing. Tech.* **39**, 706–712 (1967).
4. D. Landolt and N. Ibl, On the mechanism of anodic chlorate formation in concentrated NaCl solutions, *Electrochim. Acta* **15**, 1165–1183 (1970).
5. A. I. Beljajew, M. B. Rapoport, and L. A. Firsanowa, *Metallurgie des Aluminiums*, Vol. I, pp. 121–131, VEB Verlag Technik, Berlin (1956).
6. L. Ferrand, *Histoire de la Science et des Techniques de l'Aluminium et ses Développements Industriels*, Vol. I, pp. 398–413, Humbert, Largentière (1960).
7. K. Grjotheim, C. Krohn, M. Malinovský, K. Matiašovský, and J. Thonstad, *Aluminium Electrolysis*, pp. 227–241, Aluminium-Verlag, Düsseldorf (1977).
8. N. Ibl, Probleme des konvektiven Stofftransports bei der Elektrolyse, *Chem. Ing. Tech.* **33**, 69–74 (1961).
9. F. D. Moore and R. B. Mesler, The measurement of rapid surface temperature fluctuations during nucleate boiling of water, *AIChE J.* **7**, 620–624 (1961).
10. W. M. Rohsenow, *Developments in Heat Transfer*, p. 214, M.I.T. Press, Cambridge, MA (1964).
11. S. S. Kutateladze, *Fundamentals of Heat Transfer*, Edward Arnold Ltd., London (1963) p. 385.
12. K. Stephan, *Beitrag zur Thermodynamik des Wärmeübergangs beim Sieden*, Abh. Dt. Kältetechn. Ver. Nr. 18, C. F. Müller, Karlsruhe (1964).
13. M. Volmer, *Kinetik der Phasenbildung*, Steinkopff, Dresden (1939) and Edward Brothers, Ann Arbor, MI (1945).
14. C. A. Ward and A. S. Tucker, Thermodynamic theory of diffusion-controlled bubble growth or dissolution and experimental examination of the predictions, *J. Appl. Phys.* **46**, 233–238 (1975).
15. H. Vogt, Ein Beitrag zum Stoffübergang an gasentwickelnden Elektroden, Diss. University of Stuttgart (1977).
16. S. G. Bankoff, Entrapment of gas in the spreading of a liquid over a rough surface, *AIChE J.* **4**, 24–26 (1958).
17. R. Cole, Boiling nucleation, *Adv. Heat Transfer* **10**, 85–166 (1974).
18. R. Piontelli, B. Mazza, P. Pedefferri, and R. Tognoni, Ricerche sullo sviluppo elettrodico di gas e sugli effetti anomali che lo accompagnano. I. Sviluppo da soluzione acquose, *Electrochim. Met.* **2**, 257–287 (1967).
19. S. van Stralen and R. Cole, *Boiling Phenomena*, Vol. 1, Chapter 13, Hemisphere Publishing, Washington (1980).
20. H. Y. Cheh, On the mechanism of electrolytic gas evolution. Diss. University of California, Berkeley (1967).
21. S. Shibata, Supersaturation of oxygen in acidic solution in the vicinity of an oxygen-evolving platinum anode, *Electrochim. Acta* **23**, 619–623 (1978).
22. S. Shibata, The concentration of molecular hydrogen on the platinum cathode, *Bull. Chem. Soc. Jap.* **36**, 53–57 (1963).
23. S. Shibata, Supersolubility of hydrogen in acidic solution in the vicinity of hydrogen-evolving platinum cathodes in different surface states, *Denki Kagaku* **44**, 709–712 (1976).
24. C. K. Bon and C. W. Tobias, Supersaturation at gas-evolving electrodes, *J. Electrochem. Soc.* **115**, 91C (1968).
25. H. Vogt, Physikalische Vorgänge an gasentwickelnden Elektroden, *Chem. Ing. Tech.* **52**, 418–423 (1980).
26. H. Vogt, On the supersaturation of gas in the concentration boundary layer of gas evolving electrodes, *Electrochim. Acta* **25**, 527–531 (1980).
27. K. Stephan, Mechanismus und Modellgesetz des Wärmeübergangs bei der Blasenverdampfung, *Chem. Ing. Tech.* **35**, 775–784 (1963).

28. V. I. Kozitskii, Heat transfer coefficients during the boiling of *n*-butane on surfaces of various roughnesses. *Int. Chem. Eng.* **12**, 685–686 (1972); *Khim. Neft. Mash.* **1**, 11–12 (1972).
29. G. H. Nix, R. I. Vachon, and D. M. Hall, A scanning and transmission electron microscopy study of pool boiling surfaces. In: *Heat Transfer*, U. Grigull and E. Hahne, Eds., Vol. 5, B1.6, Elsevier, Amsterdam (1970).
30. R. Kind, Untersuchung des Stofftransports und der Rührwirkung bei gasentwickelnden Elektroden, Diss. ETH Zürich (1975).
31. N. Ibl, R. Kind, and E. Adam, Mass transfer at electrodes with gas stirring, *An. R. Soc. Esp. Fis. Quim.* **71**, 1008–1016 (1975).
32. A. C. C. Tseung and P. R. Vassie, A study of gas evolution in Teflon bonded porous electrodes, *Electrochim. Acta* **21**, 315–318 (1976).
33. Y. Heled and A. Orell, Characteristics of active nucleation sites in pool boiling, *Int. J. Heat Mass Transfer* **10**, 553–554 (1967).
34. Lord Rayleigh, On the pressure developed in a liquid during the collapse of a spherical cavity, *Phil. Mag.* **34**, 94–98 (1917).
35. J. P. Glas and J. W. Westwater, Measurements of the growth of electrolytic bubbles, *Int. J. Heat Mass Transfer* **7**, 1427–1443 (1964).
36. P. S. Epstein and M. S. Plesset, On the stability of gas bubbles in liquid–gas solutions, *J. Chem. Phys.* **18**, 1505–1509 (1950).
37. I. Langmuir, The evaporation of small spheres, *Phys. Rev.* **12**, 368–370 (1918).
38. G. Birkhoff, R. S. Margulies, and W. A. Horning, Spherical bubble growth, *Phys. Fluids* **1**, 201–204 (1958).
39. L. E. Scriven, On the dynamics of phase growth. *Chem. Eng. Sci.* **10**, 1–13 (1959).
40. W. M. Buehl and J. W. Westwater, Bubble growth by dissolution: Influence of contact angle, *AIChE J.* **12**, 571–576 (1966).
41. J. E. Burman and G. J. Jameson, Diffusional mass transfer to a growing bubble, *Chem. Eng. Sci.* **31**, 401–403 (1976).
42. H. K. Forster and N. Zuber, Growth of a vapour bubble in superheated liquid, *J. Appl. Phys.* **25**, 474–478 (1954).
43. M. S. Plesset and S. A. Zwick, The growth of vapour bubbles in superheated liquids, *J. Appl. Phys.* **25**, 493–500 (1954).
44. S. J. D. van Stralen, The growth rate of vapour bubbles in superheated pure liquids and binary mixtures, *Int. J. Heat Mass Transfer* **11**, 1467–1488 (1968).
45. N. H. Afgan, Boiling liquid superheat, *Adv. Heat Transfer* **11**, 1–49 (1975).
46. D. E. Westerheide and J. W. Westwater, Isothermal growth of hydrogen bubbles during electrolysis, *AIChE J.* **7**, 357–362 (1961).
47. H. Y. Cheh and C. W. Tobias, On the dynamics of hemispherical phase growth in nonuniform concentration fields, *Int. J. Heat Mass Transfer* **11**, 709–719 (1968).
48. J. P. Glas, Microscopic study of electrolytic bubbles, Diss. University of Illinois (1965).
49. R. Darby and M. S. Haque, The dynamics of electrolytic hydrogen bubble evolution, *Chem. Eng. Sci.* **28**, 1129–1138 (1973).
50. H. Vogt, Mass transfer at gas-evolving electrodes with superposition of hydrodynamic flow, *Electrochim. Acta* **23**, 203–205 (1978).
51. R. A. Putt and C. W. Tobias, A photographic study of incipient gas evolution, Electrochemical Society Meeting, 1976, Abstr. 253.
52. G. J. Houston, The anodic evolution and dissolution of chlorine in melts containing aluminium chloride, Thesis, University of New South Wales (1977).
53. L. J. J. Janssen and J. G. Hoogland, The effect of electrolytically evolved gas bubbles on the thickness of the diffusion layer. II, *Electrochim. Acta* **18**, 543–550 (1973).
54. I. W. Wark, The physical chemistry of flotation. I. The significance of contact angle in flotation, *J. Phys. Chem.* **38**, 623–644 (1933).

55. B. Mazza, P. Pedferri, R. Piontelli, and A. Tognoni, Ricerche sullo sviluppo elettrodico di gas e sugli effetti anomali che lo accompagnano. III. Teoria e discussione, *Electrochim. Metal.* **2**, 385–436 (1967).
56. N. Ibl, E. Adam, J. Venczel, and E. Schalch, Stofftransport bei der Elektrolyse mit Gasrührung, *Chem. Ing. Tech.* **43**, 202–215 (1971).
57. N. Ibl and J. Venczel, Die elektrolytische Gasentwicklung, *Oberfläche-Surface* **13**, 1–8 (1972).
58. U. Magrini, Tentativo di correlazione delle varibili nella trasmissione del calore in fluidi bifasi con aeriforme di origine elettrolitica, *Calore* **37**, 125–134 (1966).
59. W. Fritz, Berechnung des Maximalvolumens von Dampfblasen, *Phys. Z.* **36**, 379–384 (1935).
60. W. Fritz and W. D. Ende, Über den Verdampfungsvorgang nach kinematographischen aufnahmen von dampfblasen, *Phys. Z.* **37**, 391–401 (1936).
61. F. Bashford and J. C. Adams, *An Attempt to Test the Theories of Capillary Action*, University Press, Cambridge (1883).
62. B. Kabanow and A. Frumkin, Über die Grösse elektrolytisch entwickelter Gasblasen, *Z. Phys. Chem.* **165**, 433–452 (1933); **166**, 316–317 (1933).
63. A. M. Arthur, The solubility of aluminum in cryolite–alumina metals and the mechanism of metal loss, *Met. Trans.* **5**, 1225–1230 (1974).
64. R. C. Dorward, Reaction between aluminum and graphite in the presence of cryolite, *Met. Trans.* **4**, 386–388 (1973).
65. G. Lippmann, Beziehungen zwischen den capillaren und elektrischen Erscheinungen, *Ann. Phys. Chem.* **149**, 547 (1873).
66. H. G. Möller, Zur Theorie der Überspannung bei elektrolytischer Gasabscheidung, *Ann. Phys.* **25**, 725–744 (1908).
67. H. G. Möller, Elektrolytische Vorgänge an der Elektrodenoberfläche. Überspannung und Elektrokapillarität, *Z. Phys. Chem.* **65**, 226–254 (1909).
68. P. Drossbach and P. Krahl, Zur Kenntnis des Anodeneffekts. II, *Z. Elektrochem. Ber. Bunsenges. Phys. Chem.* **62**, 178–180 (1958).
69. R. Kind, Untersuchung des Stofftransports und der Rührwirkung bei gasentwickelnden elektroden, Diss. ETH Zürich (1975).
70. J. Venczel, Über den Stofftransport an gasentwickelnden Elektroden, Diss. ETH Zürich (1961).
71. N. Ibl and J. Venczel, Stofftransport an gasentwickelnden Elektroden, *Metalloberfläche* **24**, 365–374 (1970).
72. J. Venczel, Über Gasblasen bei elektrochemischen Prozessen, *Electrochim. Acta* **15**, 1909–1920 (1970).
73. A. Coehn and H. Neumann, Elektrostatische Erscheinungen an elektrolytisch entwickelten Gasblasen. I, *Z. Phys.* **20**, 54–68 (1923).
74. L. J. J. Janssen and J. G. Hoogland, The effect of electrolytically evolved gas bubbles on the thickness of the diffusion layer, *Electrochim. Acta* **15**, 1013–1023 (1970).
75. D. Landolt, R. Acosta, R. H. Muller, and C. W. Tobias, An optical study of cathodic hydrogen evolution in high-rate electrolysis, *J. Electrochem. Soc.* **117**, 839–845 (1970).
76. I. Roušar, J. Kačín, E. Lippert, F. Šmirous, and V. Cezner, Transport of mass or heat to an electrode in the region of hydrogen evolution. II, *Electrochim. Acta* **20**, 295–299 (1975).
77. L. J. J. Janssen, Mass transfer at gas evolving electrodes, *Electrochim. Acta* **23**, 81–86 (1978).
78. M. J. Blandamer, F. Franks, K. H. Haywood, and A. C. Tory, Effect of added solutes on the size of hydrogen bubbles liberated from a cathodic wire in aqueous solutions, *Nature (London)* **216**, 783–784 (1967).
79. J. F. Thorpe, J. E. Funk, and T. Y. Bong, Void fraction and pressure drop in a water electrolysis cell, *J. Basic Eng.* **92**, 173–182 (1970).

80. A. Coehn, Wovon hängt das Haften und die Grösse elektrolytisch entwickelter Gasblasen ab? *Z. Elektrochem.* **29**, 1–5, 88 (1923).
81. A. Coehn and H. Mozer, Über die Berührungselektrizität von Gasen gegen leitende und nichtleitende Flüssigkeiten, *Ann. Phys.* **43**, 1048–1078 (1914).
82. I. V. Kadija, B. Ž. Nikolić, and A. R. Despić, Mass transfer during gas evolution on the rotating double-ring electrode, *J. Electroanal. Chem. Interfacial Electrochem.* **57**, 35–52 (1974).
83. E. A. Ukshe, G. V. Polyakova, and G. A. Medvetskaya, Dynamics of chlorine and magnesium in electrolysis of fused chlorides, *J. Appl. Chem. USSR* **33**, 2246–2251 (1960) [*Zh. Prikl. Khim.* **33**, 2279–2284 (1960).]
84. R. C. Hannah and B. J. Welch, The behaviour of chlorine bubbles in aluminium chloride reduction cells. 107th AIME Meeting Denver, 1978, *Light Metals*, Vol. 1, pp. 165–174.
85. A. V. Lookichev and W. W. Smeltzer, The development of a grooved periodic morphology on nickel–aluminum alloys electropolished under gaseous discharge, *J. Electrochem. Soc.* **126**, 574–579 (1979).
86. M. G. Fouad and G. H. Sedahmed, Mass transfer at horizontal gas-evolving electrodes, *Electrochim. Acta* **18**, 55–58 (1973).
87. M. G. Fouad, G. H. Sedahmed, and H. A. El-Abd, The combined effect of gas evolution and surface roughness on the rate of mass transfer, *Electrochim. Acta* **18**, 279–281 (1973).
88. T. R. Beck, A contribution to the theory of electrolytic chlorate formation, *J. Electrochem. Soc.* **116**, 1038–1041 (1969).
89. M. Green and P. H. Robinson, Kinetics of the cathodic reduction of anions, *J. Electrochem. Soc.* **106**, 253–260 (1959).
90. J. Vondrák and J. Balej, Influence of mercury on hydrogen overvoltage on solid metal electrodes. I., *Electrochim. Acta* **15**, 1653–1665 (1970).
91. B. Roald and W. Beck, The dissolution of magnesium in hydrochloric acid, *J. Electrochem. Soc.* **98**, 277–290 (1951).
92. N. Ibl, Probleme des Stofftransports in der angewandten Elektrochemie, *Chem. Ing. Tech.* **35**, 353–361 (1963).
93. N. Ibl and G. Trümpler, Über zwei Elektrolyseprobleme mit linearer Diffusion bei Abwesenheit von Konvektion, *Helv. Chim. Acta* **34**, 1217–1223 (1951).
94. F. G. Cottrell, Der Reststrom bei galvanischer Polarisation, betrachtet als ein Diffusionsproblem, *Z. Phys. Chem.* **42**, 385 (1903).
95. I. Roušar and V. Cezner, Transfer of mass or heat to an electrode in the region of hydrogen evolution. I., *Electrochim. Acta* **20**, 289–293 (1975).
96. L. J. J. Janssen and S. J. D. van Stralen, Bubble behaviour on and mass transfer to an oxygen-evolving transparent nickel electrode in alkaline solution, *Electrochim. Acta* **26**, 1011–1022 (1981).
97. K. Stephan and H. Vogt, A model for correlating mass transfer data at gas-evolving electrodes, *Electrochim. Acta* **24**, 11–18 (1979).
98. H. Schlichting, *Grenzschichttheorie*, 5th ed., Braun, Karlsruhe (1965). *Boundary-Layer theory*, 4th ed., McGraw-Hill, London (1960).
99. E. Polhausen, Der wärmeaustausch zwischen festen Körpern und Flüssigkeiten mit kleiner Reibung und kleiner Wärmeleitung, *Z. Angew. Math. Mech.* **1**, 115–121 (1921).
100. V. G. Levich, *Physicochemical Hydrodynamics*, Prentice-Hall, Englewood Cliffs, NJ (1962).
101. L. J. J. Janssen and E. Barendrecht, The effect of electrolytic gas evolution on mass transfer at electrodes, *Electrochim. Acta* **24**, 693–699 (1979).
102. N. Zuber, Nucleate boiling. The region of isolated bubbles and the similarity with natural convection, *Int. J. Heat Mass Transfer* **6**, 53–78 (1963).
103. L. Sigrist, Verfahrenstechnische Aspekte von Elektrolysezellen mit stark gasenden Elektroden, Diss. ETH Zürich (1978).

104. L. Sigrist, O. Dossenbach, and N. Ibl, Mass transport in electrolytic cells with gas sparging, *Int. J. Heat Mass Transfer* **22**, 1393–1399 (1979).
105. N. Ibl, Notes on mass transfer at gas sparged electrodes, *Electrochim. Acta* **24**, 1105–1108 (1979).
106. M. G. Fouad and G. H. Sedahmed, Effect of gas evolution on the rate of mass transfer at vertical electrodes, *Electrochim. Acta* **17**, 665–672 (1972).
107. M. D. Birkett and A. Kuhn, Combined effects in mass transfer to a planar electrode, *Electrochim. Acta* **22**, 1427–1429 (1977).
108. S. S. Kutateladze, Boiling Heat Transfer, *Int. J. Heat Mass Transfer* **4**, 31–45 (1961).
109. W. G. Clark and J. A. McGeough, Temperature distribution along the gap in electrochemical machining, *J. Appl. Electrochem.* **7**, 277–286 (1977).
110. H. Vogt, Heat transfer at gas-evolving electrodes, *Electrochim. Acta* **23**, 1019–1022 (1978).
111. J. Thonstad, F. Nordmo, and K. Vee, On the anode effect in cryolite-alumina melts. I. *Electrochim. Acta* **18**, 27–32 (1973).
112. A. Kerouanton, C. Gabrielli, M. Keddad, and V. Plichon, Etude de l'effet d'anode dans le cryolithe fondue à l'aide d'une régulation à impédance interne négative, *Electroanal. Chem. Interf. Electrochem.* **57**, 273–277 (1974).
113. R. Tunold and T. Berge, The anode effect in a silver chloride/sodium chloride melt, *Electrochim. Acta* **19**, 849–854 (1974).
114. J. W. Westwater and J. G. Santangelo, Photographic study of boiling, *Ind. Eng. Chem.* **47**, 1605–1610 (1955).
115. A. Vajna de Pava, Ripresa cinematografica di alcuni fenomeni anodici nella elettrolisi ignea dell'allumina, *Electrochim. Metal.* **3**, 376–378 (1968).
116. N. Zuber, On the stability of boiling heat transfer, *J. Heat Transfer-Trans. ASME* **80**, 711–714, 718–720 (1958).
117. L. S. Tong, *Boiling Heat Transfer and Two-Phase Flow*, Wiley, New York (1965).
118. L. M. Milne-Thomson, *Theoretical Hydrodynamics*, p. 410, MacMillan, London (1960).
119. R. Lamb, *Hydrodynamics*, University Press, Cambridge (1932). a) p. 457, b) p. 462.
120. G. I. Taylor and D. J. Lewis, The instability of liquid surfaces when accelerated in a direction perpendicular to their planes, *Proc. R. Soc. Lond. A* **201**, 192–196 (1950) (Taylor). *Proc. R. Soc. Lond. A* **202**, 81–96 (1950) (Lewis).
121. N. Zuber, Comment on: P. J. Berenson, Film boiling heat transfer from a horizontal surface, *J. Heat Transfer-Trans. ASME* **83**, 357–358 (1961).
122. H. von Helmholtz, Über atmosphärische Bewegungen. Zur Theorie von Wind und Wellen, *Sitzungsber. Kgl. Preuss. Akad. Wiss. Berlin* 761–780 (1889).
123. H. von Helmholtz, Die Energie der Wogen und des Windes, *Sitzungsber. Kgl. Preuss. Akad. Wiss. Berlin* 853–872 (1890).
124. S. S. Kutateladze, A hydrodynamic theory of changes in the boiling process under free convection conditions, *Isv. Akad. Nauk. USSR Otd. Tekh. Nauk.* No. 4, 529 (1951).
125. B. Mazza, P. Pedferri, and A. Tognoni, Ricerche sull' effetto anodico nelle celle per alluminio, *Chimica Ind.* **53**, 123–132 (1971).
126. D. L. Katz, Comment on: N. Zuber, On the stability of boiling heat transfer, *J. Heat Transfer-Trans. ASME* **80**, 716 (1958).
127. B. Mazza, P. Pedferri, and G. Re, Hydrodynamic instabilities in electrolytic gas evolution, *Electrochim. Acta* **23**, 87–93 (1978).
128. O. de Nora, Anwendung maßbeständiger aktivierter Titan-Anoden bei der Chloralkali-Elektrolyse. *Chem. Ing. Tech.* **42**, 222–226 (1970).
129. J. C. Maxwell, *A Treatise on Electricity and Magnetism*, Vol. 1, 3rd ed., p. 440, Clarendon Press, Oxford (1892).
130. Z. Hashin and S. Shtrikman, A variational approach to the theory of the effective magnetic permeability of multiphase materials, *J. Appl. Phys.* **33**, 3125–3131 (1962).

131. Lord Rayleigh, On the influence of obstacles arranged in rectangular order upon the properties of a medium, *Phil. Mag.* **34**, 481–502 (1892).
132. I. Runge, Zur elektrischen Leitfähigkeit metallischer Aggregate, *Z. tech. Phys.* **6**, 61–68 (1925).
133. R. E. Meredith and C. W. Tobias, Resistance to potential flow through a cubical array of spheres, *J. Appl. Phys.* **31**, 1270–1273 (1960).
134. D. A. G. Bruggeman, Berechnung verschiedener physikalischer Konstanten von heterogenen Substanzen. I., *Ann. Phys.* **24**, 659 (1935).
135. R. E. Meredith and C. W. Tobias, Conduction in heterogeneous systems, *Adv. Electrochem. Electrochem. Eng.* **2**, 15–47 (1962).
136. K. W. Wagner, Erklärung der dielektrischen Nachwirkungsvorgänge auf Grund Maxwell'scher Vorstellungen, *Arch. Elektrotechnik* **2**, 371–387 (1914).
137. R. E. de la Rue and C. W. Tobias, On the conductivity of dispersions, *J. Electrochem. Soc.* **106**, 827–833 (1959).
138. J. C. R. Turner, Two-phase conductivity. The electrical conductance of liquid-fluidized bed of spheres, *Chem. Eng. Sci.* **31**, 487–492 (1976).
139. D. J. Jeffrey, Conduction through a random suspension of spheres. *Proc. R. Soc. Lond. A* **335**, 355–376 (1973).
140. F. N. Peebles and H. J. Garber, Studies on the motion of gas bubbles in liquids, *Chem. Eng. Prog.* **49** (2), 88–97 (1953).
141. U. Haas, H. Schmidt-Traub, and H. Brauer, Umströmung kugelförmiger Blasen mit inläufiger Zirkulation, *Chem. Ing. Tech.* **44**, 1060–1068 (1972).
142. J. Hadamard, Mouvement permanent lent d'une sphère liquide et visqueuse dans une liquide visqueuse. *C.R. Acad. Sci. Paris* **152**, 1735–1817 (1911).
143. W. Rybczyński, O ruchu postępowym kuli ciekłej w ośrodku lepkości.—Über die fortschreitende Bewegung einer flüssigen Kugel in einem zähen Medium. *Bull. Int. Acad. Sci. Cracovie, Cl. Sci. Math. Natur., Ser. A*, 1911 Nr. 1A, 40–46.
144. A. A. Kaskas, Diss. Techn. University of Berlin (1971).
145. H. Brauer and H. Thiele, Bewegung von Partikelschwärmen, *Chem. Ing. Techn.* **45**, 909–912 (1973).
146. J. F. Richardson and W. N. Zaki, Sedimentation and fluidization, *Trans. Inst. Chem. Eng.* **32**, 35–53 (1954).
147. V. A. Kryukovskii, P. V. Polyakov, G. V. Forsblom, A. M. Tsyplakov, and V. V. Burnakin, The effect of anode current density on the gas content of aluminum electrolytic cells, *Sov. J. Non-Ferrous Met.* **13**(12), 50–52 (1972). [*Tsvetn. Met.* **45**(12), 62–64 (1972)].
148. A. V. Nikitin, V. A. Kryukovskii, and N. S. Mikhailitsin, Gas impregnation and speed of anode gas flow in high-powered aluminum reduction cells, *Sov. J. Non-Ferrous Met.* **16**(8), 37–40 (1975). [*Tsvetn. Met.* **48**(8), 31–35 (1975)].
149. F. Hine, M. Yasuda, R. Nakamura, and T. Noda, Hydrodynamic studies of bubble effects on the IR-drops in a vertical rectangular cell, *J. Electrochem. Soc.* **122**, 1185–1190 (1975).
150. F. Hine and K. Murakami, Bubble effects on the solution IR-drop in a vertical electrolyzer under free and forced convection, *J. Electrochem. Soc.* **127**, 292 (1980).
151. C. W. Tobias, Effect of gas evolution on current distribution and ohmic resistance in electrolyzers, *J. Electrochem. Soc.* **106**, 833–838 (1959).
152. J. E. Funk and J. F. Thorpe, Void fraction and current density distributions in a water electrolysis cell, *J. Electrochem. Soc.* **116**, 48–54 (1969).
153. I. Roušar, Calculation of current density distribution and terminal voltage for bipolar electrolyzers. Application to chlorate cells, *J. Electrochem. Soc.* **116**, 676–683 (1969).
154. I. Roušar, A. Regner, and V. Cezner, Calculation of the current density distribution and of the terminal voltage for flow electrolyzers, *Coll. Czech. Chem. Comm.* **31**, 4193–4208 (1966).

155. I. Roušar and V. Cezner, Calculation of the current density distribution and of the terminal voltage for flow electrolyzers with the use of criterion relations, *Coll. Czech. Chem. Comm.* **32**, 1137–1151 (1967).
156. I. Roušar, V. Cezner, and J. Hostomský, Calculation of current density distribution and of terminal voltage for nonisothermal flow electrolyzers, *Coll. Czech. Chem. Comm.* **33**, 808–828 (1968).
157. I. Roušar, V. Cezner, J. Nejeřmová, M. M. Jakšić, M. Spasojević, and B. Z. Nikolić, Calculation of local current densities and terminal voltage for a monopolar sandwich electrolyzer: Application to chlorate cells, *J. Appl. Electrochem.* **7**, 427–435 (1977).
158. F. Beck, Kolbesynthese von Sebacinsäureestern in der Kapillarspaltzelle, *Electrochim. Acta* **18**, 359–368 (1973).
159. Z. Nagy, Calculations on the effect of gas evolution on the current–overpotential relation and current distribution in electrolytic cells, *J. Appl. Electrochem.* **6**, 171–181 (1976).
160. B. M. Kurgan and M. Ya. Fiošhin, A method of determining the optimum spacing between electrodes by calculation of the gas-filling, *Sov. Chem. Ind.*, No. 11, 90 (1969). [*Khim. Prom.* **45**, 870 (1969).]
161. H. Vogt, A hydrodynamic model for the ohmic interelectrode resistance of cells with vertical gas evolving electrodes, *Electrochim. Acta* **26**, 1311–1317 (1981).
162. V. Schischkin and I. Dubkof, Über die theoretische Begründung der experimentellen Abhängigkeit der Badspannung vom Druck bei der Wasserelektrolyse, *Z. Elektrochemie* **40**, 724–728 (1934).
163. J. Fleck, Chlorat-Elektrolyse, *Chem. Ing. Tech.* **43**, 173–177 (1971).
164. J. R. Hodges, U.S. Pat. 4 075 077 (Pennwalt Corp.) (1978).
165. R. B. MacMullin, In: *Chlorine. Its Manufacture, Properties and Uses*, J. S. Sconce, Ed., p. 157, Reinhold, New York (1962).
166. K. Hass, New developments in the chlorine–alkali electrolysis process, *Electrochem. Tech.* **5**, 247 (1967).
167. P. A. Danna, The effect of brine level on the voltage of mercury-type chlor-alkali cells, *J. Electrochem. Soc.* **121**, 1286–1289 (1974).
168. A. T. Kuhn, Ed., *Industrial Electrochemical Processes*, p. 553, Elsevier, Amsterdam (1971).
169. K. Hass and P. Schmittinger, Developments in the electrolysis of alkali chloride solutions since 1970, *Electrochim. Acta* **21**, 1115–1126 (1976).
170. J. Müller, Elektrodenformen gaserzeugender Elektrolysen und daraus resultierende Strömungs- und Spannungsverhältnisse, *Chem. Ing. Tech.* **49**, 326–327 (1977).
171. S. S. Kutateladze and V. M. Borishanskii, *A Concise Encyclopedia of Heat Transfer*, p. 168, Pergamon Press, Oxford (1966).
172. H. Brauer and D. Mewes, Strömungswiderstand sowie stationärer Stoff- und Wärmeübergang an Blasen und Tropfen, *Chem. Ing. Tech.* **44**, 953–956 (1972).
173. A. S. Tucker and C. A. Ward, Critical state of bubbles in liquid-gas solutions, *J. Appl. Phys.* **46**, 4801 (1975).

Annotated Author Index

- Alkire, R. and Mirarefi, A., on numerical solution for current distribution for tubular electrodes with a simultaneous electrode reactions, 307-308
- Alkire, R. and Ng, P. K., on current distribution in a three-dimensional electrode under mass transfer controlled conditions, 418
- Beenackers, A. A. C. M., *et al.*, on charge transfer in fluidized bed electrodes, 423
- Bennion, D. N. and Newman, J., on current distribution in a three-dimensional electrode under mass transfer controlled conditions, 417, 427, 428
- Berzins, T. and Delahay, P., on consecutive diffusion-controlled electrochemical reactions, 107-111
- Birkhoff, G., *et al.*, on spherical bubble growth, 450
- Cheh, H. Y. and Tobias, C. W., on hemispherical bubble growth in nonuniform concentration fields, 452
- Chilton, T. H. and Colburn, A. P., on analogies for momentum transport in electrochemical systems, 171
on prediction of limiting currents from friction force measurements, 171
- Fleischmann, M., *et al.*, on mathematical model for a bipolar particulate cell, 433
- Fleischmann, M. and Kelsall, G. H., on local potential fluctuations in fluidized bed electrodes, 424
- Fleischmann, M. and Oldfield, J. W., on charge transfer in the particulate phase of fluidized bed electrodes, 423
- Fritz, W. and Ende, W., on gas bubble departure volume, 454
- Goodridge, F., *et al.*
on design of a fluidized bed cell for copper electrowinning, 426
on a mathematical model of a bipolar packed bed electrode, 433-435
- Goodridge, F. and Vance, C. J., on a design of a circulating bed cell for zinc deposition, 426
- Guidelli, R., on a generalized numerical procedure for solving boundary value problems, 102, 103
- Hartland, S. and Spencer, A. J. M., on potential and current distribution at a bipolar three-dimensional electrode, 431
- Ibl, N., *et al.*, on the optimization of stirring rate for the reduction of chromic acid in a flow cell, 224
- Ibl, N., *et al.*, on penetration mode for mass transport at gas evolving electrodes, 457
- Ilkovic, D., on diffusion in an expanding spherical electrode, 92
- Kambara, T. and Tachi, I., on consecutive diffusion-controlled electrochemical reactions involving an arbitrary number of reactants, 112-113
- Kasper, C., on a method for determining the primary current distribution, 246-247
- King, C. J. H. and Wright, A. R., on current distribution in a thin film electrode cell, 435
- Klingert, J. *et al.*, on a finite difference

- Klingert, J. *et al.* (*cont.*)
 method for numerical integration of the Laplace equation, 251–252
- Koutecky, J., on the instantaneous current at dropping mercury electrode, 95
- Kramers, H. and Alberda, G., on cells of perfect mixing, 350
- Kreysa, G. and Heitz, E., on the effective bed thickness of three-dimensional electrodes, 413
- Levich, V. G., on diffusion at an expanding spherical electrode, 96
- Lloyd, J. L., *et al.*, on the potential distribution in a three-dimensional bipolar electrode, 430
- Mazza, B., *et al.*, on critical phenomena at gas evolving electrodes, 470
- Newman, J.
 on the determination of limiting currents without ohmic potential drop effects, 221
 on the electric potential of ionic species in solution, 16
 on the influence of migration on limiting current for a rotating disk electrode, 184
 on the primary current distribution in rotating disk electrode, 248–251
 on the tertiary current distribution at a rotating disk electrode, 292–295
- Newman, J., *et al.*, on correction factors for migration in copper electrodeposition, 197
- Newman, J. S. and Tobias, C. W., on current distribution in porous electrodes, 408, 415
- Parrish, W. R. and Newman, J., on tertiary
- Parrish, W. R. and Newman, J. (*cont.*)
 current distributions for serrated electrodes, 295–296
- Plimley, R. E. and Wright, A. R., on local potential fluctuations in fluidized bed electrodes, 424
- Raats, C. M. S., *et al.*, on design of a fluidized bed cell for metal removal from dilute effluents, 427
- Ritter, H. L. and Drake, L. C., on pore size distribution by mercury porosimetry, 325
- Rousar, I. and Cezner, V., on penetration model for mass transport at gas evolving electrodes, 459
- Tarasevich, M. R., *et al.*, on mercury porosimetry of hydrophobic electrodes, 329
- Tobias, C. W., on the effect of gas evolution on the current distribution and ohmic resistance of electrolytic cells, 476
- Vogt, H.
 on bulk liquid flow effects on mass transport at gas evolving electrodes, 465
 on mass transport at gas evolving electrodes, 461
- Wenger, R. S. and Bennion, D. N., on design of a copper concentration cell with fluidized bed electrodes, 425, 429
- Wilke, C. R., *et al.*, on approximate methods for calculating the effect of migration on limiting current, 190, 191
- Zuber, N., on heat transfer in nucleate boiling, 465

Subject Index

- Abel integral equation, 119
- Activation energies
 comparison with smooth electrodes, 366
 for porous two-phase electrodes, 365
- Activation overpotentials, 242, 292
 in electroplating, effect of organic additives, 290
 equalizing action of, 257, 263
 and concentration overpotential, 290, 295
 and current density, 294–295
 and throwing power, 273–274
 at limiting current, 299
 and local current density, 255
 in macroprofiles, 291
 at planar electrodes, 291
 and potential difference in electrode-solution interface, 293
 and secondary current distributions, 256, 260, 271
 for simultaneous reactions in tubular electrodes, 308
 Tafel equation for, 261–262
 and Wagner number, 275
- Active layer formation
 in hydrophilic electrodes, 323, 374
 in hydrophobic electrodes, 380
- Adzumi constant, 356
- Air electrodes, gas diffusion in, 373
- Alumina electrolysis
 anode effect in, 447, 468, 470
 current density, critical, at graphite, in, 467
 gas bubble departure diameter in, 455
 gas volume flux at graphite in, 467
- Aluminum electrolysis, 240
- Amalgamation, effect on mercury porosimetry, 327
- Amalgams, formation of, interfacial concentration in, 52
- Ammonium bicarbonate, 323, 326
- Analogies
 Chilton-Coburn, 171
 between concentration of energy and concentration of species, 162
 of current distribution with heat and mass transport, 245
 between heat flux by conduction and flux, 162
 between mass flux density and heat flux density in ideal solutions, 161
 between mass, heat, and momentum transport, 161–172, 222
 application of, 164
 between molar concentration differences and momentum concentration, 166
 between momentum flux and diffusion, 162
 between Ohm's law, Fick's law, and Fourier's law, 167
 between turbulent and molecular transport processes, 176
- Anode effects
 in alumina electrolysis, 447, 468, 470
- Barycentric velocity, as frame of reference, 7, 11
- Batteries, 278
 current distribution in, 240
- Bent cathode test, 310
- Bessel equations, 75
- Bessel functions, 100, 101, 381
- BET method, 328
- Bifurcation of pores, 331–335

- Binary electrolytes
 concentration-time relationship in, 74
 effective diffusion coefficient in, 74
 material balance in, 73-74
- Bipolar electrodes, 277
 characteristic lengths for electrolytic cells
 with, 270
 current distribution for electrolytic cells
 with, 270
 three dimensional copper electrodeposition
 on, 288-289
- Bipolar fluidized bed electrodes, 396, 438
- Bipolar three-dimensional electrodes, 396
 current distribution at, 429
 experimental aspects of, 436
 fixed bed type, 436
 industrial applications of, 438
 mathematical models of, 430
 polarization curve for, 431
 potential distribution at, 429
- Blasius equation, 180, 204, 210
- Boiling
 analogy with gas evolving electrode
 processes, 447
 burnout effect in, 468
 film, 447, 469
 critical wavelength for, 468, 469
 nucleate, 447, 449, 465
- Boundary layers
 mass balance in, 170
 for mass, heat, and momentum transport,
 167-168
 ratios of, 169
 simultaneous laminar and turbulent flow
 in, 181
 thickness of, 170
 enlargement in turbulent flow, 181
 in laminar flow, 167
 normalized, Sherwood and Nussett
 numbers as, 169
- Branching
 and liquid penetration, 335
 of pores, 331-335
 probability of, 335
- Breakthrough, 335
 effective electrical conductivity at, 359
 in hydrophilic three-phase electrodes, 372
 in hydrophobic electrodes, 380
 in mercury porosimetry, 344
 and percolation probabilities, 339, 341
 in square lattice model of porous media,
 337, 338, 339, 341, 359
 threshold for, 341
- Breakthrough (*cont.*)
 in triangular lattice model of porous media,
 341
- Bromine
 evolution in falling film cell, 435
 evolution in fixed bed cell, 435
 evolution at graphite fixed bed electrode,
 437
- Bubble curtain effect at gas evolving
 electrodes, 471
- Bubbles: *see* Gas bubbles
- Buoyancy, effect on gas evolution, 465
- Burnout effect in boiling, 468
- By-pass current, 435
 capillary flow, Hagen - Poiseuille equation,
 402
- Cadmium, electrodeposition from CdI_2
 solutions, 56
- Cadmium iodide, solutions
 cadmium deposition from, 56
 complex equilibria in, 26
 transport numbers for species in, 26
- Capacitative current, 39
- Capacitative current distribution, 304
- Capillary condensation, method for pore size
 distribution, 327, 328
- Capillary equilibrium, 330-345
 and effective electrical conductivity of
 porous media, 359
 experimental methods for, 342-345
 in hydrophobic electrodes, 380
 in intersecting pore model of porous media,
 333
 in packed sphere model of porous media, 345
 in three-phase hydrophilic electrodes,
 368, 372
- Capillary hysteresis, 327
- Capillary models,
 biporous
 of porous two-phase electrodes, 366, 367
 of three-phase hydrophilic electrodes,
 371-378
 of porous media, 324, 356
 comparison with serial model, 335
 Kozeny equation for, 348
 pore shape in, 348
 specific inner surface calculation, 325
- Capillary pressure, and pore filling, 330
- Carbon electrodes, porous, critical platinum
 content in, 384
- Carman - Kozeny equation, 402
- Catalysis, heterogeneous, 278

- Catalysts
 activity of, in porous media, 322
 in hydrophilic electrodes, 323
 utilization of, 376, 383
 in hydrophobic electrodes, 321
 in specific inner surface of porous media, 322
- Cells of perfect mixing
 model for porous media, 350 ff.
 average flow velocity in, 350
 characteristic length for, 351
 concentration distribution in, 351
 convective diffusion coefficient in, 351
 dispersion coefficient in, 351
 flow rate and hydrodynamic mixing in, 352
 molecular diffusion in, 352
 stagnant zones in, 352
- Channel cells
 effect of stirring on mass transport, current density and energy consumption, 224
 electrodeposition of copper in, with turbulent flow, 210
 efficiency of, size effects and, 233
 entrance effects in, 233
 local concentration variations in, 233
 local current density in, 233
 local limiting current density in, 233
- Channel flow, 58
 characteristic length in, 204
 developed
 effect of turbulence on, 204
 developing
 diffusion layer thickness in, 202, 203
 hydrodynamic boundary layer thickness in, 203
 mass transport in, with turbulence, 203
 entrance effects in, 202–204
 effect of electrode length, 204
 hydrodynamic boundary layers in, 202
 mass transport in, 203–205
 in parallel plate electrodes, 200–205
 Reynolds number for, 202
 specific stirring power of, 228
 velocity profiles in, 202
- Characteristic lengths, 158, 159, 203, 277, 289
 in cells of perfect mixing, 351
 for channel flow, 204
 and current distribution, 269
 electrode length as, 269
 in electrolytic cells with bipolar electrodes, 270
 in Grashof number, 194
 for horizontal electrodes, in natural
- Characteristic lengths
 for horizontal electrodes, in natural (*cont.*)
 convection and laminar flow, 200
 in hydrophilic three-phase electrodes, 370, 374
 in hydrophobic electrodes, 381
 interelectrode distance as, 269
 in packed sphere model of porous media, 351
 for parallel plate electrodes, 201
 in porous media, 347, 351
 and convective diffusion coefficients, 350
 and dispersion coefficients, 350
 in porous two-phase electrodes, 363, 364, 365
 for primary current distribution at plane parallel and rotating disk electrodes 248
 and secondary current distribution
 uniformity, 271
 in Sherwood number, 194
 for Wagner numbers, 257, 268
- Characteristic velocity, 179
- Charge transfer, in monopolar fluidized bed electrodes, determination of, 423
- Charge transport
 coefficients, 280
 in Cu deposition from CuSO_4 , 27–28, 43
 through diffusion layers, 27–30
 in electrolytic systems, 18 ff.
 in reduction of $\text{Fe}(3+)$, 28
 and secondary current distributions, 257
 in Swiss-roll cells, 286
- Charging curves, specific surface
 determination from, 328
- Chemical potential, 163
 and diffusion flux, 16
- Chemical yield, 394
- Chilton-Colburn analogy, 171, 203, 210, 229
 in electrochemical measurement of electrode shear stress, 222
 and form drag, 172
- Chlorine electrolysis, 270
- Chlorine evolution from NaCl electrolysis, 206–207
 concentration profile for, 206, 207
 effect of supersaturation on, 207
 equivalent reaction layer
 thickness in, 207
 gas bubble formation in, 207
- Chromic acid, reduction of, 224–226
- Chronopotentiometry, 113
 AC, 125
- Circulation patterns, use in metal winning, 426

- Collection efficiency, of monopolar three-dimensional electrode, 418
- Concentration
 gradients of, effect on electroneutrality condition, 40
 interfacial, 41
 variations of, and conservation of mass in electrolytic systems, 10
- Concentration boundary layers, in turbulent flow, 179
- Concentration distribution
 in cells of perfect mixing, 351
 for consecutive diffusion-controlled reactions, 107
 at cylindrical electrodes
 under irreversible conditions, 102
 under reversible conditions, 100
 at cylindrical interface under steady-state conditions, 81
 in diffusion layers of rotating disc electrodes, 292
 for electrochemical reoxidation of products, 107
 in hydrophilic three-phase electrodes, 373
 in hydrophobic electrodes, 383
 at infinite plane interface under steady-state conditions, 78
 for instantaneous current pulses, 117
 for irreversible reactions under non-steady-state conditions and potential step perturbation, 91
 under linear potential sweep conditions, 117
 for irreversible reactions, 121
 for reversible reactions, 118
 of oxygen in gas pores of hydrophobic electrodes, 383
 at planar electrodes
 under constant current conditions, 103–104
 in porous two-phase electrodes, 365, 368
 of reactants in electrochemical systems, 66
 of reactants in supporting electrolytes, 73
 for reactions with an arbitrary number of reactants, 112
 for reversible reactions under non-steady-state conditions and potential step perturbation, 85–87
 at semi-infinite plane under non-steady-state conditions, 85–86
 under sinusoidal current conditions, 128
 under sinusoidal potential conditions, 126
 at spherical shell interface under steady-state conditions, 80
- Concentration distribution (*cont.*)
 for step-wise electroreduction of a single species, 110
 tertiary, in three dimensional electrodes, 297
- Concentration field, 53, 54
- Concentration gradients
 in diffusion layers, 136
 relation to turbulent mass flux, 176, 177
 at surface of planar electrodes, 152
- Concentration overpotential,
 44–46, 60, 242, 243, 261, 289, 291, 292
 and current density in Nernst diffusion layer, 141
 current dependence of, 140
 effect on equalizing action of activation overpotential, 290, 295
 in electroplating, effect of organic additives, 290
 IUPAC definition for, 45
 at limiting current, 299
 and limiting current in Nernst diffusion layer, 141
 in macroprofiles, 291
 measurement of, 45
 and ohmic potential 45, 46
 at planar electrode, 291
 and potential difference in electrode-solution interface, 293
 and potential drop in diffusion layers, 140
 for simultaneous reactions in tubular electrodes, 308
 at three dimensional electrodes, 278, 296
- Concentration profiles
 analogy with temperature profiles, 165
 analogy with velocity profiles, 166
 at cathode in copper electrodeposition, 133, 195
 for chlorine evolution from NaCl, 206–207
 in diffusion layers, 134–138
 in laminar convective diffusion, calculation of, 151
 at planar electrodes, 150, 155
 at vertical electrodes, in natural convection, 193
- Conductivity
 definition, 24
 electrical
 effective, of bubble-filled electrolytes, 471, 473
 of heterogeneous systems, Maxwell's equation for, 471
 and interaction diffusion coefficients, 35
 ionic, 24

- Conformal mapping, 248
- Conjugate forces, 6, 16
relationship with local entropy, 6
- Conjugate mass flux, 164
- Consecutive reactions, 107
- Conservation
in electrochemical systems, 143, 144
of energy, in electrolytic systems, 15
equation, boundary conditions for, 51
time-averaged, 176
equation for, analogy with Navier–Stokes
equation, 145
in ideal dilute solutions, 184
laws of, in electrolytic systems, 9–13, 32, 46,
163
of mass, in electrolytic systems, 10
and concentration variations, 11
equations for, and convection, 53
and frames of reference, 11
for homogeneous reactions, 14–15
of momentum, in electrolytic systems, 15
- Constant current experiments, 154, 158
- Constant potential experiments, 155, 158
- Contact angles
and anode effect in alumina electrolysis, 470
and anode effect in molten fluoride
electrolysis, 470
for bubble departure, at gas evolving
electrodes, 455
- Continuity equation, 12, 144, 193
for porous two-phase electrodes, 364
in turbulent flow, 175
- Controlled potential experiments, 47
boundary conditions for, 53
interfacial concentrations in, 52
limiting current in, 48, 49, 53
- Convection, 2, 299
at cylindrical electrodes, under reversible
conditions, 101
effect on diffusion layer thickness, 134–135,
139
in electrochemical system, 65–67, 72
and momentum transport, 162
natural, effect on heat transport in nucleate
boiling, 466
natural, elimination of, in electrochemical
systems, 75
at porous electrodes, 319
in porous two-phase electrodes, 367–368
- Convection-free electrolysis, 199
diffusion layer thickness in, 135, 168
hydrodynamic boundary layers in, 168
thermal boundary layers in, 168
- Convective diffusion, 307
in laminar pipe flow, 349
in natural convection, 192, 226
in porous electrodes, 345–353
in porous media, 345–353
and stagnant zones, 352
in porous two-phase electrodes, 367
in turbulent flow, 175
- Convective diffusion coefficients
in cells of perfect mixing, 351
effect of stagnant zones, 352
effect of flow rate on, 351, 352
in laminar pipe flow, 349
in porous media, 348, 351
and characteristic lengths, 350
experimental methods for, 349
- Convective diffusion equation, 73–74
- Convective flux, 17
in diffusion layers, 134, 137
in electrochemical systems, 72
equations for, 143
in porous two-phase electrodes, 364, 368
relation to diffusion flux, 144
- Convective heat transport, correlation with
mass transport, 166
- Convective mass transport
industrial applications of, 220–233
introductory remarks, 134–138
measurement of, 221–222
prediction from heat and momentum
transport, 164
theoretical approaches to, 143–155
applied to copper electrodeposition,
208–217
- Convolution theorem, 110, 117
- Coordination number
average, in porous media, 323
and liquid penetration, in lattice models of
porous media, 345
- Copper
deposition at porous flow-through
electrodes, 425, 428, 429
electrodeposition, 133, 134, 167, 186–189,
194, 197, 208, 210–212, 213–216,
226–227
electrodeposition on bipolar three
dimensional electrodes, 288–289
electrodeposition from copper sulfate, 1–2
charge transport in, 27–30
concentration profile for, 29
diffusion current in, 30
diffusion layer in, 27, 28
equilibrium potential for, 44

- Copper
- electrodeposition from copper sulfate (*cont.*)
 - limiting current for, 3
 - mass transport in, 27–30
 - migration current in, 30
 - secondary current distribution for, 271
 - Wagner number for, 271
 - electrodeposition on nickel, profile of, 242
 - electrorefining of, 240
 - electrowinning
 - with fluidized bed electrodes, 425, 428
 - limiting current in, 305
 - silver content of copper deposits in, 305
 - simultaneous electrodeposition with silver, 305
- Copper sulfate, integral diffusion coefficient for, 211
- Corner electrodes
 - current lines for, 252, 253, 263–264
 - potential map for, 252, 253, 263–264
 - secondary current distributions at 263–264
- Corrosion, 22
- Cottrell method, 56
- Cottrell's equation, 158
- Coupling coefficients, 6, 15, 16
- Covering power, definition, 258
- Critical phenomena, at gas evolving electrodes, 468–470
- Crystallization
 - current density variation at preferential sites for, 290, 291
 - in electroplating, effect of current distribution on, 290–291
- Crystallization overpotential, 291
- Current concentration, 205
- Current density
 - average
 - and current distribution, 272
 - and electrode length, 232
 - at planar electrodes, 153
 - and potential distribution, 272
 - for rotating disc electrodes, 294
 - and secondary current distribution, 276
 - for serrated electrodes, 295–296
 - and Wagner number, 272
 - and current distribution in porous electrodes, 298
 - at cylindrical electrodes
 - under irreversible condition, 101
 - under reversible conditions, 100
 - at dropping mercury electrodes, 92
- Current density (*cont.*)
 - at edges of planar electrodes, relation to activation overpotential at center, 255
 - effect on applied voltage and energy consumption in industrial electrolytic cells, 223–224
 - effect on reaction rates, 223
 - in electrodes, as a scalar quantity, 244
 - in electroplating, 290, 291
 - and equalizing action of activation overpotential, 294–295
 - and flow velocity, 20
 - and frames of reference, 19
 - at hanging mercury electrodes, 92
 - in hydrophobic electrodes, 379, 381, 382, 383
 - and interfacial flux density, 185, 221
 - ionic, in three dimensional electrodes, 279–280
 - for irreversible reactions under non-steady-state conditions and potential-step perturbation, 89
 - at junctions of insulating and conducting walls, 255
 - under linear potential sweep conditions
 - for irreversible reactions, 124
 - for reversible reactions, 120
 - local, 263, 265, 293
 - and concentration overpotential in macroprofiles, 291
 - below limiting current, 231
 - edge effects and, 254, 255
 - effect on current-voltage curves, 241
 - in electrodes, 244
 - in electropolishing, 301
 - and interfacial concentration, 219
 - for multiple reaction sequences, 305
 - of planar electrodes, 254, 255
 - of rotating disk electrodes, 250, 254, 293
 - variation of along electrodes, 239
 - of vertical electrodes, 296
 - in membranes, 79
 - in metal electrodeposition, with Nernst diffusion layer model, 138–140
 - and migration, 74–75
 - partial
 - and current efficiency, 305
 - deviations from overall current density, 306
 - distribution over electrode surface, 23
 - and interfacial flux density, 22
 - of ionic solutions, 18

- Current density
partial (*cont.*)
 for tubular electrodes, 307–308
 at planar electrodes, 151, 152, 153
 in constant potential experiments, 155
 in porous electrodes, 298, 319, 356
 in porous two-phase electrodes, 364, 368
 and potential difference across electrode-solution interface, 260
 relation to polarization resistance, 256
 relation to potential and time under constant current conditions, 106
 relation to total flux, 72
 for reversible reactions under non-steady-state conditions and potential step perturbation, 87
 in rotating disk electrodes, 251
 of serrated electrodes, 256
 under sinusoidal potential conditions, 127
 in solutions, as a vector quantity, 244
 at spherical electrodes, 90
 and tertiary current distribution, 289
 in three dimensional electrodes, 279–280
 total, of ionic solutions, 18
- Current density distributions, for serrated electrodes, 296
- Current distribution, 239–315
 analogy with heat and mass transport, 245
 and average current density, 272
 in batteries, 240
 between bipolar electrodes, 270
 in bipolar three-dimensional electrodes, 429–436
 calculation from potential distribution, 412
 characteristic lengths in, 269
 comparison of Wagner number and throwing power for describing, 273–274
 and crystallization in electroplating, 290–291
 determination with dimensionless groups, 267, 268
 effect of finite electrode conductivity on, 277–287
 effect of non-conducting films on, 304
 effect of reaction overpotential on, 303–304
 effect on scale-up, 271
 over electrodes, 244
 in electrolytic cells with bubble-filled electrolytes, 476
 experimental determination of, 419
 experimental methods for, 241
- Current distribution (*cont.*)
 in fluidized bed electrodes, 240
 effect of electrode conductivity, 278
 in gas evolving electrolytic cells, 277
 historical development of theories, 308–310
 at limiting current, 299
 and powder formation, 300
 in macroprofiles, 291
 mass transport control of, 305
 and mass transport in electrochemical systems, 74
 in monopolar three-dimensional electrodes, 407–424
 and optimum interelectrode distance, 240
 for planar electrodes, effect of electrode resistance on, 277
 in porous electrodes, 240
 effect of electrode conductivity, 278
 primary, 245–255, 275
 analogic methods for, 247, 248
 analytical solutions to Laplace equation
 for plane parallel and rotating disk electrodes, 247–251
 boundary conditions for integration of Laplace equation, 245–246
 definition of, 242
 effect of solution conductivity on, 254
 and electrode conductivity, 245
 for electroplating, 258
 finite element method for, 254
 Kasper method for, 246–247
 at limiting current, 299–300
 numerical methods for, 251–254
 perturbation method for, 253
 for plating at rotating disk electrodes by periodic current reversal, 254
 potential difference across electric double layer in, 245
 for rotating disk electrodes, 248–251, 252, 254
 over sinusoidal profiles, 253
 superposition method for, at rotating disk electrodes, 252
 variational method for, 253–254
 and Wagner number, 266
 and scale-up, 230
 secondary, 243, 255–277, 306
 and activation overpotentials, 256, 260, 271
 and average current density, 276
 boundary conditions for integration of Laplace equation, 260–262

- Current distribution
 secondary (*cont.*)
 characteristic lengths for, 271
 and charge transport, 257
 for copper electrodeposition from copper sulfate, 271
 at corner electrodes, 263–264
 electrolyte conductivity and, 271
 finite difference method for, 263
 macroscopic throwing power and, 271
 microscopic throwing power and, 271
 for parallel plate electrodes, 265–267
 and reaction rates, 287
 representation by dimensionless groups, 266
 resistance models of, 256–257, 283–284
 for ring disc electrodes, 265
 for ring electrodes, 265
 at rotating disk electrodes, 263, 265–267, 276–277
 for serrated electrodes, 265–268, 271
 significance for technical applications, 287
 for Swiss-roll cells, 284, 287
 for three dimensional electrodes, 278–287
 trends in, 270–274
 uniformity of, 255, 271
 variational method for, 264
 and Wagner number 266, 271, 281, 284, 286
 for simultaneous electrode reactions, 304–408
 global, 306–307
 numerical methods for, 307
 partial, 306–30
 tubular electrode model for, 307
 for simultaneous zinc electrodeposition and hydrogen evolution, 305
 tertiary, 243, 289–303
 boundary conditions for integration of Laplace equation, 292
 and current density, 289
 and current efficiency, 289
 and diffusion, 299–300
 in electroplating, 290
 IUPAC nomenclature for, 289
 at limiting current, 295, 299–303
 over a macroprofile, 291–296, 302–303
 over a microprofile, 290–291
 for rotating disc electrodes, 292–295, 302–303
 for serrated electrodes, 295–296
 for simultaneous reactions, 306
 symmetry of, 302
- Current distribution
 secondary (*cont.*)
 theoretical approaches to, 292 ff
 for three dimensional electrodes, 296–298
 uniformity of, 294, 295, 302
 for vertical electrodes, 296
 in three dimensional electrodes, 240, 277–287
 and throwing power, 273
 for tubular electrodes, 307
 in two-phase porous electrodes, 363
 between two wire electrodes in an electrolytic cell, 246–247
 types of, 242–243
 and electrode dimensions, 271
 uniformity of, 246, 255, 295
 and ratio of electrode-solution conductivity, 278
 and Wagner number, 273
 along wire electrodes, 277
- Current efficiency, 22–23, 221, 222, 223
 and irreversible reactions, 224
 and limiting current, 232
 and partial local current densities for multiple reaction sequences, 305–307
 and scale-up, 276
 and secondary potential distributions, 276, 288
 and tertiary current distribution, 289
 in three dimensional electrodes, 288
 variation of, along electrodes, 232
- Current lines, 244
 for planar electrode facing corner electrode, 252, 253
 for secondary current distributions at corner electrodes, 263–264
- Current-voltage curves
 and current distribution, 268
 determination of Wagner number from, 273
 effect of local current density variations on, 241
 measurement of, Luggin capillary for, 142
 for porous two-phase electrodes, 365
 for steady-state in stirred electrolytes, 141
 in three dimensional electrodes, 283
 use in calculation of diffusion coefficients, 221
- Darcy's law, 347, 357
 Densification coefficients, 193, 215
 of ions, 196
 Density distribution of, in porous media, 323

- Density profiles, for copper electrodeposition
from copper sulfate-sulphuric acid,
197
- Diaphragms, 428
- Differential pulse polarography, 115
- Diffusion, 1
- in air electrodes, 373
 - analogy with momentum flux due to viscous
drag, 162
 - and convective flux in boundary layers,
136, 137
 - at cylindrical electrodes, 100–102
 - under irreversible conditions, 101
 - under reversible conditions, 100
 - as an equalizing process, 163
 - in expanding spherical electrodes, 92, 96
 - and gas bubble growth, 450
 - of gases in pores, 354–356
 - of gases through electrolyte films, in
hydrophilic electrodes, 373
 - historical development of theory, 58–60
 - in hydrophilic three-phase electrodes,
373, 375, 376
 - in hydrophobic electrodes, 381, 383
 - at limiting current, 300
 - linear
 - infinite, 76
 - semi-infinite, 76
 - at a planar electrode, 158
 - non-stationary state, 82
 - at porous electrodes, 319
 - to porous electrodes, electric current
generation and, 362
 - in porous electrodes, Fick's law deviations
in, 355
 - in porous two-phase electrodes, 365, 366
 - stationary state, 77
 - Stefanian, 373
 - and tertiary current distributions over
microprofiles at limiting current,
299–300
- Diffusion coefficients, 9, 35–37
- calculation of,
 - effect of diffusion layer equilibria on, 58
 - in real solutions, 54–56
 - effective, 34, 36
 - in binary electrolytes, 74
 - in cells of perfect mixing with stagnant
zones, 352
 - in porous media, 346
 - in porous two-phase electrodes, 364
 - of three-phase systems, 346
 - and frames of reference, 17
- Diffusion coefficients (*cont.*)
- in hydrophilic three-phase electrodes, 373
 - for ideal solution, 71
 - integral for copper sulfate, 211
 - and ion mobility, 68
 - measurement of 56, 220
 - by calculation from current-voltage
curves, 221
 - by rotating disk electrodes, 221
 - in multicomponent systems, 56
 - of neutral electrolytes, 33
 - and reaction layer thickness, 207
 - for real solutions, 71
 - relation to diffusion flux, 71
 - relation to diffusion layer thickness at
rotating disk electrode, 186
 - in strong electrolytes, 71
 - table of, 36
 - and transport coefficients, 60
- Diffusion control, 50
- Diffusion currents, in hydrophilic electrodes,
373
- Diffusion flux
- analogy with heat flux by conduction, 162
 - and chemical potential, 16
 - in diffusion layers, 134, 136–137
 - for gases in porous electrodes, 354
 - in ideal dilute solutions, 17
 - in oxygen electrodes, 354
 - at planar electrodes, 152
 - in pores, 346, 354
 - in porous layers, 346
 - in porous media, 345
 - in porous two-phase electrodes, 364
 - for real solutions, 71
 - relation to convective flux, 144
 - relation to diffusion coefficient, 71
- Diffusion flux density, 162
- limiting, 213
- Diffusion layers, 2
- charge transport through, 27–30
 - at vertical electrodes, 192
 - concentration gradients in, 294
 - concentration of nonreacting species in, 218
 - concentration profile in, 134, 136, 164, 166
 - conductivity change in, 40
 - in copper electrodeposition, 133, 167
 - density changes in, at vertical electrodes, 192
 - distinction from double layers, 42
 - electroneutrality condition in, 39
 - mass balance in, for steady-state conditions,
134–137
 - mass transport through, 27–30, 48

- Diffusion layers (*cont.*)
 Nernst model, for, 137–142
 overlap of double layers, 42
 of rotating disc electrodes concentration distribution in, 292
 of serrated electrodes, 289
 temperature profiles in, 165
 thickness of, 134–135, 293, 302
 and concentration overpotential, 289
 and convection, 137
 in developing channel flow, 202
 effect on interfacial concentration, 219
 equivalent, 139
 for gas-evolving electrodes, 303
 interfacial flux density, 232
 and local limiting current density, 232
 and local mass transfer coefficients, 164
 along macroprofiles, 291
 in Nernst model, 137
 in pulse electroplating, 300
 and reaction layer thickness, 303
 relation to diffusion coefficient, 186
 relation to Schmidt number, 150–151
 at rotating disk electrodes, 184, 296
 at serrated electrodes, 296
- Diffusion overpotential, 46
- Diffusion potential, 43
 and conductivity, 43
 and ionic mobility, 43
 minimization of, by supporting electrolytes, 43
 and space charge, 43
 total current for, 43
- Dimensional analysis, 268
 advantages of, 161
 and analogy between mass, heat and momentum transport, 161
 application to linear diffusion at a planar electrode, 158
 application to planar electrodes with parallel flow, 159
 limitations of, 161
 of mass transport in electrochemical systems, 155–161
- Dimensional matrix, for mass transport at a planar electrode in laminar flow, 157
- Dimensionless groups, 156, 157, 277, 282
 in determination of current and potential distributions, 267
 in linear approximations, 283
 in mass, heat, and momentum transport, 168
 representation of secondary current distribution by, 266
- Dimensionless groups (*cont.*)
 for shear stress, 170
 in Tafel equation, 283
- Dimensionless variables, 156, 157
- Dispersion coefficients
 in cells of perfect mixing, 351
 effect of stagnant zones, 352
 effect of flow rate on, 351, 352
 in laminar pipe flow, 349
 in porous media, 348, 351
 and characteristic lengths, 350
 experimental methods for, 349, 352
- Double layers, 42
- Double porosimetry, 330
- Driving forces,
 in electrolytic systems, 5, 13
 and mass transport control of processes, 48
 relationship with flux, 5
- Dropping mercury electrodes
 average current at, 94, 96
 current density at, 91
 diffusion in, 92
 instantaneous current at, 94, 95
 limiting current at, 94
- Duhamel's method, 122
- Economics, of industrial electrolytic cells, 223
- Eddy diffusivity, 177
- Eddy promoters, 181
- Edge effects, on local current density
 at planar electrodes, 254, 255
 at rotating disk electrodes, 254
 at serrated electrodes, 296
- Effective pore space, 321
- Effluent treatment
 with porous flow-through electrodes, 425, 428
 with fluidized bed electrodes, 425
- Einstein-Stokes equation, 68
- Electrical conductivity, effective
 of electrolytes, 422
 of porous media, 357–362
 and blind pores 359, 361
 and breakthrough, 359
 lower limit of, 361
 upper limit of, 360, 361
 of porous two-phase electrodes, 364
- Electric current
 generation of, in porous electrodes, 319, 320, 362
 pressure drop, dependence of, in porous electrodes, 320

- Electric double layers, 244
 potential difference across, in primary
 current distributions, 245
- Electric migration, 2
 effect on electrode current, 37, 38
- Electric mobility, of ions,
 definition, 23
 dependence on interaction diffusion
 coefficients, 23
 dependence on phenomenological
 coefficients, 23
 and reference velocity, 23
- Electric potential
 calculation of, 50
 and concentration overpotential, 45
 and electric current, below limiting current,
 49
 of electrodes, equilibrium, 44
 calculation of, from Nernst's Law, 47
 elimination of, from fundamental mass
 transport equations, 31
 for ideal, dilute solutions, 31, 32
 for nonideal electrolytes, 33
 and interfacial concentration, below limiting
 current, 49
 of ions in solution, 16
 and migration flux, 16
- Electrochemical activity
 of hydrophobic electrodes, 382, 383
 and catalyst utilization, 383
 and electrode temperature, 382
 and Teflon content, 379, 382, 383
 of porous electrodes, 320, 362–384
 and transport processes, 345
 of porous two-phase electrodes, 364
 and diffusion, 365
 of three-phase hydrophilic electrodes,
 369, 370, 374
 comparison of theoretical and
 experimental results for, 375
 and pore size distribution, 371
 upper limit of, 373
- Electrochemical kinetics
 at porous electrodes, 319
 at smooth electrodes, 317, 318
- Electrochemical machining, 239, 254, 260
- Electrochemical potential, 5
 and Gibbs-Duhem equation, 5
 gradients of, 5
- Electrochemical reactions, and electrode
 current, 20
- Electrochemical transducers, 362
- Electrode current, 20, 60
- Electrode current (*cont.*)
 definition, 20
 density of, average, 22
 density of, local, 22
 effect of electric migration on, 37
 in electrode reactions, 20
 sign conventions for, IUPAC, 21
- Electrodes
 reactions at, driving forces for, 48
 shear stresses on, 162, 166
 smooth, comparison with porous electrodes,
 317, 318, 319, 366
 surfaces of, distribution of partial current
 density over, 23
- Electrode-solution interface, 277
 potential difference across, 263
 and activation overpotential, 293
 and concentration overpotential, 293
 and current density, 260
 linear approximation for, 261
- Electrolyte films at three-phase hydrophilic
 electrodes, 369, 373
- Electrolytes
 bubble-filled, 471
 effective conductivity of, 471
 gas level in, 472
 gas velocity in, 473–476, 477
 concentration of, effect on current
 distribution in monopolar
 three-dimensional electrodes, 415
 conductivity of
 and electrode utilization, 287
 and primary current distributions,
 254, 278
 specific, 287
 effective conductivity of, 422
 electroneutrality condition in, 39
 flow in monopolar three-dimensional
 electrodes, 408
 flow regimes in particulate electrodes, 339
 indifferent 29, 30
 supporting and diffusion potential, 44
- Electrolytic capacitors, 304
- Electrolytic cells, 246, 247
 with bipolar electrodes
 characteristic lengths in, 270
 current distribution in, 270
 bromine evolution in, 435
 with bubble-filled electrolytes
 current distribution in, 476
 resistivity of, 476
 chemical yield of, 394
 design of, 395

- Electrolytic cells (*cont.*)
 diaphragm-less, 428
 economics of, 223–230
 effluent treatment with, 425
 electrowinning with, 426
 energy efficiency of, with bipolar fixed bed electrode, 434
 energy yield of, 394
 falling film type, 435, 438
 optimum current density in, 224
 Raschig ring type, 437
 scale-up effects in, 230–233
 space time yield of, 394, 427
 stirring of, 225
 trickle bed type, 437
- Electrolytic systems
 pressure gradients in, 6
 temperature gradients in, 7
 transport processes in, 1
- Electrometallurgy, 240
- Electroneutrality condition, 12, 14, 31, 33, 39, 60, 184, 185, 244
 departure from, for single binary electrolyte, 40
 in diffusion layers, 39
 effect of concentration gradients on, 39
 validity of, 39
- Electrophoresis, counter current, 19
- Electroplating, 240, 241, 258–260, 276, 289
 coating thickness in, 258
 and current distribution in, 239
 covering power in, 258
 crystallization in
 and current density, 291
 and current distribution, 290–291
 current distribution in, 310
 and preferential nucleation, 290–291
 primary, 258
 at rotating disk electrodes with periodic current reversal, 254, 277
 effect of current distribution on coating thickness in, 239, 258
 at limiting current, 300
 organic additives in
 and activation overpotential, 290
 catalytic effects of, 301
 and cathodic leveling, 300–301
 and concentration overpotential, 290
 as inhibitors, 301
 and potential variations along electrodes, 275–276
 pulse, diffusion layer thickness for, 300
 at rotating disc electrodes, current for periodic current reversal, 254
- Electroplating (*cont.*)
 and tertiary current distribution, 290
 on thin wire electrodes, 277
 throwing power in, 258, 259, 290
- Electropolishing, 239, 301–302
 at limiting current, 301
 local current density in, 301
- Electrowinning, 240
 with fluidized bed electrodes, 426
- Energy balances, for incompressible fluids, 163
- Energy yield, 394
- Entrainment, of particulate electrodes, 401, 404
- Entrance effects, 404, 405, 423
 in channel flow, 202–204, 233
- Entropy, local
 and conjugate forces, 6
 and flux, 6
- Equilibrium, and conservation of mass in
 homogenous reactions, 14
- Equipotential surfaces, 246, 247
- Euler-Mascheroni constant, 100
- Exchange current density, 263, 294
- Exchange currents
 in electrochemical reactions, 423
 in hydrophilic electrodes, 373
- Experimental methods
 for determination of current distributions, 241
 for determination of potential distributions, 241
 for study of capillary equilibrium, 342–345
 for study of current generation in hydrophilic electrodes, 369
 for study of porous media, 325–330
- Extrapolation, of transport property values, 216, 217
- Falling film cell, 435, 438
 by-pass currents in, 435
- Faradaic impedance, 115, 127
- Fast reactions, definition, 207
- Ferrocyanide redox system, 86
- Fick's equations
 boundary conditions for, 76, 77
 for irreversible reaction, 84
 for potential-step perturbation, 82
 for reversible reactions, 83
 general solutions for, under nonsteady-state conditions, 82
 for irreversible reactions, 84
 for potential-step perturbation, 84
 for reversible reactions at semi-infinite plane electrodes, 84

- Fick's equations (*cont.*)
 general solutions for, under steady-state conditions, 77
 at cylindrical interface, 81
 at infinite plane interface, 79
 at spherical interface, 80
 under constant current conditions, 103
 under linear potential sweep conditions, 115
 under time-dependent boundary conditions, 114
 under sinusoidal conditions, 125
Fick's first law, 68, 137
Fick's laws, 58
 analogy with Fourier's law, 59
 analogy with Ohm's law, 59
 deviations from
 in diffusion in porous electrodes, 335
 and limiting current in porous electrodes, 355
Fick's second law, 70
Field cells, 258, 310
Film gas evolution, at gas evolving electrodes, 447, 467
 burnout effect and, 468
 critical volume flux for, 468
 critical wavelength for, 468
 potential and, 468
 stability criterion for, 469
 stability of, 468
Finite difference method
 for secondary current distributions in rotating disk electrodes, 263
 for solution of Laplace equation, 251–252
Finite element method, for integration of the Laplace equation, 254
Fixed bed electrodes, 400, 420, 425
 bipolar, 433, 436
 bromine evolution at, 435
 by-pass currents in cells containing, 435
 graphite, bromine evolution at, 436
 Raschig ring type, 436
 see also Packed bed electrodes; Particulate electrodes; Three-dimensional electrodes
Flow-by electrodes, 397
Flow velocity normalized, 160
Fluidization
 homogenous, 401
 incipient, 401
 minimum velocity for, 403
 of particulate electrodes, 401, 403
 spouting bed, 401
Fluidized bed electrodes
 current distribution in, 240
Fluidized bed electrodes
 current distribution in (*cont.*)
 effect of electrode conductivity on, 278
 effect of electrolyte conductivity on, 287
 entrance effects in, 18
 mass transfer coefficient of, 21
 see also; Bipolar fluidized bed electrodes; monopolar fluidized bed electrodes
Fluids, incompressible, energy balances for, 163
Fluoroplastic: *see* Teflon
Flux
 and average velocity, 8
 in convection, 17, 72
 definition, 4
 in diffusion, 16, 68
 equation for, 17
 in migration, 16, 68, 73
 and momentum in electrolytic systems, 12
 relationship to driving forces, 5, 13
 relationship to local entropy, 6
 total, in electrochemical systems, 67, 72
Flux density
 average, at planar electrodes, 153
 in diffusion layers, 136
 in ideal, dilute solutions, 143
 normalized, 160
Form drag, 399
 in turbulent flow, 172
Fourier number, 450
 for bubble growth at gas-evolving electrodes, 452
Fourier's law, 59
Frames of reference, 7, 18
 barycentric velocity as, 7
 and current density, 18, 19
 and diffusion coefficients, 17
 and electric mobility, 23
 mass average velocity as, 7
 molar average velocity as, 8
Friction
 coefficients of, 9
 dimensionless, 170
 measurement of, use in prediction of limiting current, 171
Friction factors, dimensionless, and wall shear stress, 179
Fuel cells, 298, 317, 318, 321
Fused salts, 15, 38
 transport numbers in, 25
Galvanostatic methods, 76, 240
Gas bubbles
 buoyancy of, 465

- Gas bubbles (*cont.*)
- coalescence of, at gas evolving electrodes, 452, 453
 - departure of, from gas evolving electrodes, 448–449
 - diameter of, at gas evolving electrodes, 453–455, 465
 - formation of, effect of supersaturation on, 208
 - growth of, 449
 - hemispherical, growth of, 451, 452
 - nucleation, at gas evolving electrodes, 446, 447, 452, 459
 - rising velocity of, in bubble-filled electrolytes, 473–475, 477
 - size of, effect on coalescence, 453
 - spherical, growth of, 449
 - static force balance on, 454
 - volume of, at departure from gas evolving electrodes, 453
- Gas electrodes, 317, 353–357
- polarization characteristics of, 375–378
- Gases, dissolved, Sherwood number for, 451
- Gas evolution, at electrodes
- analogy with boiling, 447
 - buoyancy effects and, 465
 - effect on liquid density, 465
 - effect on mass transport rate, 227
 - effect on resistivity and current distribution in electrolytic cells, 476
 - film, 447, 467
 - nucleate, 447, 470
 - regimes in, 446
 - supersaturation and, 448
- Gas evolving electrodes
- bubble coalescence at, 452, 453
 - bubble curtain effect at, 471
 - bubble departure at, 448–449
 - bubble diameter at, 453–455, 465
 - bubble growth at, 449
 - bubble nucleation at, 446, 447, 452, 459
 - bubble volume at, 453
 - characterization of, 445
 - critical phenomena at, 468–470
 - current density of, 446, 452, 455
 - critical, 467
 - diffusion layer thickness at, 303
 - film gas evolution at, 447, 467
 - gas evolution at, 446, 447
 - gas flow at, 479, 480
 - gas level at, 472
 - geometry of, 465, 468, 479
 - heat transport at, 465
 - analogy with mass transport, 466
- Gas evolving electrodes (*cont.*)
- horizontal, 468, 469
 - limiting current at, 227
 - limiting current distribution for, 303
 - mass transfer coefficient of, 456
 - mass transport at, 455
 - analogy with heat transport, 466
 - effect of inter electrode space geometry on, 465
 - effect of liquid bulk flow on, 464
 - macroconvection model for, 456, 463
 - microconvection model for, 456, 461–462
 - penetration model for, 456, 457–460
 - polarity of, 453
 - supersaturation at, 448, 449
 - wetting of, 455
- Gas film evolution: *see* Film gas evolution
- Gas pores, 329
- in hydrophilic three-phase electrodes, 375, 376
 - in hydrophobic electrodes, 380, 381
 - concentration distributions in, 383
- Gibbs-Duhem equation, 5, 7, 8, 13
- and electrochemical potential, 5
- Grain size distributions, in porous media, 323
- Graphic electrodes
- fixed bed type, bromine evolution at, 436
 - Raschig ring type, 436
- Grashof number
- and heat transport at gas evolving electrodes, 194, 198, 466
- Half-wave potential
- polarographic, for systems with arbitrary number of reactants, 112
 - potential-time curves and, 113
 - for reversible reaction under non-steady-state conditions and potential-step perturbation, 88
- Hanging mercury electrode
- concentration distribution at, 98
 - current density at, 91, 92, 96, 97
- Hankel transforms, 248
- Haring-Blum cells, 241, 258–259, 273–274, 310
- partial current-potential curves from, 273
- Heat transport, 161
- analogy with current distribution, 245
 - in boiling, 465
 - effect in scale-up, 230
 - at gas evolving electrodes, 465
 - measurement with extrapolated Schmidt and Prandtl numbers, 222

- Heat transport (*cont.*)
rate of, calculation from mass transport measurements, 222
at vertical electrodes, in natural convection and laminar flow, 198
- Helmholtz instability, 469
- Horizontal electrodes
mass transport at, in natural convection and laminar flow, 200
Sherwood number for, in natural convection and laminar flow, 200
- Hull cells, 259–260, 277, 310
- Hydrodynamic boundary layers
formation, and viscosity of, 133
momentum concentration in, 166
thickness of, 170
in copper electrodeposition, 134
effect of hydrodynamic flow on, 135
equivalent, 167
at rotating disk electrodes, 184
Schmidt number and, 151
in turbulent flow, 179
- Hydrodynamic flow, 162
- Hydrodynamic velocity, and current density, 20
- Hydrogen
evolution at gas evolving electrodes, supersaturation and, 449
evolution from NaOH, 468
simultaneous evolution with zinc electrodeposition from zinc sulfate, 305
- Hydrogen electrodes, polarization characteristics of, 377
- Hydrophilic electrodes, 368–378
active layer in, 323
catalysts in, 323
comparison with hydrophobic electrodes, 321
fabrication of, 323, 372
pore formers in, 323
three-phase, 368–378
active layers in, 374
biporous capillary model of, 371–378
breakthrough in, 372
capillary equilibrium in, 368, 372
capillary models for, 368 ff
catalyst utilization in, 376
characteristic lengths in, 370, 374
concentration distributions in, 373
current generation in, 369, 370, 373, 375, 376, 378
current generation zone thickness in, 374
cylindrical capillary model of, 371–378
- Hydrophilic electrodes
three-phase (*cont.*)
depth of penetration of electrochemical processes in, 376
diffusion coefficients in, 373
diffusion current in, 373
diffusion in, 373, 375, 376
distribution of current generation across, 374, 375
electrochemical activity of, 369, 370, 371, 373, 374, 375, 376
electrochemical burning of reactant gases in, 373
electrolyte films at, 369, 373
exchange current in, 373
fabrication of, 372
function of small pores in, 372, 373
gas pores in, 375, 376
intersecting capillary model for, 370, 371
mercury porosimetry of, 372
optimization of performance of, 368
Poiseuille flow in, 373
polarization curves for, 375–378
polarization distribution across, 373, 374
polarization of, 370, 374, 376
pore size distribution in, 371
potential distributions in, 370
pressure drop in, 369, 378
reactions in, 373
thickness of, 370, 374
working pressure of, 371
- Hydrophobic electrodes, 321, 378–384
active layer structure in, 380
advantages of compared to hydrophilic electrodes, 321
breakthrough in, 380
capillary equilibrium in, 380, 381
catalysts in, 321
average grain size, 379
catalyst utilization in, 376, 383
channels for electrolyte and gas flow in, 379, 380
characteristic lengths in, 381, 382
comparison with hydrophilic electrodes, 321
current density in, 381, 382, 383
current generation in, 383
diffusion in, 381, 383
distribution of gas and electrolyte in, 38
electrochemical activity of, 382, 383
and Teflon content, 379, 382, 383
gas pores in, 380, 381
hydrophobic pores in, 380
lattice model of, 381
optimization of, 383

- Hydrophobic electrodes (*cont.*)
 Platinum-Teflon, 379, 382, 383
 polarization of, 382
 pore size distribution in, 329
 pore types in, 329, 380
 porosity of, 380, 381
 structural model of, 379
 Teflon in, 321, 380
 agglomeration of, 380
 average size of, 283, 382
 and electrochemical activity, 379, 382, 383
 optimum content, 379, 383
 temperature effects in, 382, 383
 thickness of, 382
 wetting angle, effective, of electrolyte in, 379
- Ideal solutions, 15
 charge transport in, through diffusion layers, 27
 conductivity of, 24
 conservation of mass in, 184
 convective flux in, 17
 current density in, 24
 diffusion flux in, 17
 electric mobility of ions in, 23
 flux density in, 143
 migration flux in, 17
 transport numbers in, 26
- Ilkovic equation, 92, 94
- Impedance methods, for measuring mass transport coefficients, 222
- Instantaneous current pulses, 113
 concentration distribution for, 114
- Interaction diffusion coefficients, 33, 35–36
 and electric mobility, 23
- Interelectrode distance
 as characteristic length, 160
 as characteristic length for current distribution, 269
 optimum, and current distribution, 269
- Interfacial concentration, 292, 293, 153, 218–220
 and applied potential, 77
 at planar electrodes with uniform electrode current density, 154–155
 and reaction rate for simultaneous reactions in tubular electrodes, 307–308
 and surface concentration, 67
- Interfacial flow velocity, 166
- Interfacial plane, 47
- Interfacial tension, electrode-electrolyte
 effect on nucleate to film region transition, 470
- Interfacial tension (*cont.*)
 at gas evolving electrodes, 455, 470
- Interfacial velocity, 37
- Interferometry, 220
- Intersecting sphere model
 of hydrophilic electrodes, 371
 of porous media, 333
- Ionic activity, 34
- Ionic mass transport, in solutions with moderate concentration of supporting electrolyte, 184 ff.
- Ions
 charge of, and space charge, 60
 concentration of, and double layer thickness, 42
 conductivity of, 24
 densification coefficients of, 196
 electric mobility of, definition, 23
 electric potential of, in solution, 16
 mass transport of, mechanisms, 2
 partial current density of, in solution, 18
- Irreversible reactions
 current density of
 under linear potential sweep conditions, 124
 with potential-step perturbation, 88
 at spherical electrodes, 91
 at cylindrical electrodes, 101, 102
 rate equation for, under constant current conditions, 106
- IUPAC
 definition for concentration overpotential, 45
 nomenclature conventions for transport numbers, 25
 nomenclature for tertiary current distributions, 289
 sign conventions for electrode current, 21
- Jakob number, 450
- Junction potential, 43
- Kasper method, 246–247
- Knudsen flow
 in cylindrical capillaries, 356
 in porous electrodes, 353, 354
- Kolbe reaction, 438
- Kozeny constant, 348
- Labels, use in determination of dispersion coefficients, 349–351
- Laminar flow
 boundary layer thickness in, 167

- Laminar flow (*cont.*)
and natural convection
at horizontal electrodes, 200
at vertical electrodes, 192
in pipes, dispersion coefficients for, 349
at planar electrodes, mass transport for, 147
in porous media, 347, 349
transition to turbulent flow
critical Reynolds number for, 172
on a plate, 181
velocity profiles for, 181
- Laplace equation, 243, 293
analogic methods for solution of, 245
analytical methods for solution of, 245
for current distributions at plane parallel
and rotating disk electrodes, 247–251
boundary conditions for integration of
and electrode conductivity, 277
for primary current distribution, 245–246
249
for secondary current distributions,
260–262
for tertiary current distributions, 292
finite difference method for solution of,
251–252, 262–263
mathematical methods for solution of,
245 ff.
numerical methods for solution of, 245,
262–264
finite difference, 212–213, 251–252
finite element, 254
perturbation, 253
for primary current distributions, 251–254
for secondary current distribution,
262–264
superposition, 252–253
variational, 253–254
superposition method for solution of,
252–253
variational method for solution of, 253–254
- Laplace transforms, 85, 97, 101, 110, 114,
116–118
- Lattice models, of porous media, 335–345, 359,
360
square, 336–341
triangular, 341, 342
- Law of mass action, in multicomponent
systems, 56–57
- Legendre differential equations, 250
Legendre polynomials, 250
Le Goff number
as criterion for efficiency of stirring, 229
definition, 172
- Leveling, 239
anodic, 301–302
cathodic, 300–301
- Leveque approximation, 307
- Limiting current, 47, 48, 49, 60, 243
activation overpotential at, 299
calculation of,
in channel flow, 58
from concentration field, 54
cathodic, 40
Chilton-Colburn analogy for, 171
concentration overpotential at, 299
in controlled potential experiments, 49
correction factor for, 212
in cathodic reduction at a rotating disk
electrode, 186.
effect of concentration on, 190
effect of dissociation on, 188
for stagnant semi-infinite fluid and
growing mercury drop, 189
current distribution at, 299
and current efficiency, 232
at cylindrical electrodes, 100
at DME, 94
effect on metal quality in
electroplating and electrowinning, 233
effect of migration on, 182–191
approximate method for, 190
in copper electrodeposition, from cyanide
complexes, 186
at rotating disk electrodes, 184
electroplating at, 300
electropolishing at, 301
of external diffusion at porous electrodes,
362
at gas-evolving electrodes, 227, 303
in industrial electrolytic cells, 223
interfacial concentration at, 49
mass transfer at, 218
measurement of
with mercury electrodes, 142
with rotating disk electrodes, 142, 220
in Nernst diffusion layer, 141
in oxygen electrodes, 354, 356
in porous electrodes, 355
and external diffusion, 362
relation to mass transport coefficient, 221
relative equalizing actions of concentration
and activation overpotentials at, 295
and reversibility, 49, 53
for serrated electrodes, 296
and specific stirring power, 228
tertiary current distribution at, 295, 299–303

- Limiting current (*cont.*)
 uniformity of current distribution at, 295
 at vertical electrodes
 with natural convection, 226
 in natural convection and turbulent flow, 199
 Wagner number at, 299
- Limiting current density
 average, and electrode size, 232
 calculation by transport number method, 213
 effect of migration on, 211–212
 local, 302
 in channel cells, 233
 at rotating disk electrodes, 233
 measurement of, with segmented electrodes, 221
 and Nernst model, 140
 operation of industrial electrolytic cells below, 224
 for porous electrodes, 356
 for rotating disk electrodes, 294
 for serrated electrodes, 295–296
- Limiting current technique, experimental determination of mass transfer coefficient, 406
- Linear approximations, 306
 comparison with Tafel equation for secondary current distribution at rotating disc electrodes, 265–266
 of potential difference across electrode-solution interface, 261
 for secondary current distribution in three dimensional electrodes, 280–283, 286
 comparison with Tafel equation, 282–284
 dimensionless groups in, 283
 in Swiss-roll cells, 286
 Wagner number in, 283
- Linear potential sweep voltammetry, 115
- Liquid-gas electrodes, 321
- Liquid penetration
 and coordination number, 345
 depth of, in porous media, 332, 334, 337
 method for pore size distribution, 327
 and pore branching probability, 335
 in square lattice model of porous media, 336, 345
 and supercritical pore death probability, 335
- Luggin capillary, 45, 46, 52, 142, 241, 276
- Macroconvection model, of mass transport at gas evolving electrodes, 456, 463
- Macroprofiles, 261
 activation overpotential in, 291
 concentration overpotential in, 291
 current distribution in uniformity of, 291
 diffusion layer thickness in, 291
 of planar electrodes, 291
 and reaction overpotentials, 304
 of serrated electrodes, 289
 tertiary current distributions over, 291–296
 at limiting current, 302–303
 uniformity of current distribution in, 291
- Mass average velocity, 12
 as a frame of reference, 7, 8
- Mass balances
 in boundary layers, 170
 effect of migration flux on, in diffusion layers, 134, 190
- Mass flux density
 analogy with heat flux density, in ideal solutions, 161
 at planar electrodes, 152
- Mass transfer coefficients
 of fluidized bed electrodes, 406
 of gas evolving electrodes, 456
 of porous flow-through electrodes, 405, 406
- Mass transport
 analogy with current distribution, 245
 with chemical reactions, 205
 in concentrated solution, 33–35
 and current distributions at limiting current, 299
 through diffusion layers, 27, 48
 in dilute solutions, 16
 and electrode kinetics, 3
 in electropolishing, 301
 empirical procedures for determining variables of, 54
 fundamental equations for
 in electrolytic systems, 4–10, 16, 33–35
 elimination of electric potential from, 31
 for ideal solutions, 16, 17, 31, 32
 for real solutions, 33–35
 at gas evolving electrodes, 455
 historical development of theory, 58–61
 of ions, mechanisms of, 2
 on microprofiles, 300–301
 in multicomponent systems, 56
 at planar electrodes in laminar flow, dimensional matrix for, 157
 Prandtl boundary layer simplifications for, 147–155
 Von Karman-Pohlhausen method for, 148
 in porous two-phase electrodes, 367

- Mass transport (*cont.*)
rate of
accuracy of, 217
in developing channel flow, with turbulence, 203
effect of migration on, in binary and supporting electrolytes, 183
effect of stirring on, 224
at horizontal electrodes, 200
in industrial electrolytic cells, 224–229
in turbulent flow, 173
simplified approach to, in electrolytic systems, 54–58
at three-dimensional electrodes, 404
use of dimensionless groups, in describing, 168
- Mass transport coefficients
below limiting current, 219
calculation of from interfacial flux density and electrode current density, 221
and heat transport coefficients, 165
impedance methods for measuring, 222
local
and equivalent diffusion layer thickness, 164
measurement of, with segmented electrodes, 221
and Nernst diffusion layer thickness, 139
for nonreacting species in diffusion layers, 218
at planar electrodes, 152
in turbulent mass transport, 178–179
at vertical electrodes, in natural convection and laminar flow, 194
- Mass transport control
and current distributions for multiple reaction sequences, 305
in electropolishing, 301
in simultaneous copper-silver electrodeposition, 305
- Material balance equation, 73, 74
- Material yield, 22
- Mathematical models
of bipolar fixed bed electrodes, 433
of bipolar three-dimensional electrodes, 430–435
comparison with phenomenological theories for porous electrodes, 366–367
and dimensional analysis, 161
of monopolar three-dimensional electrodes, 407–419
activation controlled, 407
mass transfer controlled, 407
- McLaurin series, 97
- Mean free path, of porous electrodes, 353
- Mechanical mobility, 24
- Membranes, 15
current density in, 79
diffusion in, 79
- Mercury porosimetry, 325–327, 331
application to hydrophilic electrodes, 372
application to hydrophobic electrodes, 329
breakthrough in, 344
comparison with calculated values, 344
effect of pore geometry on, 327
and filling of supercritical pores, 344
and intersecting pore model of porous media, 343
limitations of, 327, 344
and supercritical pore branching, 344
and supercritical pore death, 344
- Methanol, electrooxidation at porous platinum electrodes, 366
- Microconvection model, of mass transport at gas evolving electrodes, 456, 461–462
comparison with penetration model, 462
Sherwood number for, 462
- Microprofiles
in electroplating, 290
mass transport control of electrochemical reactions on, 300–301
and reaction overpotentials, 303
of serrated electrodes, 289
tertiary current distributions over, 290–291
at limiting current, 299–300
- Migration
effect on current density, 30, 74, 75
effect on limiting current, 182
approximate method for, 190
in copper electrodeposition from copper sulfate without supporting electrolyte, 211–212
in copper sulfate - sulfuric acid systems, 188, 208
correction factor for, 197
in electrodeposition of copper from cyanide complexes, 186
at rotating disk electrodes, 184
effect on limiting current density, transport number method for, 211
effect on nonreactant species concentration in diffusion layer, 218–219
effect on reactant concentration at electrode-solution interface, 218
in electrochemical systems, 65, 66, 72
flux of, 17, 68, 73

- Migration (*cont.*)
 and transport number, 32
- Migration flux, in porous two-phase electrodes, 364
- Mixed control, 50
- Molar average velocity, 8
- Molten salts, 23
- Momentum
 conservation of, in electrolytic systems, 12
 and flux in electrolytic systems, 12
- Momentum flux
 analogy with diffusion, 162
 by viscous drag, 162
- Momentum flux density, 162
- Momentum transport, 161, 164
 boundary layer in, 167
 Chilton-Colburn analogy for, 171
 correlation with heat and mass transport, 171
 dimensionless groups, use of in describing, 168
 and form drag, 171
 at a plate, analogy with heat and mass transport, 166
 relation to Schmidt number, 179
 Sherwood and Nusselt numbers in, 170, 171
 at vertical electrodes, in natural convection and laminar flow, 192
- Monopolar electrodes, 277
- Monopolar fluidized bed electrodes, 425
 charge transfer in, 423
 current density in, 421
 current efficiency of, 426
 deposition of metals on, 425
 in diaphragm-less electrolytic cells, 428
 effective bed thickness of, 413
 effluent treatment with, 425
 electrowinning with, 425
 entrance effects in, 423
 expansion of, 421
 industrial applications of, 425
 potential distribution in, 424
- Monopolar three-dimensional electrodes, 394, 407
 characteristic penetration depth of, 413
 current distribution in, 407
 effect of electrolyte concentration on, 415
 experimental determination of, 419
 and Ohm's law, 408, 410
 uniformity of, 412
 effective bed thickness of, 413
 industrial applications of, 425
 mathematical models of, 407
- Monopolar three-dimensional electrodes
 mathematical models of (*cont.*)
 under activation control, 408
 under mass transfer control, 417
 collection efficiency of, 418
 potential distribution in, 417
 polarization curve of, 407, 410, 413
 potential distribution in, 407
 experimental determination of, 419
 specific area of, 422
- Monte Carlo methods, for percolation probabilities in porous media, 338, 339, 342
 comparison with method of tree-like pseudolattices, 339, 342
 and effective electrical conductivity, 359–360
- Nalco process, 394, 425
- Natural convection, 139, 192–200
 forced convection, comparison with, 195
 at horizontal electrodes, 200
 limiting current, effect on, 195
 at vertical electrodes, 226
- Navier-Stokes equation, 12, 13, 144–145, 163, 348
 integration of, 146–147
 to obtain velocity fields, 145
 similarity variables and, 148
 mass conservation equation, analogy with, 145
 source term and momentum transport, 164
- Nernst diffusion layer, 137–142, 299
 analogy with thermal boundary layer, 165
 thickness of
 at planar electrodes, 152
 and Schmidt number, 153
- Nernst equation, 83, 105
- Nernst's law, 47, 49, 52
- Nickel
 catalysts in hydrophilic electrodes, 323
 coating thickness on rotating disc electrodes of varying radii, 271–272
 copper coatings on, profile of, 242
- Non-steady-state processes
 concentration distribution for
 irreversible reactions, 90
 reversible reactions, 86
 at spherical electrodes, 90
 Fick's equations, general solutions for, 82
- Nucleation
 active sites for, at electrodes, 449
 in boiling, 447, 449, 465

- Nucleation (*cont.*)
in electroplating
 effect on current distribution on,
 290–291
 effect on current density, 291
of gas bubbles
 at gas evolving electrodes, 446, 447,
 452, 459
 heterogeneous, 448
 homogeneous, 447
 rate of, effect on roughness on, 449
Numerical procedures, for diffusion
 in planar and spherical electrodes, 102
 with time-dependent boundary conditions,
 116, 120
Nusselt number, 159, 169
 analogy with Sherwood number, 169
 correlation with Prandtl number, 169, 171
 in momentum transport, 171
 as normalized boundary layer thickness, 169

Ohm's law, 59, 139, 408, 410
 analogy with Fick's law and Fourier's law,
 167
Onsager's law, 6, 8, 13
Orthogonal collocation method, 264
Oscillographic polarography, 115
Osmotic pressure, 60
Overpotential
 total, and mass transport, 44
 see also Activation overpotential;
 Concentration overpotential;
 Diffusion overpotential;
 Transport overpotential
 total, and mass transport, 44
Overvoltage, 89
Oxygen
 concentration distribution of, in gas pores of
 hydrophobic electrodes, 383
 diffusion of, Stefanian, in air electrodes, 373
 evolution at gas evolving electrodes
 supersaturation and, 449
Oxygen electrodes, 376, 381, 383
 diffusion flux in, 354
 limiting current of, 354, 356
 polarization curves for, 378

Packed bed electrodes
 bipolar, 433–435
 bromine evolution at, 435
 by-pass currents in cells containing, 436

Packed bed electrodes (*cont.*)
 see also Fixed bed electrodes; Particulate
 electrodes; Three-dimensional
 electrodes
Packed sphere models
 characteristic length in, 351
 of porous media, 322
 capillary equilibrium in, 345
 porosity calculation from, 322
 specific inner surface in, 322
Pan's cavity scale, 310
Parallel plate electrodes, channel flow in,
 200–205
Parital currents, 273
 in simultaneous reactions, 305–307
Particulate electrodes, 396
 entrainment of, 401
 entrance effects in, 405
 fixed bed behavior of, 400
 fluidization of, 401
 pressure loss in, 401
 and fluidization, 403
 universal equation for, 403
 see also Three-dimensional electrodes
Penetration model, of mass transport at gas
 evolving electrodes, 457–460
 comparison with microconvection model,
 462
 shape factor correction, 459
 Sherwood number for, 459
 surface coverage and, 458
 waiting time and, 458
Percolation
 in porous media, 338, 385
 probability of
 and breakthrough, 339, 340, 341
 by method of tree-like pseudolattices,
 339, 341, 342
 by Monte Carlo method, 338, 339, 342,
 359, 360
 and effective electrical conductivity,
 359, 360
 threshold of, 341
 uniformity of, 340
Permeability, of porous media, 347, 348
Perturbation methods, for solution of Laplace
 equation, 253
Phase rule, 56
Phenomenological coefficients, 5, 6, 8
 and electric mobility, 23
Pin-hole method, for the determination of
 interfacial concentration, 220
Planar electrodes

- Planar electrodes** (*cont.*)
- average current density at, 153
 - average flux density at, 153
 - boundary layer thickness at, 148
 - concentration profiles at, 150, 155
 - current density at
 - and activation overpotential, 255
 - edge effects and, 254, 255
 - current lines for, 252, 253
 - effect of resistance on current distribution, 277
 - linear diffusion at, dimensional analysis of, 158
 - macroprofile of, 291
 - mass transport at, in laminar flow
 - application of Prandtl boundary layer simplification to, 147
 - dimensional matrix for, 157
 - Von Karman-Pohlhausen method for, 148
 - in parallel flow, dimensional analysis of, 159
 - potential map for, 252, 253
 - velocity profiles at, 151
- Plane parallel electrodes**
- primary current distribution in, 248
 - analytical solutions to Laplace equation for, 247–251
 - characteristic lengths for, 248
 - secondary current distribution for, 265–267
 - and Wagner number, 265, 267
 - similarity to Swiss-roll cell, 285
- Platinum**
- catalysts in hydrophilic electrodes, 323
 - catalysts in hydrophobic electrodes, 384
 - critical content of, in porous carbon-Teflon electrodes, 384
 - hydrophobic, with Teflon, 379, 382, 383
 - porous electrodes, 366
 - reduction of Fe^{3+} at, concentration profile for, 21
- Platinum black**, 329
- Poiseuille flow**
- in cylindrical capillaries, 356
 - of reactant gases in hydrophilic electrodes, 373
- Poisson's equation**, 14
- Poisson's law**, 39, 60
- Polarization**
- of porous two-phase electrodes, 364, 365, 366
 - comparison with smooth electrodes, 366
 - at gas pores in hydrophilic electrodes, 376
 - of hydrophilic three-phase electrodes, 370, 373, 374, 376
- Polarization** (*cont.*)
- of hydrophobic electrodes, 382
- Polarization curves**
- for hydrophilic three-phase electrodes, 375–378
 - for hydrophobic electrodes, 382
 - for methanol electrooxidation of porous platinum electrodes, 366
 - of monopolar three-dimensional electrodes, 407, 410, 413
- Polarization resistance**
- relation to current density, 256
 - at serrated electrodes, 256
 - and Wagner number, 257
- Polarographic constant**, 94
- Polarography**, 30, 50, 56
- current distribution in, 240
- Pore formers**
- in hydrophilic electrodes, 323
 - in porous silver electrodes, 326
- Pores**, 321
- blind, 359, 361
 - branching of, 331–335
 - liquid penetration and, 335
 - probability for, 335
 - classification of, 323, 324
 - communicating, 321
 - critical, 331
 - cylindrical, 345
 - diffusion flux in, 346, 354
 - diffusion of gases in, 354–356
 - effective space of, 321
 - filling of, 335
 - capillary pressure and, 330
 - mechanisms in 331, 332
 - in square lattice model of porous media, 336, 337
 - with gases, 343
 - formation of in hydrophilic electrodes, 323
 - gas, 329
 - geometry of, effect on mercury porosimetry, 327
 - hydrophilic, 330
 - hydrophobic, 330, 380
 - intersecting, 333, 343
 - isolated, 321
 - looping in, 331, 332
 - shape of, 323, 324, 348
 - effect on mercury porosimetry, 327
 - and effective diffusion coefficients, 346
 - size of, 323, 324
 - and electrical conductivity of porous media, 357

- Pores
size of (*cont.*)
and gas diffusion in porous electrodes, 353
and Knudsen flow, 354
and permeability, 348
and specific inner surface, 326
specific inner surface of, 326
subcritical, 331
branching of, 344
death of, 332, 335, 344
effect on mercury porosimetry, 344
generation of, 333
in square lattice model of porous media,
336, 337
types of, 321, 323, 324, 331
in hydrophobic electrodes, 329, 330
- Pore size distributions
by capillary condensation, 327, 328
in capillary model of porous media, 324
in capillary model of porous two-phase
electrodes, 367
density of, 331
and electrochemical activity of hydrophilic
electrodes, 371
experimental methods for, 325–330
in hydrophilic three-phase electrodes, 371
of hydrophobic electrodes, 329, 330
in intersecting pore model of porous media,
343
by liquid penetration, 327
by mercury porosimetry, 325–327, 343, 344
comparison with calculations, 344
of porous silver electrodes, 326
and tortuosity, 325
- Porosimetry
double, 330
liquid, 327
mercury, 325–327
- Porosity
definition, in porous media, 322
of porous media, 322, 323, 324
calculation with capillary mode, 324
calculation with packed sphere model, 322
relation to tortuosity, 345
of three dimensional electrodes and effective
conductivity, 279
- Porous cup method, for diffusion coefficient
determination, 56
- Porous electrodes, 200, 317–391
anisotropic, 298
capillary models for, 366–367
limitations of, 367
classification of, 320, 321
- Porous electrodes (*cont.*)
comparison of phenomenological theories
and model in describing, 366–367
comparison with smooth electrodes, 318,
319, 366
convection at, 319
convective diffusion in, 345, 353
current density at, 298, 319, 356
current distribution in, 240, 298
effect of electrode conductivity on, 278
current generation in, 319, 362
pressure-drop dependence of, 320
diffusion at, 319
diffusion flux of gases in, 354
diffusion in, 355, 365, 366
electrochemical activity of, 320, 362–384
and transport processes, 345
electrochemical kinetics at, 319
exchange current in, 362
fabrication of, effect on grain size and shape,
323
flooded, outer diffusion current on, 320
gas diffusion in, 353–357
pore radius and, 353
inert layers in, 320
Knudsen flow in, 353, 354
limiting current density of, 356
limiting current in, 355, 362
mean free path in, 353
penetration of ionic current into, 298
platinum, 366
polarization curves for, 366
reacting layers in, 320
secondary current distribution for, 298
silver, 326
supercritical pores in, 331
surface area of, and limiting current, 355
thickness of, effect on kinetics at, 319
three-phase, 321
electrochemical activity of, 320
hydrophilic, 368–378
total current in, 319, 320
transfer current in, 298
transport processes in, 345–362
two-phase, 320
activation energy for, 365, 366
capillary models for, 366, 367
characteristic lengths for, 363, 364, 365
concentration distributions in, 365, 368
continuity equation for, 364
convection in, 367, 368
convective diffusion in, 367
convective flux in, 364, 368

- Porous electrodes
 two-phase (*cont.*)
 current density in, 364, 368
 current distribution in, 363
 current generation in, 362 ff
 current-voltage characteristics of, 365
 depth of reactant penetration in, 362, 363
 diffusion flux in, 364
 diffusion in, 365, 366
 effective electrical conductivity of, 364
 effective diffusion coefficient for, 364
 effective reaction rate constants for,
 365, 366
 efficiency of, 366
 electrochemical activity of, 320, 362–368
 key reactants in, 362, 365
 mass transport in, 367
 migration flux in, 364
 ohmic activation conditions in, 364, 365
 polarization characteristics of, 364,
 365, 366
 pore size distribution in, 367
 potential distribution in, 363
 specific surface area of, 366
 thickness of, 365
 transport coefficients for, 363
 types of, 320, 321
 volume reactions in, effective parameters
 for, 363
 see also hydrophilic electrodes; hydrophobic
 electrodes
- Porous flow-through electrodes, 396
 entrance effects in, 404
 industrial applications of, 425
 mass transfer coefficient of
 current technique, 406
 determination by limiting, 405, 406
 pressure loss in, 402
 see also three-dimensional electrodes
- Porous gas electrodes, 317
- Porous media, 321–330
 average coordination number in, 323, 345
 average grain radius in, 323
 branching of pores in, 331–335
 breakthrough in, 335, 337, 338, 339, 340, 359
 breakthrough threshold in, 341
 capillary equilibrium in, 330–345
 and effective electrical conductivity, 359
 experimental methods for, 342–345
 capillary model of, 324, 356
 comparison with serial model, 335
 Kozeny equation for, 348
 capillary pressure in, 330
 catalysts in, 322
- Porous media (*cont.*)
 cells of perfect mixing model of, 350 ff
 characteristic lengths in, 347
 and dispersion coefficients, 349
 convective diffusion coefficients of, 348, 349
 and characteristic lengths, 349
 convective diffusion in, 345–353
 critical pores in, 331
 current in, 357
 density distribution in, 323
 diffusion flux in, 345
 dispersion coefficients of, 348
 and characteristic lengths, 349
 effective diffusion coefficient in, 346
 electrical conductivity, effective of, 357–362
 and capillary equilibrium, 359
 and lattice models, 359–361
 and percolation, 359, 360
 three-phase systems, 358–362
 two-phase systems, 357–358
 experimental methods for studying, 325–330
 flow of liquids and gases in, 347
 random character of, 349
 gas penetration into, 342–343
 grain size distribution in, 323
 intersecting pore model of, 333
 and capillary equilibrium, 333
 mercury porosimetry and, 343
 pore size distribution in, 343
 laminar flow, 347
 lattice models of, 335–345
 liquid penetration into, 332, 334, 335,
 336, 345
 matrix of, 321, 322
 models of, 322 ff, 331–342
 intersecting sphere, 333
 packed sphere, 322, 351
 and pore size, 324
 capillary, 324, 335, 348
 serial, 334, 335
 lattice, 335–342, 359, 360
 cells of perfect mixing, 350 ff
 percolation in, 338, 339, 341
 and breakthrough, 339, 340, 341
 and effective electrical conductivity,
 359, 360
 threshold for, 341
 uniformity of, 340
 permeability of, 347
 and pore size, 348
 pore filling in, 330, 335, 337, 343
 with gases, 343
 mechanisms of, 331, 332
 pores in, types, 331

- Porous media (*cont.*)
pore size distribution of, 325–330
determination by mercury porosimetry, 325–327, 331
porosity of, 322, 323
and tortuosity, 345
properties of, 321–325
Reynolds number for, 347
serial model of, 334
comparison with capillary model, 335
spatial distribution of phases in, 330
specific inner surface of, 322, 323, 325
specific surface of
by BET method, 328
by charging curves, 328
square lattice model of, 336–341
breakthrough in, 337, 338, 339, 340, 341, 359
breakthrough threshold in, 341
clustering in, 338
depth of liquid penetration in, 337
effective electrical conductivity in, 360, 361
liquid penetration in, 336
percolation in, 338, 339, 340, 341, 385
percolation threshold, 341
permeability of links in, 336
pore filling in, 336, 337
supercritical pores in, 336, 337
subcritical pores in, 331
supercritical pore death in, 335
transport processes in, 345–362
triangular lattice model of, 341, 342
percolation in, 341
clustering in, 341
approximation by tree-like pseudolattices, 341, 342
Monte Carlo methods for, 342
breakthrough in, 341
turbulent flow in, 348, 349
- Potential distribution, 293
and average current density, 272
in bipolar three dimensional electrodes, 429
determination with dimensionless groups, 267
effect of finite electrode conductivity on, 287–289
over electrodes, 244
experimental determination of, 419
experimental methods for, 241
in hydrophilic three-phase electrodes, 370
in monopolar fluidized bed electrodes, 424
in monopolar three-dimensional electrodes, 407
- Potential distribution (*cont.*)
in porous two-phase electrodes, 363
secondary, 274–277, 287–289
and current efficiency, 276, 288
for rotating disc electrodes, 274–275
and scale-up, 276
and Wagner number, 274–275
in solutions, 250
for three dimensional electrodes, 287–289, 296
for tubular electrodes with simultaneous electrode reactions, 307, 308
between two-wire electrodes in an electrolytic cell, 246–247
types of, 242–243
- Potential maps
for planar electrode facing corner electrodes, 252, 253
for secondary current distribution at corner electrodes, 263–264
- Potential-step perturbation
of electrochemical systems, under non-steady-state conditions, 82
of irreversible reactions, 84, 88
of reversible reactions, 82, 84
- Potentiometry, 43
- Potentiostatic techniques, 240, 276
- Prandtl boundary layer simplification, 146
and integration of heat transport equations, 165
- Prandtl number
analogy with Schmidt number, 165, 168
correlation with Nusselt number, 169
deduction from Schmidt number, 170
extrapolation of, in heat transport rate measurements, 222
- Pressure gradients, 6
- Primary current distributions, 245–255
- Raschig rings, 436
- Reaction layers, 205
thickness of, and diffusion layer thickness, 303
- Reaction rates
comparison for porous and smooth electrodes, 366
and current density in electrochemical systems, 66
limitation by mass transport, 223–229
in porous two-phase electrodes, 365, 366
and secondary current distributions, 287
for simultaneous reactions in tubular electrodes, 307–308

- Resistance models, for secondary current distributions, 256–257
 in Swiss-roll cells, 284–286
 in three dimensional electrodes, 283–284
- Resistivity
 of electrolytic cells with bubble-filled electrolytes, 476
see also Conductivity
- Reversible reactions, Fick's equations, solutions for, 82
 at planar electrodes, 84
- Reynolds number, 267, 347, 348, 350, 399, 405, 406
 in channel flow, 202
 critical, 172, 181, 201
 dimensional analysis of, 159
 at gas evolving electrodes, 465
 local values of, 160
 as normalized flow velocity, 160
 and rising velocity of gas bubbles, 473–475
- Reynolds stress, 176
- Ring-disc electrodes, secondary current distribution for, 265
- Rotating cylindrical electrodes, specific stirring power of, 128
- Rotating disk electrodes
 concentration distribution in diffusion layers of, 292, 294
 conservation equations for, 184
 boundary conditions, 185
 current density in, 251, 294
 diffusion layer thickness at, 295
 effect of migration on limiting current at, 184
 effect of radius on nickel coating thickness uniformity, 271–272
 limiting current at
 correction factor for, 186–189
 method of determination, 221
 limiting current density in, 294
 local current density at, 250, 293
 edge effects and, 254
 for measurement of diffusion coefficients, 220
 primary current distribution in, 248–251, 252, 254
 analytical solutions to Laplace equation for, 247–251
 characteristic lengths for, 248
 superposition method for, 252
 for electroplating by periodic current reversal, 254, 277
 ratio of average current density to average limiting current density, 294
- Rotating disk electrodes (*cont.*)
 relative equalizing actions of concentration and activation overpotentials for, 295
 secondary current distributions in, 265–267, 276–277
 comparison of linear approximation and Tafel equation for, 265–266
 by finite difference method, 263
 secondary potential distribution for, 276–277
 and Wagner number, 274–275
 surface potentials at, 250
 tertiary current distribution for, 292–295, 302–303
 throwing power determination with, 259
 use in limiting current measurements, 142, 220
- Roughness, effect on nucleation rate, 449
- Sand's equation, 104, 158
- Scale-up
 and current efficiency, 276
 effect on current distribution on, 271
 effect of secondary potential distribution on, 276
 of industrial electrolytic cells, 230–234
 Schmidt number, 149, 150, 152, 179, 194, 405
- Segmented electrodes, 241
 use in measurement of local mass transport coefficients, 222
 use in measurement of mass transport variations in turbulent flow, 222
- Self-consistent field theory, 360
- Serial model, of porous media, 334, 335
 comparison with capillary model, 335
- Serrated electrodes
 current density at, 256
 diffusion layers at, 289
 diffusion layer thickness at, 296
 limiting current for, 296
 macroprofile of, 289
 microprofile of, 289
 polarization resistance of, 256
 ratio of average current density to average limiting current density, 295–296
 secondary current distribution for, 265–268
 comparison of theoretical and experimental results, 265, 268
 copper electrodeposition from copper sulfate, 271
 and Wagner number, 265, 267
 tertiary current distribution for, 295–296
- Shear stress
 at electrodes, 162, 164, 166

- Shear stress (*cont.*)
dimensionless groups for, 171
prediction of heat and mass transfer rates
from, 170–172, 222
turbulent, 176, 177
wall, dimensionless friction factor for, 179
- Shear stress velocity, 178
- Sherwood number, 169, 204, 210, 267
characteristic length in, 194
of a dissolved gas, 451
for horizontal electrodes, in natural
convection and laminar flow, 200
for laminar flow, 203
local values of, 160
for microconvection model of gas evolving
electrodes, 462
in momentum transport, 171
as normalized flux density, 160
for penetration model of gas evolving
electrodes, 459
in turbulent pipe flow, 180
for vertical electrodes, in natural convection
and turbulent flow, 199
- Silver
electrodes, porous, 326
mass transport control of electrodeposition,
305
- Similarity variables, 148, 149, 152
- Similitude, method of, 161
- Simultaneous reactions
current density for, 306
current distributions for, 304–308
mass transport control of, 305
tertiary, 306
current efficiency for, 305
limiting current for, 305
partial current density for, 307
partial local current density for, 305
potential distribution for, 307
in tubular electrodes, 307–308
- Solid electrolytes, 31
transport numbers in, 25
- Solutions
dilute: *see* Dilute solutions
ideal: *see* Ideal solutions
- Space charges
and diffusion potential, 43
and ionic charges, 60
- Space time yield, 394, 427
- Specific area, of monopolar three-dimensional
electrodes, 422
- Specific heat, 162
- Specific inner surface
Specific inner surface (*cont.*)
calculation of
in capillary model of porous media, 325
in packed sphere model of porous media,
322
of pores, 326, 327
of porous media, 322, 323
effect on catalyst activity, 322
- Specific resistance, of three dimensional
electrodes, 285
- Spherical electrodes, 80, 90, 45, 102
expanding, 92–99
- Stagnant zones, in cells of perfect mixing, 352
- Stanton number
definition, 180
in turbulent pipe flow, 180
- Steady-state processes, Fick's equations,
general solutions for, 77–82
- Stirring
effect on mass transport rate, optimum
current density and energy
consumption in electrolytic cells, 224
hydrodynamic model of, 226
methods of
effect on electrodeposition of copper, 227
effect on optimization of flow rate, 227
efficiency of, and Le Goff number, 229
- Stokes-Einstein equation, 190, 191
- Supercritical pore death, 332
and breakthrough, 344
effect on mercury porosimetry, 344
probability of
and liquid penetration, 335
and mercury porosimetry, 344
in serial model of porous media, 334
- Superposition method, for integration of the
Laplace equation, 252–253
- Supersaturation, at gas evolving electrodes,
448
- Surface concentration, 67
- Surface diffusion, in electrochemical systems,
75
- Surface potentials, at rotating disk electrodes,
250
- Surface profiles, of copper coatings
electroplated on nickel, 242
- Swiss-roll cells, 285–287
charge transfer resistance in, 286
electrode arrangement in, 285
electrolyte resistance in, 286
resistance model for, 284–286
secondary current distribution in, 284, 287
linear approximation for, 286

- Swiss-roll cells
 secondary current distribution in (*cont.*)
 and reaction rates, 287
 Tafel equation for, 286
 uniformity of, 287
 and Wagner number, 286
 similarity with plane parallel electrodes, 285
 similarity with three dimensional electrodes,
 285
- Tafel approximation, applied to polarization
 curves of monopolar three-
 dimensional electrodes, 407, 410, 413
- Tafel equation, 263, 271
 for activation overpotential, 261–262
 comparison with linear approximation for
 secondary current distribution at
 rotating disc electrodes, 265–266
 dimensionless groups in, 283
 for secondary current distribution in three
 dimensional electrodes, 280–283
 comparison with linear approximation,
 282–284, 286
 Wagner number in, 283, 286
 in Swiss-roll cells, 286
- Taylor instability, 469
- Teflon, 328, 329
 in hydrophobic electrodes, 321, 380, 384
 agglomeration of, 380
 average particle size of, 382, 383
 effect on electrochemical activity, 379,
 382, 383
 effect on gas and electrolyte distribution,
 380
 optimum content of, 379
- Temperature gradients, 7
- Temperature profiles, in diffusion layers, 165
- Thermal diffusivity, 162
- Three dimensional electrodes
 active surface area of, 280
 advantages of, 396
 bipolar copper electrodeposition on,
 288–289
 concentration overpotential at, 278, 296
 conductivity of
 effective, 279
 effect on depth of penetration of current
 into, 278, 284–285
 current density in, 279–280
 current distribution in, 240, 277–287
 between solid and liquid phases of, 284,
 285
 current efficiency of, 288
 cylindrical, 396
- Three dimensional electrodes (*cont.*)
 electronic current density in, 279–280
 equilibrium potential in, 288
 geometry of, 396
 hydrodynamic aspects of, 398
 ionic current density in, 279–280
 macroscopic model of, 279
 mass transport in, 404
see also; Bipolar three-dimensional
 electrodes; Fluidized bed electrodes;
 Monopolar three-dimensional
 electrodes; Particulate electrodes;
 Porous flow-through electrodes
 porosity of, 279
 potential difference between solid and liquid
 phases in, 280
 potential distributions for, 296
 pressure loss in, 402
 rectangular, 396
 secondary current distribution in, 278–287
 effect of electrodes size, 283
 and electrode utilization, 287
 and electrolyte conductivity, 287
 linear approximation for, 280–284
 and optimization of active layer thickness,
 287
 ratio of solid-liquid phase conductivities
 and, 283, 284, 285
 and reaction rates, 287
 resistance model for, 283–284
 slope of current voltage curve and, 283
 symmetry of, 283
 Tafel equation for, 280–284
 uniformity of, 284
 and Wagner number, 284
 secondary potential distribution in, 288
 similarity to Swiss-roll cell, 285
 specific resistance of, 285
 tertiary concentration distribution in, 297
 tertiary current distribution for, 296–298
 tertiary distribution of transfer current in,
 297
 tortuosity of, 279
 transfer current in, 280, 282, 284, 285
 transfer resistance of, 285
 types, 395
- Throwing power, 241, 272
 anodic, 260
 comparison with Wagner number for
 describing current distributions,
 273–274
 definition, 258–259
 determination of, 258–260
 in Field cells, 258

- Throwing power
determination of (*cont.*)
 in Haring-Blum cells, 258, 259
 in Hull cells, 259–260
 with rotating disk electrodes, 259
effect of cell geometry on, 259
and equalizing action of activation overpotential, 273–274
index limitations of, 259
limitations of, in describing current distributions, 273–279
macroscopic, 291–296
 and diffusion layer thickness, 289
 in electroplating, 290
 and secondary current distribution uniformity, 271
 and tertiary current distribution uniformity, 302
microscopic, 277, 290, 291
 and diffusion layer thickness, 289
 in electroplating, 290
 and secondary current distribution uniformity, 271
- Tortuosity
calculation of, 325
electrical, 324
geometrical definition of, 324
and porosity, 345
of three dimensional electrodes and effective conductivity, 279
- Tortuosity factor, 324, 346
and effective electrical conductivity of porous media, 357, 358
- Transfer current
in porous electrodes, 298
in three dimensional electrodes, 280, 282, 284, 285
- Transfer current distributions
tertiary, for three dimensional electrodes, 297
for three dimensional electrodes, 284–285, 297
- Transfer resistance, of three dimensional electrodes, 285
- Transition flow, 181
- Transition time, 104, 108, 110, 111, 113
- Transport controlled currents, 47
- Transport controlled experiments, 47
- Transport number, 25, 59
classical equation for, 26
effect of diffusion layers on, 32
in fused salts, 25
Hittorf's, 26
in ideal dilute solutions, 26
- Transport number (*cont.*)
and migration diffusion, 32
nomenclature for, IUPAC, 25
of real concentrated solutions, 33
in solid electrolytes, 25
- Transport number method
comparison with integral diffusivity method, 212
use in determining migration effects on limiting current density, 211
- Transport overpotential, 46
- Transport processes
conservation laws for, 163
macroscopic, 163
molecular, 163
in porous electrodes, 345–362
 effective coefficients for, 363
in porous media, 345–362
- Triangular potential sweep voltammetry, 115
- Tubular electrodes
activation overpotential in, 308
concentration distribution in, 308
current distribution for, with simultaneous electrode reactions, 307–308
partial current density in, 307
potential distribution for, with simultaneous electrode reactions, 307, 308
reaction rates for simultaneous reactions in, 307–308
- Turbulent diffusivity, 177
- Turbulent exchange coefficients
calculation of, 178
relationship to dimensionless velocity profiles, 178
- Turbulent flow, 181
concentration boundary layer thickness in, 179
concentration fluctuations in, 174
continuity equation in, 174
convective diffusion in, 175
enlargement of boundary layers in, 181
form drag in, 172
in industrial electrochemical reactors, 173
mass transport coefficient in, 178
mass transport in, 172
momentum equation in, 175
momentum transport in, 178
in pipes
 Blasius equation for, 180
 critical Reynolds number for, 181
 Sherwood number for, 180
 Stanton number for, 180
in porous media, 348, 349

- Turbulent flow (*cont.*)
 at rotating disk electrodes, effect on mass transport, 232
 velocity profiles for, 181
 at vertical electrodes, 199
- Turbulent mass flux, 176
 relation to concentration gradients, 177
- Variational methods
 for integration of the Laplace equation, 253–254
 for secondary current distributions, 264
- Velocity fields, by integration of Navier-Stokes equation, 145
- Velocity profiles
 analogy with concentration profiles, 166
 at cathode in copper electrodeposition, 198
 for channel flow, 202
 dimensionless, 178
 for laminar flow, 181
 in Nernst diffusion layer, 138
 at planar electrodes, 151
 for turbulent flow, 181
 at vertical electrodes, in natural convection, 192
- Vertical electrodes
 local current density in, 296
 tertiary current distribution for, 296
- Viscosity
 in hydrodynamic boundary layer formation, 133
 kinematic, 162
 and momentum flux, 162
- Viscous drag, 166, 399
 as an equalizing process, 163
 momentum transport by, 163
- Voltammetry, 99, 115
- Volterra integral equation, 119, 123
- Von Karman-Pohlhausen method
 and mass transport at planar electrodes, 148
 and mass transport at vertical electrodes, 194
- Wagner number, 276
 and activation overpotential, 275
 and average current density, 272
 characteristic length in, 257, 268
 comparison with throwing power for describing current distributions, 273–274
 for copper electrodeposition from copper sulfate, 271
 definition, 257
 determination of
 from current-voltage curves, 273
 for two simultaneous electrode reactions, 274
 effect of supporting electrolytes on, 272
 and electrode utilization, 287
 at limiting current, 299
 and primary current distribution, 266
 and secondary current distribution, 266, 268, 271
 of plane parallel electrodes, 265, 267
 of serrated electrodes, 265, 267
 in Swiss-roll cells, 286, 287
 of three dimensional electrodes, 281, 283, 284, 287
 and secondary potential distribution for rotating disc electrodes, 274–275
- Watt's nickel bath, 272
- Wetting
 of gas evolving electrode surfaces, 455
 of pore walls by electrolytes in hydrophobic electrodes, 379
- Wire electrodes, 246–247
 current distribution for, 277
 electroplating on, 277
- Yield
 chemical, 394
 current, 394
 energy, 394
 space-time, 394, 427